

# REPORT DOCUMENTATION PAGE

*Form Approved  
OMB No. 0704-0188*

Public reporting burden for this collection of information is estimated to average 1 hour per response, including the time for reviewing instructions, searching existing data sources, gathering and maintaining the data needed, and completing and reviewing this collection of information. Send comments regarding this burden estimate or any other aspect of this collection of information, including suggestions for reducing this burden to Department of Defense, Washington Headquarters Services, Directorate for Information Operations and Reports (0704-0188), 1215 Jefferson Davis Highway, Suite 1204, Arlington, VA 22202-4302. Respondents should be aware that notwithstanding any other provision of law, no person shall be subject to any penalty for failing to comply with a collection of information if it does not display a currently valid OMB control number. PLEASE DO NOT RETURN YOUR FORM TO THE ABOVE ADDRESS.

<b>1. REPORT DATE (DD-MM-YYYY)</b> 08/01/2002		<b>2. REPORT TYPE</b> Conference Proceedings		<b>3. DATES COVERED (From - To)</b> 01/05/2001 - 31/10/2001	
<b>4. TITLE AND SUBTITLE</b> Workshop on Quantum Transport in Semiconductors				<b>5a. CONTRACT NUMBER</b>	
				<b>5b. GRANT NUMBER</b> N00014-01-1-0115	
				<b>5c. PROGRAM ELEMENT NUMBER</b>	
<b>6. AUTHOR(S)</b> Ferry, David K.				<b>5d. PROJECT NUMBER</b>	
				<b>5e. TASK NUMBER</b>	
				<b>5f. WORK UNIT NUMBER</b>	
<b>7. PERFORMING ORGANIZATION NAME(S) AND ADDRESS(ES)</b> Arizona Board of Regents for and on behalf of Arizona State University Office for Research and Sponsored Projects Administration 270 Administration B Wing PO Box 873503 Tempe, AZ 85287-3503				<b>8. PERFORMING ORGANIZATION REPORT NUMBER</b> DWD 2651/TE (ARO) DWA 0052/TE (ONR) DWD 2652/TE (NASA)	
<b>9. SPONSORING / MONITORING AGENCY NAME(S) AND ADDRESS(ES)</b> Army Research Office, Research Triangle Park NC 27709-2211 Office of Naval Research, Arlington VA 22217-5660 National Aeronautics and Space Administration, Moffett Field CA 94035-1000				<b>10. SPONSOR/MONITOR'S ACRONYM(S)</b> ARO, ONR, NASA	
				<b>11. SPONSOR/MONITOR'S REPORT NUMBER(S)</b>	
<b>12. DISTRIBUTION / AVAILABILITY STATEMENT</b> Approved for public release					
<b>13. SUPPLEMENTARY NOTES</b>					
<b>14. ABSTRACT</b> A workshop was held on the topic of quantum transport in semiconductor devices. This workshop brought together 17 lecturers and 35 other attendees for this purpose.					
20020405 085					
<b>15. SUBJECT TERMS</b> Semiconductor devices, transport, quantum mechanics					
<b>16. SECURITY CLASSIFICATION OF:</b>			<b>17. LIMITATION OF ABSTRACT</b> None	<b>18. NUMBER OF PAGES</b> 256 plus CD	<b>19a. NAME OF RESPONSIBLE PERSON</b> David K. Ferry
a. REPORT Unclassified	b. ABSTRACT Unclassified	c. THIS PAGE Unclassified			<b>19b. TELEPHONE NUMBER (include area code)</b> 480.965.2570

# Advanced Research Workshop on Quantum Transport in Semiconductors

**Hotel Villa del Mare, Maratea, Italy 17-22 June 2001**

## Session 1

**Moderator:** John Barker, Glasgow University, "Status of the physics and modeling of ultrasmall devices"

- 1A Greg Timp, University of Illinois, "Making small MOSFETs: ballistic and quantum effects"
- 1B Max Fischetti, IBM Research, "Modeling small MOSFETs-the role of quantum and many-body effects"
- 1C Steve Goodnick, Arizona State University, "Full Band Structure Calculations for Transport in Wide-Band-Gap Semiconductors"

## Session 2

**Moderator:** Max Fischetti, IBM Research, "Semi-classical modeling of small semiconductor devices"

- 2A Asen Asenov, Glasgow University, "Discrete impurities and quantum potentials in MOSFET modeling"
- 2B Richard Akis, Arizona State University, "Effective potentials for quantum effects in MOSFETs"

## Session 3

**Moderator:** Antti-Pekka Jauho, Danish University of Technology, "Introduction to Quantum Transport"

- 3A David Ferry, Arizona State University, "Wave function approaches for self-consistent computations of transport in quantum dots and arrays"
- 3B John Barker, Glasgow University, "Trajectories in quantum mechanics"
- 3C Michael Bonitz, Rostock University, "Non-equilibrium Green's functions: transient phenomena and the role of the initial state for devices"

## Session 4

**Moderator:** Chihiro Hamaguchi, Osaka University, "The Metal-Insulator Transition"

- 4A Günther Bauer, University of Linz, "The metal-insulator transition in  $d = 2$ "
- 4B Jonathan Bird, Arizona State University, "The metal-insulator transition in open quantum dots and arrays"

## Session 5

**Moderator:** Michael Bonitz, Rostock University, "Spins and few particle problems in Semiconductors"

- 5A David Awschalom, UC Santa Barbara, "Spin coherence and optical measurements"
- 5B Daniel Loss, University of Basel, "Quantum computing in semiconductor systems"
- 5C Sankar Das Sarma, University of Maryland, "Few electron (and few impurity) systems-small system effects"

## Session 6

**Moderator:** Gerhard Klimeck, Jet Propulsion Laboratory, "Applications of quantum transport in devices"

- 6A Carlo Jacoboni, Modena University, "The Wigner function and quantum transport"
- 6B Harold Grubin, SRA, Inc., "Modeling resonant tunneling diodes with Wigner functions and density matrices"
- 6C Dejan Jovanovic, Motorola, "Non-equilibrium Green's functions for MOSFET modeling"

## Session 7

**Moderator:** Karl Hess, University of Illinois, "Applications of quantum transport in optics"

- 7A Tilmann Kuhn, University of Münster, "Quantum kinetics and the femtosecond time scale in optical excitation of semiconductors"
- 7B Rolf Haug, University of Hannover, "Single-electron charging effects in quantum dot arrays"

## Session 8

**Moderator:** Anant Anantram, NASA Ames, "Novel New Concepts"

- 8A Karl Hess, University of Illinois, "EPR Experiments: the Assumptions, and the Failure of Bell's Theorem"
- 8B Antti-Pekka Jauho, Danish University of Technology, "Scanning probe measurements of biomolecules on silicon surfaces"
- 8C Mark Lundstrom, Purdue, "The Landauer approach in device modeling"
- 8D Wolfgang Windl, Motorola, "Diffusion and clustering of impurities-a problem that cannot be ignored"

## Poster Presentations

### Poster Group 1

- 1-1 "Analytical theory for the low frequency transport and noise in Q1D conductors," G. Gomilla and L. Reggiani, Universidad Polytechnica Catalunya.
- 1-2 "Monte Carlo simulations of Wigner function tunneling: Role of the effective potential," L. Shifren and D. K. Ferry, Arizona State University.
- 1-3 "3D device Monte Carlo modeling with discrete impurities," S. Barraud, S. Galdin, P. Dollfus, Institut d'Electronique Fondamentale.
- 1-4 "3D modeling of imperfect interfaces and edges in decanano MOSFETs," S. Kaya, Ohio

University, and A. R. Brown, S. Roy, and A. Asenov, Glasgow University.

- 1-5 "Comparison of first-order quantum correction schemes in 3D drift-diffusion simulations in sub-0.1 micron MOSFETs," J. R. Watling, A. R. Brown, A. Asenov, and D. K. Ferry, Glasgow University.
- 1-6 "Quantum potential in the presence of heterointerfaces," J. R. Watling, R. C. W. Wilkins, and J. R. Barker, Glasgow University.
- 1-7 "Performance of scaled double delta doped PHEMTs," K. Kalna, J. R. Watling, A. Brown, and A. Asenov, Glasgow University.
- 1-8 "Electron transport and infrared photoconductivity in quantum dot structures," V. Ryzhii and V. Mitin, University of Aizu.
- 1-9 "Photoluminescence from hot electrons in low dimensional systems," H. Momose, Y. Inui, M. Itoh, and C. Hamaguchi, Osaka University.
- 1-10 "Nonlinear transport through an array of quantum dots," G. Kiesslich, A. Wacker, and E. Schöll, Technische Universität Berlin.

## **Poster Group 2**

- 2-1 "Quantum algorithms in the frame of a coupled-quantum-wires physical system," S. Reggiani, A. Bertoni, R. Brunetti, and M. Rudan, University of Bologna.
- 2-2 "Quantum waves in the coupled-wire Qubit," J. Harris, R. Akis, and D. K. Ferry, Arizona State University.
- 2-3 "Quantum mechanical study of nanoscale MOSFET," A. Svizhenko, M. P. Anantram, and T. R. Govindam, NASA Ames Research Laboratory.
- 2-4 "Effects of lead population on magnetic flux controlled dissipative electron transport through coupled quantum dots," N. Horing, Stevens Institute of Technology.
- 2-5 "Transport in quantum dot arrays," N. Mori, Y. Takamura, T. Ishida, and C. Hamaguchi, Osaka University.
- 2-6 "Non-equilibrium transport in nanostructures," J. Fransson, University of Uppsala.
- 2-7 "Tunneling spectroscopy of exchange-correlation interaction of electrons in Schottky barrier in quantizing magnetic field," A. Shulman, Institute of Radioengineering and Electronics.
- 2-8 "Stochastic simulation of the Barker-Ferry equation," M. Nedjalkov, Technical University of Vienna.
- 2-9 "Simulation of entanglement in semiconductor quantum wires," A. Bertoni, R. Ionicioiu, P. Zanardi, F. Rossi, and C. Jacoboni, University of Modena.
- 2-10 "Mesoscopic fluctuations of Coulomb drag between quasi-ballistic 1D wires," N. A. Mortensen, K. Flensburg, and A.-P. Jauho, Danish Technical University.

## **Poster Group 3**

- 3-1 "Spin dynamics in III-V quantum wells using Monte Carlo simulation," A. Bournel and P. Hesto, Universite Paris Sud.
- 3-2 "Electron-spin-phonon coupling and relaxation dynamics in a double quantum dot," V. Puller, L. Mourokh, and N. Horing, Stevens Institute of Technology.
- 3-3 "Quantum computing with spin qubits in semiconductors structures," V. Privman, Clarkson University.
- 3-4 "High-field transport through semiconductor heterostructures," M. Morifuji, Osaka University.
- 3-5 "Effect of electronic disorder on the phonon-drag," V. Mitin, Wayne State University.
- 3-6 "Wigner function dynamics in presence of an infinite potential barrier," P. Bordone and C. Jacoboni, Modena University.
- 3-7 "Quantum transport in 2D MOSFETs," A. P. Anantram, A. Svizhenko, and T. R. Govindan,

NASA Ames Research Center.

- 3-8 "Density-matrix modeling of terahertz photon-assisted tunneling in resonant tunneling diodes," M. Asada, Tokyo Institute of Technology.
- 3-9 "Hyperfine interaction between nuclear and electronic spins," I. D. Vagner, Holon Academic Institute of Technology.
- 3-10 "Metal-insulator transition in 2D few-electron systems," A. Filinov, M. Bonitz, and Yu. Lozovik, University of Rostock.
- 3-11 "Quantum dot modeling using NEMO-3D," G. Klimeck, F. Oyafuso, R. C. Bowen, T. B. Boykin, T. A. Cwik, E. Huang, and E. Vinyard, Jet Propulsion Laboratory.

# Quantum Transport in Semiconductors

Advanced Research Workshop  
on

## Introduction and Overview

John Barker  
University of Glasgow

Hotel Villa del Mare, Maratea, Italy  
17-22 June, 2001

# Quantum Transport in Semiconductors

Advanced Research Workshop  
on

## Introduction and Overview

Daniel E. W. Smith  
John Wiley &  
Sons, Ltd., Chichester,  
England, UK

Hall Griffin, Cambridge University Press, Cambridge

# Quantum Transport in Semiconductors

Advanced Research Workshop  
on

## Present state of play in the field

Encourage new workers  
Map out new opportunities  
Flag new directions

Our long-suffering sponsors:  
Office of Naval Research  
US Army Research Office  
NASA

1 Day Workshop on Quantum Transport Theory  
(Glasgow, May 2000)

## Origins

## Format

### Gordon Conference Style

- Introductory/tutorial material
- Advanced Topics
- Pre-publication ethics

## Sessions

- Moderator: overview and introduction (5-10 minutes)
- Speakers: 45 minutes (questions welcomed in talks)
- Questions & Discussion: 10-15 minutes per lecture

## Time Table

- Breakfast 8 00
- Morning session: 9 00-12 30 (coffee 11 10)
- Lunch 13 00
- Ad hoc sessions
- Poster session: 16 00-17 00
- Evening session: 17 00-19 30
- Dinner: 20 00

## Wednesday

- Excursion: Monastery visit + shopping in Matatea
- Please sign up: Rosella Brunetti
- Dinner: 20 00

## Session 1: Monday, June 18

### Ultra-small devices

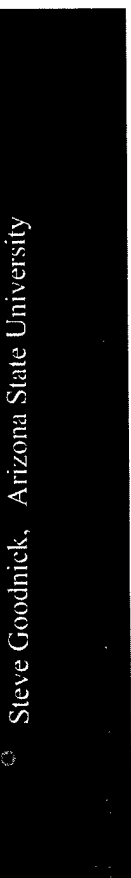
Status of Physics and Modelling of ultra-small devices

- Moderator: John Barker, University of Glasgow
- Greg Timp, University of Illinois
- Max Fischetti, IBM T J Watson Research Lab
- Steve Goodnick, Arizona State University



## Status of the physics and modelling of ultra-small semiconductor devices

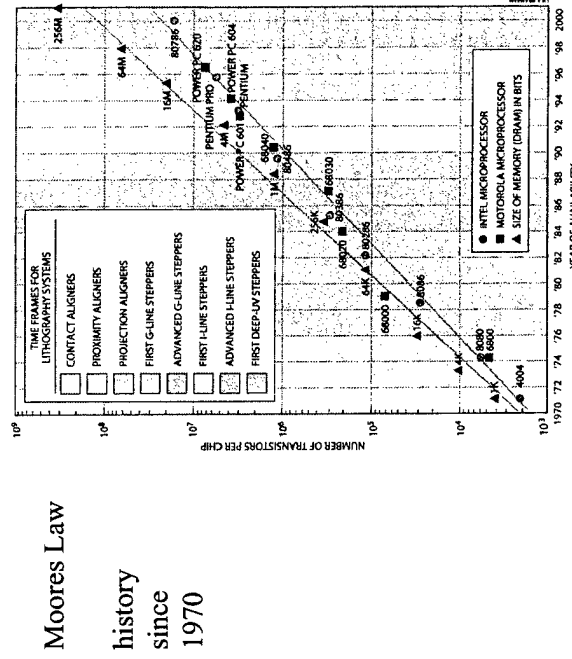
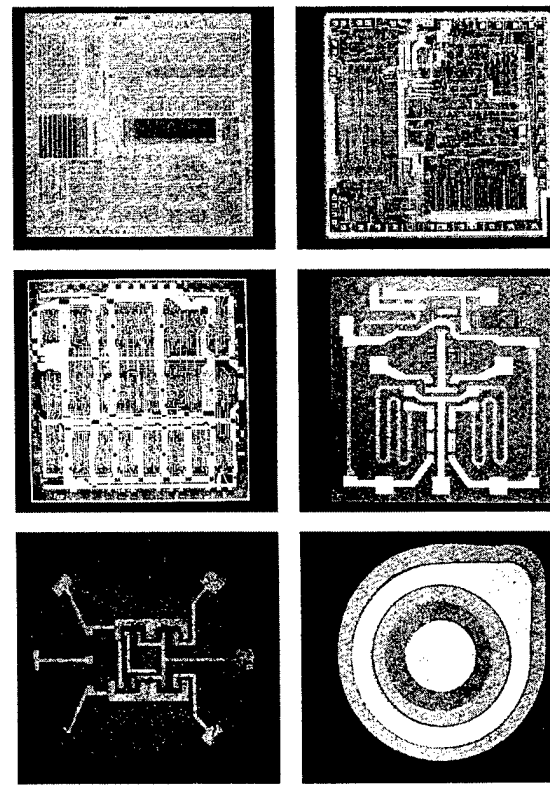
John. R. Barker  
Nanoelectronics Research Centre  
Department of Electronics and Electrical Engineering  
University of Glasgow



© NASA Ames Research Center  
This is a photograph of a 1.0-micron feature size  
wafer level chip carrier package.



Advanced Research Workshop  
on  
Quantum Transport in Semiconductors



SOURCES: ULSI Research Inc., Integrated Circuit Engineering Corporation

© 1991 Hughes 7425  
F. S. Teng, et al., Hughes  
Microelectronics Center, Tewksbury, MA  
F. S. Teng, et al., Hughes  
Microelectronics Center, Tewksbury, MA

The dinosaur model: silicon will eventually become extinct



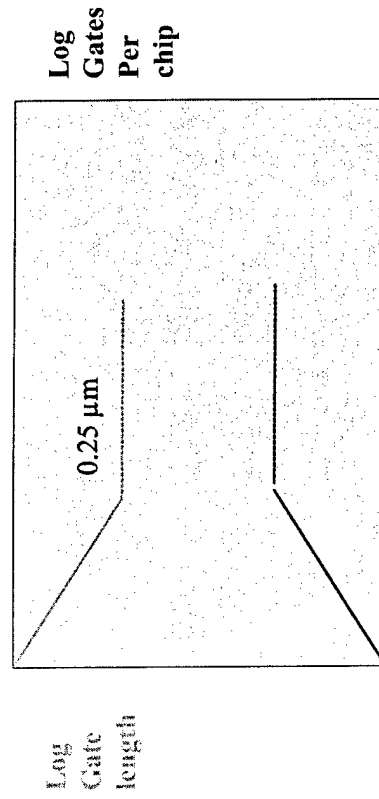
L.H. Hodder (left)  
H. H. H. Hoekstra (right)  
From: *Computer Components*,  
Society of Industrial Engineers  
1979

.... due to impending catastrophe

After the catastrophe, a long hiatus will occur and silicon's role will be replaced by new species : quantum, molecular...

### Projected Breakdown of Moore's Law

1977



(challenged by JRB/DKF  
In 1979 - 25 nm )

L.H. Hodder (left)  
H. H. H. Hoekstra (right)  
From: *Computer Components*,  
Society of Industrial Engineers  
1979

L.H. Hodder (left)  
H. H. H. Hoekstra (right)  
From: *Computer Components*,  
Society of Industrial Engineers  
1979

QuickTime™ and a  
Photo-JPEG decompressor  
are needed to see this picture.

The guiding philosophy behind semiconductor quantum transport theory strategy has often been :

- Moore's empirical Law will eventually breakdown at small enough physical scales.
- Quantum effects will likely become dominant by then.
- Prepare for new devices based on novel quantum concepts:
  - discrete energy levels
  - wave interference devices
  - tunnel devices
  - single electronics
  - quantum computing...

© A. Röcker, 2001  
Hierarchies of Device  
Technology, Springer-Verlag  
published under license  
of the International Society  
for Microelectronics and Electron

The silicon MOSFET scene

The first moves:

Ballistic transport	Serious non-equilibrium effects
Schrödinger-Poisson	Quantum levels in channel
Empirical	Density gradient or
Drift Diffusion	Quantum potential
Hydrodynamic	Corrections
Monte Carlo	Tunnelling &
	Keep charge away from interfaces
<b>Conventional device modelling:</b>	
Self-consistent via Poisson equation	
Empirical	
Drift Diffusion	
Hydrodynamic	
Monte Carlo	

© A. Röcker, 2001  
Hierarchies of Device  
Technology, Springer-Verlag  
published under license  
of the International Society  
for Microelectronics and Electron

## What has actually happened

Robert Chau (Intel) 2001

"High performance 30 nm gate length CMOS transistors operating at  $V_{cc} = 0.85$  V demonstrated for 65 nm logic technology node, which will be ready for production in 2005."

Year	1999	2001	2004	2008	2011	2014
MPU Gate Length (nm)	140	100	70			
Oxide thickness (nm)	1.9	2.5	1.5	1.9	1.2	1.5
Drain extensions (nm)	42	70	30	50		

Solution exists	
Solution Being Pursued	
No Known Solutions	

## Scaling of MOSFETs to decanano dimensions

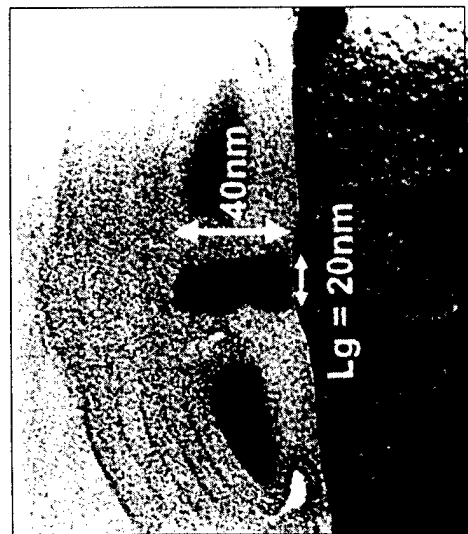
(International Roadmap for Semiconductors - 1999 Edition)

© A. Röcker, 2001  
Hierarchies of Device  
Technology, Springer-Verlag  
published under license  
of the International Society  
for Microelectronics and Electron

Year	2001	2003	2005	2007	2009
Node	150	90	65	45	30
Gate Length	70	50	30	20	15

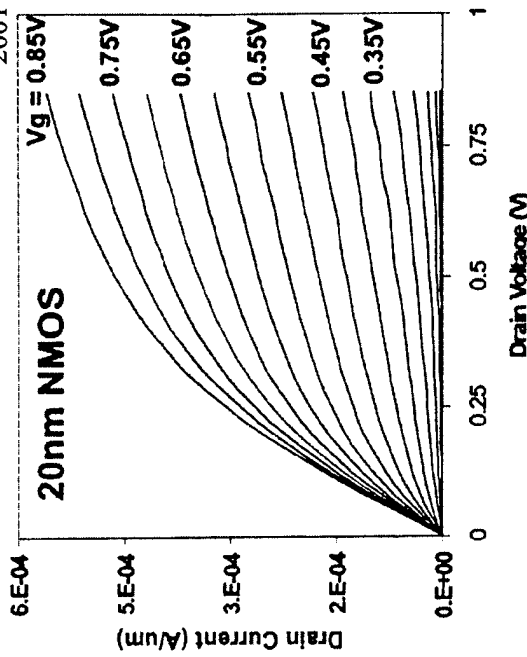
In production

© A. Röcker, 2001  
Hierarchies of Device  
Technology, Springer-Verlag  
published under license  
of the International Society  
for Microelectronics and Electron



TEM Cross section of a 20 nm gate length NMOS transistor

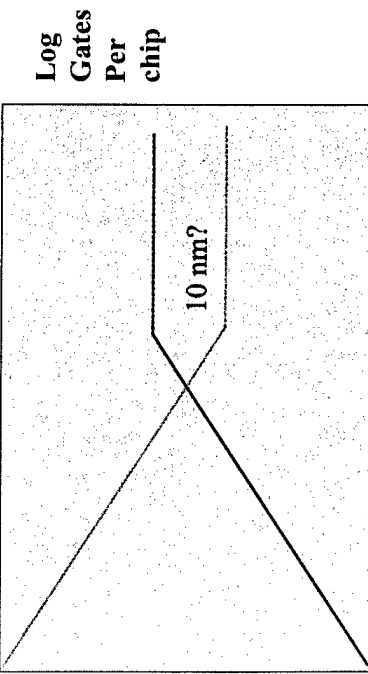
© 1999 Intel Corp.  
Published by Intel Corp.  
Reproduction in whole or in part without written permission is prohibited.



Where is the limit and what QRT is needed if any?

Single prototype MOSFETS devices have also been demonstrated with healthy I-V characteristics with gate lengths in 7-14 nm scales.

- What quantum/many-body effects occur in these devices and how do we model them?
- What are the implications of the dinosaur refusing to die for quantum devices?



© 1999 Intel Corp.  
Published by Intel Corp.  
Reproduction in whole or in part without written permission is prohibited.

© 1999 Intel Corp.  
Published by Intel Corp.  
Reproduction in whole or in part without written permission is prohibited.

Certainly, below 50 nm we expect strong atomistic effects.

The predicted high carrier densities also suggest strong **many-body effects**: Coulombic, correlations/fluctuations.

But at what level do we need to move to a true atomistic model, and where does the need for computational chemistry methods come in?

These questions are addressed in today's sessions and the role of the fundamental theoretical frameworks that underpin true QTT and fully quantum devices are discussed later.

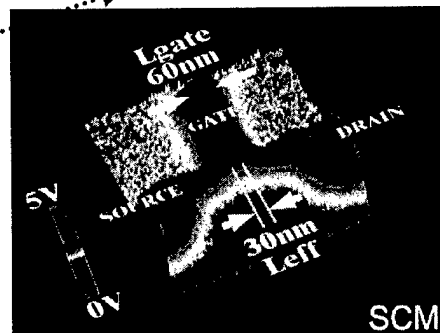
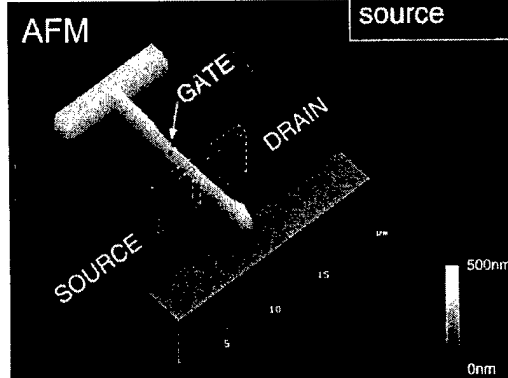
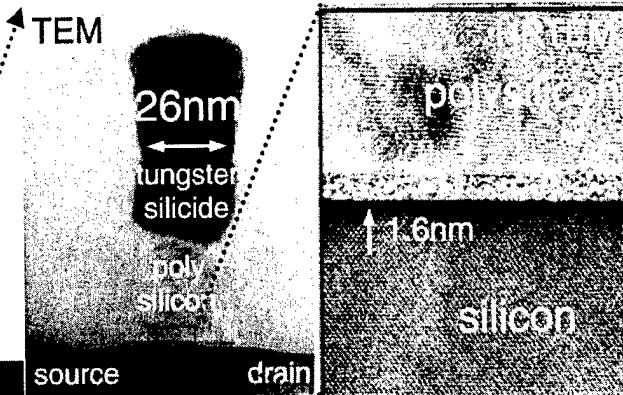
# The Nano-fabrication of Nanoscale Materials

J. Bude, F. Baumann<sup>‡</sup>, K. Evans-Lutterodt, A. Ghetti, S. Goodnick<sup>†</sup>, J. Grazul<sup>‡</sup>,  
M. Green, S. Hillenius, Y. Kim, J. Lyding<sup>+</sup>, W. Mansfield, D. Muller<sup>‡</sup>, T. Sorsch,  
K. Timp<sup>+</sup>, R. Timp<sup>+</sup>, J. Yu<sup>+</sup>.  
*Agere, Arizona State University<sup>†</sup>, Bell Laboratories, Lucent Technologies<sup>‡</sup>,  
University of Illinois<sup>+</sup>*

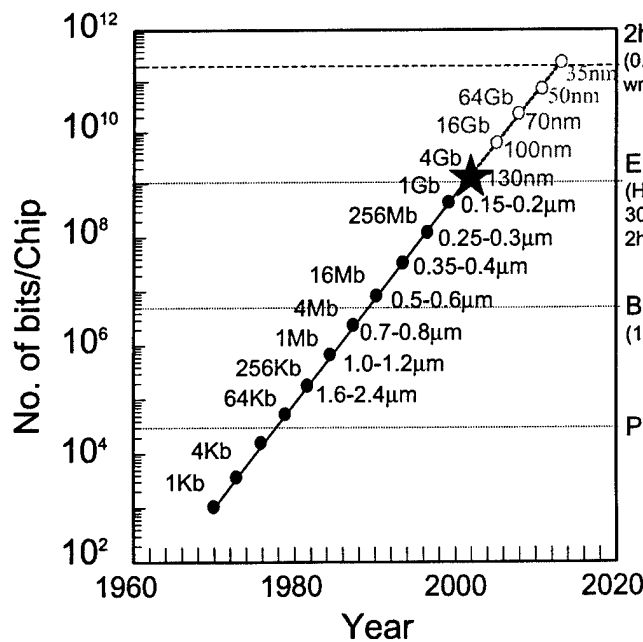
**G. Timp**  
*University of Illinois*

## *Nano-transistor*

$$\begin{aligned}L_{eff} &< 25\text{nm} \\t_{ox} &= 1.3\text{-}1.6\text{nm} \\r &< 20\text{-}30\text{nm}\end{aligned}$$



# The Secret Behind Moore's Law



2hrs. HDTV  
(0.01% of all  
written knowledge)

**Encyclopedia  
(Human DNA,  
30sec. HDTV,  
2hrs. Audio CD)**

**Book**  
(1 min. Audio CD)

Page

- D) Chip-to-chip connection:  
~1¢
- On-chip connection:  
~40µ¢

## 2000 ITRS National Roadmap Projections

30nm research is targeted at a ~15 year horizon  
Technology Generations

YEAR OF FIRST PRODUCT SHIPMENT	2001	2004	2008	2014
TECHNOLOGY GENERATIONS DENSE LINES (DRAM Half-Pitch) (nm)	130	90	60	30
Logic (High-Volume: MPU)				
Logic Transistors/chip (including SRAM)	67.3M	135M	539M	4.3B
Chip Frequency (GHz)				
On-chip local clock, high performance	2.1G	3.5G	7.1G	14.9G
TECHNOLOGY REQUIREMENTS				
Min. Logic Vdd(V) (desktop)	1.5	1.2	0.9	0.6
Nominal Ion (n/pMOS)@25C(mA/ $\mu$ m)	0.75/0.35		0.75/0.35	0.75/0.35
Nominal Ioff @25C (nA/ $\mu$ m)	5		80	160
tox equivalent (nm)	1.5-1.9		0.8-1.2	0.5-0.6
junction depth xj (nm)			16-26	8-13

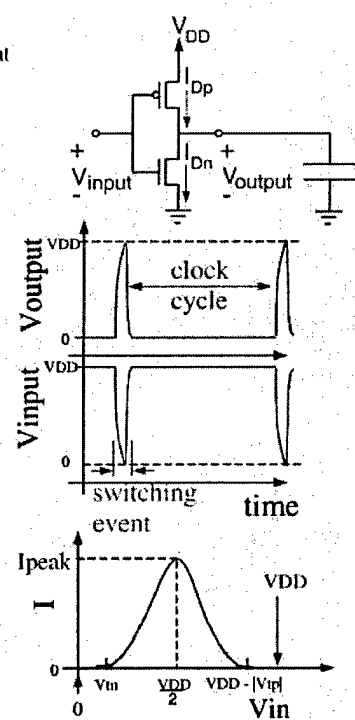
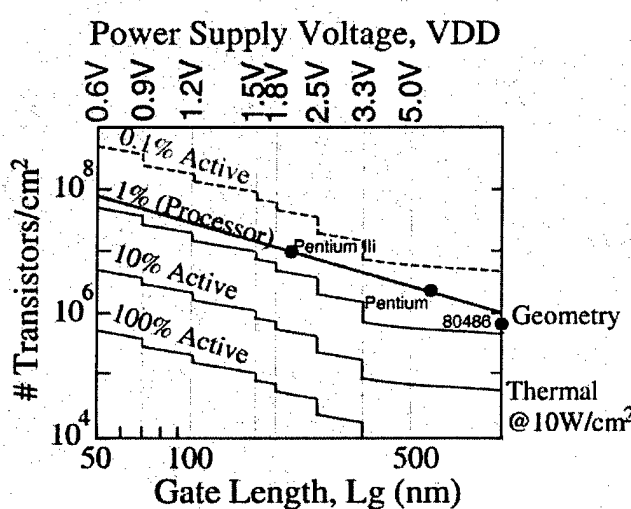


\*Drive current independent of technology

## One of the Secrets Behind the Success of CMOS

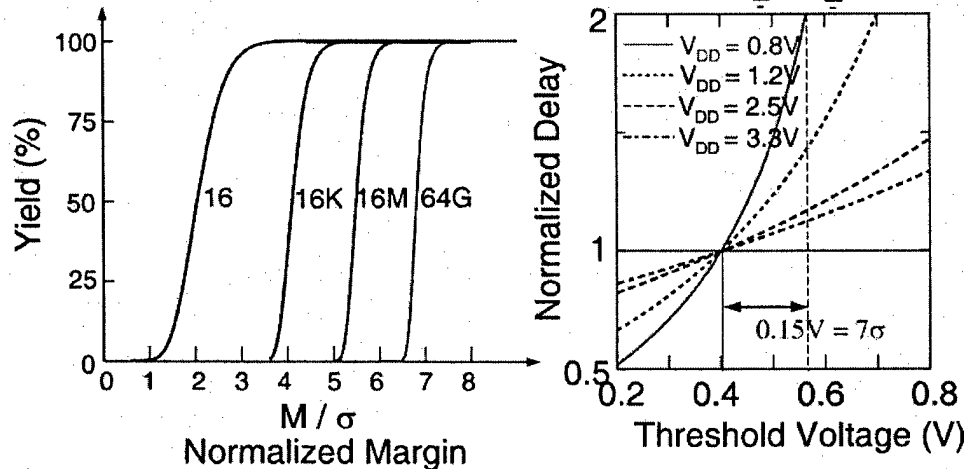
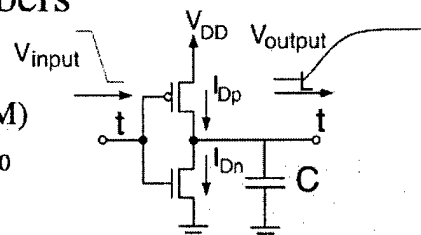
$$\text{Active Power Dissipation: } f_c C V_{DD}^2 \sim \eta V_{DD} I_{Dsat}$$

$$\text{Stand-by Power Dissipation: } V_{DD} I_{\text{leakage}}$$

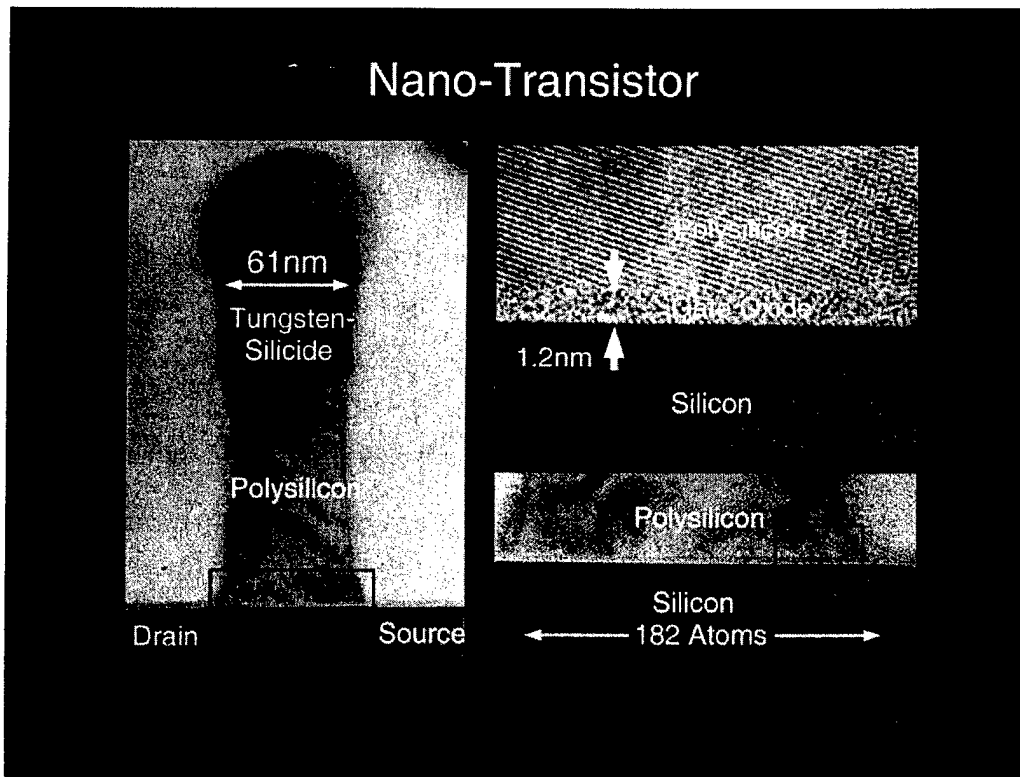


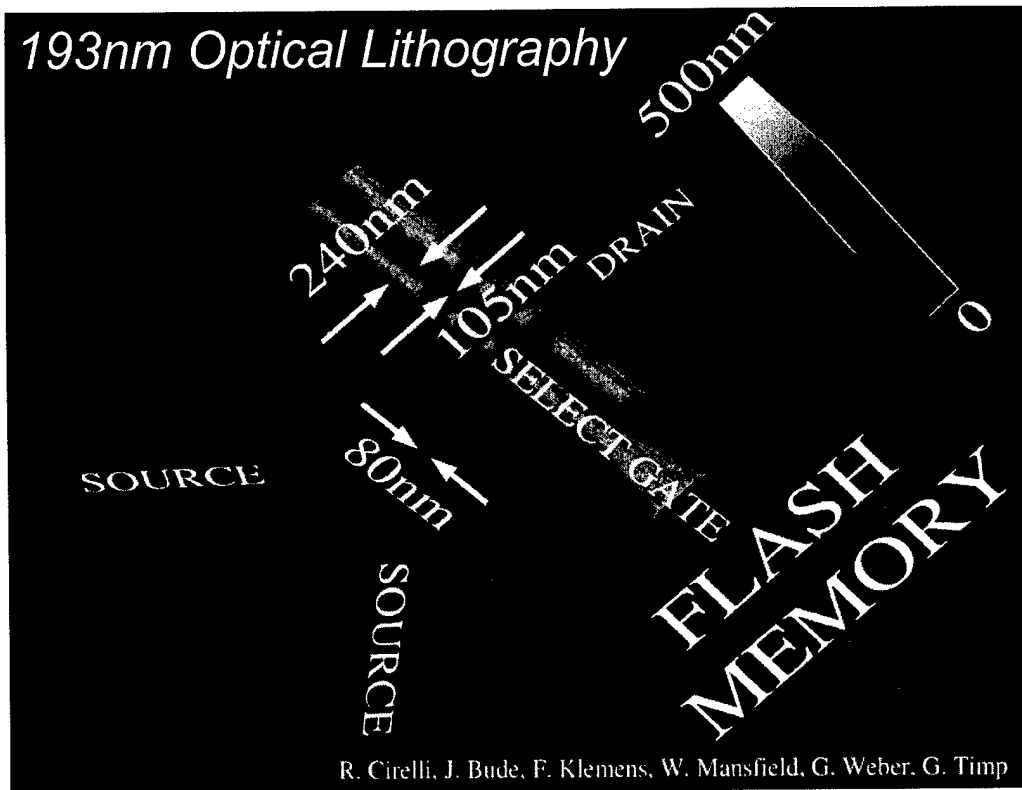
## The Tyranny of Large Numbers

circuit margin M:  $I_{D0}(1-M) < I_D < I_{D0}(1+M)$   
process control: standard deviation  $= \sigma I_{D0}$

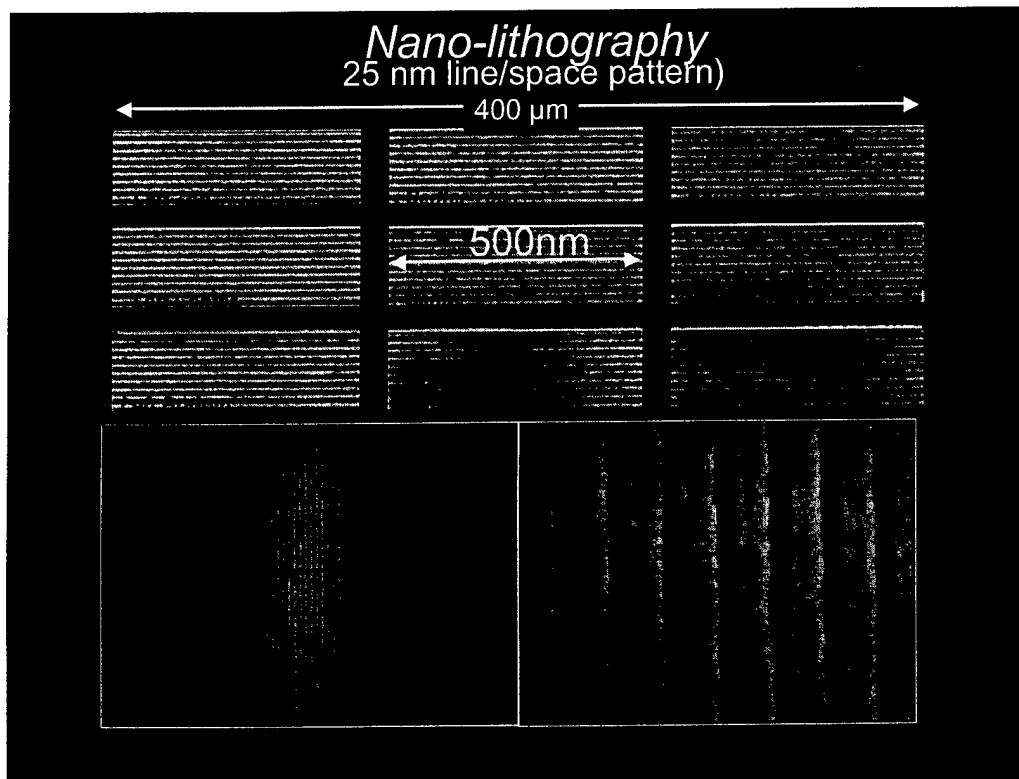


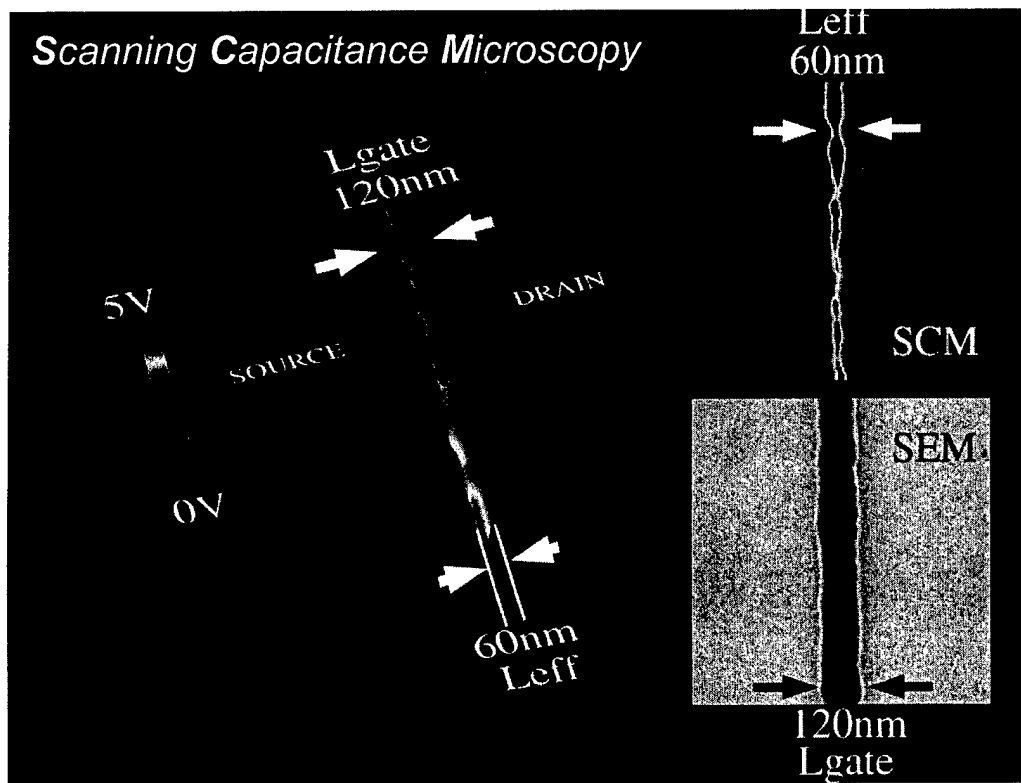
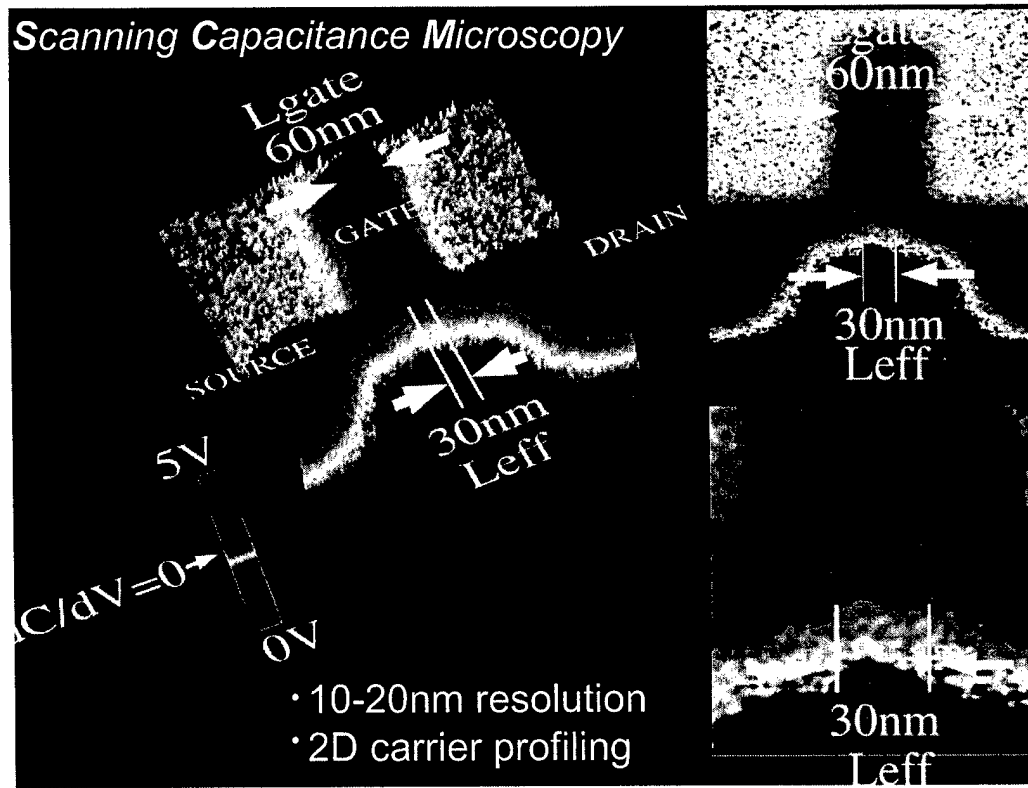
Nano-Transistor



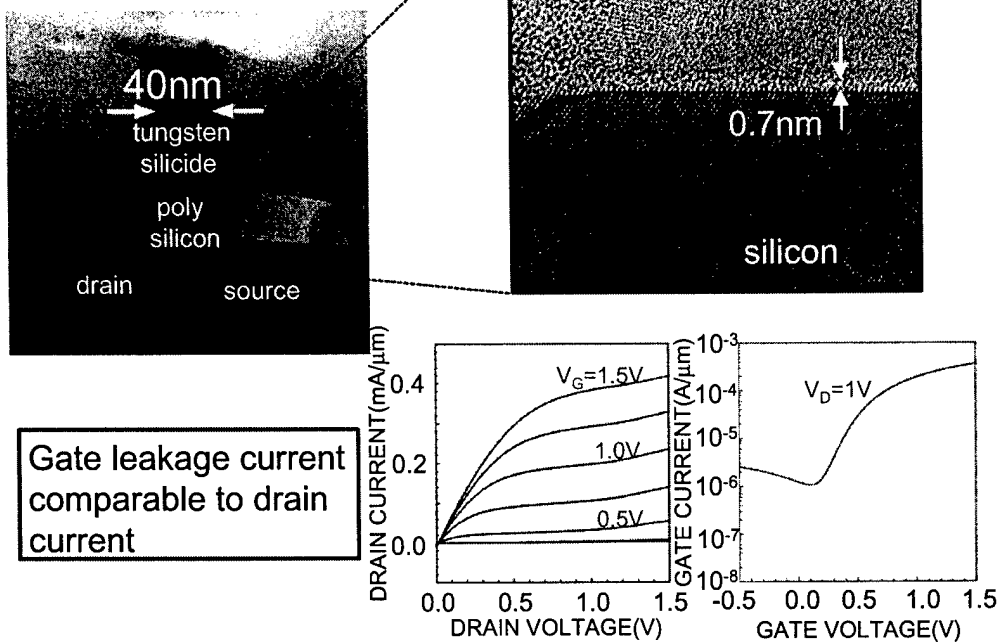


R. Cirelli, J. Bude, F. Klemens, W. Mansfield, G. Weber, G. Timp

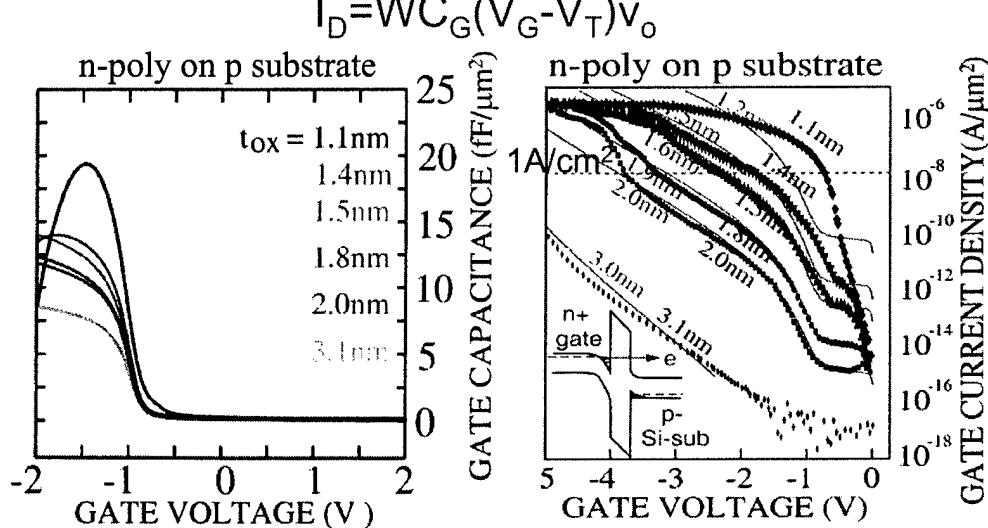




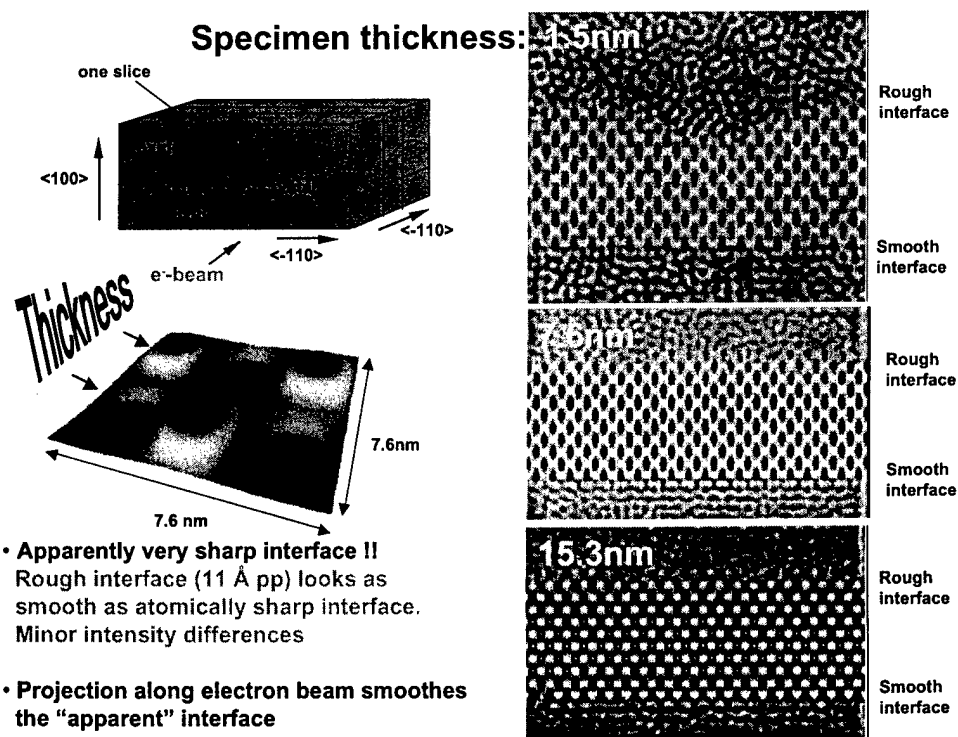
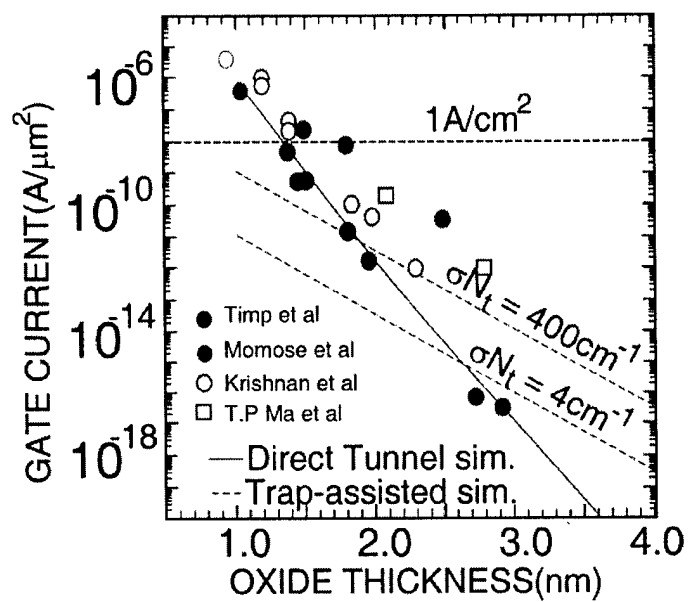
## The Nanotransistor: Hyper-thin Oxide



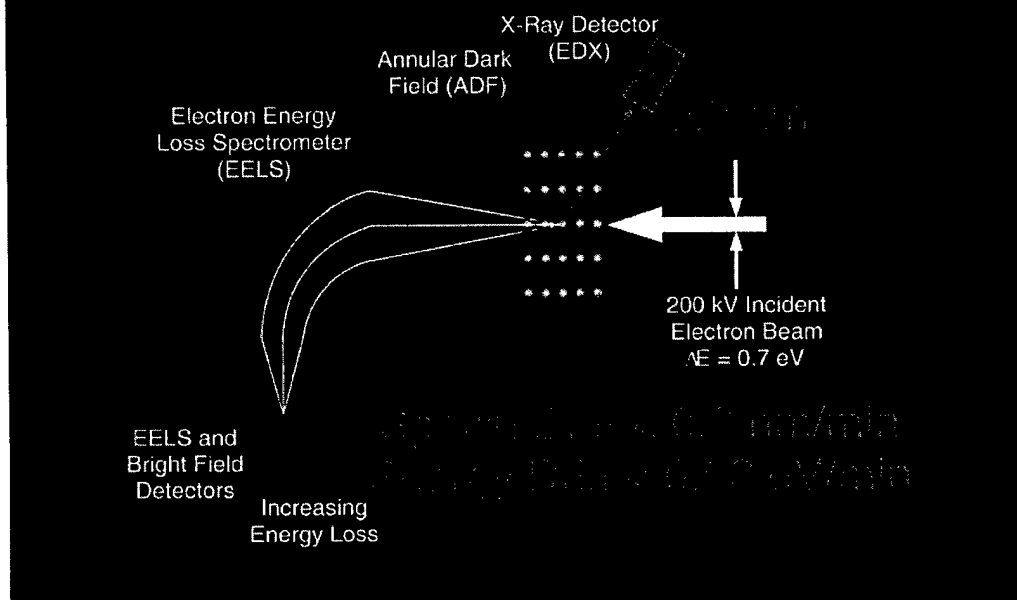
### Capacitance Improvement with decreasing $t_{ox}$



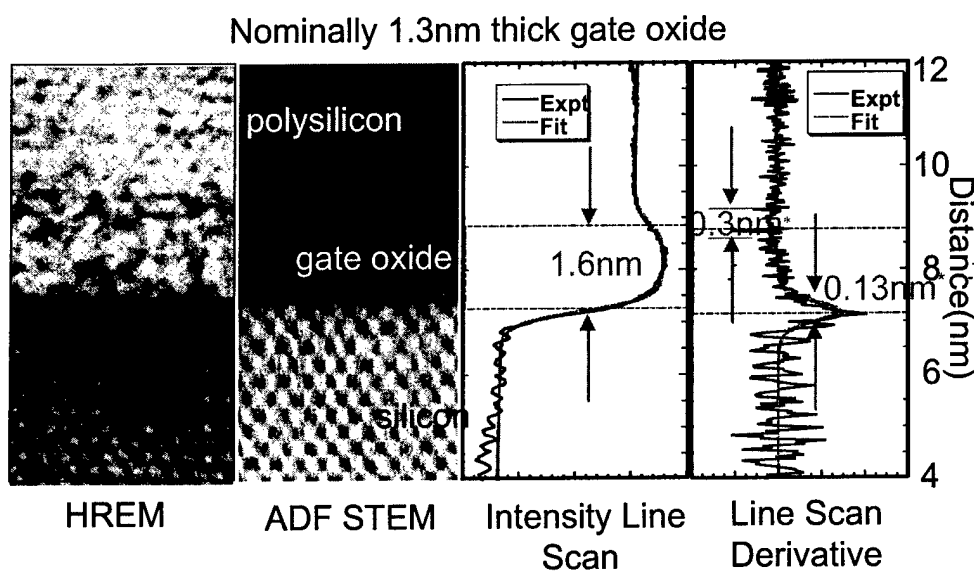
- exponential increase in leakage with increasing  $V_G$
- exponential increase in leakage with  $t_{ox}$



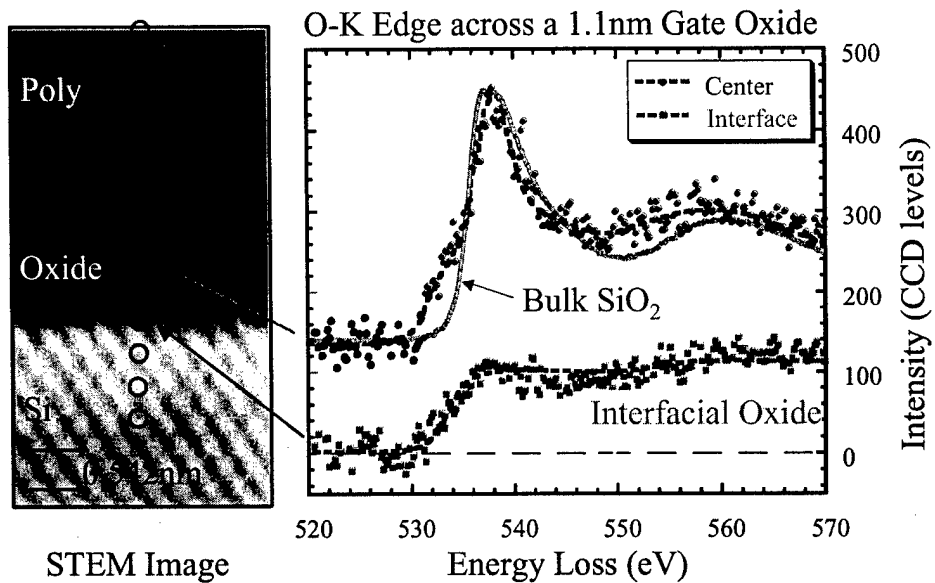
# Scanning Transmission Electron Microscopy/ Electron Energy Loss Spectroscopy



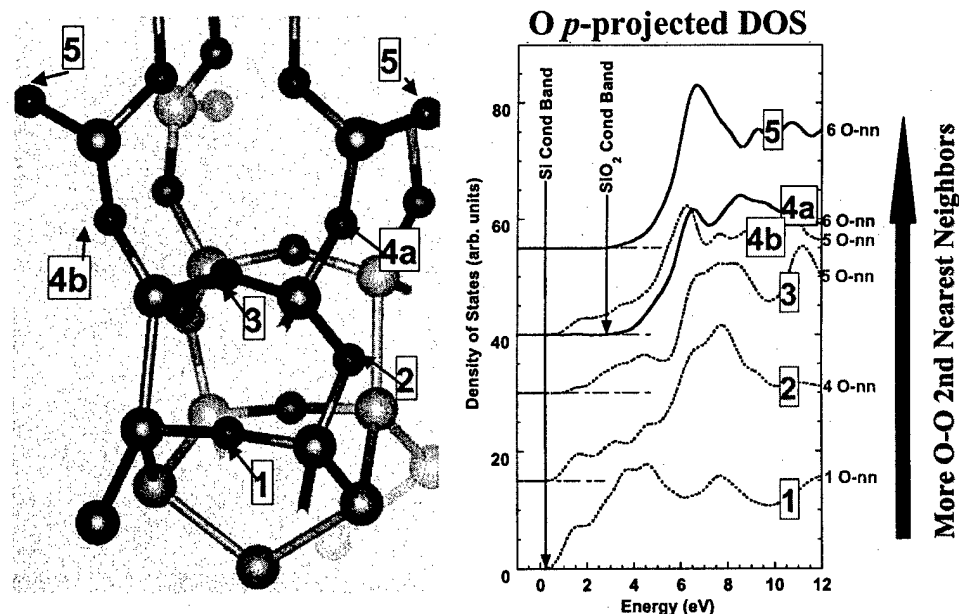
What does  $t_{ox} = 1\text{nm}$  look like?



## Oxygen Bonding from STEM/EELS (Chemistry on an Atomic Scale)



## A Model Si/SiO<sub>2</sub> Interface



(Model-3 of A. Pasquarello, M. S. Hybertson, R. Car, PRB)

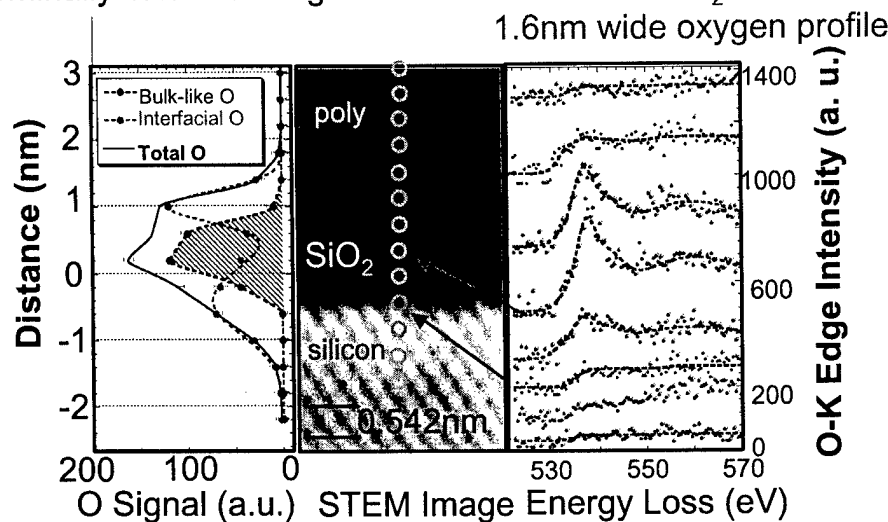
Jeff Neaton & David Muller

## When is $t_{ox} = 1\text{nm}$ ?

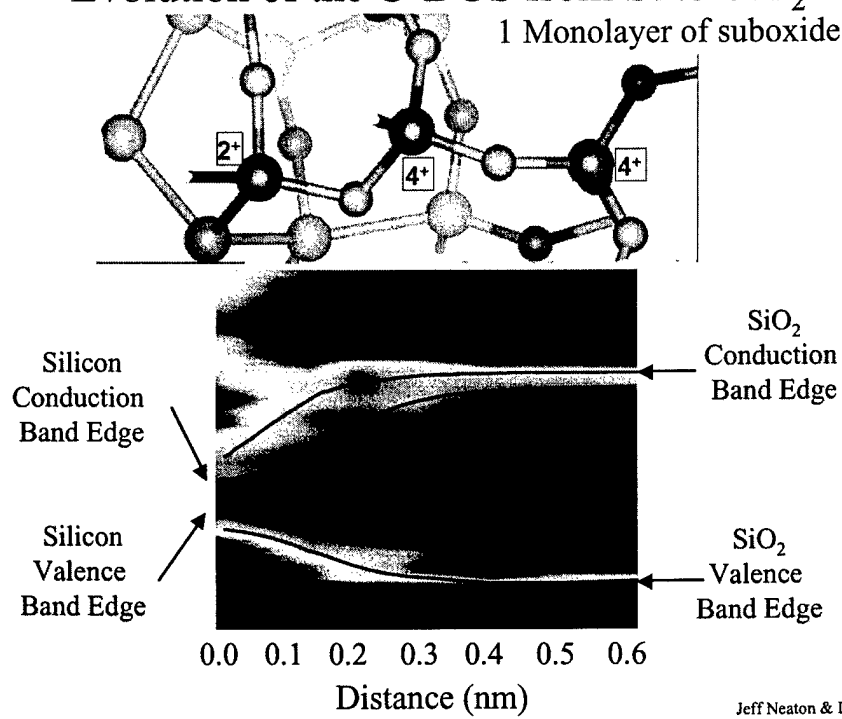
STEM/EELS

Nominally 1.1nm thick gate oxide: 0.8-1.0nm  $\text{SiO}_2$

1.6nm wide oxygen profile

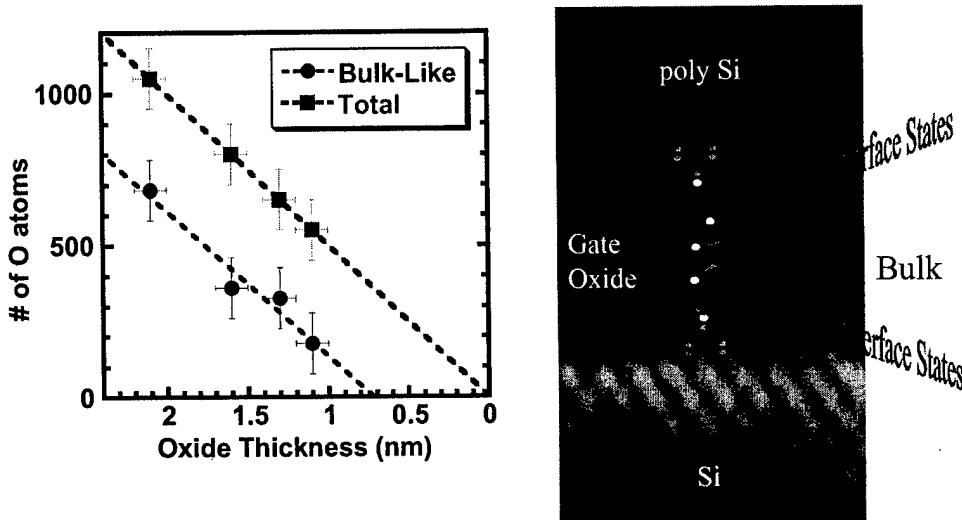


## Evolution of the O-DOS from Si to $\text{SiO}_2$



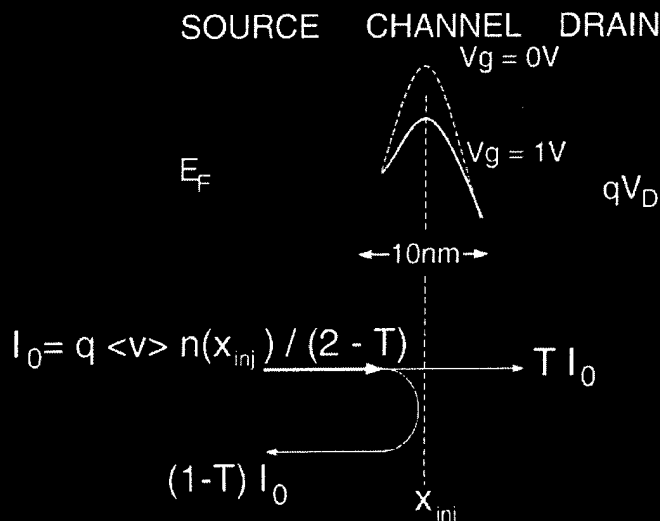
Jeff Neaton & David Muller

## The End of the Roadmap for $\text{SiO}_2$



There will be no more bulk-like bonding  
when the Oxide is less than 0.7 nm

## The MOSFET from Landauer's Perspective

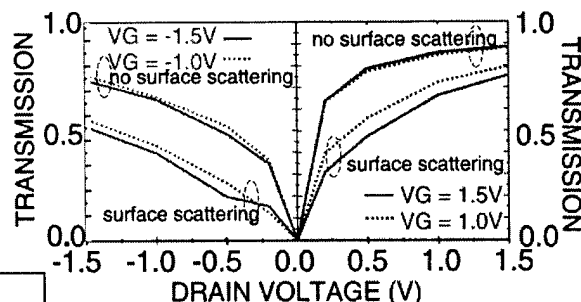
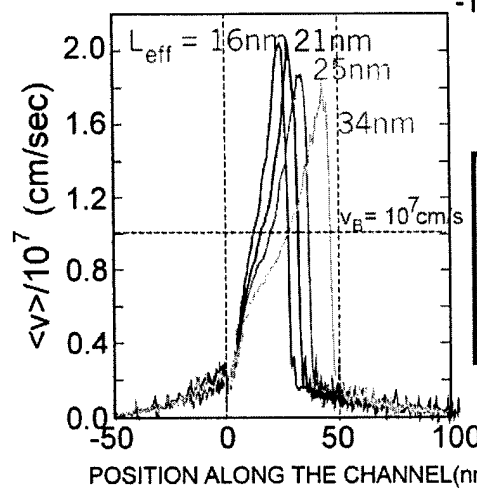


$$I_D/W = T I_0 = q \langle v \rangle n(x_{\text{inj}}) T / (2 - T)$$

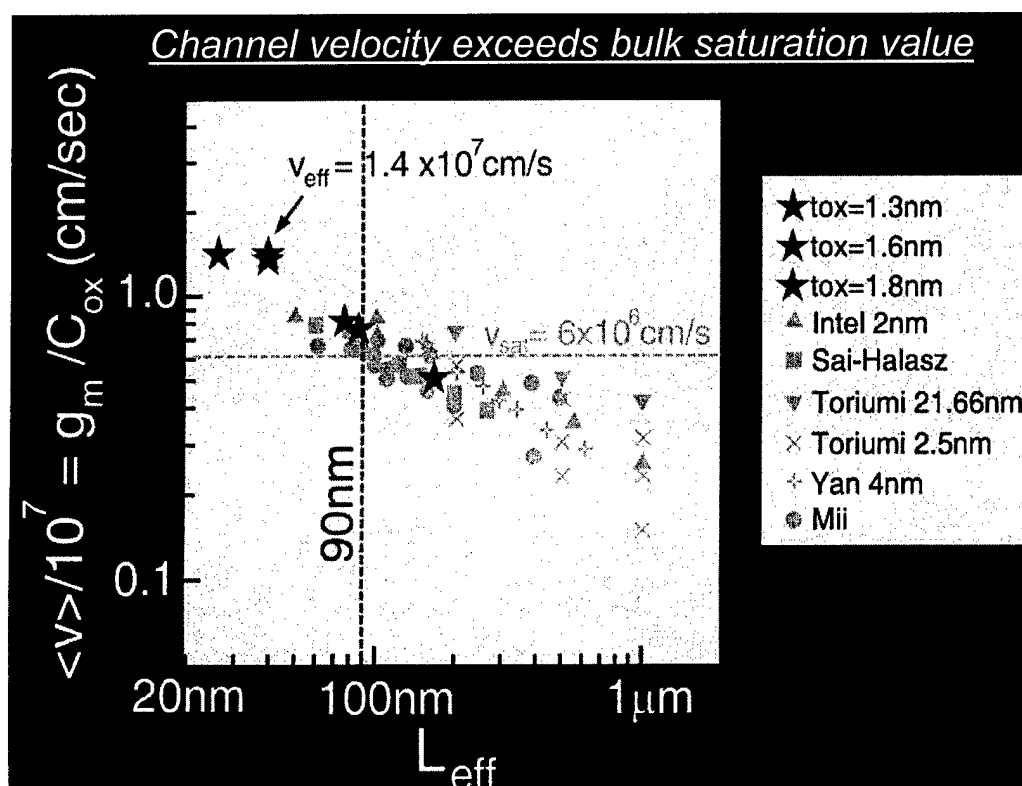
Lundstrom, S. Datta, F. Assad;  
Frank, Laux and Fischetti

## The Ballistic Nanotransistor

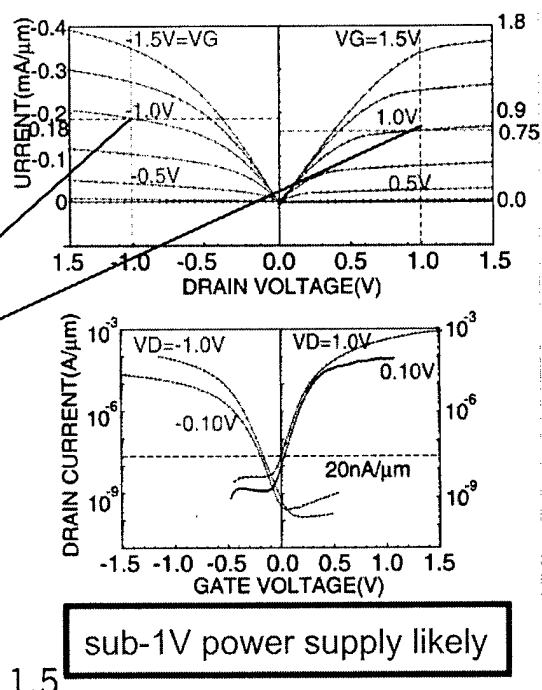
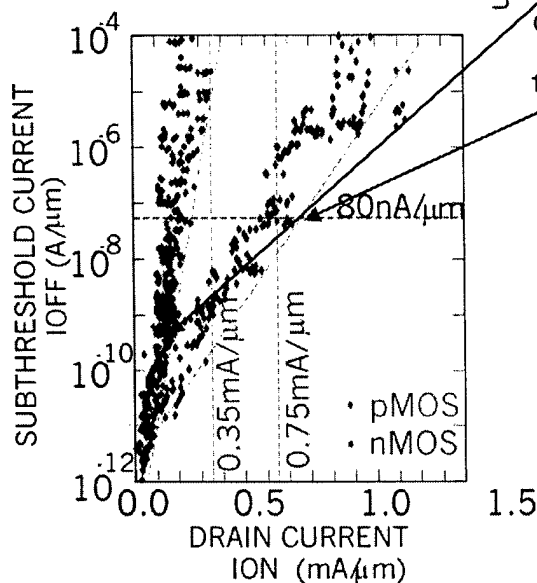
( $V_g = V_{ds} = 1V$ )



$\langle v \rangle$  exceeds bulk saturation  
the velocity (averaged over  $L_{eff}$ )  
increases as  $L_{eff}$  decreases.

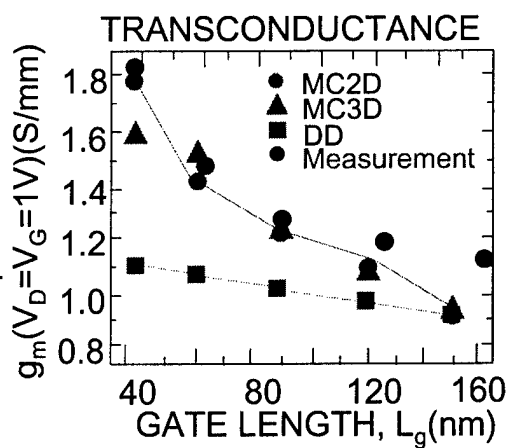
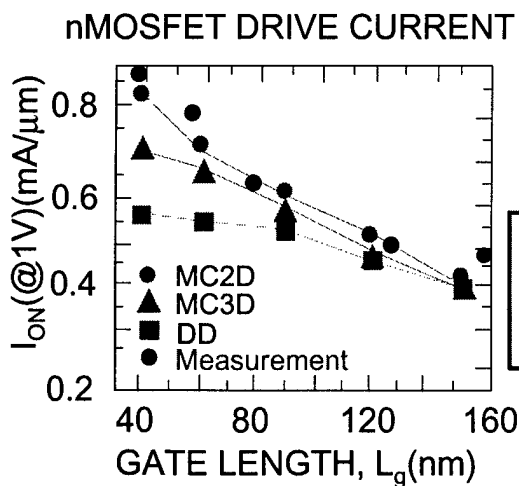


## Nanotransistor DC Performance



## Simulation versus Measurement

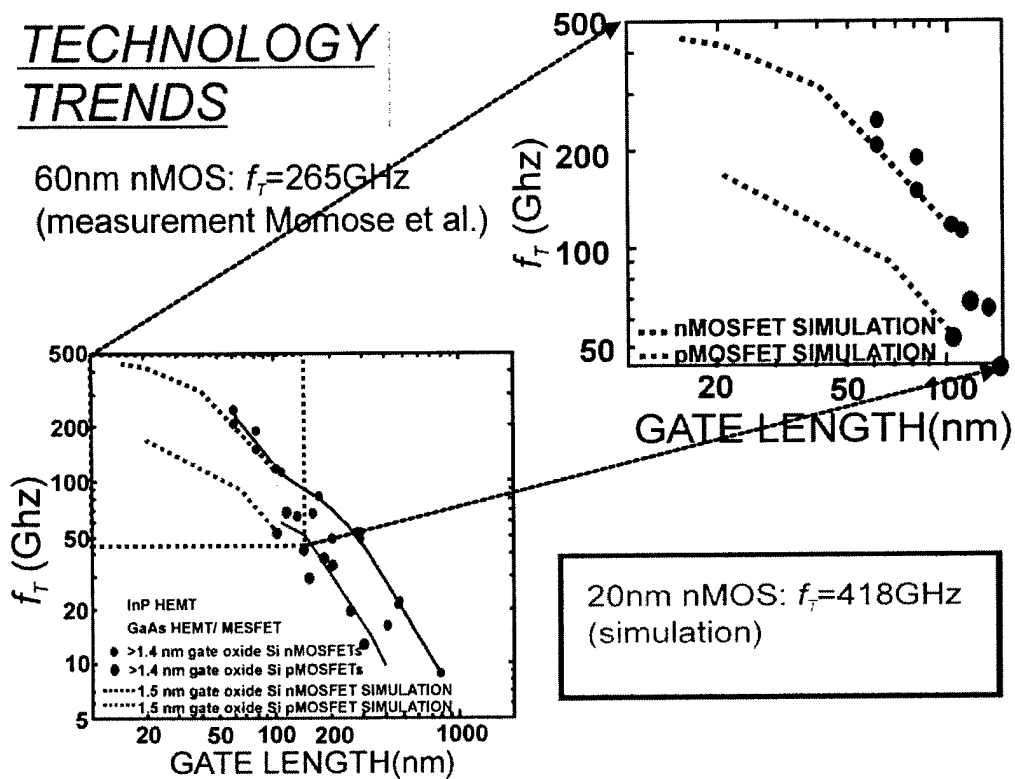
$V_{DD} = 1\text{V}$  @  $V_T = 0.4\text{V}$ ;  
 $t_{ox} = 1.5\text{nm}$  (ellips.)



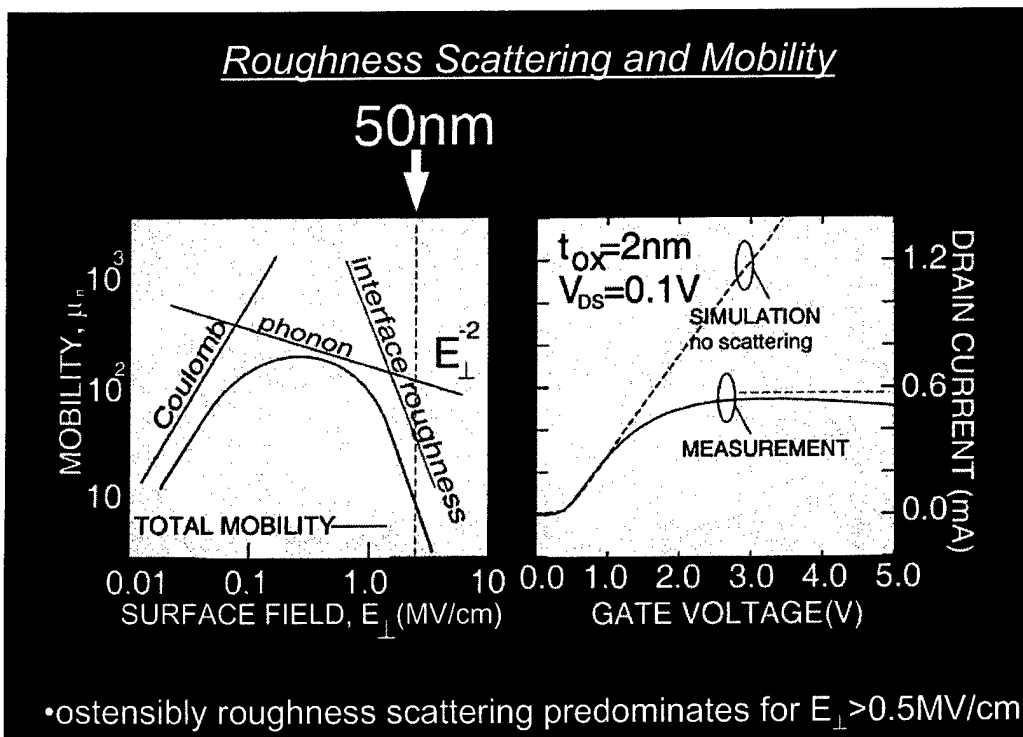
80% improvement in drive  
over DD prediction independent  
of  $t_{ox}$

## TECHNOLOGY TRENDS

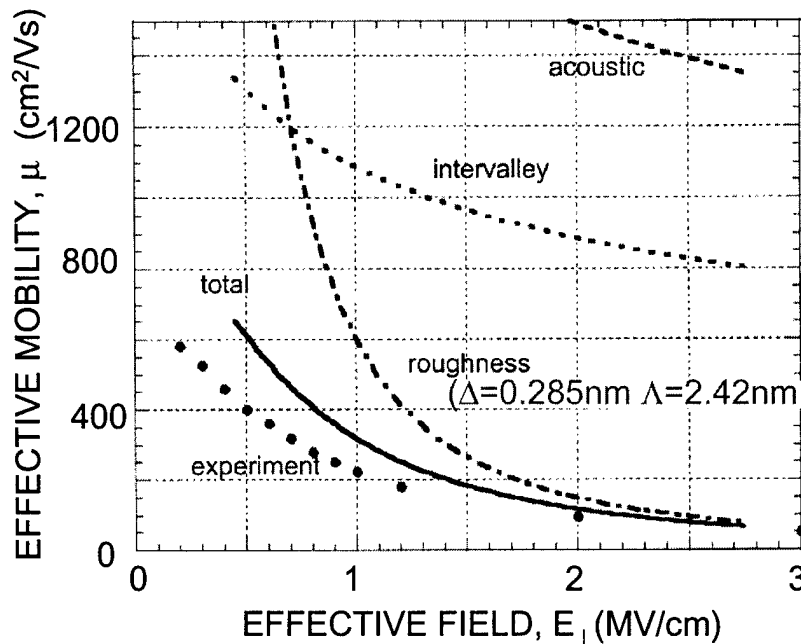
60nm nMOS:  $f_T = 265\text{GHz}$   
(measurement Momose et al.)



## Roughness Scattering and Mobility

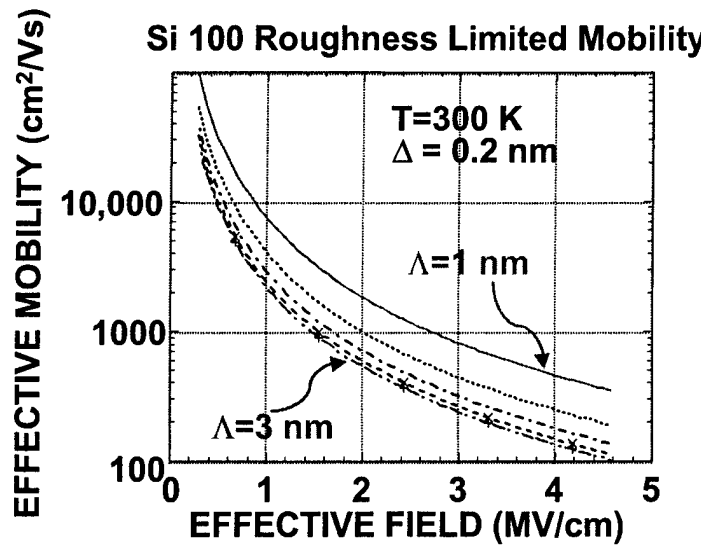


## MOBILITY RESOLVED

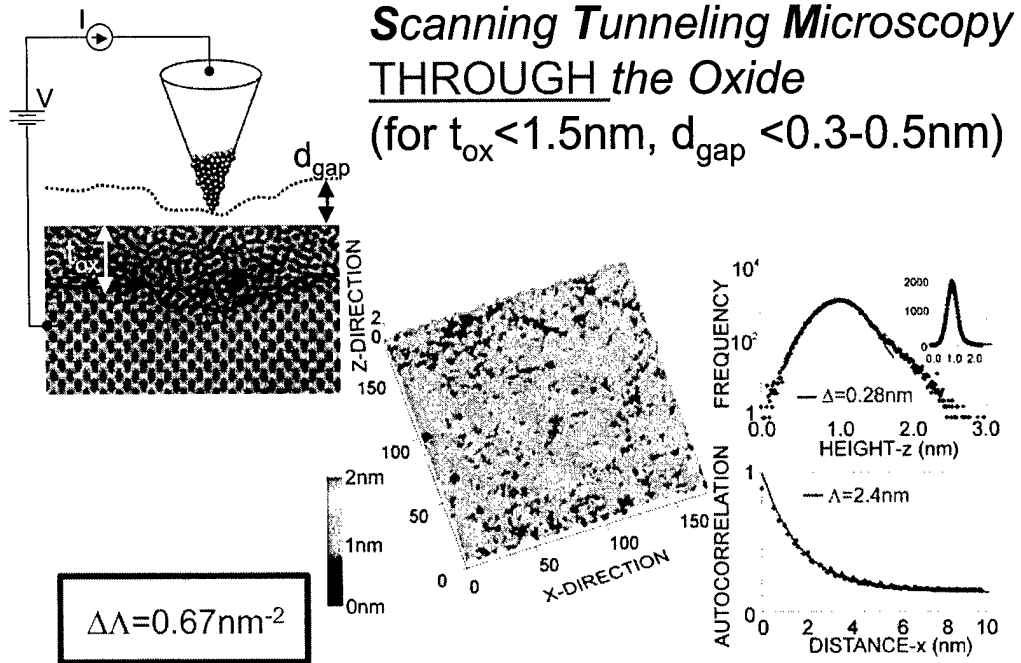


S. Goodnick

Roughness limited mobility decreases as inverse square of surface field, and as  $(\Delta\Lambda)^2$ :

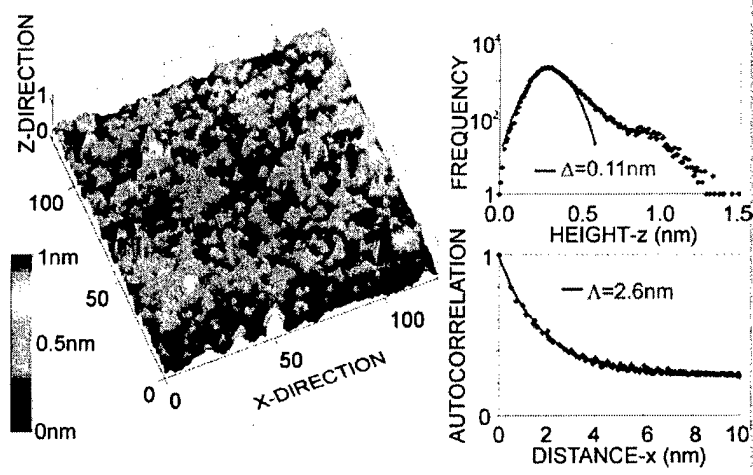


S. Goodnick

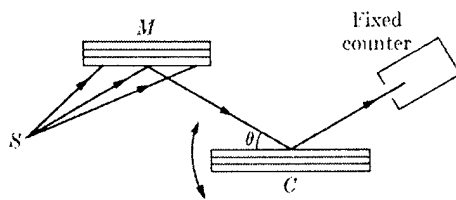


J. Yu and J. Lyding

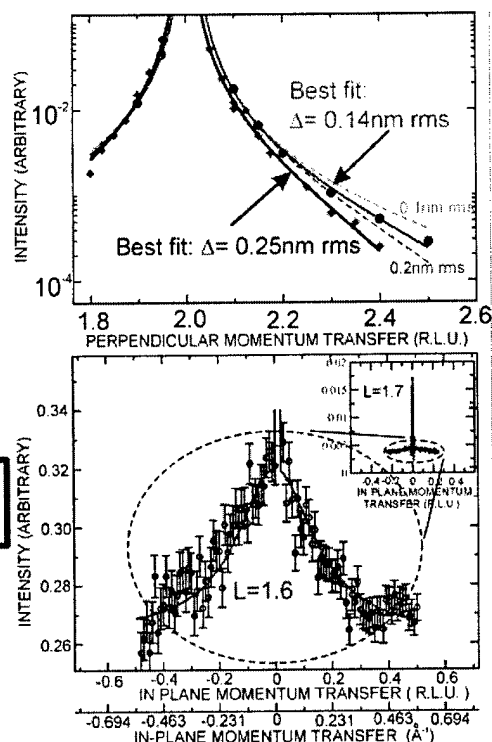
**Scanning Tunneling Microscopy  
THROUGH the Oxide**



## X-ray DIFFRACTION



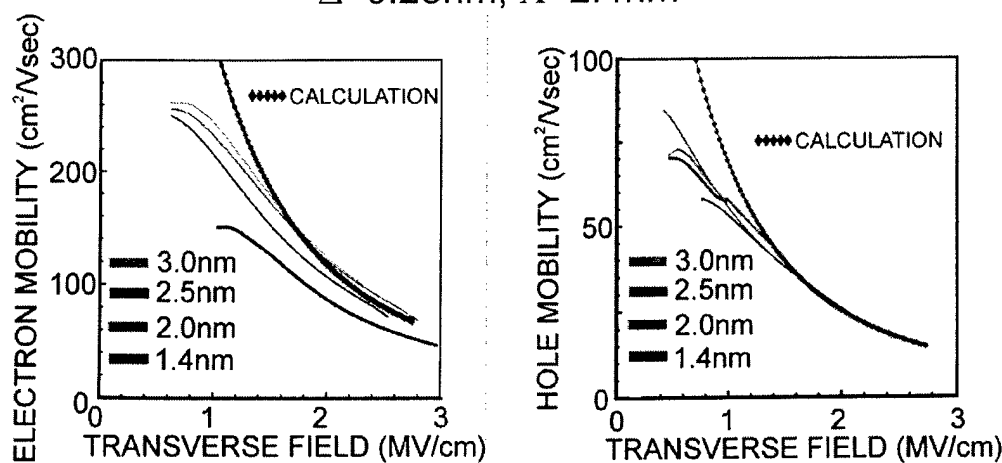
$$\Delta\Lambda = 0.67 \text{ nm}^{-2} \longrightarrow 0.35 \text{ nm}^{-2}$$



K. Evans-Lutterodt

## MOBILITY MEASUREMENTS VS. CALCULATION

$$\Delta = 0.28 \text{ nm}, \Lambda = 2.4 \text{ nm}$$



Completely constrained mobility Calculation on "rough" MOSFETS correlates well with measurements.

# *The Highlights*

- *Homeric challenges face bulk silicon technology, but the same is true of all the pretenders to the throne.*
- *Some of these challenges stem from “atomic” sensitivity (e.g. the gate oxide)*
- *As process control decreases; circuit margins must increase at an even faster rate.*

# **Long-range Coulomb interactions, coupled plasmon/insulator-TO-phonon modes, and electron mobility in Si inversion layers**

Max Fischetti

IBM Research Division

T. J. Watson Research Center  
Yorktown Heights, NY 10598

in collaboration with Deborah Neumayer and Eduard Cartier

June 2001

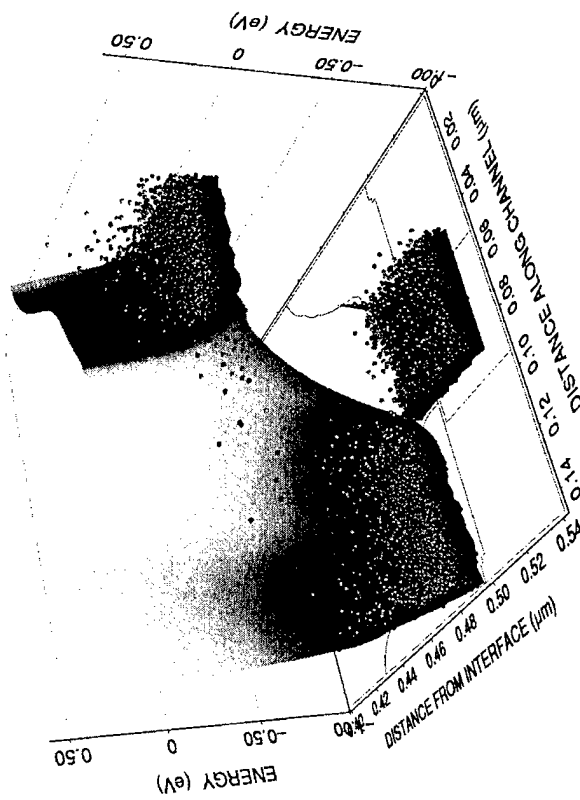
MVF

## Outline

- Long-range Coulomb interactions (a short review):
  - $g_m$  and  $v_{eff}$  degradation in short-channel/thin-oxide MOSFETs (semiclassical)
  - mobility degradation in thin-oxide MOSFETs (quantum)
- High- $\kappa$  insulators:
  - Simple picture
  - Dispersion of coupled insulator-TO-phonons/plasmon modes
  - Material parameters
  - Scattering strength
  - Electron mobility in inversion layers
  - Effect of  $\text{SiO}_2$  interfacial layers

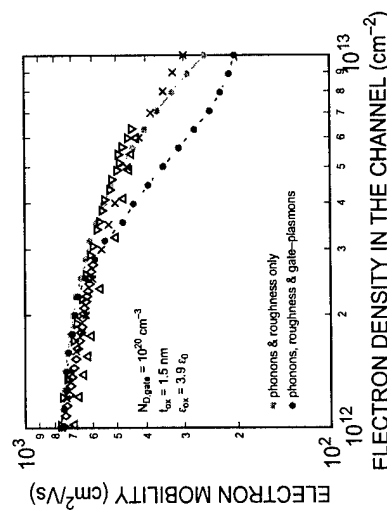
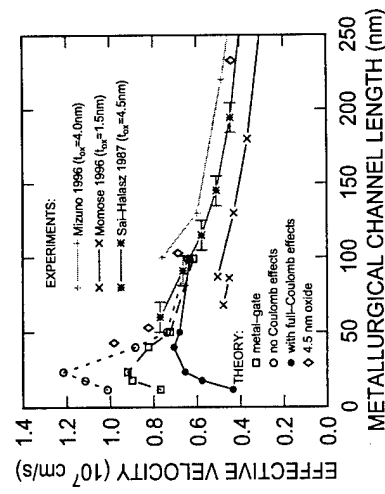
## Long-range Coulomb interactions in small MOSFETs

- Source, drain, and gate regions are high-density electron gases
- S/D separation (i.e., channel length) is shrinking below the Debye length of the channel
- Gate needs to be 1 nm (or less) away from the channel
- Collective ‘fluctuations’ in S/D perturb electrons in the channel (electron/bulk-plasmon interactions)
- Collective fluctuations in gate (interface plasmons) cause Coulomb drag



## Coulomb interactions and device speed

- S/D interactions thermalize carriers, build high-energy tails, increase momentum-loss *indirectly*
- Gate-induced Coulomb-drag subtracts momentum *directly*
- Lower transconductance, lower mobility



## High- $\kappa$ insulators

- VLSI scaling demands insulator thicknesses  $t$  approaching 1 nm for (near) future devices. But it's hard to go below 1.5 nm:
  - Gate tunneling draws too much stand-by power
  - Reliability (wear-out, breakdown) is a debated issue, but 1 nm seems to be 'too much' even to the optimist
- Lot of activity on insulators with high dielectric constant ( $\epsilon_{ox}^0 = \kappa\epsilon_0$ ), so that the gate capacitance

$$C_g = \frac{\epsilon_{ox}^0}{t} = \frac{\epsilon_{SiO_2}^0}{t_{eq}}$$

corresponds to the required small  $t_{eq}$ .

- Materials considered:
  - Metal-oxides ( $HfO_2, ZrO_2, Al_2O_3\dots$ ), with  $\kappa \approx 10-30$
  - Silicates ( $ZrSiO_4, HfSiO_4$ ), with  $\kappa \approx 15-25$
  - Perovskites, rare-earth oxides, with  $\kappa \approx 100$
  - Nitrides ( $AlN, Si_3N_4$ ), with  $\kappa \approx 10$
  - Ferroelectrics ( $\kappa \sim 10^3\dots$  but that's another story...)

## High- $\kappa$ insulators: A simple picture

- $\epsilon_{ox}^0 = \epsilon_{ion}^0 + \epsilon_{el}^0$
- $\epsilon_{el}^0 \propto E_{gap}^{-1}$  ... so, not much room left for insulators (must have large  $E_{gap}$ !)
- Large  $\epsilon_{ion}^0$  due to polarizable bonds (typically, metal-oxygen), 'soft' bonds associated with 'soft' TO phonons
- $\epsilon_{ion}^{\infty}$ , not too large (ions move slowly)
- So, for large- $\kappa$  materials,  $\epsilon_{ox}^0$  much larger than  $\epsilon_{ox}^{\infty}$
- Insulator-TO-modes at interface (surface-optical modes, SO) scatter electrons with strength  $\propto$ :

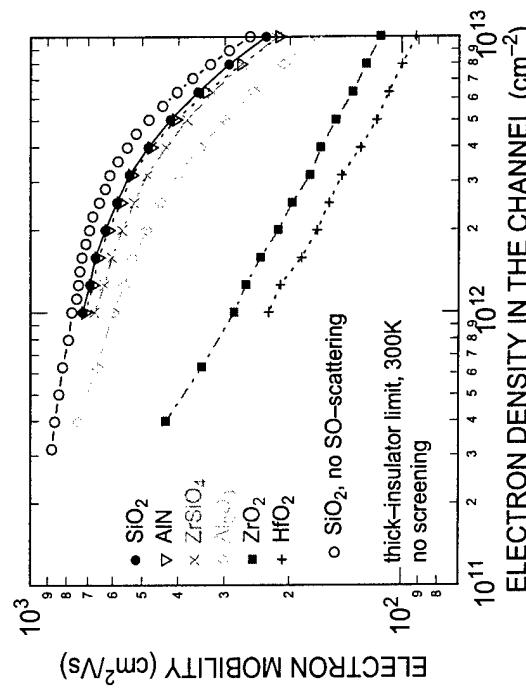
$$\hbar\omega_{SO} \left[ \frac{1}{\epsilon_{Si}^{\infty} + \epsilon_{ox}^{\infty}} - \frac{1}{\epsilon_{Si}^{\infty} + \epsilon_{ox}^0} \right]$$

(Fröhlich + images, Wang-Mahan, 72)

- Small effect ( $\sim 5\%$ ) in SiO<sub>2</sub>:  
 -  $\epsilon_{ox}^0$  ( $\approx 3.9$ ) not much larger than  $\epsilon_{ox}^{\infty}$  ( $\approx 2$  to  $2.5$ ) because Si-O bond is 'hard'
  - Small Fröhlich-like coupling constant
  - Hard bonds imply 'stiff' TO-modes,  $\hbar\omega_{TO} >> k_B T$ : too energetic to be emitted by thermal electrons, too energetic to be thermally excited (no absorption).
- But large effects in high- $\kappa$  materials:
  - Large  $\epsilon_{ox}^0$  due to polarization of 'soft' bonds
  - Large Fröhlich-like coupling constant
  - Soft bonds imply 'soft' TO-modes,  $\hbar\omega_{TO} \sim k_B T$ : energy low enough to allow emission by thermal electrons, low enough to be thermally excited (absorption possible).

## High- $\kappa$ insulators: A simple picture

- Use Wang-Mahan (Hess-Vogl, 79; Moore-Ferry, 80) matrix element
- Single insulator/Si interface (infinitely-thick insulator)
- No electronic screening
- Add Si-phonons and (shamelessly) empirical surface-roughness (Matthiessen's rule to fit experiments for SiO<sub>2</sub> at  $n_s = 10^{13} \text{ cm}^{-2}$ )



## Interface modes: A better model for thin-insulator MOSFETs

### Interface modes

- Consider a depleted-Si/insulator/inverted-Si MOS system
- Look for longitudinal eigenmodes (TM-modes or p-waves) of Maxwell's equations:  $\epsilon_{tot}(\mathbf{Q}, \omega) = 0$ .  
These give  $\mathbf{E} \neq 0$  even when  $\mathbf{D} = 0$ , while transverse modes ( $\epsilon_{tot}(\mathbf{Q}, \omega) = \infty$ ) give  $\mathbf{E} = 0$  for any  $\mathbf{D}$ , so no scattering field.
- Use non-retarded limit (OK for wavelength  $\sim \lambda_F$ ), so unknown is electrostatic potential satisfying Laplace equation.
- Chose model dielectric functions (long-wavelength-limit, two insulator TO modes).
- Impose continuity of  $\mathbf{E}_{||}$  and  $\mathbf{D}_{\perp}$  at two interfaces  
 $\rightarrow$  homogeneous linear problem of 4 equations in 4 unknowns
- Secular equation (i.e. vanishing of determinant) gives dispersion of coupled modes (4+2 of them).
- Determine phonon- and plasmon-content of each mode.
- Normalize potential (i.e. determine last unknown) somehow... (semiclassically). This defines the scattering potential.
- Account for Landau-damping (lost in taking a real  $\epsilon$  in the long-wavelength limit).
- Determine the subband structure (triangular-well).
- Compute the mobility (Kubo-Greenwood).

#### Consider MOS system:

- (poly-)Si gate,  $\epsilon_g(\mathbf{q}, \omega)$ , for  $z \leq 0$
- insulator,  $\epsilon_{ox}(\omega)$ , for  $0 < z \leq t$
- Si 2DEG,  $\epsilon_s(\mathbf{Q}, \omega)$ , for  $z > t$

- Write electrostatic potential (non-retarded limit):

$$\phi(\mathbf{R}, z, t) = \sum_{\mathbf{Q}} \phi_{\mathbf{Q}, \omega}(z) e^{i\mathbf{Q} \cdot \mathbf{R}} e^{i\omega t}$$

with

$$\phi_{\mathbf{Q}, \omega}(z) = \begin{cases} a_{\mathbf{Q}, \omega} e^{Qz} & (z < 0) \\ b_{\mathbf{Q}, \omega} e^{-Qz} + c_{\mathbf{Q}, \omega} e^{Qz} & (0 \leq z < t_{ox}) \\ d_{\mathbf{Q}, \omega} e^{-Qz} & (z \geq t_{ox}) \end{cases}$$

- Solve Laplace equation:

$$\frac{d^2 \phi_{\mathbf{Q}, \omega}(z)}{dz^2} - Q^2 \phi_{\mathbf{Q}, \omega}(z) = 0$$

with boundary-conditions (BCs):

$$\begin{cases} E_{||, \omega}(\mathbf{R}, z = 0^-, t) = E_{||, \omega}(\mathbf{R}, z = 0^+, t) \\ E_{||, \omega}(\mathbf{R}, z = t_{ox}^-, t) = E_{||, \omega}(\mathbf{R}, z = t_{ox}^+, t) \\ D_{z, \omega}(\mathbf{R}, z = 0^-, t) = D_{z, \omega}(\mathbf{R}, z = 0^+, t) \\ D_{z, \omega}(\mathbf{R}, z = t_{ox}^-, t) = D_{z, \omega}(\mathbf{R}, z = t_{ox}^+, t) \end{cases}$$

- BCs become:

$$\begin{cases} a_{\mathbf{Q}, \omega} = b_{\mathbf{Q}, \omega} + c_{\mathbf{Q}, \omega} e^{-Qt} \\ b_{\mathbf{Q}, \omega} = d_{\mathbf{Q}, \omega} e^{-Qt} \\ \tilde{\epsilon}_g(Q, \omega) a_{\mathbf{Q}, \omega} = \epsilon_{ox}(\omega) (c_{\mathbf{Q}, \omega} - b_{\mathbf{Q}, \omega}) \\ \epsilon_{ox}(\omega) [b_{\mathbf{Q}, \omega} e^{-Qt} - c_{\mathbf{Q}, \omega} e^{Qt}] = \tilde{\epsilon}_s^{(2D)}(Q, \omega) d_{\mathbf{Q}, \omega} e^{-Qt} \end{cases}$$

- Eigenmodes  $\omega(\mathbf{Q})$  given by secular equation:

$$e^{Qt} [\tilde{\epsilon}_g(Q, \omega) + \epsilon_{ox}(\omega)] [\tilde{\epsilon}_s^{(2D)}(Q, \omega) + \epsilon_{ox}(\omega)] - e^{-Qt} [\tilde{\epsilon}_g(Q, \omega) - \epsilon_{ox}(\omega)] [\tilde{\epsilon}_s^{(2D)}(Q, \omega) - \epsilon_{ox}(\omega)] = 0$$

## "Effective" dielectric functions

- Gate:
  - RPA:

$$\tilde{\epsilon}_g(Q, \omega) = \frac{1}{\pi} \int_{-\infty}^{+\infty} d\left(\frac{q_z}{Q}\right) \frac{\epsilon_g(Q, q_z; \omega)}{1 + (q_z/Q)^2} \approx \epsilon_g(q = \sqrt{2}Q, \omega)$$

- Long-wavelength limit:

$$\epsilon_g(\omega) = \epsilon_{Si}^{\infty} \left( 1 - \frac{\omega_{p,g}^2}{\omega^2} \right)$$

Getting  $\omega_{p,g}$  is not trivial: Electron density in the depleted gate is at least  $z$ -dependent. Use either surface-density or  $Q$ -dependent average.

- Substrate:
  - RPA:

$$\epsilon_s^{(2D)}(Q, \omega) = \epsilon_{Si}^{\infty} \left\{ 1 + e^{2Qt} \sum_{\mu\mu'} \frac{\beta_{\mu\mu'}(Q, \omega)}{2Q} \Phi_{Q,\omega;\mu\mu'} \Phi_{Q,\mu\mu'}^{(0)} \right\}$$

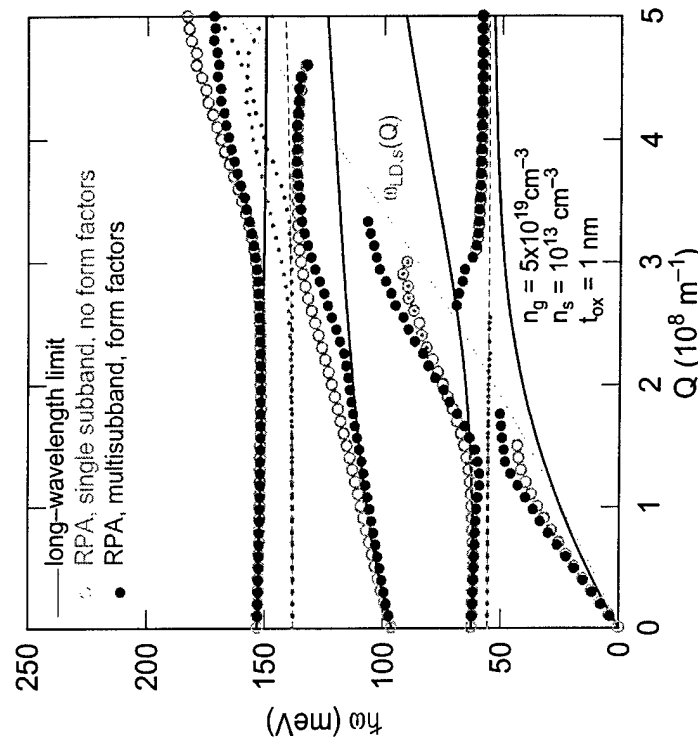
- Long-wavelength limit:

$$\epsilon_s^{(2D)}(Q, \omega) = \epsilon_{Si}^{\infty} \left[ 1 - \frac{\omega_{p,s}(Q)^2}{\omega^2} \right]$$

- Insulator (taking only 2 TO modes):

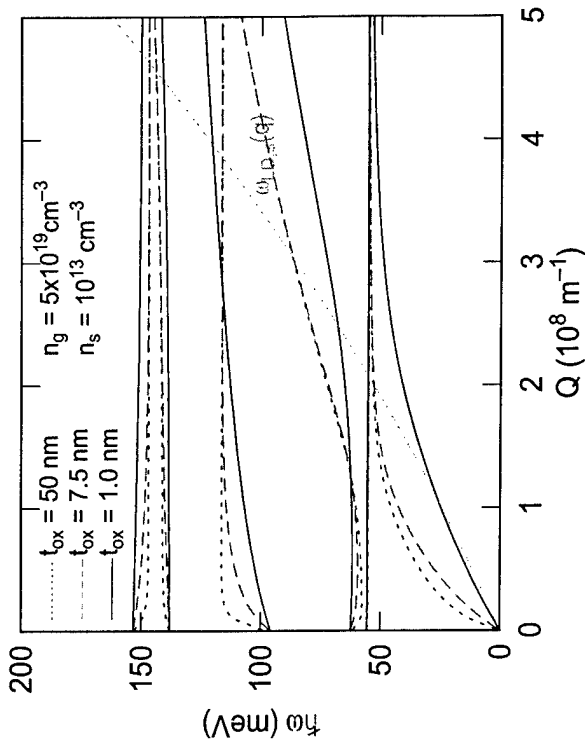
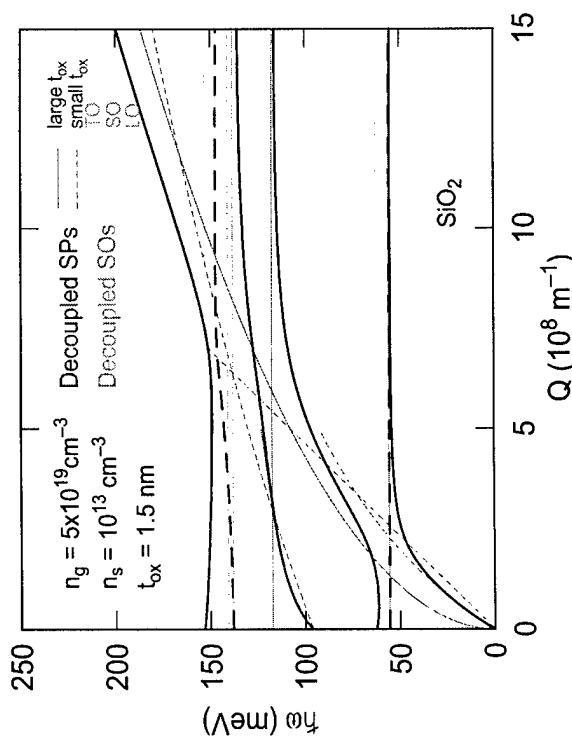
$$\epsilon_{ox}(\omega) = \epsilon_{ox}^{\infty} + (\epsilon_{ox}^i - \epsilon_{ox}^{\infty}) \frac{\omega_{TO2}^2}{\omega_{TO2}^2 - \omega^2} + (\epsilon_{ox}^0 - \epsilon_{ox}^i) \frac{\omega_{TO1}^2}{\omega_{TO1}^2 - \omega^2}$$

## RPA vs long-wavelength-limit for Si/SiO<sub>2</sub>/Si

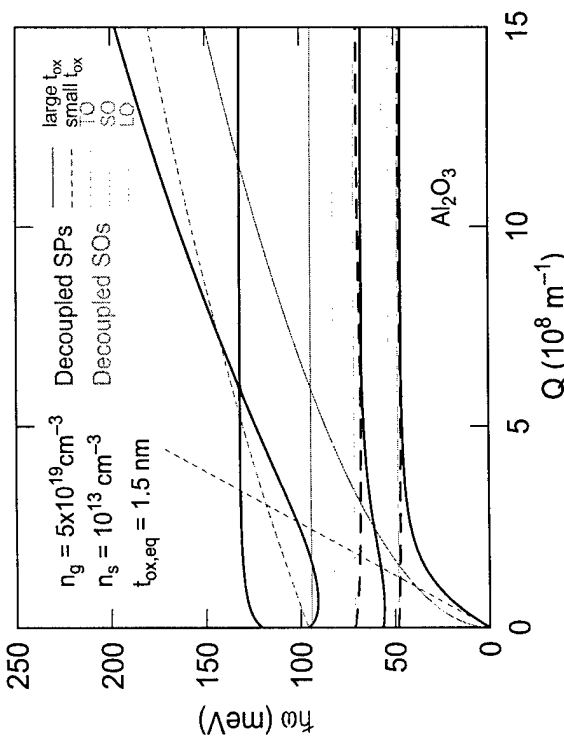


## Coupled modes for Si/SiO<sub>2</sub>/Si system: Effect of coupling

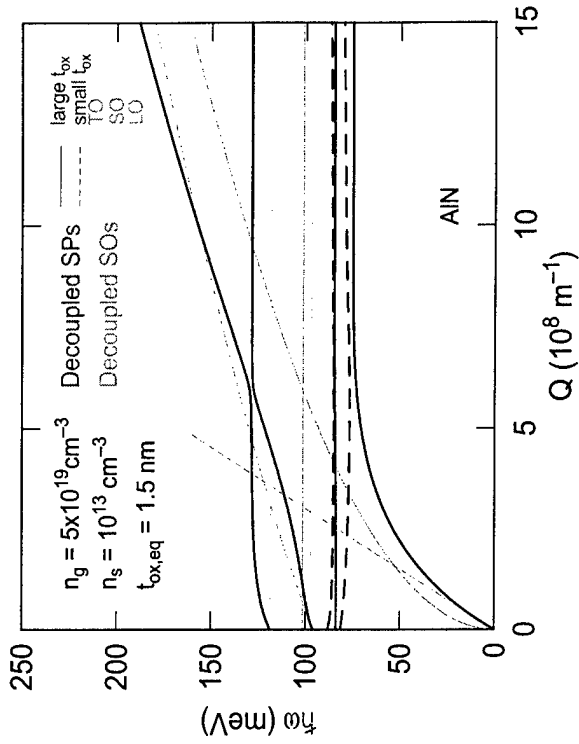
## Coupled modes for Si/SiO<sub>2</sub>/Si system: Thickness dependence



## Coupled modes for Si/Al<sub>2</sub>O<sub>3</sub>/Si system



## Coupled LO-plasmons modes for Si/AlN/Si system



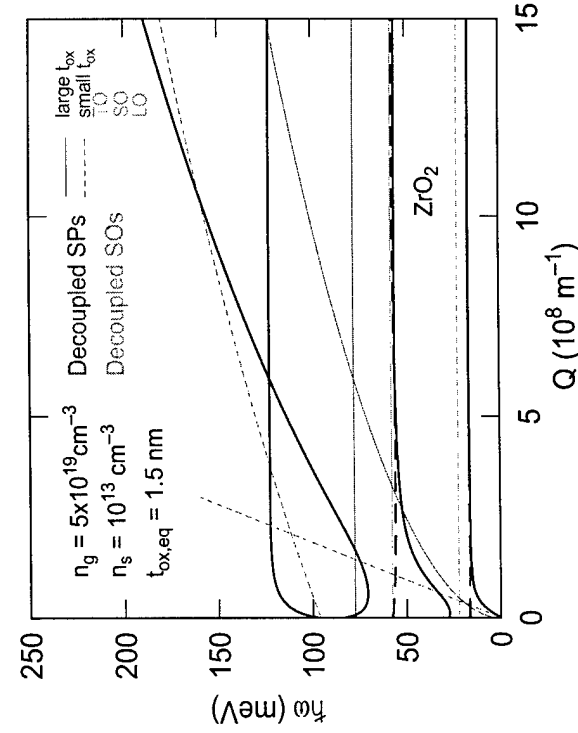
June 01 13

MVF

MVF

June 01 14

## Coupled LO-plasmons modes for Si/ZrO<sub>2</sub>/Si system



## TO- and plasmon content Landau damping

- Define 3 dispersions  $\omega_Q^{(-\alpha,j)}$  ( $j=1,3$ ) by ignoring mode  $\alpha$  ( $\alpha = \text{TO1, TO2, gate-plasma, substrate-2D-plasma}$ )
- Mode- $\alpha$  content of mode  $\omega_Q^{(i)}$  (for 4 modes):

$$\Pi^{(\alpha)}(\omega_Q^{(i)}) \approx \left| \frac{(\omega_Q^{(i)} - \omega_Q^{(-\alpha,1)^2})(\omega_Q^{(i)} - \omega_Q^{(-\alpha,2)^2})(\omega_Q^{(i)} - \omega_Q^{(-\alpha,3)^2})}{(\omega_Q^{(i)} - \omega_Q^{(j)^2})(\omega_Q^{(i)} - \omega_Q^{(k)^2})(\omega_Q^{(i)} - \omega_Q^{(l)^2})} \right|$$

with  $i, j, k, l$  cyclical.

- Content normalized so that:

$$\sum_{i=1}^4 \Pi^{(\alpha)}(\omega_Q^{(i)}) = 1$$

$$\Pi^{(G)}(\omega_Q^{(i)}) + \Pi^{(S)}(\omega_Q^{(i)}) + \Pi^{(TO1)}(\omega_Q^{(i)}) + \Pi^{(TO2)}(\omega_Q^{(i)}) = 1$$

- Landau damping (poor man's way): Ignore response of gate-plasma when gate-plasmon-like mode is in Landau-damped region; same for substrate plasma

## Scattering strength

- Field  $\phi_{Q,\omega_Q^{(i)}}(z)$  defined up to a multiplicative constant  $a_{Q,\omega_Q^{(i)}}$ :

$$\begin{aligned} b_{Q,\omega_Q^{(i)}} &= \frac{\epsilon_{ox}(\omega_Q^{(i)}) - \epsilon_g(\omega_Q^{(i)})}{2\epsilon_{ox}(\omega_Q^{(i)})} a_{Q,\omega_Q^{(i)}} \\ c_{Q,\omega_Q^{(i)}} &= \frac{\epsilon_{ox}(\omega_Q^{(i)}) + \epsilon_g(\omega_Q^{(i)})}{2\epsilon_{ox}(\omega_Q^{(i)})} a_{Q,\omega_Q^{(i)}} \\ d_{Q,\omega_Q^{(i)}} &= \frac{\epsilon_{ox}(\omega_Q^{(i)}) - \epsilon_g(\omega_Q^{(i)})}{\epsilon_{ox}(\omega_Q^{(i)}) + \epsilon_s(Q,\omega_Q^{(i)})} a_{Q,\omega_Q^{(i)}} \end{aligned}$$

- Fix  $a_{Q,\omega_Q^{(i)}}$  via second-quantization or semiclassically.

- Semiclassically (not-so-trivial extension of Kittel 63):

- Re-write potential as:

$$\phi_Q^{(i)}(\mathbf{R}, z, t) = \phi_{Q,\omega_Q^{(i)}}^{(i)}(z) \cos(\mathbf{Q} \cdot \mathbf{R} - \omega_Q^{(i)}t)$$

- Write interface charge-density as:

$$\rho_Q^{(i)}(\mathbf{R}, z, t)$$

$$\begin{aligned} &= \{ \delta(z) [ \epsilon_{gate}(\omega_Q^{(i)}) a_{Q,\omega_Q^{(i)}} + \epsilon_{insulator}(\omega_Q^{(i)}) (b_{Q,\omega_Q^{(i)}} - c_{Q,\omega_Q^{(i)}}) ] \\ &+ \delta(z-t) [ \epsilon_{insulator}(\omega_Q^{(i)}) (c_{Q,\omega_Q^{(i)}} e^{Qt} - b_{Q,\omega_Q^{(i)}} e^{-Qt}) \\ &+ \epsilon_{substrate}(Q, \omega_Q^{(i)}) d_{Q,\omega_Q^{(i)}} e^{-Qt} ] \} Q \cos(\mathbf{Q} \cdot \mathbf{R} - \omega_Q^{(i)}t). \end{aligned}$$

$\epsilon_{gate}(\omega)$ ,  $\epsilon_{insulator}(\omega)$ , and  $\epsilon_{substrate}(Q, \omega)$  to be determined: whatever response is accounted for by these functions, is not accounted for by the potential

- Get total energy (potential+kinetic, including self-energy):

$$\langle W_Q^{(i)} \rangle = 2 < U_Q^{(i)} >$$

$$\begin{aligned} &= \frac{2}{\Omega} \left\langle \int_{\Omega} d\mathbf{R} \int_{-\infty}^{\infty} dz \phi_Q^{(i)}(\mathbf{R}, z, t) \rho_Q^{(i)}(\mathbf{R}, z, t) \right\rangle \\ &= Q \epsilon_{TOT}(Q, \omega_Q^{(i)}) \left[ \frac{\epsilon_{ox}(\omega_Q^{(i)}) - \epsilon_g(\omega_Q^{(i)})}{\epsilon_{ox}(\omega_Q^{(i)}) + \epsilon_s(Q, \omega_Q^{(i)})} \right]^2 a_{Q,\omega_Q^{(i)}}^2 e^{-2Qt} \\ &\text{with} \\ &\epsilon_{TOT}(Q, \omega) = \epsilon_{gate}(\omega) \left[ \frac{\epsilon_{ox}(\omega) + \epsilon_s(Q, \omega)}{\epsilon_{ox}(\omega) - \epsilon_g(\omega)} \right]^2 e^{2Qt} \\ &\quad + \epsilon_{insulator}(\omega) \left\{ \left[ \frac{\epsilon_{ox}(\omega) + \epsilon_s(Q, \omega)}{2\epsilon_{ox}(\omega)} \right]^2 (e^{2Qt} - 1) \right. \\ &\quad \left. + \left[ \frac{\epsilon_{ox}(\omega) - \epsilon_s(Q, \omega)}{2\epsilon_{ox}(\omega)} \right]^2 (1 - e^{-2Qt}) \right\} \\ &\text{– Finally:} \\ &\phi_{Q,\omega_Q^{(i)}}^{(i)} = \left[ \frac{\hbar \omega_Q^{(i)}}{2 Q \epsilon_{TOT}(Q, \omega_Q^{(i)})} \right]^{1/2} e^{-Q(z-t)} \end{aligned}$$

- Setting:
  - \*  $\epsilon_{gate}(\omega) = \epsilon_g(\omega)$
  - \*  $\epsilon_{insulator}(\omega) = \epsilon_{ox}(\omega)$
  - \*  $\epsilon_{substrate}(Q, \omega) = \epsilon_s^{(2D)}(Q, \omega)$

the secular equation is equivalent to

$$\epsilon_{TOT}(Q, \omega) = 0$$

- Scattering field due to plasmon- and phonon-components:

- Plasmon: Set
  - $\epsilon_{substrate}(Q, \omega) = \epsilon_{Si}$ ,  $\epsilon_{gate}(\omega) = \epsilon_{Si}$   
(full plasma response lumped into the field)
  - $\epsilon_{insulator}(\omega) = \epsilon_{ox}^0$   
(TO-response excluded from the field and fully lumped into the dielectric function) in  $\epsilon_{TOT}(Q, \omega)$
  - Call it  $\epsilon_{TOT}^{(PL)}(Q, \omega)$

Then, field due to gate-plasmons:

$$\phi_{Q, \omega_Q^{(i)}}^{(i, PL)}(z) = \left[ \frac{\hbar \omega_Q^{(i)}}{2 Q \epsilon_{TOT}^{(PL)}(Q, \omega_Q^{(i)})} \Pi^{(G)}(\omega_Q^{(i)}) \right]^{1/2} e^{-Q(z-t)}$$

- TO1-mode:

- Let substrate and gate plasmas respond:
  - $\epsilon_{substrate}(Q, \omega) = \epsilon_s(Q, \omega)$ ,  $\epsilon_{gate}(\omega) = \epsilon_g(\omega)$  (so excluding plasmas from the potential)
  - Define  $\epsilon_{TOT, high}^{(TO1)}(Q, \omega_Q^{(i)})$  by setting

$$\epsilon_{insulator}(\omega) = \epsilon_{ox}^{\infty} \frac{\omega_{LO2}^2 - \omega^2}{\omega_{TO2}^2 - \omega^2}$$

(phonon 2 responds at the frequency  $\omega$ , while phonon 1 does not respond).

- Define  $\epsilon_{TOT, low}^{(TO1)}(Q, \omega_Q^{(i)})$  by setting

$$\epsilon_{insulator}(\omega) = \epsilon_{ox}^{\infty} \frac{\omega_{LO2}^2 - \omega^2}{\omega_{TO2}^2 - \omega^2} \left( \frac{\omega_{LO1}}{\omega_{TO1}} \right)^2$$

(phonon 2 responds at the frequency  $\omega$ , while phonon 1 responds fully).

Then, amplitude of (scattering) field due only to TO1 is:

$$\phi_{Q, \omega_Q^{(i)}}^{(i, PH1)}(z) = e^{-Q(z-t)} \times$$

$$\left\{ \frac{\hbar \omega_Q^{(i)}}{2 Q} \left[ \frac{1}{\epsilon_{TOT, high}^{(TO1)}(Q, \omega_Q^{(i)})} - \frac{1}{\epsilon_{TOT, low}^{(TO1)}(Q, \omega_Q^{(i)})} \right]^{1/2} \Phi^{(TO1)}(\omega_Q^{(i)}) \right\}$$

- Note: Modes 5 and 6 are SO-modes at the far (gate-insulator) interface. At small  $K_F$ , large  $n_g$ , they are screened by gate-electrons, at large  $K_F$  their effect on the mobility is depressed by a factor  $\exp(-2K_F t)$ ... so, ignore them.

- Interesting limits:
  - TO-mode (no plasma) in bulk: Scattering field  $\propto$

$$\left[ \frac{\hbar\omega_{LO}}{2q^2} \left( \frac{1}{\epsilon^\infty} - \frac{1}{\epsilon^0} \right) \right]^{1/2}$$

(usual Fröhlich coupling)

- Coupled TO-plasma modes in bulk:

$$\epsilon_{TOT}(Q, \omega) = \epsilon^\infty [(\omega^2 - \omega_{LO}^2)/(\omega^2 - \omega_{TO}^2) - (\omega_P/\omega)^2]$$

with dispersion:

$$\omega_\pm^2 = \frac{1}{2} \{ \omega_{LO}^2 + \omega_P^2 \pm [(\omega_{LO}^2 + \omega_P^2)^2 - 4\omega_{TO}^2\omega_P^2]^{1/2} \}$$

and scattering field:

$$\left\{ \frac{\hbar\omega_\pm}{2q^2} \left[ \frac{1}{\epsilon^\infty - \epsilon^\infty \omega_P^2/\omega_\pm^2} - \frac{1}{\epsilon^0 - \epsilon^\infty \omega_P^2/\omega_\pm^2} \right] \left| \frac{\omega_\pm^2 - \omega_P^2}{\omega_+^2 - \omega_-^2} \right| \right\}^{1/2}$$

(cf. Varga 65, Kim-Das-Senturia 78, Ridley 88, Sanborn 95)

- Single TO-mode at Si-insulator interface:

$$\epsilon_{TOT} = \epsilon_{ox}(\omega) + \epsilon_{Si}^\infty$$

with dispersion

$$\omega_{SO} = \omega_{TO} \left[ \frac{\epsilon_{ox}^0 + \epsilon_{Si}^\infty}{\epsilon_{ox}^\infty + \epsilon_{Si}^\infty} \right]^{1/2}$$

and scattering strength  $\propto$

$$\phi_{Q,\omega_{SO}}^{(PH)}(z) = \left\{ \frac{\hbar\omega_{SO}}{2Q} \left[ \frac{1}{\epsilon_{Si}^\infty + \epsilon_{ox}^\infty} - \frac{1}{\epsilon_{Si}^\infty + \epsilon_{ox}^0} \right] \right\}^{1/2} e^{-Q(z-t)}$$

(cf Wang-Mahan 72) which is also the unscreened  $Qt \rightarrow \infty$ -limit of the general formula

$$\alpha_i = \frac{e^2}{4\pi\hbar} \left( \frac{m_t}{2\hbar\omega_{SOi}} \right)^{1/2} \left( \frac{1}{\epsilon_{Si}^\infty + \epsilon_{ox}^\infty} - \frac{1}{\epsilon_{Si}^\infty + \epsilon_{ox}^0} \right)$$

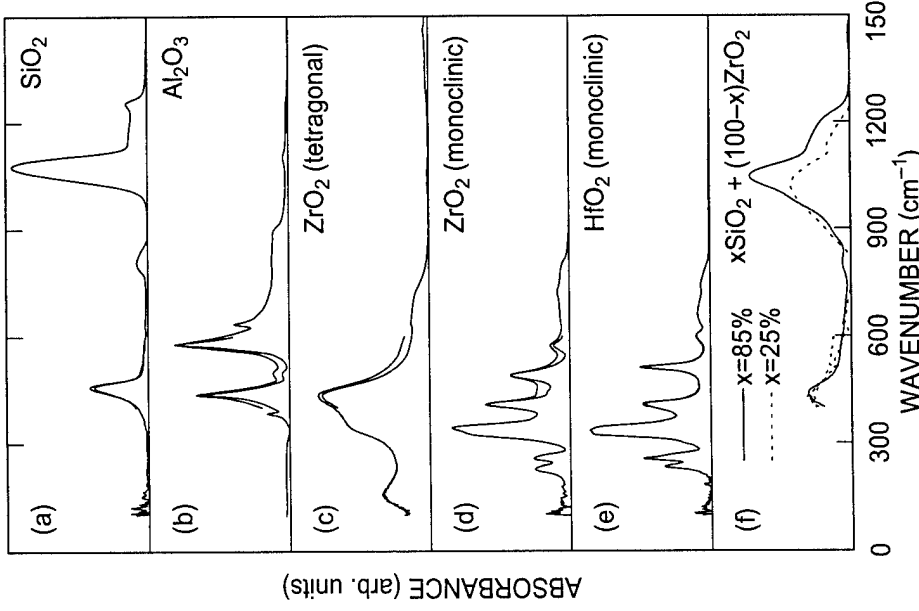
## Insulator parameters

- Select/compromise:
  - from literature (theory, experiments: FTIR, Raman, tunneling spectroscopy)
  - From 'in-house' FTIR
- Complications:
  - several modes: lump 2 stronger groups/bands into 2 discrete TO modes
  - several forms (cubic, hexagonal, monoclinic, amorphous): find closest to 'in-house' FTIR-measured films
  - process dependence (e.g., Al-ions in non-stoichiometric  $Al_2O_3$ ): assume 'ideal' films
  - interfacial layers ( $SiO_2$  for oxides and silicates,  $Si_3N_4$  for nitrides and oxynitrides): estimate effect

Quantity (units)	Material	$SiO_2$	$Al_2O_3$	AlN	$ZrO_2$	HfO <sub>2</sub>	$ZrSiO_4$
$\epsilon_{ox}^0$ ( $\epsilon_0$ )		3.90	12.53	9.14	24.0	22.00	11.75
$\epsilon_{ox}^2$ ( $\epsilon_0$ )		3.05	7.27	7.35	7.75	6.58	9.73
$\epsilon_{ox}^\infty$ ( $\epsilon_0$ )		2.50	3.20	4.80	4.00	5.03	4.20
$\omega_{TO1}$ (meV)		55.60	48.18	81.40	16.67	12.40	38.62
$\omega_{TO2}$ (meV)		138.10	71.41	88.55	57.70	48.35	116.00
$\alpha_1$		0.0248	0.0788	0.0248	0.2504	0.3102	0.0322
$\alpha_2$		0.0113	0.0814	0.0423	0.0779	0.0362	0.2942

## FTIR spectra (D. Neumayer)

### Mobility



- Scattering rate:

$$\frac{1}{\tau_{\mu\nu}(\mathbf{K})} = \frac{2\pi}{\hbar} \sum_{\mathbf{Q}} |V_{\mu\nu}(\mathbf{Q})|^2 \delta[E_{\mu}(\mathbf{K}) - E_{\nu}(\mathbf{K} + \mathbf{Q}) \pm \Delta E(\mathbf{Q})]$$

$$V_{\mu\nu}(\mathbf{Q}) = \int_0^{\infty} dz \zeta_{\mu}^{*}(z) \phi_{\mathbf{Q}}(z) \zeta_{\nu}(z)$$

- Momentum relaxation rate (along x-axis):

$$\frac{1}{\tau_{\mu\nu}^{(p,x)}(\mathbf{K})} \approx \frac{2\pi}{\hbar} \sum_{\mathbf{Q}} |V_{\mu\nu}(\mathbf{Q})|^2 \left( \frac{Q_x}{K} \right)$$

$$\times \delta[E_{\mu}(\mathbf{K}) - E_{\nu}(\mathbf{K} + \mathbf{Q}) \pm \Delta E(\mathbf{Q})]$$

- Mobility along x-axis (assuming spherical dispersion):

$$\mu_{x,x} = \sum_{\nu} \frac{\mu_{\nu} n_{\nu}}{n_s} =$$

$$\sum_{\nu} \frac{en_{\nu}}{m_{x,\nu} k_B T n_s} \int_{E_{\nu}}^{\infty} dE (E - E_{\nu}) \rho_{\nu}(E) \tau_{\nu}^{(p,x)}(E) f_{\nu}(E) [1 - f_{\nu}(E)]$$

- Screening (dynamic):

$$V_{\mu\nu}^{(s)}(\mathbf{Q}, \omega) = V_{\mu\nu}(\mathbf{Q}) - \sum_{\lambda\lambda'} \frac{\beta_{\lambda}(\mathbf{Q}, \omega)}{Q} g_{\mu\nu; \lambda\lambda'}(\mathbf{Q}) V_{\lambda\lambda'}^{(s)}(\mathbf{Q}, \omega)$$

$$g_{\mu\nu; \lambda\lambda'}(\mathbf{Q}) = \int_0^{\infty} dz' \int_0^{\infty} dz \zeta_{\mu}^{*}(z) \zeta_{\nu}(z') G_{\mathbf{Q}}(z, z') \zeta_{\lambda}(z) \zeta_{\lambda'}(z')$$

where  $G_{\mathbf{Q}}(z, z')$  is the Poisson Green's function.

In matrix form:

$$V^{(s)}(\mathbf{Q}, \omega) = [1 - \Pi(\mathbf{Q}, \omega)]^{-1} V(\mathbf{Q})$$

## Scattering processes

- Surface roughness:
  - Ando's model assumes 1st-order perturbation given by steps at interface of rms height  $\Delta$  and correlation-distance  $\Lambda$ .

- Bulk Si phonons:

$$|V_{\mu\nu}(\mathbf{Q})|^2 \propto \frac{\Delta_Q^2}{\hbar\omega_Q} F_{\mu\nu}(Q)$$

- Example: for acoustic, intravalley, one-subband, variational wavefunction

$$\frac{1}{\tau(p)} \approx \frac{3m_z b \Delta_{ac}^2}{64\hbar^3 \rho c_s^2} \rightarrow \mu_{ph} \propto b^{-1} \propto n_s^{-1/3}$$

- In general, more complicated:

1. Deformation potential is anisotropic:

$$\Delta_{LA} \rightarrow \Xi_d + \Xi_u \cos^2 \eta_Q$$

$$\Delta_{TA} \rightarrow \Xi_u \cos \eta_Q \sin \eta_Q$$

2. Subband dispersion is nonparabolic
3. Subband dispersion is non-spherical
4. Intervalley scattering (projected onto 2D BZ)
5. Are bulk Si phonons OK near the interface?
6. What about screening?

- Coulomb scattering (with dopants, oxide charges, etc):

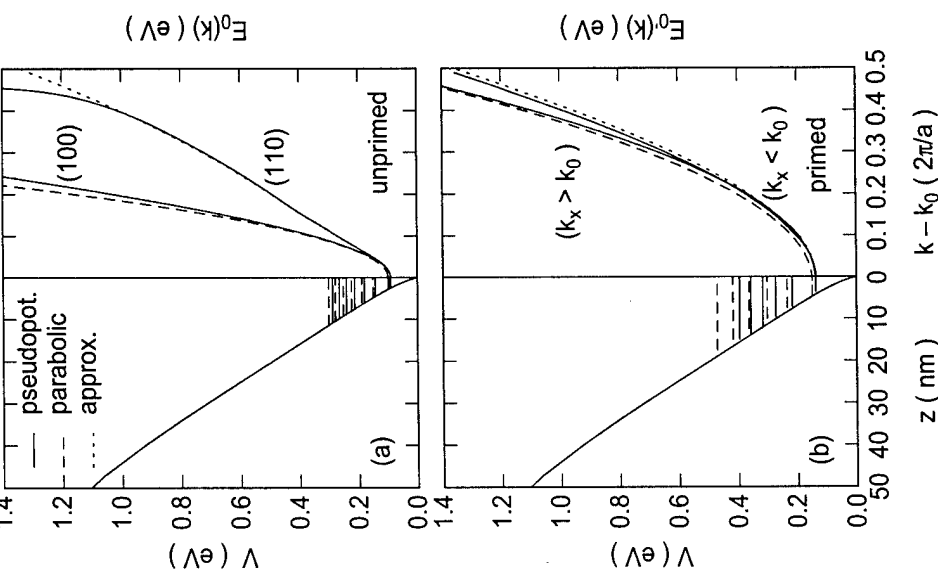
$$V_{\mu\nu}(\mathbf{Q}) \propto \frac{e^2 N_C^{1/2}}{Q^2} \tilde{G}_{\mu\mu;\nu\nu}(Q)$$

- (must be screened!) and

$$\mu_C \propto \frac{n_s^{4/3}}{N_C}$$

## Subbands

### Triangular-well approximation



MVF

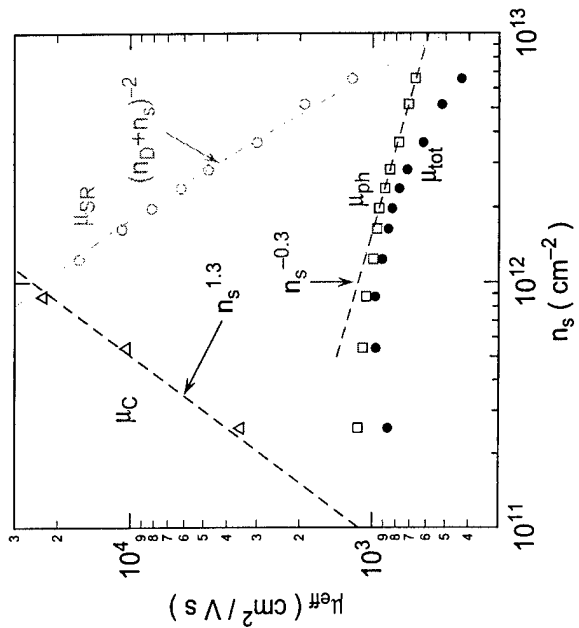
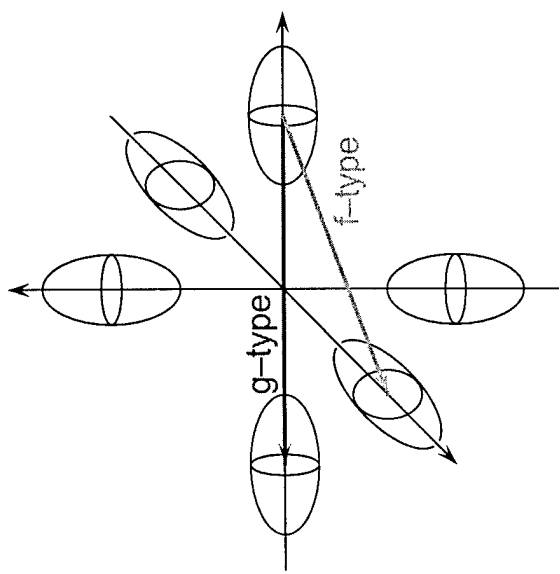
June 01 27

MVF

June 01 28

## Phonon-assisted intervalley scattering

## Mobility split into various components



June 01 29

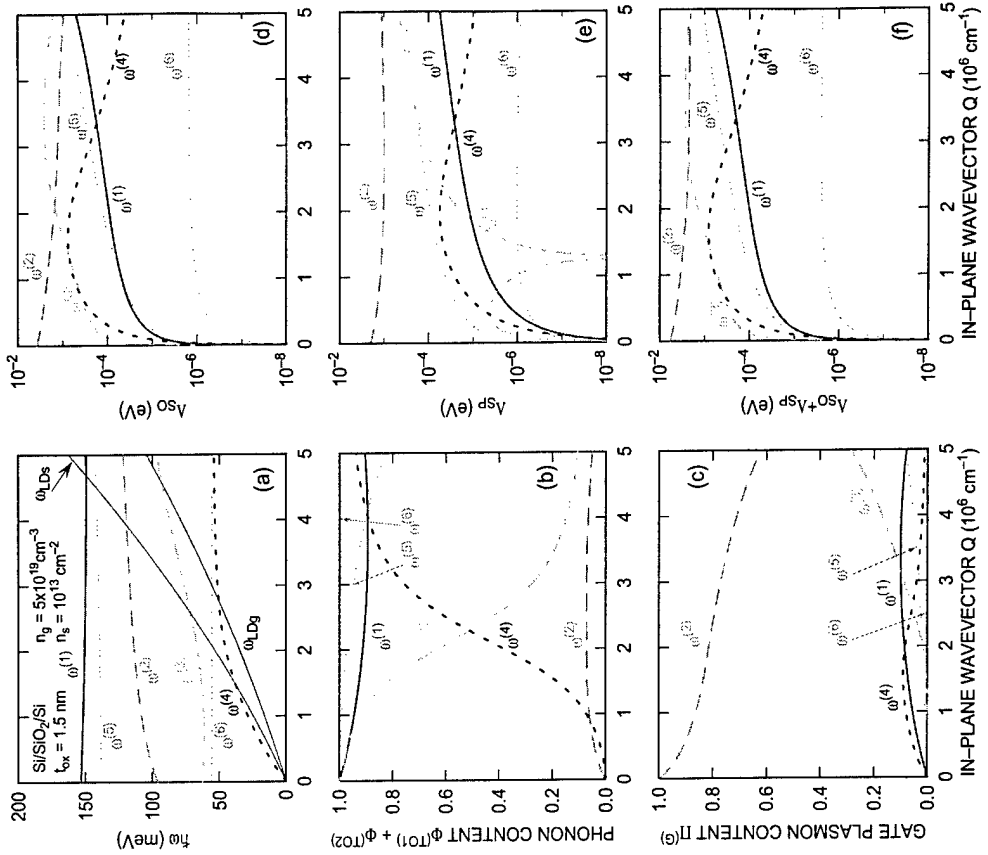
MVF

MVF

June 01 30

## The fight for the right phonon-limited mobility

### The Si/SiO<sub>2</sub>/Si system



June 01 31.

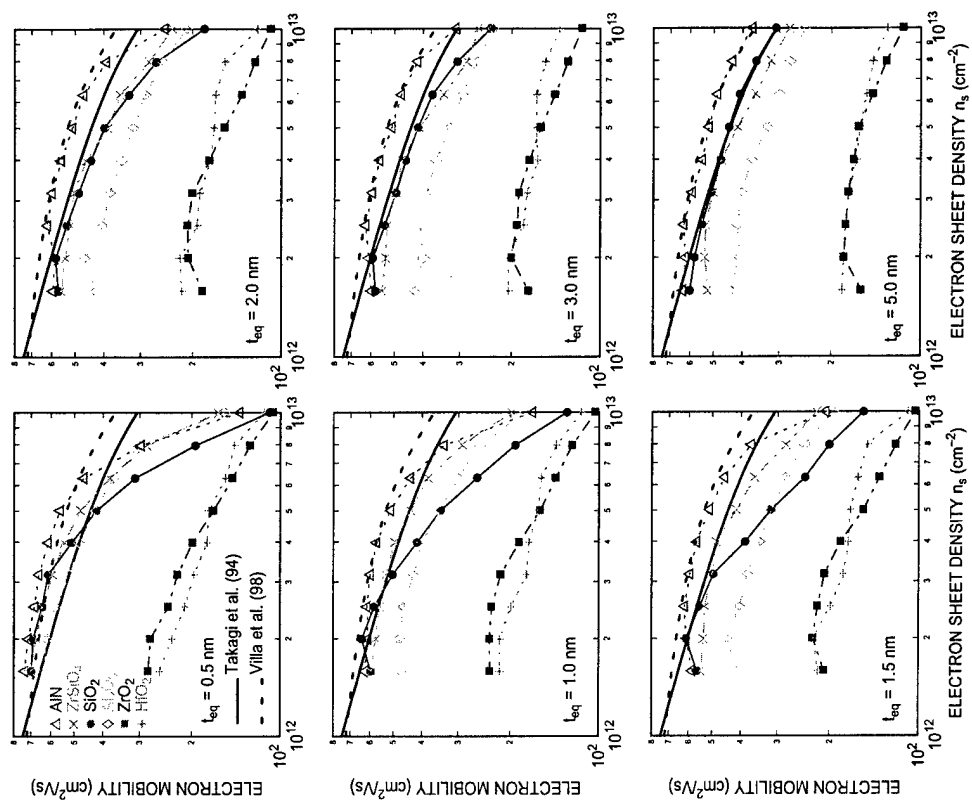
MVF

MVF

June 01 32

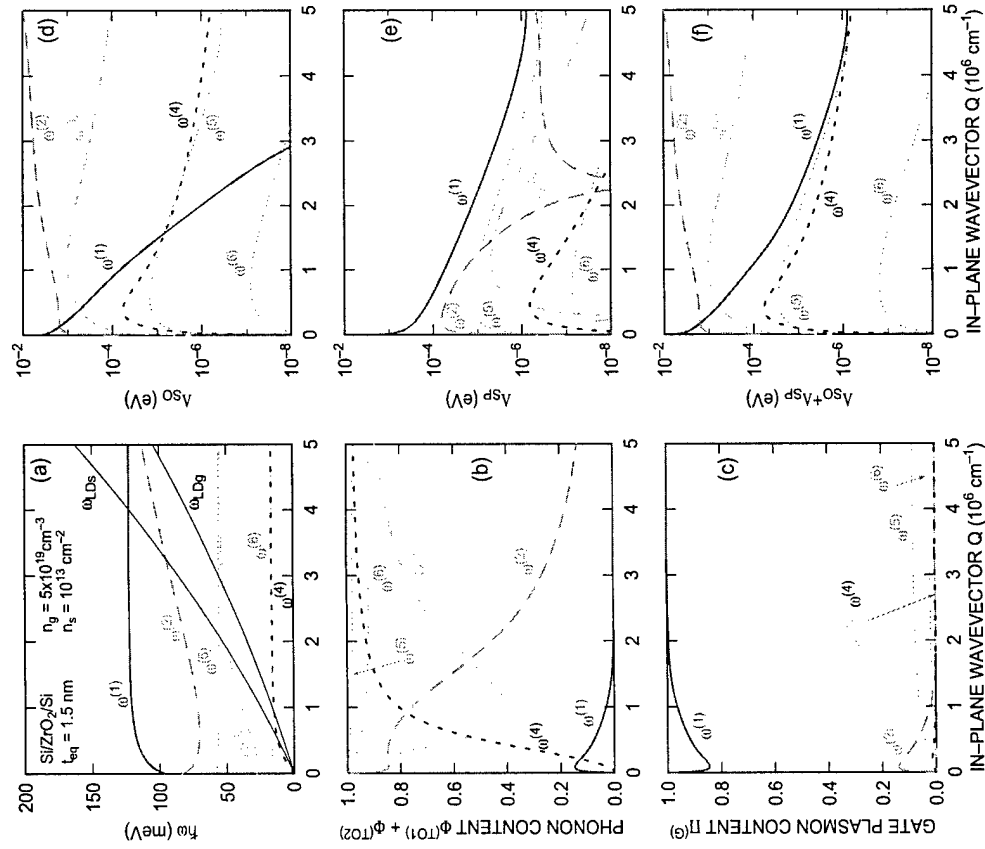
## The Si/ZrO<sub>2</sub>/Si system

### Effective mobility I (average $n_g$ )



June 01 33

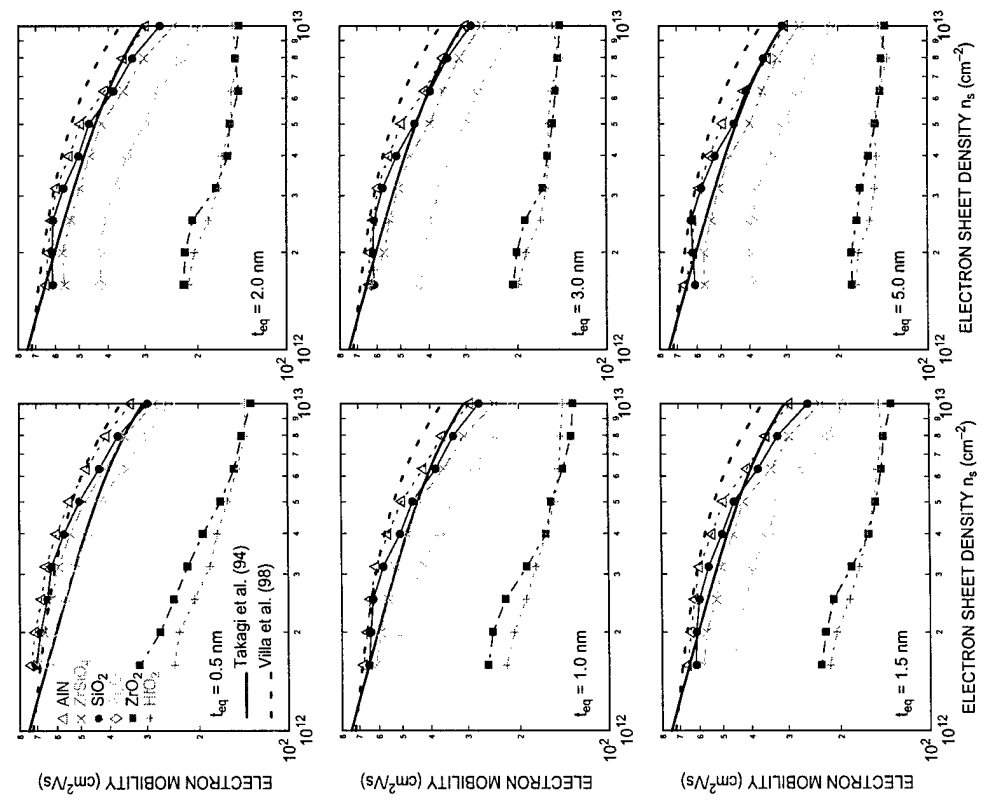
MVF



MVF

June 01 34

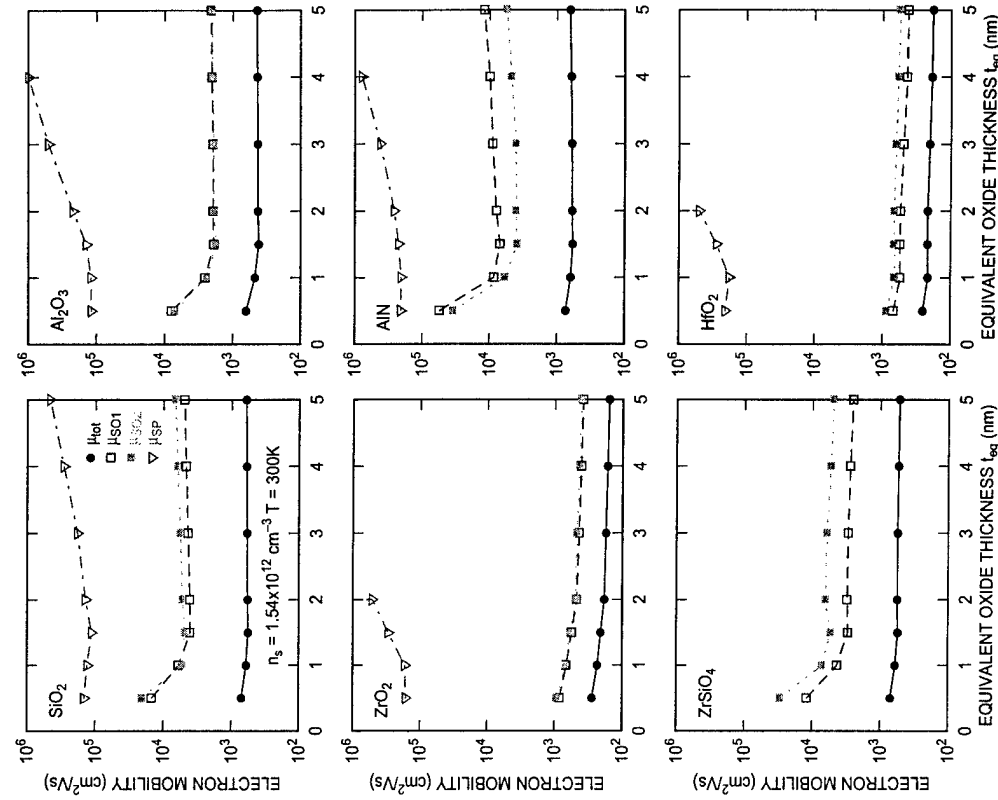
## Effective mobility II ( $Q$ -dependent $n_g$ )



June 01 35

MVF

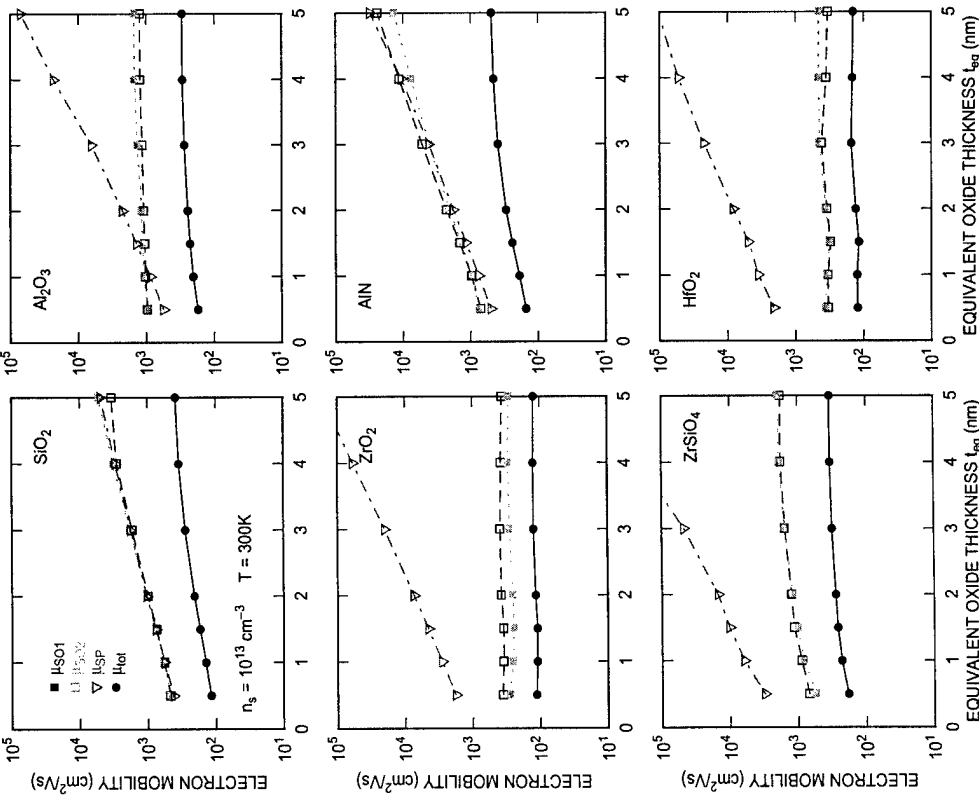
## Components of the mobility (low density)



MVF

June 01 36

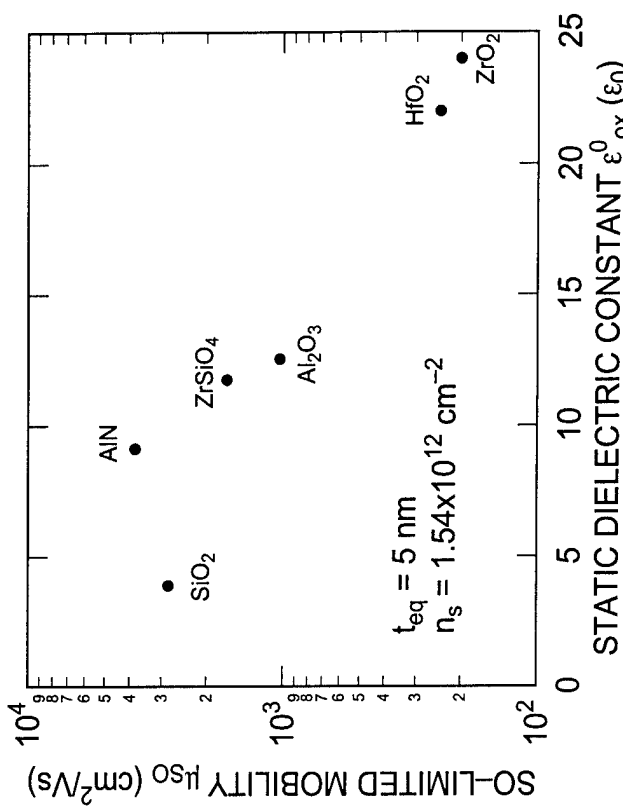
## Components of the mobility (high density)



June 01 37

MVF

## Mobility vs static dielectric constant



MVF

June 01 38

## Effect of $\text{SiO}_2$ interfacial layer

- Interfacial layer probably unavoidable, possibly desirable (with moderation...)
- Full system  $\text{Si}/\text{high-}\kappa/\text{SiO}_2/\text{Si}$  too cumbersome... secular equation

$$\begin{aligned}
 & (\epsilon_g + \epsilon_\kappa)(\epsilon_s + \epsilon_{ox})(\epsilon_{ox} + \epsilon_\kappa) + (\epsilon_g - \epsilon_\kappa)(\epsilon_s + \epsilon_{ox})(\epsilon_{ox} - \epsilon_\kappa) e^{-2Qt\kappa} \\
 & - (\epsilon_g - \epsilon_\kappa)(\epsilon_s - \epsilon_{ox})(\epsilon_{ox} + \epsilon_\kappa) e^{-2Q(t_\kappa + t_{ox})} \\
 & - (\epsilon_g + \epsilon_\kappa)(\epsilon_s - \epsilon_{ox})(\epsilon_{ox} - \epsilon_\kappa) e^{-2Qt_{ox}} = 0
 \end{aligned}$$

(16 coupled modes!)

- Consider instead 'unscreened' high- $\kappa/\text{SiO}_2/\text{Si}$  system and only one TO-mode in each insulator.

3 modes with high- $Q$ -frequencies:

1.  $\text{SiO}_2$  mode  $\Omega_{TO}$  localized at the  $\text{Si}/\text{SiO}_2$  interface:

$$\omega_Q^{(-)} \approx \Omega_{TO} \left[ \frac{\epsilon_{ox}^0 + \epsilon_{Si}^\infty}{\epsilon_{ox}^i + \epsilon_{Si}^\infty} \right]^{1/2}$$

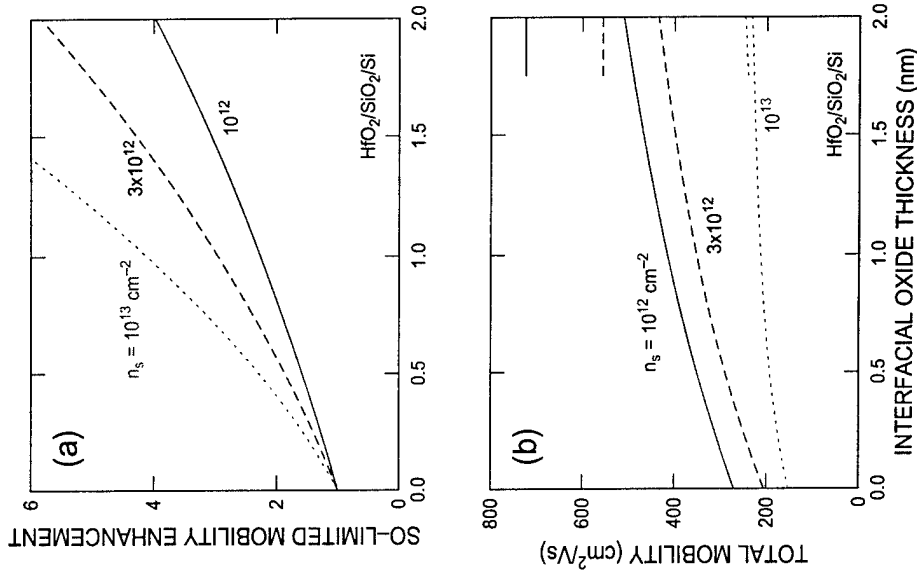
2. SiO<sub>2</sub> mode  $\Omega_{TO}$  localized at the high- $\kappa/\text{SiO}_2$  interface:

$$\omega_Q^{(+)} \approx \Omega_{TO} \left[ \frac{\epsilon_{ox}^0 + \epsilon_\kappa^\infty}{\epsilon_{ox}^i + \epsilon_\kappa^\infty} \right]^{1/2}$$

(negligible, as for modes 5 and 6 before)  
 3. remote) high- $\kappa$  mode  $\omega_{TO}$  localized at the  $\text{Si}/\text{SiO}_2$  interface:

$$\omega_Q^{(\kappa)} \approx \omega_{TO} \left[ \frac{\epsilon_\kappa^0 + \epsilon_{Si}^\infty}{\epsilon_\kappa^i + \epsilon_{Si}^\infty} \right]^{1/2}$$

## Effect of the $\text{SiO}_2$ interfacial layer



## Conclusions

- Experimental confirmation?
  - Poor mobility observed almost always, but mainly due to poor material quality (traps, interface states, non-stoichiometry, interfacial layers). Must solve these problems first!  $n_s$  hard to measure accurately.
  - Parameters: what material do we really have? How far from 'ideal'?
    - Still...trends show HfO<sub>2</sub> and ZrO<sub>2</sub> yield worst mobility (Ragnarsson, Callegari, 00-01), ZrSiO<sub>4</sub> somewhat better than ZrO<sub>2</sub> (Qi, 00), Al<sub>2</sub>O<sub>3</sub> in-between, AlN very poor (but Si<sub>3</sub>N<sub>4</sub> interfacial layer present)
- If theory is right:
  - Interfacial and many-body effects paramount in small devices:
    - \* Coulomb effects make 'ballistic limit' only a theoretical dream (metal contacts?)
      - \* there's no more 'bulk', only 'interfaces', in small devices
    - Must pay for high  $\kappa$  with poor mobility
    - Metal-oxides worst
  - Silicates promising
    - AlN promising (if we only could get rid of the Si<sub>3</sub>N<sub>4</sub> interfacial layer!)
    - Thin SiO<sub>2</sub> interfacial layer desirable
    - Assessing whether this low mobility is a fatal flaw or not is up to the circuit designers. Alternatives to high- $\kappa$  are even riskier propositions.

# Full Bandstructure Calculations for Transport in Wide-Band-Gap Semiconductors\*

Stephen M. Goodnick

Department of Electrical Engineering  
Arizona State University  
[stephen.goodnick@asu.edu](mailto:stephen.goodnick@asu.edu)  
[www.eas.asu.edu/~goodnick](http://www.eas.asu.edu/~goodnick)

\*Supported by ONR and the DARPA/Phosphor Technology Center of Excellence

ASU NRG/Maratea

## Outline

1. Wide-Bandgap Materials
2. Electronic Structure Calculations
3. Impact Ionization Rate
4. Electron-Phonon Interaction
5. Full-band Monte Carlo Simulation
6. Experimental Results

ASU NRG/Maratea

## Collaborators

- Richard Akis, Joy Barker, Manfred Dür\*, David Ferry, Trevor Thornton, Arizona State University
- Shankar Pennathur\*, John Wager, Oregon State University
- Marco Saraniti, Illinois Inst. Tech.
- Niels Fitzer, Ronald Redmer, Martin Reigrotzki\*, Universität Rostock
- Martin Städele\* and Peter Vogl, Technische Universität München
- Randy Shul, Sandia National Labs
- Daniel Koleske, Naval Research Labs

ASU NRG/Maratea

## Wide-Bandgap Semiconductors

### Column IV

SiC

### III-V Nitrides

GaN, AlN, InN

### II-VI Compounds

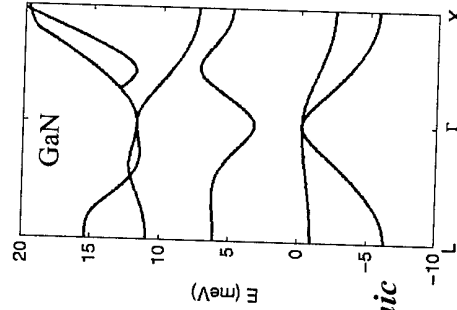
ZnS, ZnSe, MnS, SrS, CdS

Compound Semiconductors: *ionic zincblende* → *wurzite* → *rocksalt*

$E_G \sim 3\text{-}5\text{ eV}$

Breakdown field  $\sim 1\text{ MV/cm}$

ASU NRG/Maratea



## Wide-Bandgap Semiconductor Applications

### High-Frequency Power Amplifiers

- GaN MESFETs
- AlGaN/InGaN HEMTs

### Optical Sources

- ZnS/ZnSe, AlGaN/InGaN LED/Lasers (Ultraviolet, UV)

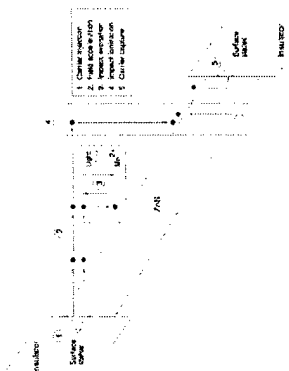
\* Phosphor materials (ZnS:Mn, Si:S:As, Ce:S:Al<sub>2</sub>O<sub>3</sub>), TFEEL.

**ASU** NRG/Maratea

## High Field Transport in TFEEL Devices

- High field phenomena affecting TFEEL performance:

- Impact excitation of luminescent impurities
  - Band to band impact ionization of electrons and holes

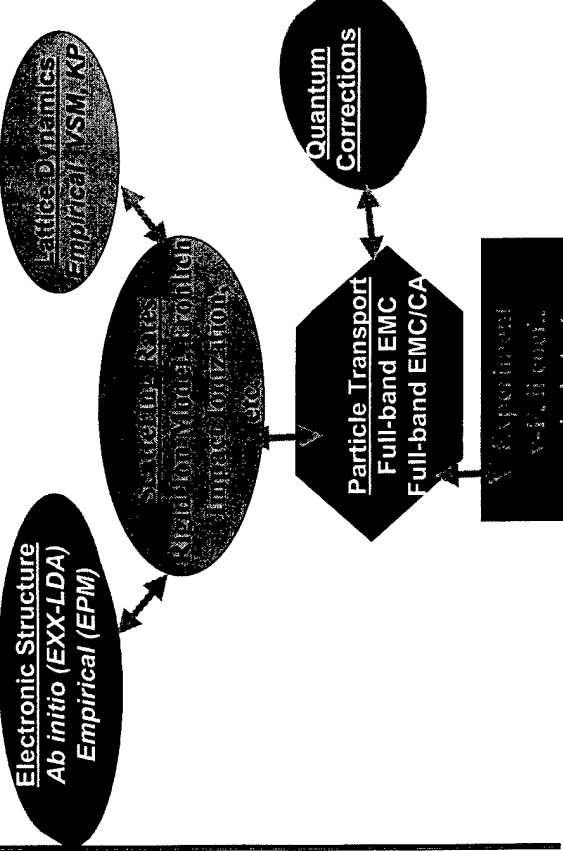


### Issues

- Average carrier energies at 1-2 MV/cm are 2-3 eV, several conduction bands occupied: Full bandstructure must be considered
- Band to band impact ionization process in wide bandgap materials not well understood
- Electron-phonon interaction at high fields is unknown experimentally in phosphor materials

**ASU** NRG/Maratea

## General Modeling Approach



**ASU** NRG/Maratea

## Bandstructure for Cubic GaN, ZnS, and SrS

### *Empirical Pseudopotential Method*

Local and nonlocal bandstructures for cubic GaN, ZnS and SrS are calculated either from formfactors in literature, or derived using least squares fit to existing critical point data.

### *ZnS*

- Local: Walter and Cohen, *Phys. Rev.* **183**, 763 (1969)
- Nonlocal: M. Dür *et al.*, *JAP* **83**, 3176 (1998)
- \* SrS
- Nonlocal- Reigrotski *et al.*, *JAP* **86**, 4458, (1999)
- \* GaN
- Oguzman *et al.*, *JAP* **80**, 4429 (1996)
- Xia *et al.*, *Phys. B* **59**, 10119 (1999)

**FSU** NRG/Maratea

## Ab Initio Bandstructure

*EXX-LDA (exact exchange-local density approximation) Method<sup>1</sup>*

- Kohn-Sham method is particular, exact realization of density functional theory which maps interacting system onto non-interacting system of the same density
- LDA approximates R( $r$ ) via exchange and correlation potential within the Kohn-Sham model

– Good ground state properties but poor band gaps

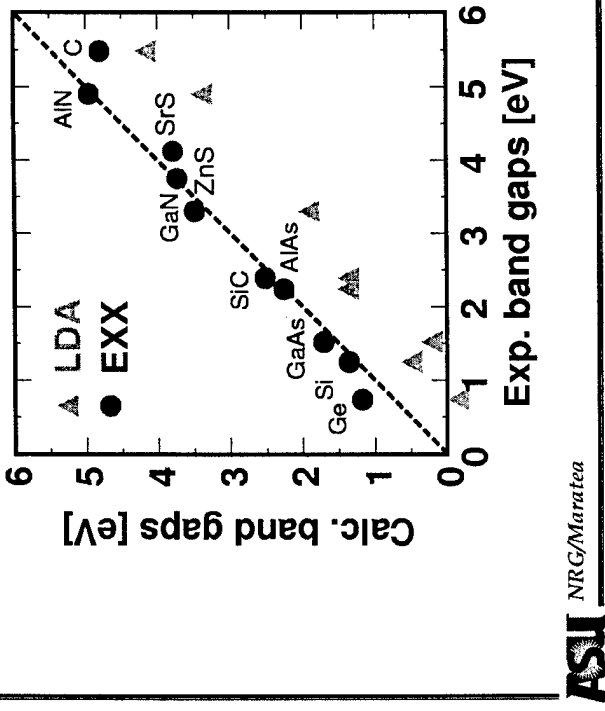
- EXX-LDA is a systematic step beyond LDA which treats the exchange potential  $E_{\text{EXX}}(V)$

– EXX+LDA yields excellent ground state properties and band gaps

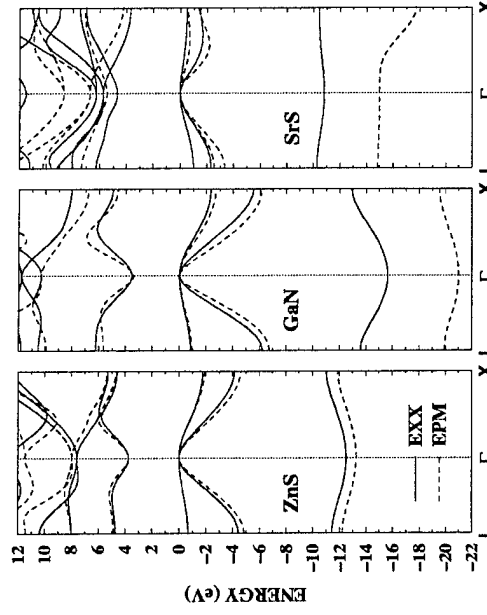
<sup>1</sup>M. Städle, J. A. Majewski, P. Vogl, and A. Görling, *Phys. Rev. Lett.* **79**, 2089 (1997)



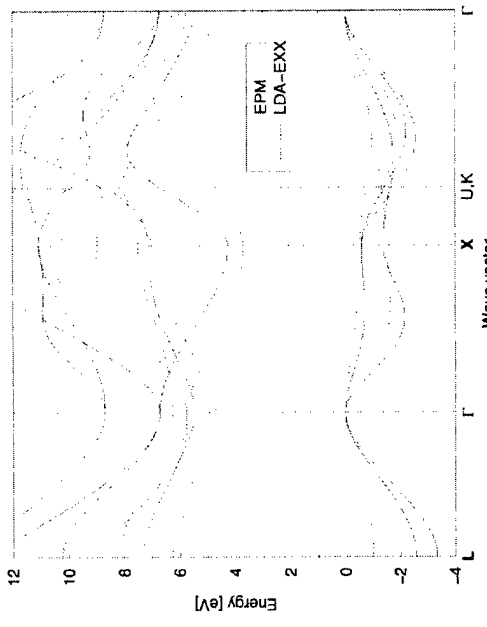
## EXX Results for Cubic Semiconductors



## Band Structure Based on EXX and Empirical Pseudopotential Method (EPM)



## SrS Band Structure Based on EXX and Empirical Pseudopotential Method (EPM)



## Comparison of EXX and EPM Results for SrS and ZnS to Experimental Data (in eV)

SrS: indirect

SrS	EXP	EXX	EPM
$E(\Gamma_v\text{-}X_c)$	4.32	3.69	4.26
$E(\Gamma_v\text{-}\Gamma_c)$	5.33	4.67	5.45
$E(X_v\text{-}X_c)$	4.83	4.21	4.86

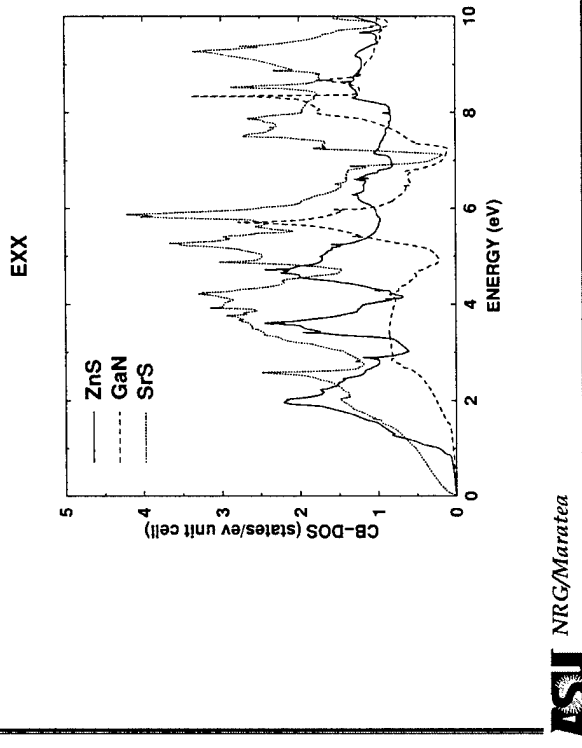
ZnS: direct

ZnS	EXP	EXX	EPM
$E(\Gamma_v\text{-}\Gamma_c)$	3.68	3.73	3.73
$E(\Gamma_v\text{-}L_c)$	5.73	5.45	5.59
$E(X_v\text{-}X_c)$	6.31	6.43	6.58

EXP: Walter and Cohen, *Phys. Rev.* **183**, 763 (1969)



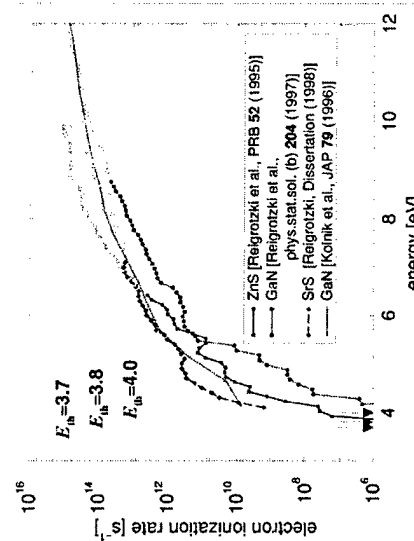
## EXX Density of States for SrS, ZnS, and GaN



## Impact Ionization Rate in Wide-Bandgap Materials

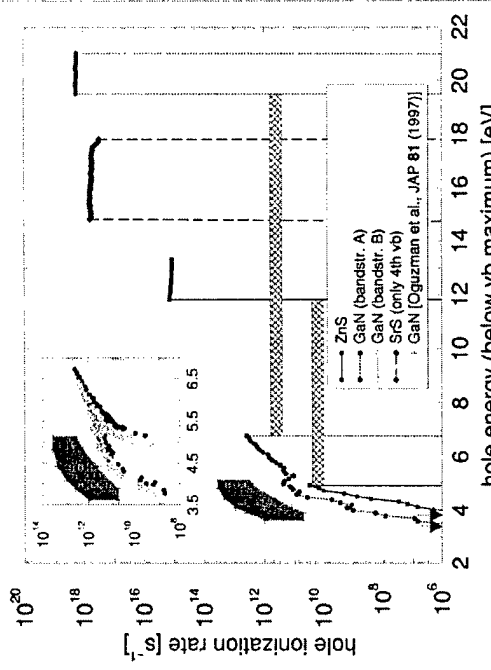
- Band to band impact ionization rate calculated directly from pseudopotential bandstructure (M. Reigrotzki *et al.*, *Phys. Rev. B* **52**, 1456 [1995]).

- Energy dependent scattering rate is fit to  $R(E) = P(E-E_{th})^a$



## Impact Ionization Rate for Holes

Cut-off in hole rate due to finite VB width



## Intercollisional Field Effect in Impact Ionization

- Quade et al. (PRB 50, 7398, 1994) ICFE in parabolic band approximation based on density matrix approach
- Redmer et al (JAP 87, 781, 2000) Extension of Quade et al. to full bandstructure, widebandgap materials using Zubarev nonequilibrium statistical operator approach.

$$\frac{\partial}{\partial t} f_{v,k}(t) + e\vec{E}_0(t) \bullet \frac{\partial}{\partial \mathbf{k}} f_{v,k}(t) = J_e(v, \mathbf{k}, t)$$

- Treating only electron-electron interactions,

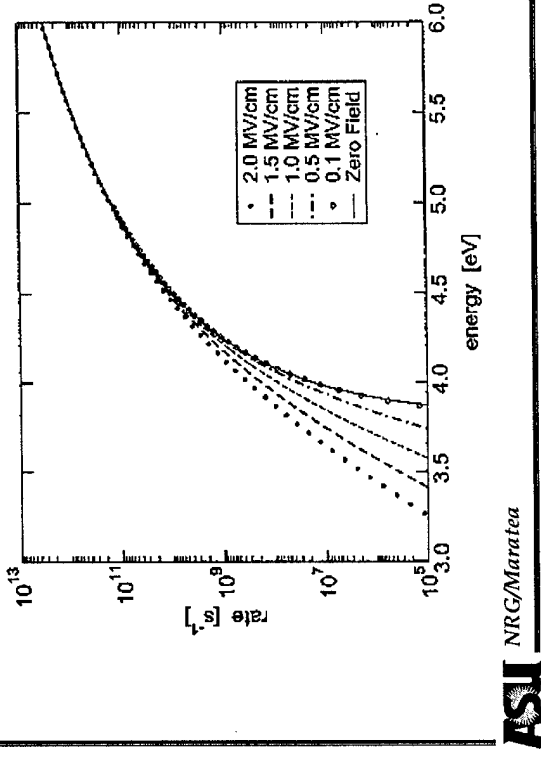
$$r_{ii}(\mathcal{E}_1, E_0) = C \int_0^{\infty} dE \left( \frac{E}{E_h} \right)^a \frac{1}{E_F^{ii}} A i \left( \frac{E_h - \mathcal{E}_1 + E}{E_F^{ii}} \right)$$

$$E_F^{ii} = \left[ \frac{(1+\alpha)(eE_0)^2}{8m_e \hbar} \right]^{1/3}$$

ASU NRG/Maratea

## Intercollisional Field Effect in Impact Ionization

- Softening of threshold field is main effect, little effect at high energy



ASU NRG/Maratea

## Direct Calculation of Electron-Phonon Scattering Rate

### MOTIVATION

- The electron-phonon coupling is the dominant scattering process controlling the high field distribution
- Deformation potential model relies on constants which are not known experimentally for phosphor materials of interest
- A method is required to obtain the electron-phonon coupling directly from the electronic and vibrational properties of the crystal

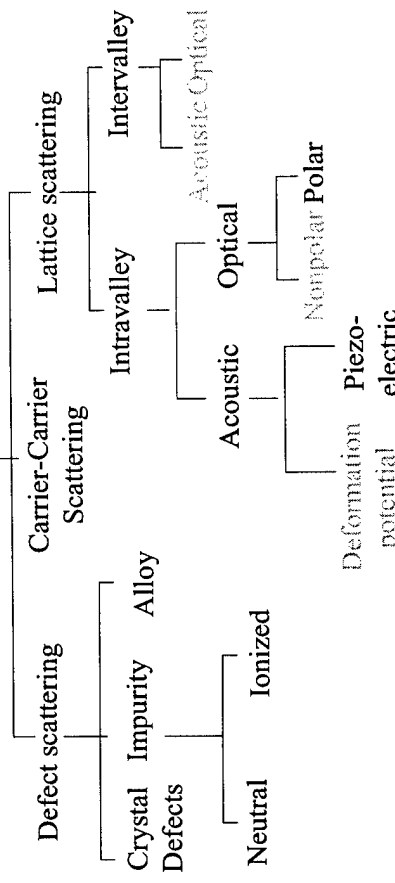
### METHOD

- Rigid-ion model (RIM) used<sup>2</sup> in which the rigid displacement of the atomic pseudo-potential (from EPM calculation) due to lattice vibrations gives the interaction potential



cation anion  
2M. V. Fischetti and J. M. Higman, 1991

## Scattering Mechanisms



ASU NRG/Maratea

## RIM electron-phonon coupling constant that enters into the scattering rate

$$\Delta_j(n\mathbf{k}; n'\mathbf{k}') = -\frac{i}{2}(M_1 + M_2)^{1/2} \times \sum_{GG'} [C_G^n(\mathbf{k})C_{G'}^n(\mathbf{k}')^*(\mathbf{Q} - \mathbf{G} + \mathbf{G}' - \mathbf{G}_u)] \sum_{\alpha} e_{g\alpha}^{\sigma} M_{\alpha}^{-1/2} V_{\alpha}(\mathbf{Q} - \mathbf{G} + \mathbf{G}' - \mathbf{G}_u) \rightarrow \sum_{\alpha} e^{-i(\mathbf{G} + \mathbf{G}' - \mathbf{G}_u) \cdot \mathbf{r}_{\alpha}} \delta_{\mathbf{k}, \mathbf{k}' + \mathbf{Q}, \mathbf{G}_u}$$

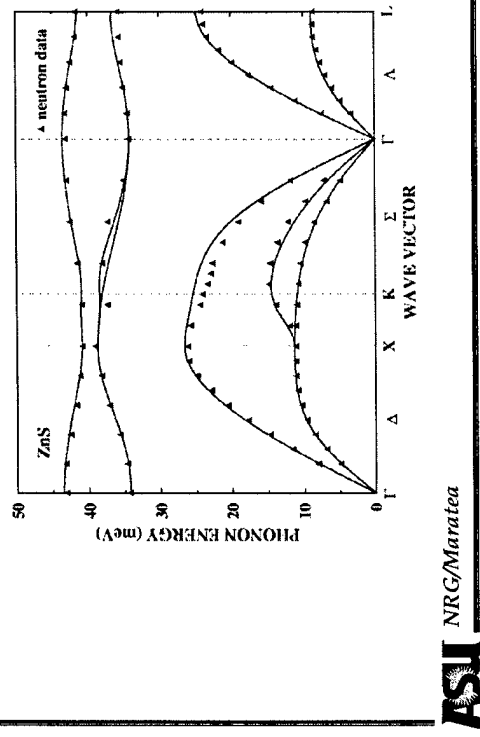
Important complication:  
require the electron potential for  
arbitrary  $\mathbf{q}$  values, not just  
the reciprocal lattice vectors

To calculate this quantity, you need the band structure,  
the pseudo wavefunctions and the phonon dispersion relations

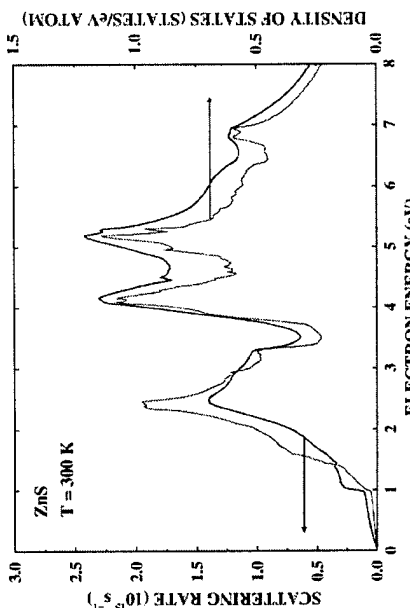
ASU NRG/Maratea

## Phonon Spectrum of ZnS

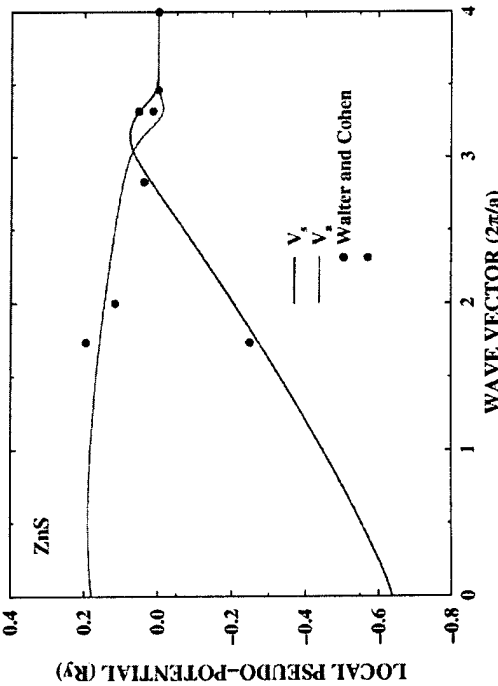
Phonon modes calculated using an empirical valence-shell model for the lattice dynamics with parameters fit to measured phonon dispersion (Vagelatos *et al.*, *J. Phys. Chem.* **60**, 3613 [1974]).



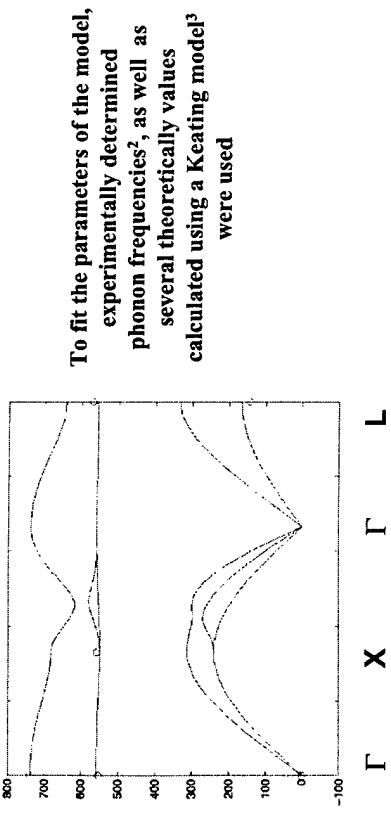
Calculated average electron-phonon scattering rate versus energy for ZnS using the rigid-ion model compared to density of states.



## Interpolation of Local Pseudopotentials for ZnS



## Phonon dispersion for zincblende GaN obtained using a ten parameter empirical Shell model<sup>1</sup>



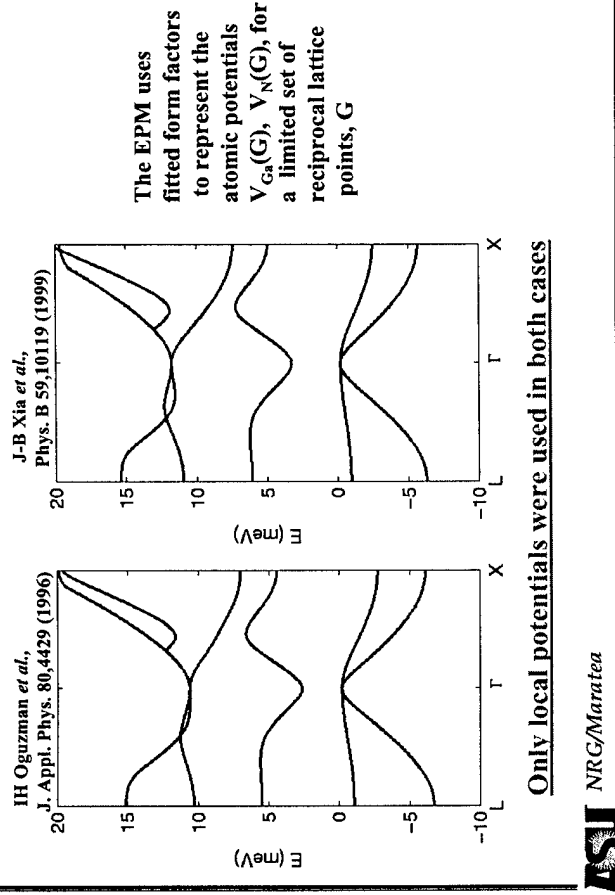
<sup>1</sup> K. Kunc, OH Neilson, Comput. Phys. Comm. 17, 413 (1979)

<sup>2</sup> T. Azuhata *et al.* J. Phys. Condens. Matter 7, L129 (1995)

<sup>3</sup> J. Zi *et al.* J. Phys. Condens. Matter 8, 6323 (1996)

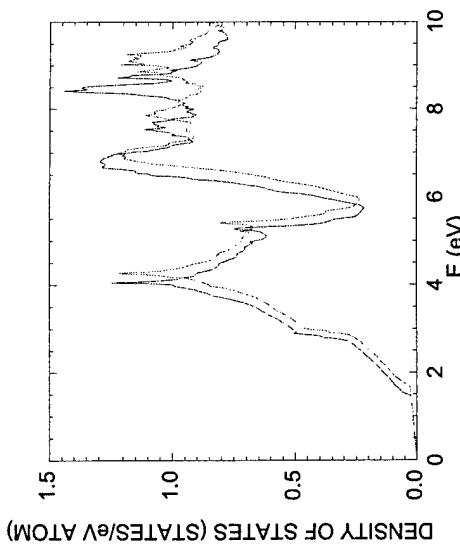
ASU NRG/Maratea

## GaN band structures used based on the Empirical Pseudopotential Method (EPM)



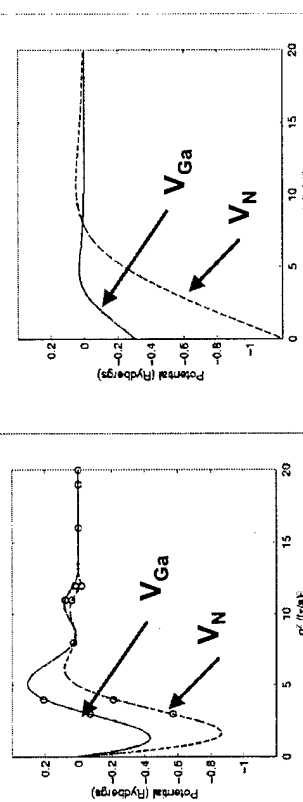
ASU NRG/Maratea

## Density of states for the two cases:



Model 1: use polynomial interpolation to fit the form factors of Oguzman *et al.* (J. Appl. Phys. 80, 4429, 1996) but impose the condition:  
 $V_1(0) = V_1'(0) = 0$

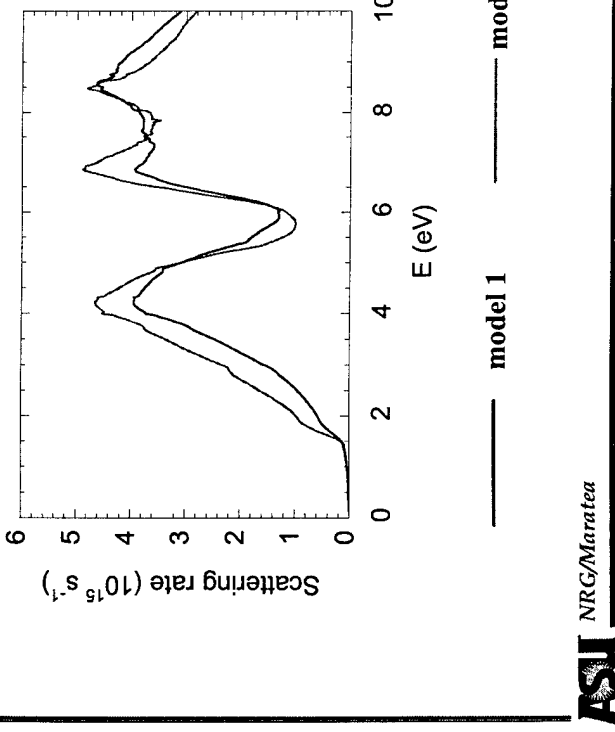
Model 2: Use the same functional form and fits used by Xia *et al.* (Phys. Rev. B 59, 10119, 1999):  
 $V_i(g) = a_i(g^2 - a_2) / [1 + \exp(a_3(g^2 - a_2))]$



Note that model 2 takes on more extreme values near zero  
Circles represent actual factors used by Oguzman *et. al.*

ASU NRG/Maratea

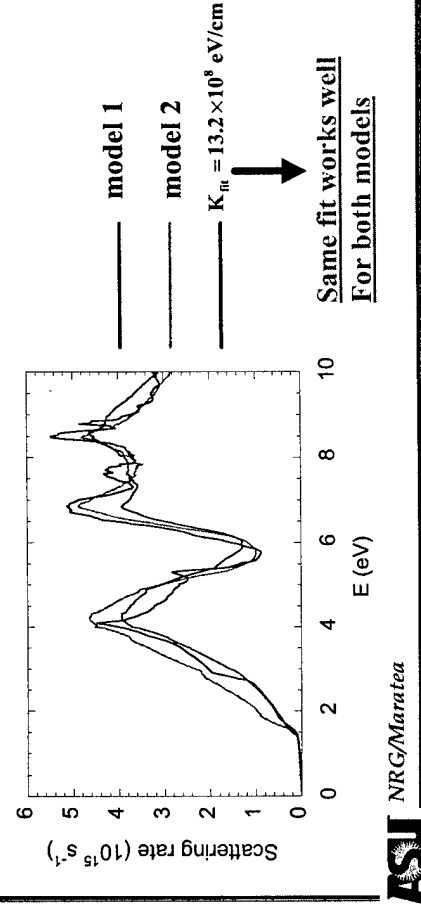
## Phonon scattering rate results for the two models



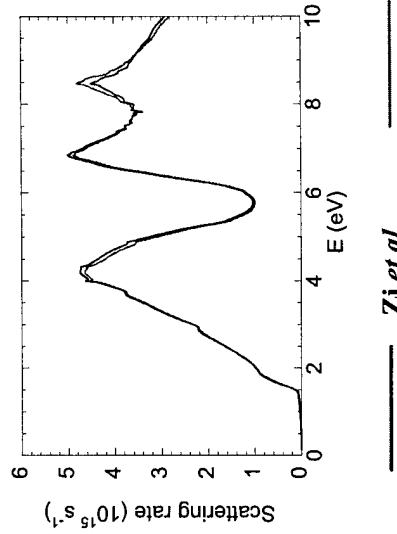
Previous work on ZnS has suggested that the high field scattering rate in wide band gap materials is dominated by optical phonon deformation potential scattering :  
 $R(E) \sim K_{fi}^2 N(E')$

$K_{fi}$  is a fitted deformation potential constant and  $N(E')$  the final density of states

**Comparison between fit and full calculations:**



## Phonon scattering rate results for the two phonon models



using Oguzman *et al.* pseudopotential parameters

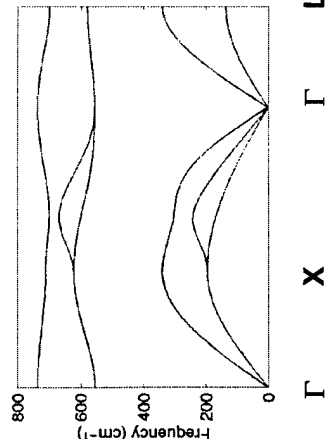
## Second phonon dispersion model for zincblende GaN was also considered

valence shell fit to the data of  
 K. Karch, J.-M. Wagner, and F. Bechstedt, Phys. Rev. B **57**, 7043 (1998)

The data of Karch *et al.* was calculated within the framework of self-consistent density functional perturbation theory.

differences:  
 More dispersion shown TO branches than with the Zi *et al.* fit.

The frequencies attained by the TA branches are significantly lower than for the Zi *et al.* case.

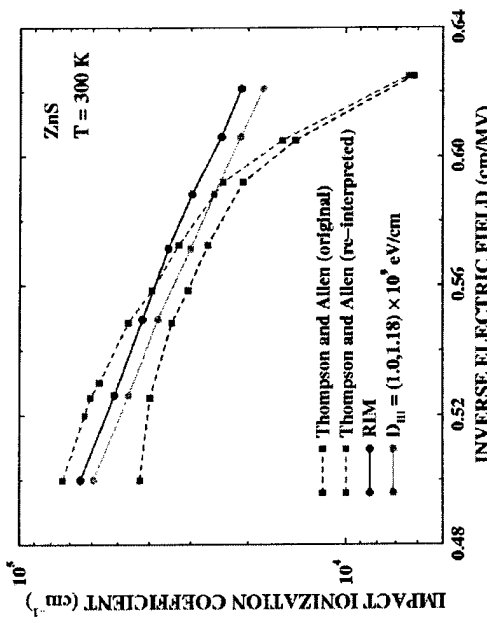


## Full Band Ensemble Monte Carlo Model

- Full band dispersion used for particle dynamics
- Scattering treated a) pseudo isotropic, energy averaged rates from full band model b) full anisotropic rates in CA model
- Deformation potential Ansatz assumed, with values chosen either from fit to experimental data or extracted from RIM calculation
- Polar optical assuming Fröhlich coupling
- Ionized impurity, other elastic mechanisms included for low energies

ASU NRG/Maratea

## Re-Evaluation of Experimental Impact ionization coefficient assuming only electrons



ASU NRG/Maratea

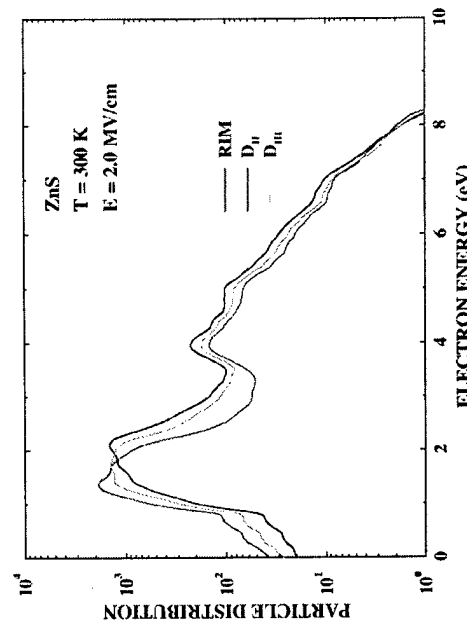
## Impact Ionization Coefficient for Electrons

- Thompson and Allen (J. Phys. C 1989) measured the impact ionization coefficient in ZnS from multiplication measurements on photoinjected carriers in reverse biased Schottky barriers
- They assumed the the e and h impact ionization rates were equal in order to relate multiplication to the ii coefficient
- Assuming the hole ionization rate is negligible, the expression relating carrier multiplication to the ionization coefficient is given by
- Using this relation, we re-evaluated the impact ionization coefficient derived by Thompson and Allen assuming equal electron and hole coefficients

$$\ln M_n = \int_0^W \alpha_n dx = \alpha_n (E_m) W_{eff}$$

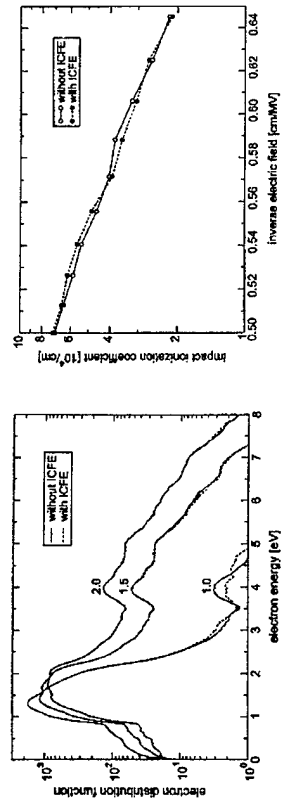
ASU NRG/Maratea

## Comparison of steady-state particle distributions in ZnS at 2 MV/cm and 300 K using rigid-ion model and deformation potential sets $D_{II}$ and $D_{III}$ .



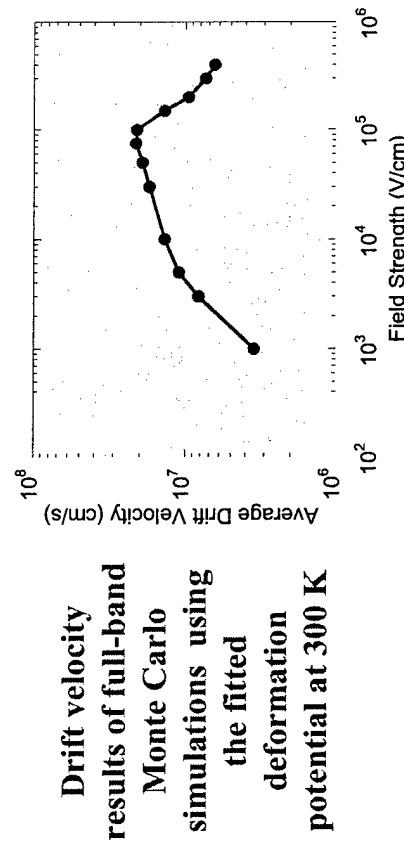
ASU NRG/Maratea

## Effect of ICFE on Distribution Function and Impact Ionization Coefficient



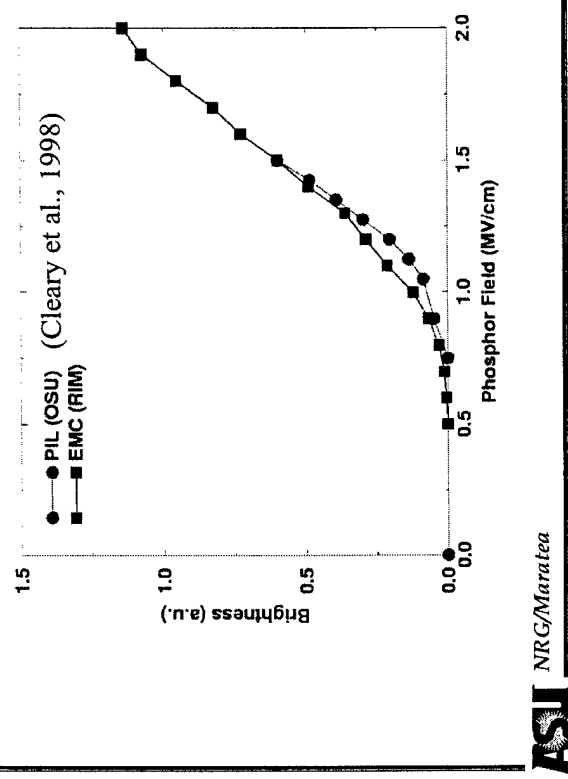
ASU NRG/Maratea

## Calculated Velocity Field Characteristics



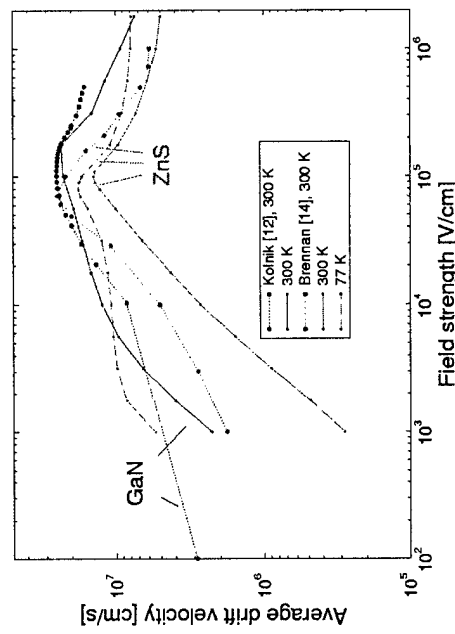
ASU NRG/Maratea

## Calculated Brightness-Field Characteristics for $\text{ZnS:Mn}^{+2}$ assuming zero space charge



ASU NRG/Maratea

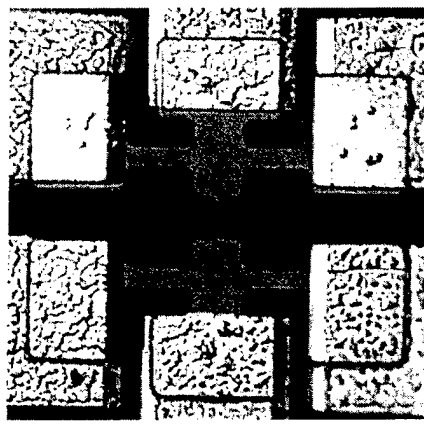
## Average Electron Drift Velocity



ASU NRG/Maratea

## *High Field Transport in GaN: Experimental*

Pulse I-V measurements of velocity field characteristics



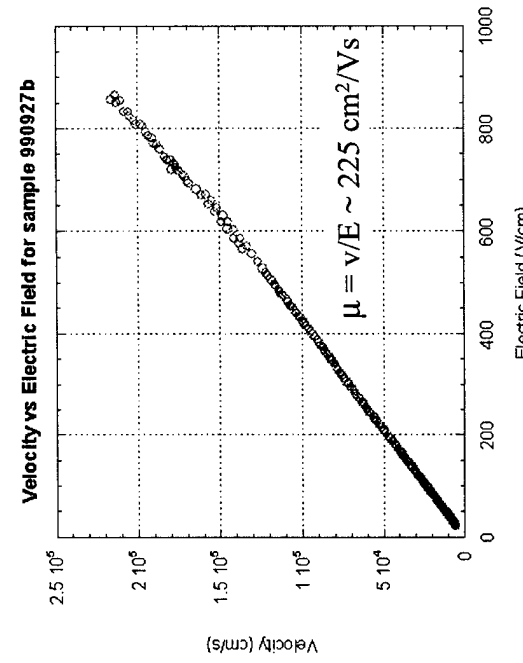
ASU NRG/Maratea

## GaN Test Structure Process Flow

- i) Mesa Etch                          Thick Films    Quantum Wells
  - ICP (Sandia)
  - Photo-chemical etching
- ii. Ti/Al Ohmic Contacts
- iii) Ti/Au Bond Pads

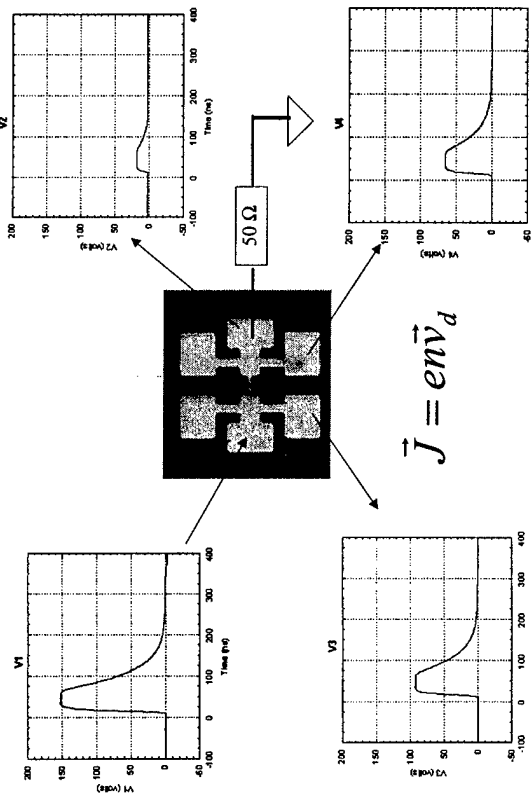
ASU NRG/Maratea

## Results at low electric fields from GaN thick films



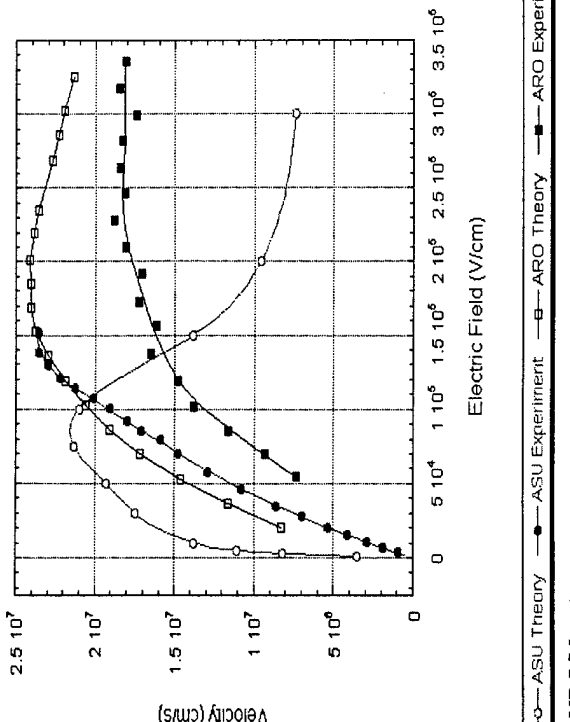
ASU NRG/Maratea

## Pulsed Measurements



ASU NRG/Maratea

## High Field Pulse Measurements in Bulk GaN



ASU  
NRG/Maratea

## Summary

- Ab initio techniques more accurate, but not necessarily better than empirical methods for transport

- Narrow valence band structure for ZnS and SrS implies impact ionization due to holes should be weak process
  - Re-evaluation of Thompson-Allen data, comparable to theory
- No effect of ICFE on impact ionization

## Velocity Field Characteristics

- Deformation potential of  $1.3 \times 10^9$  eV/cm fits RIM calculation well: dominant mechanism above intervalley threshold
- Comparison to experimental measurement by different techniques

ASU  
NRG/Maratea

# Semiclassical modeling of small semiconductor devices

Max Fischetti

IBM Research Division  
T. J. Watson Research Center  
Yorktown Heights, NY 10598

June 2001

## Semiclassical modeling of small semiconductor devices

- Asen Asenov, Glasgow University,  
*Discrete impurities and quantum potentials in MOSFET modeling*
- Richard Akis, Arizona State University,  
*Effective potentials for quantum effects in MOSFETs*

MVF

MVF

June 01 1

## Semiclassical modeling

- Various flavors:
  - Strict: may use the **bulk** (3D) Boltzmann Transport Equation (BTE), à la Kohn-Luttinger (Liouville-von Neumann with infinitely-many randomly-distributed impurities), even if Quantum Mechanics is pervasive (bands, collisions, etc.)
  - Somewhat looser: may use a lower-dimensional BTE (quantum confinement), or any Master equation (dots). No transport 'in the quantized direction'
  - Very loose ('psychologically' classical): Approximate quantum effects so to allow the concept of 'particle' or 'trajectory' (Bohm trajectories, quantum potentials, effective potentials, Wigner paths/trajectories...)
- Anticipated failures:
  - Quantum confinement (strict): channels, wires, dots
  - Tunneling (somewhat looser): band-to-band, across barrier, resonant, ...
  - Interference effects (somewhat looser): Bohm-Aharonov, current oscillations in FN-tunneling and channel current (?!), ...
  - 2D/3D confinement-effects (somewhat-looser/very-loose?): narrow channels in double-gate, point contacts, strongly-coupled dots
  - High-energy, high-field, short-time effects (Somewhat/very loose): Collisional broadening, intracollisional-field, coherent phenomena,..
- Virtues of semiclassical modeling:
  - We have survived so far...
  - 'Intuitive', leading to deeper understanding
  - Simpler (or just...doable?), allowing more accurate description of effects which *may* be dominant in many real-life experiments/devices
  - Determination of 'bulk quantum properties' (band-structures, strain, electron-phonon coupling constants, Auger/impact processes)
  - Collective/many-body effects (Coulomb effects, quantum or MD)

## Dopant fluctuations

- Important (threshold control a crucial element in VLSI)...
- but complicated:
  - BTE suspect
  - Scatterers closer than mean-free-path:
    - \* no rigorous use of mobility possible
    - \* multiple-scattering, interference, non phase-breaking
  - What's the scattering potential?
- So far limited to drift-diffusion and to electrostatics (probably good enough)

## **Quantum/effective potentials**

- From Wigner or Bohm
- 'Psychologically easy', mathematically hard
- So far approximated (equilibrium) or of a heuristic nature
- Of high appeal because of their 'intuitive' nature

## Session 4

### The Metal-Insulator Transition

- Moderator: Chihiro Hamaguchi, Osaka University

- 4A: Guenther Bauer, University of Linz,  
“The metal-insulator transition in d=2”
- 4B: Jonathan Bird, Arizona State University,  
“The metal-insulator transition in open  
quantum dots and arrays”

### Metal-insulator transition in two dimensions

Guenther Bauer, University of Linz

- No metallic state in two dimensions in  $B = 0$  (Abrahams et al. in 1979: Scaling theory).
- With decreasing temperature the resistance should rise logarithmically (weak localization) or even exponentially (strong localization) with  $R \rightarrow \infty$  for  $T \rightarrow 0$ .
- In the limit of weak localization  $R$  should grow logarithmically for  $T \rightarrow 0$ .
- For strong interactions it should end up as a Wigner crystal (or pinned Wigner crystal).
- Therefore, neither in the limit of weak nor in the limit of strong interactions, 2D systems should conduct for  $T \rightarrow 0$ .
- Early experiments confirmed these predictions.
- However, experiments with very clean high mobility samples contradict it.
  - A non zero conductivity was found.
  - Evidence for a metal-insulator transition
- A critical density was found:
  - Below the system is insulating
  - Above the system shows metallic behaviors
- Many explanations were put forward
  - Si-MOS
  - Experiments: weak localization  
 $\rightarrow$  onset of metal-insulator transition: classical effect (screening, ionized impurity scattering...)

## The metal-insulator transition in open

### quantum dots and arrays

Jonathan Bird, Arizona State University

- Much recent interest in the observation of a Kondo effect in Coulomb blockaded quantum dots.
- In open quantum dots the Coulomb blockade is suppressed.
- Transport is found to be mediated by strongly scarred wavefunction states.
- The scars correspond to quasi-bound resonant states of the open system which are characterized by long trapping times at specific energies.

- The quasi-bound nature is expected to give rise to novel signatures in transport due to electron interactions.
- The behavior of the quasi-bound states will be explored in this presentation.

# Intrinsic Fluctuations and Quantum Potentials in MOSFET Modelling

"The tyranny of the large numbers"  
G. Timp

A. R. Brown, S. Kaya, J. Watling, J. H. Davies, G. Slavcheva  
Department of Electronics and Electrical Engineering  
University of Glasgow

Sponsored by SHEFC

Quantum Transport in Semiconductors

© A. Asenov 2001



## Summary

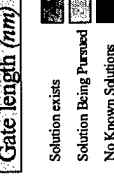
- Introduction
- Quantum corrections
- Random Dopant Fluctuations
- Oxide Thickness Fluctuations
- Conclusions

## Scaling of MOSFETs to decanano dimensions

(International Roadmap for Semiconductors - 1999 Edition)

Year	1999	2001	2004	2008	2011	2014
MPU Gate Length (nm)	0.40	0.00	70			
Oxide thickness (nm)	1.025	5.19	12-1.5			
Drain extensions (nm)	2.0	30-50				

Year	1998	2000	2003	2005	2007	2009
Technology node (nm)	0.25	0.10	0.07	0.05	0.03	0.02
Gate length (nm)	0.25	0.10	0.07	0.05	0.03	0.02



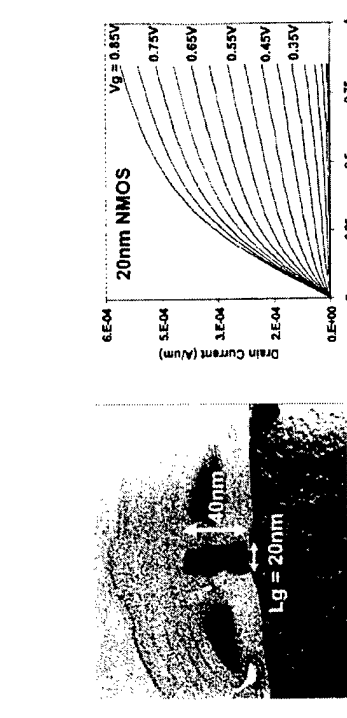
© A. Asenov 2001

Quantum Transport in Semiconductors  
Maratea, June 2001

© A. Asenov 2001

Quantum Transport in Semiconductors  
Maratea, June 2001

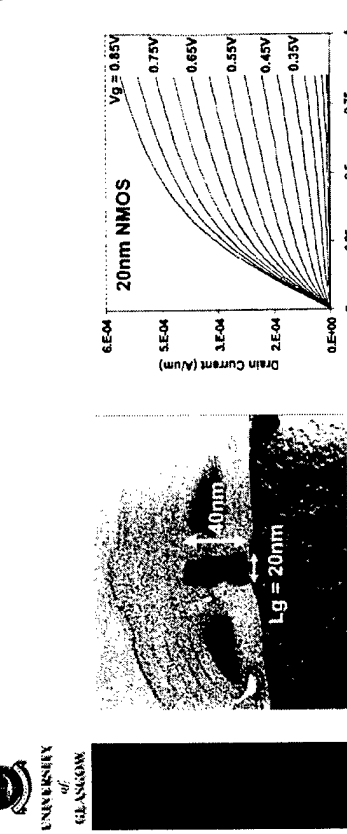
## Conventional MOSFET with 20 nm gate length



Robert Chow  
Si Nanoel, Workshop 01

Quantum Transport in Semiconductors  
Maratea, June 2001

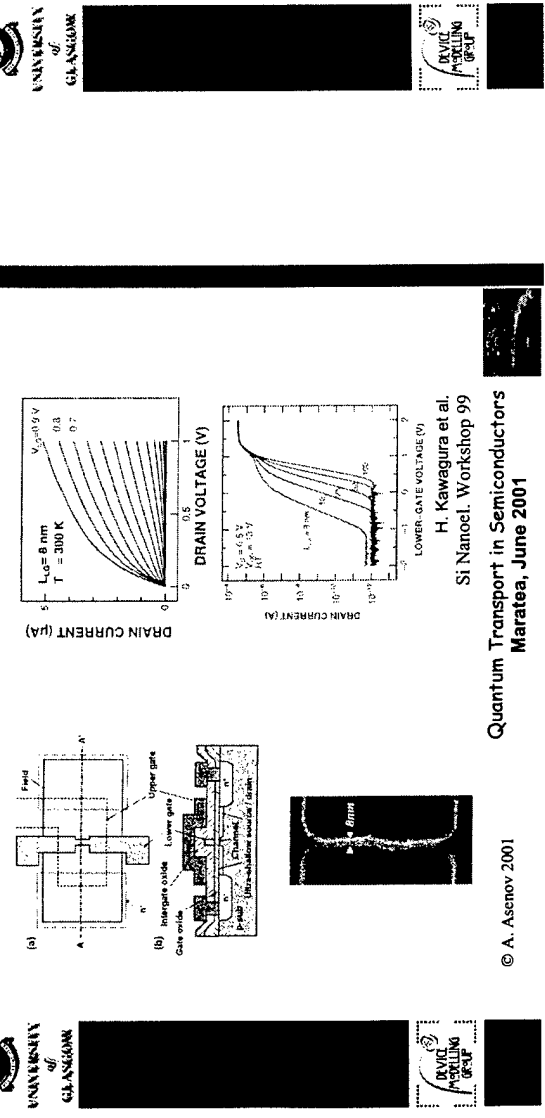
## Si-1D tunneling



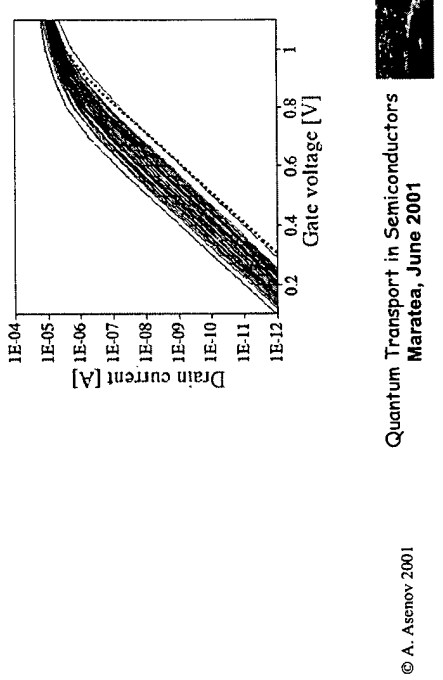
Robert Chow  
Si Nanoel, Workshop 01

Quantum Transport in Semiconductors  
Maratea, June 2001

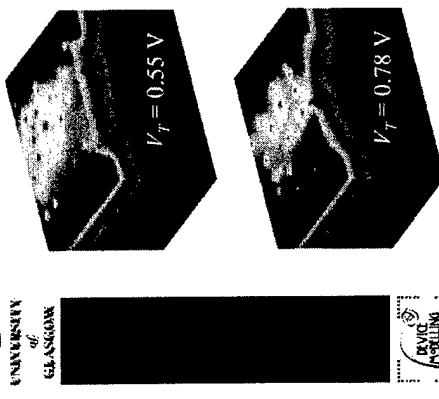
## Double gate MOSFET with 8 nm gate length



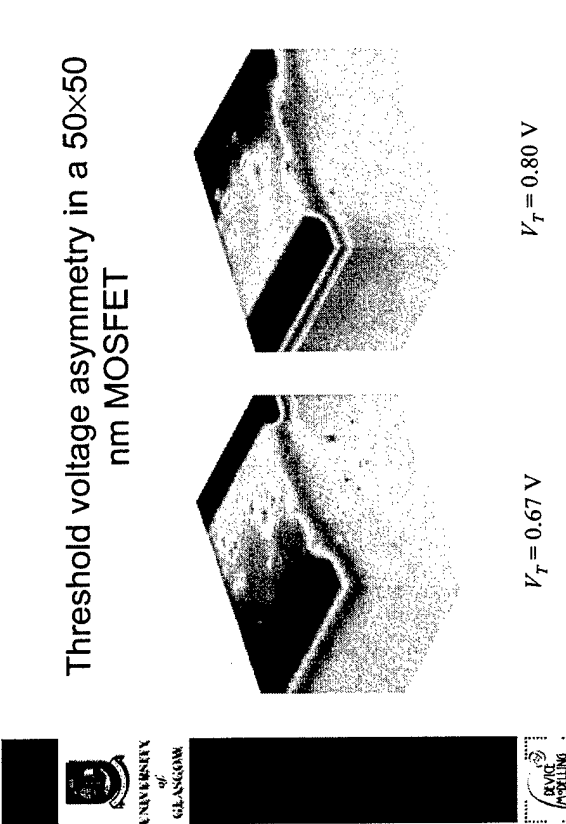
## Random Dopants Fluctuations (RDF)



## Numbers and position fluctuations



## Threshold voltage asymmetry in a 50x50 nm MOSFET



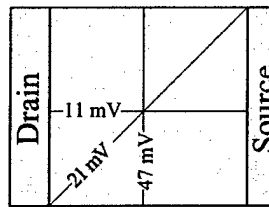
## Quantum Transport in Semiconductors Maratea, June 2001

## Quantum Transport in Semiconductors Maratea, June 2001

## The poly-Si gate (A 50x50 nm MOSFET)



UNIVERSITY  
of  
GLASGOW



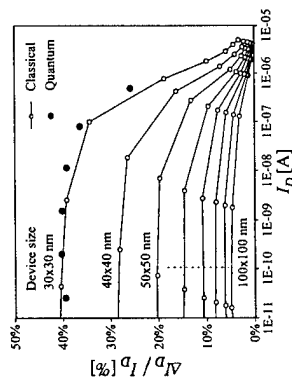
Source  
boundaries

Quantum Transport in Semiconductors  
Maratea, June 2001

© A. Asenov 2001



DEVICE  
MANUFACTURING

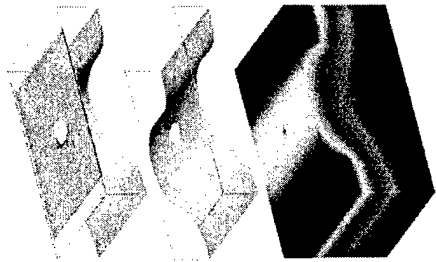


Quantum Transport in Semiconductors  
Maratea, June 2001

© A. Asenov 2001



DEVICE  
MANUFACTURING



## Single charge trapping



UNIVERSITY  
of  
GLASGOW

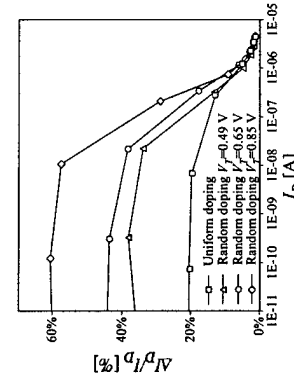


DEVICE  
MANUFACTURING

## Single charge trapping (A 50x50 nm MOSFET with discrete dopants)



DEVICE  
MANUFACTURING



Quantum Transport in Semiconductors  
Maratea, June 2001

© A. Asenov 2001



Quantum Transport in Semiconductors  
Maratea, June 2001

© A. Asenov 2001

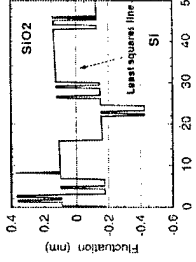
## Oxide Thickness Fluctuations (OTF)



UNIVERSITY  
of  
GLASGOW



DEVICE  
MANUFACTURING



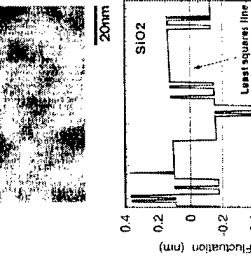
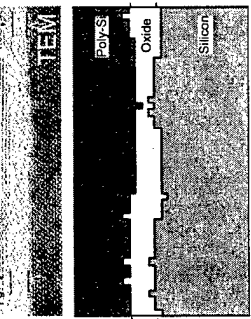
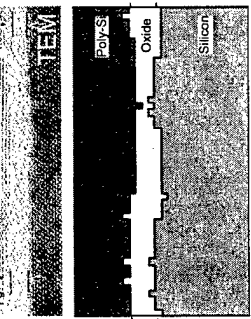
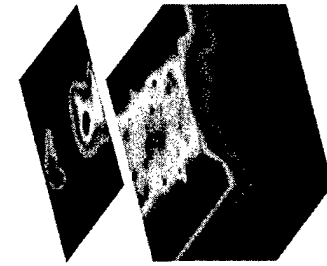
Quantum Transport in Semiconductors  
Maratea, June 2001

© A. Asenov 2001



Quantum Transport in Semiconductors  
Maratea, June 2001

© A. Asenov 2001



Quantum Transport in Semiconductors  
Maratea, June 2001

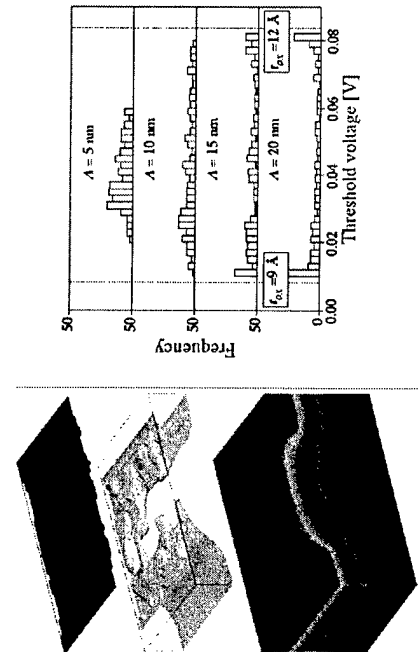
© A. Asenov 2001



Quantum Transport in Semiconductors  
Maratea, June 2001

© A. Asenov 2001

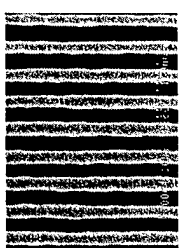
## OTF induced MOSFET parameter fluctuations (A 30x30 nm MOSFET)



## Line edge roughness (LER)



Sandia Labs – EUV



Glasgow – E-beam



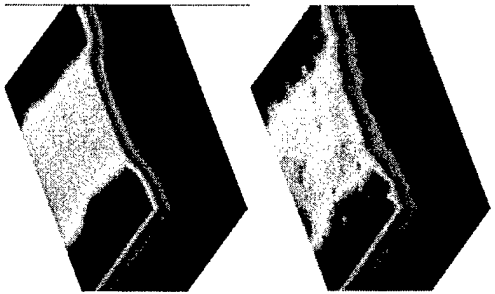
ASPFrisch  
IBM (EUV)  
SANDIA (EUV)  
SANDIA (EUV)  
NIST (ebeam)  
NIST (ebeam)

## Summary

- Introduction
- Quantum corrections
- Random Dopant Fluctuations
- Oxide Thickness Fluctuations
- Conclusions



## Line edge roughness (LER)



© A. Asenov 2001

Quantum Transport in Semiconductors Maratea, June 2001

## Solution domain in 3D 'atomistic' simulation



- 3D DD simulations + quantum corrections
- Fine grain discretisation
- Statistical ensembles of microscopically different devices
- Estimation of averages and standard deviations

50x50 nm MOSFET



© A. Asenov 2001      Quantum Transport in Semiconductors  
Maratea, June 2001

## The Density Gradient (DG) approach (C.S. Rafferty et al., SISPAD'98)

DG introduces QM corrections by introducing an extra term into carrier flux expression

$$F_n = n\mu_n \nabla \psi - D_n \nabla n + 2\mu \nabla \left( b_n \frac{\nabla^2 \sqrt{n}}{\sqrt{n}} \right)$$

where

$$b_n = \hbar / (12qm_n^*)$$

Generalised quasi-Fermi potential

$$F_n = n\mu_n \nabla \phi_n$$

Quantum Transport in Semiconductors

© A. Asenov 2001

Maratea, June 2001

## DD with DG corrections for unipolar device (C.S. Rafferty et al., SISPAD'98)

The system

$$\nabla \cdot (\epsilon \nabla \psi) = -q(p - n + N_D^+ - N_A^-)$$

$$\nabla \cdot (n\mu_n \nabla \phi_n) = 0$$

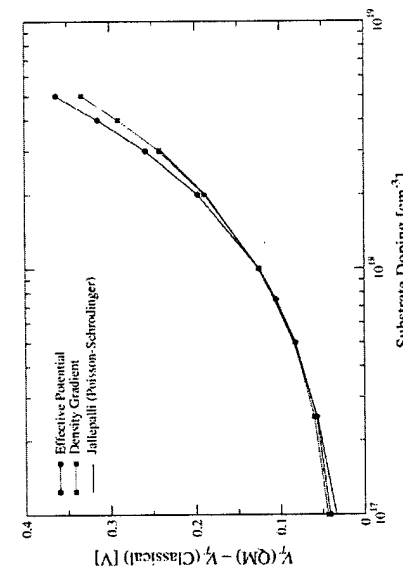
$$2b_n \frac{\nabla^2 \sqrt{n}}{\sqrt{n}} = \phi_n - \psi + \frac{kT}{q} \ln \frac{n}{n_i}$$

The variables

$$\psi, \phi_n, \sqrt{n}$$

Quantum Transport in Semiconductors  
Maratea, June 2001

Quantum Transport in Semiconductors  
Maratea, June 2001



## Quantum mechanical threshold voltage shift



Quantum Transport in Semiconductors  
Maratea, June 2001

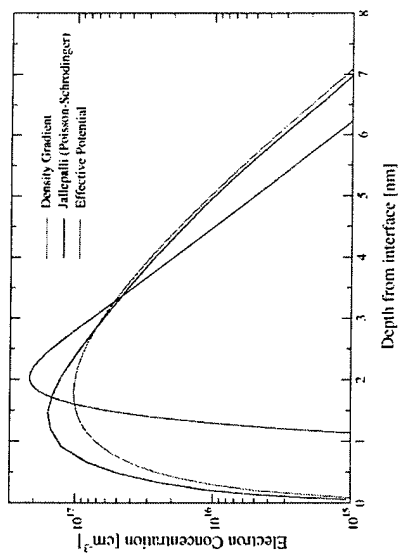


Quantum Transport in Semiconductors

© A. Asenov 2001

Maratea, June 2001

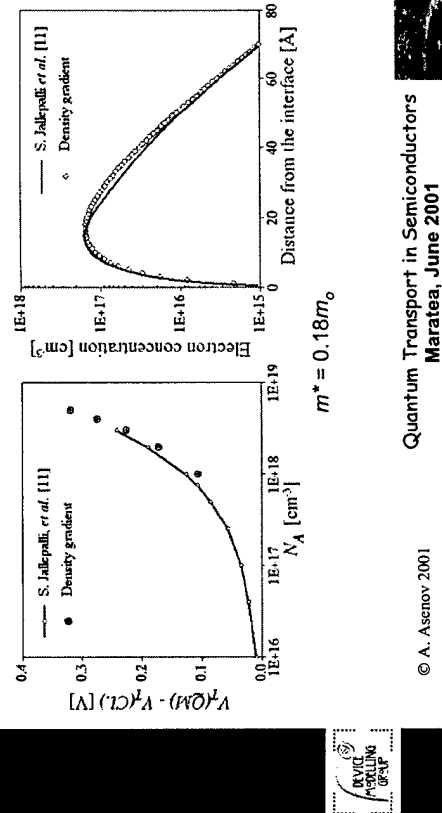
## Quantum mechanical charge distribution



Quantum Transport in Semiconductors  
Maratea, June 2001

© A. Asenov 2001

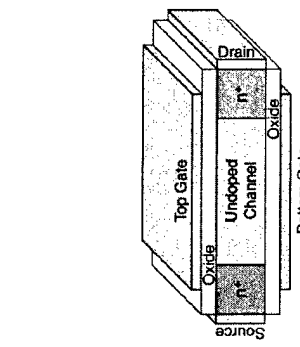
## $m^*$ is a fitting parameter



Quantum Transport in Semiconductors  
Maratea, June 2001

© A. Asenov 2001

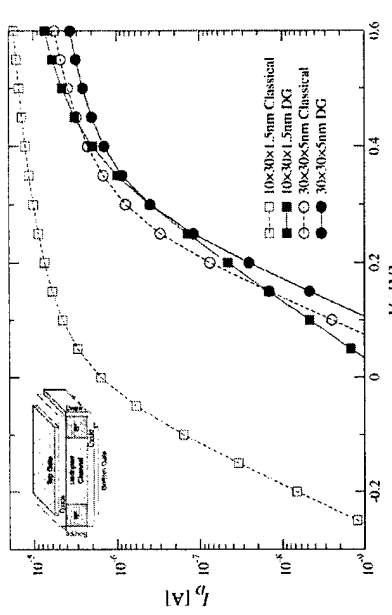
## Double gate MOSFET



Quantum Transport in Semiconductors  
Maratea, June 2001

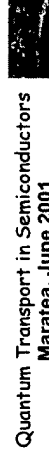
© A. Asenov 2001

## Source-to-drain tunnelling

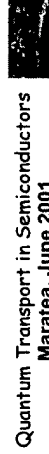


Quantum Transport in Semiconductors  
Maratea, June 2001

© A. Asenov 2001



© A. Asenov 2001



© A. Asenov 2001



## Summary

- Introduction
- Quantum corrections
- Random Dopant Fluctuations
- Oxide Thickness Fluctuations
- Conclusions



© A. Asenov 2001

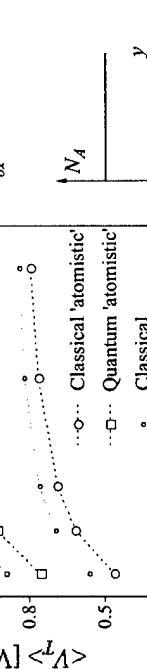
Quantum Transport in Semiconductors  
Maratea, June 2001



© A. Asenov 2001

Electron equiconcentration distribution  
(A 50x50 nm MOSFET)

QuickTime™ and a  
decompression  
are needed to see this picture.

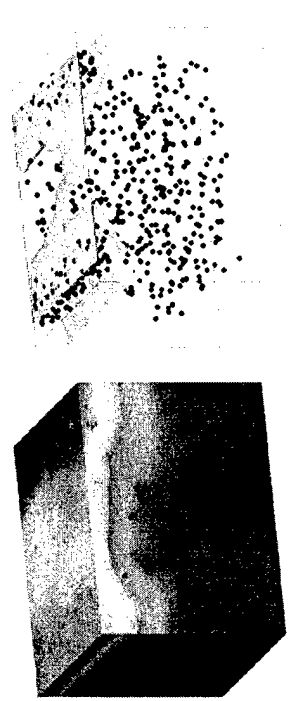


Quantum Transport in Semiconductors  
Maratea, June 2001

© A. Asenov 2001



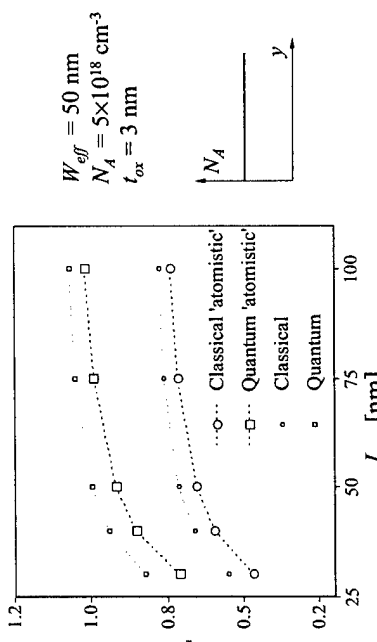
Potential and electron distribution  
(A 50x50 nm MOSFET)



Quantum Transport in Semiconductors  
Maratea, June 2001

© A. Asenov 2001

Threshold voltage as a function of the gate length

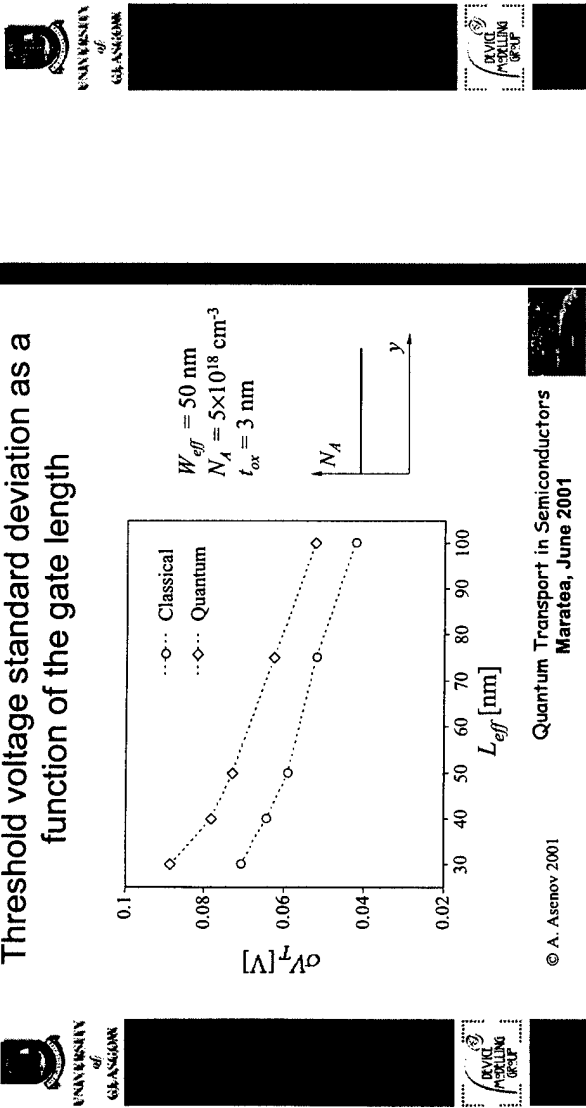


Quantum Transport in Semiconductors  
Maratea, June 2001

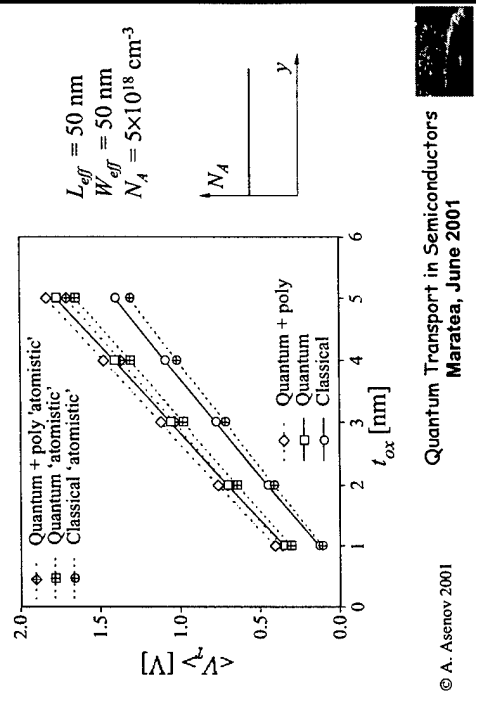
© A. Asenov 2001



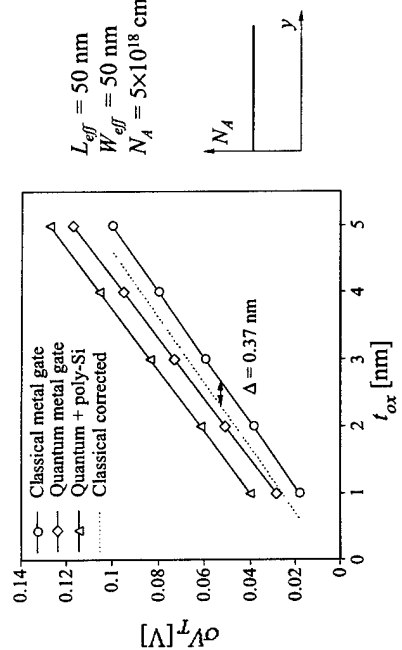
## Threshold voltage standard deviation as a function of the gate length



## Threshold voltage as a function of the oxide thickness



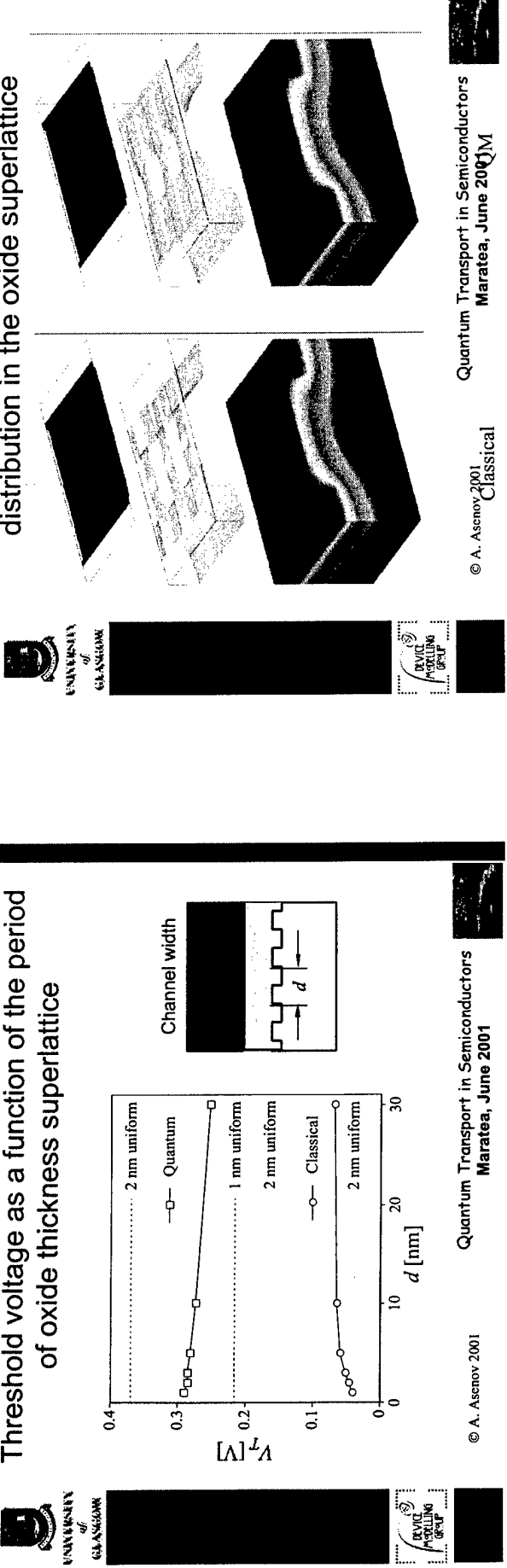
## Threshold voltage standard deviation as a function of the oxide thickness



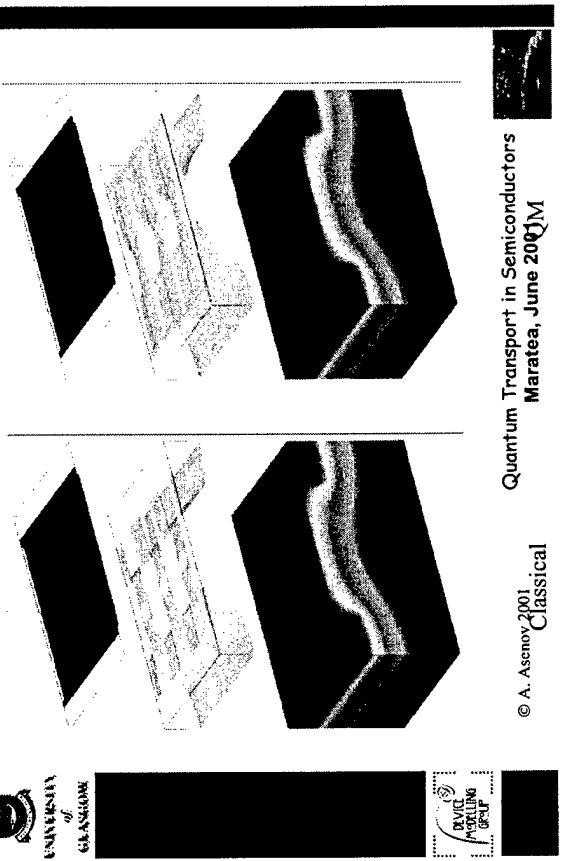
## Summary

- Introduction
- Quantum corrections
- Random Dopant Fluctuations
- Oxide Thickness Fluctuations
- Conclusions

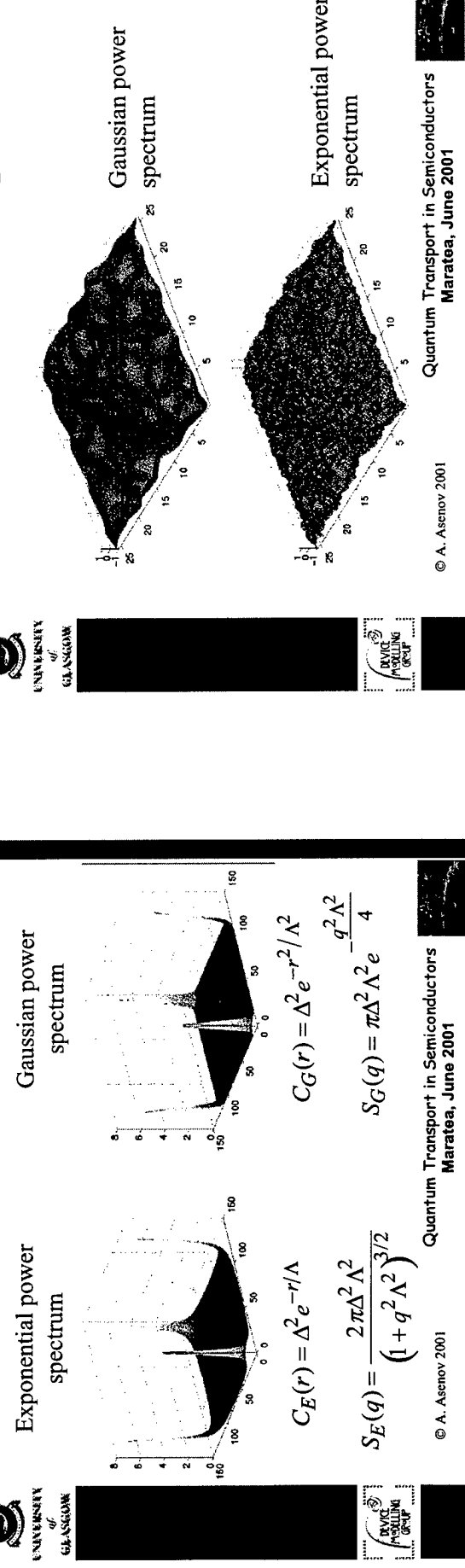
## Threshold voltage as a function of the period of oxide thickness superlattice



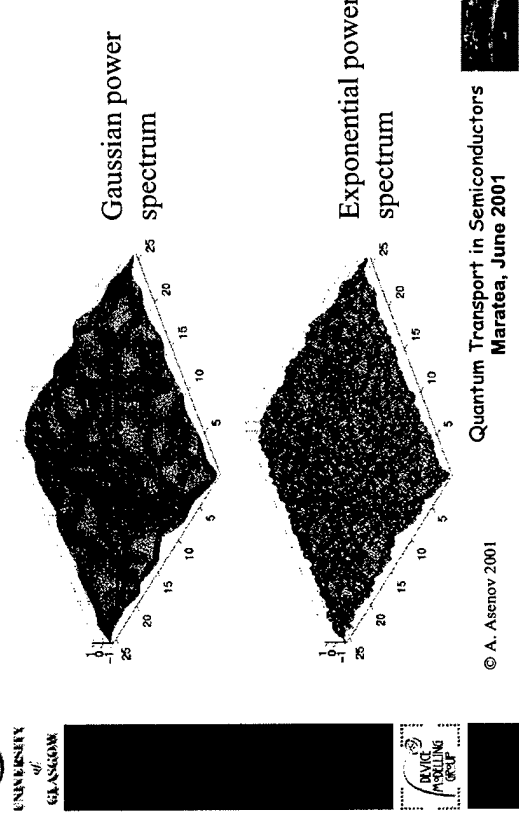
## Classical and quantum mechanical charge distribution in the oxide superlattice



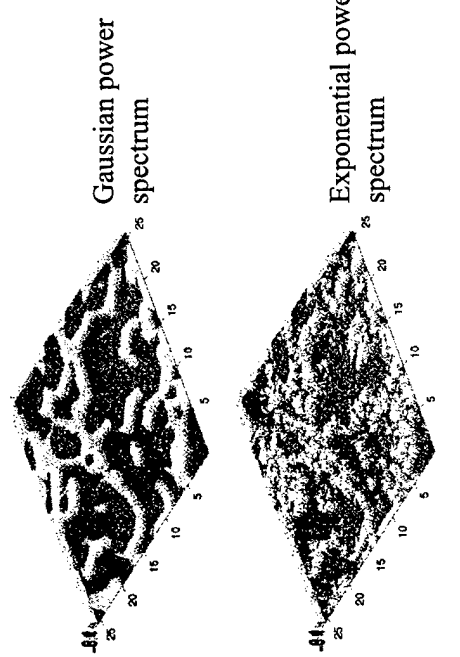
## Reconstruction of the Si/SiO<sub>2</sub> interface



## Reconstruction of the Si/SiO<sub>2</sub> interface



## Digitisation of the Si/SiO<sub>2</sub> interface

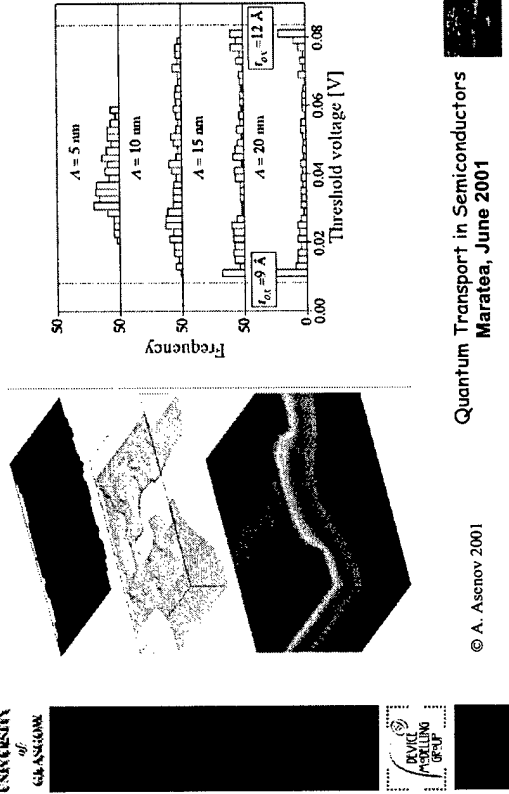


Quantum Transport in Semiconductors  
Maratea, June 2001

© A. Asenov 2001

Quantum Transport in Semiconductors  
Maratea, June 2001

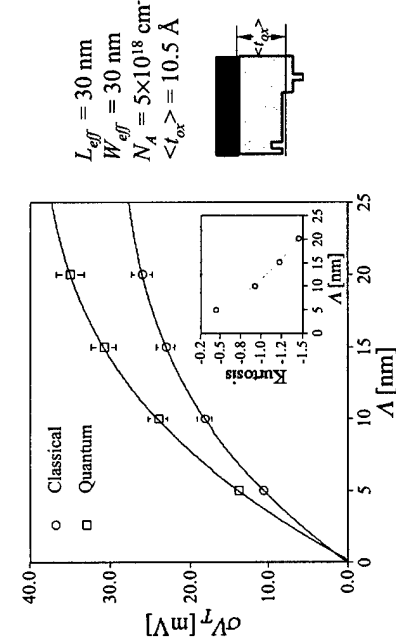
## OTF induced MOSFET parameter fluctuations (A 30x30 nm MOSFET)



Quantum Transport in Semiconductors  
Maratea, June 2001

Quantum Transport in Semiconductors  
Maratea, June 2001

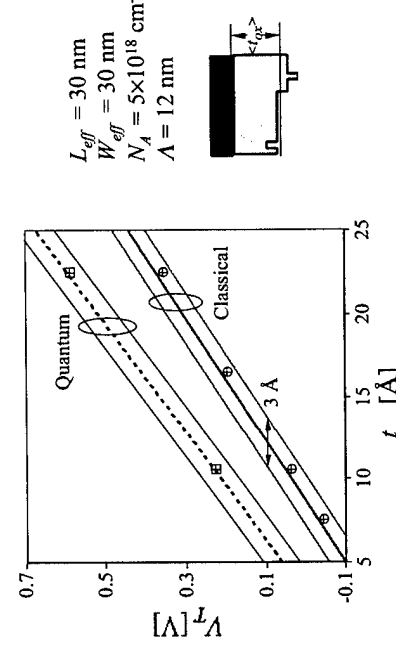
## Threshold voltage standard deviation as a function of the correlation length



Quantum Transport in Semiconductors  
Maratea, June 2001

Quantum Transport in Semiconductors  
Maratea, June 2001

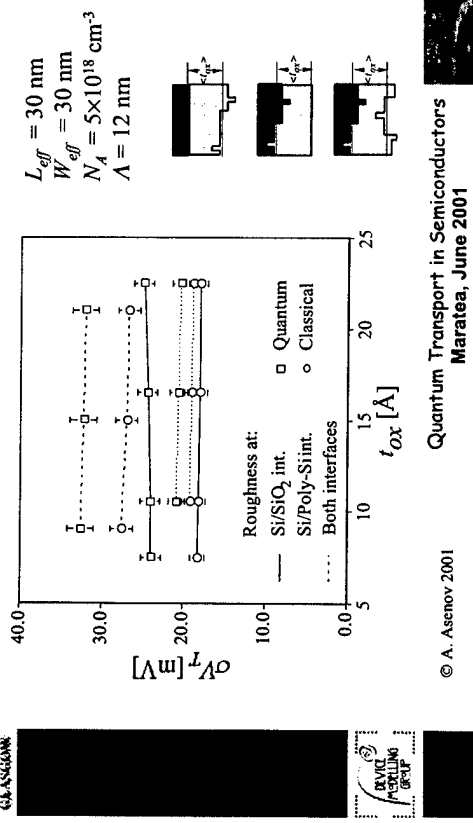
## Threshold voltage as a function of the average oxide thickness



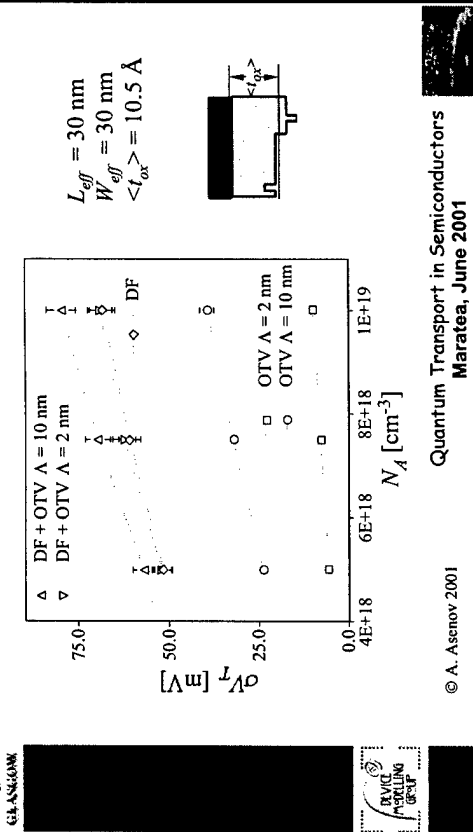
Quantum Transport in Semiconductors  
Maratea, June 2001

Quantum Transport in Semiconductors  
Maratea, June 2001

## Threshold voltage standard deviation as a function of the oxide thickness



## Threshold voltage standard deviation as a function of the doping concentration



## Conclusions

- The DG approach provides relatively simple means to include quantum correction in the 3D DD 'atomistic' MOSFET simulation.
- The inclusion of the QM corrections increases the intrinsic parameter fluctuations associated with discrete random dopants and oxide thickness variation.

Quantum Transport in Semiconductors  
Maratea, June 2001

© A. Asenov 2001



## ***Effective Potentials for Quantum Effects in MOSFETs***

**Dr. Richard Akis**

Department of Electrical Engineering  
Arizona State University

**Who else is to blame:**

L. Shifren  
S. Ramey  
S. N. Milicic  
D. Vasileska  
and, in particular  
D. K. Ferry



Work supported by ONR, NSE, and SRC

## **Outline**

**Introduction**  
**the effective potential- what is it and why should you care**

**Including the effective potential in device simulations**  
**1D simulation of a MOSFET channel**  
**2D simulation of a "standard" MOSFET**  
**simulation of SOI devices**  
**simulation of a quantum point contact**

## **Conclusions**

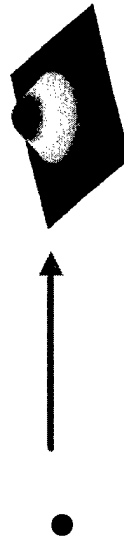
**ASU** Nanostructures Research Group  
CENTER FOR SOLID STATE ELECTRONICS RESEARCH

## **A Major Concern for Future ICs**

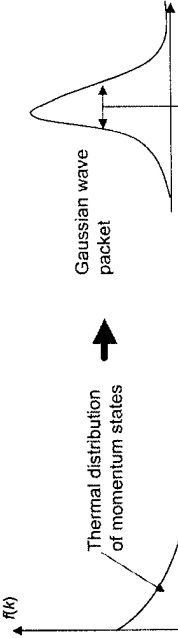
While current production devices are only at 0.18  $\mu\text{m}$ , predictions are that they will be at 50 nm by year 2012. At these sizes, we should begin to see

**quantum effects**, as  $\lambda_D \sim 3-5$  nm at 300 K. The questions are:

- ① In quantum mechanics, electrons no longer behave as point particles. How "large" is the electron wave packet?
- ② How can we include space quantization effects efficiently into what are otherwise classical device simulators?



**The smallest size will be determined by the effective size of the electron wave packet.**

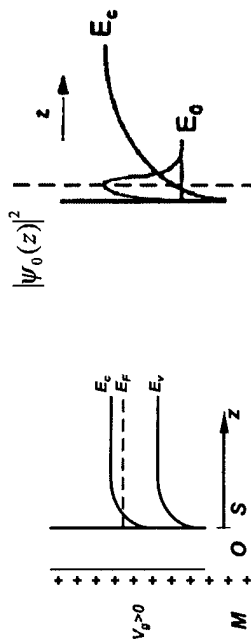


$$\psi(r) = \frac{\pi}{(\sqrt{2}\lambda_D)^{3/2}} \exp\left(-\frac{\pi r^2}{\lambda_D^2}\right)$$

**ASU** Nanostructures Research Group  
CENTER FOR SOLID STATE ELECTRONICS RESEARCH

## MOSFET conduction band profile along the growth direction

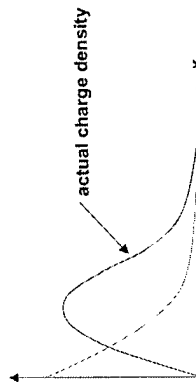
inversion layer formed → creation of 1D subbands  
carriers at interface trapped in that leads to charge set back  
a triangular well



**ASU** Nanostructures Research Group  
CENTER FOR SOLID STATE ELECTRONICS RESEARCH

## Quantization in the Channel of the MOSFET

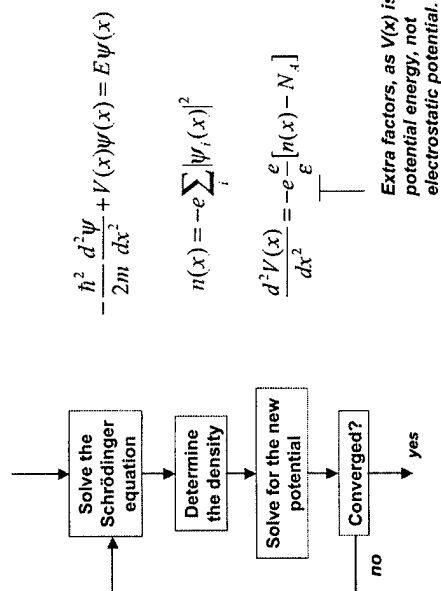
The electrons in the inversion layer are quantized—their motion normal to the interface is quantized by the potential well between the oxide and the conduction band. The actual width of the inversion layer is found from the Schrödinger equation.



$$n_s = \frac{m k_B T}{\pi \hbar^2} \ln \left[ 1 + \exp \left( \frac{E_F - E_0}{k_B T} \right) \right]$$

**ASU** Nanostructures Research Group  
CENTER FOR SOLID STATE ELECTRONICS RESEARCH

## Quantum method of finding the wave functions and energy levels



$$\begin{aligned} -\frac{\hbar^2}{2m} \frac{d^2\psi}{dx^2} + V(x)\psi(x) &= E\psi(x) \\ n(x) &= -e \sum_i |\psi_i(x)|^2 \\ \frac{d^2V(x)}{dx^2} &= -e \frac{c}{\epsilon} [n(x) - N_A] \end{aligned}$$

**ASU** Nanostructures Research Group  
CENTER FOR SOLID STATE ELECTRONICS RESEARCH

✓ The concept of the effective potential was introduced by Feynman, and has been extended by several authors.

Classically, we use  $e^{-\beta V}$ ; thus, the idea of the effective potential is to seek a modified potential  $V_{eff}$  by which we can write the density as

$$n = n_0 e^{-\beta V_{eff}}$$

→ Sharp potentials no longer appear in the problem. Rather, these are “smoothed” by a Gaussian function, here derived from the effective minimal size of the electron wave packet in the system under study.

By replacing the sharp potentials by smoothed potentials, we can return to using quasi-classical point charges in our simulations, confident that the results will be quite appropriate.

$$V_{eff}(x) = \frac{1}{\sqrt{2\pi a_0}} \int_{-\infty}^{\infty} V(x') \exp \left( -\frac{(x - x')^2}{2a_0^2} \right) dx'$$

**ASU** Nanostructures Research Group  
CENTER FOR SOLID STATE ELECTRONICS RESEARCH

## Effective Potential Approach

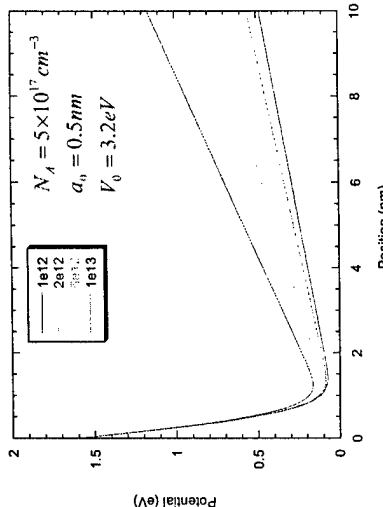
In principle, the effective role of the potential can be rewritten in terms of the non-local density as (Ferry et al.):

$$\begin{aligned} \bar{V} &= \int d\mathbf{r}' V(\mathbf{r}') \sum_i n_i(\mathbf{r}') \\ &\sim \sum_i \int d\mathbf{r}' \delta(\mathbf{r} - \mathbf{r}') \int d\mathbf{r} V(\mathbf{r}') \exp\left(-\frac{|\mathbf{r} - \mathbf{r}'|^2}{\alpha^2}\right) \delta(\mathbf{r} - \mathbf{r}') \\ &\sim \sum_i \int d\mathbf{r}' \delta(\mathbf{r} - \mathbf{r}') V_{eff}(\mathbf{r}') \\ &\sim \text{Smoothed, effective potential} \end{aligned}$$

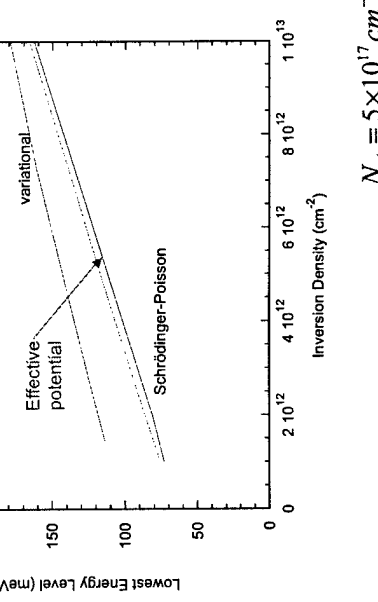
<sup>1</sup> D. K. Ferry, *Superlatt. Microstruc.* 27, 59 (2000); VLSI Design, in press.

## Use of the Effective Potential

$$V_{eff}(x) = \frac{V_0}{2} \left[ 1 - \operatorname{erf}\left(\frac{x}{\sqrt{2}a_0}\right) \right] + \frac{Fx}{2} \left[ 1 + \operatorname{erf}\left(\frac{x}{\sqrt{2}a_0}\right) \right] + \frac{Fa_0}{\sqrt{2\pi}} \exp\left(-\frac{x^2}{2a_0^2}\right)$$



## Use of the Effective Potential



## Use of the Effective Potential

Built-in potential for triangular potential approximation.

Effective potential approximation

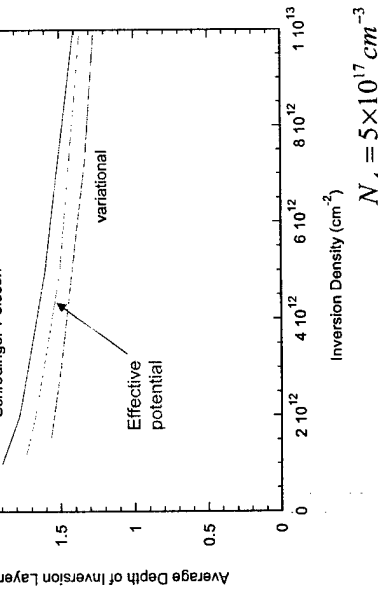
Quantization energy

"Set back" of charge quantum capacitance effects

Classical density

<sup>1</sup> D. K. Ferry, *Superlatt. Microstruc.* 27, 59 (2000); VLSI Design, in press.

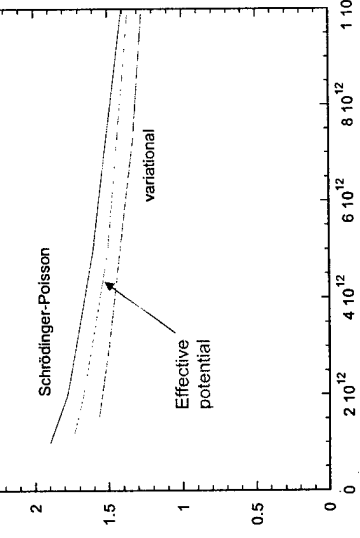
## Use of the Effective Potential



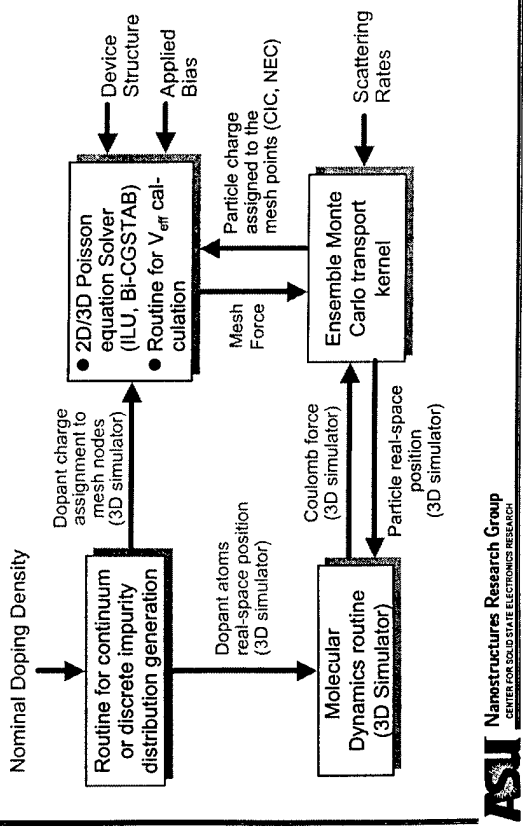
## Use of the Effective Potential

$$N_A = 5 \times 10^{17} \text{ cm}^{-3}$$

variational  
Effective potential

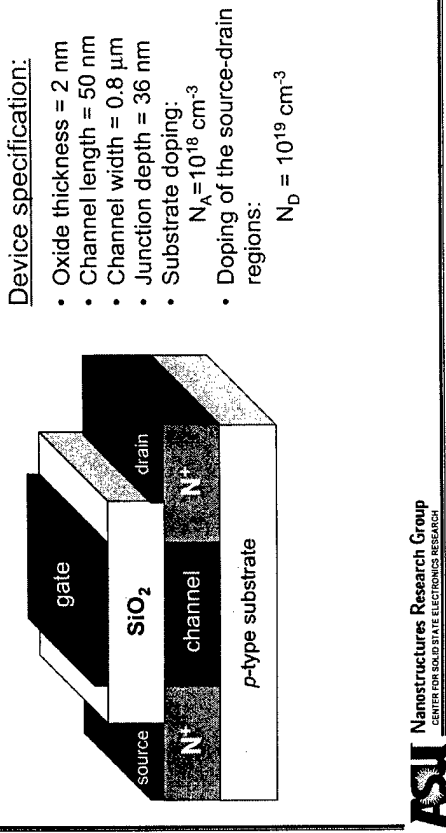


## Description of the Existing 2D/3D Device Simulators

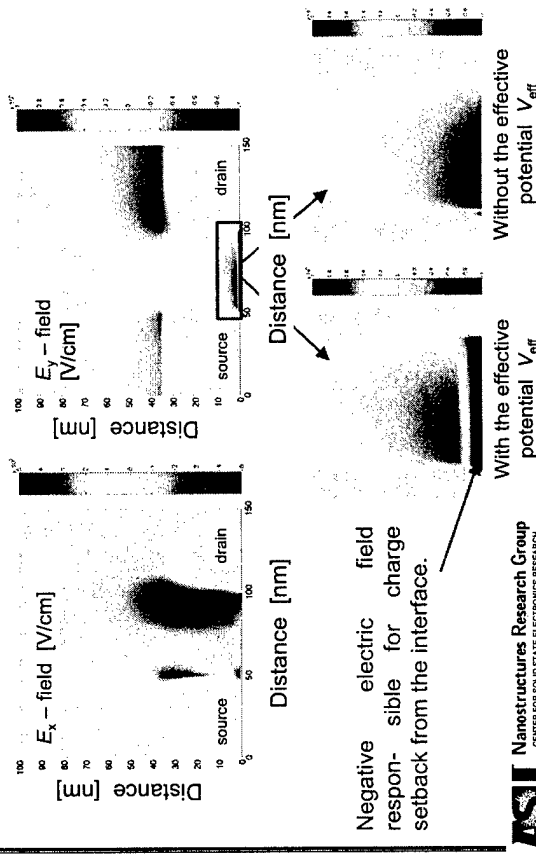


**ASU**  
NANOSTRUCTURES RESEARCH GROUP  
CENTER FOR SOLID STATE ELECTRONICS RESEARCH

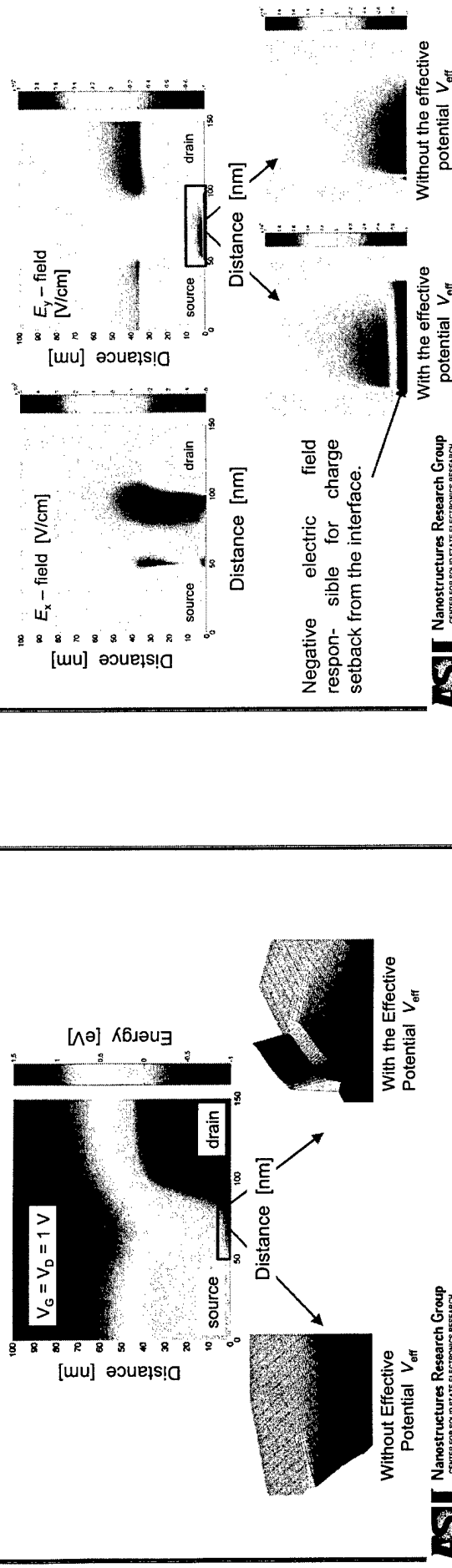
## Simulation of a 50 nm MOSFET Device



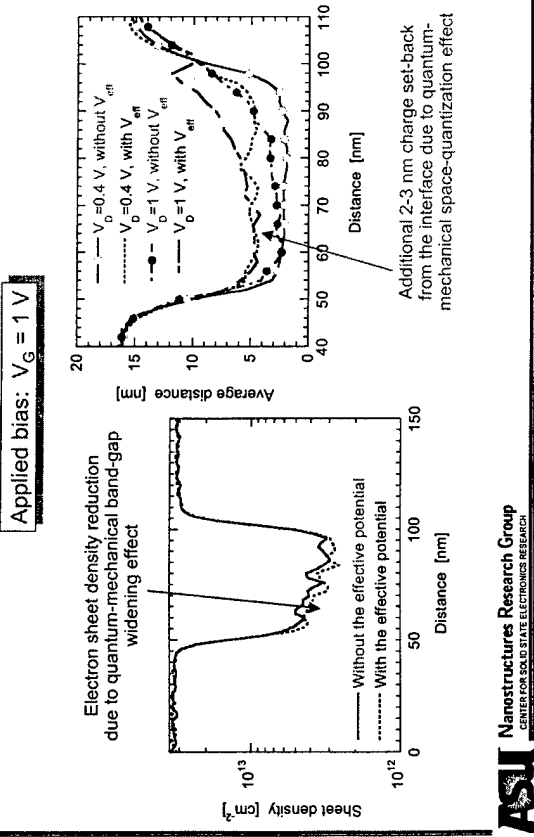
## Electric Field Profile



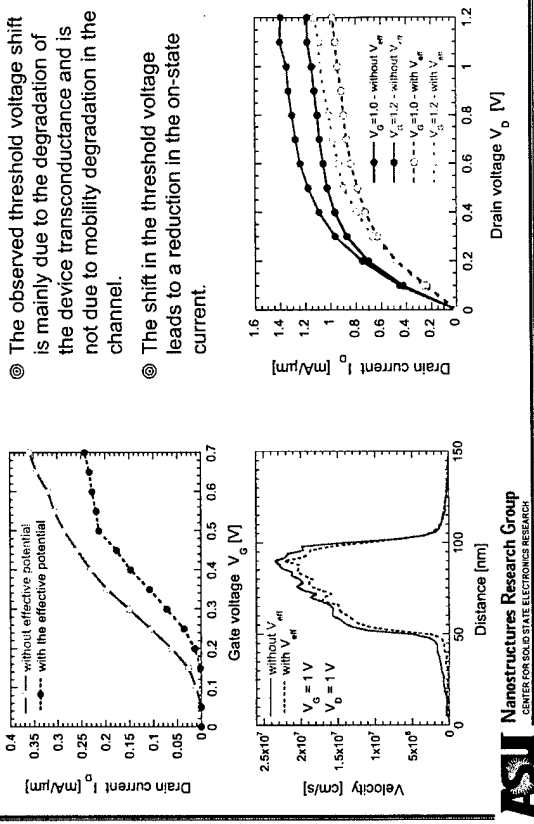
## Conduction Band Profile



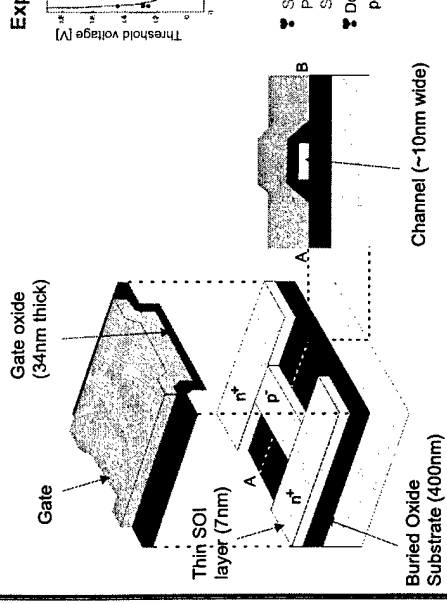
## Carrier Density and Average Distance



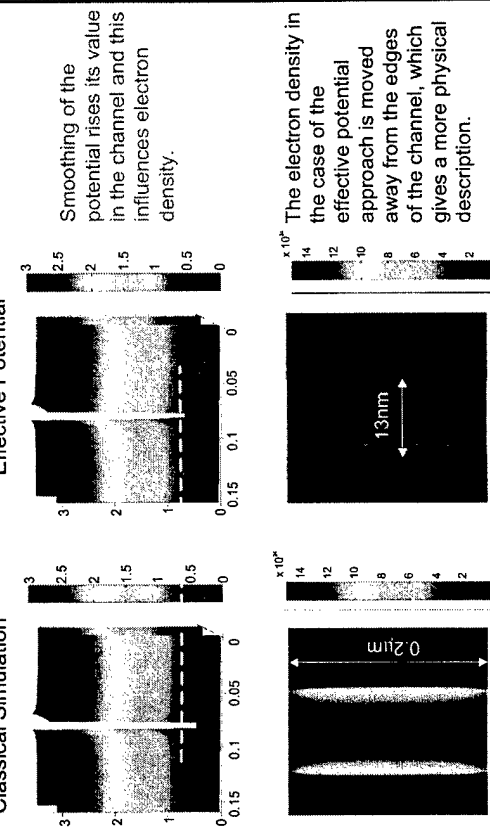
## Transfer and Output Characteristics



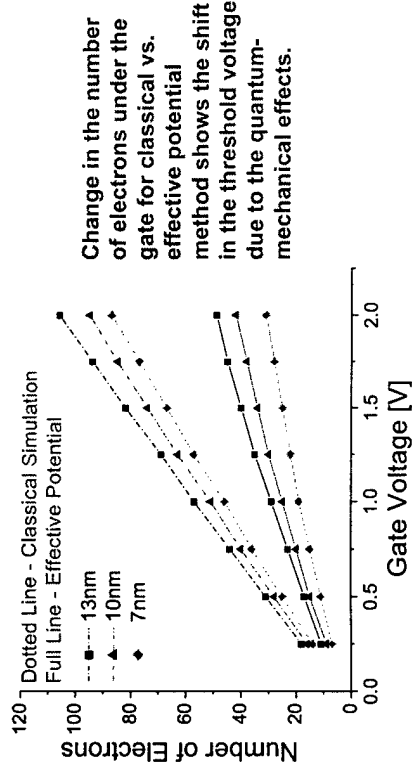
## SOI Device Structure



## Conduction Band Edge and Electron Density

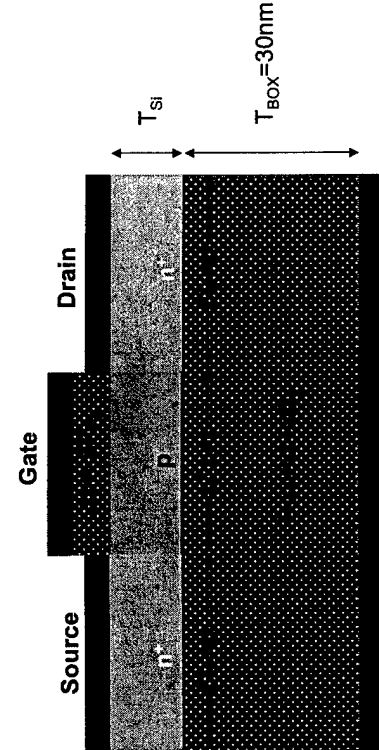


## Number of Electrons in the Channel



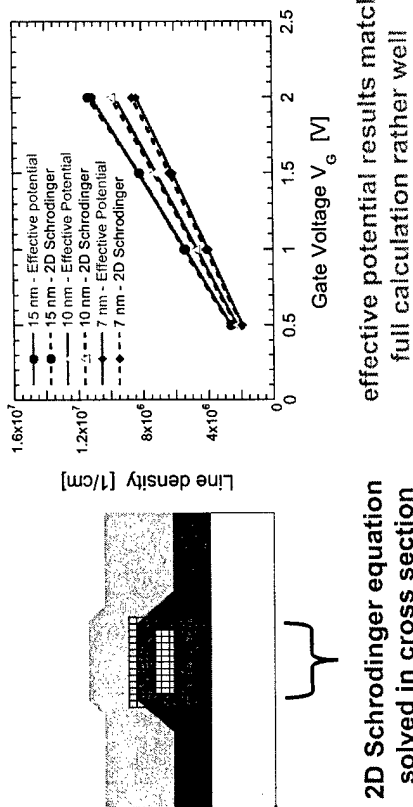
**ASU** Nanostructures Research Group  
CENTER FOR SOLID STATE ELECTRONICS RESEARCH

## SOI MOSFET Structure

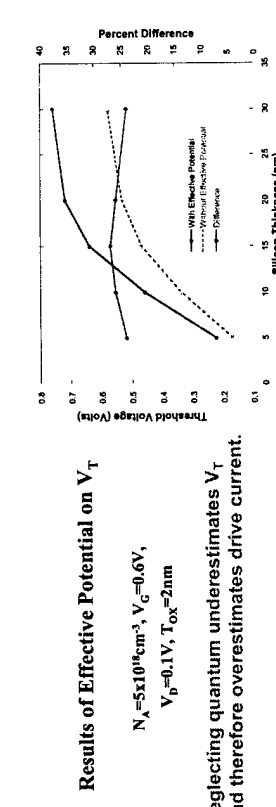
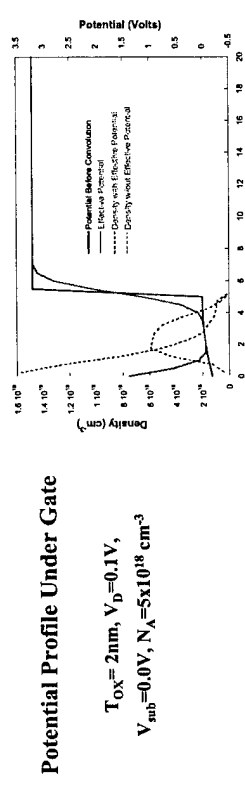


**ASU** Nanostructures Research Group  
CENTER FOR SOLID STATE ELECTRONICS RESEARCH

## Effective potential vs. 2D Schrodinger

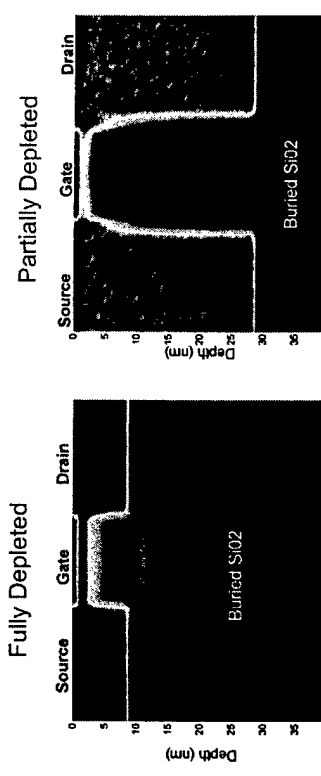


**ASU** Nanostructures Research Group  
CENTER FOR SOLID STATE ELECTRONICS RESEARCH

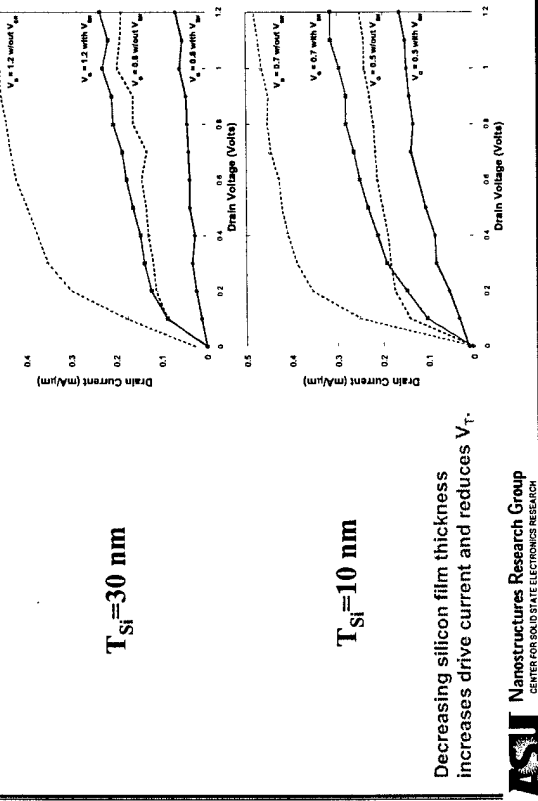


**ASU** Nanostructures Research Group  
CENTER FOR SOLID STATE ELECTRONICS RESEARCH

## Electron Density Distribution



## $I_D$ - $V_D$ Characteristics



## Madelung and Bohm's reformulation of quantum mechanics

$$\text{insert } \psi = R e^{iS/\hbar}, \quad R = \sqrt{n} = |\psi| \rightarrow -\frac{\hbar^2}{2m} \nabla^2 \psi + V\psi = i\hbar \frac{\partial \psi}{\partial t}$$

$$\text{real part yields the quantum Hamilton-Jacobi equation: } \frac{\partial S}{\partial t} + \frac{(\nabla S)^2}{2m} + V + Q = 0$$

where  $S \rightarrow$  action, and  $Q = -\frac{\hbar^2}{2m^*} \frac{\nabla^2 |\psi|}{|\psi|}$  is the "quantum potential"

$$\begin{aligned} \text{equations of motion: } & \mathbf{v}(\mathbf{x}, t) = \frac{\nabla S(\mathbf{x}, t)}{m} = \frac{\hbar}{m} \frac{\text{Im}(\psi \nabla \psi)}{|\psi|} \\ & \mathbf{a}(\mathbf{x}, t) = -\frac{\nabla(V + Q)}{m^*} \end{aligned}$$

## Connection with the effective potential

$$\begin{aligned} V_{\text{eff}}(x) &= \frac{1}{\sqrt{2\pi}\alpha} \int_{-\infty}^{\infty} V(x + \xi) e^{-\xi^2/2\alpha^2} d\xi \\ &\equiv \frac{1}{\sqrt{2\pi}\alpha} \int_{-\infty}^{\infty} V(x) + \xi \frac{\partial V}{\partial x} + \frac{\xi^2}{2} \frac{\partial^2 V}{\partial x^2} + \dots e^{-\xi^2/2\alpha^2} d\xi. \end{aligned}$$

$$\begin{aligned} V_{\text{eff}}(x) &= V(x) + \alpha^2 \frac{\partial^2 V}{\partial x^2} + \dots \\ V_{\text{eff}}(x) &= V(x) - \frac{2\alpha^2}{\beta} \frac{\partial^2 \ln(\sqrt{n/n_0})}{\partial x^2} + \dots \\ &= V(x) - \frac{2\alpha^2}{\beta \sqrt{n}} \frac{\partial^2 \sqrt{n}}{\partial x^2} + \dots \end{aligned}$$

$$Q = \frac{\hbar^2}{2m^*} \frac{\nabla^2 |\psi|}{|\psi|}$$

Within a factor of 2, the second term is now recognized as the density gradient term, but is more commonly known as the Bohm potential

## quantum point contact

1. We start by consider a quantum wire with constriction
2. We solve the system with and without self-consistently
3. We smooth the self-consistent solution to obtain the effective potential
4. We use the effective potential to generate classical trajectories and the self-consistent solution to generate quantum trajectories

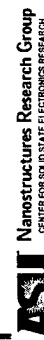
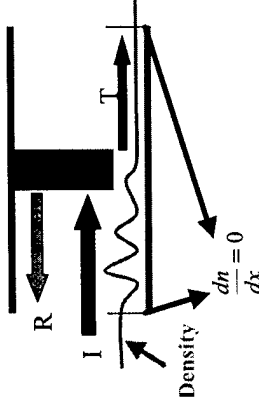
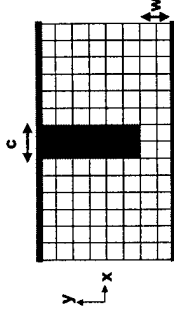


Nanostructures Research Group  
CENTER FOR SOLID STATE ELECTRONICS RESEARCH

## Self-Consistent Solutions

### Solving Schrödinger's Equation

- Solution obtained via finite difference scattering matrix cascade
- We assume:
  1. that the wire extends to  $\pm\infty$
  2. the reflected waves do not interfere with the boundary
- Therefore, solutions have continuous boundary conditions
- This is our criteria for boundary conditions

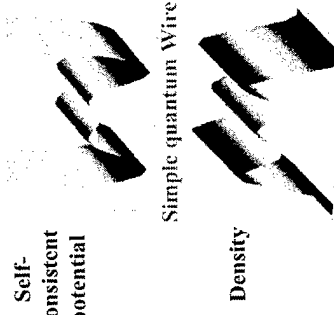


Nanostructures Research Group  
CENTER FOR SOLID STATE ELECTRONICS RESEARCH

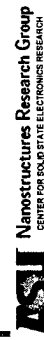
## Self-Consistent Solutions

### Dealing with the dynamic density

- Solving the self-consistent problem introduces a potential profile into the device
- The correlation energy lowers the conduction band edge, and therefore allows a build up of charge which increases the number of propagating modes and density in the device
- To keep density constant, the Fermi energy is adjusted with the lowering conduction band edge during iteration to maintain a constant density (propagating modes)



$$N = \frac{2}{\pi} \sum_{E_I < E_F} \left[ \frac{2m * (E_F - E_I)}{\hbar^2} \right]^{\frac{1}{2}}$$



Nanostructures Research Group  
CENTER FOR SOLID STATE ELECTRONICS RESEARCH

## Self-Consistent Solutions

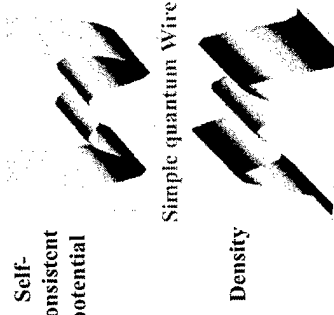
### Dealing with the dynamic density

1. Boundary conditions for the Poisson solver and the Schrödinger solver
2. Calculating the Hartree potential (via the Poisson solver) and included the exchange and correlation potentials
3. Maintaining a constant density in the system. A build up of density occurs due to the inclusion of the correlation potential which drops the conduction band edge
4. Using the correct electron density in the Poisson solver. (Taking into account the contributions of the positive ions in the system)

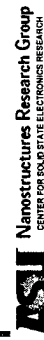
## Self-Consistent Solutions

### Dealing with the dynamic density

- Solving the self-consistent problem introduces a potential profile into the device
- The correlation energy lowers the conduction band edge, and therefore allows a build up of charge which increases the number of propagating modes and density in the device
- To keep density constant, the Fermi energy is adjusted with the lowering conduction band edge during iteration to maintain a constant density (propagating modes)



$$N = \frac{2}{\pi} \sum_{E_I < E_F} \left[ \frac{2m * (E_F - E_I)}{\hbar^2} \right]^{\frac{1}{2}}$$



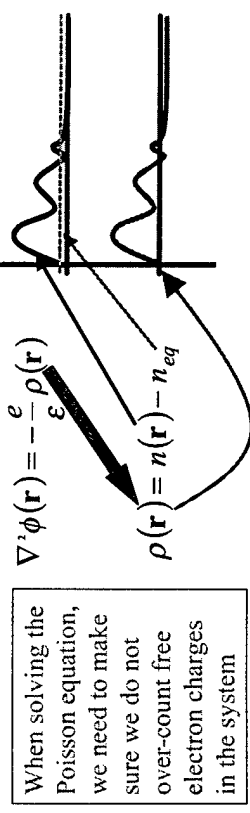
Nanostructures Research Group  
CENTER FOR SOLID STATE ELECTRONICS RESEARCH

## Self-Consistent Solutions

### Dealing with the dynamic density

## Self-Consistent Solutions

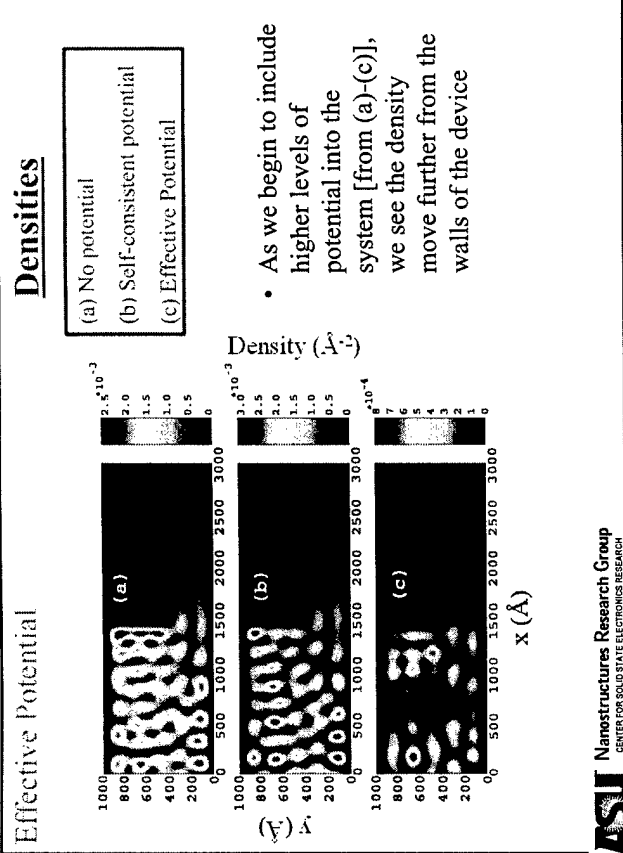
### Positive Ion Contribution



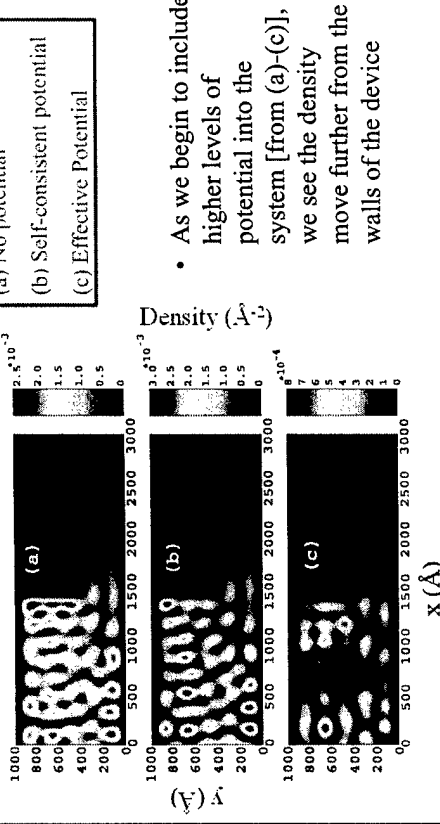
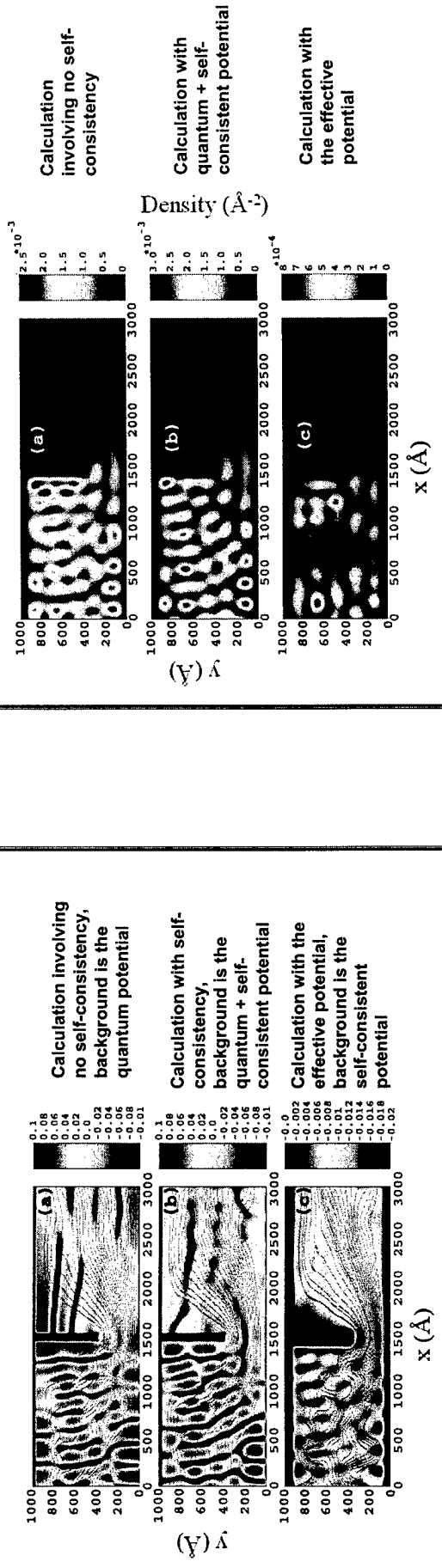
- We know there is a potential drop after the constriction
- We can interpret the drop in the Hartree potential to be the expected drop in the Fermi level

**ASU** Nanostructures Research Group  
CENTER FOR SOLID STATE ELECTRONICS RESEARCH

## Densities



Bohm trajectories flowing through the QPC. The background is the self-consistent potential.



Density ( $\text{A}^{-3}$ )

(a)  
(b)  
(c)

**ASU** Nanostructures Research Group  
CENTER FOR SOLID STATE ELECTRONICS RESEARCH

- As we begin to include higher levels of potential into the system [from (a)-(c)], we see the density move further from the walls of the device

## Conclusions

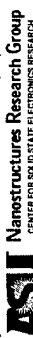
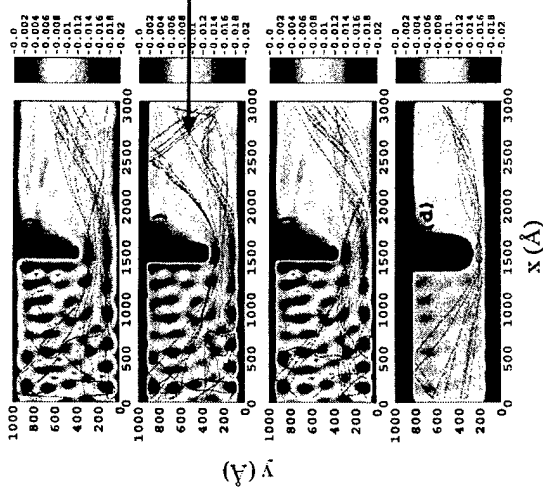
- The effective potential approach in many cases allows for a quite accurate approximation of the quantization effects in real semiconductor devices
- The numerical cost of including the effective potential is low – “more bang for the buck”
  - Some challenges remain....
  - Model valid only within the random phase approximation.
  - It is still “quasi-local”, so it does not allow proper treatment phase interference effects



Nanostructures Research Group

CENTER FOR SOLID STATE ELECTRONICS RESEARCH

## Classical particles moving in the effective potential



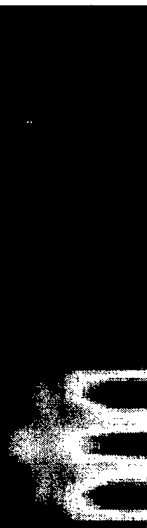
Nanostructures Research Group

CENTER FOR SOLID STATE ELECTRONICS RESEARCH

## Wave function approaches for self-consistent computations of transport in quantum dots and arrays

D. K. Ferry

Center for Solid State Electronics Research and Department of Electrical Engineering  
Arizona State University, Tempe, AZ 85287-5706



### Outline

- ❖ Discretization of the Schrödinger equation
- ❖ The Usuki mode matching technique
- ❖ Application to quantum dots
- ❖ Incorporation of Poisson's equation
- ❖ Further application to quantum dots

*Special thanks to R. Akis, L. Shifren, J. Harris for their contributions, without which there would be no content to this talk. Also, discussions with C. Jacoboni on quantum computing have been most helpful.*



- ◆ Throughout this discussion, we will consider the region of interest to be the quasi-two-dimensional electron gas at the interface of a GaAs/AlGaAs heterojunction: all parameters will be for electrons in GaAs and confining potentials will be imposed upon this 2D gas.

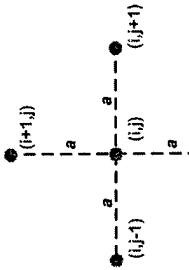
The Schrödinger equation, in 2D, can be written as

$$-\frac{\hbar^2}{2m} \left( \frac{d^2}{dx^2} + \frac{d^2}{dy^2} \right) \psi(x, y) + V(x, y) \psi(x, y) = E \psi(x, y)$$

where  $V(x, y)$  is the local "site potential." This potential will be the self-consistent potential in later usage.

$$t = \frac{\hbar^2}{2m * a^2} \quad \text{is the "hopping" energy.}$$

We now discretize the Schrödinger equation, using the 5-point scheme shown at left. This is a form of central differencing, that will introduce some unfortunate byproducts that will have to be addressed.



The Schrödinger equation, in its discretized form, now takes the shape of

$$-t[\psi(i+1, j) + \psi(i-1, j) + \psi(i, j+1) + \psi(i, j-1)] + [V(i, j) + 4t]\psi(i, j) = E\psi(i, j)$$



In general, this discretized Schrödinger equation can now be written in the form of coupled "slices" (columns  $j$ ) as

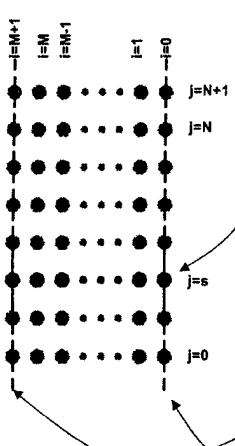
$$\mathbf{H}_0(s)\vec{\psi}(s) - t\mathbf{I}\vec{\psi}(s+1) - t\mathbf{I}\vec{\psi}(s-1) = E\vec{\psi}(s)$$

with

$$\mathbf{H}_0(s) = \begin{bmatrix} [V(M,s)+4t] & -t & 0 & \dots \\ -t & [V(M-1,s)+4t] & -t & \dots \\ \dots & -t & [V(2,s)+4t] & -t \\ \dots & 0 & -t & [V(1,s)+4t] \end{bmatrix}$$



CENTER FOR SOLID STATE ELECTRONICS RESEARCH

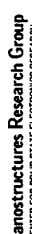


On slice  $s$ , we may write the wave function as

$$\vec{\psi}(s) = \begin{bmatrix} \psi(M,s) \\ \psi(M-1,s) \\ \vdots \\ \psi(1,s) \end{bmatrix}$$

There is an automatic assumption that

$$\psi(0,j) = \psi(M+1,j) = 0$$



CENTER FOR SOLID STATE ELECTRONICS RESEARCH

There are two approaches that can be developed now to "iterate" the solutions from one end to the other. These are:

- ❖ The "recursive" Green's function, in which a Green's function is developed for each slice, and coupling from one slice to the next is carried out by use of Dyson's equation.

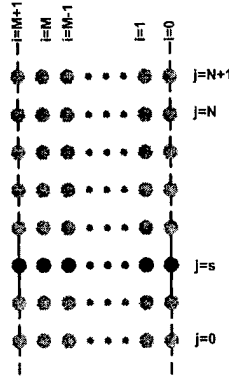
- ❖ We use the wave functions directly, matching the wave and its derivative from one slice to the next-unstable, but can be stabilized by use of the scattering matrix.

These two approaches are very nearly identical in procedure and in central iterations. They differ somewhat in the end-point processing and in extraction of the density and wave function.

We use the latter approach, since it allows us to actually follow individual modes.

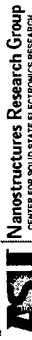


CENTER FOR SOLID STATE ELECTRONICS RESEARCH

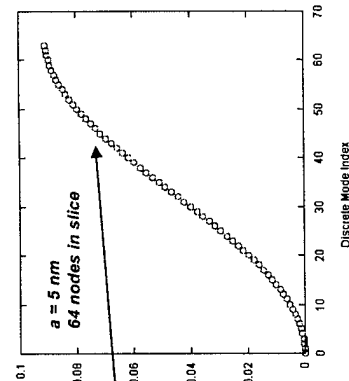


The general approach is to begin with slice "0" and propagate the excited modes toward the end of the device, as slice "N+2".

We then back propagate the density at slice "N+1" to the beginning at slice "0" in order to determine the wave function and the density in the structure.



CENTER FOR SOLID STATE ELECTRONICS RESEARCH



This creates the first "problem" as the discretization introduces an artificial band structure:  
The energy diverges from the expected parabolic band

The artificial band has a width of 4t and here t = 21.5 meV.

As a result, it is imperative that all relevant energies in the problem be < t in magnitude.

Matrix of the modes (columns) and their amplitude at each site (rows)

$$\begin{bmatrix} U(\pm) \\ U(\pm) \end{bmatrix} = ? \begin{bmatrix} U(\pm) \\ U(\pm) \end{bmatrix}$$

At slice "0", we must first determine the  $2M$  modes (left and right propagating) by solving an eigenvalue equation:

$$\text{hopping matrix } \begin{bmatrix} H_{s,s-1} \end{bmatrix}_{jk} = -te^{i\phi}\delta_{jk} \quad \phi = \frac{eBa^2}{\hbar}$$

$$\text{eigenvalues } ? = \lambda_m \delta_{mn}$$

$$\begin{bmatrix} C_1^l & C_2^l \\ 0 & 1 \end{bmatrix} = T_0 \begin{bmatrix} 1 & 0 \\ 0 & 1 \end{bmatrix} \begin{bmatrix} P_1^0 & P_2^0 \end{bmatrix}$$

We have to initialize at slice "0" with a different scheme which converts from the mode basis to the site basis:

$$T_0 = \begin{bmatrix} U(+) & U(-) \\ U(+)?(+) & U(-)?(-) \end{bmatrix}$$

$$P_2^0 = \begin{bmatrix} 0 \\ T_{21}^0 + T_{22}^0 \end{bmatrix}$$

$$P_1^0 = -P_2^0 T_{21}^0 \otimes^0 \mathbf{1}$$

This part remains unchanged.

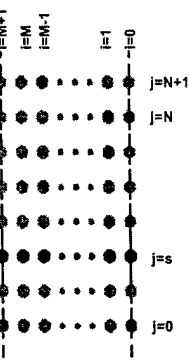
$$\begin{bmatrix} C_1^{s+1} & C_2^{s+1} \\ 0 & 1 \end{bmatrix} = T_s \begin{bmatrix} C_1^s & C_2^s \\ 0 & 1 \end{bmatrix} \begin{bmatrix} P_1^s & P_2^s \end{bmatrix}$$

The general propagation scheme for the  $s^{\text{th}}$  slice follows:

$$P_2^s = \frac{1}{[T_{21}^s C_2^s + T_{22}^s]}^{-1}$$

$$P_1^s = -P_2^s T_{21}^s C_1^s$$

This term is the  $G_0^{-1} - V_G$  that appears in the recursive Green's function approach. This is Dyson's equation.



We then back propagate from a density near the "N+2" slice in order to get the density at each point in the structure.

Once we know the wave function at slice s, near the end, we can back propagate, using:

$$F^{(N+2,s)}(i,w) = P_1^s + P_2^s F^{(N+2,s+1)}(i,w)$$

The LHS condition leads to:

$$P_2^s = [T_2^s C_2^s + T_{22}^s]^{-1}$$

$$P_1^s = -P_2^s T_{21}^s C_1^s$$

This part remains unchanged.

$$\begin{bmatrix} C_1^{N+2} & C_2^{N+2} \\ 0 & 1 \end{bmatrix} = T_{N+1} \begin{bmatrix} C_1^{N+1} & C_2^{N+1} \\ 0 & 1 \end{bmatrix} \begin{bmatrix} 1 & 0 \\ P_1^{N+1} & P_2^{N+1} \end{bmatrix}$$

$$T_{N+1} = \begin{bmatrix} 0 & [U(+)?(+)]^{-1} \\ 1 & -U(+)[U(+)?(+)]^{-1} \end{bmatrix}$$

$$t = C_1^{N+2}$$

**ASU** | Nanostructures Research Group  
CENTER FOR SOLID STATE ELECTRONICS RESEARCH

$$n_w(i,s) = |\Phi^{(N+2,s)}(i,w)|^2$$

Site "r" in the slice

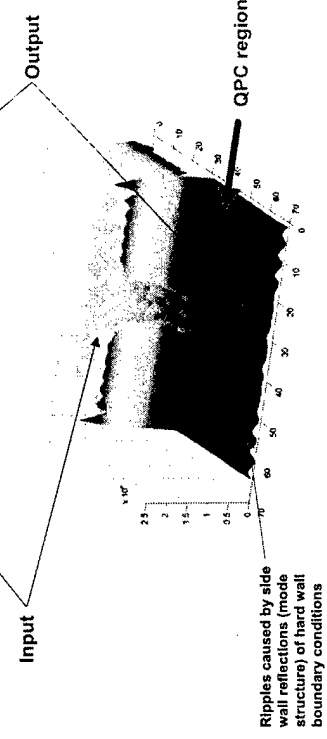
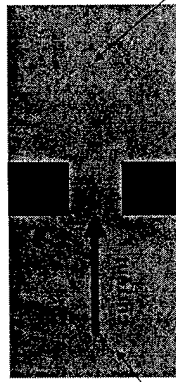
Mode "w" in the density.

The "propagated" wave function connecting slice "s" to the output modes

F^(N+2,s)(i,w)

P^s(i,s) = |Φ^(N+2,s)(i,w)|^2

n\_w(i,s) = ∑\_w |Φ^(N+2,s)(i,w)|^2



**ASU** | Nanostructures Research Group  
CENTER FOR SOLID STATE ELECTRONICS RESEARCH

Finally, we have to convert back to the mode basis at the "N+2" slice:

$$\begin{bmatrix} C_1^{N+2} & C_2^{N+2} \\ 0 & 1 \end{bmatrix} = T_{N+1} \begin{bmatrix} C_1^{N+1} & C_2^{N+1} \\ 0 & 1 \end{bmatrix} \begin{bmatrix} 1 & 0 \\ P_1^{N+1} & P_2^{N+1} \end{bmatrix}$$

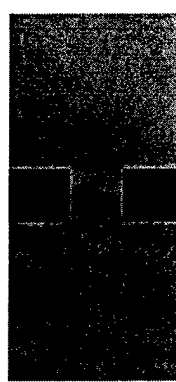
leads to:

$$P_2^s = [T_2^s C_2^s + T_{22}^s]^{-1}$$

$$P_1^s = -P_2^s T_{21}^s C_1^s$$

This part remains unchanged.

**ASU** | Nanostructures Research Group  
CENTER FOR SOLID STATE ELECTRONICS RESEARCH

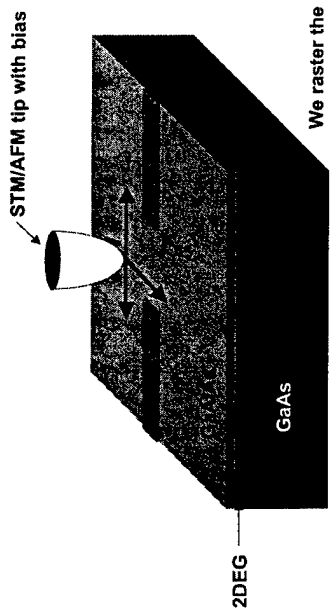


Because we initialize at one end of the structure, the result is *not* symmetric in the long axis. Thus, there is a definite input side and a definite output side, which is not often recognized.

Let us consider a simple example—that of a quantum point contact embedded in a wider wire:  
  
a = 5 nm  
width = 64 sites  
QPC opening = 12 sites

**ASU** | Nanostructures Research Group  
CENTER FOR SOLID STATE ELECTRONICS RESEARCH

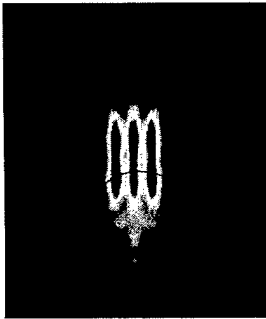
### An Interesting Experiment:



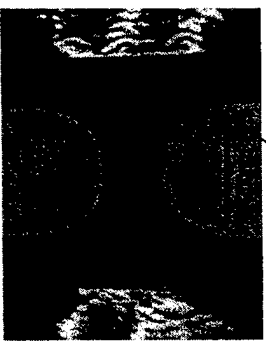
We raster the biased tip across the surface. The bias affects the 2DEG and changes the transmission through the QPC. We plot the transmission change as a function of the tip position.

**ASU**  
Nanostructures Research Group  
CENTER FOR SOLID STATE ELECTRONICS RESEARCH

### simulation



### experiment



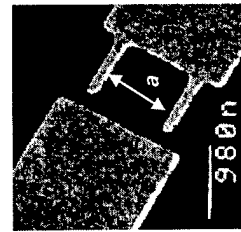
M. A. Topinka et al., Science 289, 2323 (2000).

The three-fold pattern of the conduction change is seen only on the input side of the QPC (experiment is done in a.c. fashion rather than d.c. fashion assumed in the calculations).

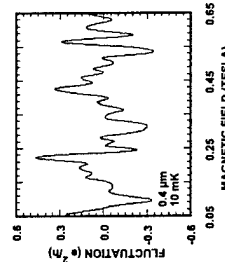
**ASU**  
Nanostructures Research Group  
CENTER FOR SOLID STATE ELECTRONICS RESEARCH

As a second example, we consider an open quantum dot.

Dots can be of many shapes, even multiple dots:



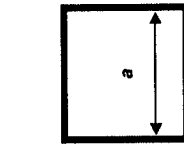
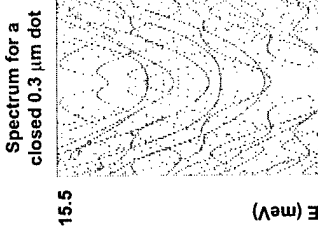
Typical fluctuations as  $B$  or  $V_G$  is varied:



- A magnetic field mixes the states and produces an entangled state.

**ASU**  
Nanostructures Research Group  
CENTER FOR SOLID STATE ELECTRONICS RESEARCH

### THE CLOSED DOT



$$\Psi_{nm}(x, y) = \frac{2}{a} \sin\left(\frac{n\pi x}{a}\right) \sin\left(\frac{m\pi y}{a}\right)$$

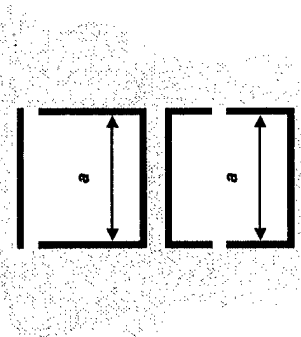
$n, m = 1, 2, \dots$

**ASU**  
Nanostructures Research Group  
CENTER FOR SOLID STATE ELECTRONICS RESEARCH

## The Open Dot

Opening the dot does NOT destroy the quantization within the dot!

The dot states hybridize (entangle) with the environment states.



**Dot:** states  $\{\alpha_d\}$   
parameters (ops., var.)

**Environment:** states  $\{\alpha_e\}$   
parameters (ops., var.)

$$H = H_d + H_e + H_{ed}$$

## The Open Dot

Define the *system* density matrix  $\rho_s$   
and the *reduced*, device density matrix  $\rho_d = \text{Tr}_e\{\rho_s\}$

$$H = H_d + H_e + H_{ed}$$

Use a projection super-operator  $\hat{P}$  to remove the environment variables

This leads to the new Liouville equation for the device density matrix:

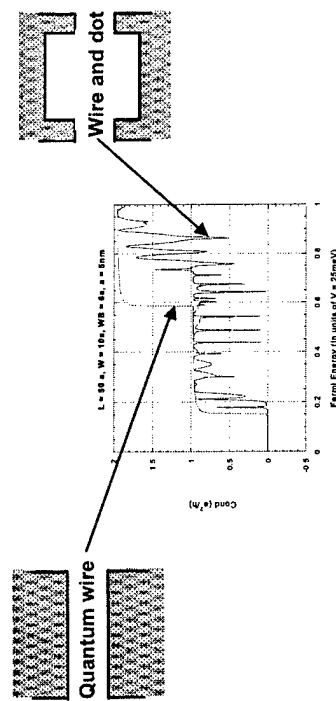
$$i\hbar \frac{\partial \rho_d}{\partial t} = (\hat{H}_d + \hat{H}_{ed} + \hat{\Sigma}(t \rightarrow \infty))\rho_d$$

Where (in Laplace transform notation):

$$\begin{aligned} \hat{H}_{ed} &\rho_d(s) \equiv \text{Tr}\{\hat{P}\hat{H}_{ed}\hat{P}\rho_d(s)\} \\ \hat{\Sigma}(s) &= \hat{P}\hat{H}\hat{Q}(i\hbar s - \hat{Q}\hat{H}\hat{Q})^{-1}\hat{Q}\hat{H}\hat{P} \end{aligned}$$

## Environmental Effects

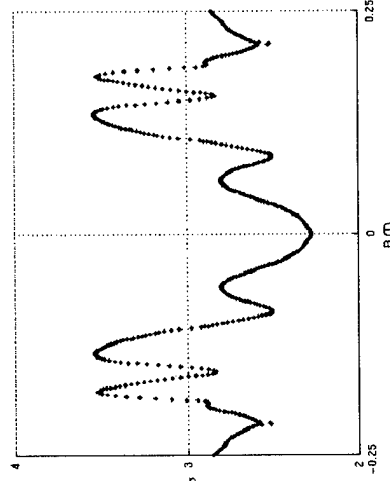
We can understand how the QPCs and the dot work together to provide the "spectrum" of conductance.

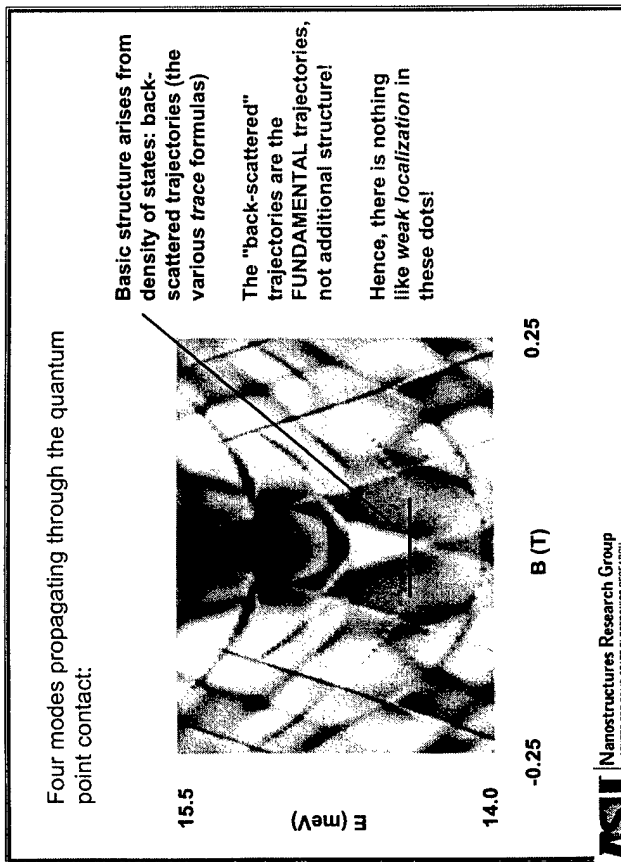
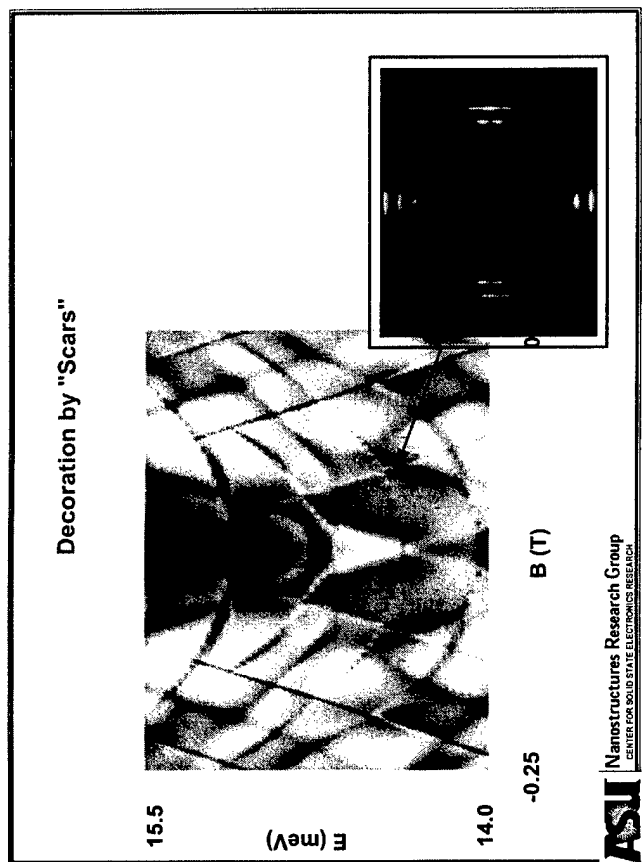
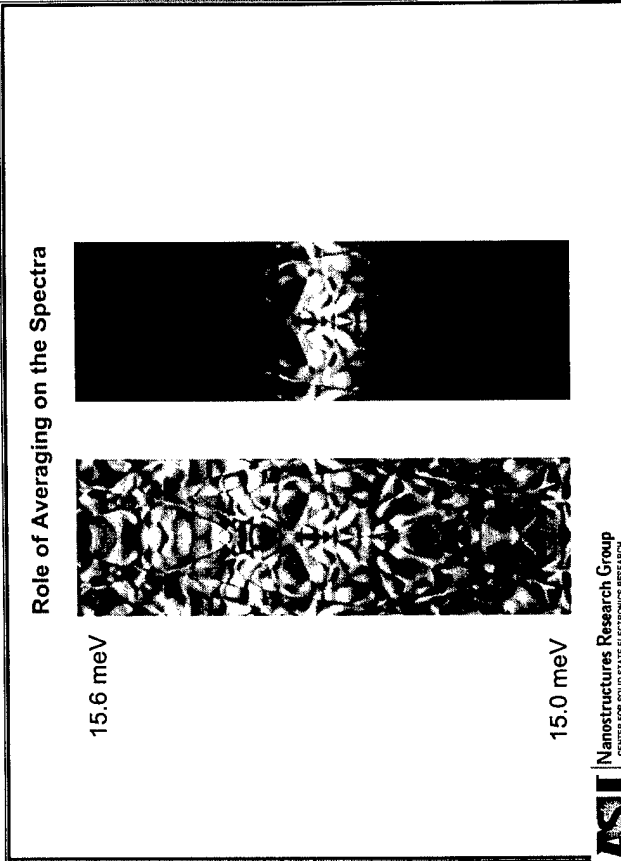
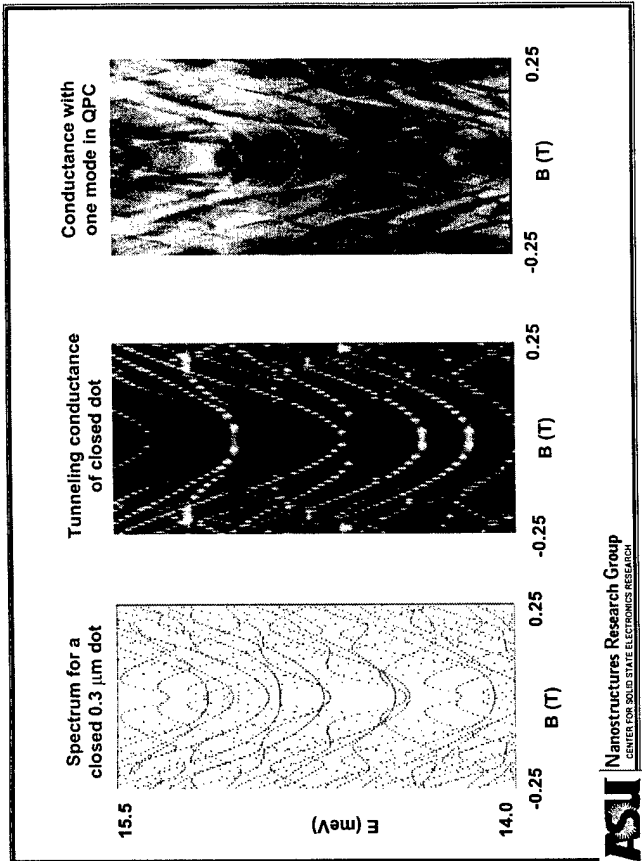


Dot modes, which are excited, work to provide modulation of the overall transmission.

## The Open Dot

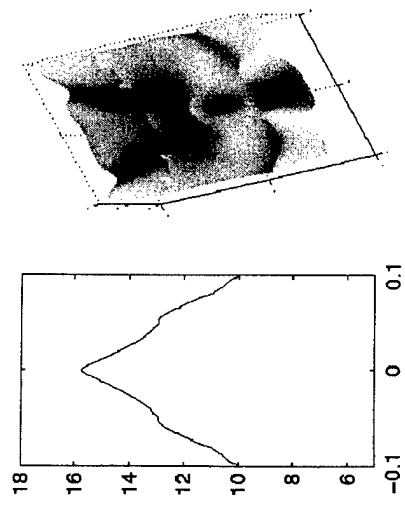
We determine the "spectrum" of the open dot from the conductance through the dot:  
 $G \sim$  density of states  
 $DOS \sim$  energy levels





## Role of Averaging on the Spectra

Moving average



Let us now turn to the problem of self-consistency of the potential in the calculation--

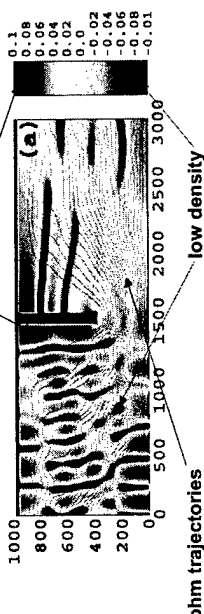
The potential that is included in the site energy  $V(j)$  can be included as a self-consistent quantity. Here, the charge density is

$$\rho(x,y) = -\frac{e}{\epsilon_s} (|\psi(x,y)|^2 - 1) n_0$$

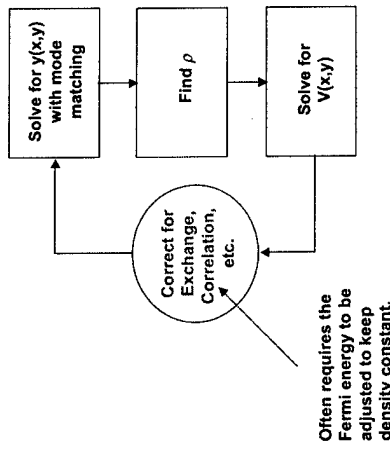
Uniform electron density set by  
remote dopants in AlGaAs

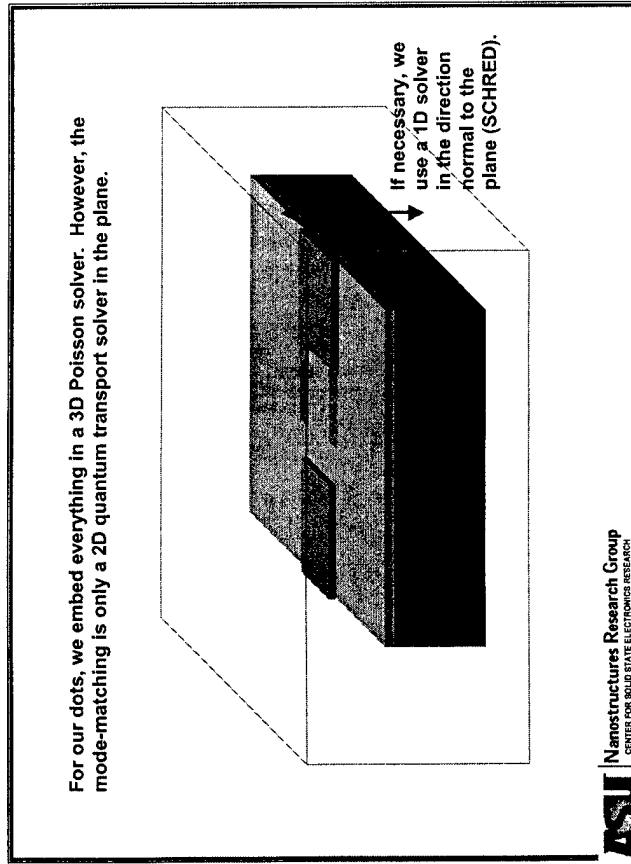
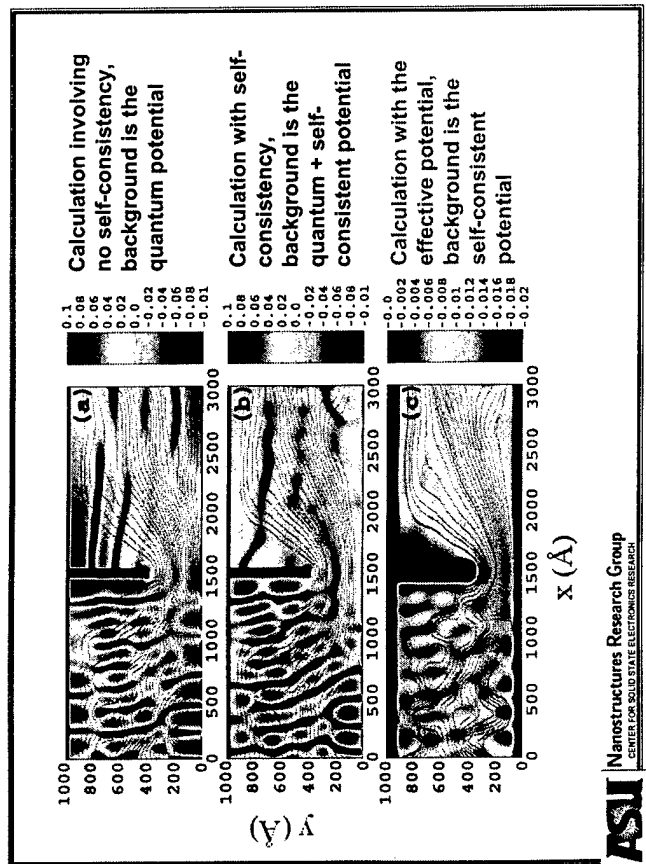
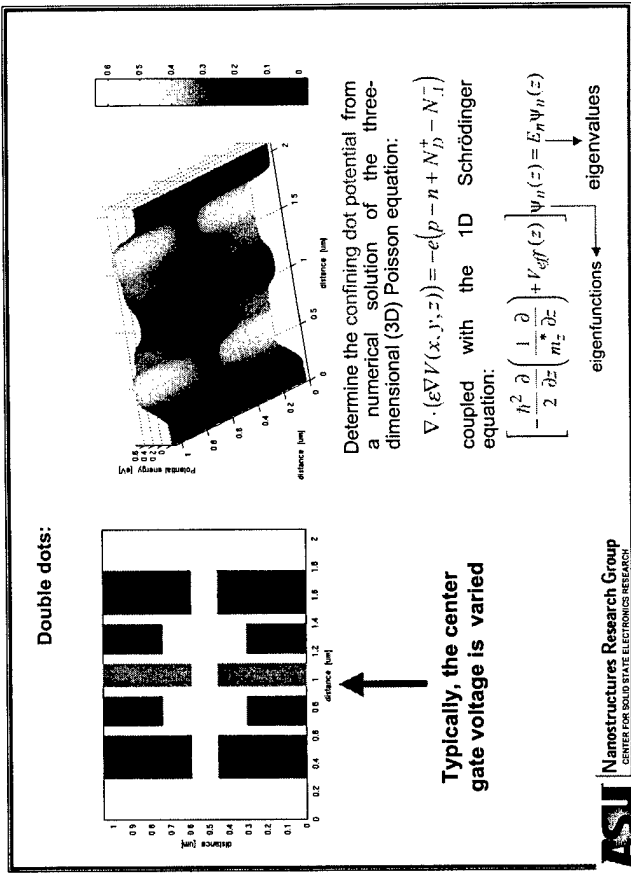
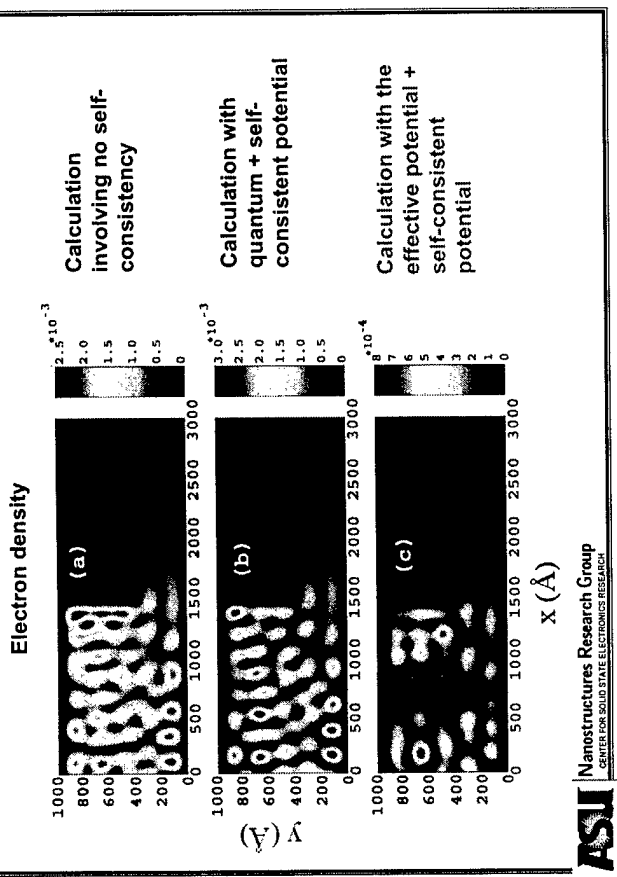
Consider a simple quantum wire with an embedded QPC. Here, we move the QPC to one side of the wire:

barriers



For simple systems, we can generate a relatively straight-forward loop to find the solutions:



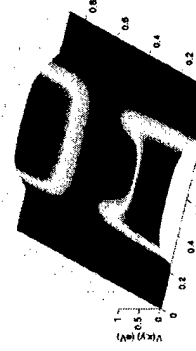


**Problems with simple mode matching when:**

- ❖  $V(x,y)$  is not a simple function
- ❖ A magnetic field is applied

**Then the modes can no longer be expressed as well characterized analytical functions.**

**Example: a realistic quantum dot potential obtained by a self-consistent calculation**



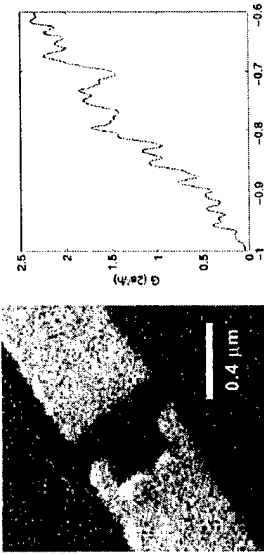
For better flexibility and accuracy it is advantageous to do the problem on a discrete lattice.

Our use of a solver for the modes, with a lattice representation solves this problem.

**Scarring notches** has the form of a

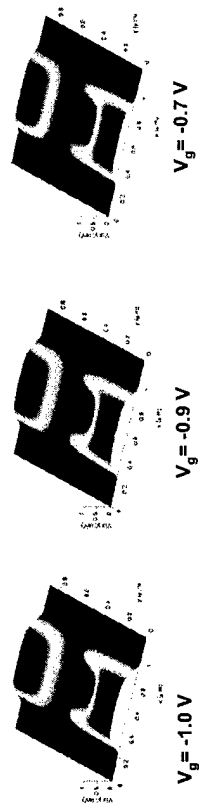
Nanostructures Research Group  
CENTER FOR SOLID STATE ELECTRONICS RESEARCH

**Split gate pattern**



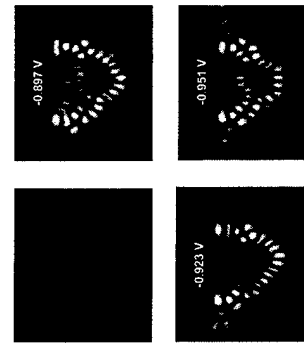
**Measured conductance**

In the normal direction, the Exchange and correlation corrections to the ground state energy of the are included by using the Local Density Approximation.



Nanostructures Research Group  
CENTER FOR SOLID STATE ELECTRONICS RESEARCH

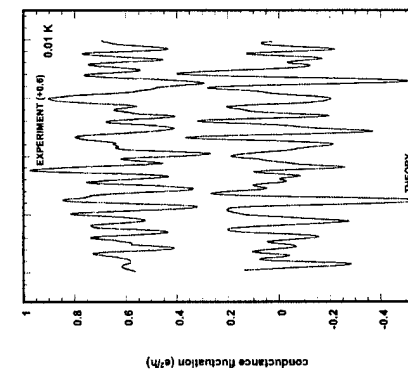
**Gate voltage comparison revisited**



Simulations also reveal that certain scars may RECUR as gate voltage is varied. The resulting periodicity agrees WELL with that of the conductance oscillations

Persistence of the scarring at zero magnetic field indicates its INTRINSIC nature

The scarring is NOT induced by the application of the magnetic field



Nanostructures Research Group  
CENTER FOR SOLID STATE ELECTRONICS RESEARCH

Nanostructures Research Group  
CENTER FOR SOLID STATE ELECTRONICS RESEARCH

- ❖ Mode matching approaches are a viable method of computing the conduction in mesoscopic systems.
- ❖ This can easily be incorporated with the Poisson equation for self-consistent solutions.
- ❖ In addition, the energy dependence can be converted to a temperature dependence for near-equilibrium systems. It is also possible to do non-equilibrium approaches with only slight changes in the program (in principle).

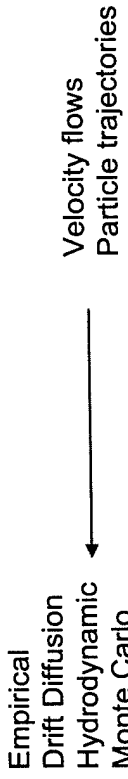
# Trajectories in quantum mechanics

John R. Barker  
Nanoelectronics Research Centre  
Department of Electronics and Electrical Engineering  
University of Glasgow



Advanced Research Workshop  
on  
Quantum Transport in Semiconductors

© R. Barker, 2003. This material is not to be reproduced without permission.



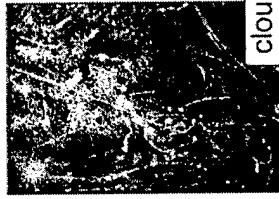
Self-consistent via Poisson equation

**Can we obtain a trajectory description  
of quantum transport?**

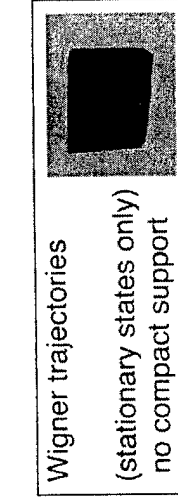
In principle, the the surprising answer is yes

© R. Barker, 2003. This material is not to be reproduced without permission.

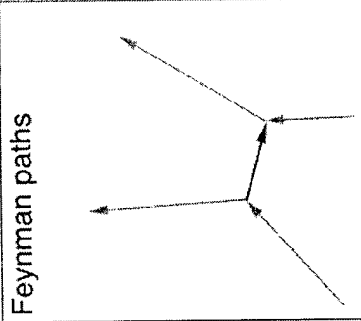
1. Without any extension of quantum theory we may define velocity flows.
2. With special assumptions we may define trajectories
3. Bohm has also proposed deterministic extension to QM which uses trajectories calculated in 1 or 2.
4. Others have defined stochastic trajectories in extensions to QM
  - Position-momentum uncertainty relations
  - Non-locality of quantum mechanics



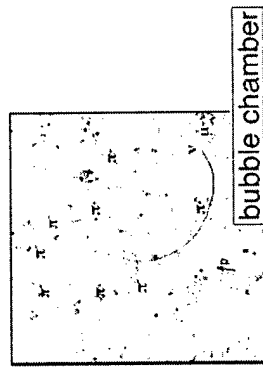
cloud chamber



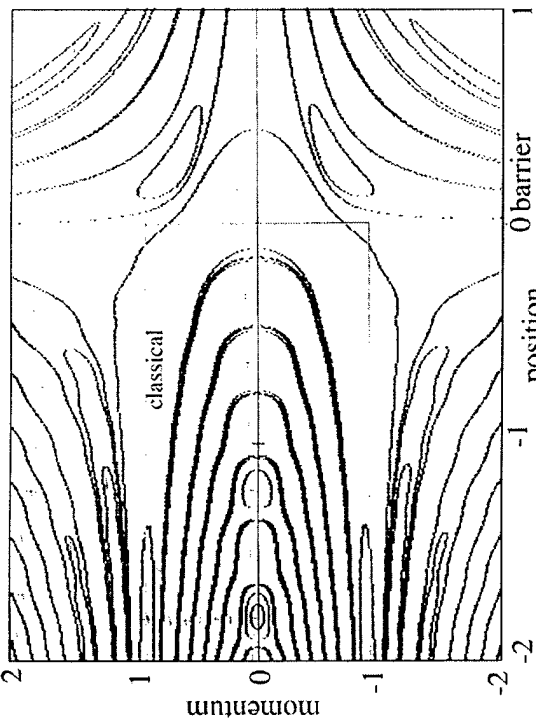
Wigner trajectories  
(stationary states only)  
no compact support



Feynman paths



bubble chamber



© J.P. Bozler, M. Müller, F. Püttmann, T. Schäfer, 2001, Universität Regensburg, Institut für Theoretische Physik und Kosmologie, Heisenbergstrasse 1, D-9304 Regensburg, Germany

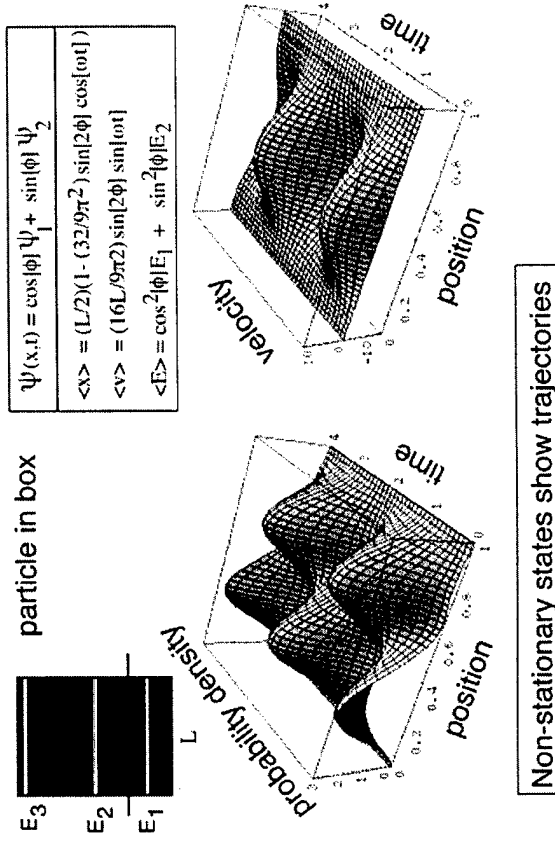
What do we want from a quantum transport theory?

A self-consistent treatment of the local charge and current density fields which describe

- tunnelling
- scattering
- interference effects
- size quantisation
- time-dependence
- de-coherence effects
- many-body issues

### FOR FINITE REGIONS OF OPEN SYSTEMS

© J.P. Bozler, M. Müller, F. Püttmann, T. Schäfer, 2001, Universität Regensburg, Institut für Theoretische Physik und Kosmologie, Heisenbergstrasse 1, D-9304 Regensburg, Germany



Non-stationary states show trajectories

© J.P. Bozler, M. Müller, F. Püttmann, T. Schäfer, 2001, Universität Regensburg, Institut für Theoretische Physik und Kosmologie, Heisenbergstrasse 1, D-9304 Regensburg, Germany

A rigorous approach to trajectories

Velocity Flow Picture

Probability density  $n(x,t)$

Particle Current density  $j(x,t)$

Define a velocity field:

$$\mathbf{v}(x,t) = j(x,t)/n(x,t)$$

© J.P. Bozler, M. Müller, F. Püttmann, T. Schäfer, 2001, Universität Regensburg, Institut für Theoretische Physik und Kosmologie, Heisenbergstrasse 1, D-9304 Regensburg, Germany

## Schrödinger Equation

*A posteriori* quantum hydrodynamics

Express wave function in polar form:  $\Psi = R \exp(iS/\hbar)$

$$i\hbar \frac{\partial \Psi}{\partial t} = H\Psi(x, t)$$

$$H = -\frac{\hbar^2}{2m} \nabla^2 + \Phi$$

$$n(x, t) = \Psi^*(x, t)\Psi(x, t)$$

$$\mathbf{j}(x, t) = \frac{-i\hbar}{2m} \{ \Psi^* \nabla \Psi - \Psi \nabla \Psi^* \}$$

$$V_Q = -\frac{\hbar^2}{2m} \frac{\nabla^2 \sqrt{n}}{\sqrt{n}} \quad n = R^2 \quad m\mathbf{v} = \nabla S$$

Newton's 2nd law for carriers:  
 $m^* \frac{d\mathbf{v}}{dt} = q\nabla(\psi - \varphi) - \frac{D}{n\mu} \nabla n - q \frac{\mathbf{v}}{\mu}$

Take the gradient of  
the phase equation

$$m \frac{\partial \varphi}{\partial t} + m\mathbf{v} \cdot \nabla \varphi = -\nabla \Phi(\mathbf{x}, t) - \nabla V_Q(\mathbf{x}, t)$$

Quantum Euler Eqn

Continuity Equation

$$\frac{\partial n}{\partial t} + \nabla \cdot n\mathbf{v} = 0$$

The first equation is not  
quite correct and we need  
further constraints as we  
shall see

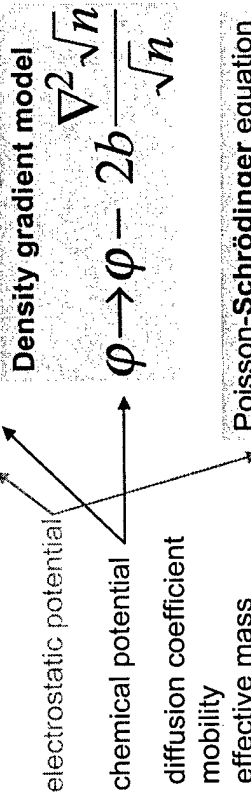
$$V_Q = -\frac{\hbar^2}{2m} \frac{\nabla^2 \sqrt{n}}{\sqrt{n}} \quad n = R^2 \quad m\mathbf{v} = \nabla S$$

Quantum potential

$n, \mathbf{v}, \psi$

Newton's 2nd law for carriers:

$$m^* \frac{d\mathbf{v}}{dt} = q\nabla(\psi - \varphi) - \frac{D}{n\mu} \nabla n - q \frac{\mathbf{v}}{\mu}$$



Poisson-Schrödinger equation

Quantum potential causes repulsion from boundaries  
But also lowers barrier energies to allow tunnelling

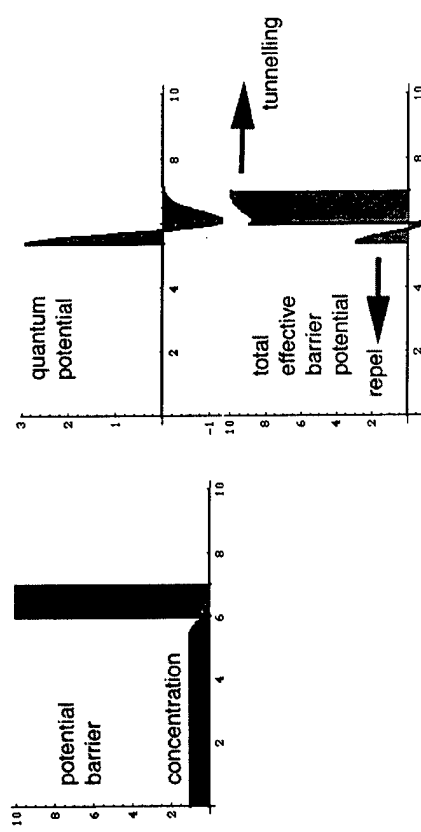
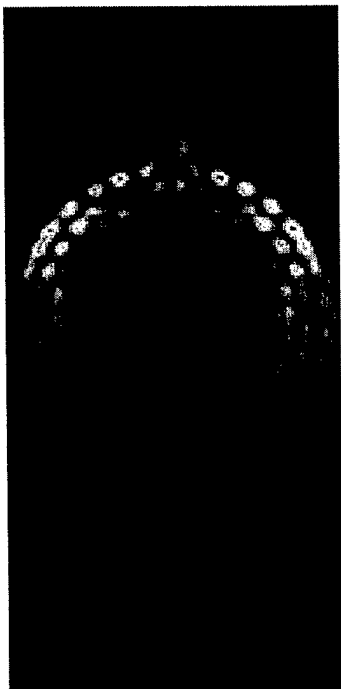
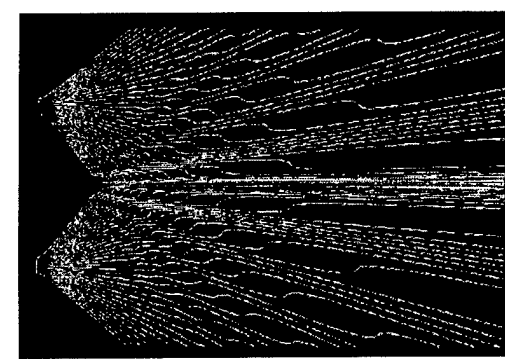


Fig. 1. Illustration of the quantum potential barrier effect. The potential barrier is represented by a black rectangle. The quantum potential is shown as a red curve. The total effective barrier potential is the sum of the potential barrier and the quantum potential.

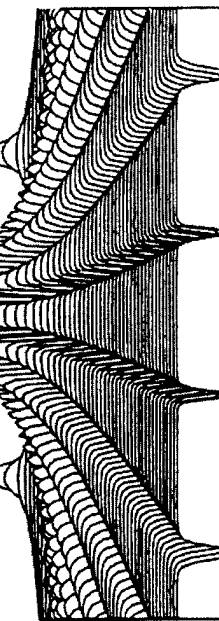
### 2-slit interference



Quantum Potential

Trajectories  
equivalent to  
streamlines  
in steady state

First reported by  
Dewdney et al



Interpretation: discover a trajectory

© 1998 Blackwell Science Ltd, *Journal of Experimental Biology*, 25, 131–138. The model of quantum potential barrier effect proposed by Dewdney et al. (1998) is presented here.

## Uncertainty Relations

$$\Delta x \Delta p \geq \hbar / 2$$

## Entanglement

$$\Delta x = \langle (x - \langle x \rangle)^2 \rangle^{1/2} = \{ \int x^2 n(x) dx - [\int x n(x) dx]^2 \}^{1/2}$$

Factorisable wave-function  $\rightarrow$  physical independence

Sum of factorisable wave-functions :

$$\Delta p = \langle (p - \langle p \rangle)^2 \rangle^{1/2} =$$

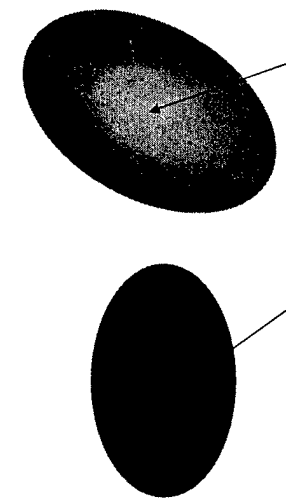
$$\{ \int (p^2(x) + 2mV_Q(x)n(x)dx - [\int p(x) n(x)dx]^2 \}^{1/2}$$

$$p = \partial S / \partial x$$

Barker (1992)

For the sake of simplicity, this diagram illustrates the principle of entanglement.

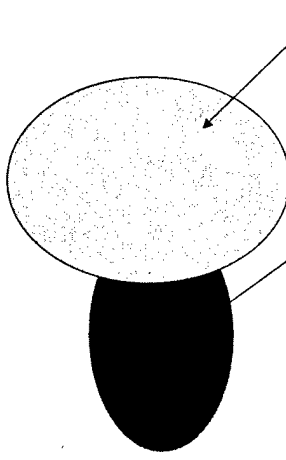
## Configuration Space



$$\Psi(\mathbf{r}_1, \mathbf{r}_2) = C[\Psi_\alpha(\mathbf{r}_1)\Psi_\beta(\mathbf{r}_2) + \Psi_\gamma(\mathbf{r}_1)\Psi_\delta(\mathbf{r}_2)]$$

No overlap: effective statistical mixture,  
System point is in one or the other sub-state

## Configuration Space



$$\Psi(\mathbf{r}_1, \mathbf{r}_2) = C[\Psi_\alpha(\mathbf{r}_1)\Psi_\beta(\mathbf{r}_2) + \Psi_\gamma(\mathbf{r}_1)\Psi_\delta(\mathbf{r}_2)]$$

Overlap: entangled state,  
Correlation

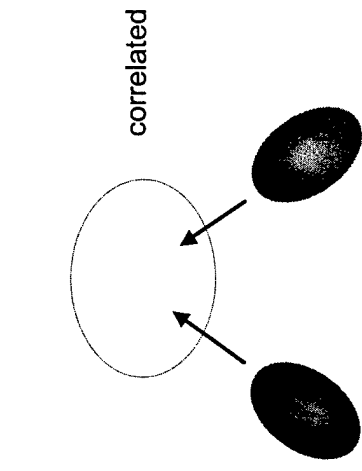
For the sake of simplicity, this diagram illustrates the principle of entanglement.

IP Nuclear Physics, Institute of Physics, University of Cologne, Germany, with permission.

© JINR Letter 1992, University of Cologne. This material is not peer-reviewed prior to publication.

## Fermions

## 2 fermions in a harmonic oscillator potential

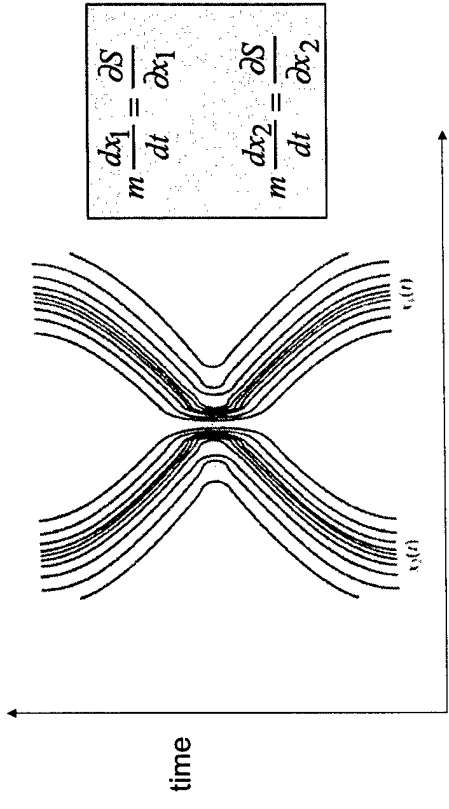


$$\Psi(\mathbf{r}_1, \mathbf{r}_2) = C[\Psi(\mathbf{r}_1, \mathbf{r}_2) - \Psi(\mathbf{r}_2, \mathbf{r}_1)]$$

Effectively factorisable at long distances

© K. E. Cahill, 2001. All rights reserved. This material is based upon work supported by the National Science Foundation under grants No. DMR-9623073 and No. DMR-9996494.

Vigier, Dewdney, Holland and Kyriandis (1987) *Friction and time evolution. The standard model for the interaction of matter with its environment*



© K. E. Cahill, 2001. All rights reserved. This material is based upon work supported by the National Science Foundation under grants No. DMR-9623073 and No. DMR-9996494.

Vigier, Dewdney, Holland and Kyriandis (1987) *Friction and time evolution. The standard model for the interaction of matter with its environment*

## Topological properties of quantum flows

Velocity  $\mathbf{v}$  derived from gradient of phase  $S$

Wave function  $R \exp(iS/\hbar)$  is single-valued

Streamlines do not cross

Velocity circulation is quantised

Position coordinates form an autonomous system:  
flow determined topologically by fixed points in the flow.

## 2D example

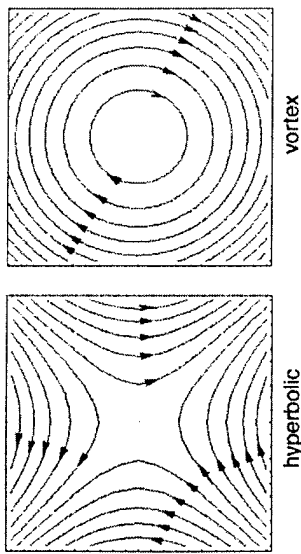
$$\frac{dx}{dt} = v_x = m^{-1} \frac{\partial S}{\partial x}; \quad \frac{dy}{dt} = v_y = m^{-1} \frac{\partial S}{\partial y}$$

$$\frac{dy}{dx} = \frac{\frac{\partial S(x, y)}{\partial y}}{\frac{\partial S(x, y)}{\partial x}}$$

© K. E. Cahill, 2001. All rights reserved. This material is based upon work supported by the National Science Foundation under grants No. DMR-9623073 and No. DMR-9996494.

© K. E. Cahill, 2001. All rights reserved. This material is based upon work supported by the National Science Foundation under grants No. DMR-9623073 and No. DMR-9996494.

## Flow near singularities



At velocity nodes

© J. K. Barker 2001. University of Exeter. This material is subject to copyright. It is made available under the terms of the Creative Commons Attribution Non-Commercial-ShareAlike 2.0 Licence. For full details see the copyright page.

## The quantisation of velocity circulation

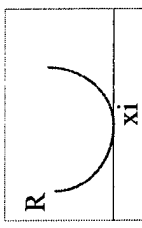
The *a posteriori* QHD equations automatically satisfy the velocity circulation theorem:

$$\oint \nabla S \cdot d\mathbf{r} = Nh \quad (N : \text{integer})$$

$$\oint \mathbf{v} \cdot d\mathbf{r} = Nh / m$$

© J. K. Barker 2001. University of Exeter. This material is subject to copyright. It is made available under the terms of the Creative Commons Attribution Non-Commercial-ShareAlike 2.0 Licence. For full details see the copyright page.

## Vortices occur at strong nodal points/lines (Barker 2001)

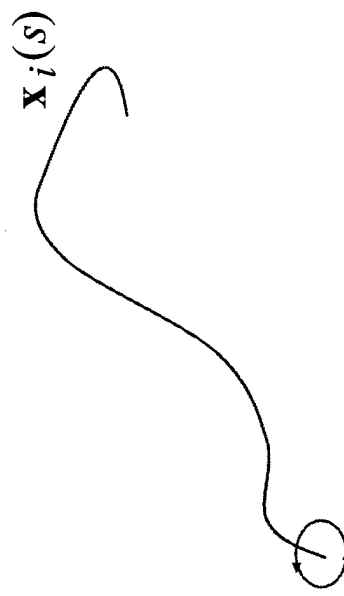


$$R \approx |\mathbf{r} - \mathbf{x}_i| N_i$$

Or generally,

$$R \approx [(\mathbf{r} - \mathbf{x}_i) \cdot \Lambda \cdot (\mathbf{r} - \mathbf{x}_i)]^{1/2}$$

$$V_Q = -(\hbar^2 / 2m) \nabla^2 R / R \approx -(\hbar^2 / 2m) N_i^2 / |\mathbf{r} - \mathbf{x}_i|^2$$



## Vortex line

$$\nabla \times \mathbf{v} = N_i (h / m) \int \delta(\mathbf{r} - \mathbf{x}_i(s)) (d\mathbf{x}_i / ds) ds$$

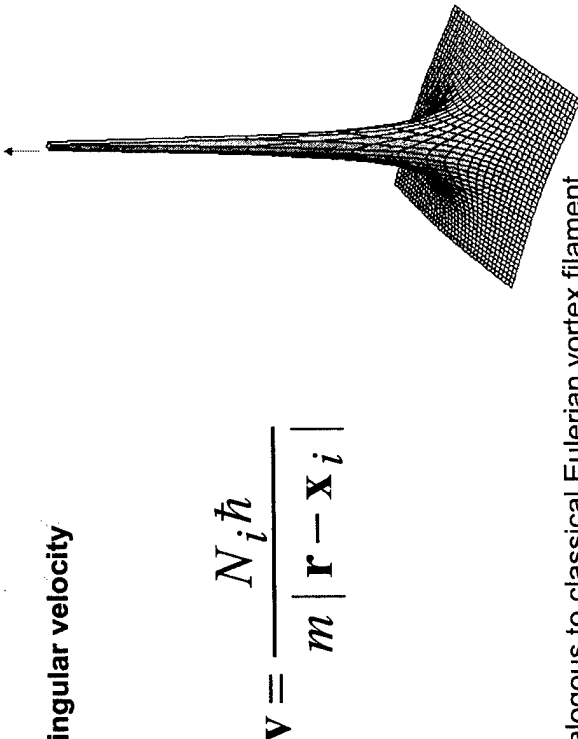
© J. K. Barker 2001. University of Exeter. This material is subject to copyright. It is made available under the terms of the Creative Commons Attribution Non-Commercial-ShareAlike 2.0 Licence. For full details see the copyright page.

© J. K. Barker 2001. University of Exeter. This material is subject to copyright. It is made available under the terms of the Creative Commons Attribution Non-Commercial-ShareAlike 2.0 Licence. For full details see the copyright page.

Near the strong nodal point:

$$\begin{aligned}\frac{1}{2} m v^2 \approx -V_Q &= (\hbar^2 / 2m) \nabla^2 R / R \\ &\approx (\hbar^2 / 2m) N_i^2 / |\mathbf{r} - \mathbf{x}_i|^2\end{aligned}$$

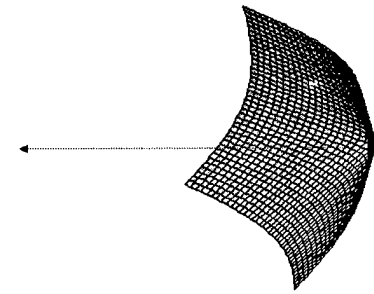
### Singular velocity



$$\mathbf{v} = \frac{N_i \hbar}{m |\mathbf{r} - \mathbf{x}_i|}$$

### Non-singular current density

$$\mathbf{J} \propto |\mathbf{r} - \mathbf{x}_i|^{2N_i-1}$$



$$\text{Phase } S = N_k \text{Arctan}(y/x) \quad x, y \neq 0$$

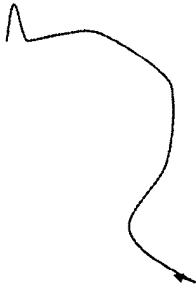
$$\Psi \approx |\mathbf{r} - \mathbf{x}_k|^{N_k} \exp[iN_k \phi]$$

Re-constructed wave-function

$$\oint \nabla S \cdot d\mathbf{r} = N_k h$$

### Traversal Time

requires Bohm interpretation

$$t = \int_{\eta_1}^{\eta_2} \frac{\mathbf{v} \cdot d\mathbf{r}}{\mathbf{v}^2}$$


$$= \int_{\eta_1}^{\eta_2} \frac{\mathbf{p} \cdot d\mathbf{r}}{2T}$$

Kinetic energy appears as metric

On a vortex, one loop executed in time  $t = Nh/2T$

Barker (1992)

This is a later publication. This one is much more traditional, and does not mention vortices.

At this stage, I will not discuss this topic. This is a very interesting topic, but it is not covered in this book. A reference is given at the end of the section.

To describe vortex motion with *ab initio* quantum hydrodynamics

we need to introduce a vector quantum potential  $\mathbf{a}_Q(\mathbf{r}, t)$

$$\oint_C \mathbf{a}_Q \cdot d\mathbf{r} = nh$$

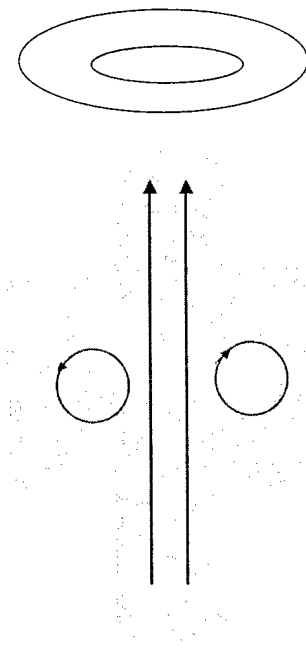
$$\boxed{m \frac{\partial \mathbf{v}}{\partial t} + m \mathbf{v} \cdot \nabla \mathbf{v} = -\nabla \Phi(\mathbf{x}, t) \\ - m \mathbf{v} \times \nabla \times \mathbf{a}_Q(\mathbf{x}, t) - \nabla V_Q(\mathbf{x}, t)}$$

where

$$\nabla \times \mathbf{a}_Q = \sum_i N_i (h/m) \delta(\mathbf{r} - \mathbf{x}_i(s)) (\mathbf{d}\mathbf{x}_i / ds) ds$$

### Quantum smoke ring

Ballistic flow  
in open quantum dots



Compare Lord Kelvin's cigar box!

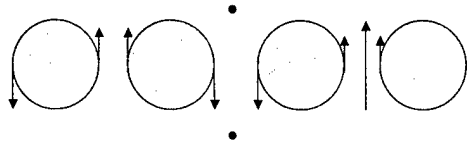
J. P. P. Dyer, AMI University of Technology, has permission to copy this material for internal, non-profit purposes.

© J. P. P. Dyer, 2001, University of Technology, has permission to copy this material for internal, non-profit purposes.

## Density evolution

### Current density evolution

QuickTime™ and a  
Animation decompressor  
are needed to see this picture.



4 vortices  
formed

## Travelling wave in single transverse mode

### Transmission Maximum

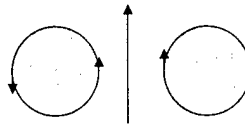
QuickTime™ and a  
Animation decompressor  
are needed to see this picture.

QuickTime™ and a  
Animation decompressor  
are needed to see this picture.

### Transmission Maximum

## Density plot

### Current Density And Particle density



QuickTime™ and a  
Animation decompressor  
are needed to see this picture.

## Lower energy, transmission minimum (reflection)

### Smoke ring 2 vortices formed

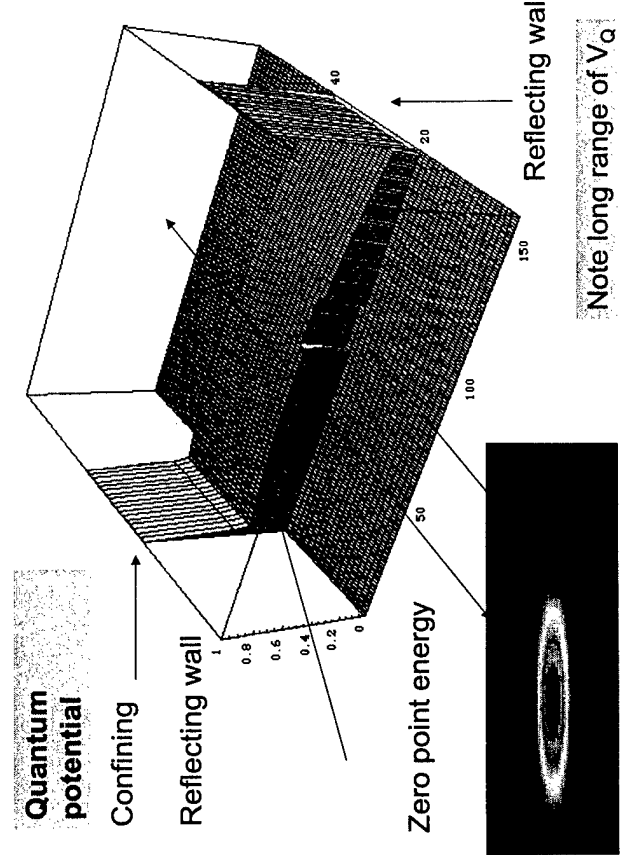
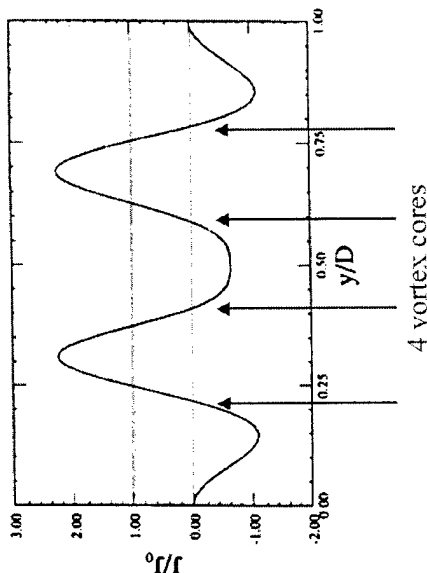
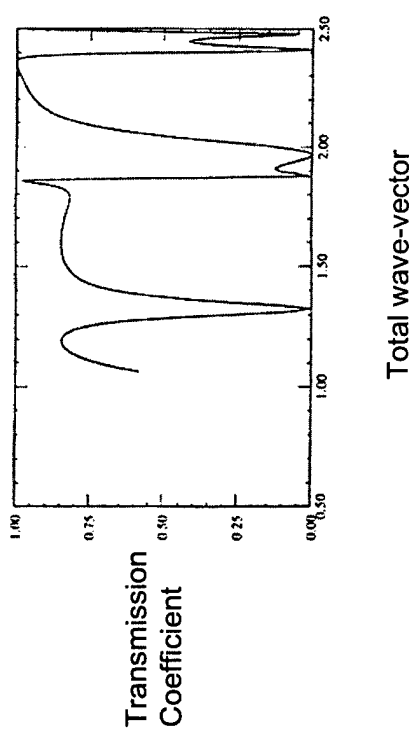
QuickTime™ and a  
Animation decompressor  
are needed to see this picture.

QuickTime™ and a  
Animation decompressor  
are needed to see this picture.

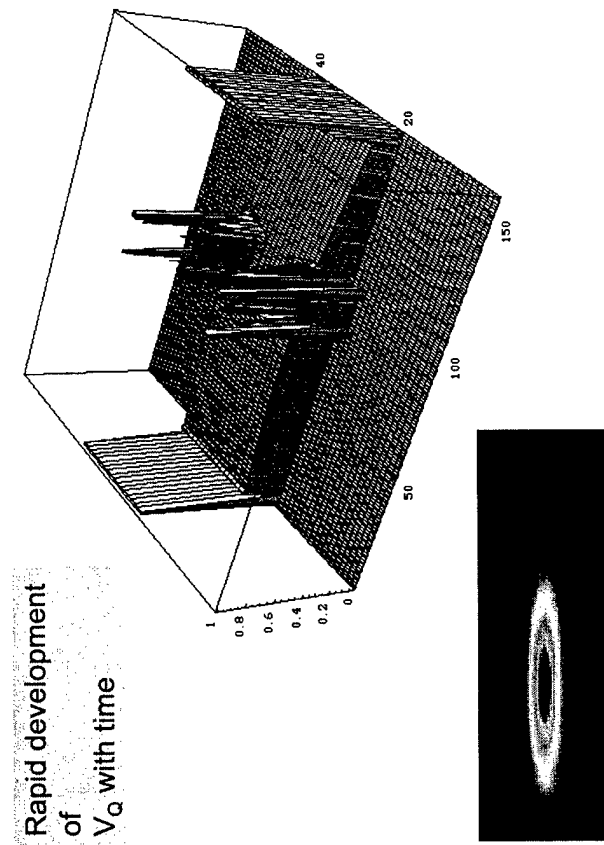
QuickTime™ and a  
Animation decompressor  
are needed to see this picture.

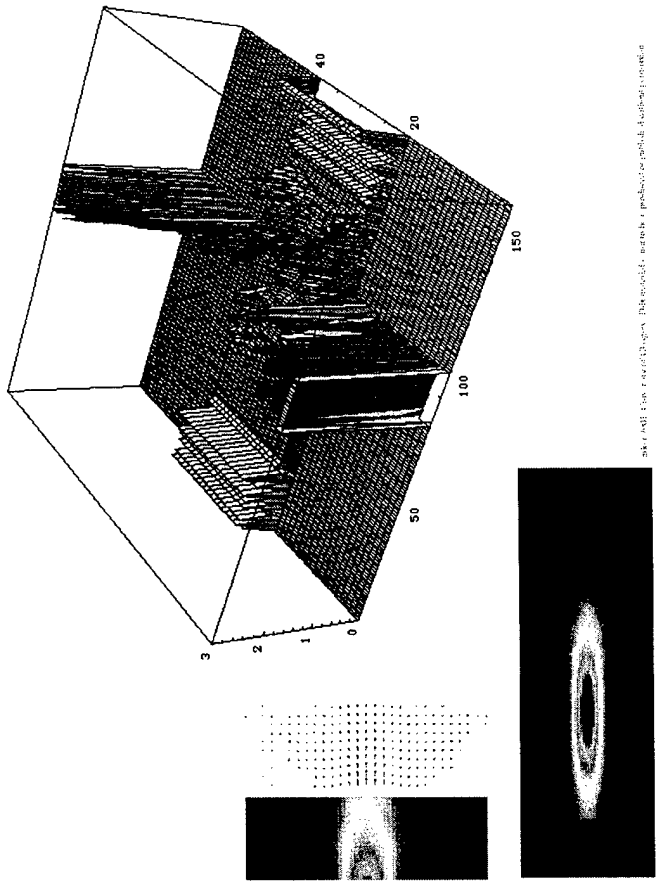
QuickTime™ and a  
Animation decompressor  
are needed to see this picture.

## Current density magnitude transverse across the cavity

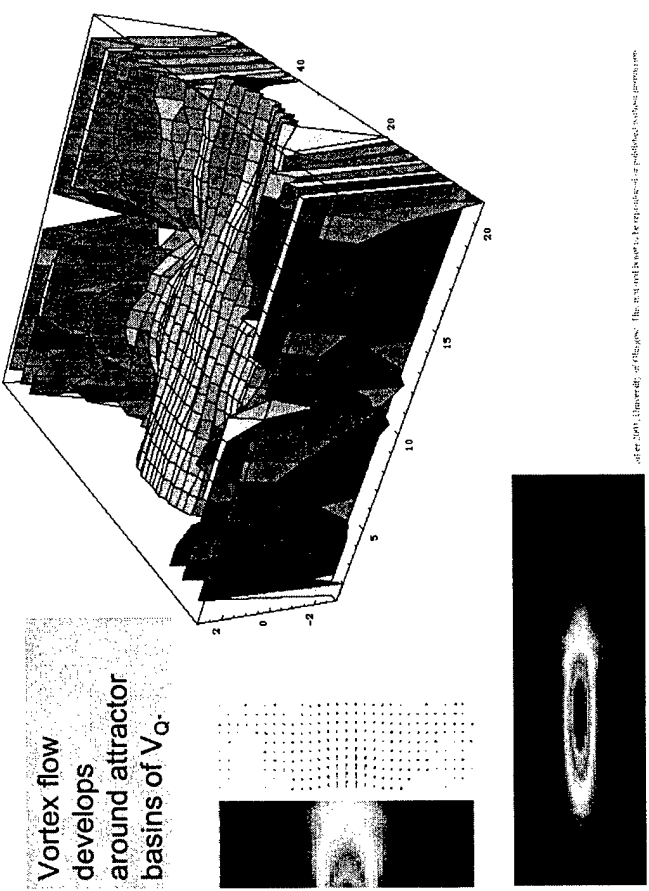


**Rapid development**  
of  
 $V_Q$  with time



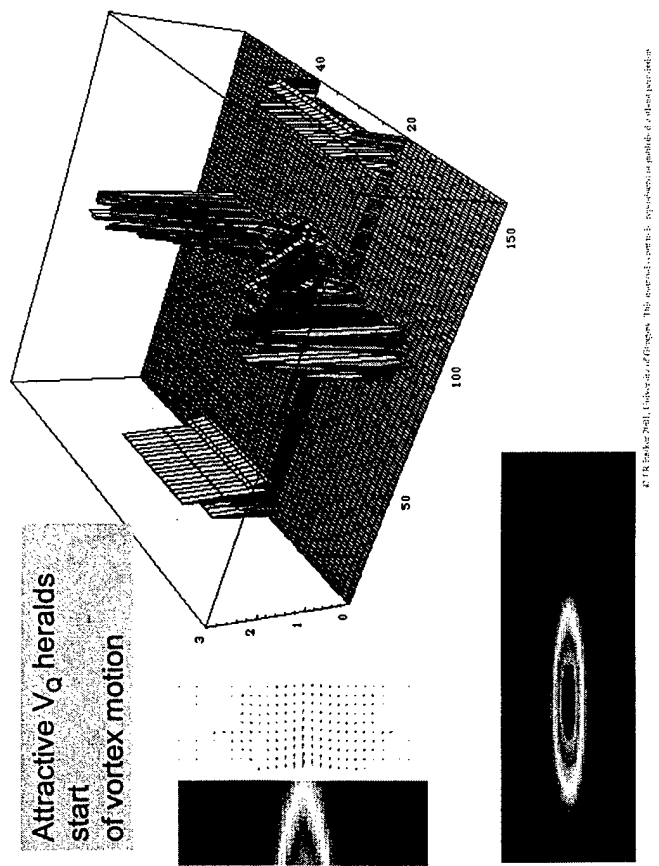


After 2001, University of Cologne. This simulation matches a prediction of a self-excited pattern formation

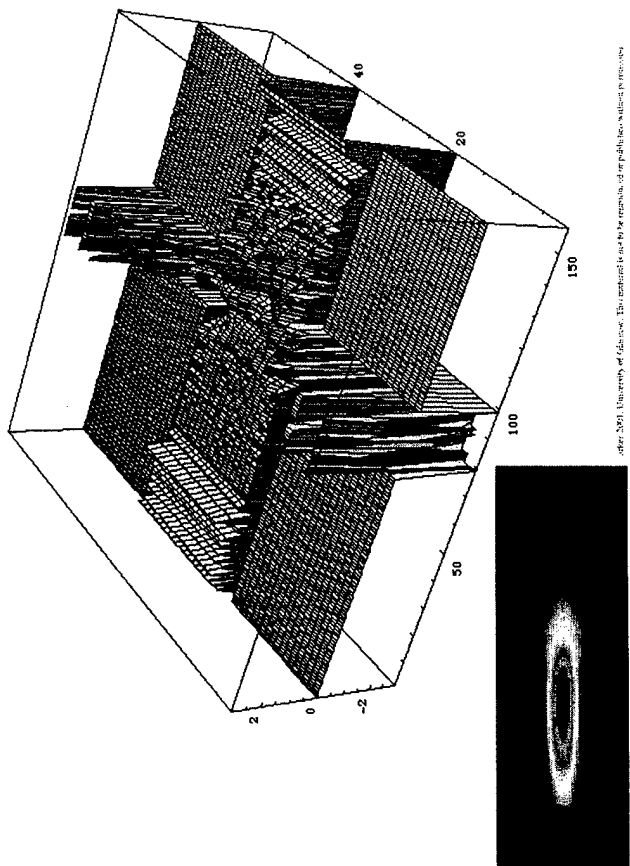


Vortex flow  
develops  
around attractor  
basins of  $V_Q$ .

After 2001, University of Cologne. The simulation matches a prediction of a self-excited pattern formation



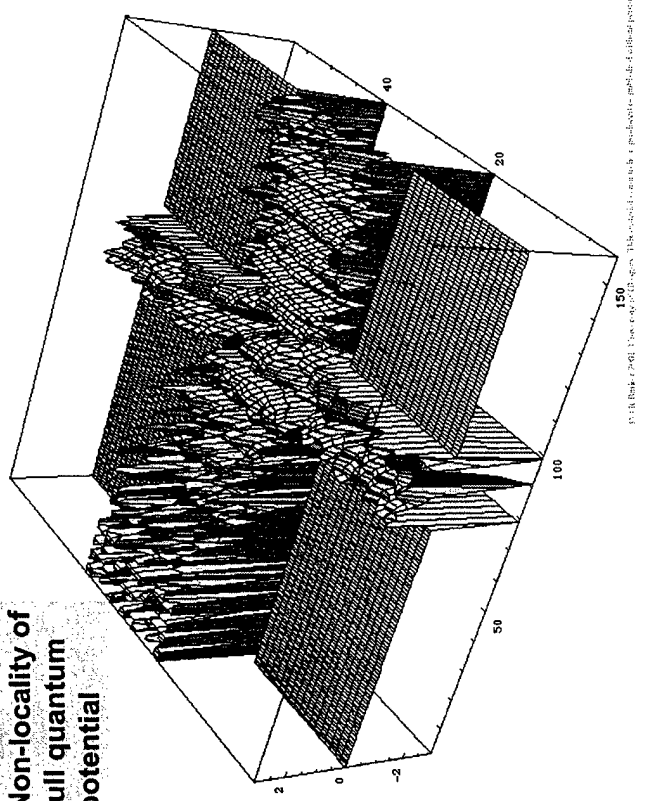
After 2001, University of Cologne. This simulation matches a prediction of a self-excited pattern formation



**Attractive  $V_Q$  heralds  
start  
of vortex motion**

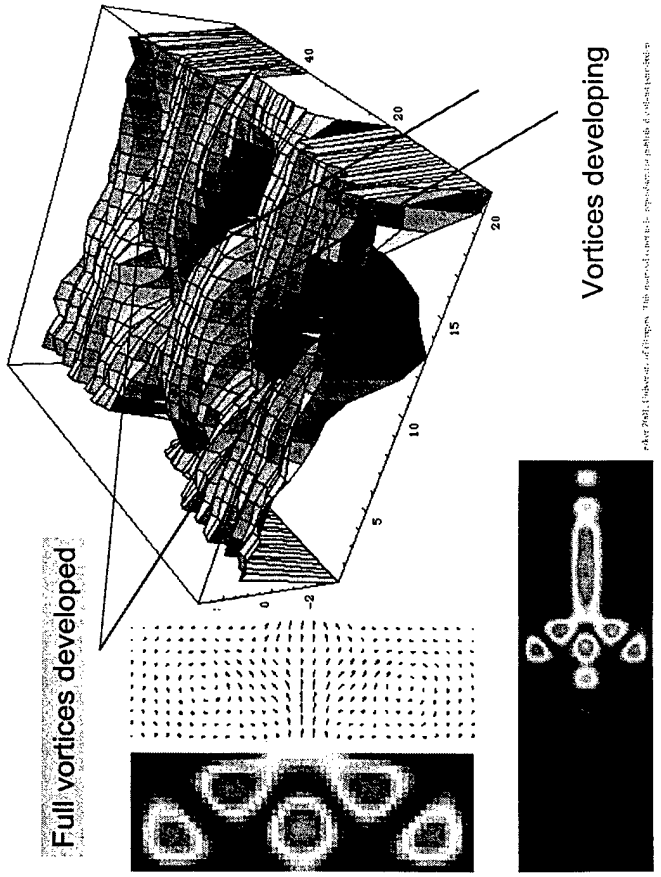
After 2001, University of Cologne. The simulation matches a prediction of a self-excited pattern formation

Non-locality of  
full quantum  
potential



© P. B. Blakie & P.G.L. Drazin. This material is subject to copyright protection by the author(s) and/or the copyright holder(s). It is made available under a Creative Commons Attribution Non-Commercial-ShareAlike 4.0 International license.

Full vortices developed



© P. B. Blakie & P.G.L. Drazin. This material is subject to copyright protection by the author(s) and/or the copyright holder(s). It is made available under a Creative Commons Attribution Non-Commercial-ShareAlike 4.0 International license.

Vortices developing

Angular momentum

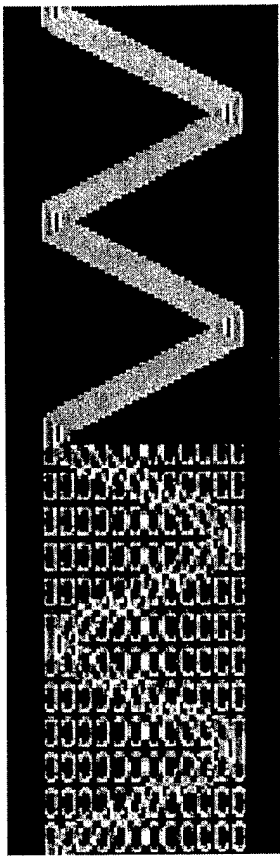
$$\mathbf{L} = \mathbf{r} \times \nabla S$$

$$\mathbf{L}_z = N\hbar$$

$$\mathbf{L}^2 = l^2 + L_Q^2$$

Leads to stability

Example: Wave incident on a 2DEG throttle



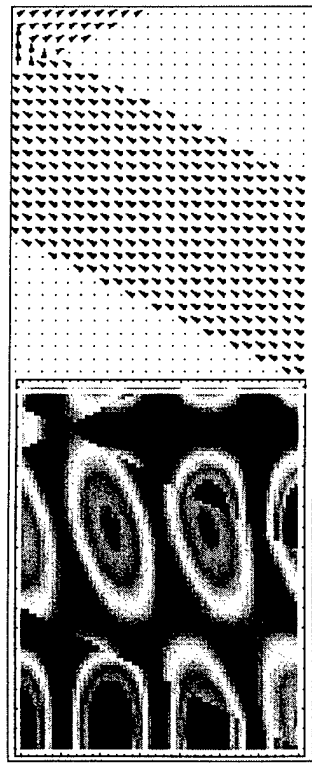
Incident travelling wave in high transverse mode

© P. B. Blakie & P.G.L. Drazin. This material is subject to copyright protection by the author(s) and/or the copyright holder(s). It is made available under a Creative Commons Attribution Non-Commercial-ShareAlike 4.0 International license.

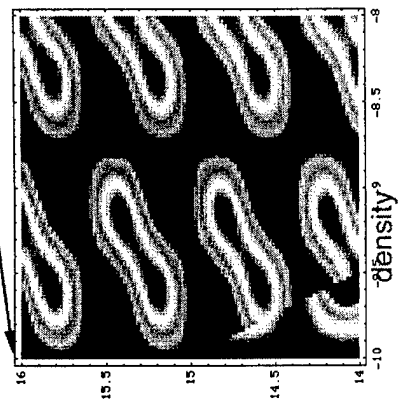
© P. B. Blakie & P.G.L. Drazin. This material is subject to copyright protection by the author(s) and/or the copyright holder(s). It is made available under a Creative Commons Attribution Non-Commercial-ShareAlike 4.0 International license.

## Detail of upstream density and velocity flow

Upstream flow: full form



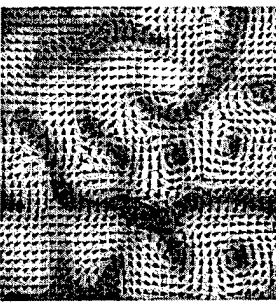
Scattered wave-function  
Ray approximation



© 1998 Kluwer Academic Publishers. This material is based upon work supported by the National Science Foundation under grant number DMR-9505763.

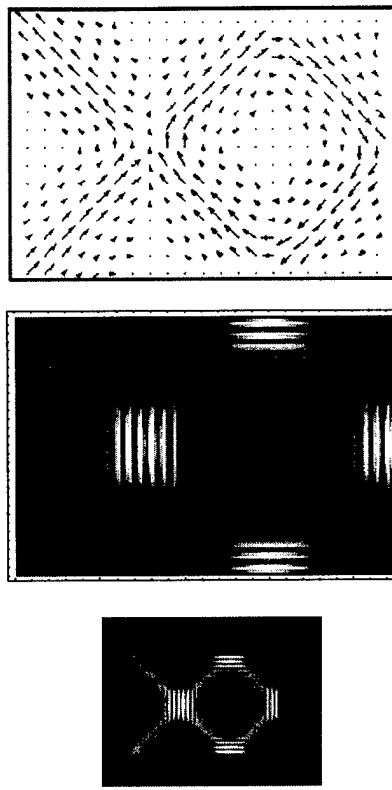
## Quantum Flows

Barker  
Ferry & Akis (2000)

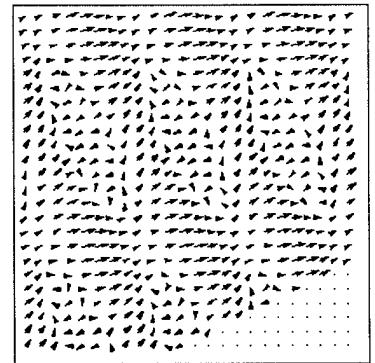


- Velocity field in quantum dot
- Meandering open orbits
- Trapped flows - vortices

Flow of an extended wave packet  
in a double throttle = open quantum dot



© 1998 Kluwer Academic Publishers. This material is based upon work supported by the National Science Foundation under grant number DMR-9505763.



© 1998 Kluwer Academic Publishers. This material is based upon work supported by the National Science Foundation under grant number DMR-9505763.

## A posteriori quantum hydrodynamics

Calculate  $\mathbf{J}$  and  $n$ , form  $\mathbf{v}$

Quantum Euler equations automatically satisfied, including quantization of circulation.

**Ab initio** quantum hydrodynamics

To be of predictive power rather than purely explanatory the velocity flow approach must become *ab initio*.

Quantum Euler equations, + scalar & vector quantum potentials  
A neat way to put QM in Monte Carlo, Hydrodynamic, DD models.

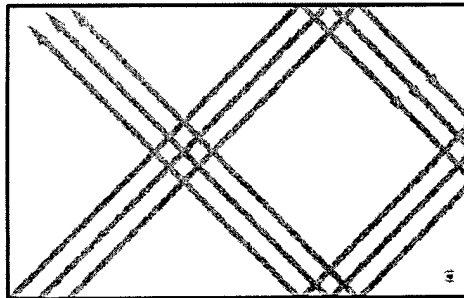
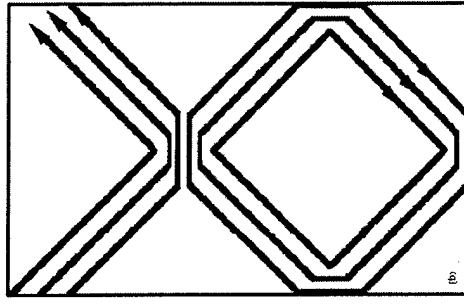
Difficult to solve in general.

© 1994-2001 University of Chicago. This material is subject to copyright protection.

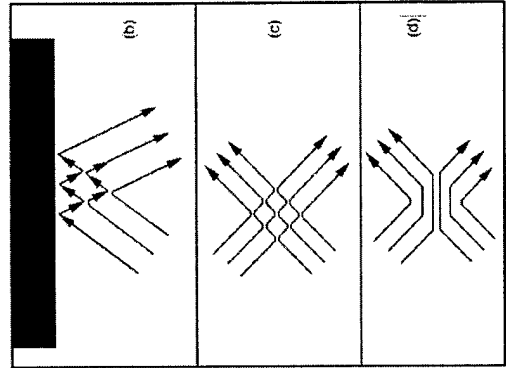
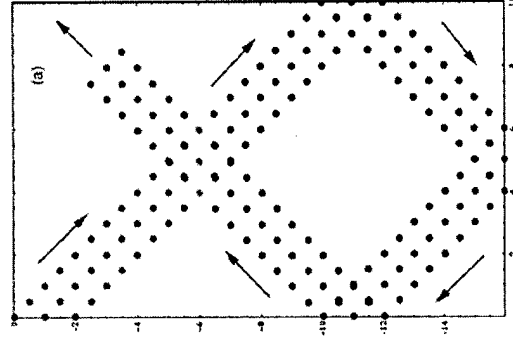
The open quantum dot analysis suggests:  
Can we construct the quantum flow by first

constructing the classical flow and then replacing any trajectory crossing points by flow separation?

## Classical and quantum ray paths



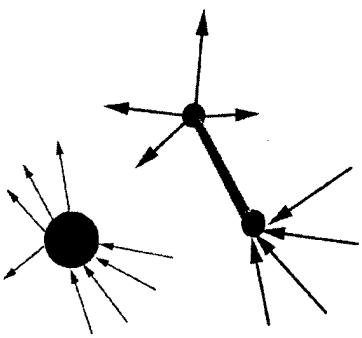
## Spatially correlated virtual particles



## conjecture

## Dissipative quantum hydrodynamics

Conventional QHD has used classical HD model for scattering processes.  
Less empirical approach



Use transient scattered wave or use non-hermitian

Hamiltonian:  
leads to description of trapping/de-trapping,  
elastic and inelastic scattering  
with extended collision zones  
and intra-collisional field effect  
Barker and Ferry, APL 74 582 (1999),  
Barker and Watling, Superlattices and microstructures,  
27, 347 (2000)

New  
Topological  
features

\* Institut für Angewandte Physik, Universität Regensburg, The standard version is copyrighted by Springer-Verlag, Berlin Heidelberg 2009.

## Inelastic Scattering

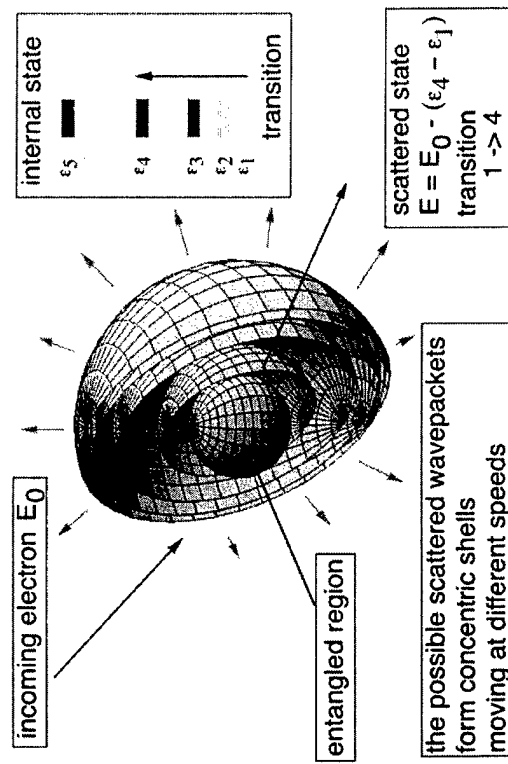
Flow occurs in configuration space  
Electron coordinate  $\mathbf{r}$   
Scatterer generalised coordinate(s)  
 $X, \dots$

Trajectories cannot cross in configuration space.

But trajectories may now cross in real space  
PROVIDED... Scatterer coordinates are different - a new result.

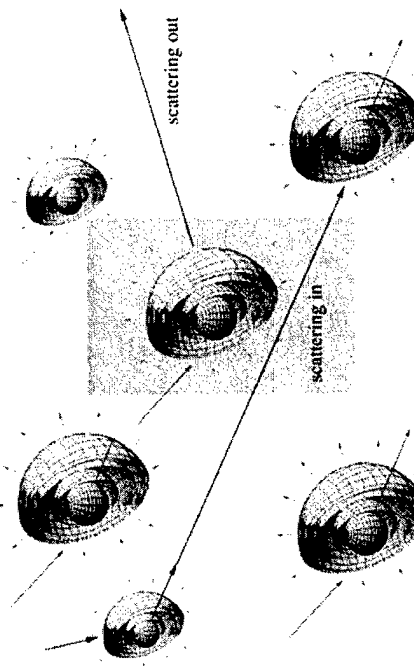
\* Institut für Angewandte Physik, Universität Regensburg, The standard version is copyrighted by Springer-Verlag, Berlin Heidelberg 2009.

## Inelastic Scattering



\* IPB Stuttgart University of Education. This material is subject to copyright. Any use outside of the narrow limits of the copyright law without the permission of the copyright owner is illegal and liable to prosecution.

## Inelastic Scattering



superposition of randomly selected output trajectories > Boltzmann transport theory

10

Dissipation may be shown to leads to crossings of quantum trajectories in the carrier space.

The trajectories in the full phase space do not cross.

Pure state, coherent

$$f(x, p; t) = n(x, t) \delta(p - \nabla S)$$

Pure state developing incoherence

$f \rightarrow$  solution of a BTE-like transport eqn.

corresponds to evolution of mixed states

© 1997 R. Zwier, J. van der Pol, University of Groningen. This material is based upon work supported by the National Science Foundation under grant No. DMR-9522273.

Recall the temperature tensor: the covariance matrix of the velocity

$$k\mathbf{T} = m <(\mathbf{v} - \mathbf{V})(\mathbf{v} - \mathbf{V})>$$

Taking quantum mechanical averages this is just:

$$kT_Q = m <\mathbf{v}\mathbf{v}> - m <\mathbf{V}\mathbf{V}>$$

Choosing  $N = 3$  we get

$$\frac{\partial(nP)}{\partial t} + \frac{\partial(nU_0)}{\partial x} + n \frac{\partial}{\partial x} (\varphi + V_Q) = 0 \quad U_0 = mV^2$$

$$U = U_0 + kT_Q$$

which is essentially the finite temperature QHD result

$$NkT_Q = mV^2 + 2V_Q - mV^2 = 2V_Q$$

$$(N = 1, 2, 3)$$

A more detailed examination of the closure relations indicates further reconciliation of the two pictures although the finite temperature case involves coupling to a full hierarchy of moment equations.

## Comparison between finite temperature mixed state quantum hydrodynamics and pure state QHD (vortex free)

$$\boxed{\frac{\partial(nP)}{\partial t} + \frac{\partial(nU)}{\partial x} + n \frac{\partial}{\partial x} (\varphi + \frac{1}{3}V_Q) = 0} \quad U = mV^2 + kT$$

$$\boxed{\frac{\partial(nP)}{\partial t} + \frac{\partial(nU_0)}{\partial x} + n \frac{\partial}{\partial x} (\varphi + V_Q) = 0}$$

Paradox: Pure state is not zero temperature limit?

© 1997 R. Zwier, J. van der Pol, University of Groningen. This material is based upon work supported by the National Science Foundation under grant No. DMR-9522273.

© 1997 R. Zwier, J. van der Pol, University of Groningen. This material is based upon work supported by the National Science Foundation under grant No. DMR-9522273.

© 1997 R. Zwier, J. van der Pol, University of Groningen. This material is based upon work supported by the National Science Foundation under grant No. DMR-9522273.

## Mixed states

For mixed states, existing quantum hydrodynamic and density gradient models are not complete.

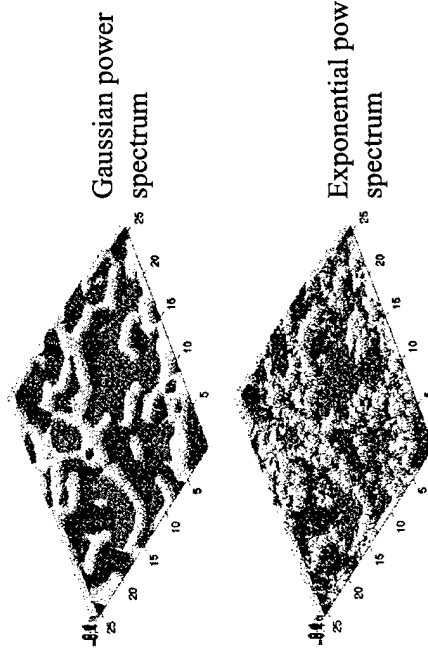
If vortex formation may be ignored then empirical quantum potential is the most pragmatic approach.

However, if coherent flow occurs with scattering off more than one obstacle we expect vortex flows and QHD and DD needs to be solved under the constraint of a generalised velocity circulation theorem By solving for nodal lines and computing the Vector quantum potential.

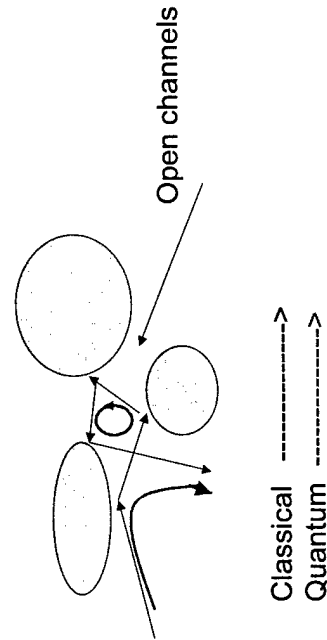
© J.P. Boffetier 2001, Université de Bretagne, Brest, France. This material is subject to copyright protection by the author(s) and/or other rights holders.

© J.P. Boffetier 2001, Université de Bretagne, Brest, France. This material is subject to copyright protection by the author(s) and/or other rights holders.

## Digitisation of the Si/SiO<sub>2</sub> interface topology



Possibility of  
Diffraction, interference effects-> vortex flows  
And meandering orbits.



© J.P. Boffetier 2001, Université de Bretagne, Brest, France. This material is subject to copyright protection by the author(s) and/or other rights holders.

© J.P. Boffetier 2001, Université de Bretagne, Brest, France. This material is subject to copyright protection by the author(s) and/or other rights holders.

## Application to MOS device modelling

At Glasgow, we have begun a systematic inclusion of quantum effects into finite MOSFET models at decanano dimensions.

The first level uses a phenomenological quantum potential model.

The effect is to keep charge away from interfaces and to induce some tunnelling effects.

## Conclusions

- Quantum flow formalism is close to spirit of drift diffusion and hydrodynamic models.
  - Vortex motion is ubiquitous
  - In the immediate future, density gradient QHD may be parameterised from deeper quantum simulations in analogy with using BTE to re-parameterise Drift Diffusion and HD models beyond their normal range of validity.

# Coulomb correlations in semiconductors and transient phenomena.

## Nonequilibrium Greens functions and beyond

### Outline

1. Introduction: Coulomb correlations in semiconductors
2. Short-time phenomena and Initial correlations
3. Nonequilibrium Greens functions:
  - main ideas
  - application to optics and high field transport
4. Strong correlations in semiconductors:
  - excitons, biexcitons, electron-hole liquid
  - Wigner crystal
5. Summary and Outlook

*Michael Bonitz, Universität Rostock*

Workshop „Quantum Transport in Semiconductors“

Moritzburg, June 17-22, 2004

© Michael Bonitz, all rights reserved

In collaboration with

1. Dirk Semkat (Rostock), Nai Kwong, Sigurd Köhler, Rolf Binder (Tucson)
2. Antigoni Alexandrou (Paris/Seoul)
3. Hartmut Haug (Frankfurt), Ronald Redmer, Justino Madureira (Rostock)
4. Vladimir Filinov (Moscow), Stephan Koch, Walter Hoyer (Marburg)
5. Alexei Filinov, Yuri Lozovik (Moscow)

## Coulomb correlations in semiconductors

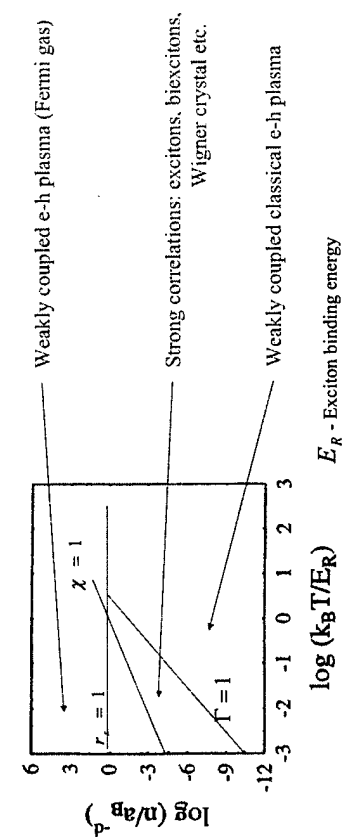
Coulomb interaction between electrons / holes  $U(r) = \pm e^2/r$

Coupling strength: Ratio of Interaction energy/kinetic energy

$$\Gamma \equiv \langle U(r) \rangle / k_B T \quad r_s \equiv \langle U \rangle / E_F \propto \langle r \rangle / a_B$$

$E_F$  - Fermi energy  $a_B$  - exciton Bohr radius

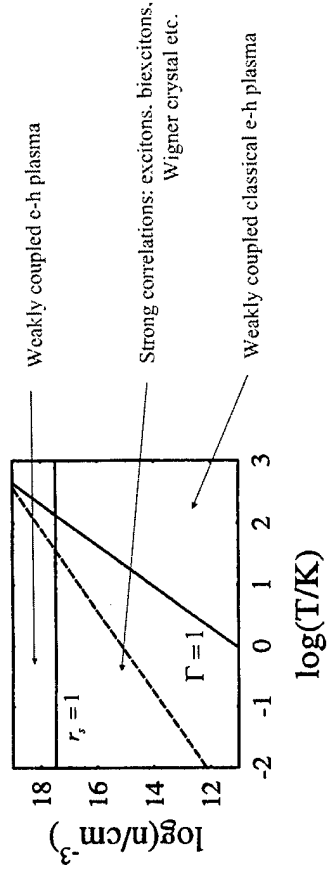
Quantum degeneracy:  $\chi \equiv n\lambda^d$   $\lambda$  - electron quantum wave length, d - dimension



## Coulomb correlations in insulators

$\Gamma \equiv \langle U(r) \rangle / k_B T$   $r_s \equiv \langle r \rangle / a_B$

$$\begin{aligned} \Gamma &\equiv \langle U(r) \rangle / k_B T & r_s &\equiv \langle U \rangle / E_F \propto \langle r \rangle / a_B \\ \chi &\equiv \langle U \rangle / E_F \propto \langle r \rangle / a_B & E_F &- Fermi energy \quad a_B - exciton Bohr radius \\ \lambda &- electron quantum wave length & \lambda &- electron Bohr radius \end{aligned}$$



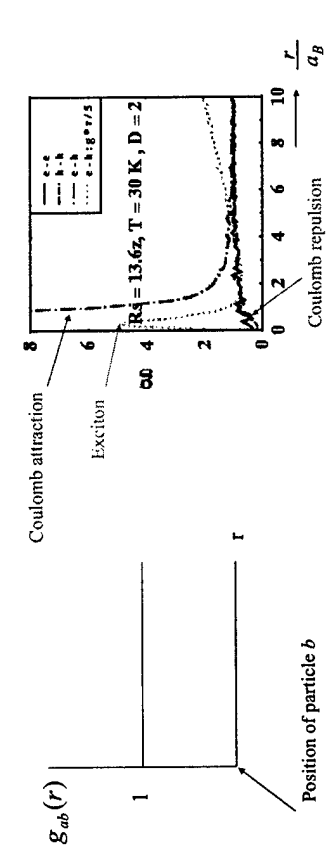
## Statistical treatment of correlations

→ Pair distribution function  $g_{ab}(r)$  ; a,b - electrons, holes

= probability of finding particle  $a$  at distance  $r$  from particle  $b$

$$\text{Normalization: } \int g_{ab}(r) dV = 1 \quad \text{Interaction energy: } \langle U \rangle = \int U(r) g_{ab}(r) dV$$

Non-interacting particles



Interacting 2D e-h plasma



Pair correlation function:  $c_{ab}(r) \equiv g_{ab}(r) - 1$

## Relaxation processes in electron-hole systems

Pre-excited e-h plasma (doping/prepulse,  
correlated contacts etc.)

Initially correlated e-h ensemble  
 $t = t_0$

Excitation: e.g. optical or electric field

Finite duration  
 $\Delta\tau_{exc}$

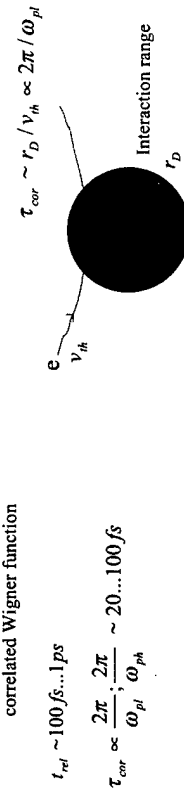
Creation of nonequilibrium electrons/holes

Decay of initial correlations  
Correlation buildup  
 $t \leq \tau_{corr}$

Relaxation towards equilibrium/stationary state  
due to scattering processes (collisions)

Formation of stationary distribution  $f^{EQ_{e,h}}$ :  
 $t \leq t_{rel}$

Example: buildup of Coulomb correlations/screening  
e-h pairs created uncorrelated



## When are initial correlations important?

Transient processes before stationary state

1. Short times:  $t_0 \leq t \leq \tau_{corr}$  (Or high-frequency switching:  $\omega_s \geq 2\pi/\tau_{corr}$ )

2. Strongly correlated initial state:  $|\langle U_{corr} \rangle| (t_0) \geq \langle E_{kin} \rangle (t_0)$

- materials with strong electron-phonon coupling
- materials with strong Coulomb interaction

In this case also:  $\tau_{corr} \geq t_{rel}$

3. „bottle neck“ situations, threshold processes:

- carrier excitation below phonon energy, impact ionization etc.
- modified plasmon spectrum in p-doped semiconductors

4. Long-living initial correlations: e.g. bound states (excitons, impurities etc.), Wigner crystal, Bose condensate etc.

- weak damping (slow decay) of initial correlations

## Idea of Green's functions

1. Classical N-body system: statistical properties given by distribution function  $f(r, p, t)$

$$\int \frac{d^3 p}{(2\pi\hbar)^3} f(r, p, t) = n(r, t), \quad \int d^3 r n(r, t) = N(t)$$

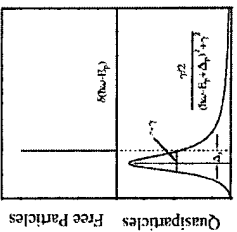
2. Quantum N-body system:

$$\begin{cases} - Wigner („quasi“)-distribution function  $f(r, p, t)$  \\ - Wave properties, energy „spectrum“  $A(E)$  \end{cases}$$

Idea: combine into „generalized distribution“  $g(r, p, t; E)$

E - independent variable

Green's function



Equilibrium:  $g(p; E) = if(E)A(p, E), \quad f(E) = 1/(e^{\beta(E-\mu)} + 1)$

- non-interacting particles:  $A(p, E) = 2\pi \delta(E - p^2/2m)$

- interacting (correlated) particles:  $A(p, E) \propto \frac{\gamma^{1/2}}{(E - p^2/2m + \Delta)^2 + \gamma^2}$

Correlated Wigner distribution  $g(p)$

Finite line width (finite life time), related to pair correlations  $g(r)$

Correlations included into single-particle properties (quasi-particle)

## Nonequilibrium Green's functions

Spectral function of interacting electrons

$g(r, p, t; E)$  Equivalent to function of two-times:

$$\text{I. Fourier transform: } \int dE g(r, p, t; E) e^{iEt/\hbar} \rightarrow g(r, p, t, \tau)$$

$$\text{II. Define } t_{1,2} = t \pm \tau/2 \quad \rightarrow g(r, p, t_1, t_2)$$

III. Build in spin: relate  $g$  to fermion field operators:

$$\psi^+(r, t), \psi(r, t), \psi^*(r_1, t), \psi(r_1 - r_2)$$

Anticommutation:  $\psi^*(r_1, t)\psi(r_2, t) + \psi(r_2, t)\psi^*(r_1, t) = \delta(r_1 - r_2)$

IV. Two-operator averages – two possibilities:  $\langle \psi^*(2)\psi(1) \rangle \rightarrow g^<(1,2); 1 \equiv r_1, t_1, s_1$   
 (two independent functions)

$$\langle \psi(1)\psi^*(2) \rangle \rightarrow g^>(1,2)$$

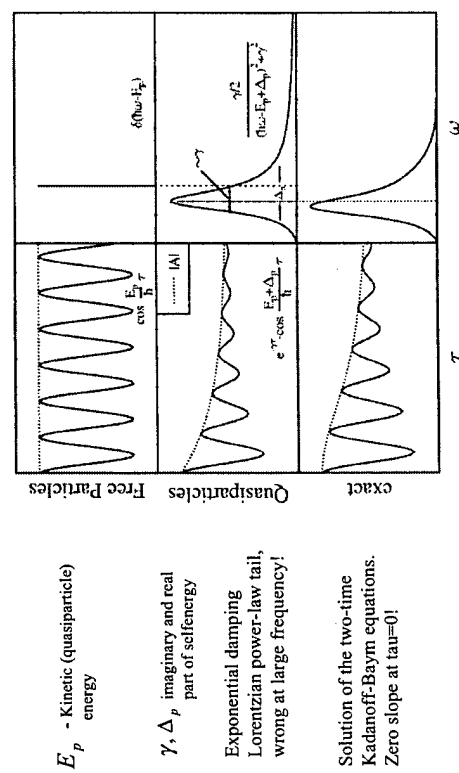
V. Physical contents: on time diagonal:  $g^<(r_1, t, r_2, t) \propto f(r_1, r_2, t)$  Density matrix,  
 Wigner distribution etc.

Across diagonal:  $g^>(1,2) - g^<(1,2) \propto A(1,2)$  Spectral function,  
 Density of states etc.

VI. Heisenberg equations for  $\psi^*, \psi$   $\rightarrow$  (Kadanoff-Baym/Keldysh) equations of motion for  $g^>, g^<$

→ Fully selfconsistent treatment of relaxation, correlations and energy spectrum

→ Clear recipe for treatment of complex processes and systematic approximations



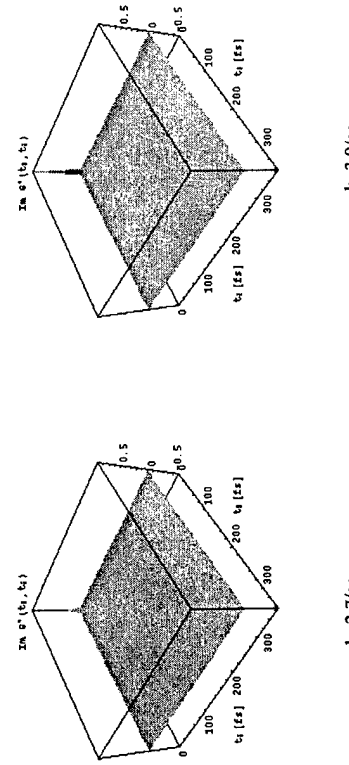
## Direct Solution of the Kadanoff-Baym equations

Exact spectral function with Coulomb scattering

Imaginary part of  $g^<(k, t_1, t_2)$  for fixed momentum  $k$

1. Relaxation of nonequilibrium electron distribution (peaked at  $k=3.9/\text{ao}$ )

2. Build up of electron spectrum (of Coulomb correlations) across time diagonal



Homogeneous bulk GaAs  $n = 10^{17} \text{ cm}^{-3}$

$k=2.7/\text{ao}$

$k=3.9/\text{ao}$

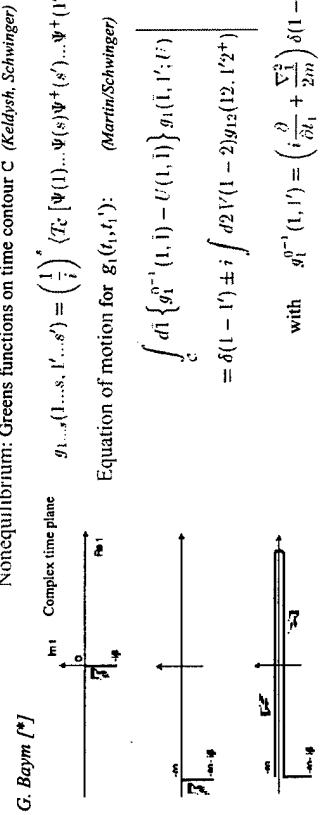
Dirk Semkat/Michael Bonitz

Semkat/Kwong/Köhler/Binder/MB

## Kadanoff-Baym equations with initial correlations

*Kadanoff-Baym equations with initial correlations, contd.*

N-particle system, binary interaction  $V(\mathbf{r})$ , external potential  $U(\mathbf{r})$



Nonequilibrium: Greens functions on time contour C (Keldysh, Schwinger)

Condition:  $\lim_{t_1 \rightarrow t_0 + i -\infty} g_{1...s}(1, \dots, s, t_1, \dots, t_s) = \left(\frac{1}{i}\right)^s \langle T_C [\Psi(1) \dots \Psi(s)] \Psi^+(s') \dots \Psi^+(1') \rangle$

Equation of motion for  $g_1(t_1, t_1')$ : (Martin/Schwinger)

$$\int_C d\bar{t} \left\{ g_1^{0-1}(1, \bar{t}) - U(1, \bar{t}) \right\} g_1(\bar{t}, 1'; \bar{t}')$$

$$= \delta(1 - 1') \pm i \int d2 V(1 - 2) g_{12}(12, 1'2')$$

$$\text{with } g_1^{0-1}(1, 1') = \left( i \frac{\partial}{\partial t_1} + \frac{\nabla_1^2}{2m} \right) \delta(1 - 1')$$

$$+ c(\mathbf{r}_1, \mathbf{r}_2, \mathbf{r}_1', \mathbf{r}_2', t_0)$$

$$+ \Sigma^{HF}(1, 1') + \Sigma^c(1, 1') + \Sigma^{in}(1, 1')$$

$$\Sigma^{in}(1, 1') = \Sigma^{in}(1, \mathbf{r}_1' t_0) \delta(t_1' - t_0)$$

\* In: „Progress in Nonequilibrium Green's functions“, M. Bonitz (Ed.), 2000

Semkat, Kremp, Bonitz 1999, 2000

Haug/Jauho „Quantum Kinetics...“

Non-equilibrium: Greens functions on time contour C (Keldysh, Schwinger)

Condition:  $\lim_{t_1 \rightarrow t_0 + i -\infty} g_{1...s}(12, 1'2')|_{t_0} = [g_1(1, 1')g_1(2, 2') \pm g_1(1, 2)g_1(2, 1')]|_{t_0}$

$$+ c(\mathbf{r}_1, \mathbf{r}_2, \mathbf{r}_1', \mathbf{r}_2', t_0)$$

Equation of motion for  $g_1(t_1, t_1')$ :

$$\delta(1 - 1') + \int_C d\bar{t} [\Sigma^r(1, \bar{t}) + \Sigma^{in}(1, \bar{t})] g_1(\bar{t}, 1')$$

\* In: „Progress in Nonequilibrium Green's functions“, M. Bonitz (Ed.), 2000

Semkat, Kremp, Bonitz 1999, 2000

Haug/Jauho „Quantum Kinetics...“

Formal closure of hierarchy (generalized\*): introduce selfenergy

$$\begin{aligned} \int_C d\bar{t} \Sigma(1, \bar{t}) g_1(\bar{t}, 1') &= \pm i \int d2 V(1 - 2) g_{12}(12, 1'2') \\ &= \pm i \int d2 V(1 - 2) \left\{ \pm \frac{\delta g_1(1, 1'; \bar{t})}{dU(2+, 2)} + g_1(1, 1') g_1(2, 2') \right\} \end{aligned}$$

Boundary condition:

$$\lim_{t_1 \rightarrow t_0 + i -\infty} \int_C d\bar{t} \Sigma(1, \bar{t}) g_1(\bar{t}, 1') = \pm i \int d2 V(\mathbf{r}_1 - \mathbf{r}_2) [c(\mathbf{r}_1, \mathbf{r}_2, \mathbf{r}_1', \mathbf{r}_2', t_0) \\ + g_1(\mathbf{r}_1, \mathbf{r}_1', t_0) g_1(\mathbf{r}_2, \mathbf{r}_2', t_0)]$$

Result: additional selfenergy contribution

$$\begin{aligned} \Sigma(1, 1') &= \Sigma^{HF}(1, 1') + \Sigma^c(1, 1') + \Sigma^{in}(1, 1') \\ \Sigma^{in}(1, 1') &= \Sigma^{in}(1, \mathbf{r}_1' t_0) \delta(t_1' - t_0) \end{aligned}$$

\*Semkat, Kremp, MB, J. Math. Phys., 41, 7458 (2000)

## Generalized Kadanoff-Baym equations

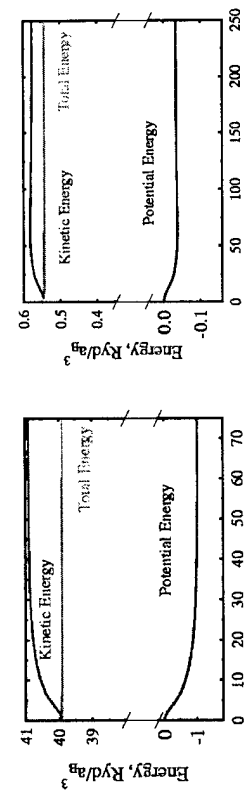
*Short-time relaxation with initial correlations*

Solution of KB-equations with initial correlation selfenergy

Example: bulk GaAs, uncorrelated vs. over-correlated initial state

- Correct conservation of total energy (kinetic + correlation)

- Energy relaxation reflects correlation build up/decay for  $t \leq \tau_{cor}$



Selfconsistent evolution and decay of initial correlations

*Short-time relaxation with initial correlations*

Solution of KB-equations with initial correlation selfenergy

Example: bulk GaAs, uncorrelated vs. over-correlated initial state

- Correct conservation of total energy (kinetic + correlation)

- Energy relaxation reflects correlation build up/decay for  $t \leq \tau_{cor}$

$$\begin{aligned} \text{Result: } \int_C d\bar{t} [g_1^{0-1}(1, \bar{t}) - U(1, \bar{t}) - \Sigma^{HF}(1, \bar{t})] g_1(\bar{t}, 1') \\ = \delta(1 - 1') + \int_C d\bar{t} [\Sigma^r(1, \bar{t}) + \Sigma^{in}(1, \bar{t})] g_1(\bar{t}, 1') \end{aligned}$$

Matrix equations on the time contour

Result on the physical (real) time axis:

$$\begin{aligned} \left( i \frac{\partial}{\partial t_1} + \frac{\nabla_1^2}{2m} \right) g_1^2(1, 1') - \int d2 V(1, \bar{t}) g_1^2(\bar{t}, 1') - \int d\bar{t}_1 \Sigma^{HF}(1, \bar{t}) g_1^2(\bar{t}, 1') \\ = \int_{t_0}^{\infty} d\bar{t} \Sigma^R(1, \bar{t}) g_1^2(\bar{t}, 1') + \int_{t_0}^{\infty} d\bar{t} [\Sigma^r(1, \bar{t}) + \Sigma^{in}(1, \bar{t})] g_1^2(\bar{t}, 1') \end{aligned}$$

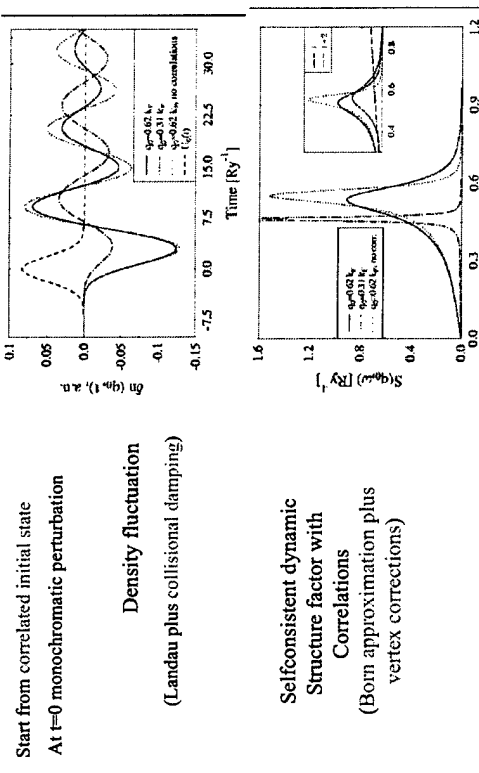
Result for selfenergy:

$$\begin{aligned} \Sigma^{in}(1, 1') &= \pm i \int d2 V(1 - 2) \int d\bar{t}_1 d\bar{t}_2 d\bar{t}_1' d\bar{t}_2' \\ &\times g_{12}^R(12, \bar{t}_1 t_0, \bar{t}_2 t_0) c(\bar{t}_1 t_0, \bar{t}_2 t_0, 1', \bar{t}_1' t_0, 2') \delta(t_1' - t_0) \end{aligned}$$

$n = 0.277 a_B^{-3}$  (intermediate coupling)  
 $n = 2.77 a_B^{-3}$  (weak coupling)

## Dynamic Structure factor of interacting electrons

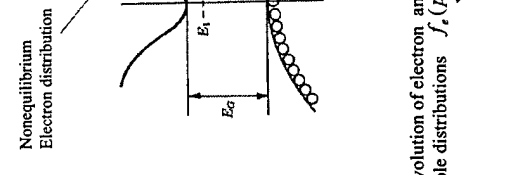
Solution of inhomogeneous Kadanoff-Baym Equations



Kwong, Bonitz, Phys. Rev. Lett. **84**, 1768 (2000)

## Electron dynamics in semiconductors

Example: Optical Excitation



## Interband-Kadanoff-Baym equations

$\mu_1, \mu_2$  – Band indices,  $E_\mu(p)$  – Semiconductor band structure

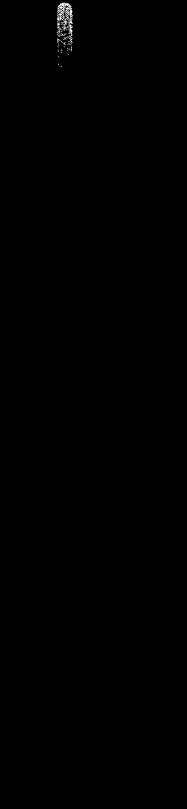
$$\begin{aligned} & \left\{ i\hbar \frac{\partial}{\partial t_1} - \epsilon_{\mu_1} \right\} g_{\mu_1 \mu_2}^>(t_1, t_2) - \sum_{\vec{\mu}} \hbar \Omega_{\mu_1 \vec{\mu}}(t_1) g_{\vec{\mu} \mu_2}^>(t_1, t_2) = I_{\mu_1 \mu_2}^>(t_1, t_2) \\ & \left\{ -i\hbar \frac{\partial}{\partial t_2} - \epsilon_{\mu_2} \right\} g_{\mu_1 \mu_2}^>(t_1, t_2) - \sum_{\vec{\mu}} g_{\mu_1 \vec{\mu}}^>(t_1, t_2) \hbar \Omega_{\vec{\mu} \mu_2}(t_2) = -I_{\mu_2 \mu_1}^>(t_2, t_1) \\ & \hbar \Omega_{\mu_1 \mu_2}(t) = -\mathbf{d}_{\mu_1 \mu_2} \mathcal{E}(t) (1 - \delta_{\mu_1 \mu_2}) + i\hbar \sum_{\vec{\mu}} g_{\mu_1 \vec{\mu}}^<(k' t) V_{\mu_1 \mu_2}(k - k') \end{aligned}$$

Dipole moment      Laser field      Hartree-Fock mean field

Kwong, Bonitz, Binder, Köhler, phys. stat. sol. (b) **206**, 197 (1998)

3.2.

3. Nonequilibrium Greens functions:  
- application to optics and high field transport

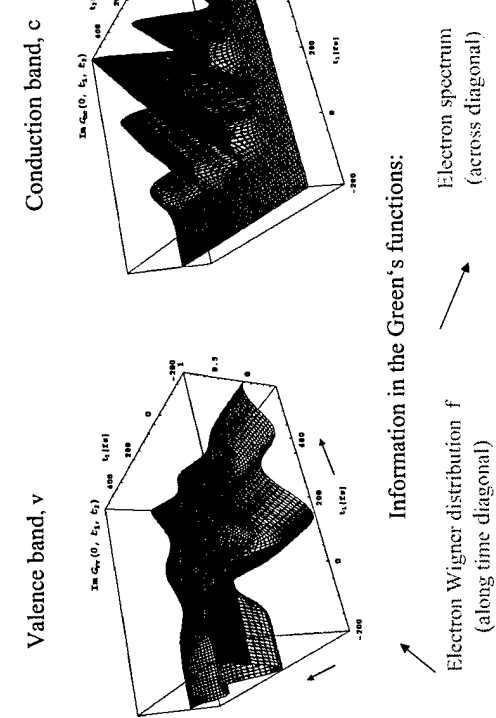
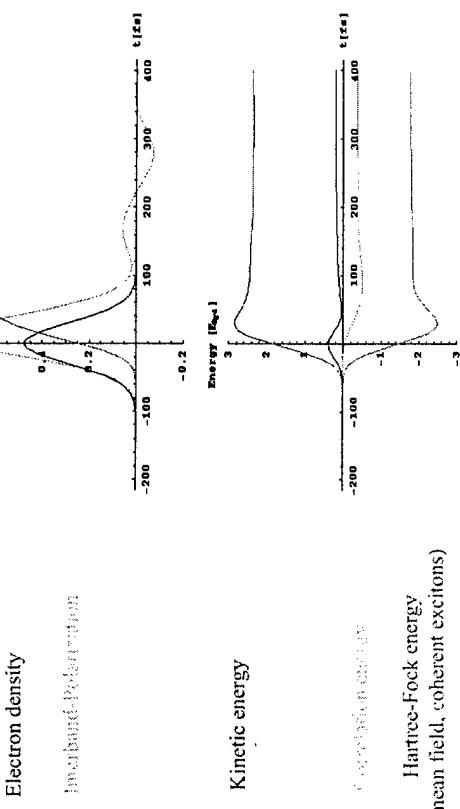


## Laser pulse excitation of a s.c. quantum well

### *Electron dynamics in a semiconductor*

Laser „lifts“ Electrons from valence band to conduction band

(50fs-Pulse, Maximum at t=0)

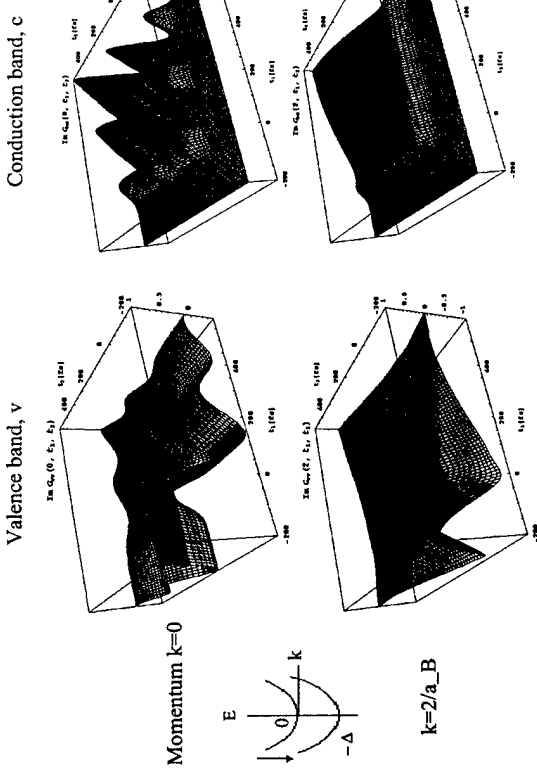


Hartree-Fock energy  
(mean field, coherent excitons)

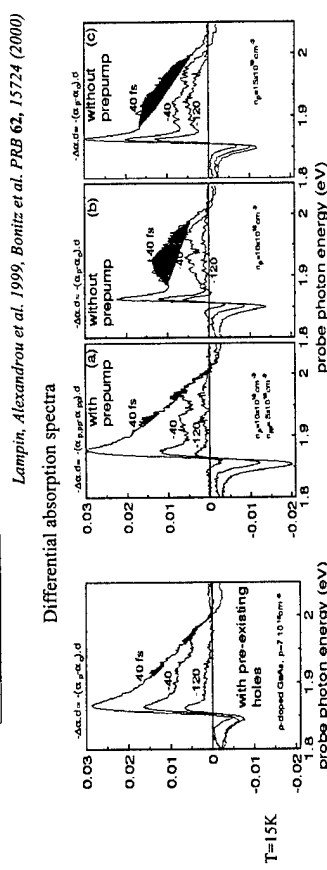
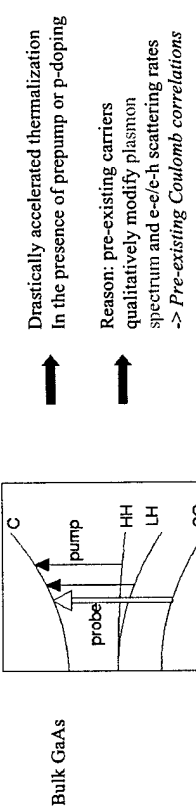
Information in the Green's functions:  
Electron Wigner distribution  $f$   
(along time diagonal)

Information in the Green's functions:  
Electron spectrum  
(across diagonal)

## Damping of the Electrons and Renormalization of the energy bands

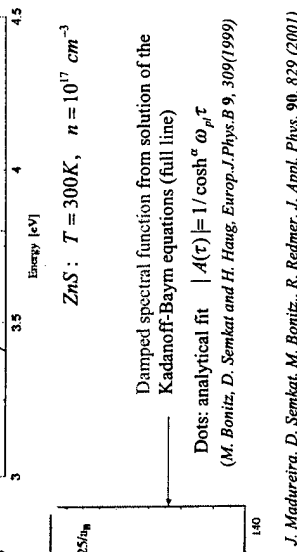
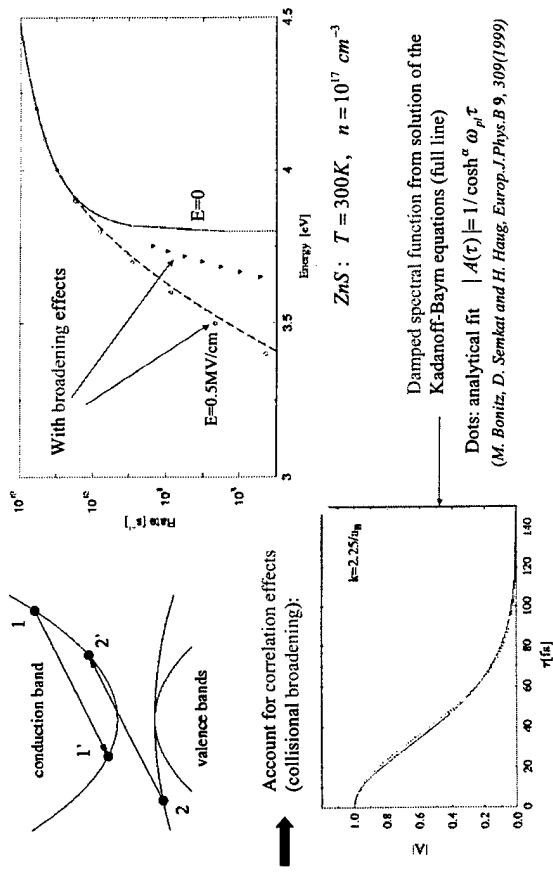


## Relaxation in the presence of preexcited electrons/holes



Lampit, Alexandrou et al. 1999, Bonitz et al. PRB 62, 15724 (2000)

## Impact Ionization rates in semiconductors



J. Madureira, D. Semkat, M. Bonitz, R. Redmer, J. Appl. Phys. **90**, 829 (2001)

## Strong Coulomb correlations

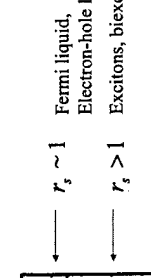
$$\Gamma \equiv \langle U \rangle / k_B T$$

$$r_s \equiv \langle U \rangle / E_F \propto <r> / a_B$$

$$E_F - \text{Fermi energy}$$

Expected behavior:

$$r_s \ll 1 \quad \text{Fermi gas}$$



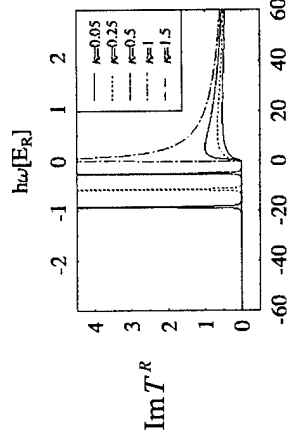
- $r_s \sim 1$  Fermi liquid, Electron-hole liquid
- $r_s > 1$  Excitons, biexcitons
- $r_s \geq 37$  Electron Wigner crystal
- Non-perturbative theories needed

- Greens functions: ladder diagrams
- Path integral Monte Carlo
- Quantum Molecular Dynamics

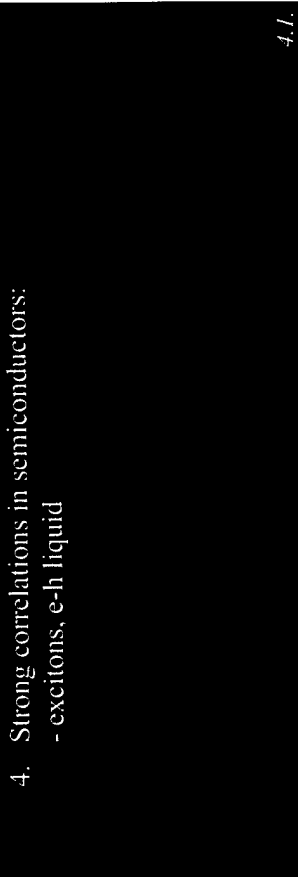
## Greens functions treatment of Strong Coulomb correlations

Problem: strong Coulomb correlations, bound states, exciton formation etc.  
not possible in Born approximation

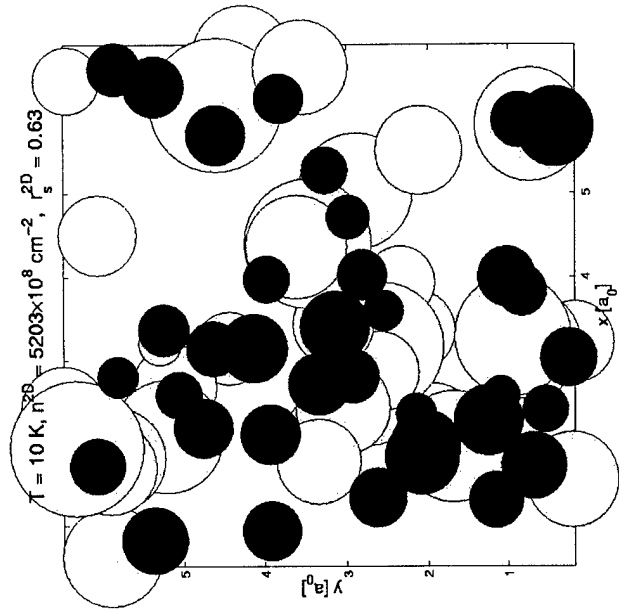
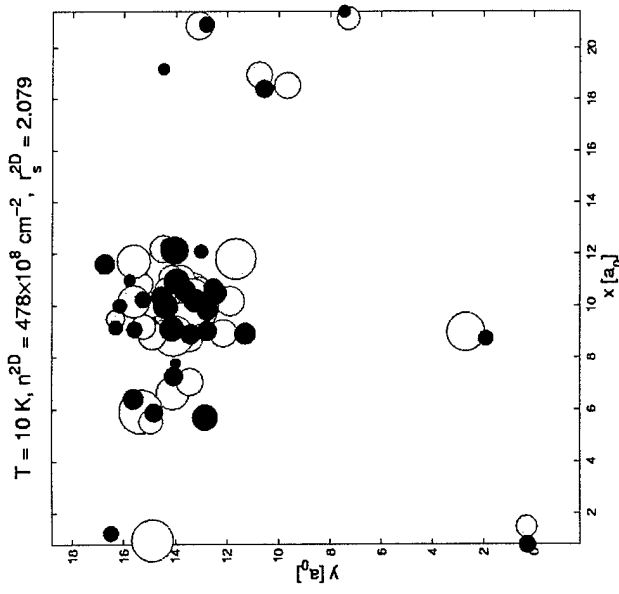
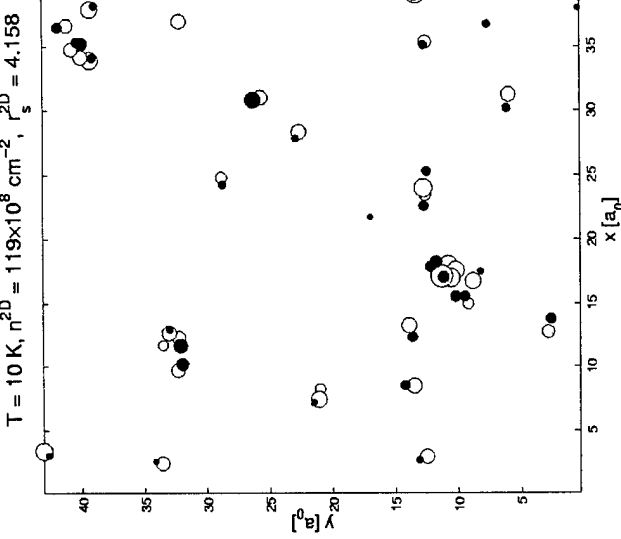
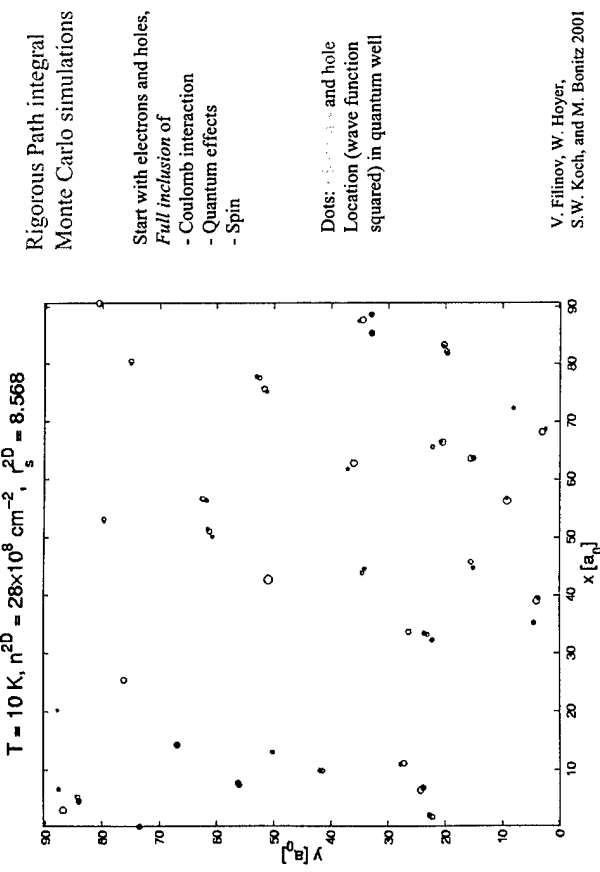
- Need selfenergies in T-matrix (ladder) approximation
- Electron spectrum: continuum and bound states



- Screening parameter  $\kappa = 4\pi me^2 / kT$
- Semkat, Bonitz, Kramp (2001)

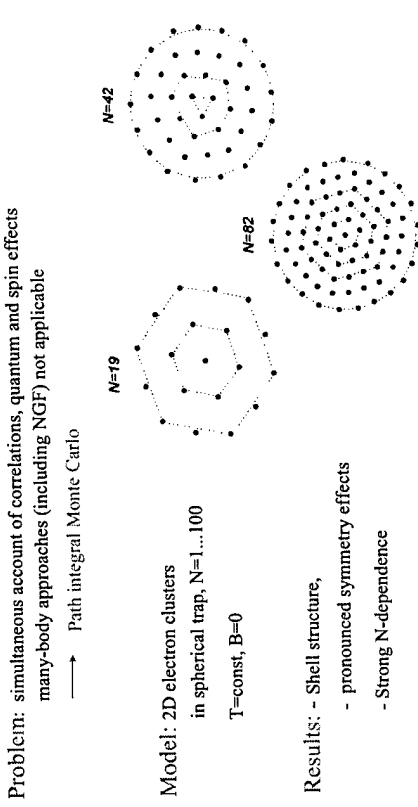


4. J.



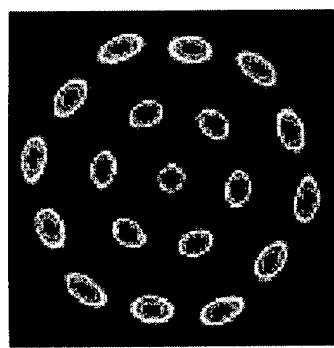
## Mesoscopic electron clusters

Easy realization of strong correlations  
many-body approaches (including NGF) not applicable  
Question: possibility of Wigner crystallization?  
Is there a metal-insulator transition?

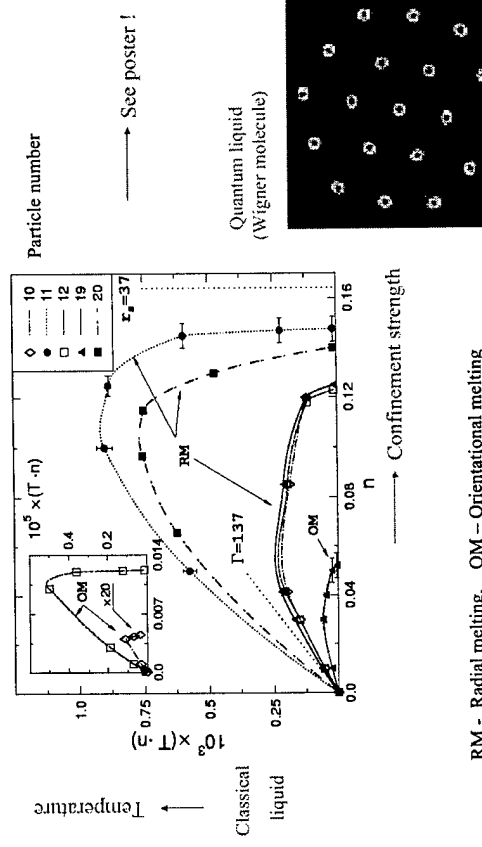


## Wigner crystallization of electron clusters

Variation of temperature or density (confinement)  
Existence of two crystal phases: *intra-shell* and *inter-shell* ordering



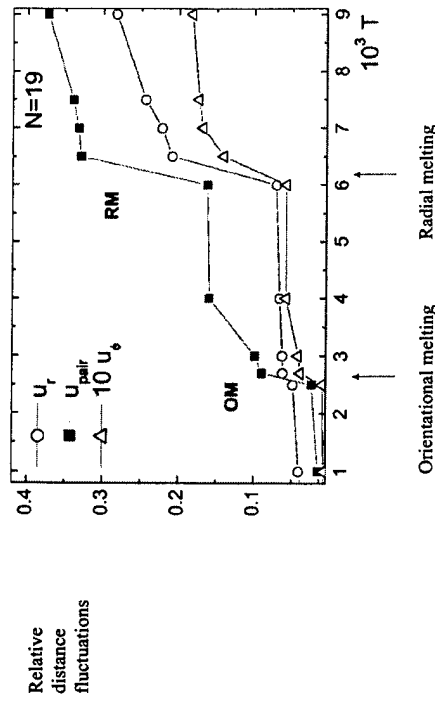
## Phase diagram of the mesoscopic Wigner crystal



# Crystal melting and mobility increase

At the melting point: drastic increase of angular and radial distance fluctuations

→ Mobility and conductivity increase



## Summary and Outlook

- I. Nonequilibrium Greens functions powerful tool
  - extended to arbitrary initial correlations
  - well applicable to ultrafast/transient phenomena
  - useful for high field transport
- II. Strong correlations in semiconductors
  - excitons, droplets, Wigner crystal
  - quantum Monte Carlo and molecular dynamics
- III. Future: combination of NGF and quantum simulations

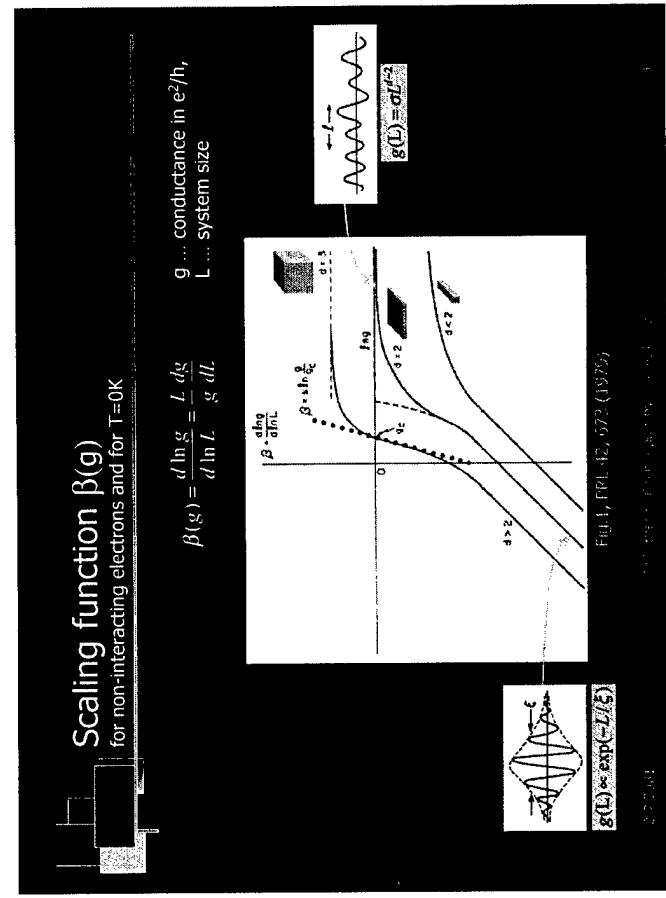
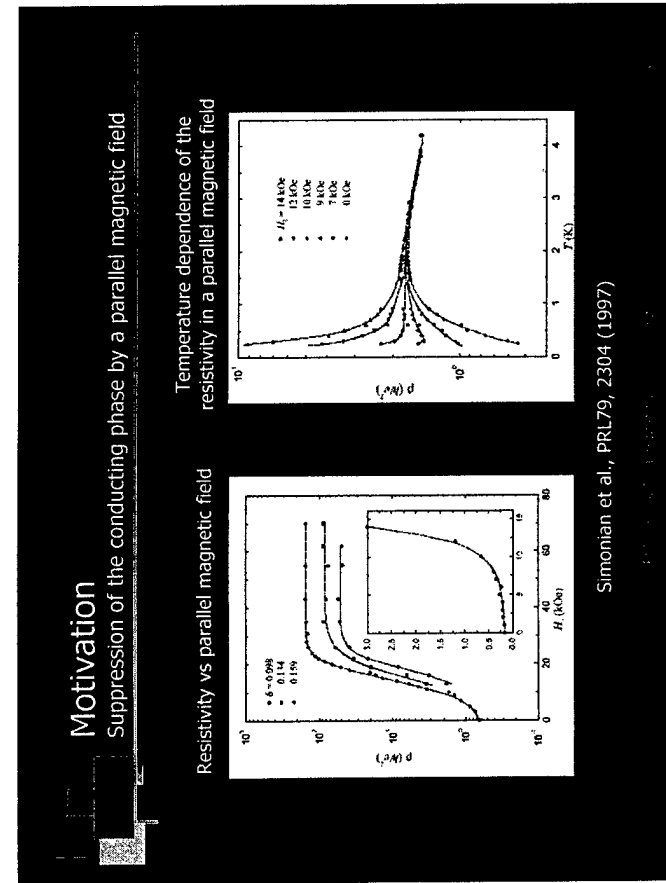
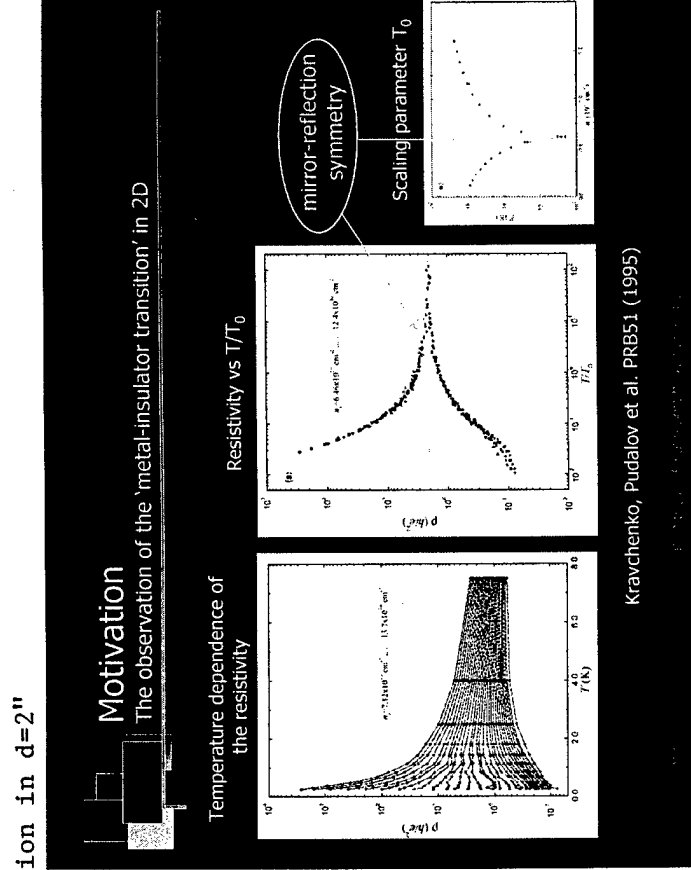
## References

1. Quantum kinetic theory with density operators and Greens functions, see M. Bonitz „Quantum Kinetic Theory“, B.G. Teubner, Stuttgart-Leipzig 1998
2. An overview (review articles) on Kadanoff-Baym equations can be found in „Progress in Nonequilibrium Greens Functions“, M. Bonitz (ed.), World Scientific, Singapore 2000
3. Kadanoff-Baym equations with initial correlations, see D. Semkat, D. Kremp, and M. Bonitz, J. Math. Phys. **41**, 7458 (2000) and references therein
4. Greens functions applications to high-field transport, see e.g., Mladurevic, Semkat, Bonitz, Redner, J. AP **91**, S29 (2001)
5. Greens functions applications to semiconductor optics, see e.g., Kwong, Bonitz, Binder, Kohler, physica solid. **106**, 197 (1998)
6. Fermionic path integral Monte Carlo (bound state formation etc.); see V.S.伊里诺夫, M. Bonitz, W. Ebeling, and V.E. Fortov, Plasma Phys. Contr. Fusion **43**, 743 (2001) and references therein
7. Wigner crystallization in mesoscopic electron clusters (open quantum dots); A.伊里诺夫, M. Bonitz, and Yu. Lozovik, Phys. Rev. Lett. **86**, 3851 (2001); Physical Review Focus April 19 (2001)

For updated references, please look at <http://elte.mpg.uni-potsdam.de/nb>

## Content

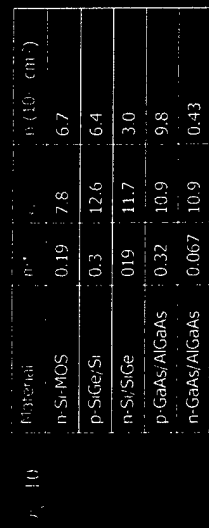
- Motivation
  - The observation of the 'metal-insulator transition' in 2D
- Scaling theory of localization
  - Scaling Function and phase coherence length
  - Importance electron-electron interaction
- Experiments
  - Measurement technique and Si-MOSFET devices
  - Standard transport measurements with and without magnetic field
- Weak localization
  - The role of quantum interference on the MIT
- The trap model
  - The capability and the limits
- Conclusions



## Importance Electron-Electron Interaction

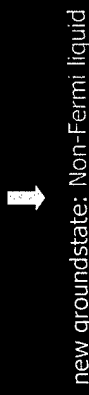
Coulomb energy versus Fermi energy:

$$\frac{1}{E_c} = \frac{E_{c,\text{in}}}{E_i} \propto \frac{\mu'}{E_i} \propto \frac{\sqrt{n_D}}{\mu'} \propto \frac{m^*}{\mu'} \propto \frac{1}{\sqrt{n_D}}$$



## Possible explanations for the phenomenon

Failure of the quasi-particle picture of Landau due to EEI

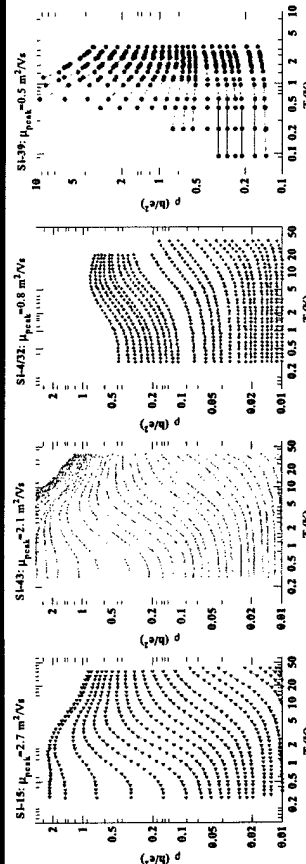


Superconductivity

or just a 'classical' effect?

## Transport measurements in zero B-field

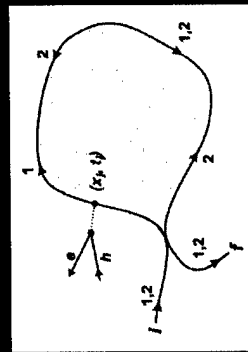
Temperature dependence of the resistivity



Comparison of different samples

## Weak Localization

Overview

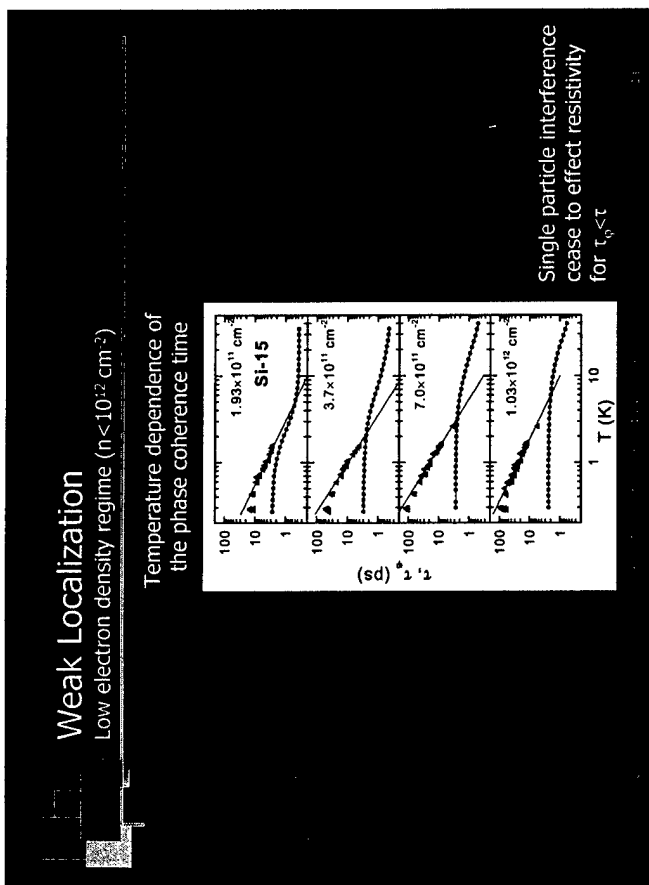
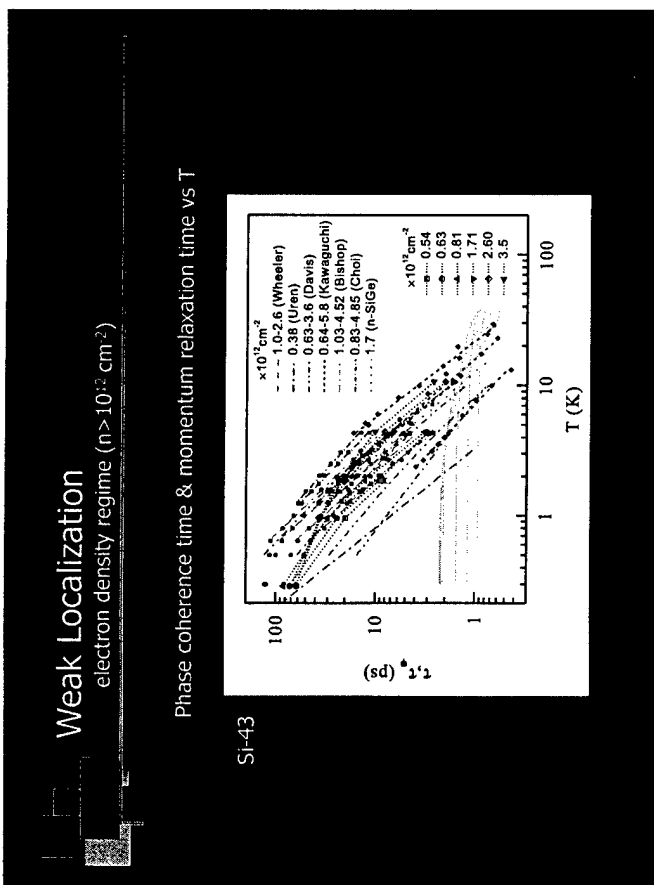
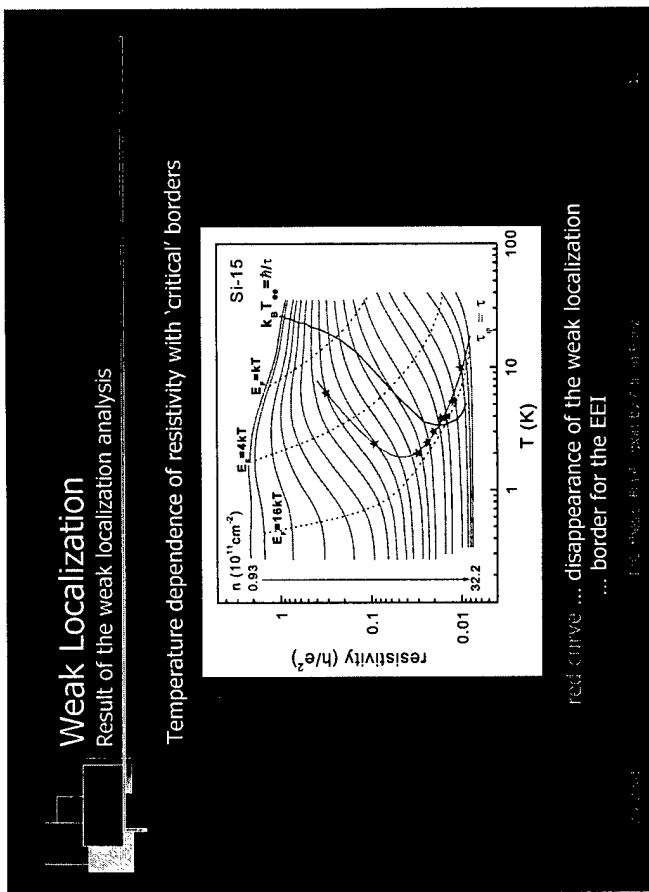
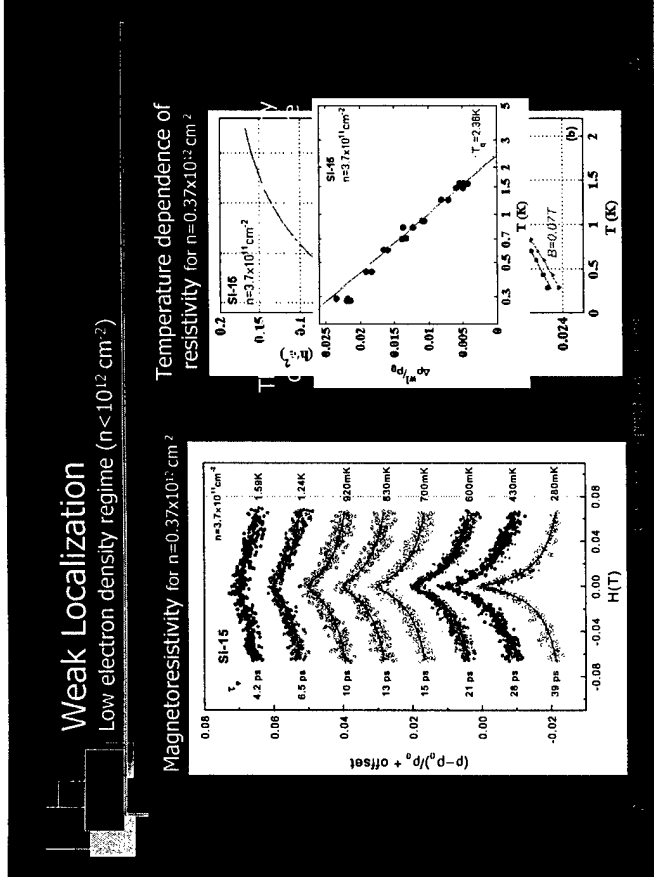


Quantum mechanical interference enhances back scattering

The exponential drop increases with the peak mobility !

2 features of weak localization are important :

- (1) logarithmic temperature dependence of the conductivity
- (2) negative magnetoresistance



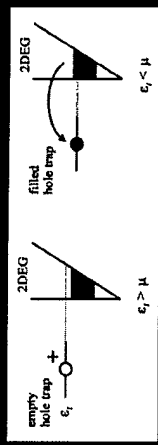
## Trap Model after B.L. Altshuler and D.L. Maslov

Overview

### Assumptions:

- traps are distributed homogeneously in the oxide
- all the traps have the same energy  $\epsilon_t$
- traps are due to weak Si-Si bonds (occupied by  $1e^-$  or  $2e^-$ )
- traps can be easily charged and discharged

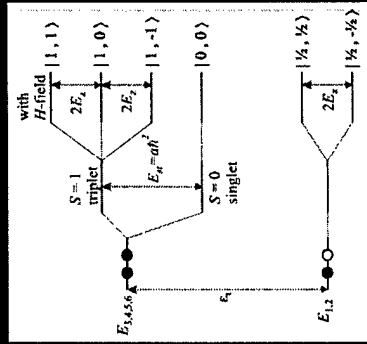
Charge state of the trap depends on the Fermi energy of the 2D electron gas



## Trap Model

The effect of the magnetic field

Splitting of the trap energy levels  
in a magnetic field



## Conclusions

■ The experimentally determined **phase coherence time** is about 10 smaller than theoretically predicted, but is in agreement with prior works on low-mobility samples

■ From analysis of the weak localization, **quantum interference** can be excluded as an origin for the metallic state and the MIT

■ There is no indication of a non-Fermi liquid in the metallic regime  
→ **no quantum phase**

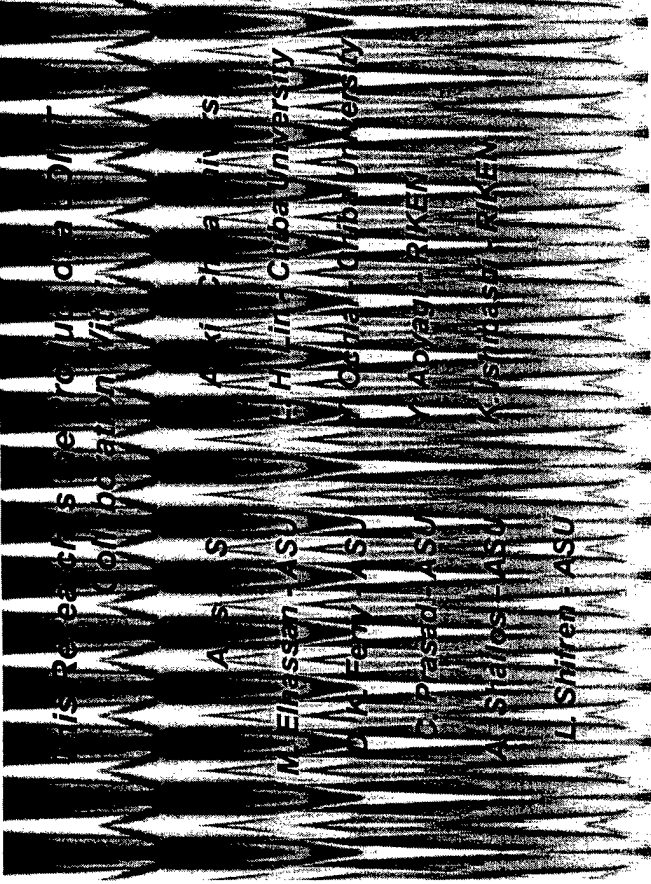
■ The trap model can explain qualitatively certain feature of the MIT, but fails to give quantitative results

# The "Metal-Insulator Transition" in Open Quantum Dots & Dot Arrays

**Jonathan P. Bird**

Department of Electrical Engineering &  
Center for Solid State Electronics Research  
Arizona State University  
Tempe, AZ 85287-5706

S4700 15.0kV 12.3mm x11.0k SE(U) 5/31/00 15:31 5.00um



NANOSTRUCTURES RESEARCH GROUP

ASU

NANOSTRUCTURES RESEARCH GROUP

ASU

Work at ASU is Supported By:



Office of  
Naval Research



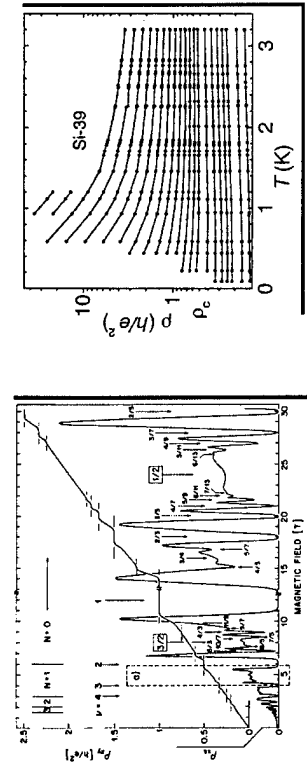
National  
Science  
Foundation

## OUTLINE

- INTRODUCTION
- TRANSPORT IN QUANTUM DOTS
- DEVICE FABRICATION & BASIC CHARACTERIZATION
- EXPERIMENTAL RESULTS
- CONCLUSIONS

- The study of the transport properties of LOW-DIMENSIONAL systems has lead to the discovery of a number of novel MANY-BODY effects in recent years

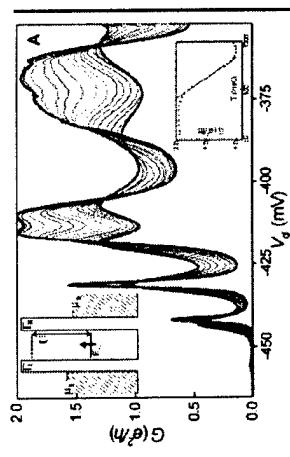
- Striking examples include the recent discovery of COMPOSITE FERMIONS in the fractional quantum-Hall effect and the METAL-INSULATOR TRANSITION in two dimensions



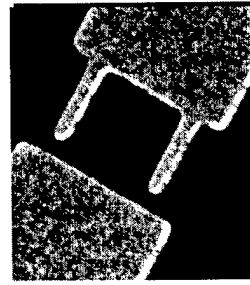
R. Willet et al.  
Phys. Rev. Lett. 59, 1776 (1987)

V. M. Pudalov et al.  
Physica E 3, 79 (1998)

- When the dots are coupled to their external reservoirs by means of WEAK tunnel barriers many-body effects have been argued to give rise to KONDO-LIKE behavior
- Here electrons confined WITHIN the dot play the role of the magnetic impurity in the more conventional Kondo effect

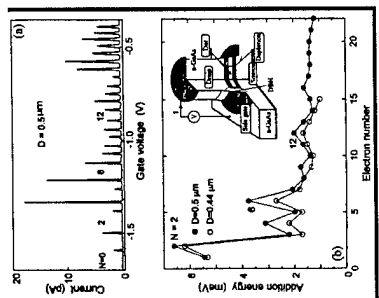


- In contrast to these studies our interest will lie in a discussion of transport in OPEN quantum dots
- These dots are coupled to their external reservoirs by means of quantum-point-contact LEADS that are configured to support a SMALL number of PROPAGATING modes
- Since transport through these structures is typically BALLISTIC in nature their electrical properties strongly reflect the details of the electron BOUNDARY scattering they generate



D. Goldhaber-Gordon et al.  
Nature 331, 158 (1991)  
J. Schmid et al.  
Phys. Rev. Lett. 85, 5824 (2000)  
W. G. van der Wiel  
Science 289, 2105 (2000)

- In mesoscopic QUANTUM DOTS electron interactions are known to play an important role when the dots are coupled to their reservoirs by means of weakly transmitting TUNNEL BARRIERS
- In this regime the COULOMB BLOCKADE of transport gives rise to SINGLE-ELECTRON behavior which can be used to demonstrate SHELL-LIKE filling of electron states

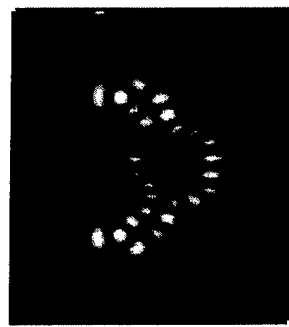


S. Tarucha et al.  
Phys. Rev. Lett. 72, 3613 (1994)

- While the Coulomb blockade is QUENCHED in open dots electrons may still be confined for LONG times in such structures

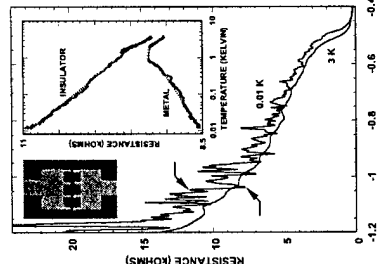
• We might therefore expect that the transport properties of open dots should exhibit NOVEL signatures that arise due to the MANY-BODY interactions of carriers trapped within them

\* FEW studies to date appear to have explored this possibility however



R. Akis et al.  
Physica E 17, 745 (2003)

- We investigate evidence for MANY-BODY interactions in open quantum dots and quantum-dot arrays by studying the variation of their resistance with TEMPERATURE
- \* We find evidence for novel LOCALIZATION behavior that we speculate arises due to an ENHANCED electron-electron interaction in these mesoscopic structures

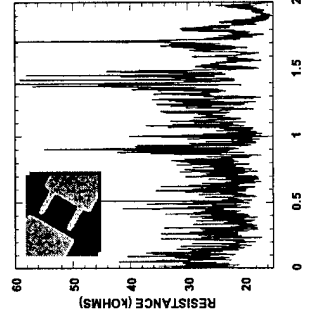


R. Akis et al.  
Phys. Rev. B 63, 241302 (2001)

## OUTLINE

- It is well known that at low temperatures the DISCRETE level spectrum of ISOLATED quantum dots can be RESOLVED in experiment
- \* When the dot is OPENED to the outside world the coupling between to the reservoirs gives rise to a NON-UNIFORM broadening of the dot states
- \* Discrete states that SURVIVE the coupling can be driven past the Fermi level by applying a magnetic field or gate voltage which gives rise to OSCILLATIONS in the conductance

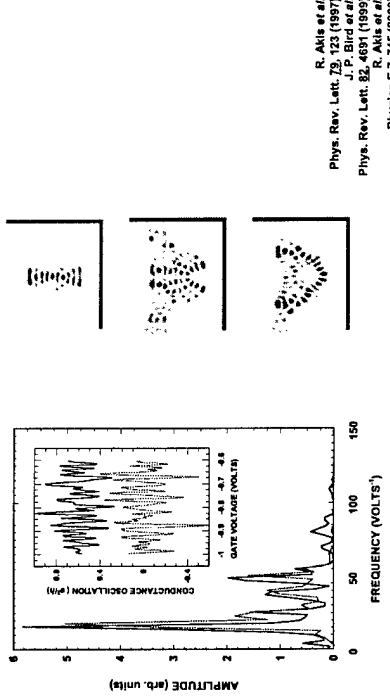
- TRANSPORT IN QUANTUM DOTS
- DEVICE FABRICATION & BASIC CHARACTERIZATION
- EXPERIMENTAL RESULTS
- CONCLUSIONS



J. P. Bird et al.  
Europhys. Lett. 35, 539 (1996)

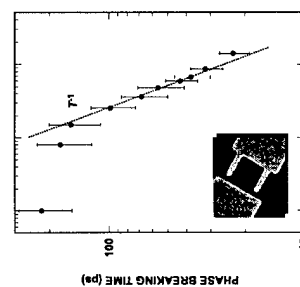
- The particular states that persist in the open dots are found to correspond to strongly SCARRED wavefunctions

\* The conductance oscillations observed in experiment therefore represent MEASURABLE signatures associated with these wavefunction scars



- From an analysis of the magneto-conductance fluctuations we can determine the electron PHASE-BREAKING time which is a measure of the time over which the coherent WAVE-LIKE nature of the electron is PRESERVED within the dot

\* At low temperatures this time scale is several ORDERS of magnitude longer than the time required to traverse the dot thus allowing confinement effects to be strongly RESOLVED



J. P. Bird *et al.*  
Phys. Rev. B **51**, 18037 (1995)  
D. P. Pinn *et al.*  
Phys. Rev. Lett. **72**, 4687 (1994)

R. Akis *et al.*  
Phys. Rev. Lett. **73**, 123 (1997)  
J.-P. Bird *et al.*  
Phys. Rev. Lett. **82**, 4691 (1999)  
R. Akis *et al.*  
Physica E **17**, 745 (2000)

R. Akis *et al.*  
Phys. Rev. B **52**, 17705 (1995)  
Phys. Rev. Lett. **73**, 123 (1997)

## OUTLINE

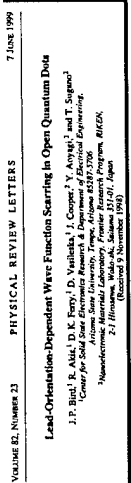
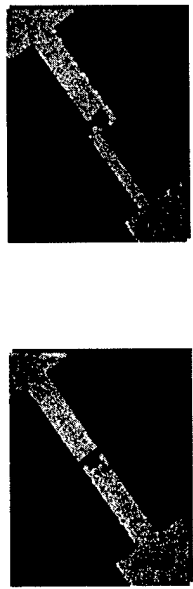
- INTRODUCTION

- TRANSPORT IN QUANTUM DOTS

- DEVICE FABRICATION & BASIC CHARACTERIZATION

- EXPERIMENTAL RESULTS

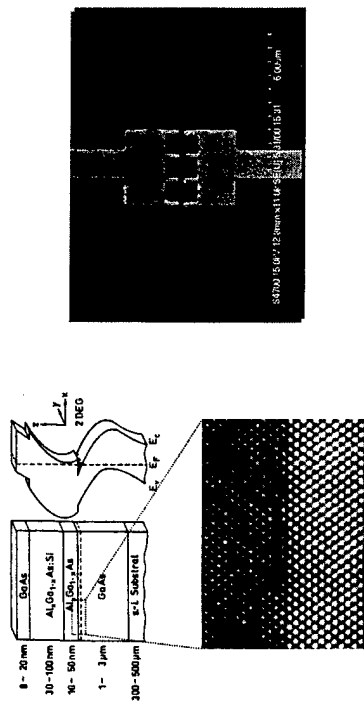
- CONCLUSIONS



- By changing the ORIENTATION of the leads that couple the dot to the reservoirs DIFFERENT groups of states can be selected to mediate the transport behavior

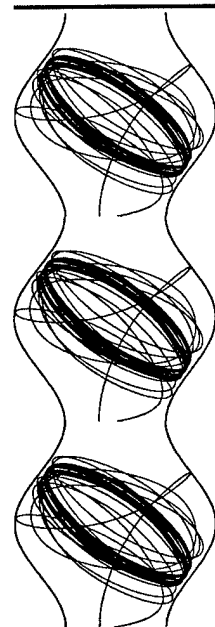
\* Evidence for this process of SCAR SELECTION can be observed directly in experiment

- In this report we discuss the transport properties of multiply-coupled QUANTUM-DOT ARRAYS
  - \* The arrays are realized using the SPLIT-GATE technique in which a depleting voltage is applied to lithographically-defined Schottky gates to induce LATERAL confinement of the high-mobility two-dimensional electron gas formed at the heterointerface



- Some further COMMENTS on the transport characteristics of the arrays

- \* The carrier density within the arrays is found to remain UNCHANGED with gate voltage
- \* The transport mean free path ( $>10 \mu\text{m}$ ) is very much LONGER than the size of the arrays so that transport within them is expected to be highly BALLISTIC in nature
- \* At low temperatures the electron phase-breaking length is of order 100 ps corresponding to a TOTAL coherent path length in EXCESS of  $50 \mu\text{m}$

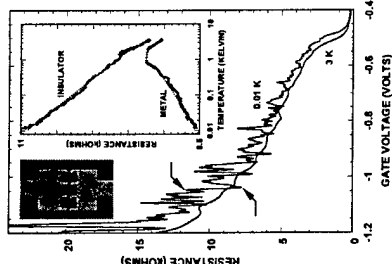


## OUTLINE

- INTRODUCTION
- TRANSPORT IN QUANTUM DOTS
- DEVICE FABRICATION & BASIC CHARACTERIZATION
- EXPERIMENTAL RESULTS
- CONCLUSIONS

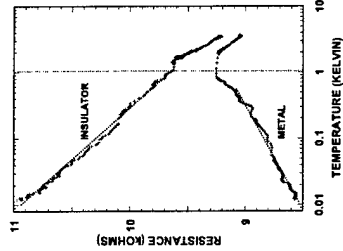
- The details of quantum transport in the arrays are investigated by studying the TEMPERATURE dependence of their resistance

\* These studies reveal evidence for behavior reminiscent of a METAL-INSULATOR transition



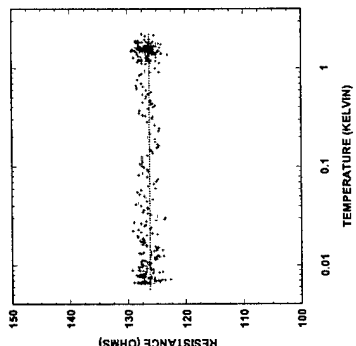
A. Andersen et al.  
Phys. Rev. B 50, 18050 (1999)  
Phys. Rev. B 50, 18051 (1999)  
A. Shalots et al.  
Phys. Rev. B 63, 241302 (2001)

- The main characteristics of the metal-insulator behavior are an EXPONENTIAL increase of the resistance at intermediate temperatures and for ALL gate voltages
- This gives way to a LOGARITHMIC variation of the resistance at lower temperatures that may be either METALLIC or INSULATING in nature

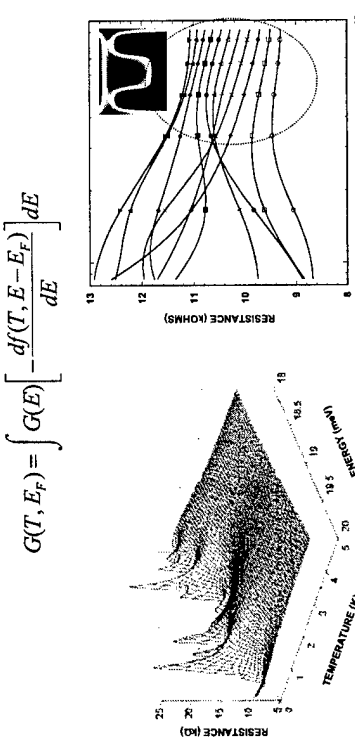


A. Andersen et al.  
Phys. Rev. B 50, 18050 (1999)  
A. Shalots et al.  
Phys. Rev. B 63, 241302 (2001)

- No evidence for the temperature-dependent variations found in the arrays is seen in studies performed with the gates GROUNDED
- \* This indicates that these variations are INTRINSIC to the dot ARRAYS rather than being a property of the two-dimensional electron-gas layer



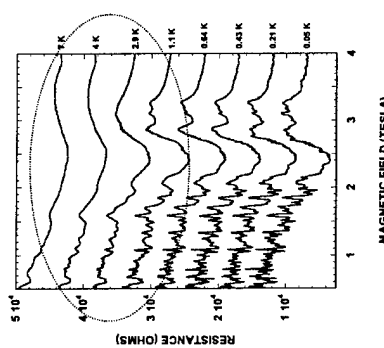
A. Andersen et al.  
Phys. Rev. B 50, 18050 (1999)  
L.-H. Lin et al.  
Phys. Rev. B 50, R16299 (1999)  
A. Shalots et al.  
Phys. Rev. B 63, 241302 (2001)



A. Shalots et al.  
submitted for publication

- \* We suggest the exponential regime indicates a transition from THERMALLY-BROADENED to ENERGETICALLY-DISCRETE levels in the dots with decreasing temperature

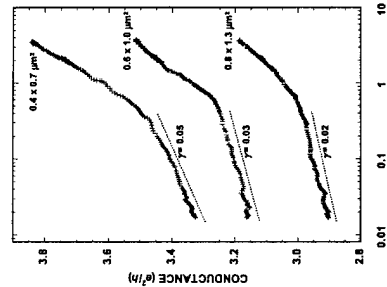
\* This assertion is further supported by studies of the temperature dependence of the MAGNETO-RESISTANCE which show a large change in amplitude in the exponential regime



A. Shalots et al.  
submitted for publication

- \* The amplitude of the logarithmic term is found to be LARGER in the arrays composed of smaller dots

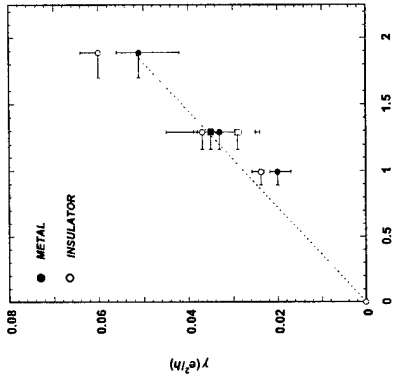
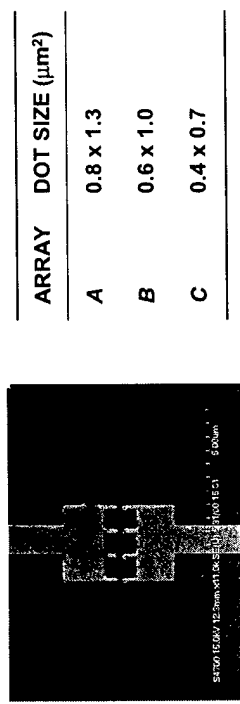
\* We quantify this effect in terms of the SLOPE of the logarithmic variation ( $\gamma$ ) in this regime



A. Shalots et al.  
Phys. Rev. B 53, 241302 (2001)

- \* While our simulations show features reminiscent of the exponential regime found in experiment they are UNABLE to reproduce the LOGARITHMIC behavior seen at much lower temperatures

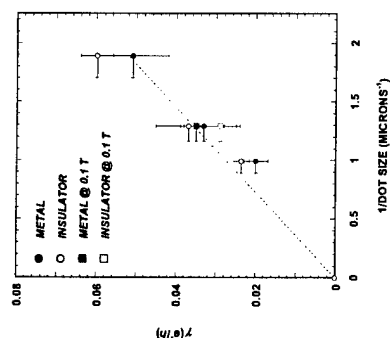
\* To further investigate the properties of this term we have fabricated quantum dot arrays of DIFFERENT size



A. Shalots et al.  
Phys. Rev. B 63, 241302 (2001)

- We also find that the magnitude of the logarithmic term is **INSENSITIVE** to the application of a magnetic field sufficient to BREAK time-reversal symmetry

\* This indicates that this term is **NOT** associated with a weak-localization effect in the dots

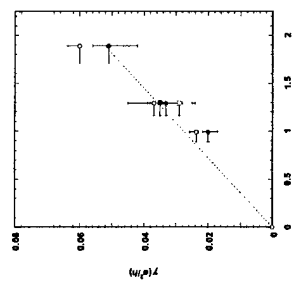


A. Shabotov et al.  
Phys. Rev. B 63, 241302 (2001)

- Based on experiment we have suggested that the logarithmic term in the conductance results from an **ENHANCEMENT** of the electron-electron interaction inside the dots

\* The basic idea is that confining electrons within the ballistic dots should **AMPLIFY** the Coulomb many-body interaction by **SUPPRESSING** the tendency for charge separation

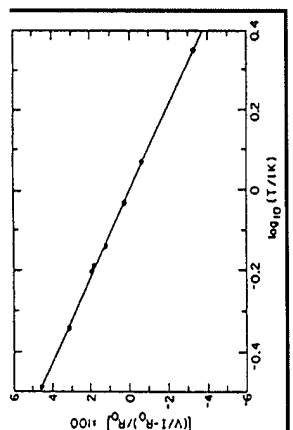
\* In fact the **SCALING** of the logarithmic term with **INVERSE** dot size is consistent with an Interaction that scales in inverse proportion to the PERIMETER LENGTH



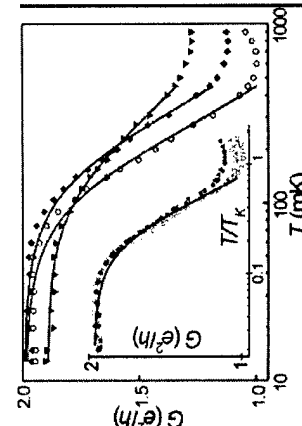
A. Shabotov et al.  
Phys. Rev. B 63, 241302 (2001)

- Logarithmic conductance variations are well known from studies of **DISORDERED** mesoscopic systems in which they can result from **WEAK LOCALIZATION** or **ELECTRON INTERACTIONS**

\* In order to distinguish between these two effects it is necessary to apply a sufficient MAGNETIC FIELD to break time-reversal symmetry and so quench weak localization

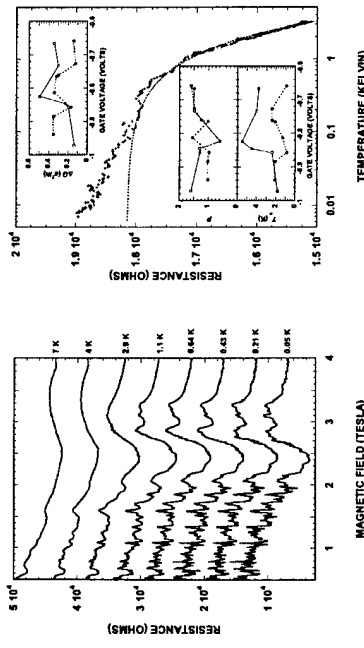


G. J. Dolan and D. C. Osherson  
Phys. Rev. Lett. 33, 721 (1974)



W. G. van der Wiel  
Science 285, 2105 (2000)

- We therefore arrive at the following MODEL to account for the different temperature variations
  - At temperatures in EXCESS of a few Kelvin the discrete dot states are thermally OBSCURED
  - Lowering the temperature In this regime allows the dot states to become RESOLVED and it is this transition that is reflected in the EXPONENTIAL- resistance



A. Shalaev et al.

submitted for publication

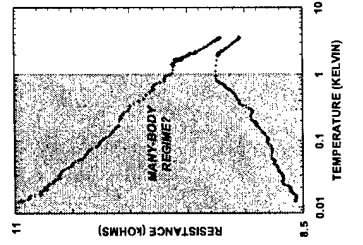
## CONCLUSIONS

- WE HAVE STUDIED THE TEMPERATURE-DEPENDENT TRANSPORT IN COUPLED QUANTUM-DOT ARRAYS AND FIND VERY DIFFERENT BEHAVIOR COMPARED TO THAT OF THE UNDERLYING TWO-DIMENSIONAL ELECTRON GAS

- THE REGIME OF EXPONENTIAL RESISTANCE VARIATION IS SUGGESTED TO SIGNIFY THE EMERGENCE FROM THERMALLY-BROADENED TO ENERGETICALLY-RESOLVED DOT LEVELS WITH DECREASING TEMPERATURE

- THE LOGARITHMIC VARIATION SEEN AT EVEN LOWER TEMPERATURES CANNOT BE ACCOUNTED FOR BY EXISTING THEORIES AND MAY SIGNIFY THE EMERGENCE OF A NOVEL MANY-BODY STATE AT LOW TEMPERATURES THAT RESULTS FROM AN ENHANCEMENT OF ELECTRON INTERACTIONS IN THE CONFINED DOTS

- IT IS OUR HOPE THAT THIS WORK WILL STIMULATE RENEWED THEORETICAL INTEREST IN THE STUDY OF ELECTRON INTERACTIONS IN OPEN MESOSCOPIC SYSTEMS



- As the temperature is lowered below a KELVIN we enter the regime of strongly-resolved dot states and it is here that the LOGARITHMIC variation of resistance is observed
- An INTRIGUING issue concerns whether this variation signals the emergence of some NOVEL many-body state once the quantum nature of these structures is well resolved?

Wednesday, June 20

Session 5:

- Also related posters Thursday:

  1. David Awschalom ..Spin coherence and optical measurements
  2. Daniel Loss ..Quantum Computing in semiconductor systems
  3. Sankar Das Sarma ..Few electron (and few impurity) systems
  - 3-1 Brunel et al.
  - 3-2 Pöller et al.
  - 3-3 Pravman
  - 3-4 Wagner
  - 3-10 Ilinov et al.

Workshop „Quantum Transport in Semiconductors“

Mărițea, June 17-22 2001

Welcome to the spin doctors!

1. What disease?  
2. Who's sick?



Quantum Transport in Semiconductors

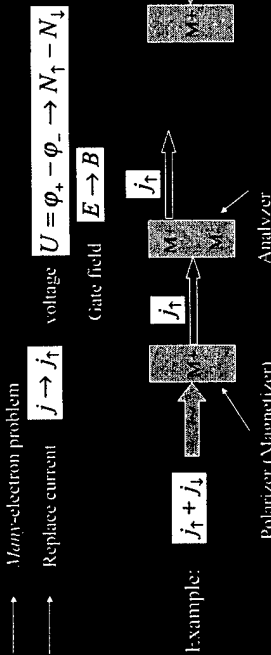
Workshop 1

## *Spintronics (alternative medicine?)*

Ideal: control devices by controlling the electron spin (instead of the charge)

Spin already in use: M-RAMs, read heads of hard drives etc.  
But, metal based "Challenger" semiconductors (integrability)

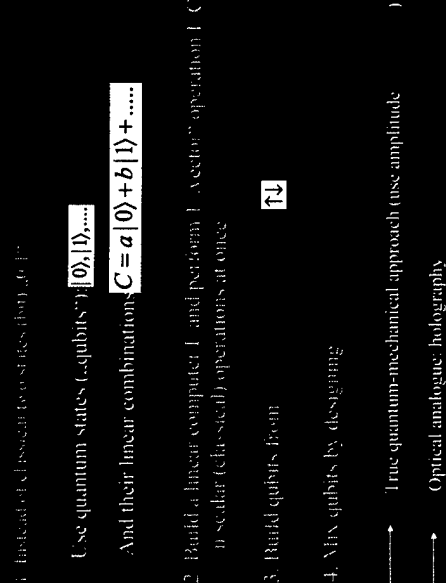
- ## **L. Improve classical devices (computers)**



Problems: creation/injection/transport/storage..... (possible side effects?)

# Spintronics II.

III. Create new *quantum* computers ( $f_{\text{CNOT}}$ - $f_{\text{alpha}}$ -problem)



## Semiconductor electrons in E/B fields

E-Field (couples to charge)

$$e \cdot e\vec{E} \rightarrow \vec{v} \rightarrow \vec{j} \text{ current}$$

→ Transport (intraband)

2. Interband transport (optics)

$$e \rightarrow d_{cv} \sim e \int dV \psi_c^*(r) r \psi_v(r)$$

Interband current (polarization)  $\vec{P}$

$$\left[ \frac{\partial}{\partial t} + i \frac{\tilde{\epsilon}_{cv}(k)}{\hbar} \right] P_k = -i \tilde{d}_{cv} E(t) [f_{c+}(t) - f_{c-}(t)]$$

- Coherent oscillations of  $P$ ,

Rabi flops, photon echo etc.,  
coherent excitons, biexcitons

- Dephasing due to scattering  $\sim -\frac{P_{av}}{T_2}$

B-Field (couples to mag. moment)

$$\vec{s} \rightarrow \vec{m}: \vec{m}\vec{B} \rightarrow \omega_L = g\mu_B B/\hbar$$

→ Lamor precession

$$\begin{array}{c} \overline{M_x} \\ \overline{f_{c+}} \\ \overline{f_{c-}} \end{array}$$

$$\left[ \frac{\partial}{\partial t} + i \frac{\tilde{\epsilon}_z(k)}{\hbar} \right] M_z = i g \tilde{\mu}_z B(t) [f_{c+}(t) - f_{c-}(t)]$$

- Coherent oscillations of  $M_z$ ,...Larmor flops

spin echoes?

- very long dephasing times  
- bound states (cooper pairs)??

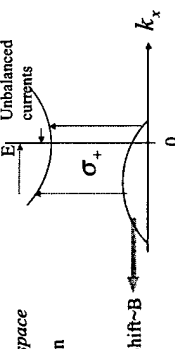
## Outlook

Number of quantum computing papers (title and abstract):  
from 1994-2001 (June 14): 1, 6, 10, 15, 38, 59, 81, 122

→ On track with Moore's law

Number of spintronics papers:  
from 1999-2001 (June 14-11.32 a.m. ET): 2, 8, 10

→ Way ahead of Moore's law



## Electrons in E/B-fields, contd.

### 3. Spin meets optics



-spin-sensitive absorption/emission of  
circular-polarized light (old)

-spin-modulated polarization of laser emission [Hallstein et al. PRB 56, R7076 (1997)]

$$\left[ \frac{\partial}{\partial t} + i \frac{\tilde{\epsilon}_z(k)}{\hbar} \right] M_z = i g \tilde{\mu}_z B(t) [f_{c+}(t) - f_{c-}(t)]$$

### 4. Spin meets intraband transport

- „Conversion of spin into directed electric current in Quantum Wells“, Ganichev et al. PRL 86, 4356 (2001)
- B-field induced separation of  $+3/2$  and  $-3/2$  hh bands in k-space
- current direction determined by helicity of light polarization

Workshop „Quantum Transport in Semiconductors“

Maratea, June 17-22 2001

*Listen to (and interrupt!)  
the spin doctors!*



Workshop „Quantum Transport in Semiconductors..

Mareta, June 17-22 2001



## SPIN ELECTRONICS

**Group of Sankar Das Sarma, University of Maryland**  
**Igor Žutić, Jaroslav Fabian, Xuedong Hu, et al.**

- theory of bipolar spin-polarized transport in inhomogeneous semiconductors (magnetic and nonmagnetic) and their heterostructures
- spin devices: proposal and modeling of spin-polarized and magnetic p - n junctions and solar cells, magnetic field sensors, spin transistors, ...
- dynamical mean field theory for critical temperature in ferromagnetic semiconductors (e.g., GaMnAs)
- spin entanglement and interactions in quantum dots:
- assessment of feasibility for spin-based quantum computing

## Group Publications (partial list):

Theory of spin-polarized transport in inhomogeneous magnetic semiconductors, LANL preprint cond-mat/0106085

Spin Electronics and Spin Computation, to appear in Solid State Commun., LANL preprint cond-mat/0105247

A proposal for spin-polarized solar battery. to appear in Appl. Phys. Lett. (8/27/01); LANL preprint cond-mat/0104416

Spin transport in inhomogeneous magnetic fields: a proposal for Stern-Gerlach-like experiments with conduction electrons, LANL preprint cond-mat/0104146

Spin injection through the depletion layer: a theory of spin-polarized p-n junctions and solar cells, to appear in Phys. Rev. B, Rapid Commun. (8/15/01); LANL preprint cond-mat/0103473

Issues, Concepts, and Challenges in Spintronics, IEEE 58th DRC Device Research Conference Digest, p. 95 (2000)

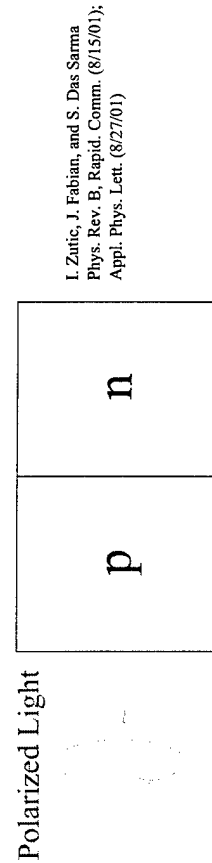
Theoretical Perspectives on Spintronics and Spin-Polarized Transport. IEEE Trans. Magn. 36, 2821 (2000)

Issues Concepts, and Challenges in Spintronics, Superlattice Microst. 27, 289 (2000)

Spin-polarized transport and Andreev reflection in semiconductor/superconductor hybrid structures. Phys. Rev. B 60 Rapid Commun., R16 322 (1999).

publications also available at :  
<http://www.physics.umd.edu/rgroups/spin/papers.html>

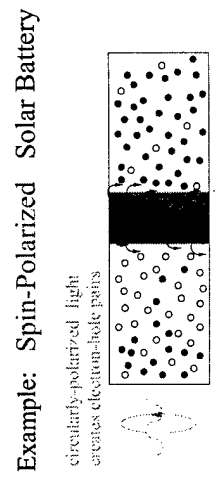
## Spin - Polarized p - n Junction



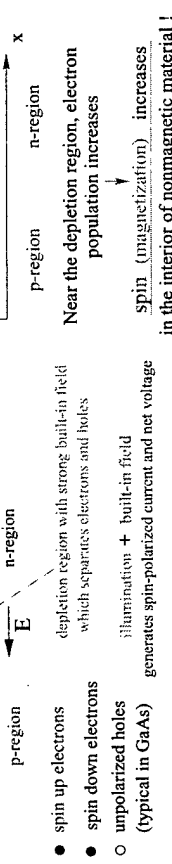
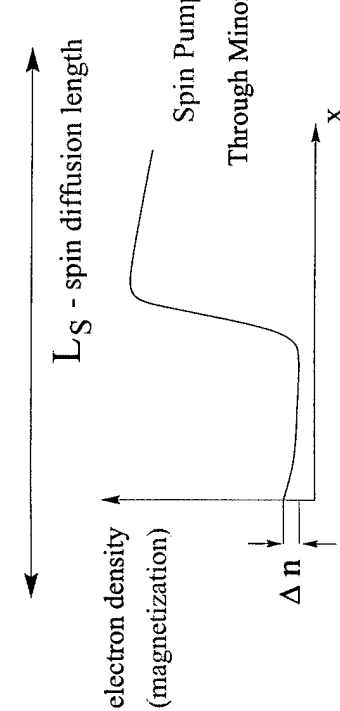
I. Zutic, J. Fabian, and S. Das Sarma  
 Phys. Rev. B, Rapid. Comm. (8/15/01);  
 Appl. Phys. Lett. (8/27/01)

## Spin-Polarized and Magnetic p - n Junctions and Solar Batteries

spin-polarized p - n junction -- building block for semiconductor spin electronics , feasible with the current technology and available materials (e.g., GaAs with the appropriate doping)  
 spin polarization can be created by circularly polarized light, electrical spin injection, applied magnetic field, ...



Example: Spin-Polarized Solar Battery



Near the depletion region, electron population increases  
 spin (magnetization) increases in the interior of nonmagnetic material !

## Spin - Polarized Drift - Diffusion Equations

$$\nabla^2 \phi = -\frac{e}{\epsilon} (p - n + N_A - N_D)$$

and

4 Continuity equations for  $n_\uparrow$ ,  $n_\downarrow$ ,  $p_\uparrow$  and  $p_\downarrow$

Generation - Recombination ( $\tau_n, \tau_p$ )

Spin Relaxation ( $T_1$ )

Results based on realistic GaAs parameters

$$p_\uparrow = p_\downarrow$$

$(n_\uparrow - n_\downarrow) / n \leftarrow$  max polarization 50%  
(with circularly-polarized light)

$T_1 \sim 0.2\text{ms}$

Continuity Equation for  $n_\uparrow$

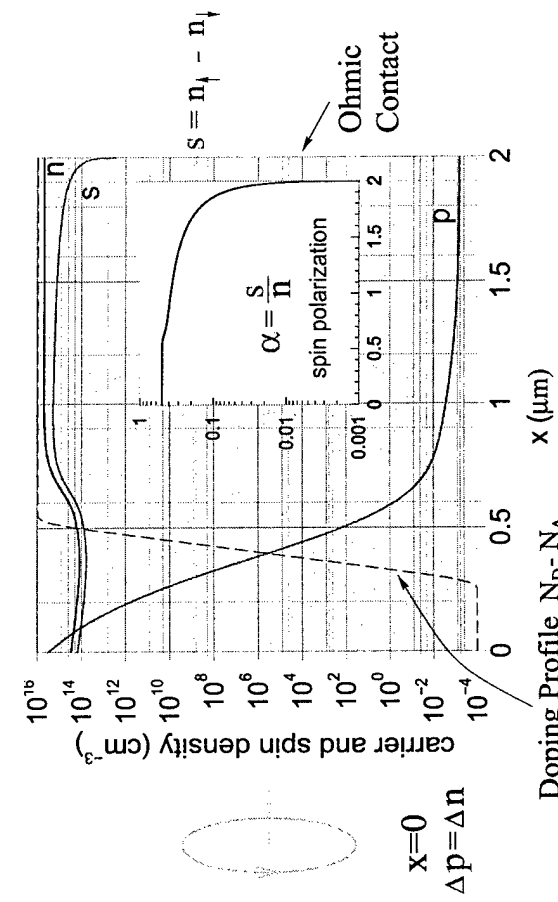
$$J_{n_\uparrow} = -n_\uparrow \mu_{n_\uparrow} E - D_{n_\uparrow} \nabla n_\uparrow \quad (\text{for nonmagnetic p-n junction})$$

$$\frac{dn_\uparrow}{dt} + \nabla \cdot J_{n_\uparrow} = -w_{n_\uparrow} (n_\uparrow p - \frac{n_0 p_0}{2}) - \frac{n_\uparrow - n_\downarrow}{2 T_1} + G_\uparrow$$

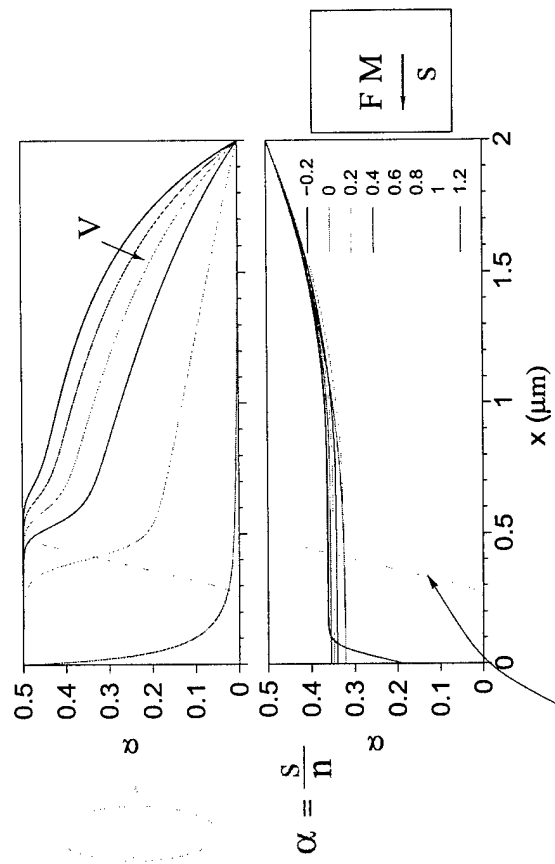
$w_{n_\uparrow}$  - Generation - Recombination rate

$G_\uparrow$  - Photo-excitation rate for  $n_\uparrow$

Spin Injection through the  $p - n$  junction



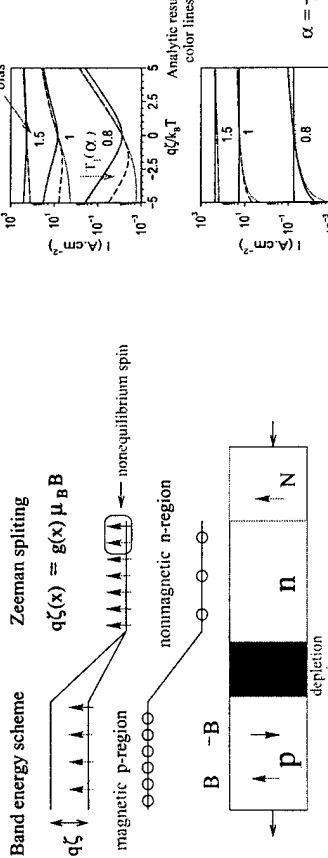
Spin Polarization Profiles for different voltages



Doping Profile  $N_D - N_A$

## Magnetic / Nonmagnetic p - n Junctions

I. Zutic, J. Fabian, and S. Das Sarma, LANL preprint cond-mat/0106085



p-region:  $n_0 \approx (n_i^2 N_A) \cosh(q\zeta/kT)$

at low bias, current  $\sim$  minority carriers  $\rightarrow$  exponentially large magnetoresistance with the increase in  $|B|$  (i.e.  $|\zeta|$ )

$J = J_n + J_p \rightarrow$  nonequilibrium spin-induced current

$$J_{n,p} \sim (e^{(qV/kT)-1})^{1/2} J_n \sim \alpha \sinh(q\zeta/kT) e^{(qV/kT)}$$

current can flow at zero bias!  
(spin analogue of photovoltaic effect)

zero bias current changes sign  
with the change of  $\alpha$  and/or  $B$

## Applications of Spin-Polarized and Magnetic p - n Junctions and Solar Batteries

- Generation of spin and charge currents
- Spin injection through the depletion layer
- Electronically tunable spin polarization
- Amplification of spin density
- Extension of the spin-diffusion range
- Exponential magnetoresistance and spinovoltaic effect
- Magnetic field sensors
- Electrical detection of spin polarization and spin relaxation

- Generation of spin and charge currents
- Spin injection through the depletion layer
- Electronically tunable spin polarization
- Amplification of spin density
- Extension of the spin-diffusion range
- Exponential magnetoresistance and spinovoltaic effect
- Magnetic field sensors
- Electrical detection of spin polarization and spin relaxation

## Applications of Quantum transport in devices

Gerhard Klimeck

Jet Propulsion Laboratory,  
California Institute of Technology

gelko@jpl.nasa.gov, 818-354-2182  
<http://hpc.jpl.nasa.gov/PEP/gelko>

Gerhard Klimeck

## Application of Quantum Transport in Devices

- What is the focus of the research?

- Quantum Transport  
=> Devices/Structures are a tool to explore the needed theory
- Relevant Theories:  
Green Functions, Wigner Functions, Rate Equations
- Relevant Structures:  
quantum dots/wires, molecules, RTDs (for time dependence only)

### Devices / Applications

- => Quantum transport is a tool to design/optimize devices
- Relevant devices: super-scaled FETs, RTDs, Esaki diodes
- Need quantitative agreement between experiment and theory
  - DC, high bias performance
  - AC / time-dependent high bias performance
- Need realistically sized devices - contacts/reservoirs.
- Need realistic electron interactions with environment:  
phonons, light, bandstructure.

Gerhard Klimeck

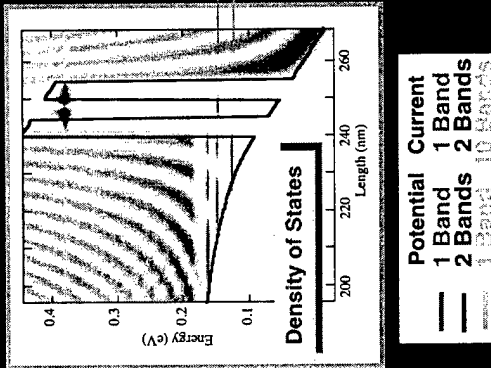
## Quantitative Modeling of Devices

### Quick review of DC transport simulations in RTDs - NEMO 1-D

- Realistic contacts:
- Quantized and continuous states in the emitter
- Realistic bandstructure:
  - Band-non parabolicity - emitter states and RTD state alignment
- Putting it together:
  - Valley current at high temperatures due to bandstructure effects (thermionic emission)
  - Bistability (in symmetric structures) a numerical problem due to limited device models
- Test matrix - comparison to experiments

Gerhard Klimeck

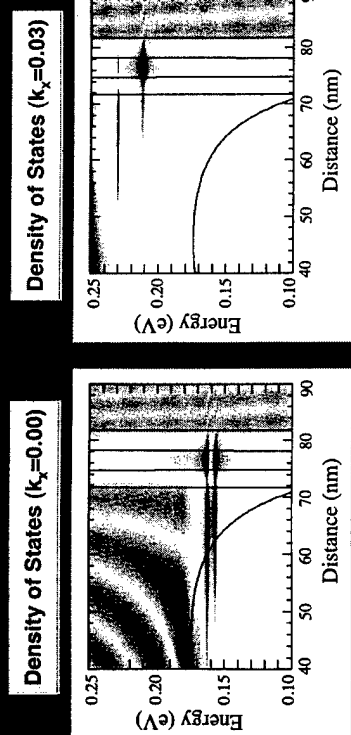
## Realistic Devices have Extended Contacts



Quantum selfconsistent potential

Work on this slide performed by NEMO team at Texas Instruments / Raytheon 1995-1997

## Band non-parabolicity modifies momentum dependence in emitter-RTD coupling



Resonance coupling depends on the transverse momentum

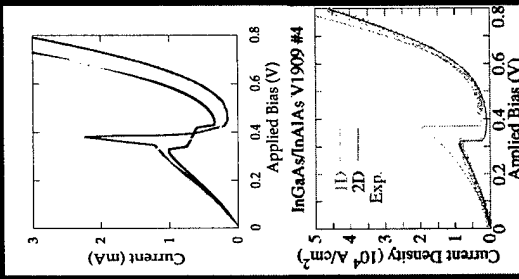
Gerhard Klimeck Work on this slide performed by NEMO team at Texas Instruments / Raytheon 1995-1997

## Full Band Simulation of Electron Transport

- 1D integration assuming parabolic subbands can lead to unphysical current overshoots.

- 2 Examples on InGaAs/InAlAs simulations:

- Sp3s\* simulation with partial charge self-consistency  
→ sharp spike at turn-off
- Parameterized single band simulation which incorporates the band-non-parabolicity  
→ overall current overshoot.
- 2D integration with good bandstructure fixes these unphysical results.

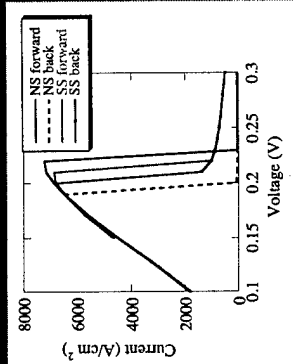


Gerhard Klimeck Work on this slide performed by NEMO team at Texas Instruments / Raytheon 1995-1997

## Scattering also reduces the numerical bi-stability

- Current Model:

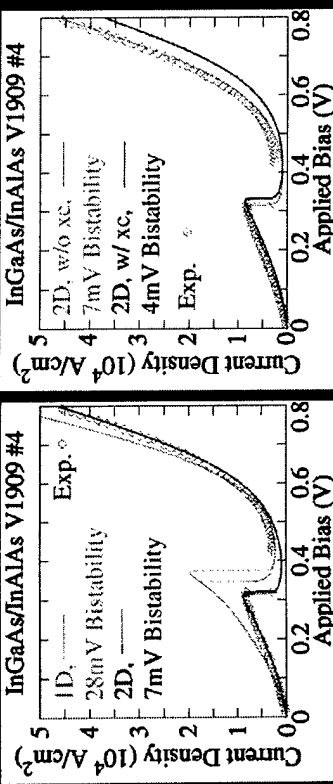
- self-consistent elastic and single tridiagonal POP scattering
- Potential Models:
- Hartree self-consistency
  - no scattering
  - selfconsistent elastic and tridiagonal POP scattering
- Compare forward to reverse bias sweep:
  - Scattering reduces the width of the bistability region.
  - not shown: inclusion of exchange correlation does not change the width of the bistability in this device.



Gerhard Klimeck Work on this slide performed by NEMO team at Texas Instruments / Raytheon 1995-1997

## Spurious Bistability: More Physics → Better results

Full band integration + Exchange&Correlation

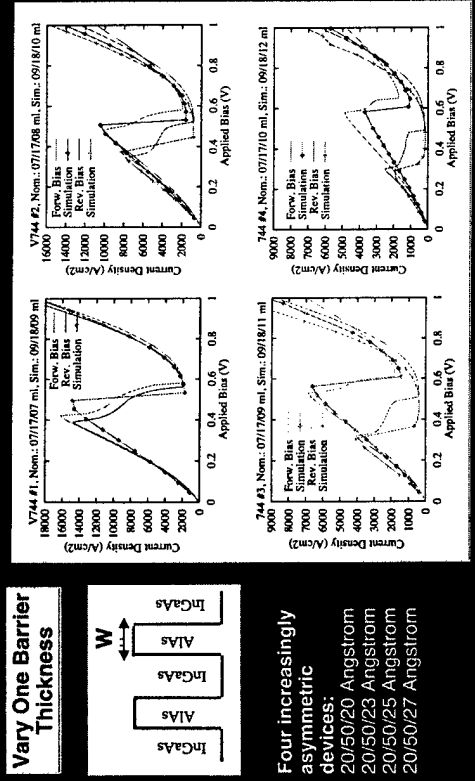


- Calculate the exchange and correlation potential in LDA.
- Exchange and correlation energy does not eliminate (in general) the bistability, it does reduce it however.
- Inclusion of scattering in the simulation reduces the bistability region as well.

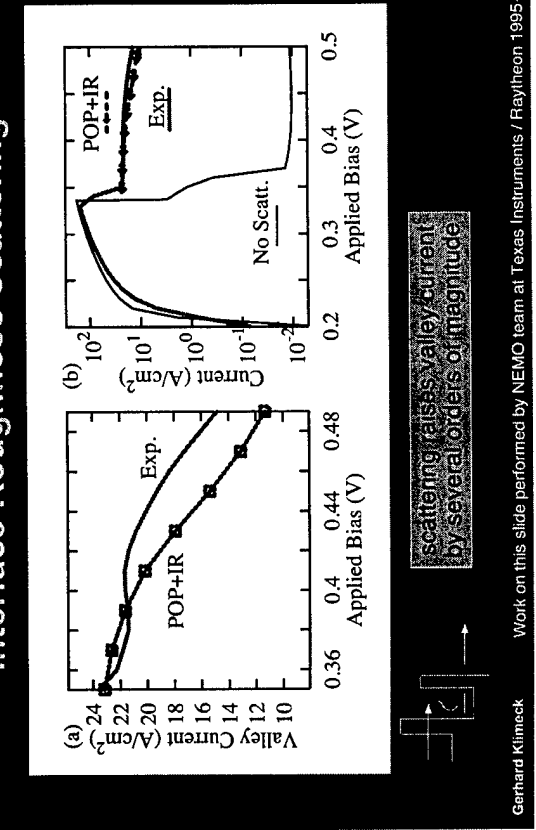
Gerhard Klimeck Work on this slide performed by NEMO team at Texas Instruments / Raytheon 1995-1997

Gerhard Klimeck Work on this slide performed by NEMO team at Texas Instruments / Raytheon 1995-1997

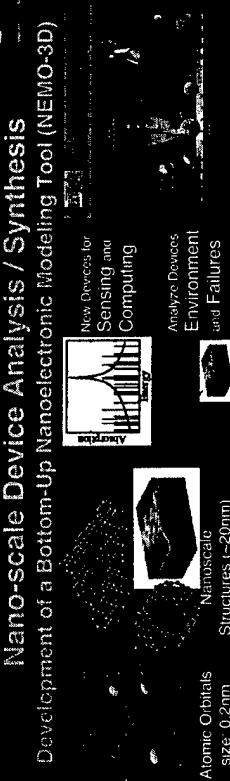
## TestMatrix-Based Verification (room temperature) Strained InGaAs/AlAs 4 Stack RTD with Asymmetric Barrier Variation



## Tow Temperature: Polar Optical Phonon and Interface Roughness Scattering



## Nano-scale Device Analysis / Synthesis



## Speakers in the Program

- Harold Grubin,  
SRA, Inc.,  
“Modeling resonant tunneling diodes with Wigner functions and density matrices”
- Dejan Jovanovic,  
Motorola,  
“Non-equilibrium Green’s functions for MOSFET modeling”
- Carlo Jacoboni,  
Modena University,  
“The Wigner function and quantum transport”

Gerhard Klimeck *Modeling will narrate: the empirical search space!*

## Speakers in the Program

- Harold Grubin,  
SRA, Inc.,  
“Modeling resonant tunneling diodes with Wigner functions and density matrices”
- Dejan Jovanovic,  
Motorola,  
“Non-equilibrium Green’s functions for MOSFET modeling”
- Carlo Jacoboni,  
Modena University,  
“The Wigner function and quantum transport”

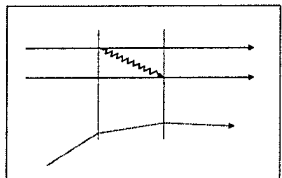
Gerhard Klimeck

**WIGNER-FUNCTION AND QUANTUM TRANSPORT  
 IN SEMICONDUCTORS**

Carlo Jacoboni

INFM - Istituto Nazionale per la Fisica della Materia  
 Dipartimento di Fisica - Università di Modena  
 Via Campi 213/A - I 41100 Modena, ITALY

Partially supported by O.N.R. and MURST



Rossella Brunetti  
 Paolo Bordone  
 Andrea Bertoni  
 Stefano Monastra

Antonio Abramico  
 Marco Pascoli  
 Fausto Rossi

- Spectral density

# Contents

**Elementary definition and properties**

**Dynamical equations**

- Classical force
- Infinite potential barrier

**Electron - phonon interaction**

**Wigner paths and MC simulation**

- Paths and diagrams
- Multiplicity of Wigner paths
- Quantum self scattering

**Two-time Wigner function**

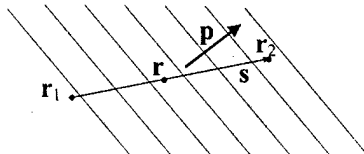
$$f_w(p, \omega)$$

## THE WIGNER FUNCTION

The Wigner-function approach is a phase-space formulation of quantum mechanics that allows to establish many analogies with the semiclassical theory based on the concept of distribution function

Elementary definition:

$$\rho(r_1, r_2)$$



$$f_w(r, p, t) = \int ds e^{-ips/\hbar} \Psi(r + s/2, t) \Psi^*(r - s/2, t)$$

## Properties of the Wigner function

$$\frac{1}{\hbar^3} \int f_w(r, p, t) dp = |\Psi(r, t)|^2$$

$$\frac{1}{\hbar^3} \int f_w(r, p, t) dr = |\Phi(p, t)|^2$$

$$\langle A \rangle = \frac{1}{\hbar^3} \int dr \int dp f_w(r, p, t) A_w(r, p)$$

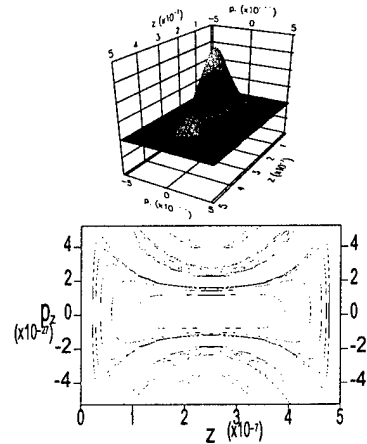
$$A_w[\mathbf{a}, p] = \sum_s e^{-ips/\hbar} \langle r+s/2 | A | r-s/2 \rangle$$

Linear in  $f$

NOT positive definite  
Strong oscillations  
 $\neq 0$  also where  $\Psi = 0$

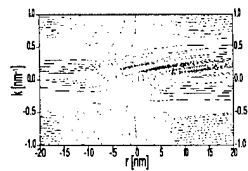
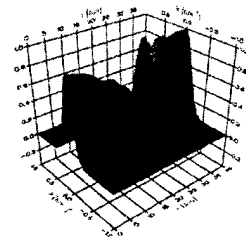
## WIGNER FUNCTION

*Ground state in a box:*

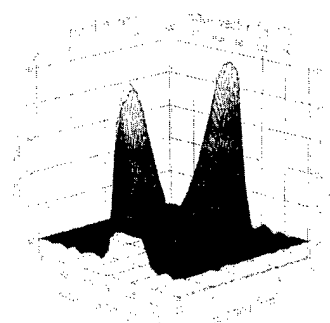


## WIGNER FUNCTION

Potential step with scattering states:



## WIGNER FUNCTION FOR A DOUBLE BARRIER



## COHERENT PROPAGATION OF THE W.F.

## DYNAMICAL EQUATION OF THE W.F. (1)

From the Liouville – Von Neumann

If

$$\mathbf{H}|\varphi_n\rangle = \hbar\omega_n|\varphi_n\rangle$$

then

$$f_w(\mathbf{r}, \mathbf{p}, t) = \sum_{n,m} f_{n,m}(\mathbf{r}, \mathbf{p}) e^{-i(\omega_n - \omega_m)(t-t_0)} \frac{1}{\hbar^3} \int d\mathbf{r}' \int d\mathbf{p}' f_{n,m}^*(\mathbf{r}', \mathbf{p}') f_w(\mathbf{r}', \mathbf{p}', t_0)$$

Linear

where

$$f_{n,m}(\mathbf{r}, \mathbf{p}) = \int ds e^{-ips/\hbar} \langle \mathbf{r} + s/2 | \varphi_n \rangle \langle \varphi_m | \mathbf{r} - s/2 \rangle$$

$$i\hbar \frac{d}{dt} \rho = [\mathbf{H}, \rho]$$

with

$$\mathbf{H} = \mathbf{H}_o + \mathbf{V}(\mathbf{r})$$

$$\mathbf{H}_o = -\frac{\hbar^2}{2m} \nabla^2$$

Obtain

$$\frac{\partial}{\partial t} f_w(\mathbf{r}, \mathbf{p}, t) = \int ds e^{-ips/\hbar} \times \langle \mathbf{r} + s/2 | \mathcal{V}_h[\mathbf{H}_o + \mathbf{V}(\mathbf{r}), \rho] | \mathbf{r} - s/2 \rangle$$

With standard elaboration:

$$\int ds e^{-ips/\hbar} \langle \mathbf{r} + s/2 | \mathcal{V}_h[\mathbf{H}_o, \rho] | \mathbf{r} - s/2 \rangle = -\frac{\mathbf{p}}{m} \nabla f_w$$

and

$$\begin{aligned} \int ds e^{-ips/\hbar} \langle \mathbf{r} + s/2 | \mathcal{V}_h[\mathbf{V}(\mathbf{r}), \rho] | \mathbf{r} - s/2 \rangle \\ = \int d\mathbf{p}' V_w(\mathbf{r}, \mathbf{p} - \mathbf{p}') f_w(\mathbf{r}, \mathbf{p}', t) \end{aligned}$$

where

$$V_w(\mathbf{r}, \mathbf{p}) = \frac{1}{i\hbar} \frac{1}{\hbar^3} \int ds e^{ips/\hbar} [V(\mathbf{r} - s/2) - V(\mathbf{r} + s/2)]$$

## DYNAMICAL EQUATION OF THE W.F. (2)

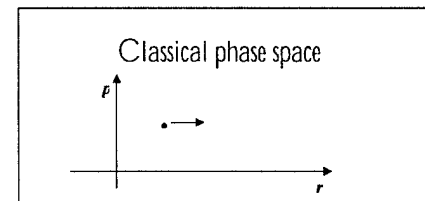
Collecting the above:

$$\frac{\partial}{\partial t} f_w(\mathbf{r}, \mathbf{p}, t) + \frac{\mathbf{p}}{m} \frac{\partial}{\partial \mathbf{r}} f_w = \frac{\partial f_w}{\partial t} \Big|_{\mathbf{r}}$$

For "regular" potential (up to quadratic):

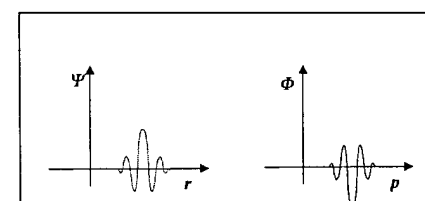
$$\frac{\partial}{\partial t} f_w(\mathbf{r}, \mathbf{p}, t) + \frac{\mathbf{p}}{m} \frac{\partial}{\partial \mathbf{r}} f_w + \mathbf{F} \frac{\partial}{\partial \mathbf{p}} f_w = 0$$

as in Liouville theorem.

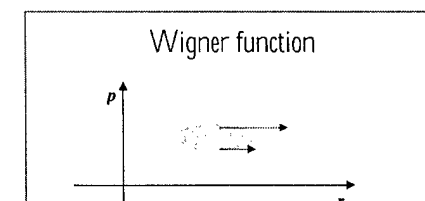


### WIGNER PATHS:

The Wigner function of electrons in presence of potentials up to quadratic evolves as an ensemble of classical particles: each point follows a classical path in the Wigner phase space (Wigner path)

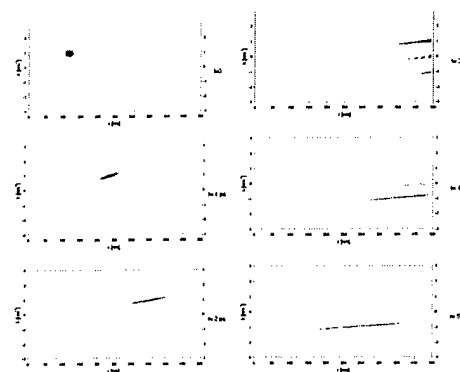
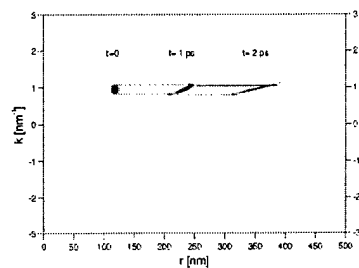


Quantum mechanics



## Time evolution of the Wigner Function of a wave packet

Time evolution of the Wigner Function reflected by an infinite potential barrier



13

## WIGNER PATHS WITH POTENTIAL SCATTERING

$$V = V_o + V' \quad F = -\nabla V_o$$

$V_o$  linear or quadratic - Integro-differential equation

$$\frac{\partial}{\partial t} f_w(r, p, t) + \frac{p}{m} \frac{\partial}{\partial r} f_w + F \frac{\partial}{\partial p} f_w = \sum_{\vec{p}'} V_w(r, p - p') f_w(r, p', t)$$

where

$$V_w(r, p) = \frac{1}{h^3} \sum_s e^{-ips/h} [V'(r+s/2) - V'(r-s/2)]$$

path variables:

$$r(\tilde{t}) = r - \sum_{t'} p(t') / m \quad p(\tilde{t}) = p - \sum_{t'} F(r(t')) dt'$$

time integration:

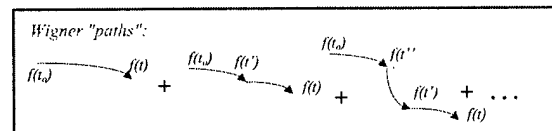
$$f_w(r, p, t)$$

$$= f_w(r(t_0), p(t_0), t_0) + \sum_{t'} \sum_{p'} V_w(r(t'), p' - p(t')) f_w(r(t'), p', t')$$

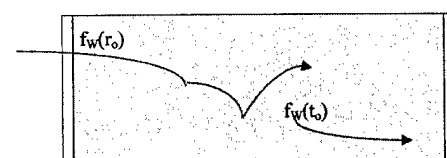
as in Chambers kinetic integral equation, without scattering "out", with similar interpretation:

$$f(t_0) \xrightarrow{f(t)} + \xrightarrow{f(t')} f(t)$$

Neumann expansion



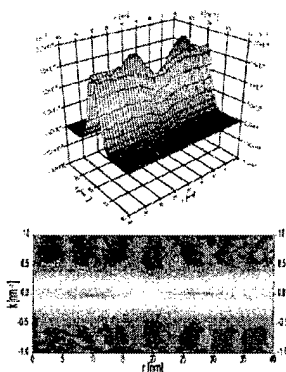
## Boundary conditions



Phys.Rev.B 58, 3503 (1998)

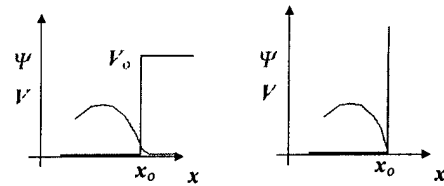
Phys.Rev.B 59, 3060 (1999)

## Single barrier (4nm x .05eV)



Obtained by means of W. Paths with potential scattering in a Monte Carlo approach

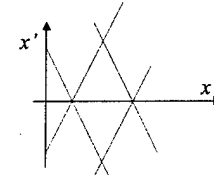
## Wigner Function confined by an infinite potential barrier



For the infinite barrier the Schröd. eq. holds only inside.  
For a box (a,b)

$$f_w(x, p, t) = \int_{-\xi(x)}^{\xi(x)} ds e^{-ips/\hbar} \Psi(x+s/2, t) \Psi^*(x-s/2, t)$$

where



$$\xi(x) = V(r+s/2) \begin{cases} 2(x-a) & \text{if } x < (a+b)/2 \\ 2(b-x) & \text{if } x \geq (a+b)/2 \end{cases}$$

16

17

## Wigner Function confined by an infinite potential barrier (ii)

In the derivation of the dynamical equation, the derivatives at the boundaries do not vanish, and we have an extra integral term

$$\frac{\partial f_w}{\partial t} + \frac{p}{m} \frac{\partial f_w}{\partial x} = \frac{1}{\hbar} \int dp' V_w(x, p-p') f_w(x, p', t) + \frac{1}{\hbar} \int dp' B(x, p-p') \frac{\partial}{\partial x} f_w(x, p', t)$$

where

$$B(x, p) = \frac{2\hbar}{m} \sin \left[ \frac{p}{\hbar} \xi(x) \right]$$

simulation ...

## SEPARATION BETWEEN CLASSICAL FORCE AND QUANTUM EFFECTS

$$\frac{\partial f_w}{\partial t} + \frac{p}{m} \frac{\partial f_w}{\partial r} = \frac{1}{\hbar^2} \int dp' V_w(r, p-p') f_w(r, p', t)$$

where

$$V_w(r, p) = \frac{1}{i\hbar} \int ds e^{-ips/\hbar} \beta(r, s)$$

$$\beta(r, s) = V(r+s/2) - V(r-s/2)$$

or

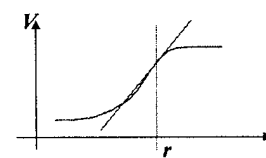
$$\frac{\partial f_w}{\partial t} + \frac{p}{m} \frac{\partial f_w}{\partial r} + F \frac{\partial f_w}{\partial p} = \frac{1}{\hbar^2} \int dp' \tilde{V}_w(r, p-p') f_w(r, p', t)$$

where

$$F = -\frac{\partial V f_w}{\partial r}$$

$$\tilde{V}_w(r, p) = \frac{1}{i\hbar} \int ds e^{-ips/\hbar} \tilde{\beta}(r, s)$$

$$\tilde{\beta}(r, s) = \left[ V(r+s/2) - \frac{\partial V}{\partial r} s/2 \right] - \left[ V(r-s/2) + \frac{\partial V}{\partial r} s/2 \right]$$



18

19

## ELECTRON-PHONON SCATTERING WITH THE WIGNER FUNCTION

Extend the definition of Wigner function:

$$f_w(\mathbf{r}, \mathbf{p}, \{n_q\}, \{n'_q\}, t)$$

$$= \int d\mathbf{s} e^{-ips/\hbar} \langle \mathbf{r} + s/2, \{n_q\} | \rho(t) | \mathbf{r} - s/2, \{n'_q\} \rangle$$

Hamiltonian:

$$\mathbf{H} = \mathbf{H}_o + \mathbf{H}_{ph} + \mathbf{H}_{e-p} + \mathbf{V}_o(\mathbf{r}) + \mathbf{V}'(\mathbf{r})$$

where

$$\begin{aligned} \mathbf{H}_o &= -\frac{\hbar^2}{2m} \nabla^2 \\ \mathbf{H}_{ph} &= \sum_q \mathbf{b}_q^\dagger \mathbf{b}_q \hbar \omega_q \\ \mathbf{H}_{e-p} &= \sum_q i\hbar F(q) (\mathbf{b}_q e^{i\mathbf{q}\cdot\mathbf{r}} - \mathbf{b}_q^\dagger e^{-i\mathbf{q}\cdot\mathbf{r}}) \\ \mathbf{V}_o(\mathbf{r}) &= e\mathbf{E} \cdot \mathbf{r} \end{aligned}$$

$\mathbf{V}'(\mathbf{r})$  = potential profile

Differentiate the definition above and use

$$i\hbar \frac{d}{dt} \rho = [\mathbf{H}, \rho]$$

Obtain

$$\begin{aligned} \frac{\partial}{\partial t} f_w(\mathbf{r}, \mathbf{p}, \{n_q\}, \{n'_q\}, t) &= \int d\mathbf{s} e^{-ips/\hbar} \times \\ &\langle \mathbf{r} + s/2, \{n_q\} | \gamma_h [\mathbf{H}_o + \mathbf{H}_{ph} + \mathbf{H}_{e-p} + \mathbf{V}_o(\mathbf{r}) + \mathbf{V}'(\mathbf{r}), \rho] | \mathbf{r} - s/2, \{n'_q\} \rangle \end{aligned}$$

## ELECTRON-PHONON SCATTERING WITH THE WIGNER FUNCTION - II

Several terms:

$$\int d\mathbf{s} e^{-ips/\hbar} \langle \mathbf{r} + s/2, \{n_q\} | \gamma_h [\mathbf{H}_o, \rho] | \mathbf{r} - s/2, \{n'_q\} \rangle = -\frac{p}{m} \nabla f_w$$

$$\int d\mathbf{s} e^{-ips/\hbar} \langle \mathbf{r} + s/2, \{n_q\} | \gamma_h [\mathbf{H}_{ph}, \rho] | \mathbf{r} - s/2, \{n'_q\} \rangle = -\gamma_h [e(\{n_q\}) - e(\{n'_q\})] f_w$$

$$\int d\mathbf{s} e^{-ips/\hbar} \langle \mathbf{r} + s/2, \{n_q\} | \gamma_h [\mathbf{V}_o(\mathbf{r}), \rho] | \mathbf{r} - s/2, \{n'_q\} \rangle = -F \frac{\partial}{\partial p} f_w$$

$$\begin{aligned} \int d\mathbf{s} e^{-ips/\hbar} \langle \mathbf{r} + s/2, \{n_q\} | \gamma_h [\mathbf{V}'(\mathbf{r}), \rho] | \mathbf{r} - s/2, \{n'_q\} \rangle \\ = \int d\mathbf{p}' V_o(\mathbf{r}, \mathbf{p} - \mathbf{p}') f_w(\mathbf{r}, \mathbf{p}', \{n_q\}, \{n'_q\}, t) \end{aligned}$$

Electron-phonon term:

$$\begin{aligned} \int d\mathbf{s} e^{-ips/\hbar} \langle \mathbf{r} + s/2, \{n_q\} | \gamma_h [\mathbf{H}_{e-p}, \rho] | \mathbf{r} - s/2, \{n'_q\} \rangle = \\ \sum_{q'} F(q') \{ e^{iq'\mathbf{r}} \sqrt{n_{q'}+1} f_w(\mathbf{r}, \mathbf{p} - \frac{\hbar q'}{2}), n_1 \dots n_{q'}+1 \dots, \{n'_q\}, t) \\ - e^{-iq'\mathbf{r}} \sqrt{n_{q'}} f_w(\mathbf{r}, \mathbf{p} + \frac{\hbar q'}{2}), n_1 \dots n_{q'}-1 \dots, \{n'_q\}, t) \\ - e^{iq'\mathbf{r}} \sqrt{n_{q'}+1} f_w(\mathbf{r}, \mathbf{p} + \frac{\hbar q'}{2}), \{n_q\}, n_1' \dots n_{q'}'-1 \dots, t) \\ + e^{-iq'\mathbf{r}} \sqrt{n_{q'}+1} f_w(\mathbf{r}, \mathbf{p} - \frac{\hbar q'}{2}), \{n_q\}, n_1' \dots n_{q'}'+1 \dots, t) \} \end{aligned}$$

Path variables, time integration, Neumann expansion ...

## PHONON AVERAGE

Reduction to electron Wigner function

Trace over phonon variables:

$$f_w \mathbf{a}_{\mathbf{p},t} = \sum_{\mathbf{q}, \mathbf{r}} f_w \mathbf{d}_{\mathbf{p}, \mathbf{q}} \mathbf{n}_{\mathbf{q}} \mathbf{s}_{\mathbf{q}} \mathbf{s}_{\mathbf{r}}$$

Assume separate equilibrium initial density matrix:

$$f_w \mathbf{d}_{\mathbf{p}, \mathbf{q}} \mathbf{n}_{\mathbf{q}} \mathbf{s}_{\mathbf{q}} \mathbf{s}_{\mathbf{r}} = \mathbf{i}_{\infty} \prod_q P_{eq} \mathbf{G}_q \mathbf{i}$$

For final diagonal terms, with initial diagonal W.f., each Monte Carlo term contains a phonon mode twice and has factors like

$$\Delta f_w \mathbf{d}_{\mathbf{p}, \mathbf{q}} \mathbf{n}_{\mathbf{q}} \mathbf{s}_{\mathbf{q}} \mathbf{s}_{\mathbf{r}} \propto n_{q_1} \dots n_{q_l} + 1 \dots f_w \mathbf{d}_{\mathbf{p}, \mathbf{q}} \mathbf{n}_{\mathbf{q}} \mathbf{s}_{\mathbf{q}} \mathbf{s}_{\mathbf{r}}$$

The simulation must be thought of as repeated a 'large number' of times for each  $\{n_q\}$ . Then, if hot-phonon effects are ignored,

⇒ for absent  $q$ :

$$\sum_{\mathbf{q}, \mathbf{r}} P_{eq} \mathbf{G}_q \mathbf{h}_1$$

⇒ for real or virtual absorptions:

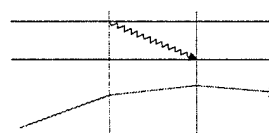
$$\sum_{n_q} \mathbf{G}_q + 1 \mathbf{h}_{eq} \mathbf{G}_q + 1 \mathbf{h} \langle n_q \rangle \quad \sum_{n_q} \mathbf{G}_q \mathbf{h}_{eq} \mathbf{G}_q \mathbf{h} \langle n_q \rangle$$

⇒ for real or virtual emissions:

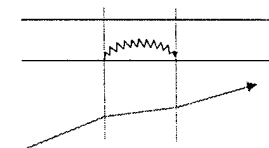
$$\sum_{n_q} n_q P_{eq} \mathbf{G}_q - 1 \mathbf{h} \langle n_q + 1 \rangle \quad \sum_{n_q} \mathbf{G}_q + 1 \mathbf{h}_{eq} \mathbf{G}_q \mathbf{h} \langle n_q + 1 \rangle$$

## Phonon scattering

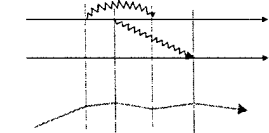
Real emission ("in")



Virtual emission ("out")



Multiple scattering

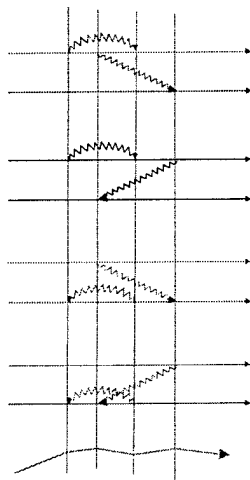


Intracollisional field effect, interference with potential scattering, ...

MONTE CARLO

## Multiplicity of Wigner paths

Each multiple path can be obtained with different diagrams



Each graph contributes with a factor

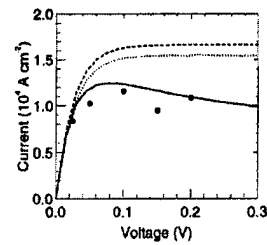
$$e^{i(qr_j - \omega t_j)}$$

Summing up all terms, the contribution becomes

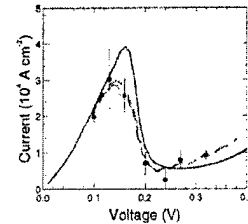
$$2\cos(qr_j - \omega t_j) 2\cos(q'r_k - \omega't_k) \rightarrow 2^m \prod \cos$$

24

## Potential step – one phonon scattering



## Double barrier – one phonon scattering



25

## Quantum self-scattering

IN STRICT FORMAL ANALOGY WITH SELF SCATTERING IN SEMICLASSICAL TRANSPORT SIMULATION

Define:

$$\tilde{f}_w(\mathbf{r}, \mathbf{p}, \{n_q\}, \{n'_q\}, t) = e^{\Gamma(t-t_0)} f_w$$

By substitution into the dynamical equation, an extra term is added to the interaction, proportional to  $\Gamma$ .

Each "free flight" in the Wigner paths is multiplied by a factor

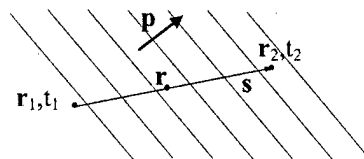
$$e^{-\Gamma(t_i - t_f)}$$

corresponding to an approximate constant life-time of the electron state (imaginary part of the self energy).

At each "scattering event" a choice is made between self or actual scattering, thus correcting, at each order, the approximate self energy with the exact one.

## TWO-TIME WIGNER FUNCTION

$$\rho(\mathbf{r}_1, t_1; \mathbf{r}_2, t_2)$$



$$\mathbf{r} = \frac{\mathbf{r}_1 + \mathbf{r}_2}{2} \quad \mathbf{s} = \mathbf{r}_2 - \mathbf{r}_1$$

$$t = \frac{t_1 + t_2}{2} \quad \tau = t_2 - t_1$$

$$f_w(\mathbf{r}, \mathbf{p}, \omega, t) = \int d\tau e^{i\omega\tau} \int ds e^{-ips/\hbar} \langle r+s/2 | \Psi(\mathbf{d}+\tau/2) \rangle \langle \Psi(\mathbf{d}-\tau/2) | r-s/2 \rangle$$

26

27

## TWO-TIME WIGNER F. WITH PHONONS (1)

$$G^c(r_1, t_1; r_2, t_2) = \frac{i}{\hbar} \langle \Psi^\dagger(r_2, t_2) \Psi(r_1, t_1) \rangle$$

$$= \frac{i}{\hbar} \langle \Phi(t_2) | \Psi^\dagger(r_2) U(t_2, t_1) \Psi(r_1) | \Phi(t_1) \rangle$$

$$\Phi(r, \{n_q\}, t) = \langle r, \{n_q\} | \Phi(t) \rangle$$

$$\mathbb{H} = \mathbb{H}_e + \mathbb{H}_p + \mathbb{H}_{ep}$$

$$G^c = \frac{i}{\hbar} \sum_{\{n_q\}} \sum_{\{n'_q\}} \langle 0, \{n_q\} | e^{-iH_p(t_2-t_1)/\hbar} | 0, \{n'_q\} \rangle \Phi^*(r_2, \{n_q\}, t_2) \Phi(r_1, \{n'_q\}, t_1)$$

$$= \frac{i}{\hbar} \sum_{\{n_q\}} e^{-i\omega_p(t_2-t_1)} \Phi^*(r_2, \{n_q\}, t_2) \Phi(r_1, \{n_q\}, t_1)$$

Put

$$g(r, \{n_q\}, t) = e^{i\omega(\{n_q\})t} \Phi(r, \{n_q\}, t)$$

Then

$$G^c(r_1, t_1; r_2, t_2) = \frac{i}{\hbar} \sum_{\{n_q\}} g^*(r_2, \{n_q\}, t_2) g(r_1, \{n_q\}, t_1)$$

28

29

## TWO-TIME WIGNER F. WITH PHONONS (3)

Dynamical equation

$$\begin{aligned} \frac{\partial}{\partial t} f_w(r, p, \{n_q\}, \{n'_q\}, t, \omega) &= \int e^{ipr/\hbar} dr' \\ \int e^{-i\omega r} d\tau \left[ \left[ \frac{\partial}{\partial t} g(r - r'/2, \{n_q\}, t - \tau/2) \right] g^*(r + r'/2, \{n'_q\}, t + \tau/2) + g \frac{\partial}{\partial t} g^* \right] & \\ \frac{\partial}{\partial t} g(r, \{n_q\}, t) &= i\omega(\{n_q\}) g + \frac{1}{i\hbar} \mathbb{H} g \end{aligned}$$

If

$$\mathbb{H} = \mathbb{H}_e + \mathbb{H}_p + \mathbb{H}_{ep}$$

with

$$\mathbb{H}_p = \sum_q \mathbf{b}_q^\dagger \mathbf{b}_q \hbar \omega_q$$

then

$$\begin{aligned} \frac{\partial}{\partial t} g(r, \{n_q\}, t) &= i\omega(\{n_q\}) g + \frac{1}{i\hbar} (\mathbb{H}_e + \mathbb{H}_p + \mathbb{H}_{ep}) g \\ &= i\omega(\{n_q\}) g + \frac{1}{i\hbar} (\mathbb{H}_e + \mathbb{H}_{ep}) g + \frac{1}{i\hbar} \hbar \omega(\{n_q\}) g \end{aligned}$$

Thus the free-phonon dynamics is eliminated

## TWO-TIME WIGNER F. WITH PHONONS (2)

Perform traditional transformation:

$$t = \frac{t_1 + t_2}{2}, \quad \tau = t_2 - t_1 \quad \mathbf{r} = \frac{\mathbf{r}_1 + \mathbf{r}_2}{2}, \quad \mathbf{r}' = \mathbf{r}_2 - \mathbf{r}_1$$

and Fourier transform:

$$\begin{aligned} f_w(r, p, t, \omega) &= -i\hbar G^c(r, p, t, \omega) = \sum_{\{n_q\}} \int e^{ipr/\hbar} dr' \\ \int e^{-i\omega \tau} d\tau g(r - r'/2, \{n_q\}, t - \tau/2) g^*(r + r'/2, \{n_q\}, t + \tau/2) & \end{aligned}$$

For dynamical equation generalize to non diagonal phonon states:

$$\begin{aligned} f_w(r, p, \{n_q\}, \{n'_q\}, t, \omega) &= \int e^{ipr/\hbar} dr' \\ \int e^{-i\omega \tau} d\tau g(r - r'/2, \{n_q\}, t - \tau/2) g^*(r + r'/2, \{n'_q\}, t + \tau/2) & \end{aligned}$$

and

$$f_w(r, p, t, \omega) = \sum_{\{n_q\}} f_w(r, p, \{n_q\}, \{n_q\}, t, \omega)$$

## TWO-TIME WIGNER F. WITH PHONONS (4)

The various terms in the dynamical equations are treated as in the standard case:

$$\mathbb{H}_v = -\frac{\hbar^2}{2m} \nabla^2$$

yields

$$\frac{\partial}{\partial t} \Big|_{t_o} f_w(r, p, \{n_q\}, \{n'_q\}, t, \omega) = -\frac{p}{m} \nabla_r f_w$$

$$\nabla = V(r)$$

yields

$$\begin{aligned} \frac{\partial}{\partial t} \Big|_{t_o} f_w(r, p, \{n_q\}, \{n'_q\}, t, \omega) & \\ = \int_{-\infty}^{\infty} dp' V_w(r, p - p') f_w(r, p', \{n_q\}, \{n'_q\}, t, \omega) & \end{aligned}$$

where

$$V_w(r, p) = \frac{1}{i\hbar} \frac{1}{(2\pi\hbar)^3} \int dr' e^{ipr'/\hbar} [V(r - r'/2) - V(r + r'/2)]$$

For a constant or harmonic force F

$$\frac{\partial}{\partial t} \Big|_{t_o} f_w(r, p, \{n_q\}, \{n'_q\}, t, \omega) = -F \frac{\partial}{\partial p} f_w$$

30

31

## TWO-TIME WIGNER F. WITH PHONONS (5)

Taking into account that

$$\begin{aligned} b_q g(r - r'/2, \{n_q\}, t - \tau/2) \\ = e^{i\omega[n_q](t-\tau/2)} \langle r - r'/2, \{n_q\} | b_q | \Psi(t - \tau/2) \rangle \\ = e^{-i\omega_q(t-\tau/2)} \sqrt{n_q + 1} g(r - r'/2, \{n_1, \dots, n_q + 1, \dots\}, t - \tau/2) \end{aligned}$$

and similar,

the electron-phonon interaction

$$H_{ep} = i\hbar \sum_q F(\mathbf{q}') (b_q e^{i\mathbf{q}' \cdot \mathbf{r}} - b_q^\dagger e^{-i\mathbf{q}' \cdot \mathbf{r}})$$

yields

$$\begin{aligned} \frac{\partial}{\partial t} \Big|_{ep} f_w(r, p, \{n_q\}, \{n'_q\}, t, \omega) = \sum_q F(\mathbf{q}') \{ \\ e^{i(\mathbf{q}' \cdot \mathbf{r} - \omega_q t)} \sqrt{n_q + 1} f_w(r, p - \hbar\mathbf{q}'/2, \{n_1, \dots, n_q + 1, \dots\}, \{n'_q\}, t, \omega - \omega_q/2) \\ - e^{-i(\mathbf{q}' \cdot \mathbf{r} - \omega_q t)} \sqrt{n_q} f_w(r, p + \hbar\mathbf{q}'/2, \{n_1, \dots, n_q - 1, \dots\}, \{n'_q\}, t, \omega + \omega_q/2) \\ + e^{-i(\mathbf{q}' \cdot \mathbf{r} - \omega_q t)} \sqrt{n'_q + 1} f_w(r, p - \hbar\mathbf{q}'/2, \{n_q\}, \{n'_1, \dots, n'_q + 1, \dots\}, t, \omega - \omega_q/2) \\ - e^{i(\mathbf{q}' \cdot \mathbf{r} - \omega_q t)} \sqrt{n'_q} f_w(r, p + \hbar\mathbf{q}'/2, \{n_q\}, \{n'_1, \dots, n'_q - 1, \dots\}, t, \omega + \omega_q/2) \} \end{aligned}$$

## TWO-TIME WIGNER F. WITH PHONONS (6)

The general equation

$$\frac{\partial}{\partial t} f_w(r, p, \{n_q\}, \{n'_q\}, t, \omega) + \frac{p}{m} \frac{\partial}{\partial r} f_w + F \frac{\partial}{\partial p} f_w = \frac{\partial f_w}{\partial t} \Big|_r + \frac{\partial f_w}{\partial t} \Big|_p$$

here

$$\begin{aligned} \frac{\partial}{\partial t} \Big|_r f_w(r, p, \{n_q\}, \{n'_q\}, t, \omega) &= \int dp' V_w(r, p - p') f_w(r, p', \{n_q\}, \{n'_q\}, t, \omega) \\ V_w(r, p) &= \frac{1}{i\hbar(2\pi\hbar)} \int dr' e^{i\mathbf{p}' \cdot \mathbf{r}'} [V(r - r'/2) - V(r + r'/2)] \end{aligned}$$

and

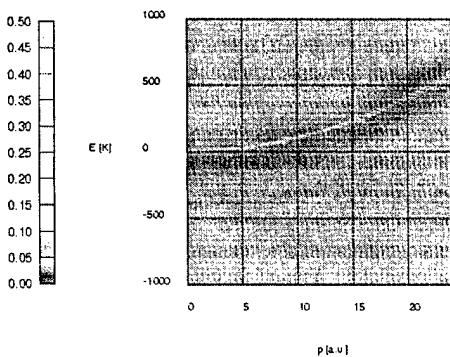
$$\begin{aligned} \frac{\partial}{\partial t} \Big|_p f_w(r, p, \{n_q\}, \{n'_q\}, t, \omega) &= \sum_q F(\mathbf{q}') \{ \\ e^{i(\mathbf{q}' \cdot \mathbf{r} - \omega_q t)} \sqrt{n_q + 1} f_w(r, p - \hbar\mathbf{q}'/2, \{n_1, \dots, n_q + 1, \dots\}, \{n'_q\}, t, \omega - \omega_q/2) \\ - e^{-i(\mathbf{q}' \cdot \mathbf{r} - \omega_q t)} \sqrt{n_q} f_w(r, p + \hbar\mathbf{q}'/2, \{n_1, \dots, n_q - 1, \dots\}, \{n'_q\}, t, \omega + \omega_q/2) \\ + e^{-i(\mathbf{q}' \cdot \mathbf{r} - \omega_q t)} \sqrt{n'_q + 1} f_w(r, p - \hbar\mathbf{q}'/2, \{n_q\}, \{n'_1, \dots, n'_q + 1, \dots\}, t, \omega - \omega_q/2) \\ - e^{i(\mathbf{q}' \cdot \mathbf{r} - \omega_q t)} \sqrt{n'_q} f_w(r, p + \hbar\mathbf{q}'/2, \{n_q\}, \{n'_1, \dots, n'_q - 1, \dots\}, t, \omega + \omega_q/2) \} \end{aligned}$$

- The left hand side of the above equation is the same Liouvillian as in the Boltzmann equation
- Path variables and integral form of the transport equation
- Neumann expansion
- Wigner Paths
- Monte Carlo

• At each interaction “vertex” half phonon momentum and half phonon energy is transferred to or taken from the electron

Spectral Density  
 $A(p, \omega) = f_w(p, \omega)/f_w(p)$

GaAs  
 Polar optical phonons  
 $T=300\text{ K}$   
 up to 3 scattering  
 $t=150\text{ fs}$



## Conclusions

Wigner paths can be defined as ballistic “flights” separated by scattering processes

The Wigner-function approach allows a description of quantum transport in terms of phase-space analogous to the semiclassical case

A Monte Carlo algorithm can be implemented that accounts for given initial and boundary conditions

Momentum and frequency can be considered as independent variables in a two-time Green function approach, maintaining the path Monte Carlo approach

PROBLEMS ...

## Modeling Resonant Tunneling Devices With Wigner Functions and Density Matrices

H. L. Grubin

Scientific Research Associates, Inc

hal@sraassoc.com

SRA

Nanostructures & Transients

## Quantum Transport RTD Studies

- Use Wigner Function (primarily) and Density Matrix to describe **transient** transport in nanoscale devices
- Go beyond using switching speed as a primary characteristic of a device. Instead we also determine the **recovery** time.
- We do this within the framework of an RTD as a self-excited sustained relaxation oscillator (RTD-RO) and seek the highest frequency of oscillation.

SRA

Nanostructures & Transients

## WF/DM Equation

- Can be obtained in simple cases directly from Schrodinger's equation or formally as follows:

SRA

Nanostructures & Transients

- Collaborators:  
R.C. Buggeln and J. P. Kreskovsky
- Supported by Office of Naval Research

SRA

Nanostructures & Transients

## Simulation Requirements

- Suitable transient quantum transport equation—Wigner equation/Density Matrix
- Poisson's equation + flat band boundary conditions
- Circuit equations/transmission line equations—treated as boundary conditions
- Suitable description of reservoirs and dissipation

SRA

Nanostructures & Transients

## Density Operator

$$\rho_{op}(t) = \sum_i |i(t)\rangle P(i) \langle i(t)|$$

Single time  
Density Operator

SRA

Nanostructures & Transients

## Density Operator

$$\rho_{op}(t) = \sum_i |i(t)\rangle P(i) \langle i(t)|$$

Coordinate representation

$$\begin{aligned} \langle \mathbf{x} | \rho_{op}(t) | \mathbf{x}' \rangle &= \sum_i \langle \mathbf{x} | i(t) \rangle P(i) \langle i(t) | \mathbf{x}' \rangle \\ &= \sum_i P(i) \Psi_i^*(\mathbf{x}', t) \Psi_i(\mathbf{x}, t) \end{aligned}$$

SRA  
Nanostructures & Transients

## Time Dependence/Liouville Eq.

$$\begin{aligned} i\hbar \frac{d\rho_{op}(t)}{dt} &= [H(t), \rho_{op}(t)] \\ i\hbar \frac{\partial \langle \mathbf{x} | \rho(t) | \mathbf{x}' \rangle}{\partial t} &= \\ &= \left\{ -\frac{\hbar^2}{2m} \left( \frac{\partial^2}{\partial \mathbf{x}^2} - \frac{\partial^2}{\partial \mathbf{x}'^2} \right) + V(\mathbf{x}) - V(\mathbf{x}') \right\} \langle \mathbf{x} | \rho(t) | \mathbf{x}' \rangle \\ \xrightarrow{\text{dissipation}} &+ i\hbar \left\{ \frac{\partial \langle \mathbf{x} | \rho(t) | \mathbf{x}' \rangle}{\partial t} \right\}_{\text{scattering}} \end{aligned}$$

SRA  
Nanostructures & Transients

## Density & Current Density Matrix

$$\rho(\mathbf{x}, \mathbf{x}') = \langle \mathbf{x} | \rho_{op}(t) | \mathbf{x}' \rangle$$

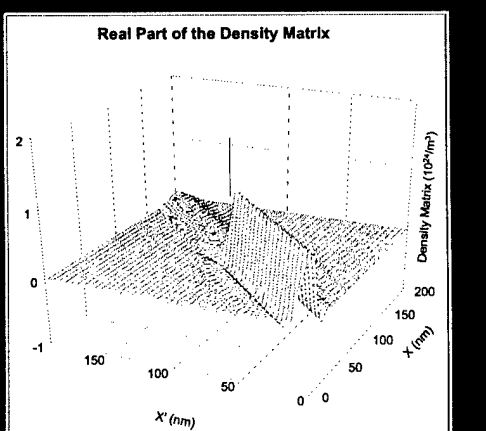
$$\text{Density} \quad \rho(\mathbf{x}) = \langle \mathbf{x} | \rho_{op}(t) | \mathbf{x} \rangle$$

$$\mathbf{j}(\mathbf{x}, \mathbf{x}') = \frac{\hbar}{2mi} (\nabla_{\mathbf{x}} - \nabla_{\mathbf{x}'}) \langle \mathbf{x} | \rho_{op}(t) | \mathbf{x}' \rangle$$

$$\text{Current Density} \quad \mathbf{j}(\mathbf{x}) = \lim_{\mathbf{x}' \rightarrow \mathbf{x}} \mathbf{j}(\mathbf{x}, \mathbf{x}')$$

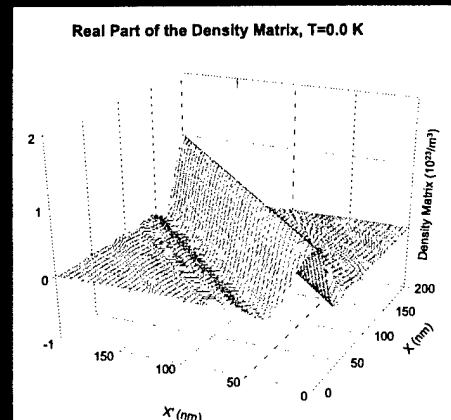
SRA  
Nanostructures & Transients

## Density Matrix Hetero-structure



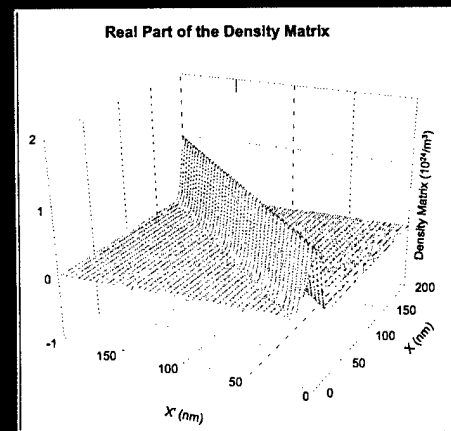
SRA  
Nanostructures & Transients

## Density Matrix Flat Profile



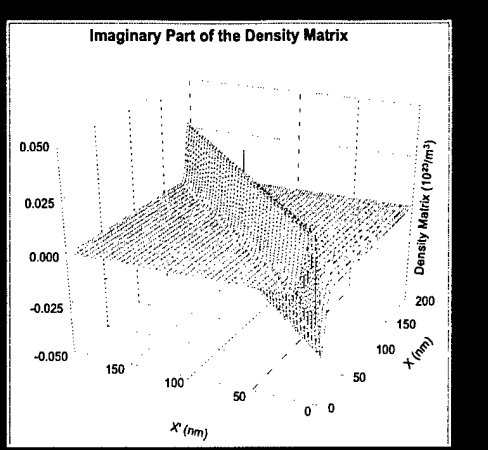
SRA  
Nanostructures & Transients

## Real Part Flat Profile, 300K



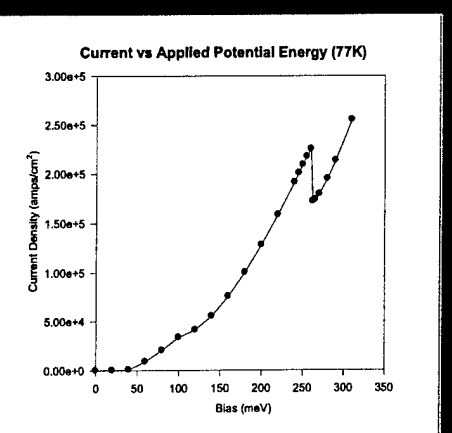
SRA  
Nanostructures & Transients

## Imag. Part Flat Profile, 300K



SRA  
Nanostructures & Transients

## IV Double Barrier RTD



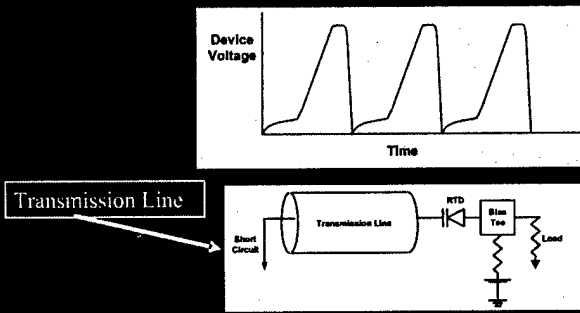
SRA  
Nanostructures & Transients

### What do we do with the RTD?

- Switching device!
  - There are many of these
- Logic device-particularly multiple value logic elements
- Quantum Van der Pol oscillator
  - Negative differential resistance can (sometimes) yield sustained oscillations.

SRA  
Nanostructures & Transients

### RTD as a Relaxation Oscillator: (Vergheese, C. D. Parker, E.R. Brown APL 1998)



SRA  
Nanostructures & Transients

### Quantum Van der Pol Oscillator

- It should be of interest to physicists because it is capable of providing a practical measure of the speed and response time of resonant tunneling diode.
  - How?
  - Determine the maximum frequency of a controlled oscillation that can *drive or affect* the total system
  - Use the RTD/RO as a clock.

SRA  
Nanostructures & Transients

### There are non-Van der Pol Oscillations

- We have observed weak (above threshold) voltage oscillations at frequencies near 700 GHz!

SRA  
Nanostructures & Transients

We will concentrate on the Wigner Function

- More success than with using the DM.
- Not as fast as the DM.

SRA  
Nanostuctures & Transients

Wigner Function/Equation from the Density Matrix through the Weyl Transformation

$$f_w(\mathbf{k}, \mathbf{r}) = \frac{1}{2} \int d\mathbf{s} \langle \mathbf{r} + \frac{\mathbf{s}}{2} | \rho_{\text{eff}}(t) \cdot \mathbf{r} - \frac{\mathbf{s}}{2} \rangle \exp - i \mathbf{k} \bullet \mathbf{s}$$

SRA  
Nanostuctures & Transients

## The Wigner Equation

$$0 = \frac{\partial f_w(\mathbf{k}, x)}{\partial t} + \frac{f_w(\mathbf{k}, x) - f_{w0}(\mathbf{k}, x)}{\tau(x)} + \frac{\hbar k_z}{m} \frac{\partial f_w(\mathbf{k}, x)}{\partial x}$$

$$- \frac{1}{\pi \hbar} \lim_{t \rightarrow \infty} \int_t^{\infty} d\xi \left[ \frac{V(x+\xi)}{-V(x-\xi)} \right] \int dk_z' f_w(k_z', k_z, k_z, \eta_z) \sin[2(k_z' - k_z)\xi]$$

Quantum Mechanics: The Wigner integral represents a correlation of states in the coordinate representation.

SRA  
Nanostuctures & Transients

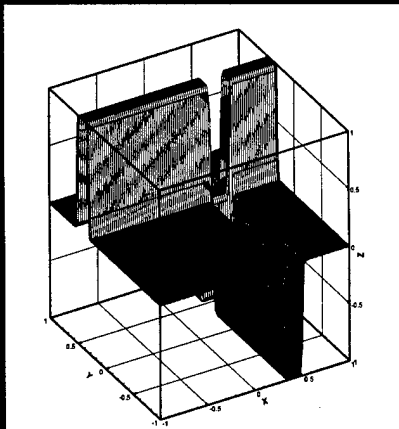
The Wigner Integral Treated Analytically-Highlights Correlations

$$\lim_{t \rightarrow \infty} \int_t^{\infty} dy \left[ \begin{matrix} V(x+y) \\ -V(x-y) \end{matrix} \right] \sin[2(k_z' - k_z)y]$$

$$= \frac{2V_0 \sin[2(k_z' - k_z)(x_0 - x)] \sin[(k_z' - k_z)\Delta]}{i(k_z' - k_z)}$$

SRA  
Nanostuctures & Transients

$V(x)-V(x')$  for a single asymmetrically placed barrier



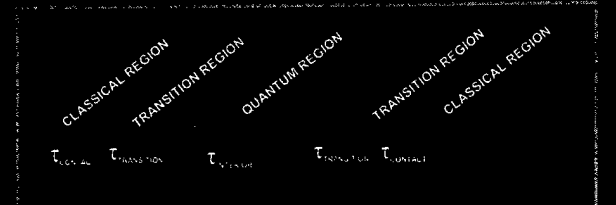
SRA  
Nanostuctures & Transients

## The Five Zone Structure

- Five zone structure:
  - The end regions (two) represent the contact regions;
  - The central region (one)-- incorporates the quantum barriers and wells;
  - The transition region (two)
- Variable scattering time, smallest in contact region.

SRA  
Nanostuctures & Transients

## Device Geometry



SRA  
Nanostructures & Transients

## Structure Emphasized *The Baseline Study, cont.*

- New derivative boundary conditions on Wigner function show flat-band and qualitative displacement momentum contributions.
- Do not need to assert displaced Fermi boundary conditions.
- Equilibrium distribution obtained first.

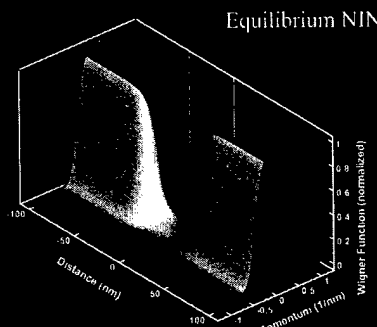
SRA  
Nanostructures & Transients

## Structure Emphasized *The Baseline Studies*

- 200 nm, DBRTD, 250/300mev-5nm-5nm-5nm, low doped central region
- DC and transient studies
- Hysteresis studies
- (Note: In the absence of barriers can compute IV of an NIN structure as well as linear resistor)

SRA  
Nanostructures & Transients

## Wigner Function NIN



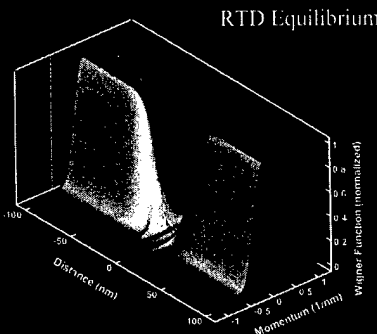
SRA  
Nanostructures & Transients

## Structure Emphasized *The Baseline Study, cont.*

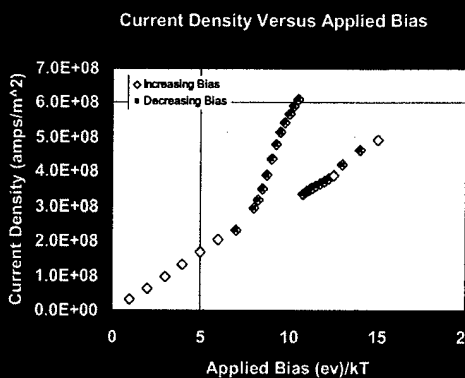
- Converged dc solutions via small bias increments show **no hysteresis!**
- Large signal transients show hysteresis.
- Relaxation to steady state occurs within a pico-sec and is bias dependent
- Devices sustain steady relaxation oscillations!

SRA  
Nanostructures & Transients

## Wigner Function RTD



SRA  
Nanostructures & Transients



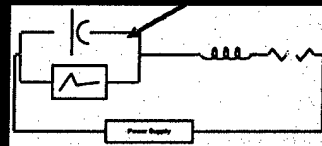
SRA  
Nanostructures & Transients

## RTD as a Relaxation Oscillator

(Lumped Circuit Elements, RTD Represented by Wigner Equation)

Wigner Equation  
Represents the  
RTD

Realistic Device  
Response



SRA  
Nanostructures & Transients

## RO Equations

$$\frac{dv_D}{dt} = \frac{2\pi Z_0}{R_D} \{ i(t) - i_D(v_D) \}$$

$$\frac{di}{dt} = \frac{R_D}{2\pi Z_0} \left\{ v_{APPLIED}(t) - v_D(t) + i(t) \frac{R_{LOAD}}{R_D} \right\}$$

SRA  
Nanostructures & Transients

## RO Equations

$$\frac{dv_D}{dt} = \frac{2\pi Z_0}{R_D} \{ i(t) - i_D(v_D) \}$$

$$\frac{di}{dt} = \frac{R_D}{2\pi Z_0} \left\{ v_{APPLIED}(t) - v_D(t) + i(t) \frac{R_{LOAD}}{R_D} \right\}$$

$$v_D = V_D / V_P, \quad i = I / I_P, \quad t = \tau / T_{ref}$$

SRA  
Nanostructures & Transients

## RO Equations

$$\frac{dv_D}{dt} = \frac{2\pi Z_0}{R_D} \{ i(t) - i_D(v_D) \}$$

$$\frac{di}{dt} = \frac{R_D}{2\pi Z_0} \left\{ v_{APPLIED}(t) - v_D(t) + i(t) \frac{R_{LOAD}}{R_D} \right\}$$

$$v_D = V_D / V_P, \quad i = I / I_P, \quad t = \tau / T_{ref}$$

Z<sub>0</sub> =  $\sqrt{L/C_D}$ , T<sub>ref</sub> =  $2\pi\sqrt{LC_D}$ , R<sub>D</sub> = V<sub>P</sub> / I<sub>P</sub>

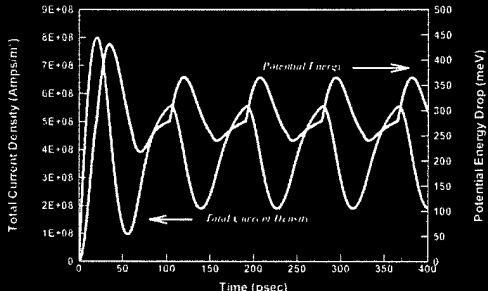
## RO Equation Parameters

$$\begin{cases} Z_0 = \sqrt{L/C_D} \\ T_{ref} = 2\pi\sqrt{LC_D} \\ R_D = V_P / I_P \end{cases}$$

Observation: For a fixed Z, oscillation characteristics are the same for all oscillatory periods provided the NDR is not dynamic.

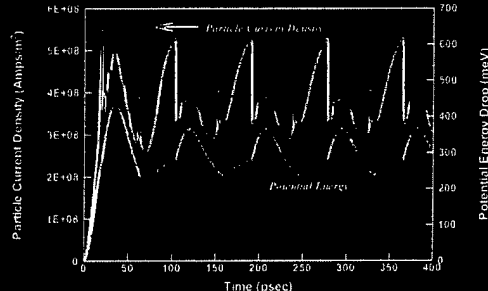
SRA  
Nanostructures & Transients

## RO at 11.5 GHz: Total Current Density and Potential Energy Drop



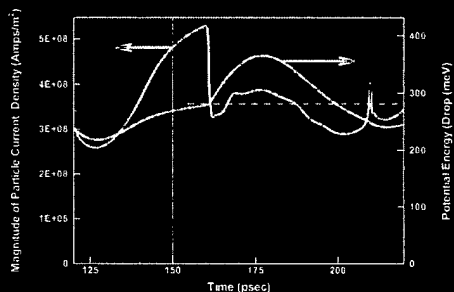
SRA  
Nanostructures & Transients

## RO at 11.5 GHz: Particle Current Density and Potential Energy Drop



SRA  
Nanostructures & Transients

## Details of the RO at 11.5 GHz: Particle Current Density and Potential Energy Drop



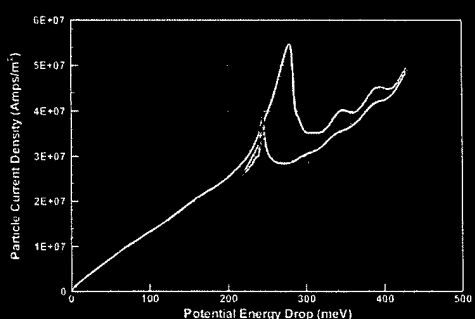
SRA  
Nanostructures & Transients

## Details of the RO at 11.5 GHz: Particle Current Density and Potential Energy Drop

- First part of the oscillation  
Linear I versus V, L/R rise time
- Second part of the oscillation  
Drop in particle current and increase in potential drop
- Third part of the oscillation
  - Decrease in potential drop, particle current remains below values associated with first part of the oscillation

SRA  
Nanostructures & Transients

## RO at 11.5 GHz: Dynamic 'IV'



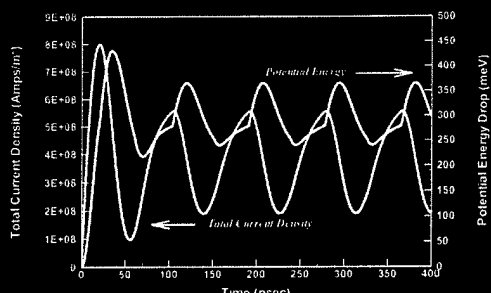
SRA  
Nanostructures & Transients

## 'Temporal Invariance'

*When the device oscillates, its characteristics are independent of oscillatory period!*

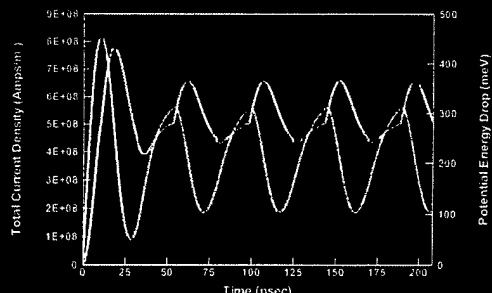
SRA  
Nanostructures & Transients

### RO at 11.5 GHz: Total Current Density and Potential Energy Drop



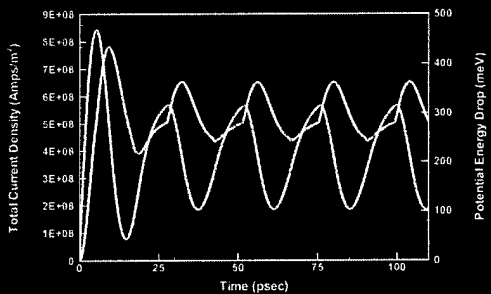
SRA  
Nanostructures & Transients

### RO at 22.0 GHz: Total Current Density and Potential Energy Drop



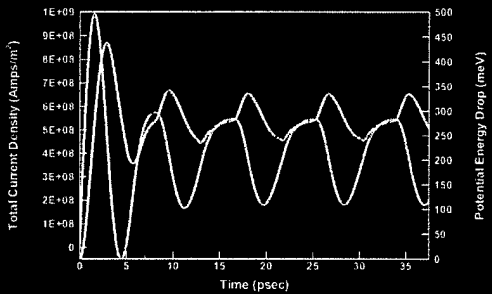
SRA  
Nanostructures & Transients

### RO at 41.8 GHz: Total Current Density and Potential Energy Drop



SRA  
Nanostructures & Transients

### RO at 113.7 GHz: Total Current Density and Potential Energy Drop

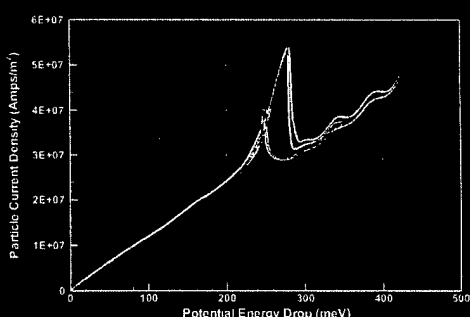


SRA  
Nanostructures & Transients

Dynamic 'IV'

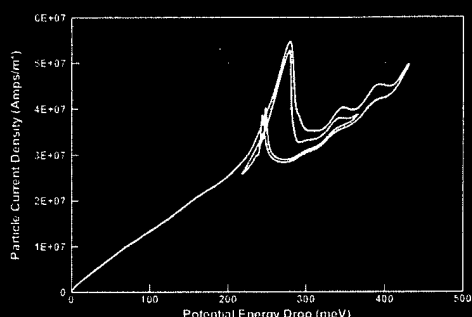
SRA  
Nanostructures & Transients

### RO at 6 GHz: Dynamic 'IV'



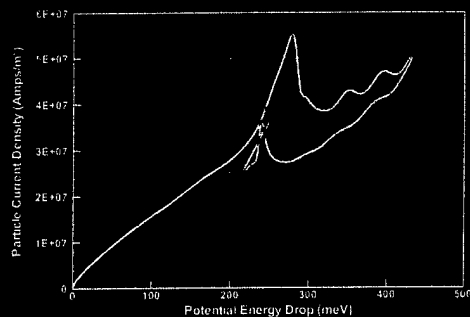
SRA  
Nanostructures & Transients

### RO at 11.5 GHz: Dynamic 'IV'



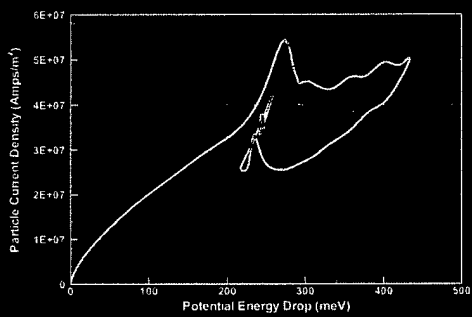
SRA  
Nanostructures & Transients

### RO at 22.0 GHz: Dynamic 'IV'



SRA  
Nanostructures & Transients

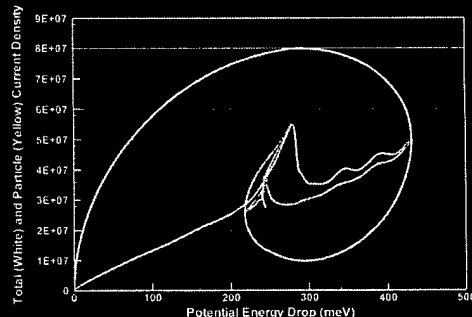
### RO at 41.8 GHz: Dynamic 'IV'



SRA  
Nanostructures & Transients

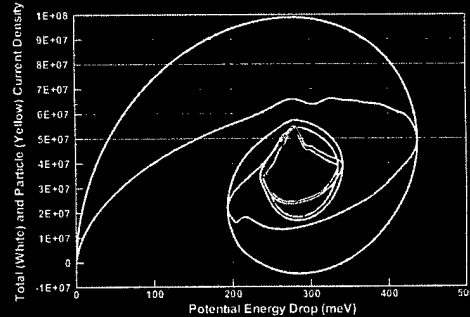
### Total and Dynamic 'IV'

### RO at 6 GHz: Total and Dynamic 'IV'



SRA  
Nanostructures & Transients

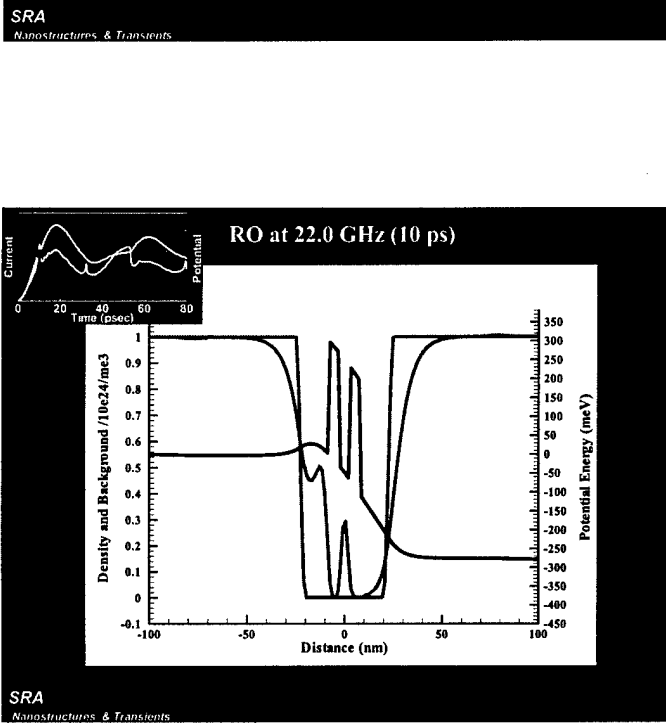
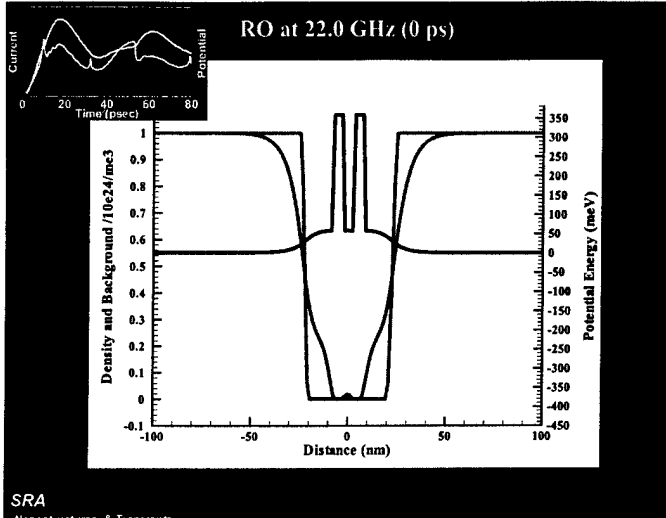
### RO at 113.72 GHz: Total and Dynamic 'IV'



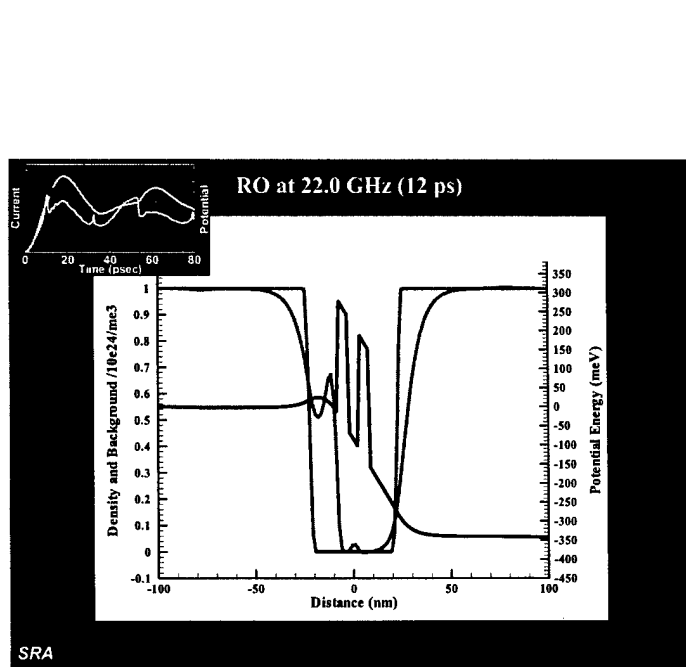
SRA  
Nanostructures & Transients

## Summary of Charge and Current for the 22.0 GHz RO

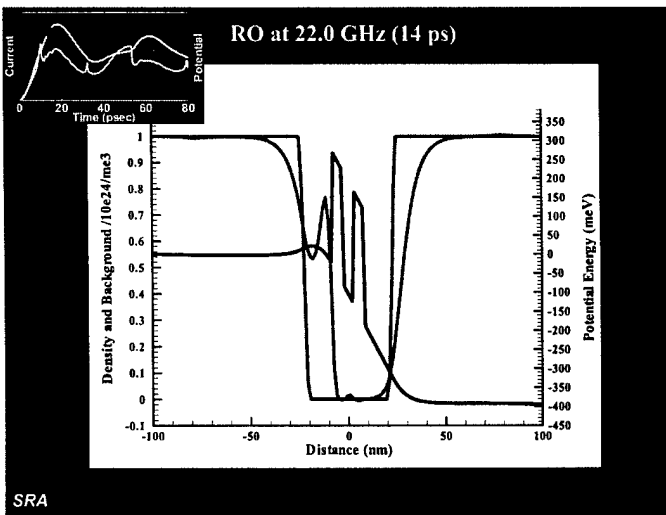
SRA  
Nanostructures & Transients



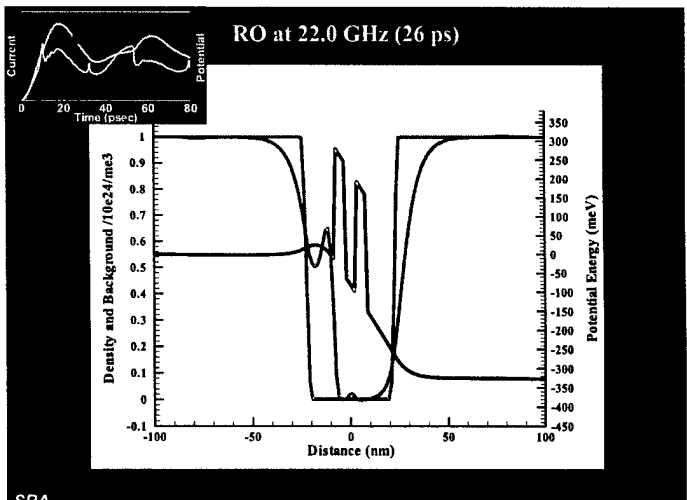
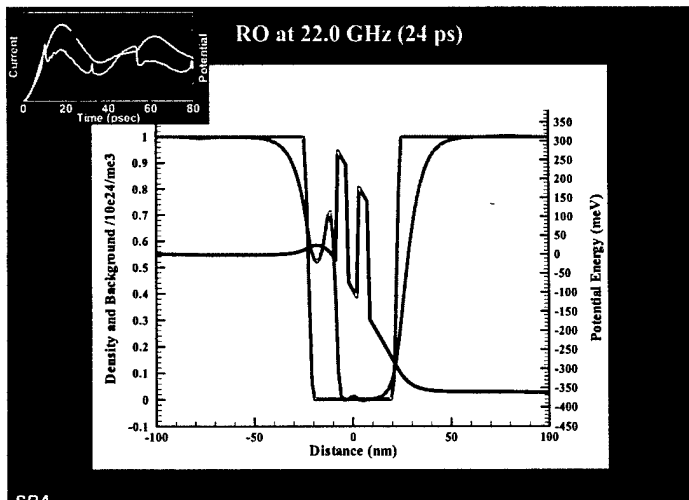
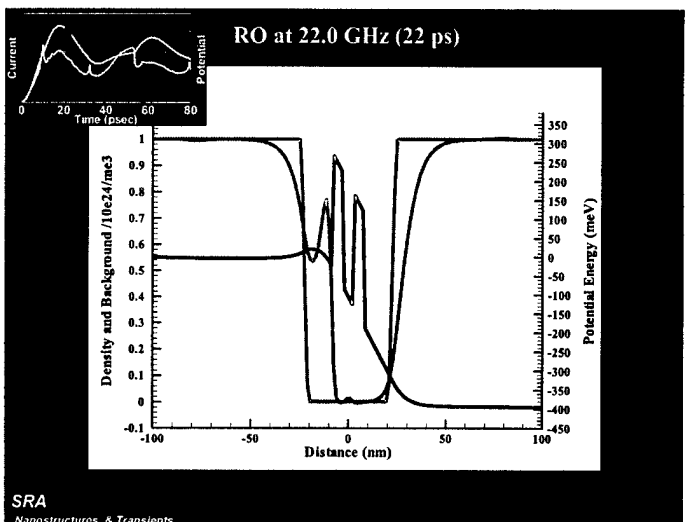
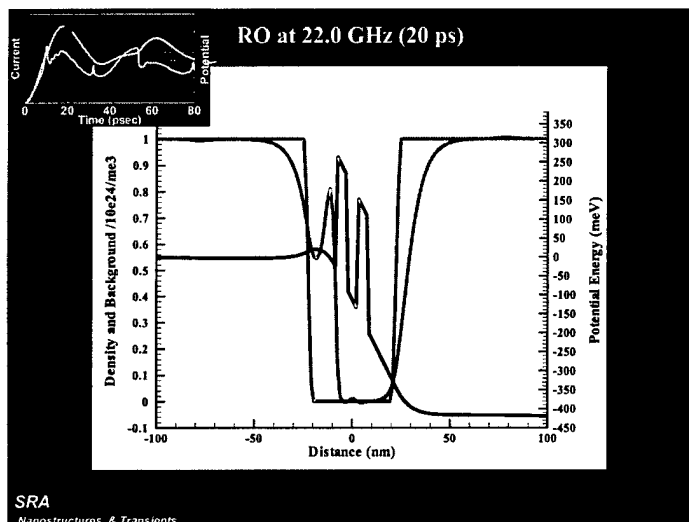
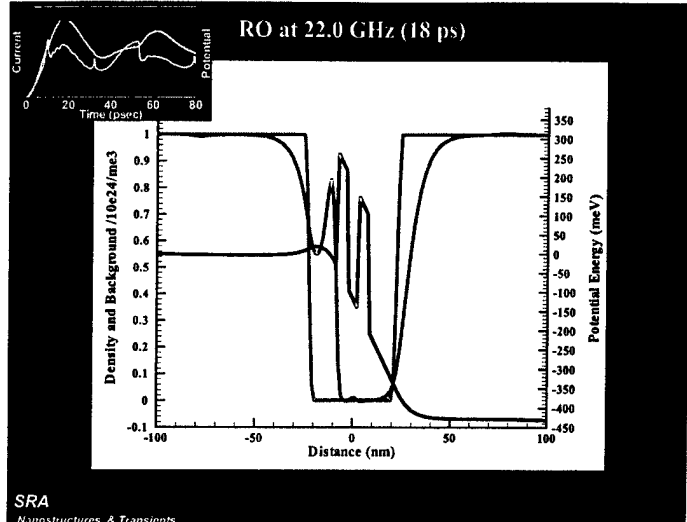
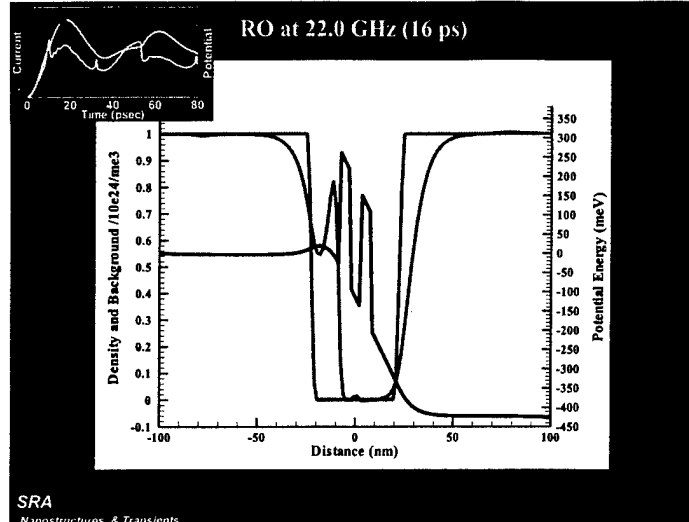
SRA  
Nanostructures & Transients

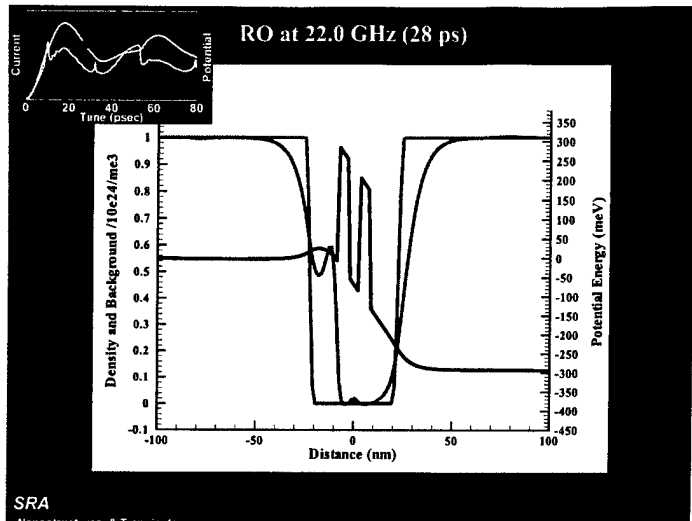


SRA  
Nanostructures & Transients

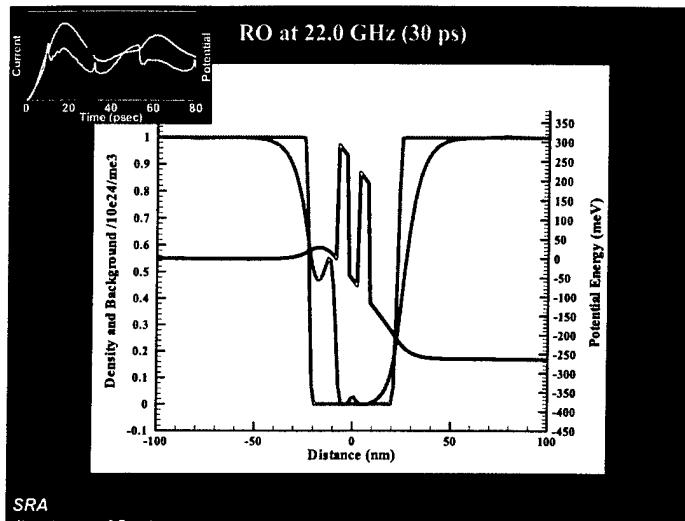


SRA  
Nanostructures & Transients

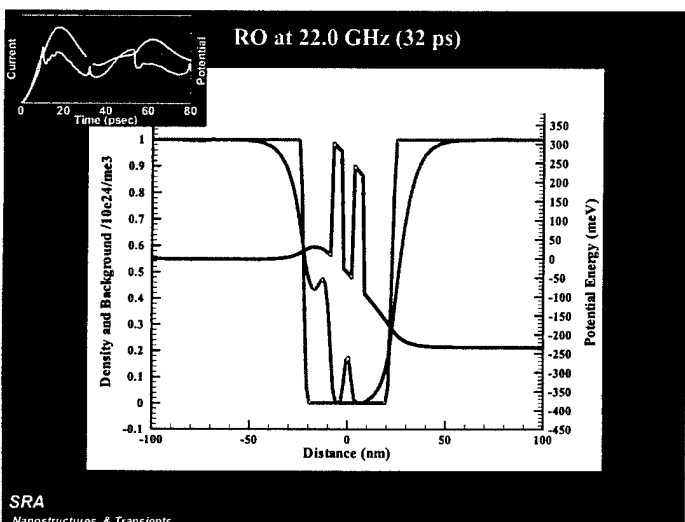




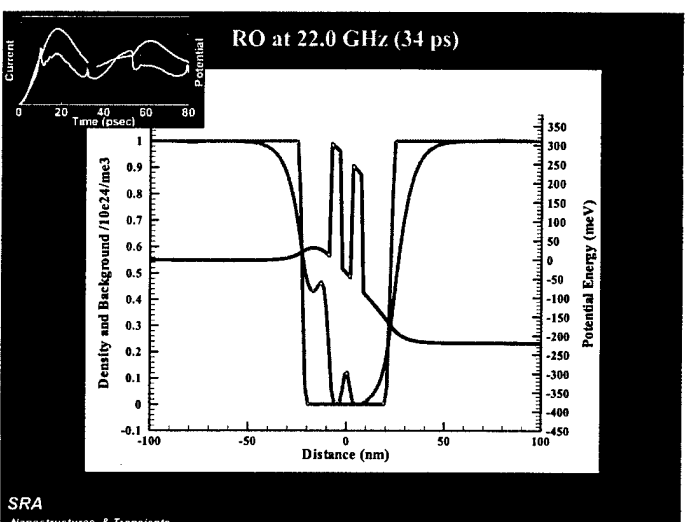
SRA  
Nanostructures & Transients



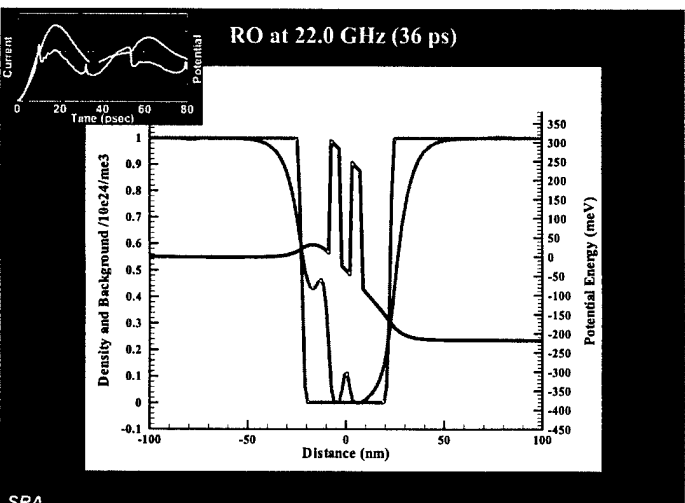
SRA  
Nanostructures & Transients



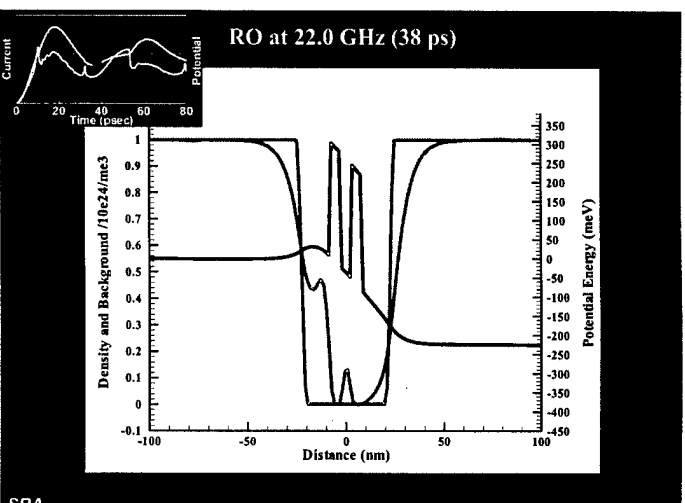
SRA  
Nanostructures & Transients



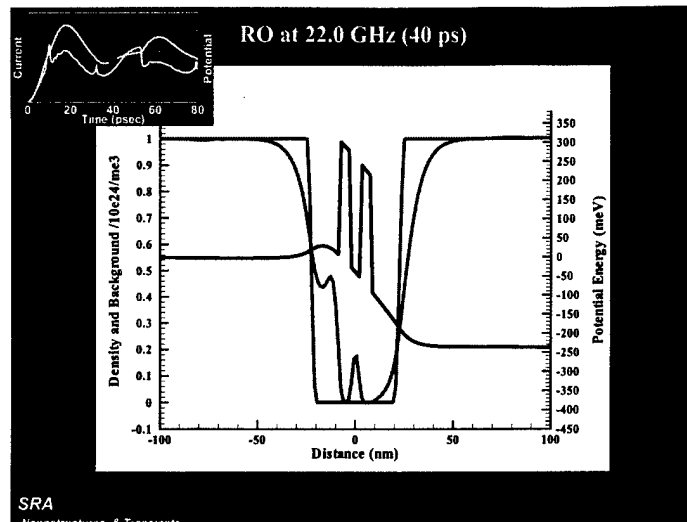
SRA  
Nanostructures & Transients



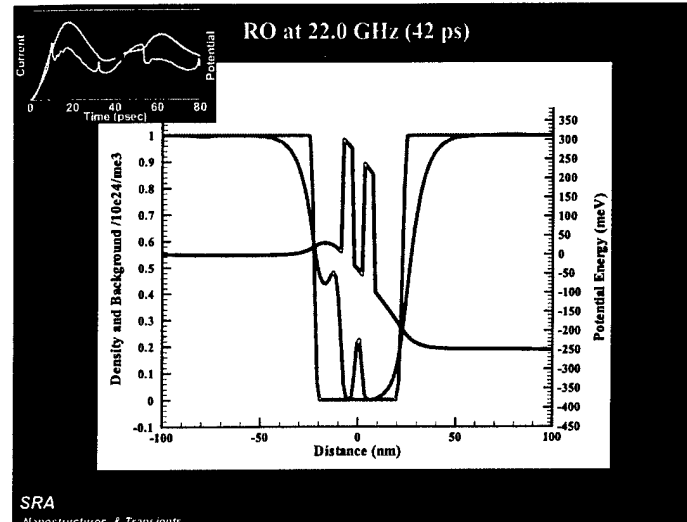
SRA  
Nanostructures & Transients



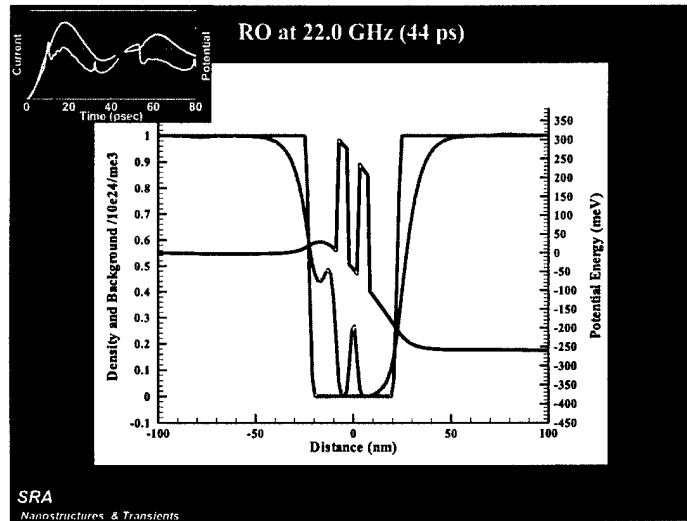
SRA  
Nanostructures & Transients



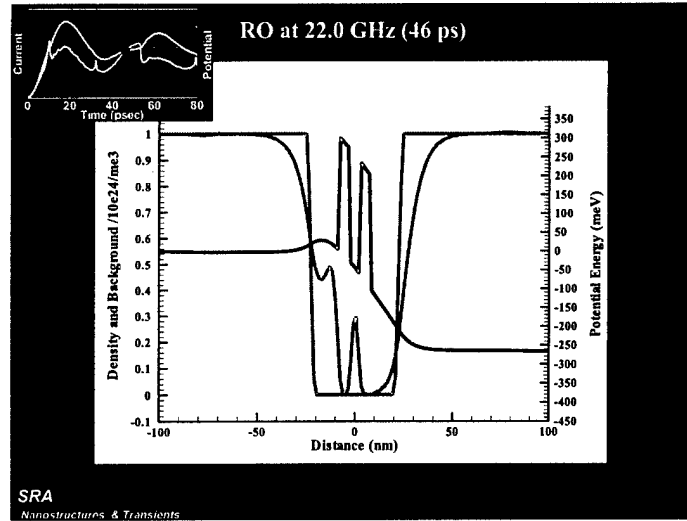
SRA  
Nanostructures & Transients



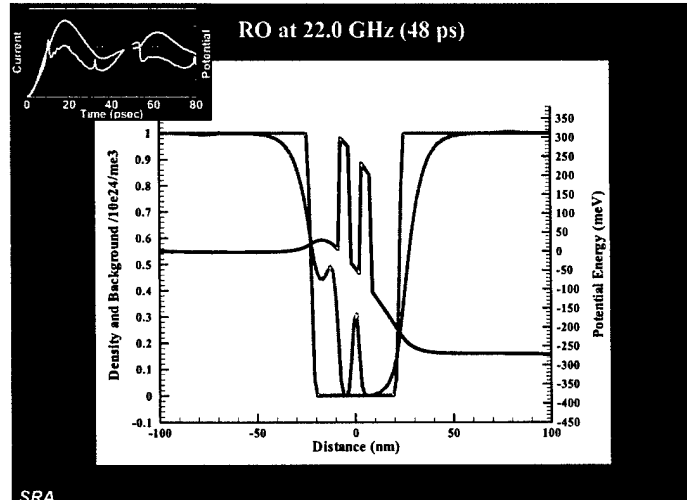
SRA  
Nanostructures & Transients



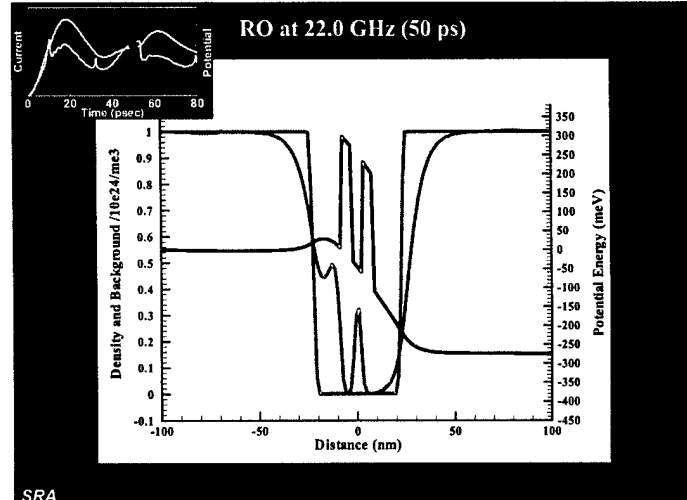
SRA  
Nanostructures & Transients



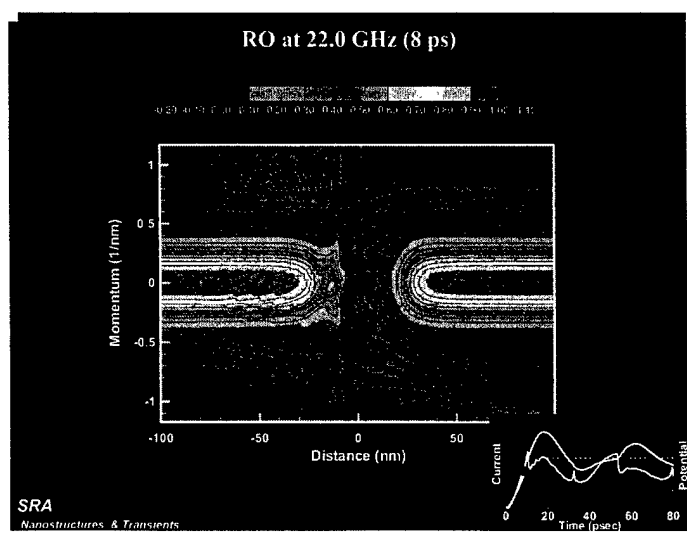
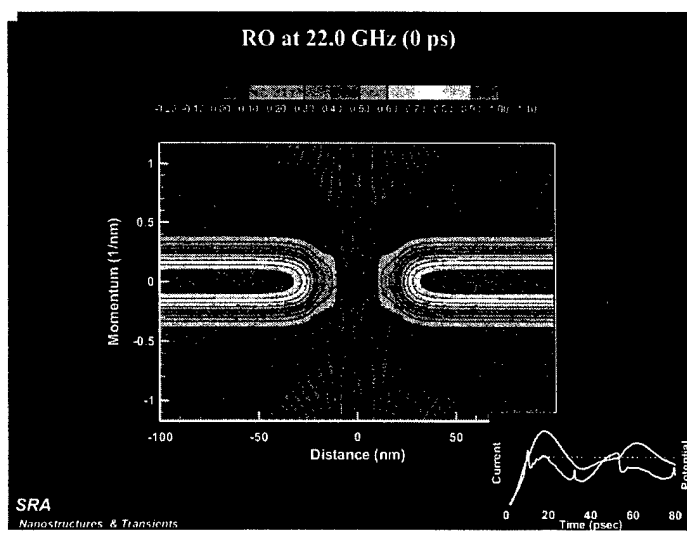
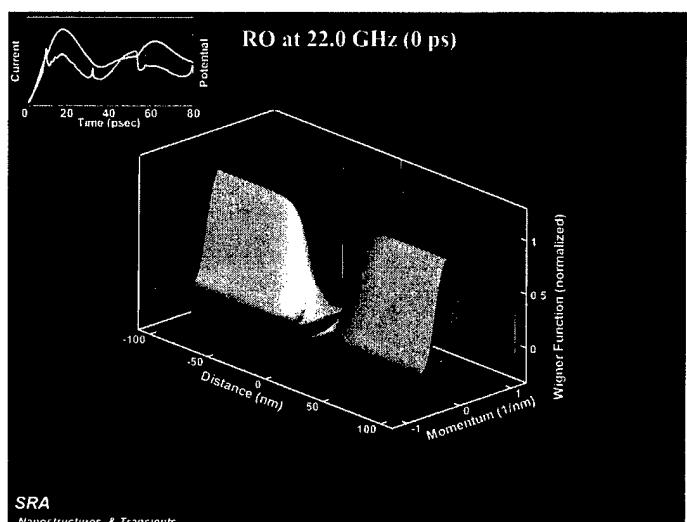
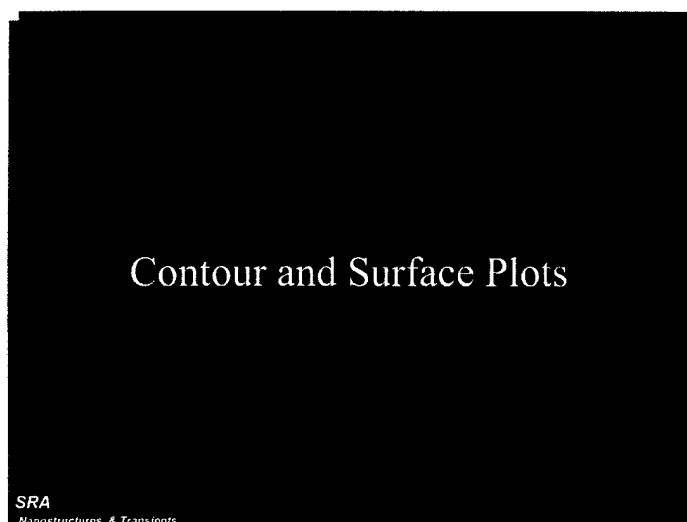
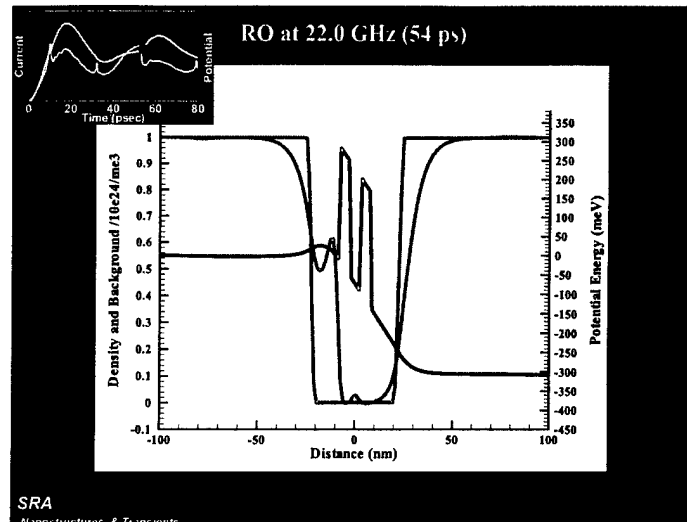
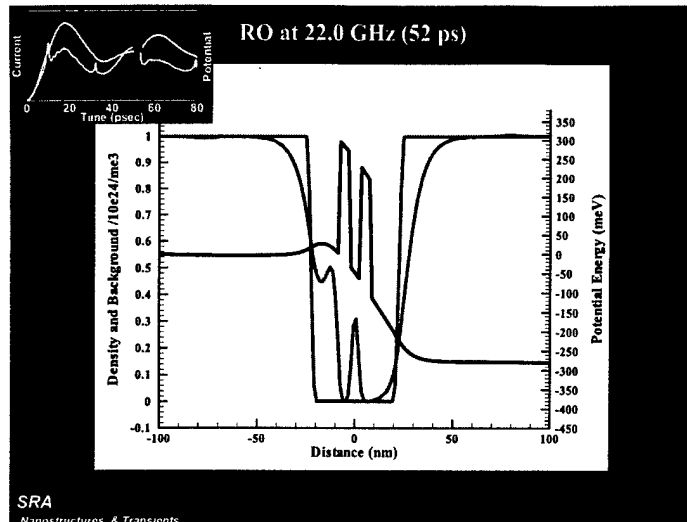
SRA  
Nanostructures & Transients



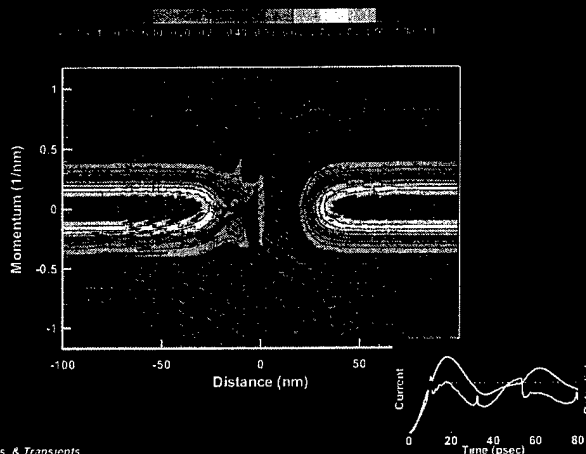
SRA  
Nanostructures & Transients



SRA  
Nanostructures & Transients



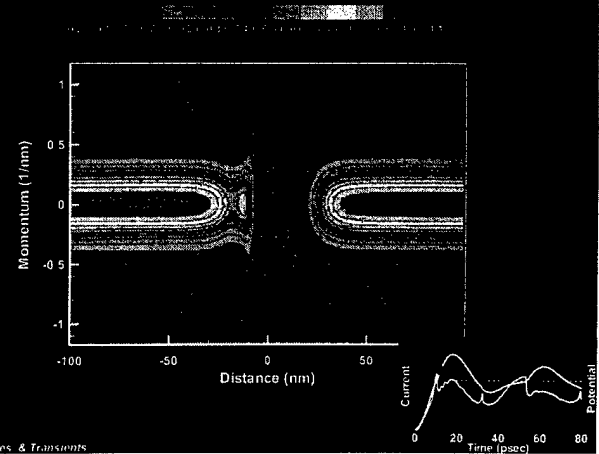
RO at 22.0 GHz (10 ps)



SRA

Nanostructures & Transients

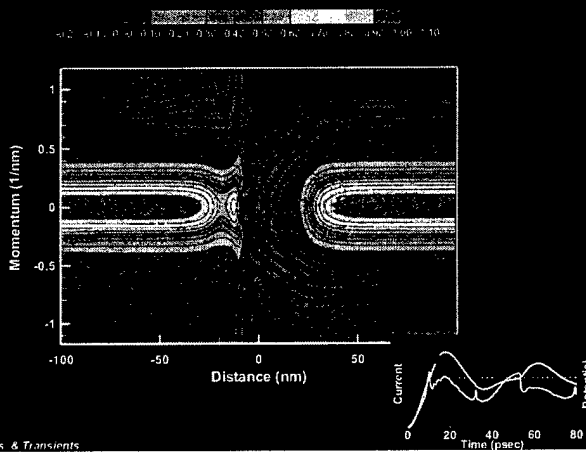
RO at 22.0 GHz (12 ps)



SRA

Nanostructures & Transients

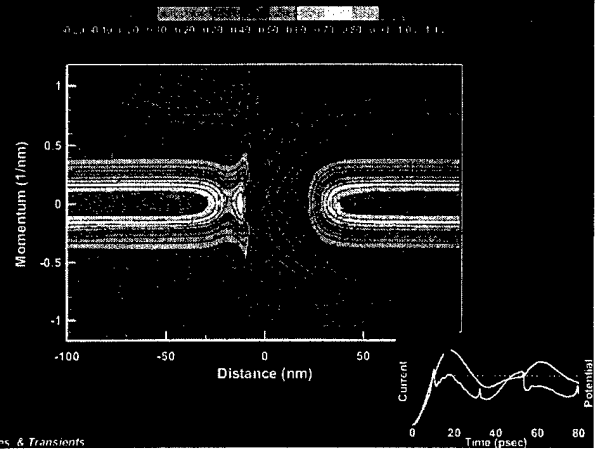
RO at 22.0 GHz (14 ps)



SRA

Nanostructures & Transients

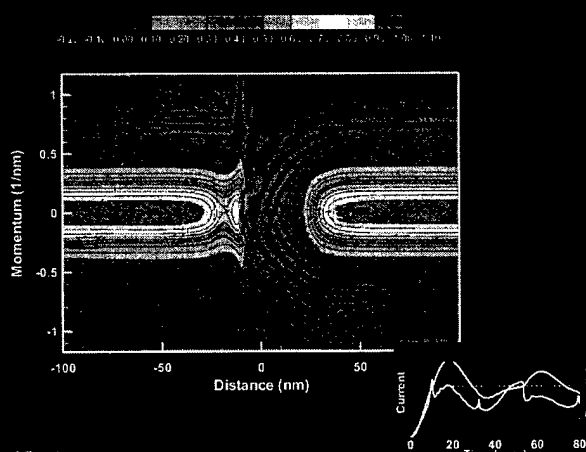
RO at 22.0 GHz (16 ps)



SRA

Nanostructures & Transients

RO at 22.0 GHz (18 ps)



SRA

Nanostructures & Transients

## Observations

- Increasing circuit frequency results in increased looping of IV.
- Oscillations cease at approximately 120GHz for these device parameters.
- There is an invariant quantity prior to the current drop-back. This quantity is the "Bohm Quantum Potential".
- Oscillations are stable to circuit noise and device fluctuations.
- Noise characteristics can probably be explained by early discussions of M. Lax.

## The Bohm Quantum Potential and the Steady State Schrodinger Equation

$$\frac{-\hbar^2}{2m} \frac{\partial^2 \psi}{\partial x^2} + V(x)\psi = E\psi$$

$$\psi(x) = R \exp[iS(x)/\hbar]$$

SRA

*Nanostructures & Transients*

## Quantum Potential

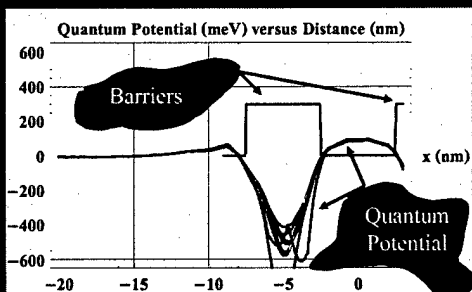
$$a. \frac{(\partial_x S)^2}{2m} + V + Q = E$$

$$b. \frac{\partial}{\partial x} \left( R^2 \frac{\partial_x S}{m} \right) = 0$$

$$c. Q = -\frac{\hbar^2}{2m} \frac{\partial_{xx} R}{R}$$

Q represents the ground state for simple double barrier problems

### From Simulations (Post Processed): Quantum Potential, Within and to the Left of the Barrier—For Different Values of Bias



SRA

*Nanostructures & Transients*

## Conclusions Suggested by the Quantum Potential

- Simulations are consistent with the filling of a well defined quantum state prior to the drop-back in current.
- Quantum potential is not well defined after the drop-back.
  - Certainly there are computational difficulties with small values of charge. But we may be dealing with a mixture of a large number of quantum states, scattering states and dissipation.

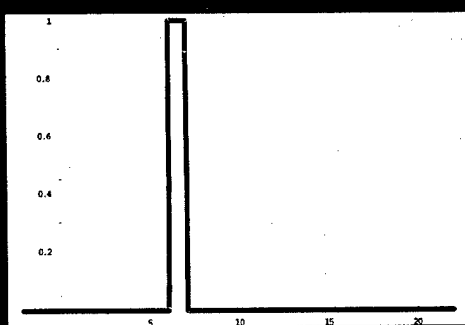
## Noise Considerations

- For nonlinear systems amplitude noise is not an issue (M. Lax and our studies)
- Phase noise is additive.
- Amount of phase noise depends on time of disturbance.
- Recovery from disturbance occurs within one cycle.
- Illustrate with ODE and Quantum RO

SRA

*Nanostructures & Transients*

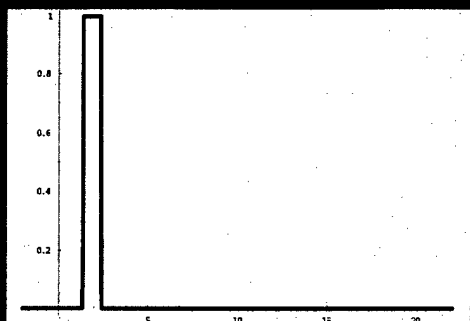
## Injected Current Source at a Particular Instant of Time



SRA

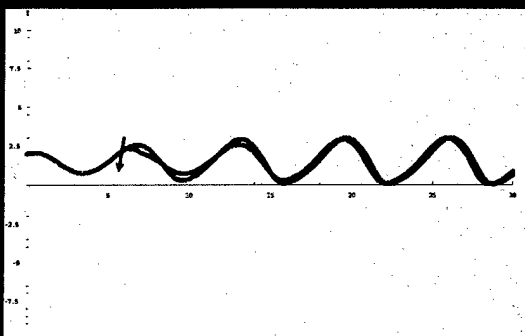
*Nanostructures & Transients*

Same type of current source:  
different time



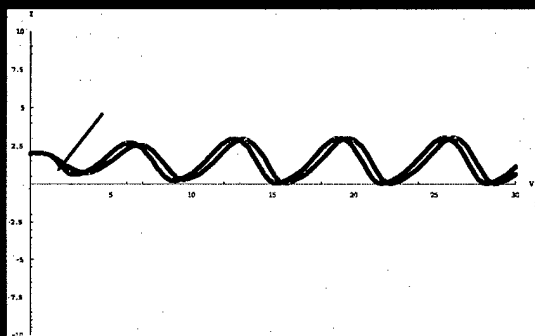
SRA  
Nanostructures & Transients

## ODE/RO Circuit Response



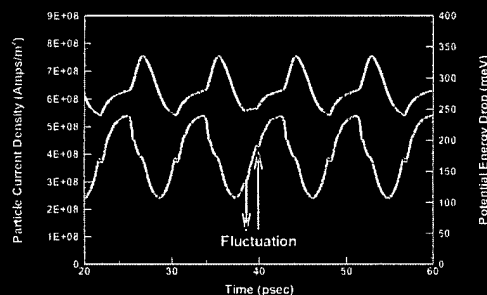
SRA  
Nanostructures & Transients

## ODE/RO Circuit Response



SRA  
Nanostructures & Transients

## Quantum RO at 113.7 GHz: Fluctuation Response of Particle Current and Potential Energy



SRA  
Nanostructures & Transients

## Conclusions

- Quantum Van der Pol oscillator provides quantitative values for the large signal switching and recovery times of RTD.
- Large signal frequencies near 120 GHz for non-optimized structure.
- Small signal oscillations sustained at higher frequencies. ( $f > 670$  GHz).
- Quantum Van der Pol oscillators recover from fluctuations within one cycle.
- Phase noise dominates.

SRA  
Nanostructures & Transients

## Speculations

- Periodic invariance is probably due to time increments. If use was made of femtosecond increments would probably see high frequency contributions.
- Quantum potential interpretation not as simple for higher ( $> 300$  meV) barriers.

SRA  
Nanostructures & Transients

## Non-Equilibrium Green's Functions for MOSFET Modeling

Dejan Jovanovic  
Benjamin Liu  
Roland Stumpf  
Keith Beardmore  
Ramesh Venugopa (Purdue)  
Mark Lundstrom (Purdue)  
Supriyo Datta (Purdue)

**Motorola**  
Computational Materials Group  
4200 W. Jemez Rd., Suite 300  
Los Alamos, NM 87544

Physical Sciences Research Laboratory

Computational Materials Group



## Device Model Deployment

### CALIBRATION

#### Advanced Models

PURPOSE: Calibrate TCAD models for sub-0.1 $\mu\text{m}$  Tech. Nodes and provide platform for novel structures research

- Full physics models with emphasis on global accuracy
- Provide detailed transport and material understanding
- Minimal calibration required

Monte-Carlo  
Quantum Transport

#### TCAD

PURPOSE: Create Rev. 0 compact models and support lot design

- Physics-based device models with emphasis on performance
- Provide interface between process and device behavior
- Will require experimental (~100 days) or TCAD-based (~30 days) calibration

Drift-diffusion  
Hydrodynamic  
Density Gradient

#### Compact Models

PURPOSE: Enable circuit-level simulation

- High-performance device models based on analytic equations
- Provide interface between devices and circuits
- Requires experimental (~100 days) or TCAD-based (~30 days) calibration

SPICE: BSIM3, SSIM, etc.

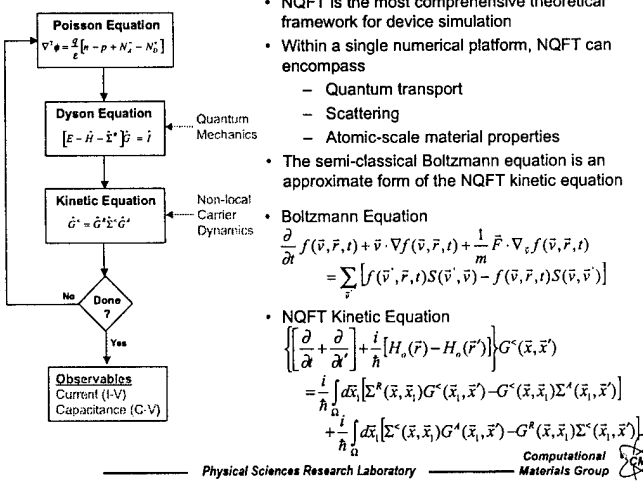
### DESIGN

Physical Sciences Research Laboratory

Computational Materials Group



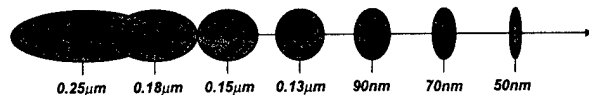
## Nonequilibrium Quantum Field Theory



Physical Sciences Research Laboratory Computational Materials Group

## Conventional TCAD

- Process-Device simulation (TCAD) is used by the semiconductor industry to expedite and optimize process development
- TCAD enables the efficient use of experimental cycles and provides major cost/time savings during early design iterations
- TCAD device models are based on semi-classical transport theory which relies on approximations to facilitate performance efficiency
- Semiclassical transport models will become increasingly inaccurate with decreasing  $L_{\text{gate}}$  due to the onset of quantum effects



Experimental calibration will be increasingly required to calibrate TCAD device simulators which will undermine their usefulness

Computational Materials Group

## Comparison of Contemporary Device Simulators

Device Simulator	Transport Model	Scattering	Quantum Effects	Leakage	Material Properties	Biasing		Performance
						$V_c < V_r$	$V_c > V_r$	
Drift-Diffusion	Semi-Classical	Mobility based		Sub-threshold				Good
Hydro-Dynamic	Semi-Classical	Mobility based		Sub-threshold				Average
Density Gradient	Semi-Classical	Mobility based	Quantum Potentials	Sub-threshold				Poor
Monte Carlo	Semi-Classical	Detailed	Sub-threshold		Advanced			-1 hr/bias
Quantum Transport	Quantum Mechanical	Exact	Exact	Exact				

Good  
Average  
Poor

Computational Materials Group

### Principal Equations

$$[E - \hat{H}_o(\vec{k}_\perp) - \hat{\Sigma}^R(E, \vec{k}_\perp)] \hat{G}^R(E, \vec{k}_\perp) = \hat{I} \quad \text{Impulse response}$$

$$G_{i,j}^R(E, \vec{k}_\perp) = \sum_{i,j} G_{i,k}^R(E, \vec{k}_\perp) \Sigma_{i,j}^R(E, \vec{k}_\perp) G_{j,l}^R(E, \vec{k}_\perp) + g_{i,j}^R(E, \vec{k}_\perp) \quad \text{Convolution Integral}$$

### Scattering

$$\Sigma_{i,j}^R(E, \vec{k}_\perp) = \frac{1}{(2\pi)^3} \sum_i \int dE' \int d\vec{k}'_1 V_{i,k}(E, \vec{k}_\perp, E', \vec{k}'_1) G_{i,j}^R(E', \vec{k}'_1)$$

$$\Sigma_{i,j}^R(E, \vec{k}_\perp) = \frac{1}{(2\pi)^3} \sum_i \int dE' \int d\vec{k}'_1 V_{i,k}(E, \vec{k}_\perp, E', \vec{k}'_1) G_{i,j}^R(E', \vec{k}'_1)$$

$$\frac{1}{\tau_{ij}^{tot}(E)} \Leftrightarrow -\frac{2}{\hbar} \text{Im}[\Sigma_{i,j}^R(E, \vec{k}_\perp)]$$

Scattering is both the key and impediment to numerical quantum transport simulation

### Definitions

- $\hat{H}_o(\vec{k}_\perp)$  - Tight-binding Hamiltonian
- $g_{i,j}^R(E, \vec{k}_\perp)$  - Zero-order correlation function
- $\hat{\Sigma}^R(E, \vec{k}_\perp)$  - Retarded self-energy (out-scattering)
- $\Sigma_{i,j}^R(E, \vec{k}_\perp)$  - Causal Self-Energy (in-scattering)
- $\hat{G}^R(E, \vec{k}_\perp)$  - Retarded Green Function (Propagator)
- $G_{i,j}^R(E, \vec{k}_\perp)$  - Full correlation function
- $V_{i,j}(E, \vec{k}_\perp, E', \vec{k}'_1)$  - Interaction Potential (Green Function)

Computational Materials Group

Physical Sciences Research Laboratory Computational Materials Group

## Nonequilibrium Quantum Field Theory

### Physical Observables

- Density of States

$$A_g(E, \vec{k}_\perp) = -2 \text{Im}[G^R(E, \vec{k}_\perp)] \quad (\text{quantum mechanical DOS})$$

- Electrons

$$G_u^c(E, \vec{k}_\perp) = i f(E, \phi_F) A_u(E, \vec{k}_\perp) \quad (\text{equilibrium})$$

$$= i f(E, \phi_F^*) A_u^*(E, \vec{k}_\perp) + i f(E, \phi_F^*) A_u^*(E, \vec{k}_\perp) \quad (\text{non-equilibrium})$$

$$n_i = -2i \int \frac{dE}{2\pi} \int \frac{d\vec{k}_\perp}{(2\pi)^2} G_u^c(E, \vec{k}_\perp) \quad (\text{electron density})$$

$$J_i = \frac{2e}{\hbar} \int \frac{dE}{2\pi} \int \frac{d\vec{k}_\perp}{(2\pi)^2} [H_{i,i+1}(\vec{k}_\perp) G_{i,i+1}^c(E, \vec{k}_\perp) - G_{i,i+1}^c(E, \vec{k}_\perp) H_{i,i+1}(\vec{k}_\perp)] \quad (\text{electron current})$$

- Holes

$$G_u^s(E, \vec{k}_\perp) = -i[1 - f(E, \phi_F)] A_u(E, \vec{k}_\perp) \quad (\text{equilibrium})$$

$$= -i[1 - f(E, \phi_F^*)] A_u^*(E, \vec{k}_\perp) - i[1 - f(E, \phi_F^*)] A_u^*(E, \vec{k}_\perp) \quad (\text{non-equilibrium})$$

$$p_i = -2i \int \frac{dE}{2\pi} \int \frac{d\vec{k}_\perp}{(2\pi)^2} G_u^s(E, \vec{k}_\perp) \quad (\text{hole density})$$

$$J_i = \frac{2e}{\hbar} \int \frac{dE}{2\pi} \int \frac{d\vec{k}_\perp}{(2\pi)^2} [H_{i,i+1}(\vec{k}_\perp) G_{i,i+1}^s(E, \vec{k}_\perp) - G_{i,i+1}^s(E, \vec{k}_\perp) H_{i,i+1}(\vec{k}_\perp)] \quad (\text{hole current})$$

Physical Sciences Research Laboratory

Computational Materials Group

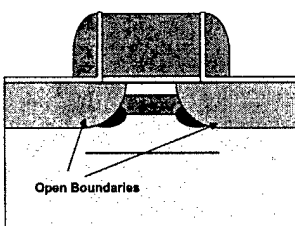


## Nonequilibrium Quantum Field Theory

### Boundary Conditions for Green's and Correlation Functions

- Boundary condition assumptions

- Contacts are modeled as translationally invariant open boundaries and are assumed to be in local equilibrium
- Closed boundaries are set where  $G^R$  and  $G^c$  can be safely assumed to be negligible



- Boundary eigenvalue problem

$$\left[ Z_m + (Z_m)^{-1} - \frac{E - \varepsilon_j}{t_j} \right] \phi_{j,m} = 0$$

- Boundary Green's function

$$\tilde{g}_{0,1}^R = Q Z Q^{-1} g_{0,1}^R$$

$$\tilde{g}_{0,0}^R = [E - \hat{\varepsilon} - i Q Z Q^{-1}]^{-1}$$

$$\tilde{g}_{0,0}^c = -i 2 f(\phi_F^*) \text{Im}[\tilde{g}_{0,0}^R]$$

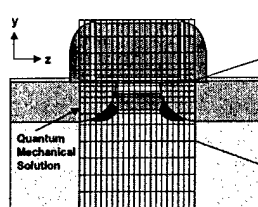
Physical Sciences Research Laboratory

Computational Materials Group

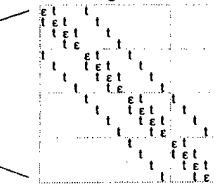


## Nonequilibrium Quantum Field Theory

### Spatial Discretization



Block Tri-Diagonal Hamiltonian



- Presently using multi-valley effective-mass based discretization
- Simulated bandstructure is intrinsically linked to grid morphology in lateral (z) direction

$$E(k_z) = \frac{\hbar^2}{m_i \Delta_z} [1 - \cos(k_z \Delta_z)]$$

- Uniform grid is required for the lateral (z) direction to avoid spurious reflections
- Non-uniform grid can be used in vertical (y) direction

Physical Sciences Research Laboratory

Computational Materials Group



## Nonequilibrium Quantum Field Theory

### Recursive Solution of Dyson and Kinetic Equations

- General Dyson equations for  $G^R$  and  $G^c$

$$\hat{G}_{i,i}^R = g_{i,i}^R + \sum_{j,k} \hat{g}_{i,j}^R \hat{\Sigma}_{j,k}^R \hat{G}_{k,i}^R$$

$$\hat{G}_{i,i}^c = \hat{g}_{i,i}^c + \sum_{j,k} \hat{g}_{i,j}^c \hat{\Sigma}_{j,k}^c \hat{G}_{k,i}^c + \sum_{j,k} \hat{g}_{i,j}^R \Sigma_{j,k}^R \hat{G}_{k,i}^c + \sum_{j,k} \hat{g}_{i,j}^c \Sigma_{j,k}^c \hat{G}_{k,i}^R$$

- Recursive Greens Function (RGF) Technique

- Direct solution of the Green's functions is computationally prohibited ( $N_x N_y$ )<sup>3</sup>
- Physical observables are clustered along the Green's function diagonals
- Dyson equations can be used to recursively construct Green and correlation function diagonals in a two-step manner  $N_x N_y$ <sup>3</sup>
- Perturbative elements are the off-diagonal elements of the Hamiltonian

$$\tilde{g}_{i,i}^R = g_{i,i}^R + \sum_{j,k} g_{i,j}^R t_{j,k} \tilde{g}_{k,i}^R$$

$$\tilde{g}_{i,i}^c = g_{i,i}^c + \sum_{j,k} g_{i,j}^c t_{j,k} \tilde{g}_{k,i}^c + \sum_{j,k} g_{i,j}^R t_{j,k} \tilde{g}_{k,i}^c$$

- Self-consistent scattering can be efficiently incorporated into the RGF approach

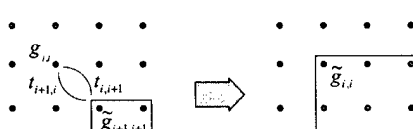
Physical Sciences Research Laboratory

Computational Materials Group



## Nonequilibrium Quantum Field Theory

### Recursive Solution of Semi-infinite Green/Correlation Functions



$$\tilde{g}_{i,i}^R = g_{i,i}^R + g_{i,i}^R t_{i,i+1} \tilde{g}_{i+1,i+1}^R$$

$$= g_{i,i}^R + g_{i,i}^R t_{i,i+1} \tilde{g}_{i+1,i+1}^R t_{i+1,i+1} \tilde{g}_{i+1,i+1}^R$$

$$= g_{i,i}^R + g_{i,i}^R t_{i,i+1} \tilde{g}_{i+1,i+1}^R t_{i+1,i+1} \tilde{g}_{i+1,i+1}^R + g_{i,i}^R t_{i,i+1} \tilde{g}_{i+1,i+1}^R t_{i+1,i+1} \tilde{g}_{i+1,i+1}^R$$

$$\tilde{g}_{i,i}^R = [g_{i,i}^R]^{-1} - t_{i,i+1} \tilde{g}_{i+1,i+1}^R t_{i+1,i+1}^{-1}$$

$$\tilde{g}_{i,i}^c = \tilde{g}_{i,i}^R | \sigma_{i,i}^c + t_{i,i+1} \tilde{g}_{i+1,i+1}^c t_{i+1,i+1} \tilde{g}_{i+1,i+1}^R$$

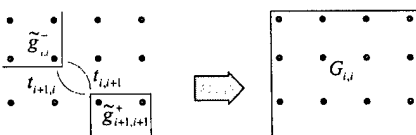
Physical Sciences Research Laboratory

Computational Materials Group



## Nonequilibrium Quantum Field Theory

### Recursive Solution of Full Green/Correlation Functions



$$G_{i,i}^R = \tilde{g}_{i,i}^R + \tilde{g}_{i,i}^R t_{i,i+1} G_{i+1,i+1}^R t_{i+1,i+1} \tilde{g}_{i+1,i+1}^R$$

$$= [\tilde{g}_{i,i}^R]^{-1} - t_{i,i+1} \tilde{g}_{i+1,i+1}^R t_{i+1,i+1}^{-1}$$

$$G_{i,i}^c = \tilde{g}_{i,i}^c + \tilde{g}_{i,i}^c t_{i,i+1} G_{i+1,i+1}^c t_{i+1,i+1} \tilde{g}_{i+1,i+1}^c + \tilde{g}_{i,i}^R t_{i,i+1} G_{i+1,i+1}^c t_{i+1,i+1} \tilde{g}_{i+1,i+1}^c$$

$$= G_{i,i}^R [g_{i,i}^c | \sigma_{i,i}^c + t_{i,i+1} \tilde{g}_{i+1,i+1}^c t_{i+1,i+1} \tilde{g}_{i+1,i+1}^R] G_{i,i}^A$$

Physical Sciences Research Laboratory

Computational Materials Group



## Nonequilibrium Quantum Field Theory

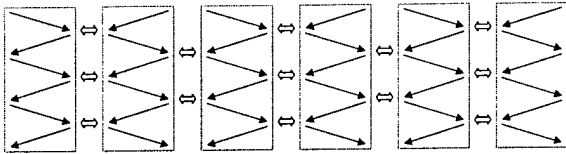
### Parallel Implementation of the Recursive Green's Function Method

- Parallel energy integration

- Green's function calculations at each energy are distributed to slave processors
- Found to be highly inefficient for scattering simulations due to varying execution time per node

- Parallel Recursive Green's function algorithm

- Spatial grid topology is distributed across processors
- Cross element coupling terms are calculated in parallel
- Boundary Green's functions are calculated and distributed to enable parallel calculation of GR
- Correlation functions are then iteratively calculated until scattering self-consistency is achieved



~ 80% parallel efficiency is exhibited for 60 processor simulations

Physical Sciences Research Laboratory

Computational Materials Group

## Scattering Model

- Kinetic Equation

$$\left[ \left[ \frac{\partial}{\partial t} + \frac{\partial}{\partial \vec{r}} \right] + \frac{i}{\hbar} [H_o(\vec{r}) - H_o(\vec{r}')] \right] G^<(\vec{x}, \vec{x}') = \frac{i}{\hbar} \int d\vec{x}_1 \left[ \Sigma^R(\vec{x}, \vec{x}_1) G^<(\vec{x}_1, \vec{x}') - G^<(\vec{x}, \vec{x}_1) \Sigma^A(\vec{x}_1, \vec{x}') + \Sigma^C(\vec{x}, \vec{x}_1) G^A(\vec{x}_1, \vec{x}') - G^R(\vec{x}, \vec{x}_1) \Sigma^C(\vec{x}_1, \vec{x}') \right]$$

- Current Continuity

$$\left[ \left[ \frac{\partial}{\partial t} + \frac{\partial}{\partial \vec{r}} \right] + \frac{i}{\hbar} [H_o(\vec{r}) - H_o(\vec{r}')] \right] G^<(\vec{x}, \vec{x}') = \frac{\partial}{\partial t} n(\vec{r}, t) + \vec{\nabla} \cdot \vec{J}(\vec{r}, t) = 0$$

$$\int d\vec{x}_1 \left[ \Gamma(\vec{x}, \vec{x}_1) G^<(\vec{x}_1, \vec{x}') - \Sigma^C(\vec{x}, \vec{x}_1) A(\vec{x}_1, \vec{x}') \right] = 0$$

- Rate-Based Scattering Model

$$\Sigma_{i,j,f,i'}^R(E, \vec{k}) \equiv i \delta_{i,f} \delta_{j,i'} \int \frac{dE'}{2\pi} \int \frac{dk'}{2\pi} \lambda_{i,j}(E, \vec{k}, E', \vec{k}') = -i \frac{\Gamma_{i,j}(E, \vec{k})}{2}$$

$$\Sigma_{i,j,f,i'}^C(E, \vec{k}) = -2 \delta_{i,f} \delta_{j,i'} \frac{G_{i,j}^<(E, \vec{k})}{A_{i,j}(E, \vec{k})} \int \frac{dE'}{2\pi} \int \frac{dk'}{2\pi} \lambda_{i,j}(E', \vec{k}', E, \vec{k}) = -\frac{\tilde{\Gamma}_{i,j}(E, \vec{k})}{A_{i,j}(E, \vec{k})} G_{i,j}^<(E, \vec{k})$$

Approximation:

$$\Gamma_{i,j}(E, \vec{k}) = \tilde{\Gamma}_{i,j}(E, \vec{k}) \equiv \Gamma_{i,j}^*(E) \delta_{i,j}$$

- Enables efficient self-consistent scattering calculation
- Simple calibration
- Accounts for resistive effects (e.g.  $L_{eff}$  scaling)

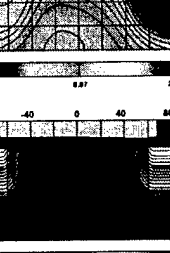
Physical Sciences Research Laboratory

Computational Materials Group

## MIT Reference MOSFETs

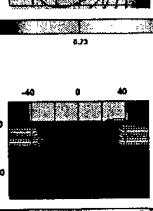
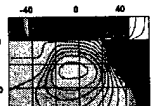
**MIT 90nm MOSFET**

- $L_{poly}=0.13\mu m$
- $t_{ox}=4.5nm$



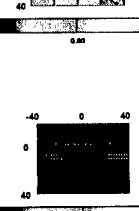
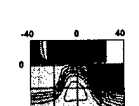
**MIT 50nm MOSFET**

- $L_{poly}=85nm$
- $t_{ox}=2.0 nm$



**MIT 25nm MOSFET**

- $L_{poly}=50nm$
- $t_{ox}=1.5 nm$



## Quantum Mechanical Simulation of MOSFETs

### Numerical Issues and Computational Platforms

- Algorithms

- Numerical NQFT solutions rely heavily on matrix inversion and multiplication

- Computing Platforms

- Commodity clusters are the enabling platforms for 2D NQFT simulation
- All runs were performed on a 110 node 2xP4/1.45GHz Linux cluster which cost under \$250,000

- Performance

- 90nm Ballistic simulations: ~1 hour/bias point
- 90nm Scattering simulations: ~8 hour/bias point

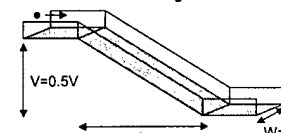


Computational Materials Group

Physical Sciences Research Laboratory

## Empirical Scattering Model

- Resistive electron wave-guide

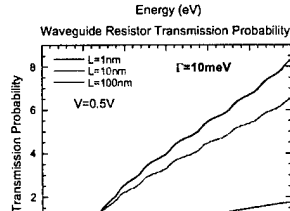
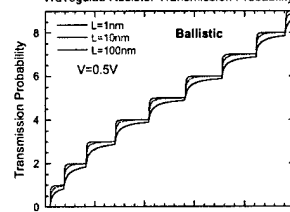


- Ballistic Case

- Subband structure is apparent and retained up to 100nm
- Variation in L causes subband smearing but no change in transmission envelope
- Resistive effects are not accounted for

- Constant-Rate model

- Accounts for incoherence effects and back-scattering
- Subband structure disappears for L=100nm
- Attenuation of transmission envelope occurs for increasing L
- Can account for resistive effects with proper calibration

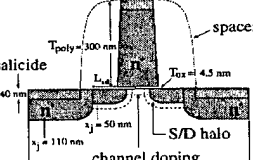


Computational Materials Group

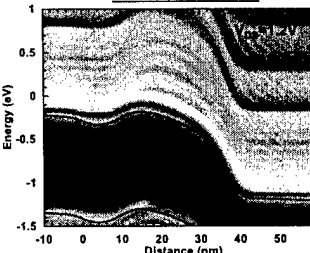
## MOSFET Quantum Mechanical Effects

### Sub-bands

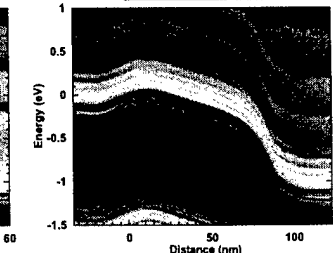
- Quantum mechanical DOS (spectral function) data taken at Si-SiO<sub>2</sub> interface
- Striations in DOS plots are sub-bands
- Spectral shift evident near source barrier
- Multiple sub-bands are required for accurate scattering calculations



25nm MIT MOSFET



90nm MIT MOSFET

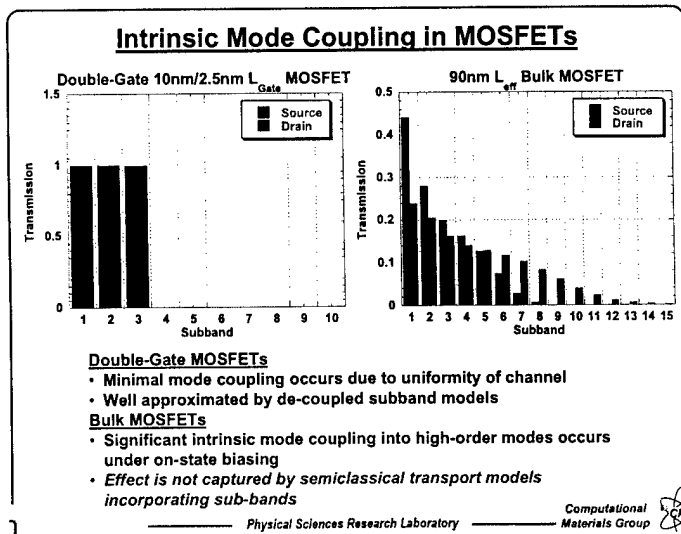
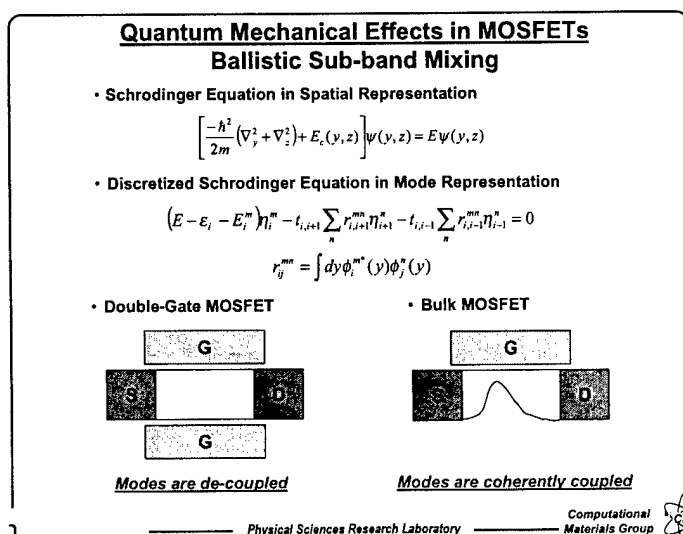
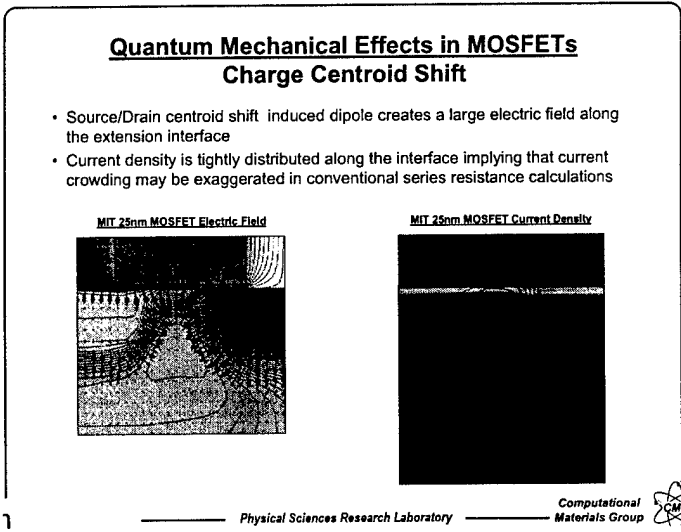
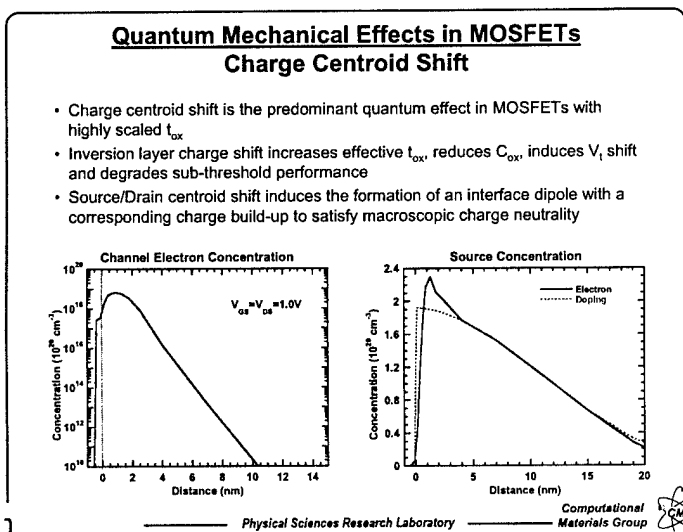
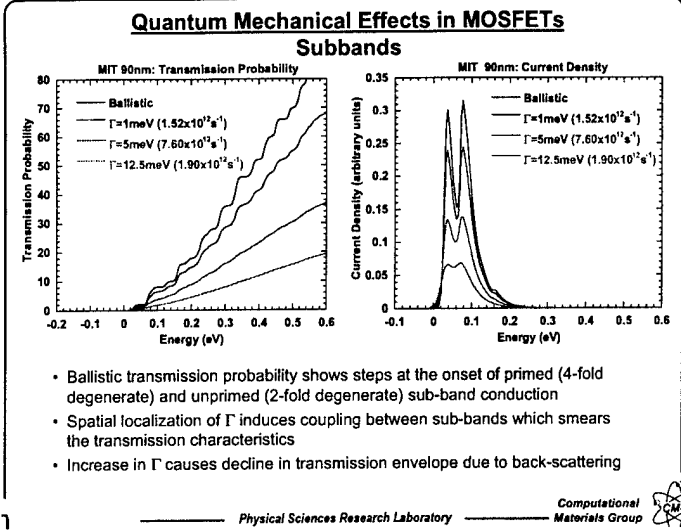
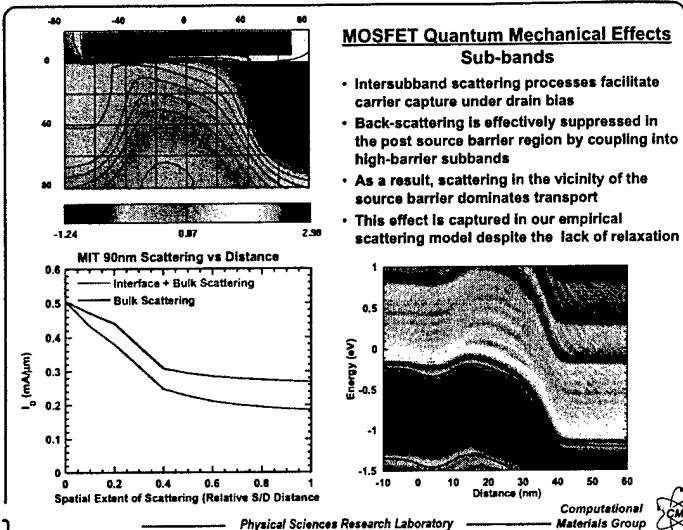


Computational Materials Group

Physical Sciences Research Laboratory

Physical Sciences Research Laboratory

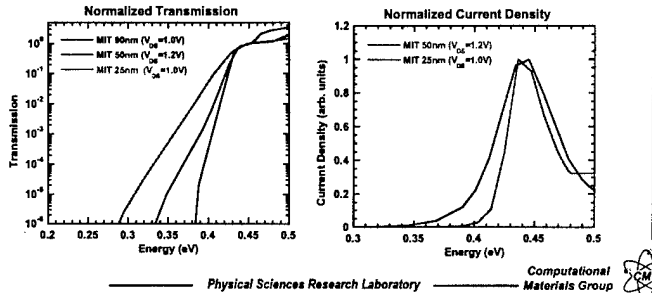
Computational Materials Group



## Quantum Mechanical Effects in MOSFETs

### Sub-Threshold Tunneling

- Sub-threshold tunneling through the source barrier enhances off-state leakage and compromises the  $I_{on}/I_{off}$  trade-off
- 50nm  $L_{eff}$  MOSFET exhibits a ~25%  $I_{off}$  increase
- 25nm  $L_{eff}$  MOSFET exhibits a ~40%  $I_{off}$  increase
- Further complications may arise from trap-assisted tunneling due to S/D extension lateral dopant diffusion into the channel

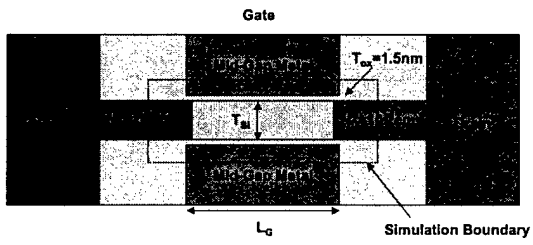


Physical Sciences Research Laboratory

Computational Materials Group

## Quantum Mechanical Effects in MOSFETs

### $I_D$ - $V_{GS}$ Saturation



- Double-Gate MOSFETs are predicted to display optimal scaling properties and carry the potential of realizing (sub?) 10nm  $L_G$  technologies
- However, electrostatics dictates that  $L_G/T_{Si}$  remain roughly constant to suppress short-channel effects and achieve target  $I_{on}/I_{off}$

#### Scaling Study

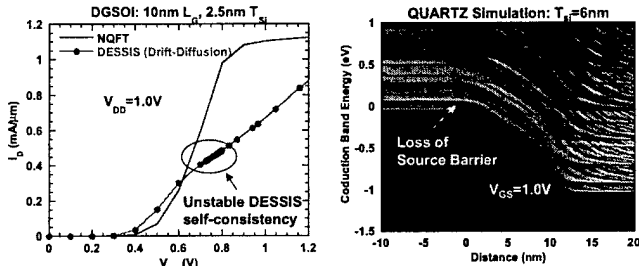
- Set  $L_G/T_{Si} = 4$  to control SCE ... keeping  $t_{ox}=1.5\text{ nm}$  constant
- Evaluate device performance for  $10\text{ nm} < L_G < 80\text{ nm}$

Physical Sciences Research Laboratory

Computational Materials Group

## Double-Gate SOI Simulation Study

### Saturation of Gate Control



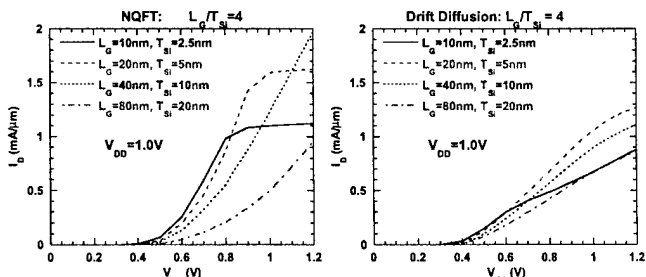
- Drift-diffusion simulations show an instability in self-consistency for  $V_{GS} > 0.8\text{ V}$  due to breakdown of macroscopic charge neutrality at the source boundary
- Boundary charge neutrality is maintained for quantum transport simulations by invoking the equilibrium approximation in the S/D extensions
- Quantum transport simulation predicts current saturation with  $V_{GS} = 0.8\text{ V}$  due to elimination of source barrier

Physical Sciences Research Laboratory

Computational Materials Group

## Double-Gate SOI Simulation Study

### Impact of Current Saturation on Device Scaling



- Cases studied have  $L_g/T_{Si} = 4$  to maintain control of SCE with  $L_g$  scaling
- QUARTZ predicts  $I_{Dsat}$  @  $V_{DD}=1.0\text{ V}$  increases with decreasing  $L_g$  down to ~30-40nm
- Subsequent reductions in  $L_g$  lead to reduced  $I_{Dsat}$  @  $V_{DD}=1.0\text{ V}$  due to elimination of source barrier and current bottleneck with decreasing  $T_{Si}$
- A technology with  $V_{DD}=0.6\text{ V}$  show increasing  $I_{Dsat}$  with  $L_g$  for all cases studied
- DESSIS shows reduction of  $I_{Dsat}$  at  $L_g=10\text{-}20\text{ nm}$

Physical Sciences Research Laboratory

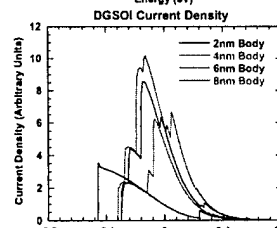
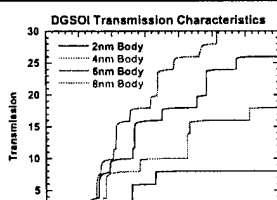
Computational Materials Group

## Double-Gate SOI Simulation Study

- Decreasing  $T_{Si}$  is predicted to enhance mobility by breaking valley degeneracy and preferentially occupying low  $m_{eff}$  valleys
- Macroscopic charge neutrality must be satisfied in the source
- Velocity enhancement is cancelled out by decrease in density of states in transmission characteristics

Decreasing  $T_{Si}$  degrades max  $I_D$  ... cannot scale  $T_{Si}$  indefinitely

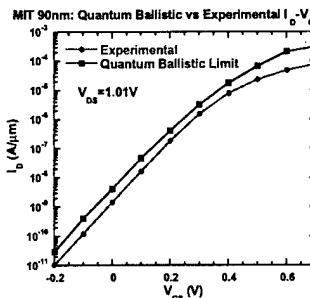
Electron Density vs. Body Thickness



Physical Sciences Research Laboratory

Computational Materials Group

## Quantum Transport Simulations of MOSFETs Scattering Model Calibration

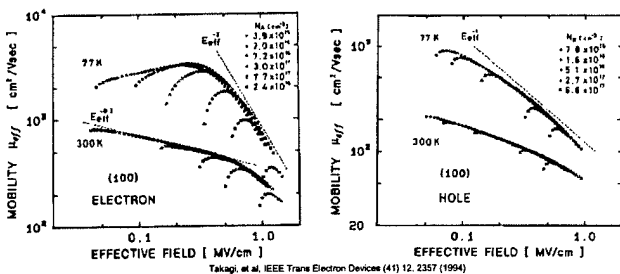


- Discrepancy in quantum mechanical sub-threshold current is due to non-locality of self-consistent charge
- Device drive current is 25% of theoretical limit

Physical Sciences Research Laboratory

Computational Materials Group

## CMOS Effective Mobility

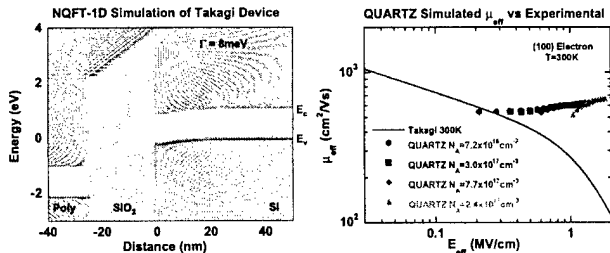


- Effective mobility is a measure of the local mobility averaged over the vertical carrier density in the channel
- Both nMOS and pMOS show a decrease in effective mobility with increasing effective field (inversion charge density)
- Roll-off of mobility has been generally attributed to interface roughness
- Atomistic interpretation has been lacking

Physical Sciences Research Laboratory

Computational Materials Group

## Non-Equilibrium Quantum Field Theory Mobility Model Single Parameter Scattering

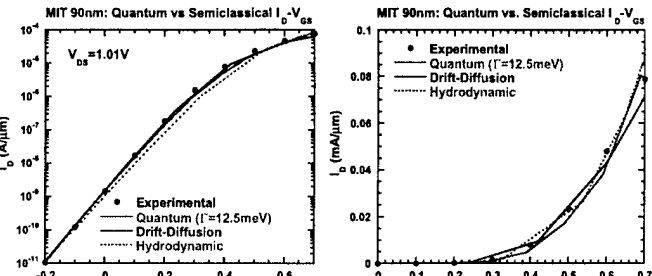


- Single-parameter scattering model brings mobility into empirical range for  $\Gamma=8\text{meV}$
- Universal mobility behavior is exhibited with the NQFT mobility model
- Strong disagreement with empirical universal mobility curve begins to occur for high effective fields ( $E_{\text{eff}} > 0.3 \text{ MV/cm}$ )
- Single-parameter scattering model alone is insufficient for capturing effective mobility behavior

Physical Sciences Research Laboratory

Computational Materials Group

## MIT 90nm Device Quantum Mechanical vs Semiclassical Transport



- Hydrodynamic model shows minor current discrepancy in sub-threshold regime
- Drift-diffusion model shows minor current discrepancy for saturation biases
- Quantum-mechanical simulation using single parameter rate-based scattering model shows good overall fit with experimental data

Physical Sciences Research Laboratory

Computational Materials Group

## Non-Equilibrium Quantum Field Theory Calibration Mobility Model

### Linear Response Conductivity

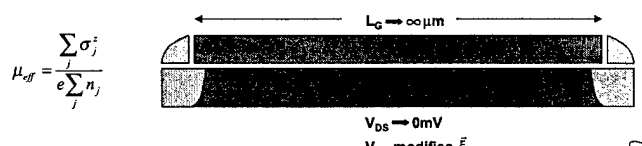
$$\langle \sigma_z \rangle = \lim_{\omega \rightarrow 0} \text{Im} \left[ \frac{\prod(\vec{x}, \vec{x}')}{\omega} \right] \quad (\text{Current-Current Response Function})$$

$$= \frac{e^2 \hbar^3}{8m^2} \lim_{\vec{r}_i \rightarrow \vec{r}_1} [\nabla_{\vec{r}_i} - \nabla_{\vec{r}_1}] \int \frac{dE}{2\pi} \frac{\partial f(E)}{\partial E} \int \frac{dk_z}{2\pi} \int d\vec{r}_{11} \lim_{\vec{r}_z \rightarrow \vec{r}_{11}} [\nabla_{\vec{r}_z} - \nabla_{\vec{r}_{11}}] \mathcal{A}(\vec{r}'_1, \vec{r}_{11}, k_x, E) A(\vec{r}_{12}, \vec{r}_1, k_z, E)$$

### Conductivity: Final Form

$$\sigma_j^z = \frac{2e^2}{h} \int dE \frac{\partial f(E)}{\partial E} \int \frac{dk_z}{2\pi} \sum_m \phi_{jm} \phi_{mj}^* a \text{Re} \left\{ \frac{(e^{i\lambda_m} - e^{-i\lambda_m})^2}{v_m \Gamma_m(E)} + \frac{(e^{i2\lambda_m} - e^{-i2\lambda_m})}{v_m^2} \right\}$$

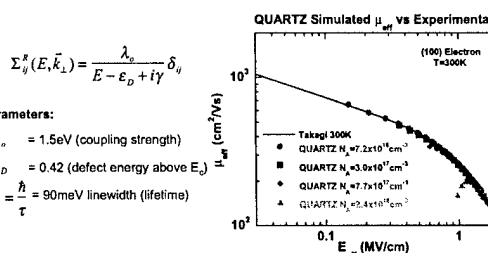
### Effective Mobility and Corresponding MOSFET Test Structure



Physical Sciences Research Laboratory

Computational Materials Group

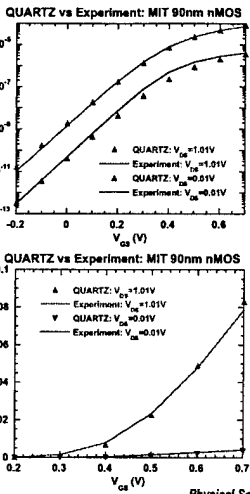
## Quantum Transport Simulated Mobility: Bulk + Interface Scattering Model



- Interface model assumes a strong peak of localized states exists in the Si conduction band due to atoms in the Si-SiO<sub>2</sub> transition layer
- Qualitative view of the interface suggests that there should be a transition layer that averages Si and SiO<sub>2</sub> conduction/valectance band properties
- Bulk + interface scattering model produces universal mobility behavior

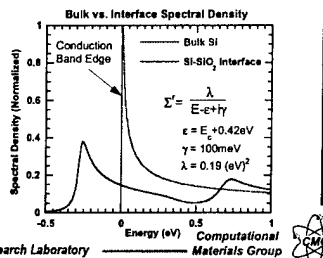
Physical Sciences Research Laboratory

Computational Materials Group



### 90nm MIT MOSFET Comparison

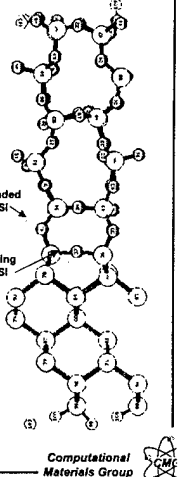
- Calibrated bulk+interface scattering model shows good agreement between theory and experiment
- Band-gap re-normalization leads to states extending into the Si band-gap
- Model agrees with recent gap-state measurements by Lacaita, Pacelli, et al.



### Si-SiO<sub>2</sub> Mobility Model Validation

#### Validation:

- Direct experimental validation is difficult due to mixing of interface and bulk states
- Density Functional Theory (DFT) electronic structure calculations can provide information on structure and density of states
- Existing DFT work has not focused on the detailed interface properties

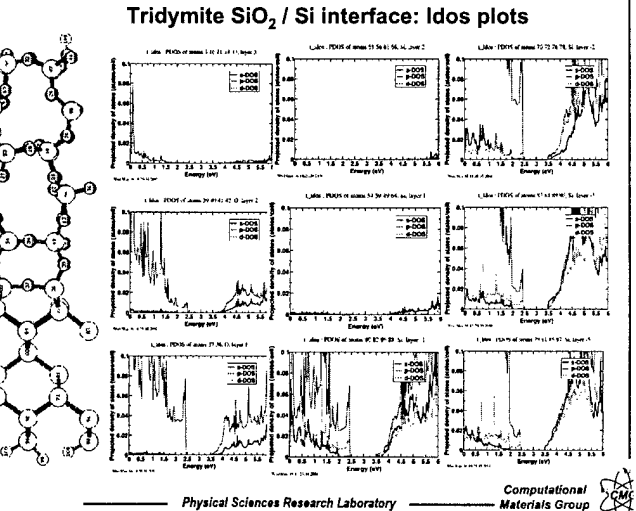


#### DFT Calculations (Liu and Stumpf)

- Performed using VASP on CMG Linux cluster
- Examined three interface structures:
  - Si - SiO<sub>2</sub> ( $\beta$ -quartz)
  - Si - SiO<sub>2</sub> (tridymite)
  - Si - SiO<sub>2</sub> ( $\beta$ -cristobalite)
- Two basic interface Si-O-Si bonding structures observed:
  - Si-O-Si Bridging bonds
  - Si-O-Si Extended bonds
- The bridging and extended interface bonds are present in all SiO<sub>2</sub> structures and are periodically distributed along the interface

Physical Sciences Research Laboratory

Computational Materials Group

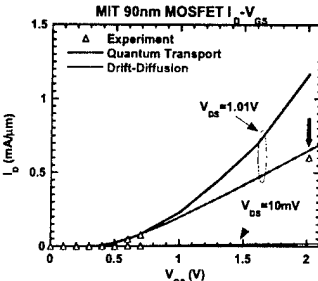


Physical Sciences Research Laboratory

Computational Materials Group

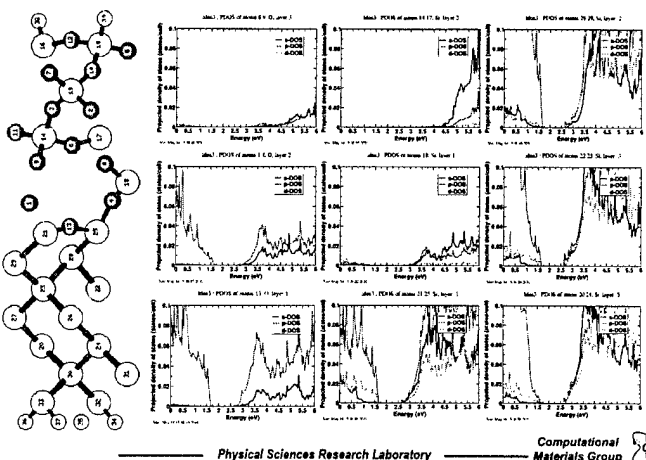
### 90nm MIT MOSFET Comparison

Calibrated localized interface scattering model shows poor agreement with both experimental data and drift-diffusion simulation for high  $V_{GS}$



Physical Sciences Research Laboratory Computational Materials Group

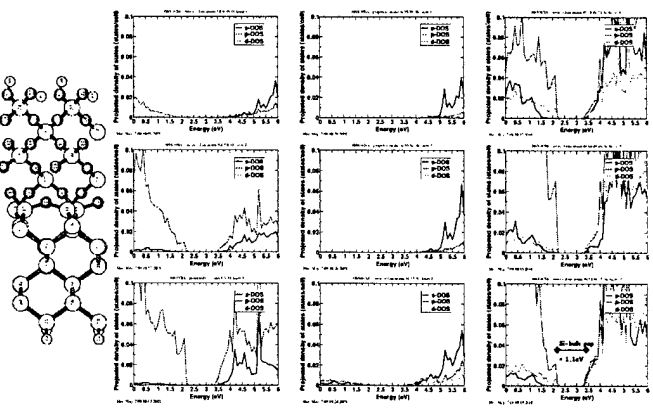
### $\beta$ Quartz SiO<sub>2</sub> / Si interface: Idos plots



Physical Sciences Research Laboratory

Computational Materials Group

### Si(001)/SiO<sub>2</sub> $\beta$ -cristobalite

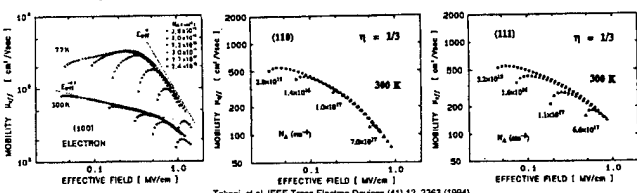


Physical Sciences Research Laboratory

Computational Materials Group

## Effective Mobility Dependence on Si Orientation

- Interface scattering may depend on
  - Non-tetrahedral atomic arrangement of bridging and extended interfacial O atoms
  - Distortion of Si atomic positions below the Si-SiO<sub>2</sub> interface
- If interfacial O and/or distorted Si atomic positions are responsible for high-field  $\mu_{eff}$  behavior, there should be some correlation to Si areal density ( $\rho_S$ )
- Takagi's data shows that (110) Si orientation should have the strongest interface scattering followed by (111) then (100)



Scattering from Interfacial O and/or distorted Si lattice as the cause of Interfacial  $\mu_{eff}$  degradation is supported by experimental data for orientation dependence

Physical Sciences Research Laboratory

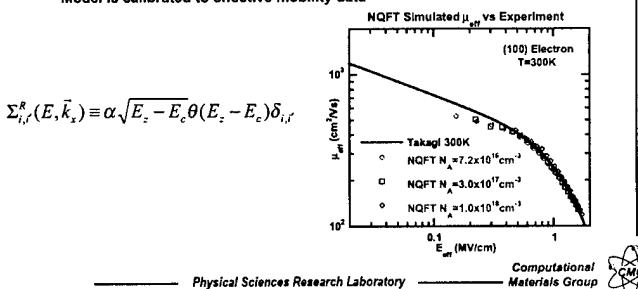
Computational Materials Group

Computational Materials Group

## Quantum Transport Simulated Mobility: Atomistic Interface Scattering Model Calibration

### Interface scattering model calibration:

- A monotonically increasing  $\Sigma^R$  is used to account for the increasing interfacial O and distorted Si DOS
- The interface model is spatially extended 0.5nm into both the SiO<sub>2</sub> and Si to account for the spatial extent of the interfacial O and distorted Si
- Model is calibrated to effective mobility data



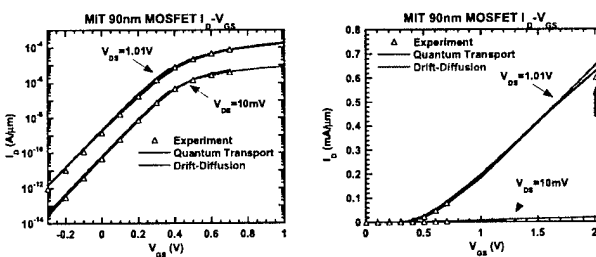
Physical Sciences Research Laboratory

Computational Materials Group

Computational Materials Group

## Quantum Transport Simulated Mobility: Atomistic Interface Scattering Model Calibration

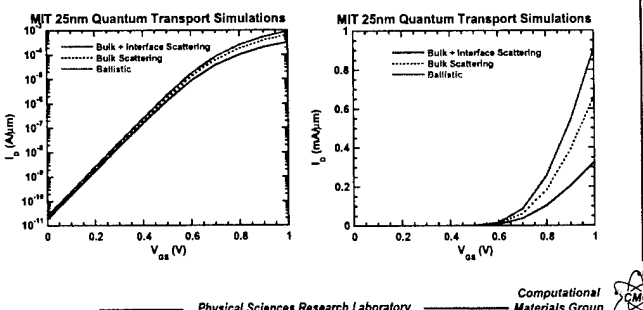
- Incorporation of the effective mobility calibrated interface model leads to excellent theory-experiment agreement for 2D MOSFET quantum transport simulation
- Quantum transport MOSFET simulation can now serve as the basis for TCAD device simulator calibration and device engineering studies



Physical Sciences Research Laboratory Computational Materials Group

## Quantum Transport Simulated Mobility: Ballistic Transport vs Scattering

- Ballistic quantum transport simulations reveal that the MIT 25nm device is operating at ~30% of the ballistic limit
- Interface scattering dominates 25nm MIT device  $I_{Dsat}$
- If the atomic interface scattering model is to be believed, there is little hope of ever achieving ballistic performance in MOSFETs

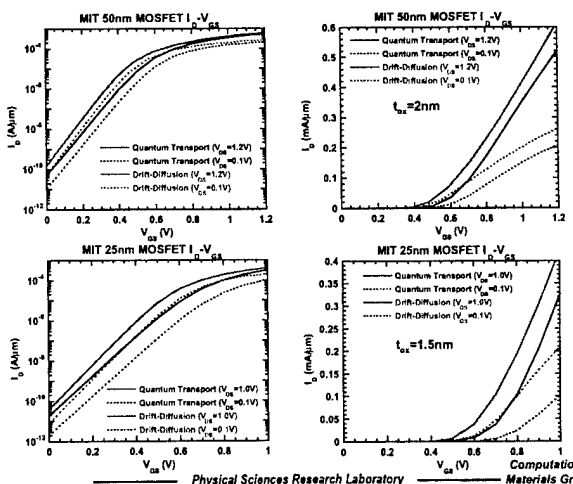


Physical Sciences Research Laboratory

Computational Materials Group

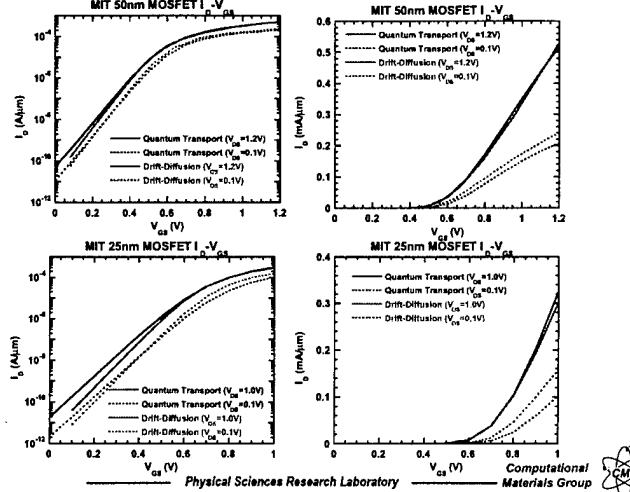
Computational Materials Group

## MIT MOSFET Simulation Comparison



Physical Sciences Research Laboratory Computational Materials Group

## MIT MOSFET Simulation Comparison Eliminating $V_t$ Shift



## MIT MOSFET Simulation Comparison

### Comparison Summary

- Centroid induced  $V_t$  shift is approximately 50meV for the 50nm MIT MOSFET ( $t_{ox}=2\text{nm}$ ) and 100meV for the 25nm MIT MOSFET ( $t_{ox}=1.5\text{nm}$ ) as compared to drift diffusion data
- Increasing DIBL, sub-threshold slope, and  $I_{off}$  are observed with decreasing  $L_{poly}$  (and  $t_{ox}$ ) indicating the centroid shift may be compromising resistance to short channel effects
- Sub-threshold slope and  $I_{off}$  increase are also influenced by increasing sub-threshold tunneling with decreasing  $L_{poly}$  ... further study into relative effects of sub-threshold tunneling and centroid shift is required
- Drift-diffusion model show excellent agreement with calibrated quantum transport theory in predicting post-threshold behavior

### Conclusion

*Appropriately calibrated effective potential corrections applied to drift diffusion models will provide all the essential physics required for TCAD device simulation for the foreseeable future*

**Physical Sciences Research Laboratory** **Computational Materials Group**

# Quantum kinetics and the femtosecond time scale in optical excitation of semiconductors

V. M. Axt, M. Glanemann, M. Herbst,  
J. Schlip, T. Wolterink



WESTFÄLISCHE  
WILHELMUS-UNIVERSITÄT  
MÜNSTER

Institut für Festkörpertheorie

Work supported by the European Commission (TMR network "Ultrafast Quantum Optoelectronics") and by the Deutsche Forschungsgemeinschaft (Schwerpunktprogramm "Quantenkohärenz in Halbleitern")

AFW Quantum Transport in Semiconductors Maratea, 17-22 June 2001

## Quantum kinetics in semiconductors introduction

### Semiclassical transport and kinetics

Free flights  
electrons accelerated by local electric field ( $\sim \text{grad } V$ )

Scattering processes  
instantaneous in time  
local in space  
between well-defined  $k$ -states  
different mechanisms additive

Dynamical equation  
Boltzmann equation

### Quantum effects on short time and length scales

Energy-time uncertainty  
single-particle energies not conserved  
on short time-scales

Momentum-position uncertainty  
no local transitions between  
well-defined momentum states

Memory effects  
dynamics of distribution functions and  
polarizations non-local in time and space

Quantum-mechanical correlations  
scattering between renormalized states  
phonon-assisted transitions  
intracollisional field effect

## Quantum kinetics in semiconductors introduction

## Quantum kinetics in semiconductors overview

### Introduction

#### Phonon quantum kinetics in homogeneous systems

density-matrix theory

relaxation to NGFs

energy-time uncertainty

nonequilibrium phonons

scattering between renormalized states

phonon quantum beats

intracollisional field effect

#### Phonon quantum kinetics in inhomogeneous systems

different representations

wave-packet dynamics

coherent phonons

carrier-trapping dynamics

### Conclusions

## Electron-phonon quantum kinetics hierarchy

### Carrier-phonon interaction 1-band model

#### Hamiltonian

$$H = \sum_k \epsilon_k c_k^\dagger c_k + \sum_q \hbar \omega_q b_q^\dagger b_q + \sum_{k,q} (g_q^* c_{k+q}^\dagger b_q c_k + h.c.)$$

#### dynamical variables

$$\langle c_{k-q}^\dagger c_k^\dagger + c_k c_{k-q} \rangle$$

$$\langle b_{k-q}^\dagger b_{k-q} \rangle$$

#### distribution functions

$$f_k^* = \langle c_k^\dagger c_k \rangle$$

$$n_q = \langle b_q^\dagger b_q \rangle$$

#### phonon-assisted density matrix

$$S_{k+q,k}^* = \frac{i}{\hbar} g_q^* c_{k+q}^\dagger b_q c_k$$

#### equations of motion

$$\langle c_{k-q}^\dagger c_k^\dagger b_{k-q} b_q \rangle \approx f_k n_q \delta_{k-k-q} \delta_{q,q'}$$

#### neglecting higher order correlations

#### factorized equation of motion

$$\frac{d}{dt} S_{k+q,k}^* = \frac{i}{\hbar} (\epsilon_k - \epsilon_{k+q} - \hbar \omega_q) S_{k+q,k}^*$$

$$+ \frac{1}{\hbar^2} |g_q^*|^2 [f_k^* (1 - f_{k+q}) - (1 - f_{k+q}^*) f_k^*]$$

#### ⇒ quantum kinetic second Born approximation

$$\frac{d}{dt} n_q = \sum_k [2\text{Re} \{ S_{k+q,k}^* \} - 2\text{Re} \{ S_{k+q,k}^* \}]$$

$$\frac{d}{dt} f_k^* = \sum_q [2\text{Re} \{ S_{k+q,k}^* \} - 2\text{Re} \{ S_{k+q,k}^* \}]$$

## Electron-phonon quantum kinetics memory effects and Markov limit

## Electron-phonon quantum kinetics two-particle correlations

## Electron-phonon quantum kinetics two-particle correlations

formal solution

$$\begin{aligned} S_{k,k}(t) &= S_{k,k}^0 \exp \left[ \frac{i}{\hbar} (\epsilon_k - \epsilon'_k - \hbar\omega_q) t \right] \\ &+ \frac{1}{\hbar^2} |g'_q|^2 \int_0^t d\tau \exp \left[ \frac{i}{\hbar} (\epsilon'_k - \epsilon'_k - \hbar\omega_q) \tau \right] \\ &\times [f'_k (1 - f'_k) (n_q + 1) - (1 - f'_k) f'_k n_q] (t - \tau) \\ \Rightarrow & \text{Dynamics with memory} \end{aligned}$$

Markov limit

$$\begin{aligned} \frac{d}{dt} f'_k &= 2\pi \sum_{q,\pm} |g'_q|^2 [\delta(\epsilon'_k - \epsilon'_{k-q} \mp \hbar\omega_q) \\ &\times [(1 - f'_k) \left( n_q + \frac{1}{2} \mp \frac{1}{2} \right) f'_{k-q} - f'_k (1 - f'_{k-q}) \left( n_q + \frac{1}{2} \pm \frac{1}{2} \right)] \\ &+ \frac{d}{dt} n_q = 2\pi \sum_k |g'_q|^2 \delta(\epsilon'_k - \epsilon'_{k-q} - \hbar\omega_q) \\ &\times [(1 - f'_k) n_q f'_{k-q} - f'_k (1 - f'_{k-q}) (n_q + 1)] \end{aligned}$$

$\Rightarrow$  Boltzmann equations

## Electron-phonon quantum kinetics diagonal approximation

Classification of higher-order contributions

equation of motion for  $S_{k,k'}$  involves terms

(a)  $\sim S_{k,k'}$

(b)  $\sim \sum_{q,q'} S_{k+q,k'+q'}$

assumption: (b) small due to random phases of  $S$

$\Rightarrow$  diagonal approximation:  $k$ -components decoupled

Markov approximation for  $T^{(r)}$

$$\begin{aligned} \frac{d}{dt} S_{k,k}^r &= \left[ \frac{i}{\hbar} (\epsilon_k - \epsilon'_k - \hbar\omega_q) - \Gamma_k - \Gamma_1 \right] S_{k,k}^r \\ &+ \frac{1}{\hbar^2} |g'_q|^2 [f'_k (1 - f'_k) (n_q + 1) - (1 - f'_k) f'_k n_q] \end{aligned}$$

with

$$\begin{aligned} \Gamma_k &= \frac{\pi}{\hbar} \sum_{q,\pm} |g'_q|^2 \delta(\epsilon'_k - \epsilon'_{k+q} \pm \hbar\omega_q) \\ &\times [n_q + \frac{1}{2} \pm \frac{1}{2}] f'_{k+q} + (n_q + \frac{1}{2} \mp \frac{1}{2}) (1 - f'_{k+q}) \end{aligned}$$

$\Rightarrow$  polaron self energy (real part neglected)

$\Rightarrow$  quantum kinetics with damped memory

including deviations from factorization:

$$(c_k^\dagger b_k^\dagger b_{k-q} c_k) \approx \delta_{k,-q} n_q (c_k^\dagger b_{k-q} c_k) + \delta_{k,q} n_q (c_k^\dagger b_{k+q} c_k)$$

factorized equation of motion for  $T$

$$\begin{aligned} \frac{d}{dt} T_{k,k,q}^{(1)} &= \frac{i}{\hbar} (\epsilon'_{k+q} - \epsilon'_k + \hbar\omega_q - \hbar\omega_q) T_{k,k,q}^{(1)} \\ &+ \frac{1}{\hbar^2} |g'_q|^2 [(1 + n_q - f'_k) S_{k+q,k+q}^r - (n_q + f'_k) S_{k+q,k}^r] \end{aligned}$$

exact equation of motion for  $S$

$$\begin{aligned} \frac{d}{dt} S_{k,k}^r &= \frac{i}{\hbar} (\epsilon'_k - \epsilon'_k - \hbar\omega_q) S_{k,k}^r \\ &+ \frac{1}{\hbar^2} |g'_q|^2 [f'_k (1 - f'_k) (n_q + 1) - (1 - f'_k) f'_k n_q] \\ &+ \sum_l [T_{k,k+q,l}^{(1)} - T_{k,k+q,l}^{(1)} + T_{k,k+q,l}^{(2)} - T_{k,k+q,l}^{(2)}] \end{aligned}$$

(with  $q = k - k'$ )

required: equations of motion for  $T^{(i)}$

## Electron-phonon quantum kinetics density matrices and Greens functions

Generalized Kadanoff-Baym Equation

$$\begin{aligned} \frac{d}{dt} R(t) &= -i \frac{d}{dt} G_K^<(t,t) \\ &= - \int_{-\infty}^t dt' [S_K^>(t,t') G_K^<(t',t) - \Sigma_K^<(t,t') G_K^>(t',t) \\ &\quad - G_K^>(t,t') \Sigma_K^<(t',t) + G_K^<(t,t') \Sigma_K^>(t',t)] \end{aligned}$$

self-energy

$$\Sigma_K^<(t,t) = \frac{i}{\hbar^2} \sum_q |g'_q|^2 D_K^<(t,t') G_{k+q}^<(t,t')$$

quantum kinetic

Generalized Kadanoff-Baym Ansatz (GKBA)  
 $G_K^<(t,t') = -G_K^>(t,t') f'_k(t') + f'_k(t) G_K^>(t,t')$

Second Born approximation:

GKBA with  $G^r(0), G^a(0)$  (no  $\Sigma$ )

fourth Born approximation, diagonal terms:

GKBA with  $G^r, G^a$  including  $\Sigma$

relaxation from given initial distribution

$\Rightarrow$  time-dependent broadening

truncation by factorization on 5-point level

$$(c_k^\dagger b_k^\dagger b_{k-q} c_k) \approx \delta_{k,-q} n_q (c_k^\dagger b_{k-q} c_k) + \delta_{k,q} n_q (c_k^\dagger b_{k+q} c_k)$$

factorized equation of motion for  $T$

$$\begin{aligned} \frac{d}{dt} T_{k,k,q}^{(1)} &= \frac{i}{\hbar} (\epsilon'_{k+q} - \epsilon'_k + \hbar\omega_q - \hbar\omega_q) T_{k,k,q}^{(1)} \\ &+ \frac{1}{\hbar^2} |g'_q|^2 [(1 + n_q - f'_k) S_{k+q,k+q}^r - (n_q + f'_k) S_{k+q,k}^r] \end{aligned}$$

exact equation of motion for  $S$

$$\begin{aligned} \frac{d}{dt} S_{k,k}^r &= \frac{i}{\hbar} (\epsilon'_k - \epsilon'_k - \hbar\omega_q) S_{k,k}^r \\ &+ \frac{1}{\hbar^2} |g'_q|^2 [(1 + n_q - f'_k) S_{k+q,k+q}^r - (n_q + f'_k) S_{k+q,k}^r] \end{aligned}$$

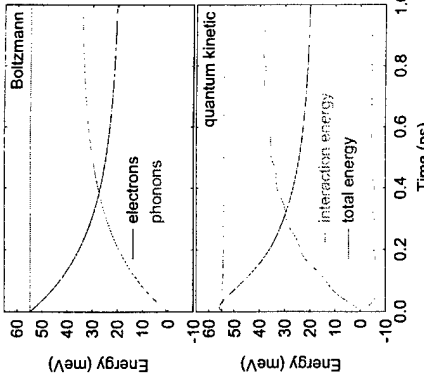
formal solution yields  $T_{k,k,q}^{(1)}(t) = T_{k,k,q}^{(1)}[f'_k, n_q, S_{k,k}^r](t)$

$\Rightarrow$  Closed integro-differential equation for  $S$

$\Rightarrow$  quantum kinetic fourth Born approximation

## Carrier-phonon interaction

### Boltzmann 1-band model



mean energy per electron  
⇒ energy conservation with interaction

### CARRIER-PHONON INTERACTION

#### EQUATIONS OF MOTION

##### DISTRIBUTION FUNCTIONS AND POLARIZATION

**dynamical variables**

$$f_k^h = \langle d_k^\dagger b_k \rangle \quad n_q = \langle b_k^\dagger b_q \rangle$$

**distribution functions**

$$f_k^h = \langle d_k^\dagger d_k \rangle \quad n_q = \langle d_q^\dagger d_q \rangle$$

**interband polarization**

$$p_k = \langle d_{-k} c_k \rangle$$

**phonon-assisted density matrices**

$$S_{k,k}^h = \frac{i}{\hbar} g_q^* \langle c_k^\dagger b_q c_k \rangle \quad S_{-k,-k}^h = \frac{i}{\hbar} g_q^h \langle d_{-k}^\dagger b_q d_{-k} \rangle$$

$$\tau_{-k,k}^{(+)} = \frac{i}{\hbar} g_q^* \langle d_{-k} b_q c_k \rangle \quad \tau_{-k,k}^{(-)} = \frac{i}{\hbar} g_q^* \langle c_k^\dagger b_q d_{-k} \rangle$$

mean energy per electron  
⇒ energy conservation with interaction

#### EQUATIONS OF MOTION

##### PHONON-ASSISTED DENSITY MATRICES

$$\frac{d}{dt} f_k^h = 2R \{ i \tilde{\mu}_k p_k \} + \sum_q [2R \{ S_{k+q,k}^h \} - 2R \{ S_{-k,-k-q}^h \}]$$

$$\frac{d}{dt} n_q = \sum_k [2R \{ S_{k+q,k}^h \} + 2R \{ S_{-k+q,-k}^h \}]$$

$$\frac{d}{dt} p_k = -i \Omega_k^p p_k - i \tilde{\mu}_k (1 - f_k^h - f_{-k}^h)$$

$$+ \sum_q [T_{-k,q,k}^{(+)} - T_{-k,q,k}^{(-)*} - T_{-k,k-q}^{(+)} + T_{-k,k+q}^{(-)*}]$$

$$\Rightarrow \text{semiconductor Bloch equations}$$

$$\text{with } \tilde{\mu}_k = M_k \cdot E_0(t) e^{-i \omega_k t} - \sum_q V_q p_{k+q}$$

**coherent generation, Boltzmann scattering**

$$\text{with } \tilde{\mu}_k = M_k \cdot E_0(t) e^{-i \omega_k t} - \sum_q V_q f_{k+q}^h$$

$$\tilde{\epsilon}_k^h = \epsilon_k^h - \sum_q V_q f_{k+q}^h$$

**CROSS TERMS (RENORMALIZATIONS)**

“Boltzmann” terms (scattering processes)

Polarization scattering (eh-coherence/c.c.)

excitation with 100 fs pulse  
⇒ broadening of generation

### EQUATIONS OF MOTION

#### DISTRIBUTION FUNCTIONS AND POLARIZATION

#### CARRIER-PHONON INTERACTION

##### 2-BAND MODEL

**quantum kinetic**

$$\frac{d}{dt} f_k^h = \sum_k [2R \{ S_{k+q,k}^h \} + 2R \{ S_{-k+q,-k}^h \}]$$

$$\frac{d}{dt} n_q = \sum_k [T_{-k,q,k}^{(+)} - T_{-k,q,k}^{(-)*} - T_{-k,k-q}^{(+)} + T_{-k,k+q}^{(-)*}]$$

**quantum kinetic with renormalizations**

$$\tilde{\epsilon}_k^h = \epsilon_k^h - \sum_q V_q f_{k+q}^h$$

**excitation with 100 fs pulse**

⇒ time-dependent broadening

#### CARRIER-PHONON INTERACTION

##### 2-BAND MODEL

**Boltzmann generation and scattering**

$$\frac{d}{dt} S_{k,k}^h = \frac{i}{\hbar} (\tilde{\epsilon}_k - \tilde{\epsilon}_k - \hbar \omega_{kp}) S_{k,k}^h$$

$$+ i \tilde{\mu}_k^* T_{-k,k}^{(+)} - i \tilde{\mu}_k T_{-k,k}^{(-)}$$

$$+ \frac{1}{\hbar^2} |g_q|^2 [(n_q + 1) (1 - f_k^h) f_k^h - n_q f_k^h (1 - f_k^h)]$$

$$- \frac{1}{\hbar^2} \tilde{\epsilon}_k^h \tilde{\epsilon}_k^h \tilde{\epsilon}_k^h \tilde{\epsilon}_k^h$$

$$\tilde{\epsilon}_k^h = \epsilon_k^h - \sum_q V_q f_{k+q}^h$$

**coherent generation, Boltzmann scattering**

$$\text{with } \tilde{\mu}_k = M_k \cdot E_0(t) e^{-i \omega_k t} - \sum_q V_q p_{k+q}$$

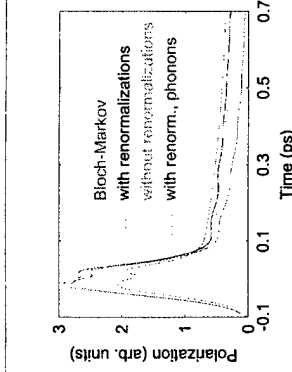
**CROSS TERMS (RENORMALIZATIONS)**

“Boltzmann” terms (scattering processes)

Polarization scattering (eh-coherence/c.c.)

## Carrier-phonon interaction

### 2-band model with constant field



decay of incoherently summed polarization  
 $(P = \sum |p_k|)$   
 $\Rightarrow$  phonon quantum beats

$$\begin{aligned} \frac{d}{dt} f'_k &= \frac{eE}{\hbar} \frac{\partial}{\partial k_z} f'_k + 2\text{Re}\{f'_k p_k\} \\ &+ \sum_q [2\text{Re}\{S_{k+q,k}\} - 2\text{Re}\{S'_{k,-q,k}\}] \\ \frac{d}{dt} p_k &= \frac{eE}{\hbar} \frac{\partial}{\partial k_z} p_k - i(\tilde{\epsilon}_k + \tilde{\epsilon}_k^*) p_k - i\tilde{\nu}_k (1 - f'_k - f_k) \\ &+ \sum_q [T_{-k+q,k}^{(+)} - T_{-k+q,k}^{(-)*} - T_{-k+q,k}^{(+)} + T_{-k+q,k}^{(-)*}] \\ \frac{d}{dt} S'_{k,k} &= \frac{eE}{\hbar} \left( \frac{\partial}{\partial k_z} + \frac{\partial}{\partial k'_z} \right) S'_{k,k} + \frac{i}{\hbar} (\tilde{\epsilon}'_k - \tilde{\epsilon}'_k^* - \hbar\nu_{L0}) S'_{k,k} \\ &+ i\tilde{\mu}_k T_{-k,k}^{(+)} - i\tilde{\mu}_k T_{-k,k}^{(-)} - \frac{1}{\hbar^2} g'_k g'_k p'_k p_k \\ \text{with } \tilde{\nu}_k \tilde{f}_k &= -M E - M_k E_0(t) e^{-i\omega_k t} - \sum_q V_q p_{k+q} \end{aligned}$$

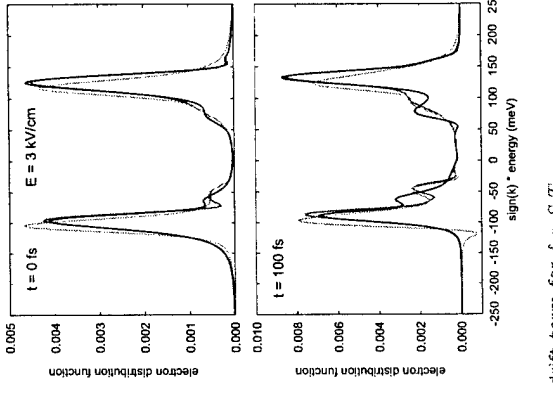
$$\tilde{\epsilon}'_k^h = \epsilon'_k^h - \sum_q V_q f'_{k+q}^h$$

acceleration terms

Zener term

### Intracollisional field effect

#### 2-band model, quantum wire



drift term for  $f, p, S, T$   
 drift term for  $f, p$   
 drift term for  $S, T$

## Electron-phonon quantum kinetics

### Spatially inhomogeneous system

#### equations of motion

$$\begin{aligned} \frac{d}{dt} f'_{k,k} &= \frac{i}{\hbar} \sum_k [\mathcal{E}'_{kk} f'_{kk} - \mathcal{E}'_{kk} f''_{kk} + U'_{kk} p_{kk} - U_{kk} p'_{kk}] \\ &+ \sum_q [S'_{k+q,k+q} - S''_{k+q,k+q} + S'_{k+q,k+q} - S'_{k,q,k-q}] \\ \text{coherent phonon amplitude} \\ \frac{d}{dt} B_q &= -i\omega_{qp} B_q + \frac{i}{\hbar} g_{qq} \sum_k [f'_{kk+q} - f'_{kk+q}] \\ \text{energy matrices:} \\ \mathcal{E}'_{kk}^h &= \left[ \epsilon'_k \pm \frac{icE}{2} \left( \frac{\partial}{\partial k_z} - \frac{\partial}{\partial k'_z} \right) \right] \delta_{kk} + V_{kk}^h \\ \text{incoherent phonon distribution function} \\ n_{kk'} &= \langle (b'_k - B'_k)(b_{k'} - B_{k'}) \rangle \\ \text{phonon assisted density matrices} \\ S'_{k,q,k} &= \frac{i}{\hbar} g_q (c'_k (b'_q - B'_q) c_k) \quad S''_{k,q,k} = -\frac{i}{\hbar} g_q (d'_k (b'_q - B'_q) d_k) \\ T'_{k,q,k}^{(+)} &= \frac{i}{\hbar} g_q (d_{-k} (b'_q - B'_q) c_k) \quad T'_{k,q,k}^{(-)} = -\frac{i}{\hbar} g_q (d_{-k} (b'_q - B'_q) c_k) \end{aligned}$$

renormalization of scattering dynamics due to:  
 external field (intracollisional field effect)  
 incoherent phonons  
 coherent phonons  
 exchange energy and Coulomb enhancement  
 spatial inhomogeneities

$\pm g_{k+q-k} (B_{k+q} - B_{k+q})$

effective field matrices:

$$U_{kk} = EM_1 \delta_{kk} + M_1 (n_{kk} + \sum_q V_{qk+q}) - \sum_q V_{qk+q}$$

single-particle potential

external field (drift and Zener term)

exchange energy and Coulomb enhancement

induced field (Ulfarce term)

coherent phonons

## Spatially inhomogeneous system Wigner representation

## Spatially resolved kinetics density and mean energy

$$\begin{aligned} f'(\mathbf{k}, \mathbf{r}) &= \sum_{\mathbf{q}} e^{i\mathbf{q}\cdot\mathbf{r}} (c_{\mathbf{k}-\mathbf{q}}^{\dagger} c_{\mathbf{k}+\frac{1}{2}\mathbf{q}}) \\ p(\mathbf{k}, \mathbf{r}) &= \sum_{\mathbf{q}} e^{i\mathbf{q}\cdot\mathbf{r}} (a_{\mathbf{k}+\frac{1}{2}\mathbf{q}}^{\dagger} c_{\mathbf{k}+\frac{1}{2}\mathbf{q}}) \\ B(\mathbf{r}) &= \sum_{\mathbf{q}} e^{i\mathbf{q}\cdot\mathbf{r}} B_{\mathbf{q}} \end{aligned}$$

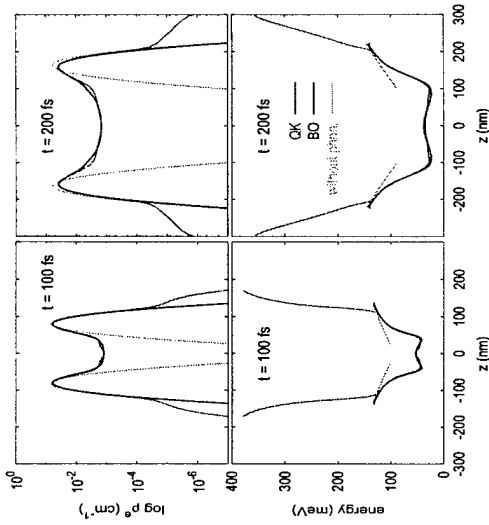
spatially resolved variables:

$$\text{electron density } n'(\mathbf{r}) = \sum_{\mathbf{k}} f'(\mathbf{k}, \mathbf{r})$$

$$\text{energy density } u'(\mathbf{r}) = \sum_{\mathbf{k}} \epsilon_{\mathbf{k}} f'(\mathbf{k}, \mathbf{r})$$

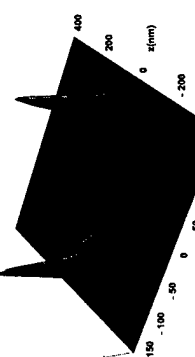
$$\text{mean kinetic energy per carrier } E(\mathbf{r}) = \frac{u'(\mathbf{r})}{n'(\mathbf{r})}$$

$$\text{lattice polarization } P(\mathbf{r}) = \frac{-ie_0}{e} \sum_{\mathbf{q}} q \rho_q e^{i\mathbf{q}\cdot\mathbf{r}} (B_{\mathbf{q}} - B_{-\mathbf{q}})$$



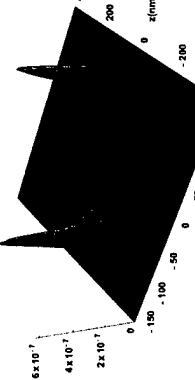
## Spatially resolved kinetics Wigner function

$t = 100 \text{ fs}$

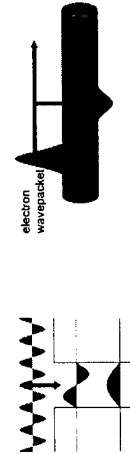


## Spatially resolved kinetics Wigner function

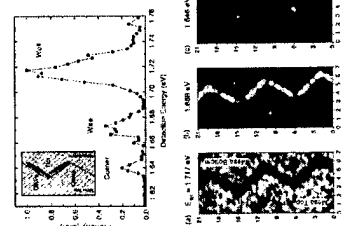
$t = 100 \text{ fs, quantum kinetic}$



$t = 100 \text{ fs, carrier trapping process}$



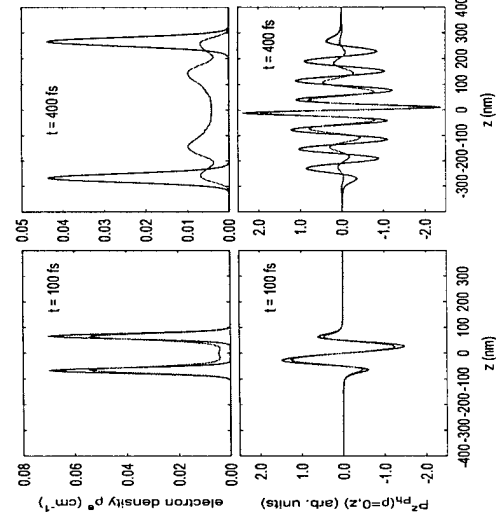
$t = 100 \text{ fs}$   
transitions between states of different dimensions



Ch. Lienau et al., phys. stat. sol. (a) 178, 471 (2000)

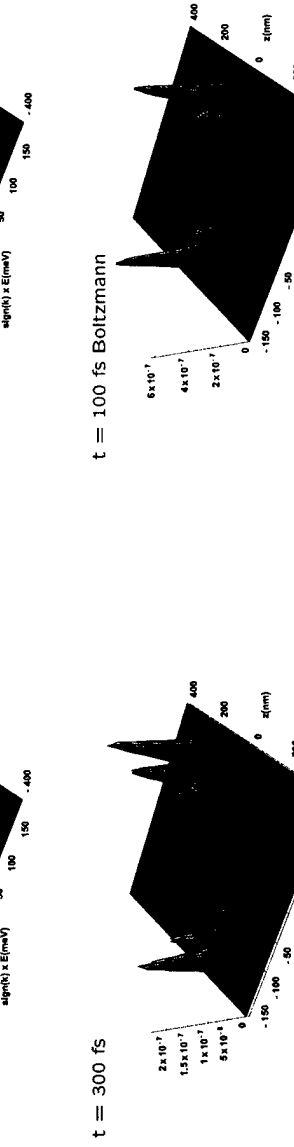
## Kinetics of charge separation coherent phonons

without/with incoherent phonons



## Dynamics with inhomogeneous potential Carrier trapping process

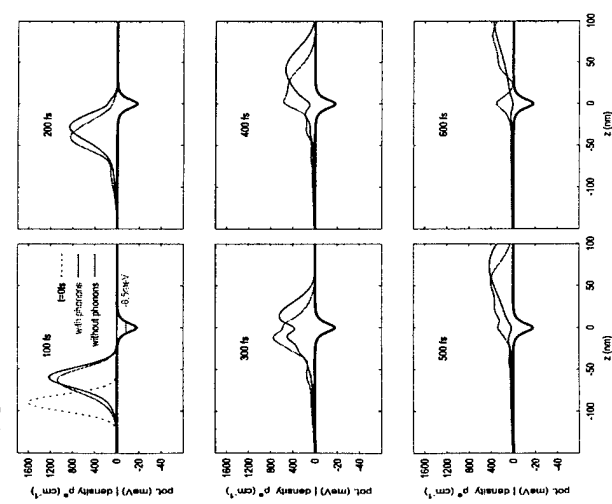
$t = 100 \text{ fs}$   
experimental realization & near-field spectroscopy



### Carrier trapping in dot states

#### Shallow smooth potential

initial energy: 18 meV, width: 7.5 meV



**Carrier trapping in dot states  
smooth potential, resonant case**

100 fs

200 fs

300 fs

400 fs

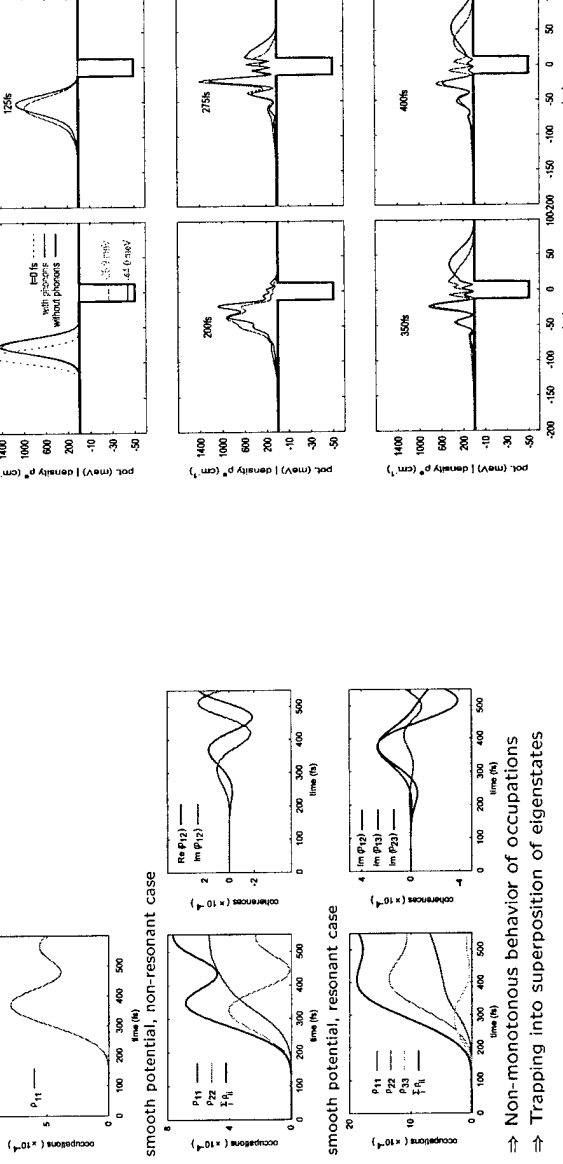
500 fs

600 fs

z (nm)

**Carrier trapping in dot states  
density matrix of bound states**

shallow smooth potential, non-resonant case

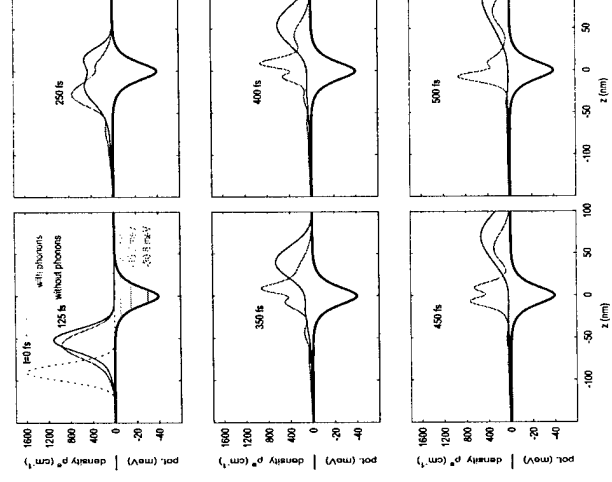


Non-monotonous behavior of occupations  
⇒ Trapping into superposition of eigenstates

### Carrier trapping in dot states

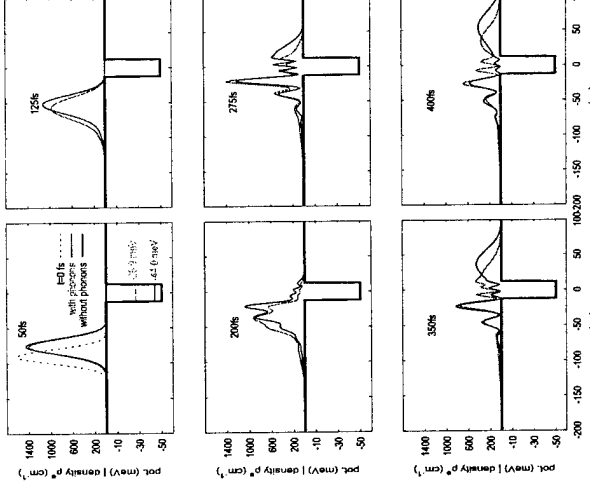
#### Shallow smooth potential

initial energy: 18 meV, width: 7.5 meV



**Carrier trapping in dot states  
square well potential**

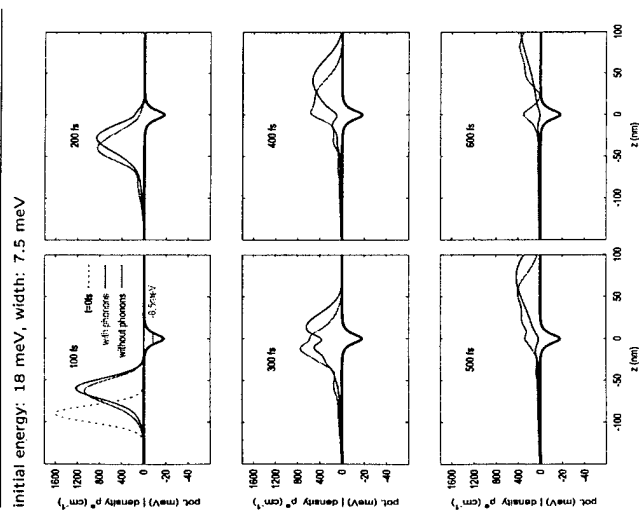
initial energy: 18 meV, width: 7.5 meV



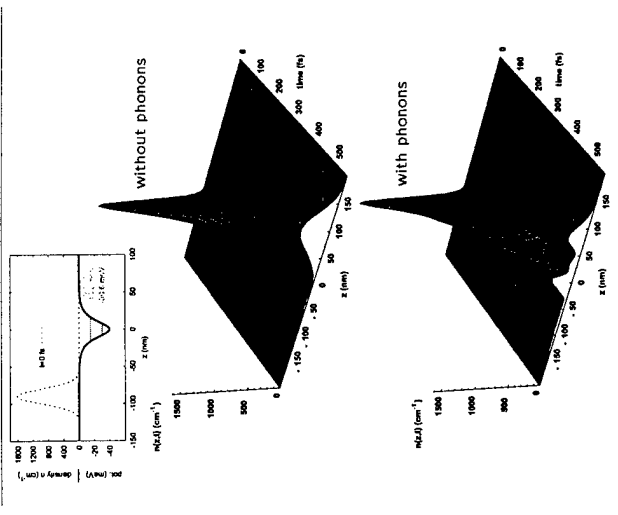
Non-monotonous behavior of occupations  
⇒ Trapping into superposition of eigenstates

### Carrier trapping in dot states

#### Shallow smooth potential

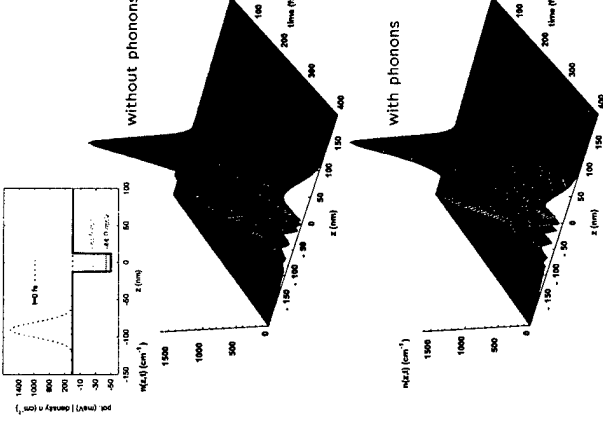


**Carrier trapping in dot states  
smooth potential, resonant case**



Non-monotonous behavior of occupations  
⇒ Trapping into superposition of eigenstates

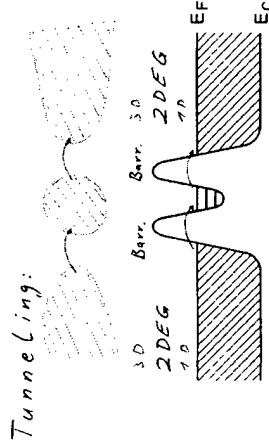
## Carrier trapping in dot states square well potential



## Quantum kinetics in semiconductors conclusions

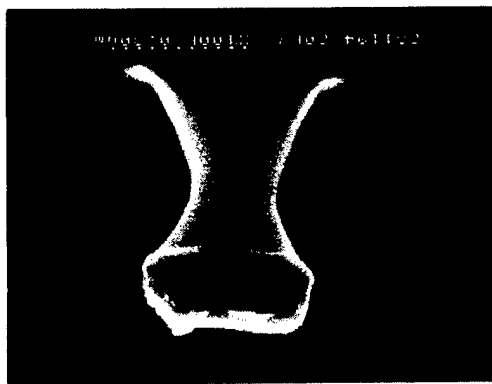
- Phonon quantum kinetics in homogeneous systems
  - density-matrix theory
  - relation to NGFs
  - energy-time uncertainty
  - nonequilibrium phonons
  - scattering between renormalized states
  - phonon quantum beats
  - intracollisional field effect
- Phonon quantum kinetics in inhomogeneous systems
  - different representations
  - wave-packet dynamics
  - coherent phonons
  - carrier-trapping dynamics

## Transport through a Quantum Dot:



Tunneling:

- Discrete Energy Levels (Confinement)
- Charging Energy ( $E_c = \frac{e^2}{2C}$ ) (Capacitance C)



## Overview:

- Single-Electron Tunneling
- Transport through Quantum Dots
- Spectroscopy
- Influence of Emitter States
- Spin Effects
- Conclusions

# Single-Electron Tunneling through Quantum Dots (Single-Electron Charging in Quantum Dot Arrays)

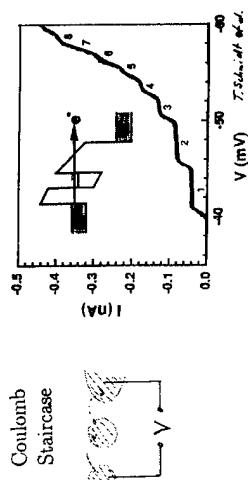
Rolf J. Haug

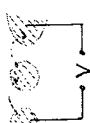
University of Hannover  
Germany

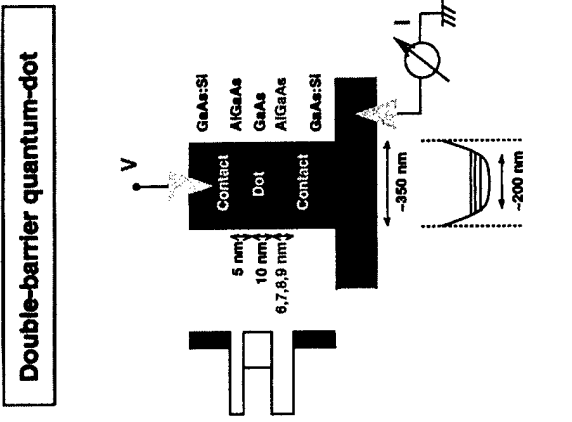
$$\text{NANOSTRUKTUREN} \quad \text{an Hannover}$$

Advanced Research Workshop on Quantum Transport in Semiconductors, 21.-22.2001

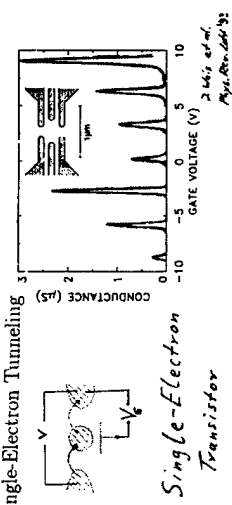
## Charging Effects

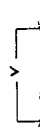


Coulomb  
Staircase  




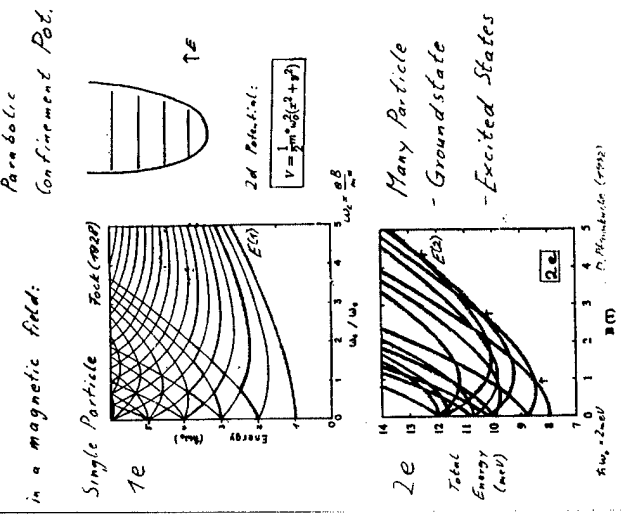
## Double-barrier quantum-dot



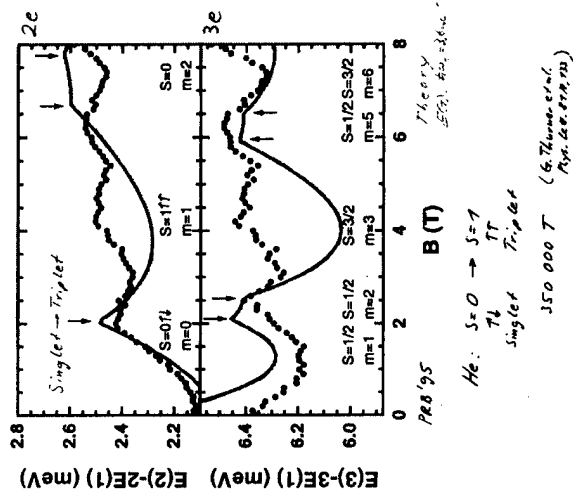
Coulomb Blockade  
and  
Single-Electron Tunneling  
Transistor  


*T. Schmid et al.,  
Phys. Rev. B 59, 15155*  
*J. Phys. Chem. B 103, 2463*

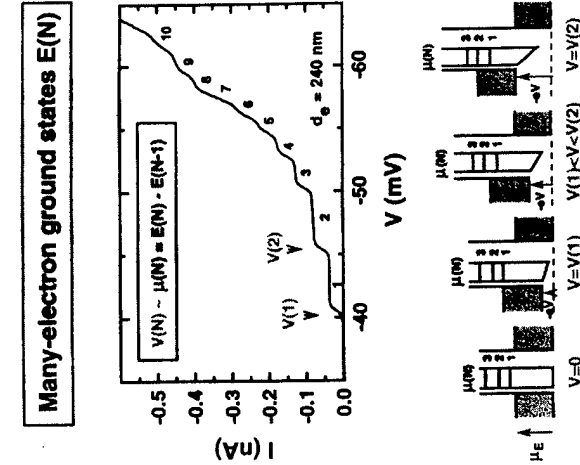
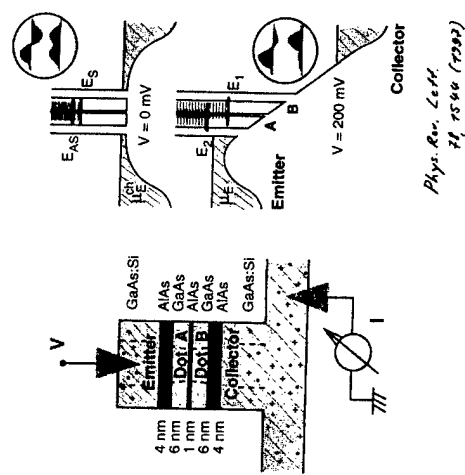
## Transport Spectroscopy of Artificial 'Atoms'?



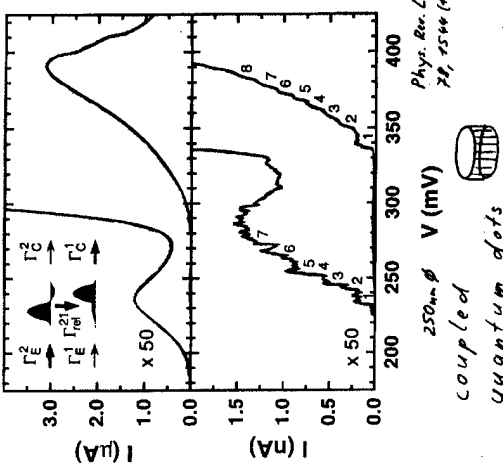
## Quantum-dot Helium and Lithium



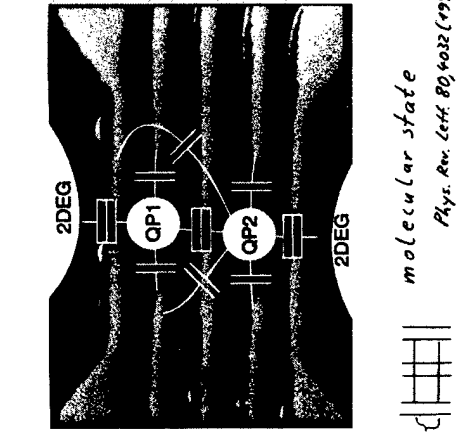
## Coupled Quantum Dots



## Lateral Double Quantum Dot



## Coupled quantum wells



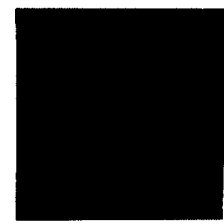
Phys. Rev. Lett. 80, 4032 (1998)  
Phys. Rev. Lett. 80, 4032 (1998)  
Phys. Rev. Lett. 80, 4032 (1998)

Rabi oscillations

Phys. Rev. Lett. 80, 4032 (1998)

## Transport through Several Quantum Dots

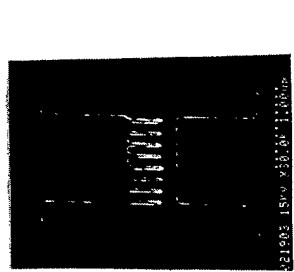
- Gate level



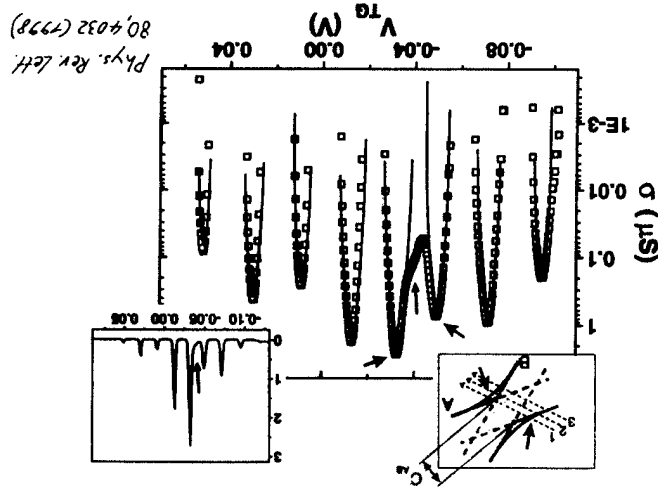
### One-Dimensional Superlattice

with a period of 150nm

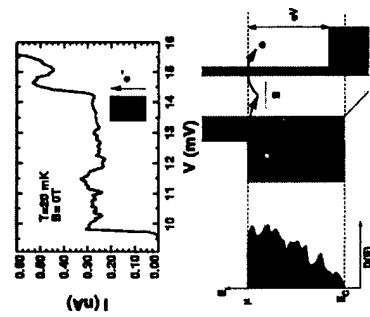
- Gate level



IBM



## Quantum Dot as Spectrometer



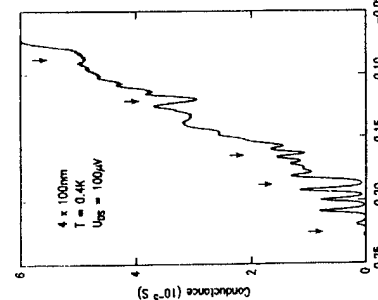
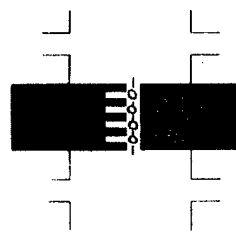
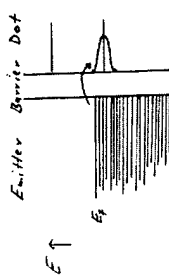
Spectrometer discrete and localized in space  
(10nm)  
local density of states fluctuations

R. J. Haug  
et al.  
Proc. of 20th ICDS,  
Takaike, Soc. Chem.,  
Suppl. 5, 111  
(1992)  
Electron Microscop.

R. J. Haug  
et al.  
Proc. of 20th ICDS,  
Takaike, Soc. Chem.,  
Suppl. 5, 111  
(1992)  
Electron Microscop.

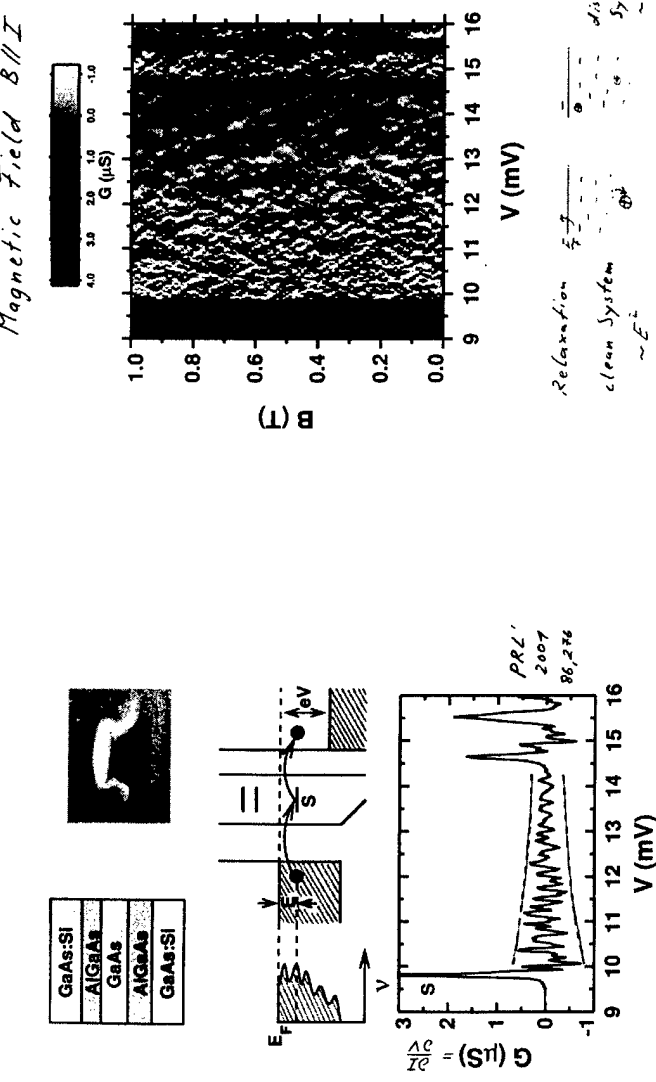
Influence of Contacts  
3d 0d 3d Tunneling  
• Density-of-States

- Interaction Effects

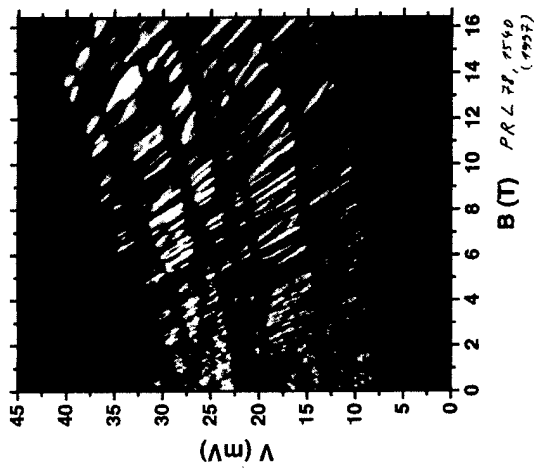
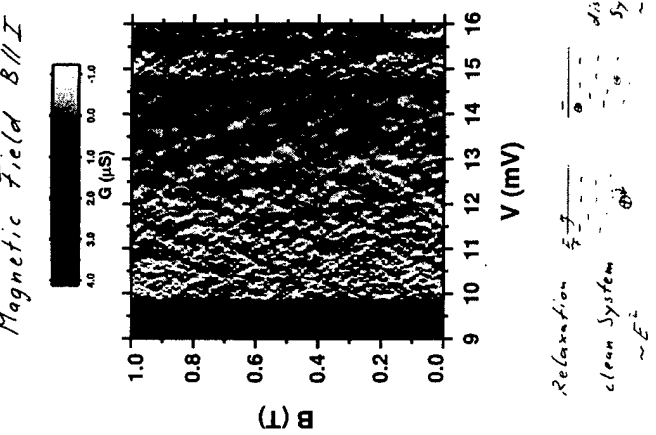
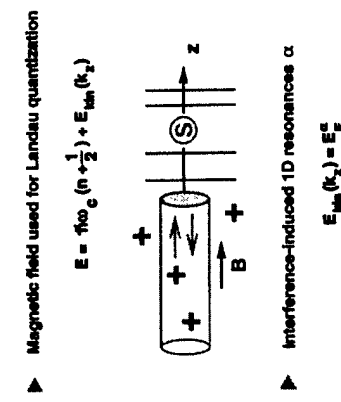


Theory: S. Das Sarma and B. I. Shalom  
Phys. Rev. Lett. 72, 2576 (1994)

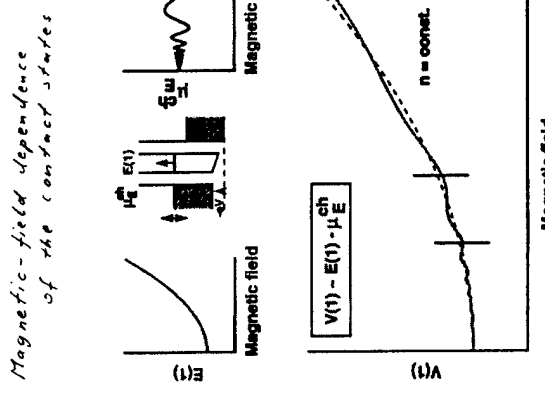
### Diff. Conductance



### Quantum Interference in high magnetic fields

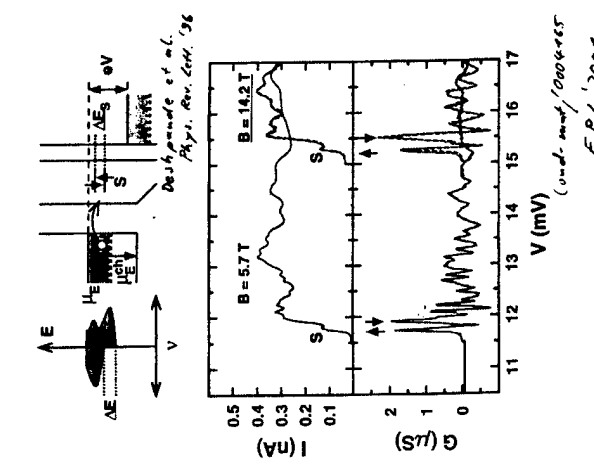


▲  $\omega_c \gg 1$ , Landau band formation relevant

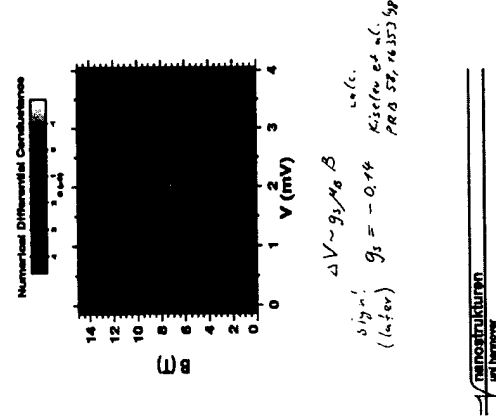


## Two Spin-Levels in the Dot

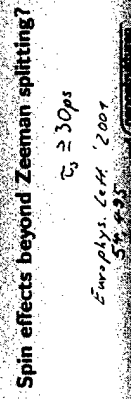
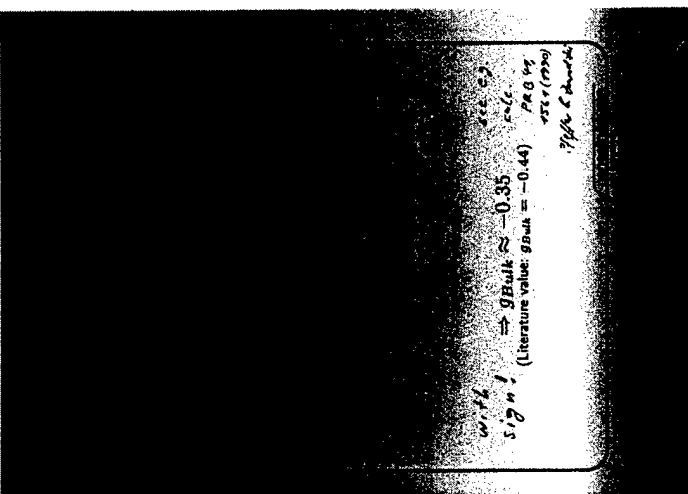
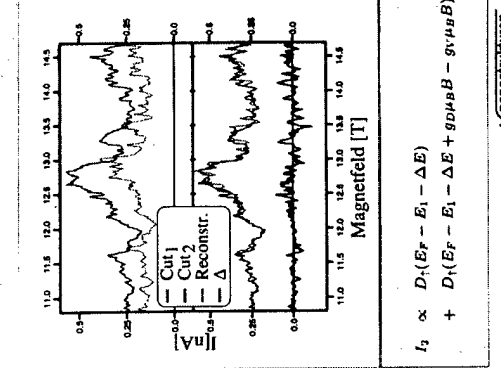
Calculations of  $I$  and  $G$  for  $\uparrow$  and  $\downarrow$  in a magnetic field



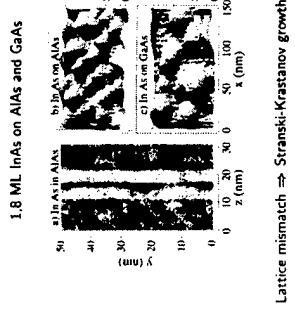
## Zeeman Splitting



## The Reconstructed Current

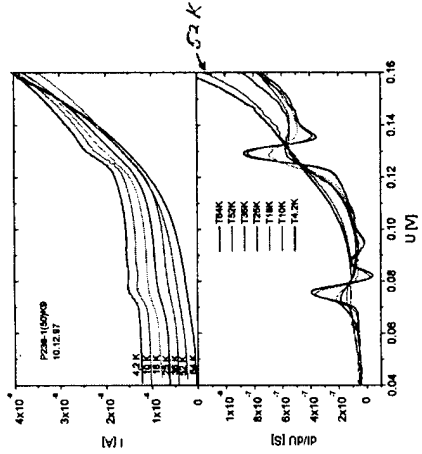
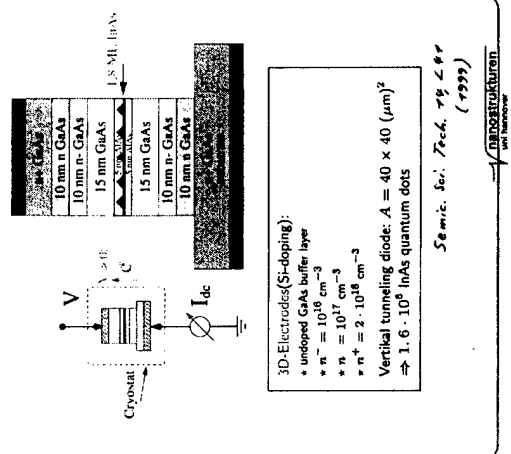


## InAs Quantum dots



InAs on	height (nm)	$\theta$ (nm)	density ( $\mu\text{m}^{-2}$ )
GaAs	4	30	250
AlAs	4	15	1000

## Sample structure

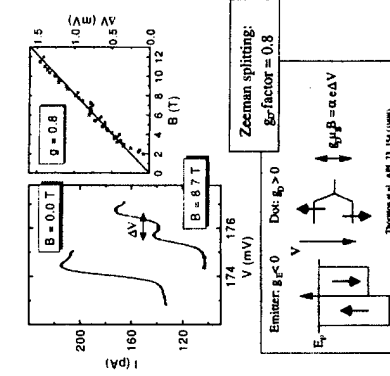


$\ln \beta_3 \text{ dots } \phi = \tau_{\text{eff}} \omega$   
 $(\text{from edge specific drift})$

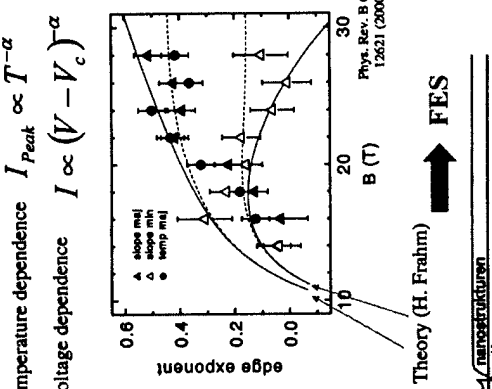
$(\text{single dots!})$

## Small magnetic fields $B \parallel I$

Positive bias



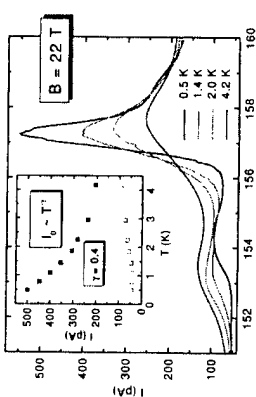
## Temperature dependence



## Exponents

Temperature dependence  $I_{\text{Peak}} \propto T^{-\alpha}$

Voltage dependence  $I \propto (V - V_c)^{-\alpha}$



Peak form  $I \sim (V - V_c)^{\alpha} \Theta(V - V_c)$   
 $(\tau = 0)$

—> nanostrukturen und nanowiren

## Peaks:

Fermi-Edge Singularity

(Mahan 1987)

Interaction of Charge on Dot  
with States in the Emitter

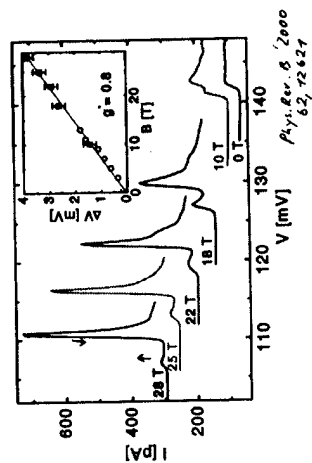


FES in Tunneling:  
see Geim et al. Phys. Rev. Lett. 72, 2061  
Cobden et al. Phys. Rev. Lett. 75, 4274

= nanostrukturen

## InAs quantum dots

High magnetic fields  
 $B \parallel I$



= nanostrukturen

## Theory:

lowest Landau level  $n=0$   
wave function  $\psi = \psi_0(r, \theta) \sin k_z z$   
as  $m \rightarrow \infty$ ,  $m=0$   
 $\psi_0(r, \theta) \propto \exp(-i\mu r^2/\epsilon_0 \hbar^2)$   
 $\epsilon_0 = 1/e^2$

main effect:  
FES from tunneling from  
lowest n-state  
( $L_d =$  dot diameter)

I. Hapke-Wurst  
U.F. Keyser  
J. Könenmann  
P. König  
H.W. Schumacher  
U. Zeitler  
T. Schmidt

## Conclusions

- Transport through Quantum Dot Arrays
- Single and Coupled Quantum Dots
- Lateral and Vertical Devices
- Spectroscopy
- Local Density of States of Emitter Relaxation
- Spin
- InAs-Quantum Dots
- Interaction Effects (FES)

= nanostrukturen

A. G. M. Jansen  
K. Pierz  
A. Förster, H. Lüth  
K. Eberl

= nanostrukturen

## Modeling Ballistic Current Flow in Carbon Nanotube Wires

M. P. Anantram

Nanoelectronics & Device Modeling Group

NASA Ames Research Center

Moffett Field, CA  
U. S. A.

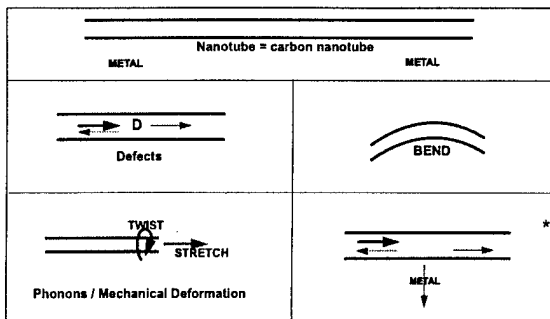
### Acknowledgements:

T. R. Govindan  
Jie Han  
Supriyo Datta  
Liu Yang  
Natalio Mingo

### Outline:

- \* Role of Defects
- \* Bragg reflection
- \* Metal-nanotube coupling
- wave vector conservation
- Armchair versus Zigzag

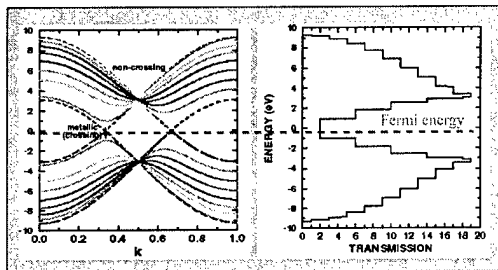
## Topics Studied



\* Bragg reflec.: Intrinsic mechanism, which exists even in an ideal situation

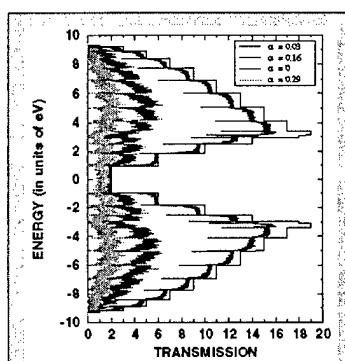
\* = This Talk

### Transmission vs Energy of a (10,10) Nanotube



- Close to  $E=0$ , Resistance =  $6 \text{ k}\Omega$ ; At higher energies, less than  $300 \text{ }\Omega$
- Experimentally:
  - Max. small bias conductance  $\sim 12.5 \text{ k}\Omega$
  - Max. large bias conductance  $\sim 4 \text{ k}\Omega$

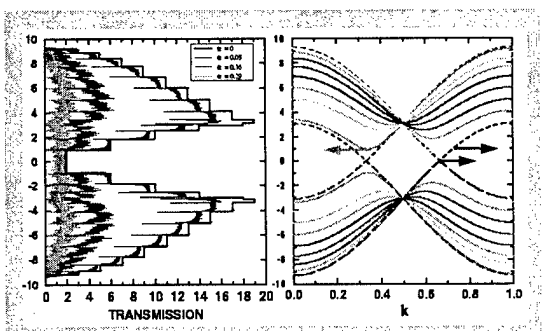
### Transmission versus Energy with Defects



#### Transmission Probability:

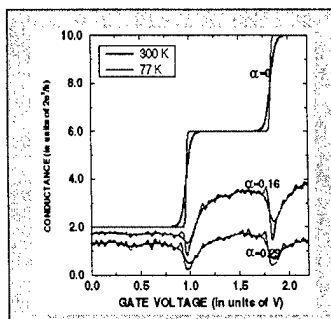
- Decreases with disorder
- Large Dips at some energies
- Very small decrease around  $E=0$  (WIRES?)
- Localization length

### Physical explanation of the transmission dips



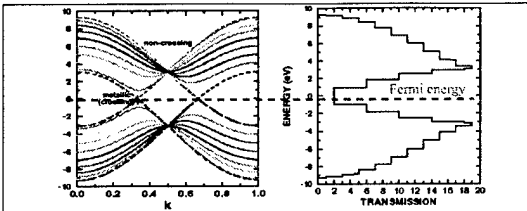
- $E=0$ , Crossing bands: Large velocity ( $dE/dk$ )
- Large velocity states ( $\rightarrow$ ) at higher energies are prone to REFLECTION as they couple to low velocity states ( $\leftarrow$  and  $\leftarrow$ )

### Conductance vs. Gate Voltage



- DIPS IN THE CONDUCTANCE WHEN THE FERMI ENERGY IS CLOSE TO THE SUB-BAND OPENINGS
- FERMI ENERGY AT THE BAND CENTER: GOOD WIRE

### Current-carrying capacity of carbon nanotubes

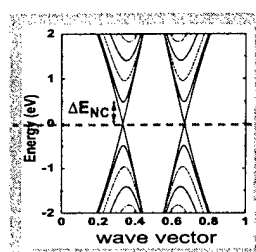


- Close to  $E=0$ , only two sub-bands, Conductance =  $\frac{4e^2}{h}$  ( $6\text{ k}\Omega$ )
- At higher energies, Conductance =  $\frac{(20-30)e^2}{h}$  ( $< 1\text{ k}\Omega$ )

An important question is if subbands at higher energies be accessed to drive large currents through these molecular wires?

Experiments by various groups have shown that the differential resistance of a nanotube decreases by small amounts with increase in applied voltage, i.e., the current carrying capacity does not increase better than an ordinary resistor with applied bias.

### At what applied voltage are electrons injected into higher subbands?



Bias at which electrons are injected into non crossing subbands is  $\Delta E_{NC}$

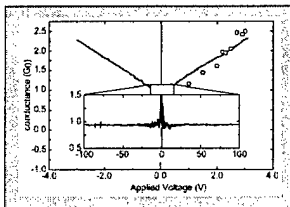
7 Å                            56 Å

size	(5,5)	(10,10)	(20,20)	(40,40)
$\Delta E_{NC}$ (eV)	1.9	0.98	0.5	0.25

For example, in a (20,20) nanotube electrons are injected into over 20 subbands at an energy of 2.5 eV.

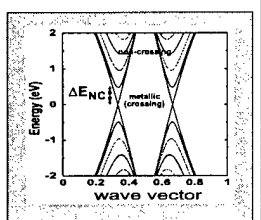
The maximum conductance if the Fermi energy is at 2.5 eV is  $\approx 40\text{ e}^2/\text{h}$

One exception is the experiment by Frank et. al in Science 280 (1998) which showed a modest decrease in differential resistance with bias.



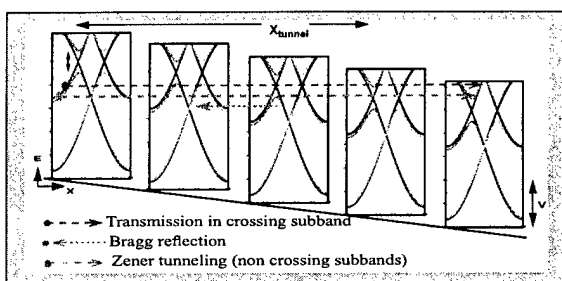
Main experimental features are:

- $V_{APPLIED} < 200\text{ mV}$ , conductance =  $G_0$
- $V_{APPLIED} > 200\text{ mV}$ , conductance increases modestly to about  $1.75\text{ G}_0$



- For large diameter nanotubes such as used in the experiments, the non-crossing subbands open at about 100 meV.
- Further there are about 80 subbands at an energy of about 2 eV.
- Yet the conductance is only  $\sim 1.75\text{ G}_0$

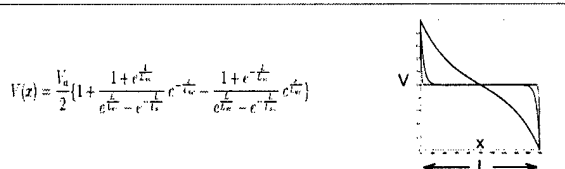
### Semiclassical picture is useful



- The strength of the two processes are determined by:
  - Tunneling distance ( $X_{tunnel}$ )  $\rightarrow$  Screening length
  - Barrier height,  $2\Delta E_{NC}$
  - Scattering and Defects
- $\Delta E_{NC} \propto 1/\text{Diameter}$ . So, the importance of Zener tunneling increases with increase in nanotube diameter.

### Model

- pi-orbital based tight binding calculation [Phys. Rev. B 58, 4882 (1998)]
- Ideal contacts - reflection less contacts
- Electrostatic potential drop
  - Linear
  - Exponential (Screening length,  $L_{sc}$ )



- $L=2400\text{ \AA}$ ,  $L_{sc}=6, 50, 500\text{ \AA}$

- e-e and e-p scattering are not included

$L=10\text{ \AA}$

- $dI/dV = 4\text{ e}^2/\text{h}$  for  $V_a < 2\Delta E_{NC}$
- Threshold changes with diameter
- Barrier height ( $\Delta E_{NC}$ ) decreases with increase in diameter
- Total Current increases with increase in diameter
- $dI/dV > 0$  for  $V_a > 3.1\text{ V}$ , except for the (5,5) nanotube
- (5,5) nanotube  $\Delta E_{NC} \approx 1.9\text{ eV}$

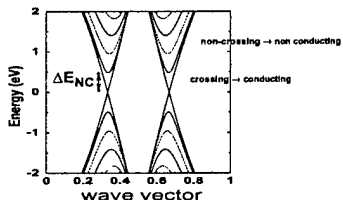
The differential conductance is NOT comparable to the increase in the number of subbands.

For a (20,20) nanotube, there are 35 subbands at  $E = \pm 3.5\text{ V}$ .

Bragg reflection severely limits the current carrying capacity

The crossing metallic-type bands conduct current.

The non crossing semiconductor type bands do not conduct current



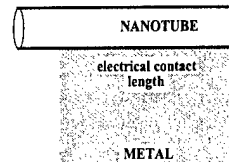
Large diameter nanotubes: non-crossing bands will partially conduct due to Zener-type tunneling.

### Coupling of carbon nanotubes to metallic contacts

The electronic properties of nanotubes are closely related to chirality. The metallic versus semiconducting nature of nanotubes and the bandgap change with deformation depend on chirality.

Questions:

- Is there a preferable nanotube chirality to maximize current flow?
- Role of wave vector conservation?
- Explain experimentally observed scaling of conductance with contact length

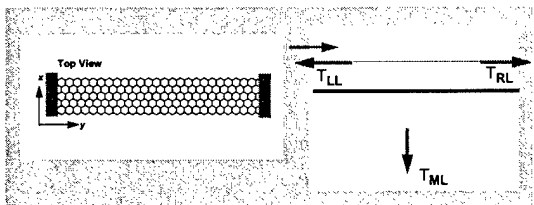


Parameters that influence current flow:

- Strength of coupling to metal
- Length of metal-nanotube contact
- Defects
- Metal Fermi wave vector

### How do we model the system?

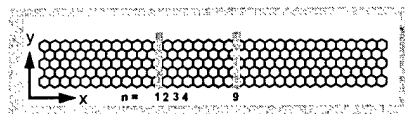
- Same code as in our MOSFET work
- $\pi$  electron tight binding model
- Metal is modeled as a free electron gas ( $k_F$ )



- $T_{RL} + T_{ML} + T_{LL} = 2$ .
- Phys. Rev. B, v.58, p. 4882 (1998) and v. 61, p. 14219 (2000)
- Compute self energy due to: (i) metal & (ii) semi-infinite CNT leads

Calculation of the total transmission from nanotube to metal,  $T_{ML}$  are presented for armchair and zigzag nanotubes:

### Scattering rate



$$\text{The wave function of a nanotube is } \Psi = e^{ink_x L} \phi$$

$n$  is an integer and  $\phi$  is wave func. of atoms in a 1D unit cell

The scattering rate from metal to nanotube (Born approx.) is,

$$1/\tau \propto |\langle \Psi_{nt} | V_{m-nt} | \Phi_m \rangle|^2$$

$$\delta(k_x - k_x^m) \quad |\langle \phi | V_{m-nt} | \Phi_m \rangle|^2$$

This implies that

- $k_x$  is conserved
- $k_y$  conservation is relaxed due to finite width of contact area

As a result of the difference in  $k_y$  corresponding to  $E=0$  (Fermi energy), important differences should arise as a function of chirality.

### ARMCHAIR

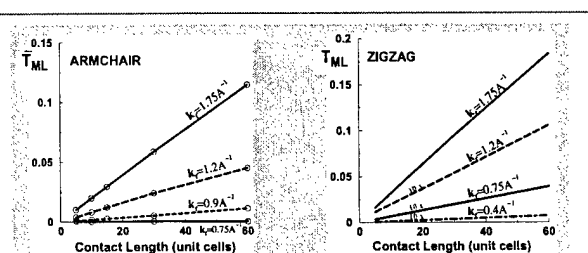
$E=0$  at  $k_y = 2\pi/3a_0 = 0.85 \text{ \AA}^{-1}$

Metal with  $k_{Fermi} < 0.85 \text{ \AA}^{-1}$  couples weakly

### ZIGZAG

$E=0$  at  $k_y = 0$

No threshold for  $k_{Fermi}$

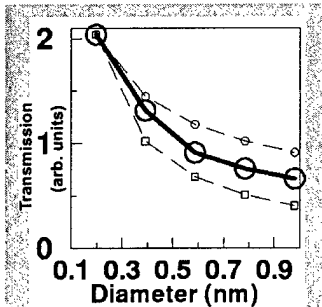


- Note that threshold value is the value of  $k_f$  below which the transmission does not scale with contact length

The main differences between the armchair and zigzag case are:

- Threshold value of  $k_f$  is  $\frac{2\pi}{3a_0} = 0.85 \text{ \AA}^{-1}$  for armchair nanotubes (see  $k_f = 0.75 \text{ \AA}^{-1}$ ) and is 0 for zigzag nanotubes (see  $k_f = 0.4 \text{ \AA}^{-1}$ ).
- Beyond the threshold  $k_f$ , transmission increases with contact length as seen in experiment by Tans et al., Nature, vol. 386, 474 (1997)
- For zigzag tubes,  $T_{LM}$  is small for  $k_f \leq 1.2 \text{ \AA}^{-1}$  as a result of the large angular momentum in the circumferential direction.

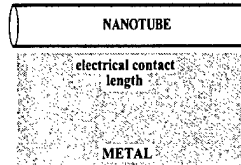
### Diameter dependence of Transmission



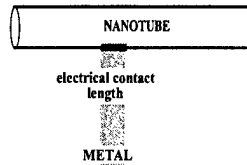
Transmission decreases as the diameter increases because the nanotube tends to a graphite sheet.

The previous values of T are small compared to the maximum possible value of 2. Two possible scenarios to increase T are:

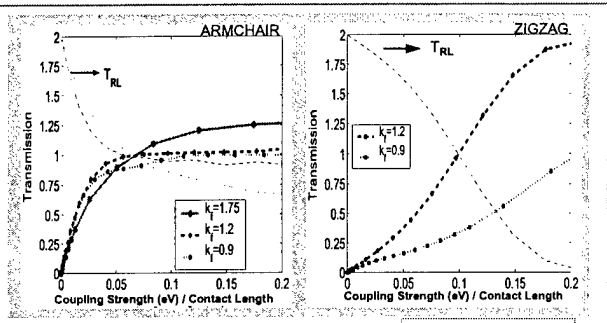
- \* Large contact length - Small coupling



- \* Small contact length - Large coupling



- For nanoelectronics, the second option (right) is better.
- We model a contact length of 30 unit cells (72 Å for armchair and 125 Å for zigzag nanotubes), and vary the coupling strength. The main results of the calculation are rather surprising and are presented below:



- Armchair: Transmission is pinned at values close to unity for metal  $k_F$  of 0.9 and  $1.2 \text{ \AA}^{-1}$
- Zigzag: Transmission increases to two (maximum possible value)
- At small coupling strengths, transmission increases more rapidly in the armchair case

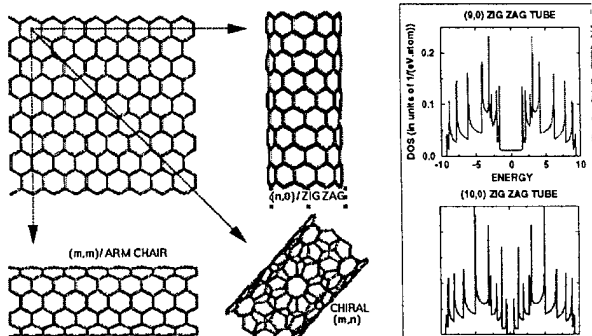
Metallic-zigzag are preferable from metal-nanotube coupling viewpoint

### Conclusions

- $dI/dV$  versus V does not increase in a manner commensurate with the increase in number of subbands.
- The increase in  $dI/dV$  with bias is much smaller than the increase in the number of subbands - a consequence of bragg reflection
- Requirement for axial wave vector conservation:
  - ARMCHAIR cut-off  $k_{\text{Fermi}} = 2\pi/3a_0 = 0.85 \text{ \AA}^{-1}$
  - ZIGZAG cut-off  $k_{\text{Fermi}} = 0$
- Our calculations show an increase in transmission with length of contact, as seen in experiments.
- It is desirable for molecular electronics applications to have a small contact area, yet large coupling. In this case, the circumferential dependence of the nanotube wave function dictates:
  - Transmission in armchair tubes saturates around unity
  - Transmission in zigzag tubes saturates at two

### WHAT ARE CNT?

- STRIP OF A GRAPHENE SHEET ROLLED INTO A TUBE

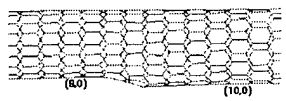


- Varying the diameter and  $(m,n)$ : metal, semiconductor
- $n-m = 3 \cdot \text{integer}$ : metal

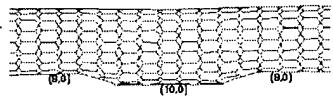
WIRE



METAL-SEMICONDUCTOR  
JUNCTION: RECTIFICATION?

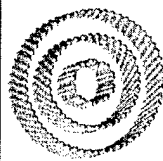


MSM JUNCTION:  
BARRIER?



Observed in nature

Branched Nanotube



# A POSSIBLE LOOPHOLE IN THE THEOREM OF BELL

Karl Hess<sup>1</sup> and Walter Philipp<sup>2</sup>

<sup>1</sup> Beckman Institute, Department of Electrical Engineering and Department of Physics, University of Illinois, Urbana, IL 61801

<sup>2</sup> Beckman Institute, Department of Statistics and Department of Mathematics, University of Illinois, Urbana, IL 61801

## Abstract

The celebrated inequalities of Bell are based on the assumption that local hidden parameters exist. When combined with conflicting experimental results these inequalities appear to prove that local hidden parameters cannot exist. This suggests to many that only instantaneous action at a distance can explain Einstein, Podolsky, Rosen (EPR) type of experiments. The Bell inequalities are based on a simple mathematical model of the EPR- experiments. They have no experimental confirmation since they contradict the results of EPR-experiments. Furthermore, in addition to the assumption that hidden parameters exist, Bell tacitly makes a variety of other assumptions which could contribute to his being able to obtain the desired contradiction. For instance, Bell assumes that the hidden parameters are governed by a single probability measure independent of the analyzer settings. Moreover, we argue that the mathematical model of Bell excludes a large set of local hidden variables and a large variety of probability densities of these local (in the sense of Einstein) variables. These exclusions have neither a physical nor a mathematical basis but are based on Bell's translation of the concept of Einstein locality into the language of probability theory. Our additional set of local hidden variables includes time like correlated parameters and a generalized probability density. We prove that our extended space of local hidden variables does not permit Bell-type proofs to go forward. This opens the possibility to explain EPR-experiments within Einstein's space-time continuum, with a finite velocity of light and without recourse to spooky action at a distance.

## 1 Introduction

Einstein, Podolsky and Rosen (EPR) [1] challenged Bohr [2] and the completeness of quantum mechanics by designing a "Gedanken" experiment that suggested the existence of "hidden parameters" and of a theory that was more complete than quantum mechanics. The

EPR design was later realized in various implementations [3] with experimental results close to the quantum mechanical prediction. These experimental results by themselves do not have any bearing on the EPR claim that quantum mechanics was incomplete, nor on the existence of hidden parameters. However, inequalities derived by Bell [4] that are based on the assumption that local hidden parameters exist, taken together with the experimental results that happen to be inconsistent with the result of the Bell inequalities, do appear to prove that local hidden parameters cannot exist. This has been discussed in great detail in [5] and [6].

The Bell theorem is based on a mathematical model of the EPR- experiments. It has, by itself, no experimental confirmation since its result contradict the results of the EPR-experiments. The standing of the Bell theorem has therefore unique features in the history of modern physics: the mathematical model and the theorem of Bell are taken to be correct and seen by many as valid as the second law of thermodynamics is, while there exists no experimental confirmation. However, instead of discarding altogether a mathematical model that contradicts experiment, the contradiction to the experiment is used to prove that the basic assumption of the theorem, the existence of local hidden parameters is incorrect. The framework of research that has developed around the Bell theorem claims the necessity of "gross non-localities". In simple words, the correlated spins of the EPR-experiment are in some contact over arbitrary space like distances of our space-time continuum and if one spin is measured in one station, the correlated spin in another station is instantaneously influenced. This contradicts the locality conditions of Einstein and Einstein's very argument for the lack of completeness of quantum mechanics. Einstein called the instantaneous interaction of the spatially separated spins "spukhafte Fernwirkungen (spooky action at a distance)". He did not accept the possibility of such spooky action and since quantum mechanics appeared to demand it, it had to be at least incomplete. The Bell theorem and its standard interpretation has turned the logic around. Its supporters now claim that local hidden parameters do not exist and cannot explain the EPR-experiments. Quantum mechanics does agree with experiments and spooky action at a distance must be accepted as a fact of nature. However, it has been shown in a serious of papers of which we cite only two of the more recent [7] [8], that Bell's theorem does contain more than self-evident locality assumptions. These are related to the role of time in the experiments and the admissibility of more general probability measures.

We show in this paper that the assumption of the existence of local hidden variables is not the only assumption in the proof of the Bell inequalities. We show that the mathematical model of Bell excludes a large set of hidden variables and a large variety of probability densities of these variables that all fulfill Einstein's locality conditions perfectly. This exclusion has neither a physical nor a mathematical basis but is based on Bell's mathematical interpretation of what Einstein locality means in terms of probability theory. Our additional set of hidden variables or, as we will call them, parameter random variables includes time like correlated parameters and a generalized probability density which is a sum of what we later define as setting dependent subspace product measures (SDSPM's). We demonstrate that Bell type proofs cannot go forward using our extended space of hidden variables.

The paper is organized as follows. We first review the theorem of Bell. We then analyze

the restrictions that Bell's proof puts on the parameter space and probability measure and show that a much larger space and a more general probability measure can be constructed without violation of Einstein locality conditions. We demonstrate that a variety of proofs of theorems similar to that of Bell cannot be performed in this larger parameter space and with the more general probability measure, and that these theorems and inequalities are therefore not valid in this space. We finally point toward a mathematical model that uses this larger space and permits the construction of a hidden parameter theory that does agree with EPR-experiments.

## 2 The theorem of Bell

We first present a short summary of the work of Bell. In EPR experiments, two particles having their spins in a singlet state are emitted from a source and are sent to spin analyzers (instruments) at two spatially separated stations,  $S_1$  and  $S_2$ . The spin analyzers are described by Bell using unit vectors  $\mathbf{a}$ ,  $\mathbf{b}$ , etc. of three dimensional Euclidean space and functions  $A = \pm 1$  (operating at station  $S_1$ ) and  $B = \pm 1$  (operating at station  $S_2$ ): furthermore A does not depend on the settings  $\mathbf{b}$  of station  $S_2$ , nor B on the settings  $\mathbf{a}$  of station  $S_1$  (Einstein separability or locality). Bell permits particles emitted from the source to carry arbitrary hidden parameters  $\lambda$  of a set  $\Omega$  that fully characterize the spins and are "attached" to the particles with a probability density  $\rho$  (we denote the corresponding probability measure by  $\mu$ ). Neither the parameters  $\lambda$  nor the probability measure  $\mu$  are permitted to depend on the settings at the stations. Einstein separability is again cited as the reason for this restriction. The analyzer settings are changed rapidly in the experiments and do change after emission from the source. Therefore the source parameters and their probability measure must not depend on the settings at the time of measurement. Bell further assumes that the values of the functions A and B are determined by the spin analyzer settings and by the parameters such that:

$$A = A_{\mathbf{a}}(\lambda) = \pm 1 \text{ and } B = B_{\mathbf{b}}(\lambda) = \pm 1 \quad (1)$$

Thus  $A_{\mathbf{a}}(\lambda)$  and  $B_{\mathbf{b}}(\lambda)$  can be considered as stochastic processes on  $\Omega$ , indexed by the unit vectors  $\mathbf{a}$  and  $\mathbf{b}$  respectively. Quantum theory and experiments show that, for a given time of measurement for which the settings are equal in both stations, we have for singlet state spins

$$A_{\mathbf{a}}(\lambda) = -B_{\mathbf{a}}(\lambda) \quad (2)$$

with probability one. Bell further defines the spin pair expectation value  $P(\mathbf{a}, \mathbf{b})$  by

$$P(\mathbf{a}, \mathbf{b}) = \int_{\Omega} A_{\mathbf{a}}(\lambda) B_{\mathbf{b}}(\lambda) \rho(\lambda) d\lambda = - \int_{\Omega} A_{\mathbf{a}}(\lambda) A_{\mathbf{b}}(\lambda) \mu(d\lambda) \quad (3)$$

From Eqs.(1)-(3), Bell derives his celebrated inequality [4]

$$1 + P(\mathbf{b}, \mathbf{c}) \geq |P(\mathbf{a}, \mathbf{b}) - P(\mathbf{a}, \mathbf{c})| \quad (4)$$

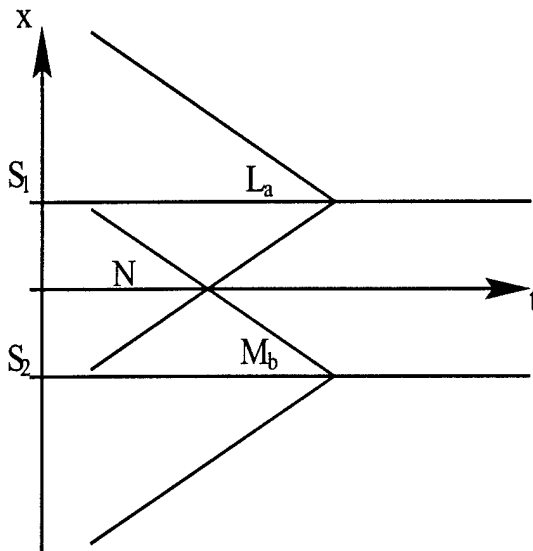


Figure 1: Light cone used by Bell. X denotes the space coordinate and t the time

and observes that this inequality is in contradiction with the result of Quantum Mechanics:

$$P(\mathbf{a}, \mathbf{b}) = -\mathbf{a} \cdot \mathbf{b} \quad (5)$$

Here  $\mathbf{a} \cdot \mathbf{b}$  is the scalar product of  $\mathbf{a}$  and  $\mathbf{b}$ .

The proof of Bell's inequality is based on the obvious fact that for  $x, y, z = \pm 1$  we have

$$|xz - yz| = |x - y| = 1 - xy \quad (6)$$

Substituting  $x = A_b(\lambda)$ ,  $y = A_c(\lambda)$ ,  $z = A_a(\lambda)$  and integrating with respect to the measure  $\mu$  one obtains Eq.(4) in view of Eq.(3). Thus, from the vantage point of mathematics, the Bell inequality is a straight-forward consequence of the set of hypotheses and assumptions that are imposed.

### 3 Extension of Bell's parameter space and probability measure

We are going to argue below that Bell's parameter space is not general enough and excludes without any necessity a manifold of parameters that has at least the cardinality of the continuum. Bell's probability measure is, correspondingly, not as general as the physics of relativity would permit. To show this we start with a discussion of the parameter space and corresponding probabilities out of Bell's book [9].

Bell [9] defines the following parameter sets that are in the backward light cone, as defined by relativity and as illustrated in Fig. 1. He lets  $N$  denote the specification of all entities that are represented by parameters and belong to the overlap of the backward light cones

of both space-like separated stations  $S_1$  and  $S_2$ . In addition he considers sets of parameters  $L_a$  (our notation) that are in the remainder of the backward light cone of  $S_1$  and  $M_b$  for  $S_2$  respectively. Bell (see p56 of ref. [9]) denotes the conditional probability that the function  $A_a$  assumes a certain value with  $A_a = \pm 1$  by  $\{A_a|L_a, N\}$  and similarly for  $B_b = \pm 1$ . Then he claims that in a local causal theory we have:

$$\{A_a|L_a, N, B_b\} = \{A_a|L_a, N\} \text{ and } \{B_b|M_b, N, A_a\} = \{B_b|M_b, N\} \quad (7)$$

Eq.(7) appears entirely plausible as a consequence of the finite speed of light: whatever happens at station  $S_1$  to the result of  $A_a$  cannot be causally connected to the result of  $B_b$  in station  $S_2$  within a local theory. When the switching of the settings is fast enough, the probability that  $A_a$  assumes a certain value must be the same no matter what value  $B_b$  might assume. While this conclusion is undoubtedly correct at a given instance of measurement, Bell's use of Eq.(7) as identical and valid for all times of measurement with a given setting is fatally flawed. The reason is the possible dependence of  $A_a$  and  $B_b$  on time-like correlated parameters that may be setting dependent. The mathematics of Bell-type proofs requires complete statistical independence of  $A_a$  and  $B_b$  for the whole set of measurements and not only at a given time. It also contains the assumption of identical  $L_a$  and  $M_b$  for all measurements of a run. This, however, cannot be guaranteed because physical phenomena other than the setting of the polarizer by the experimenter can occur in the stations and these can be correlated.

Consider, for example, two clocks, one in each station. These clocks may have different settings (e.g. pendulum length and/or starting time etc.). The time that one clock shows is certainly not the causal reason for the time of the other clock. It is the same physical law that is at work in both stations and that causes a correlation in the periodicity of the processes in the clocks or in some general periodic processes for that matter. It is, of course well known that two gyroscopes in the two stations could also be used as clocks as they may indicate the rotation of the earth. As mentioned, there may be also other periodic processes that cause correlations and these correlations may be influenced by the settings **a** and **b**. Although there are clear analogies of gyroscopes and spin properties, we do not wish to push this comparison too far. We do, however, wish to point out the dangers of using of Eq.(7) without proper caution. Bell's argument resulting in Eq.(7) does not include the vital fact that the experiments are made in a time sequence and that the backward light cones change and evolve with time. The situation is illustrated in Fig.2 which shows that for each instant of measurement there is a different light cone. Fig. 2 illustrates our point for measurements at two different times  $t_1$  and  $t_2$ .

The backward light cones contain sets of parameters  $L_{a,t_1}$ ,  $M_{b,t_1}$ ,  $N_{t_1}$  and  $L_{a,t_2}$ ,  $M_{b,t_2}$ ,  $N_{t_2}$  respectively. It is clear, that the set  $L_{a,t_1}$  and the set  $L_{a,t_2}$  may contain setting dependent parameters  $\lambda_a^*$  with different probability densities. It is also clear from the discussion with clocks that the sets  $L_{a,t_1}$ ,  $L_{a,t_2}$ ,  $M_{b,t_1}$ ,  $M_{b,t_2}$  etc. need not be statistically independent. This has several consequences that do not permit Bell-type proofs to go forward. We outline below the most crucial problems.

Bell uses combinations of Eq.(7) for different settings in his proofs as follows (see e.g.

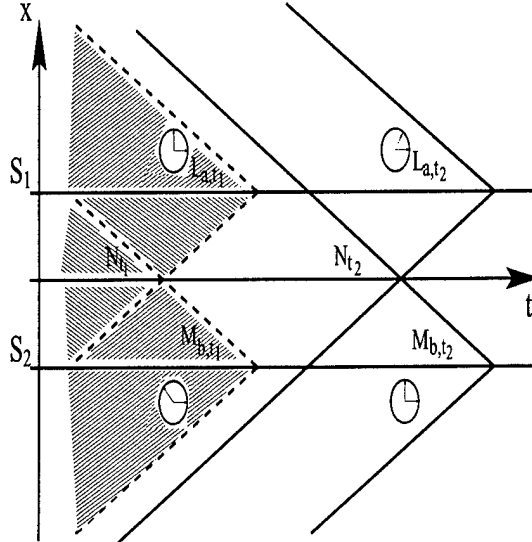


Figure 2: Light cones at randomly chose times  $t_1$  and  $t_2$  of the measurements. The clocks indicate time-like and setting dependent correlations of parameters in stations  $S_1$  and  $S_2$  (in this example, the difference between the times indicated by the clocks in the two stations stays constant).

Bell's Eq.(10) of ref. [9] on page 56):

$$\{A_{\mathbf{a}}|L_{\mathbf{a}}, N, B_{\mathbf{b}}\} = \{A_{\mathbf{a}}|L_{\mathbf{a}}, N, B_{\mathbf{c}}\} = \{A_{\mathbf{a}}|L_{\mathbf{a}}, N\} \quad (8)$$

However, since the measurements with setting  $\mathbf{b}$  and  $\mathbf{c}$  are necessarily taken at different times, this needs to be written in the form:

$$\{A_{\mathbf{a}}|L_{\mathbf{a},t_1}, N_{t_1}, B_{\mathbf{b},t_1}\} = \{A_{\mathbf{a}}|L_{\mathbf{a},t_2}, N_{t_2}, B_{\mathbf{c},t_2}\} \quad (9)$$

which is, in general, clearly incorrect.

The above arguments also demonstrate that Bell's use of a single probability density  $\rho(\lambda)$  that is valid for all times of a run of measurements is in contradiction to physical intuition and facts: the parameter space related to light cones changes and evolves, in general, with time. To describe this physical reality (if this word is permitted), one needs at least to admit a time dependence of  $\rho(\lambda)$  i.e. one needs to replace  $\rho(\lambda)$  by

$$\sum_{t_i} \rho_{t_i}(\lambda) \quad (10)$$

In addition one needs to include, again in general, setting dependent parameters denoted e.g. by  $\lambda_{\mathbf{a}}^*(t)$  in station  $S_1$  and by  $\lambda_{\mathbf{b}}^{**}(t)$  in station  $S_2$  with

$$\lambda_{\mathbf{a}}^*(t) = \lambda_{\mathbf{a}}^{**}(t) \quad (11)$$

if  $\mathbf{b} = \mathbf{a}$  in order to make it possible to fulfill Eq.(2). Bell has included into his later proofs (after publication of reference [10]) setting dependent parameters. However, he and everyone

else assumed that the  $\lambda_a^*$  and  $\lambda_b^{**}$  be statistically independent. He argued this independence from the fact that the parameters are in different stations and he did not consider time-like correlations as described above. Bell assumes that setting dependent parameters in the stations analyzers (called instruments by Bell) must be statistically independent or do not exist. This is explicitly stated in his book ([9] p 38): "...it is necessary that the equality holds in (8) (which is equal to our Eq.(1)), i.e. for this case the possibility of the results depending on hidden variables in the instruments can be excluded from the beginning ..". Of course, in a run with all different settings that still would be true. However,  $P(\mathbf{a}, \mathbf{b})$  is evaluated from measurements with fixed  $\mathbf{a}$  and  $\mathbf{b}$ . Therefore a possible time dependence can cause statistical correlations. To visualize this, assume that the parameters  $\lambda_a^*$  and  $\lambda_b^{**}$  are identified with the hour pointers of two clocks in the two stations. The clock in station  $S_1$  is connected to a plane that is perpendicular to the setting  $\mathbf{a}$  and the clock in station  $S_2$  to a plane perpendicular to  $\mathbf{b}$ . Let the direction of the pointers be idealized by unit vector  $\lambda_a^*$  in station  $S_1$  and  $\lambda_b^{**}$  in  $S_2$  at each instant of measurement. Clearly, these parameters will exhibit time correlations. Note that it is of no concern that the measurements are taken at random times. It is the time correlation in the two stations at any given time that matters.

In addition to the generalization of Bell's probability densities shown in Eq.(10), one needs a further generalization and replace  $\rho(\lambda)$  by

$$\sum_{t_i} \rho_{t_i}(\lambda, \lambda_a^*, \lambda_b^{**}) \quad (12)$$

Of course, to obey Einstein locality,  $\lambda_a^*$  and  $\lambda_b^{**}$  must be station specific and can only be correlated by time like correlations i.e. by some relation to local periodic processes. It is also important to note that the station parameters  $\lambda_a^*$  and  $\lambda_b^{**}$  cannot be emulated by the parameter pair  $\mathbf{a}, \lambda$  or  $\mathbf{b}, \lambda$ , as always implied by Bell by use of his functions  $A$  and  $B$ . The source parameters  $\lambda$  of Bell appear with a given probability density. Since the parameters  $\lambda_a^*$  and  $\lambda_b^{**}$  can have different probability distributions for different  $\mathbf{a}$  and  $\mathbf{b}$ , that are not related in any way to the parameters  $\lambda$ , it becomes clear that the joint density  $\rho_{t_i}(\lambda, \lambda_a^*, \lambda_b^{**})$  can depend, a priori, on the setting vectors  $\mathbf{a}$  and  $\mathbf{b}$ . It is irrelevant that by lucky coincidence, the triples  $(\mathbf{a}, \lambda, \lambda_a^*)$  and  $(\mathbf{b}, \lambda, \lambda_b^{**})$  could perhaps be written as  $\mathbf{a}, \Lambda$  and  $\mathbf{b}, \Lambda$  for some  $\Lambda$  incorporating  $\lambda$  and the station parameters. The probability density that must be considered, in general, for all these parameters is therefore also different from that of Bell and must exhibit a time dependence. This implies the necessity of a more general probability measure that includes time-like correlated parameters.

We have shown [8], that a properly chosen sum of what we call setting dependent subspace product measures (SDSPM) does not violate Einstein-separability and does lead to the quantum result of Eq.(5) while still always fulfilling Eq.(2). By this we mean the following. The probability space  $\Omega$  is partitioned into a finite number  $M$  of subspaces  $\Omega_m$

$$\Omega = \bigcup_{m=1}^M \Omega_m \quad (13)$$

For given  $\mathbf{a}$  and  $\mathbf{b}$ , a setting dependent measure  $(\mu_{ab})_m$  is defined on each subspace  $\Omega_m$ . This measure can be extended to the entire space  $\Omega$  by setting

$$(\mu_{ab})_m(\Omega_j) = 0 \text{ if } j \neq m \quad (14)$$

The final measure  $\mu$  is then defined on the entire space  $\Omega$  by

$$\mu = \sum_{m=1}^M (\mu_{ab})_m \quad (15)$$

and the index  $m$  indicates the time correlations. In the above notation we would have  $m = t_i$ . We have shown in reference [8] that a product measure can be found such that

$$(\mu_{ab})_m = (\mu_a \times \mu_b)_m \quad (16)$$

This is of minor concern for the main argument presented here but does provide flexibility to completely avoid any hint of spooky action within our system of setting dependent subspace product measures (SDSPM's).

It is clear that Bell's proof does not go through with such a probability measure since integrating Eq.(6) to obtain Eq.(4) works only with a single setting independent probability measure. In addition, one can show in a rather intricate proof [8] that the quantum result of Eq.(5) can be obtained with a probability measure as in Eq.(15). In other words hidden parameters are possible if the parameter space is properly extended. We also have shown in [8] that the parameters that are considered that way show no trace of spooky action.

## 4 Conclusions

We have presented a mathematical framework that is more extensive than that of Bell and permits the possibility of describing the spin-pair correlation in EPR-type experiments by use of hidden parameters. A key-element of our approach is contained in the introduction of time-like correlated parameter random variables that also depend on the setting of the station in which they influence the measurements. This leads in a natural way to a setting dependent probability measure composed of subspace product measures (SDSPM's). Use of such SDSPM's does not permit the proof of Bell to go forward (nor any other proofs of similar theorems known to us as given e.g. in references [9] and [11]). We conclude that setting and time dependent parameter random variables present a possible loophole in theorems a la Bell.

## 5 Acknowledgement

The work was supported by the Office of Naval Research N00014-98-1-0604.

## References

- [1] A. Einstein, B. Podolsky, and N. Rosen, Phys. Rev. Vol. 47, 777 (1935).
- [2] N. Bohr, Phys. Rev. Vol. 48, 696 (1935).
- [3] A. Aspect, J. Dalibard and G. Roger, Phys. Rev. Letters Vol. 49, 1804 (1982)

- [4] J. S. Bell, Physics, Vol. 1, 195 (1964).
- [5] N. D. Mermin, Physics Today, Vol. 38, No. 4, 38-47 (1985).
- [6] A. J. Leggett, The Problems of Physics, Oxford University Press (1987).
- [7] Y. Aharonov, A. Botero and M. Scully, Z. Naturforsch. Vol. 56 a, 5-15 (2001).
- [8] Karl Hess and Walter Philipp, quant-ph, see <http://xxx.lanl.gov/abs/quant-ph/0103028>, March 7 (2001).
- [9] J.S. Bell, "Speakable and Unspeakable in Quantum Mechanics", Cambridge University Press, 1993
- [10] L.E. Ballentine and Jon P. Jarrett, Am. J. Phys. Vol. 55, 696 (1987)
- [11] D. M. Greenberger, M. A. Horne, A. Shimony and A. Zeilinger, Am. J. Phys. Vol. 58, 1131 (1990)

# First principles modelling of electron transport in atomic-scale systems

Antti-Pekka Jauho  
MIC, Technical University of Denmark

- 1) Motivation: Atomic/Molecular-scale Electronics
- 2) Modelling: Challenges
- 3) Nonequilibrium Green function formalism
- 4) The *TranSIESTA ab initio* transport program.
- 5) Results for atomic gold wires.
- 6) A toy molecular device.

Collaboration of several groups:

Mads Brandbyge, Kurt Stokbro, Jeremy Taylor, MIC, Denmark



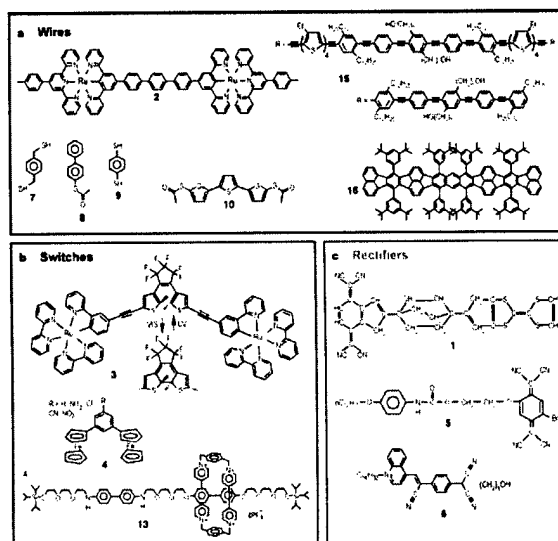
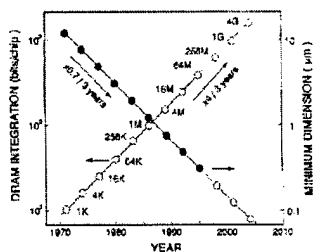
Pablo Ordejon, Jose-Luis Mozos, UAB, Spain

ICMAB

## Molecular-scale Electronics - Why ??

Smallest functional unit: The single molecule (Aviram & Ratner, 1974)

- “Top-down” silicon technology cannot continue to shrink in component size (dissipation, tunneling, cost of fabs...)  
*“End of the road map”*



- “Bottom-up”: The single molecule = Smallest functional unit
- Chemists can synthesize organic molecules with a range of properties
- Use novel quantum effects

J. Reichert<sup>1</sup>, R. Ochs<sup>1</sup>, D. Beckmann<sup>1</sup>, H. B. Weber<sup>1</sup>, M. Mayor<sup>1</sup>, and H. v. Löhneysen<sup>2,3</sup>

<sup>1</sup>Forschungszentrum Karlsruhe, Institut für Nanotechnologie, D-76021 Karlsruhe

<sup>2</sup>Forschungszentrum Karlsruhe, Institut für Festkörperphysik, D-76021 Karlsruhe

<sup>3</sup>Physikalisches Institut, Universität Karlsruhe, D-76128 Karlsruhe

(June 12, 2001)

We investigate electronic transport through two types of conjugated molecules. Mechanically controlled break-junctions are used to couple thiol endgroups of single molecules to two gold electrodes. Current-voltage characteristics (IVs) of the metal-molecule-metal system are observed. These IVs reproduce the spatial symmetry of the molecules with respect to the direction of current flow. We hereby unambiguously detect an intrinsic property of the molecule, and are able to distinguish the influence of both the molecule and the contact to the metal electrodes on the transport properties of the compound system.

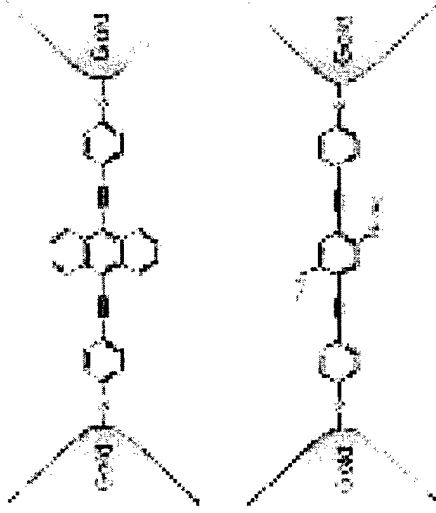


FIG. 1. Scheme of the experimental setup: a spatially symmetric (9,10-Bis((2'-para-mercaptophenyl)-ethynyl)-anthracene) and an asymmetric molecule (1,4-Bis((2'-para-mercaptophenyl)-ethynyl)-2-acetyl-2-amino-5-nitro-phenyl) in between two gold electrodes.

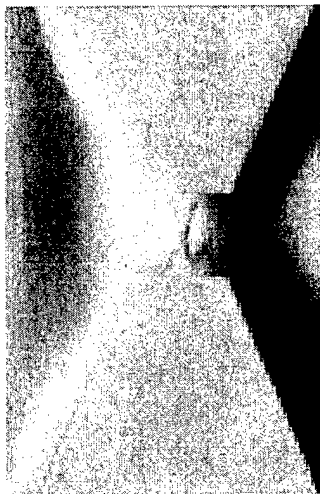


FIG. 2. Scanning electron microscope picture of the lithographically fabricated break junction. The setup consists of a metallic plate, covered by an insulating layer of polyimide. On top of this, a gold film with a small constriction (smallest diameter  $50 \times 50 \text{ nm}^2$ ) is deposited, laterally structured by e-beam lithography. Two electrodes lead outside to connect the bridge electrically. The polyimide is partially etched away so that in the constriction region, the bridge is freely suspended over the polyimide substrate.

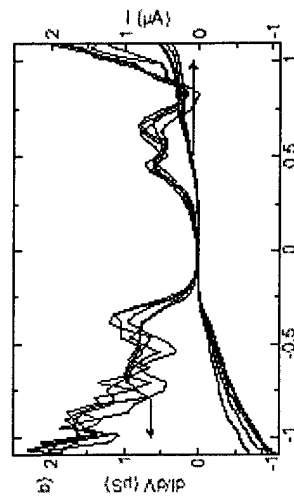
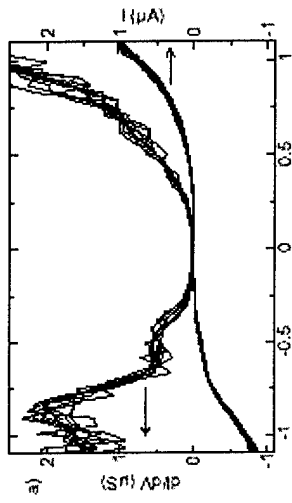
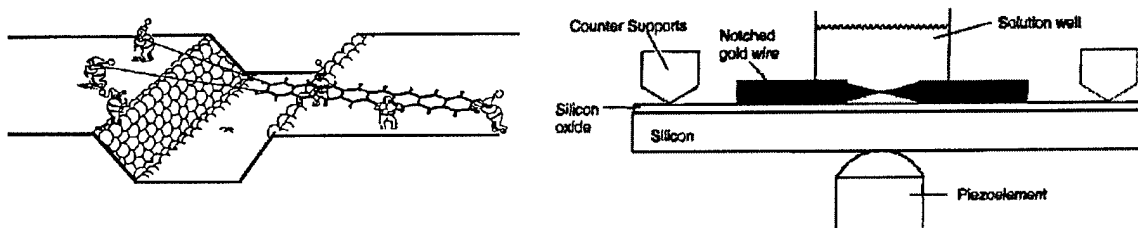


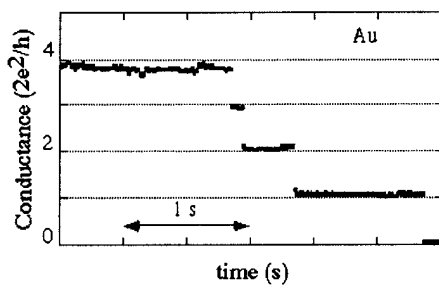
FIG. 3. Transport data of the asymmetric molecule. a) Current-voltage (IV) raw data (dashed lines, nine subsequent voltage sweeps) on a stable junction and the numerically differentiated data  $dI/dV$  (solid lines) from the above IV. b) Data from a subsequent junction.

## Mechanical Break Junction Experiments

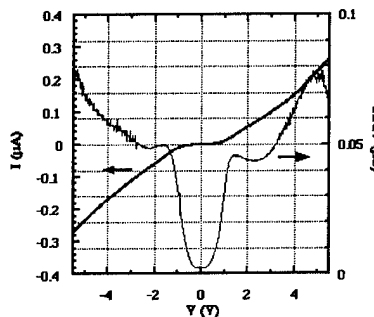


### No Molecules/Solution

Conductance Quantization: Atomic short circuit



### Molecules in solution

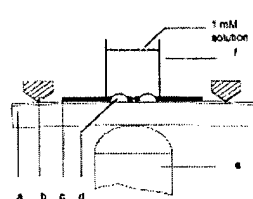


"Conductance of a Molecular Junction," M.A. Reed et al., Science, 278, 252 (1997).

## “Single” Molecule Experiments



**SELF-ASSEMBLY** occurs spontaneously as molecules with a specially “tethered” group tend to attach themselves to a substrate material. Typically the molecules do not end up perpendicular to the substrate.



a Gold Wire

1. Add THF  
2. Add benzene 1,4-dithiol

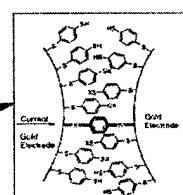
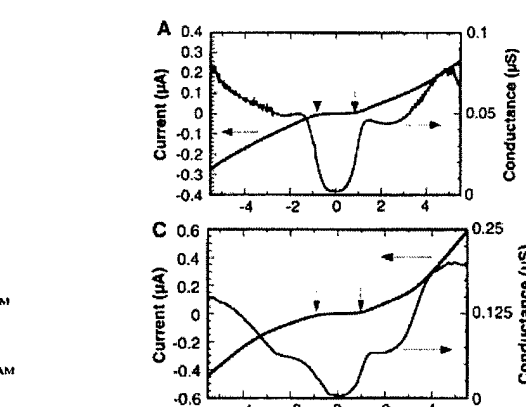
b Gold Wire SAM

Pulling of wire until cleavage results in metal tip formation

c Gold Electrode

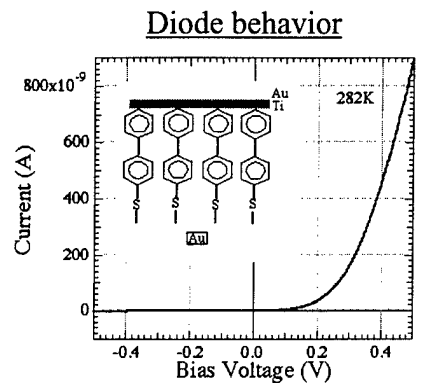
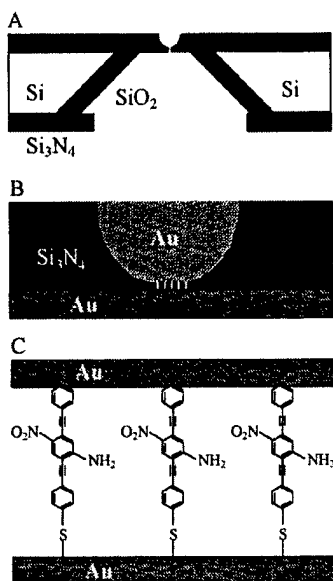
1. Evaporation of volatiles  
2. Slowly moving tips together until conductance onset

d Gold Electrode

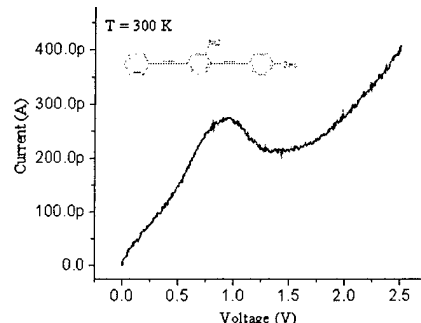


"Conductance of a Molecular Junction,"  
M.A. Reed et al., Science, 278, 252  
(1997).

# Nano-pore

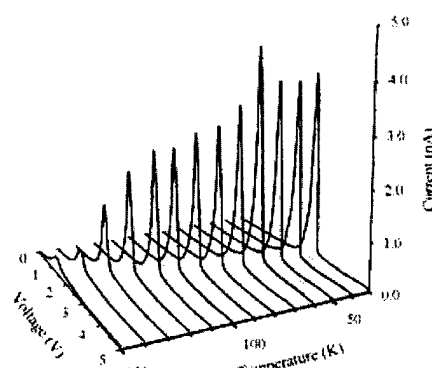
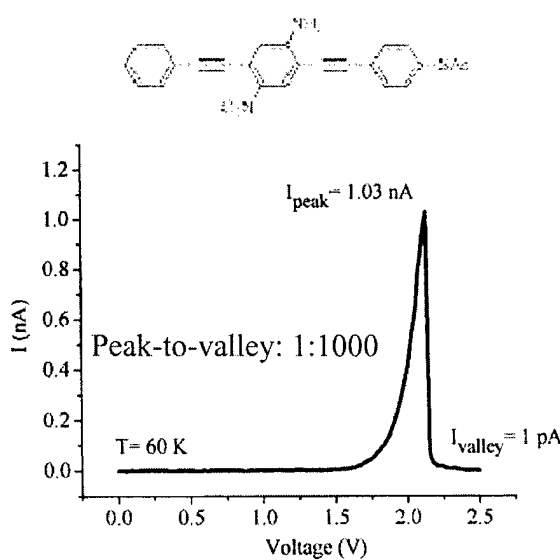


## Negative Differential Resistance



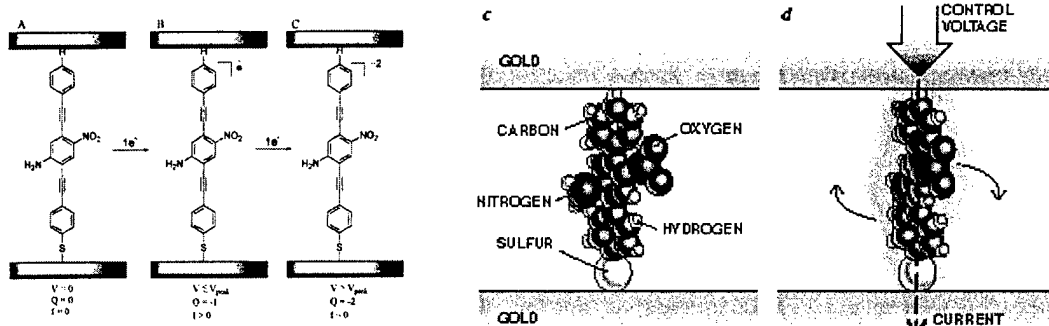
- C. Zhou et al., "Nanoscale Metal/Self-Assembled Monolayer/Metal Heterostructures", Appl. Phys. Lett., 71, 611 (1997)  
 J. Chen et al., "Room-Temperature Negative Differential Resistance in Nanoscale Molecular Junctions", Appl. Phys. Lett., 21, 1224 (2000)

# The Tour wire: “Giant” NDR



NDR has strange temperature dependence

## The Tour wire: Mechanism ???



No explanation yet

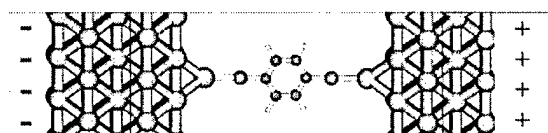
From Mark A. Reed and James M. Tour, Scientific Am. June 2000

Possible factors:

- A) Change in molecular states
- B) Change in geometry
- C) Change in charge states
- D) Interaction of molecular dipole with external field

Only calculations for the *isolated* molecule has been published

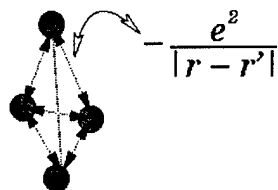
## Modelling atomic-scale conductors: Challenges



- Model a molecule coupled to bulk (infinite) electrodes
- Model the molecule-electrode system from “first principles”: No parameters fitted to the particular system
- Include finite bias voltage/current
- Calculate the conductance (quantum transmission through the molecule)
- Determine geometry: Relax the atomic positions to an energy minimum

# Density Functional Theory

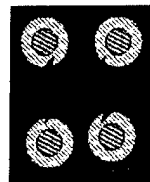
**Challenge:** Many interacting electrons



Interacting electrons + real potential

**Way out: DFT**

If the electron density is correct so is the total energy,  
W. Kohn, Nobel prize 1998.



DFT gives a good description of energy and geometry of isolated molecules and perfect crystals

Non-interacting, fictitious particles + effective potential ( $V_{eff}$ )  
 $V_{eff}[n(r)]$ ,  $n(r)$  is the electron density

**Schrödinger's equation**

$$H\Psi = E\Psi, \quad H = T + V_{eff}$$

instead of solving this we solve for G:

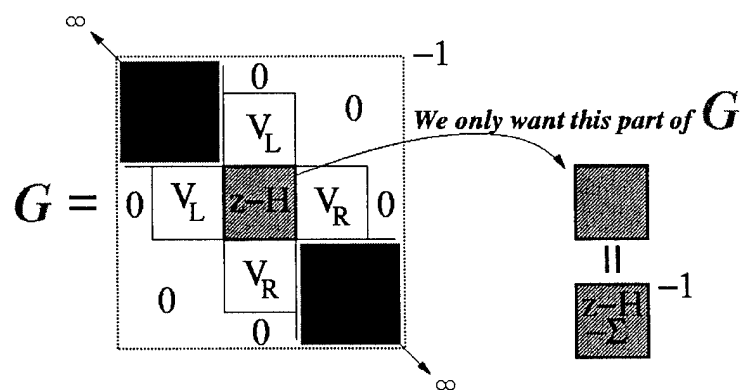
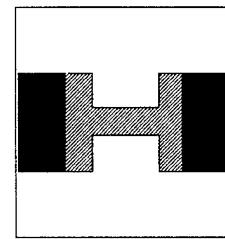
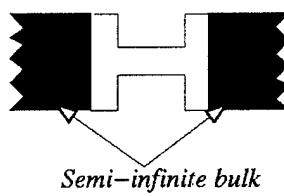
$$G(z) = (z - H)^{-1}$$

We can get the density from G



## Open/infinite System

**Challenge:** Coupling to *infinite* electrodes



The selfenergy:  $\Sigma = \Sigma_L + \Sigma_R$   
(can be calculated from  $1/(z-H^{bulk})$ )



## Summary of important relations from Nonequilibrium Green Function Theory

We consider the Hamiltonian:

$$H = \sum_{k,\alpha} \epsilon_\alpha(t) c_{k,\alpha}^\dagger c_{k,\alpha} + \sum_{k,\alpha;n} \left[ V_{k,\alpha;n}(t) c_{k,\alpha}^\dagger d_n + \text{h.c.} \right] + H_{\text{cen}}[\{d_n\}, \{d_n^\dagger\}, t]$$

Current is calculated as follows (Caroli et al.(70's), Meir and Wingreen (1992), Jauho et al. (1994)):

$$\begin{aligned} J_L(t) &= \langle (-e) \dot{N}_L(t) \rangle \\ &= \frac{2e}{\hbar} \text{Re} \left\{ \sum_{k,\alpha;n} V_{k,\alpha;n}(t) G_{n,k\alpha}^<(t,t) \right\} \\ &= -\frac{2e}{\hbar} \int_{-\infty}^t dt_1 \int d\epsilon \text{ImTr} \left\{ e^{-i\epsilon(t_1-t)} \Gamma^L(\epsilon, t_1, t) \right. \\ &\quad \left. [\mathbf{G}^<(t, t_1) + f_L^0(\epsilon) \mathbf{G}^r(t, t_1)] \right\}. \end{aligned}$$

Here the Green functions are *matrices* in the indices  $(m, n)$ , and the linewidth functions  $\Gamma$  are defined as (here given for time-independent situation)

$$[\Gamma^L(\epsilon_k)]_{mn} = 2\pi \sum_{\alpha \in L} \rho_\alpha(\epsilon_k) V_{\alpha;m}^*(\epsilon_k) V_{\alpha;n}(\epsilon_k)$$



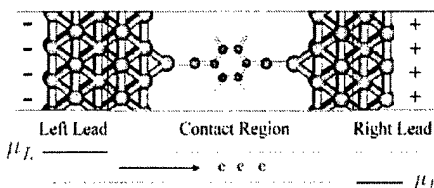
Time-independent case (Meir-Wingreen):

$$\begin{aligned} J &= \frac{ie}{2h} \int d\epsilon \text{Tr} \left\{ [\Gamma^L(\epsilon) - \Gamma^R(\epsilon)] \mathbf{G}^<(\epsilon) \right. \\ &\quad \left. + [f_L^0(\epsilon) \Gamma^L(\epsilon) - f_R^0(\epsilon) \Gamma^R(\epsilon)] [\mathbf{G}^r(\epsilon) - \mathbf{G}^a(\epsilon)] \right\} \\ &= \frac{e}{h} \int d\epsilon [f_L^0(\epsilon) - f_R^0(\epsilon)] \text{Tr} \left\{ \mathbf{G}^a \Gamma^R \mathbf{G}^r \Gamma^L \right\}, \end{aligned}$$

where the second line holds, if the central region can be described in terms of an *effective one-body potential* (such as in density-functional theory).

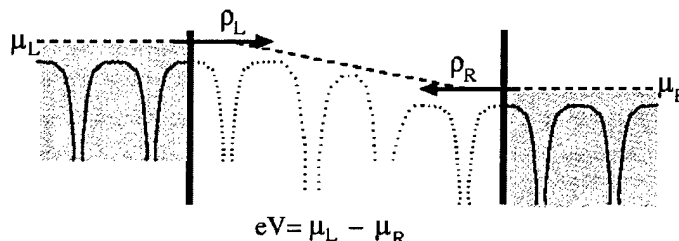
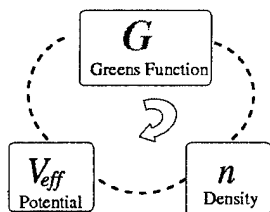
# Finite Voltage Bias/Current

**Challenge:** non-equilibrium electron distribution



## The Non-equilibrium Density Matrix

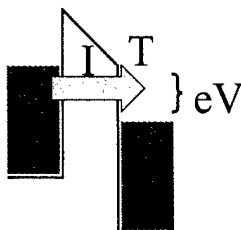
*Selfconsistent solution*



$$\mathbf{D}_{\alpha,\beta} = \int_{-\infty}^{\infty} dE \rho_{\alpha,\beta}^L(E) n_F(E - \mu_L) + \rho_{\alpha,\beta}^R(E) n_F(E - \mu_R)$$

$$\rho_{\alpha,\beta}^L(E) = \frac{1}{\pi} (G(E + i\delta) \text{Im} [\Sigma_L(E + i\delta)] G^\dagger(E + i\delta))_{\alpha,\beta}$$

Conductance = Transmission



## Conductance (Landauer-Büttiker)

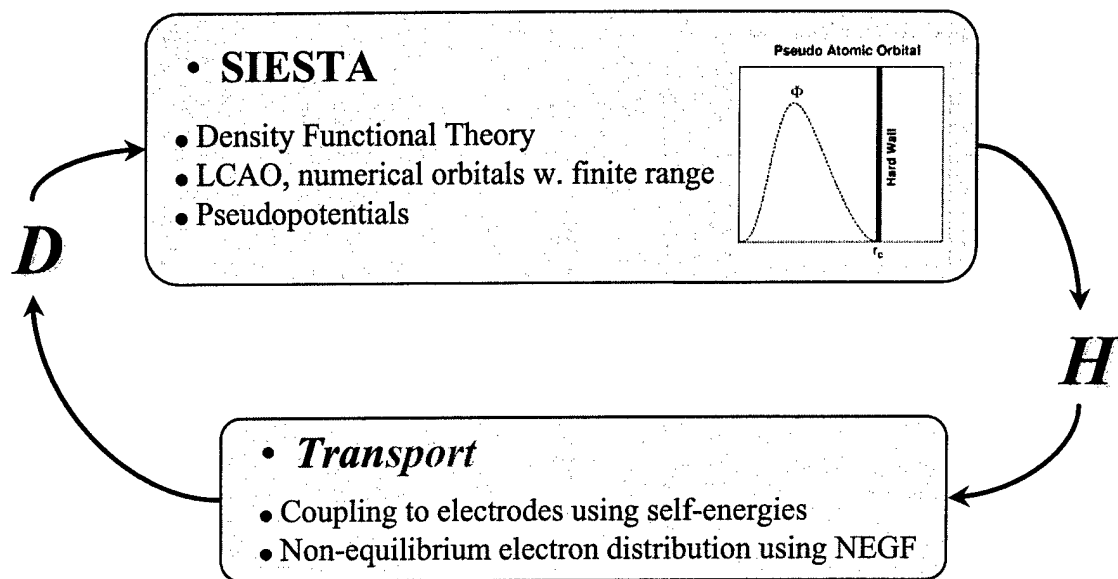
$$I = \frac{2e^2}{h} \int dE (f_R(E) - f_L(E)) T_{\text{tot}}(E)$$

$T_{\text{tot}}(E)$ : Total Quantum Transmission

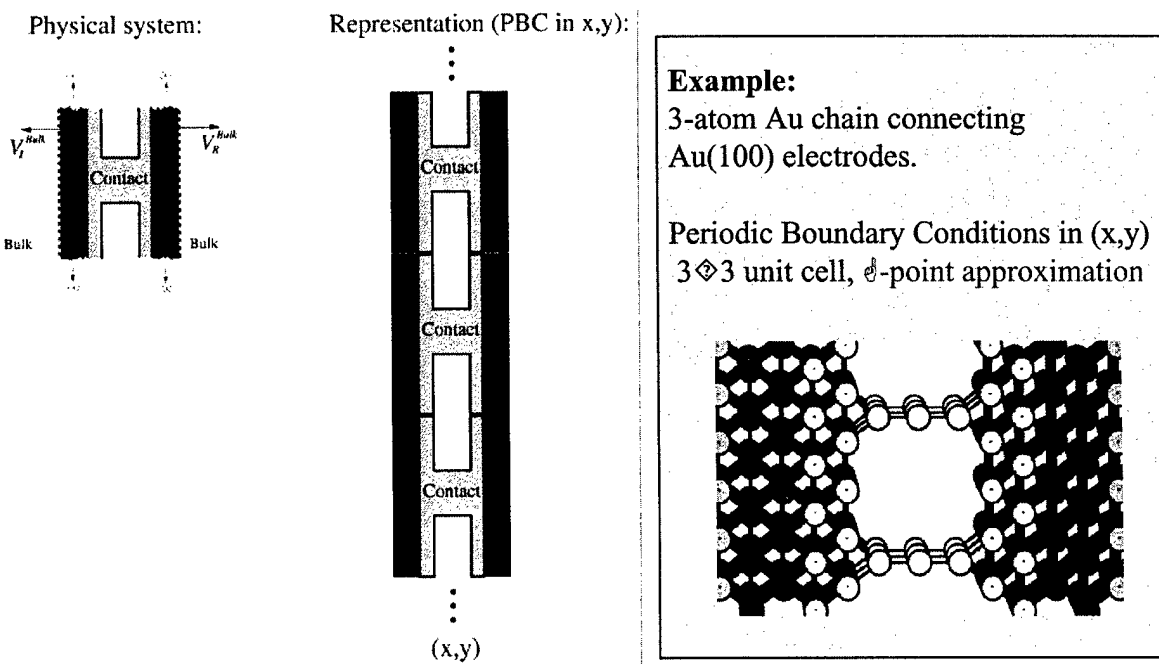
$$T_{\text{tot}}(E) = \text{Tr}[t^\dagger t](E)$$

$$t(E) = (\text{Im} [\Sigma_R](E))^{1/2} G(E) (\text{Im} [\Sigma_L](E))^{1/2}$$

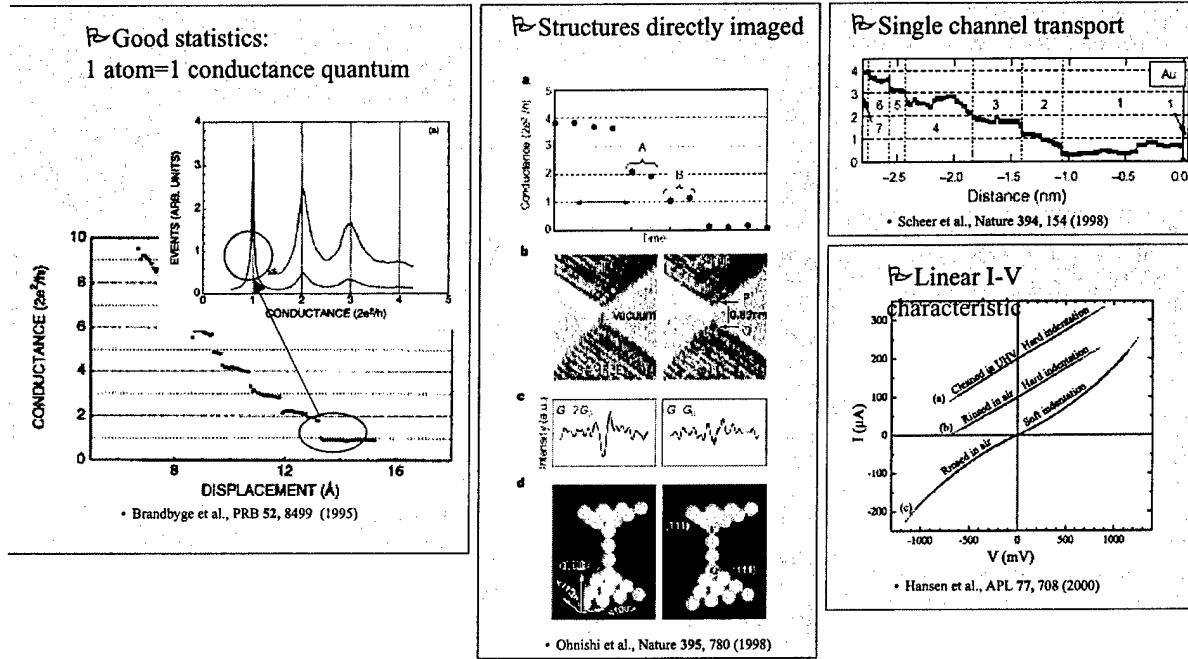
# Implementation: TranSIESTA



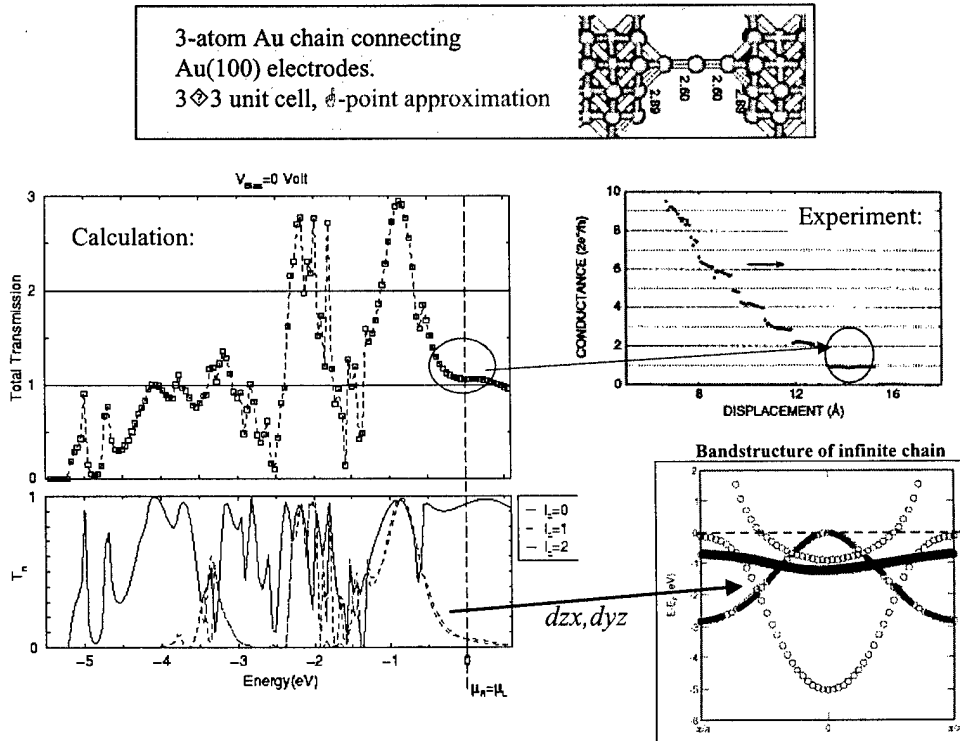
## Setup



# Benchmark atomic-scale conductors: Single-atom gold contacts

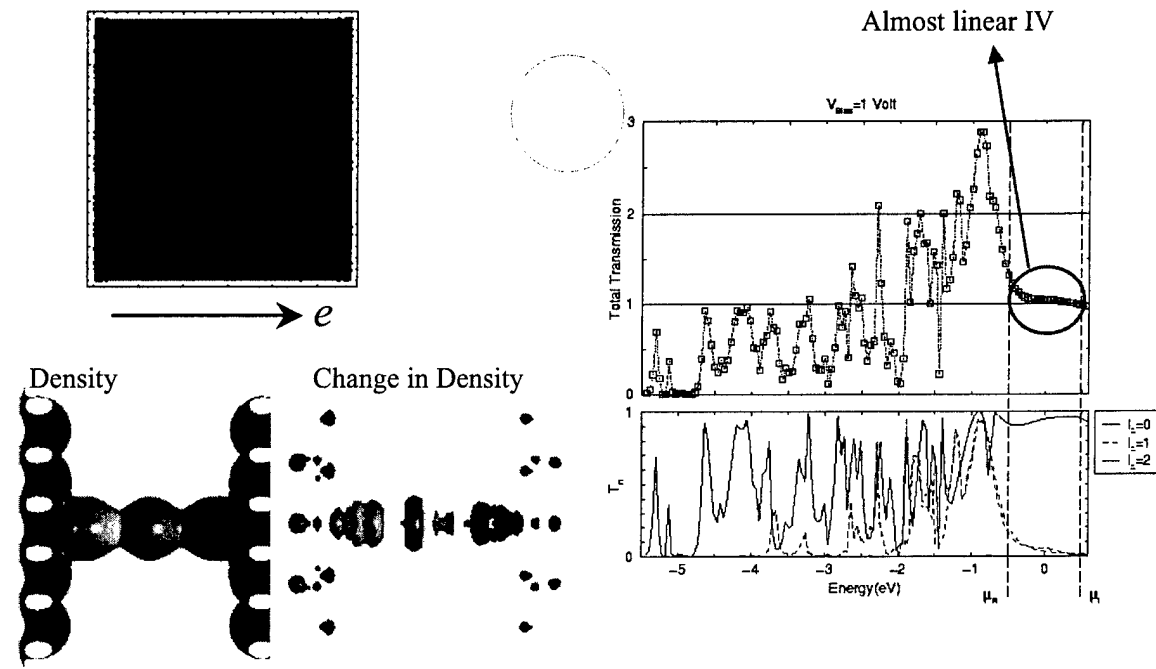


## Atomic short circuit: Single-atom contact



# Single atomic contact: 1 Volt Bias

Voltage drop through the contact



## Zig-zag chains

VOLUME 83, NUMBER 19

PHYSICAL REVIEW LETTERS

8 NOVEMBER 1999

### Stiff Monatomic Gold Wires with a Spinning Zigzag Geometry

Daniel Sanchez-Portal,<sup>1</sup> Emilio Artacho,<sup>2</sup> Javier Junquera,<sup>2</sup> Pablo Ordejón,<sup>1</sup> Alberto García,<sup>4</sup> and José M. Soler<sup>2</sup>

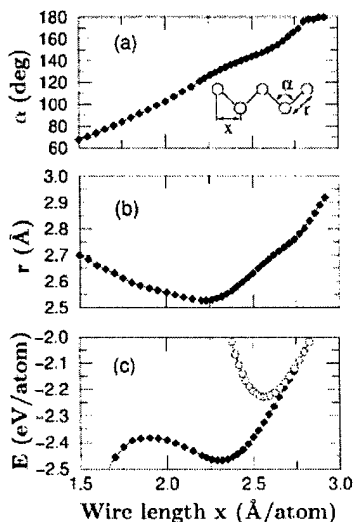


FIG. 1. First-principles, density-functional results for the bond angle  $\alpha$  (a), and bond length  $r$  (b) in a monatomic gold wire with zigzag geometry, as a function of its length per atom. (c) Binding energy  $E$  in the zigzag (solid symbols) and linear wires (open symbols).

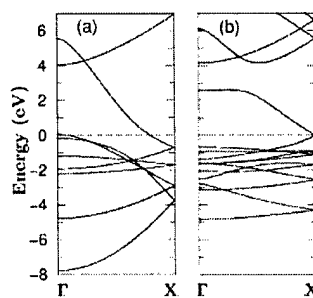
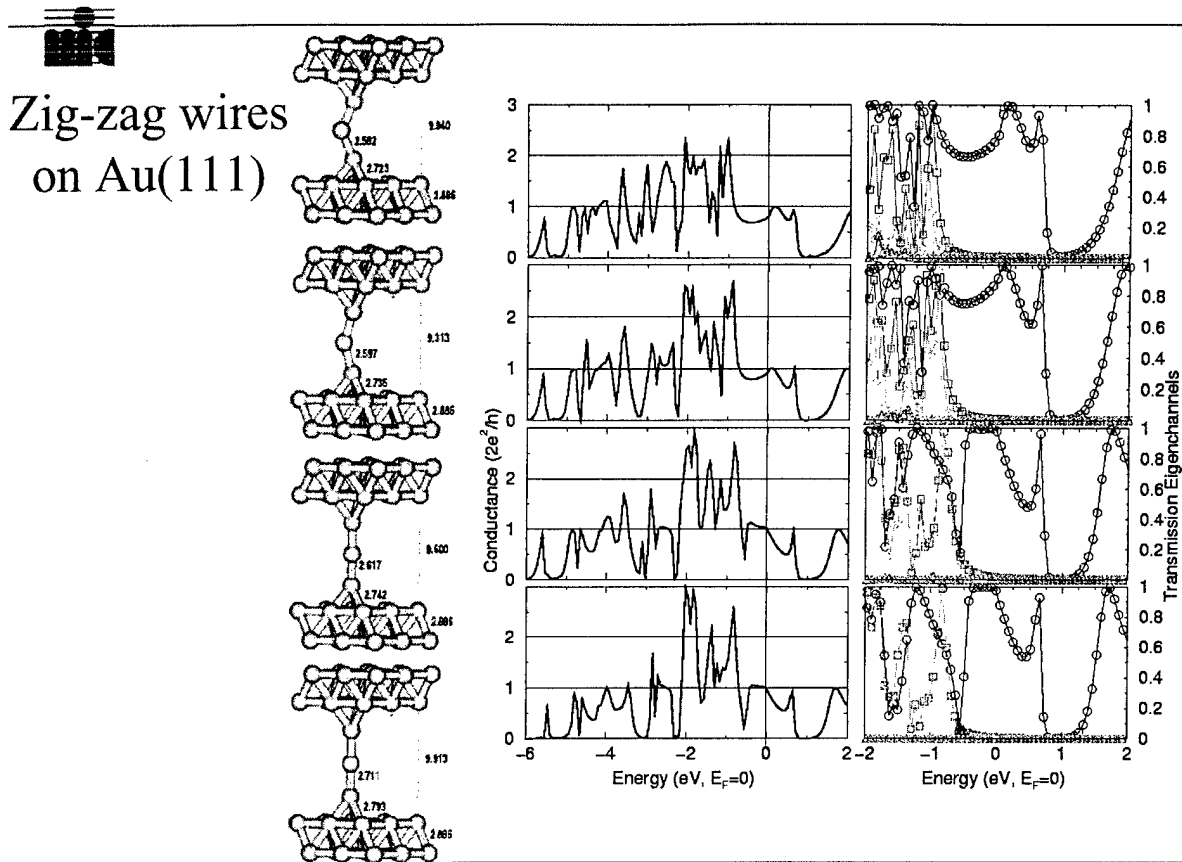
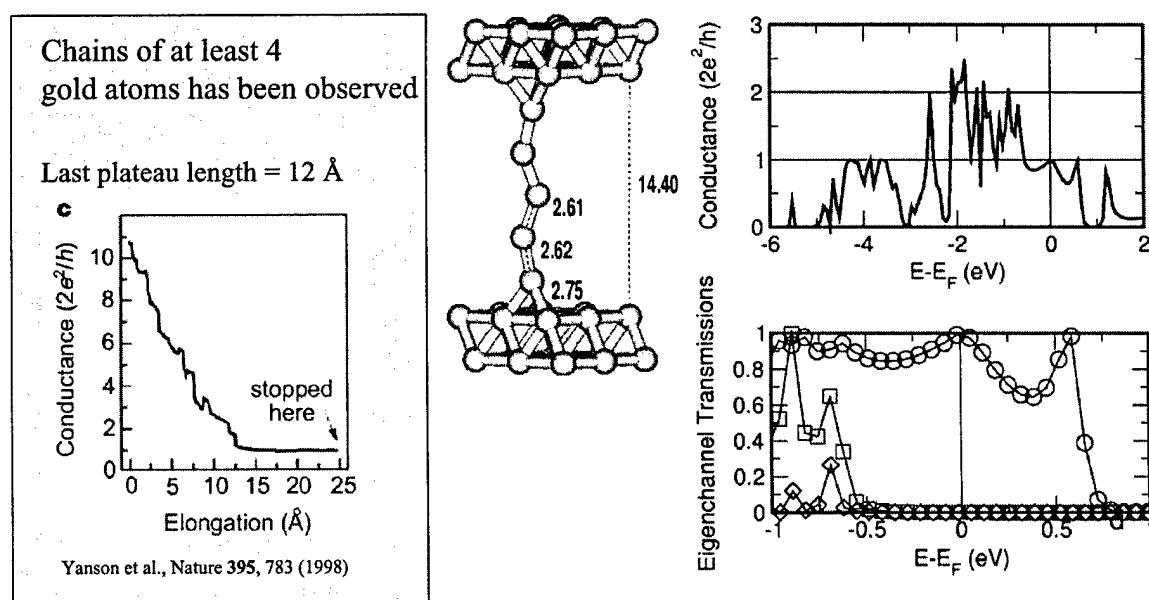


FIG. 2. Electronic band structure of the linear (a) and zigzag (b) wires for a length of 2.32 Å/atom. The linear-wire bands have been folded onto a two-atom Brillouin zone to facilitate the comparison. The energies are relative to the Fermi level.



### 5 atom long gold chain

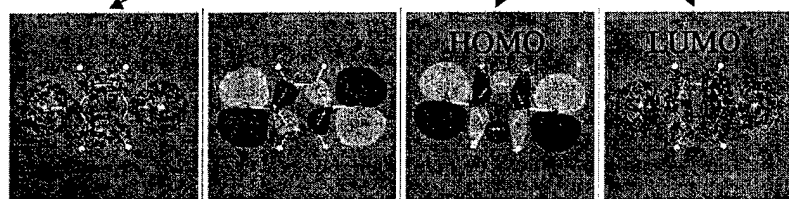
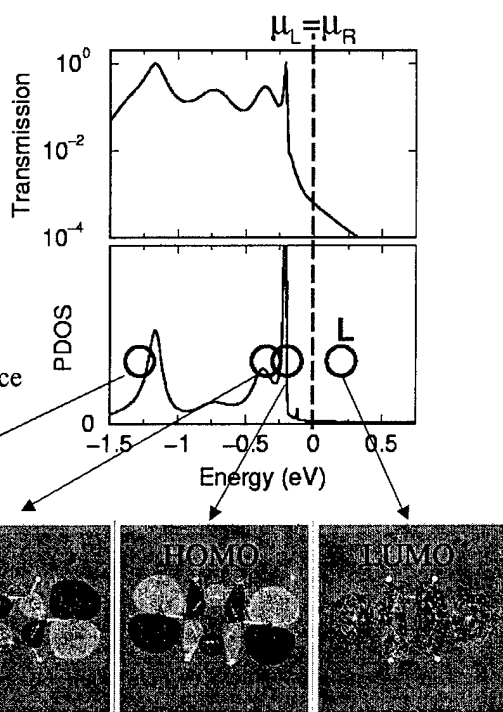


## “Toy model”

Benzene-1,4-dithiolate coupled to gold chains

- The molecular states have a node plane
- The chain band states are rot. symmetric at the Fermi energy

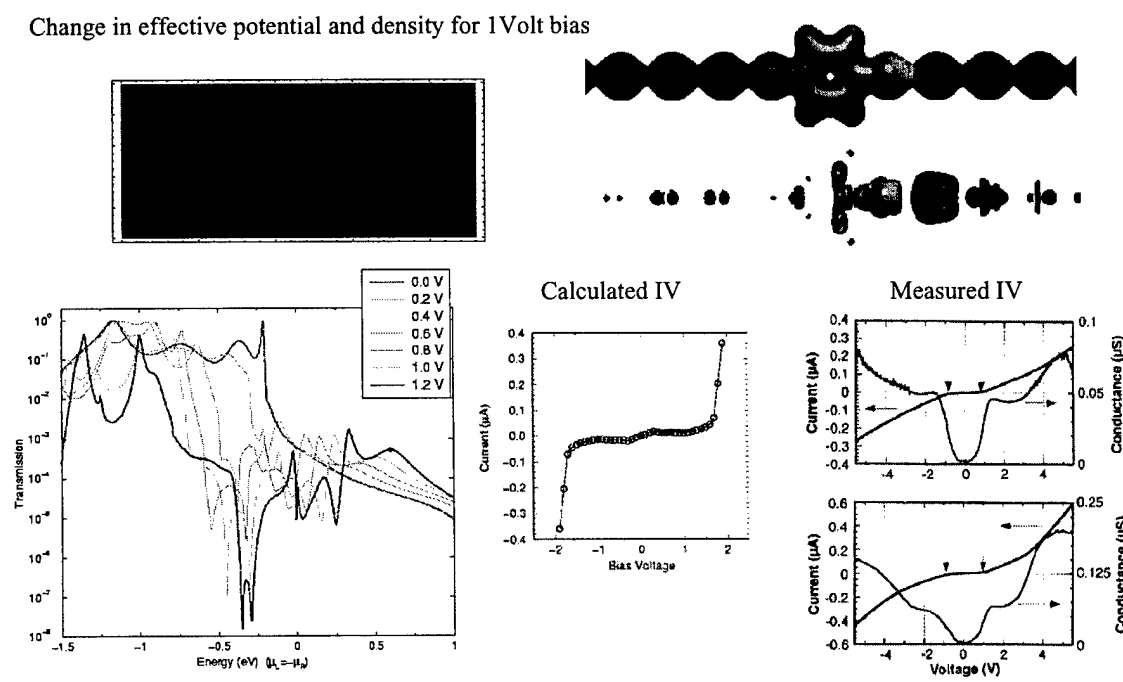
Low conductance



Brandbyge et al., Proceedings MRS fall meeting 2000, D9.25

## Benzene-1,4-dithiolate coupled to gold chains: Finite Bias

Change in effective potential and density for 1 Volt bias

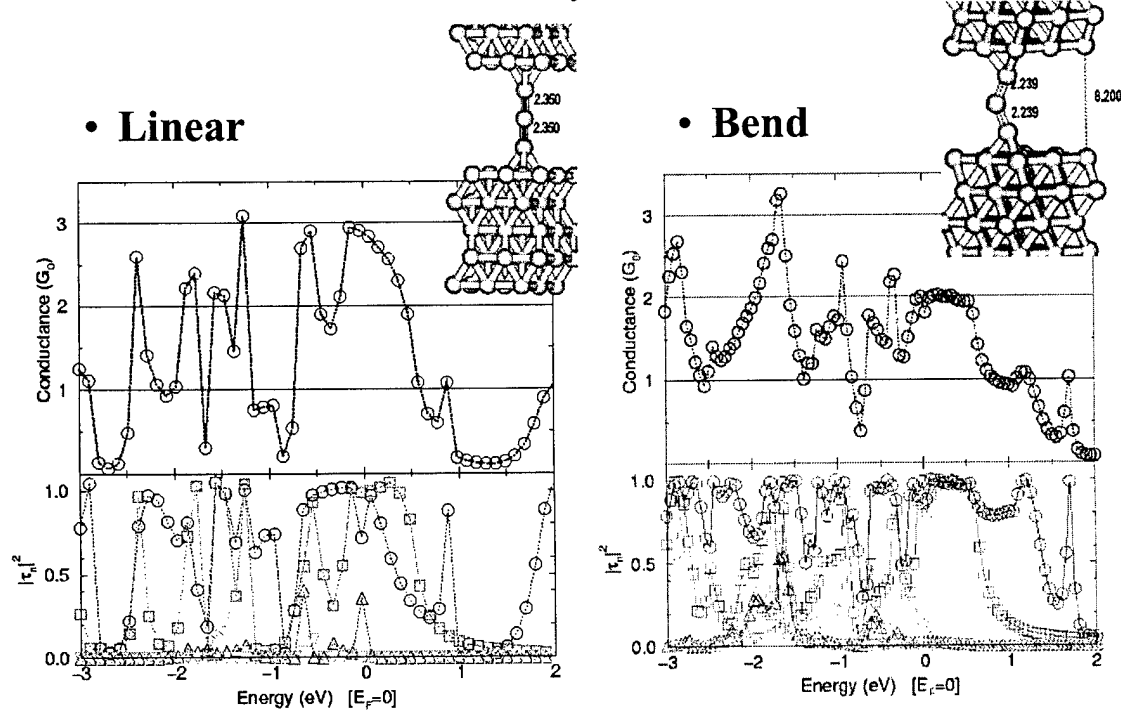


From Reed et al., Science 278, 252 (1997)

# Summary

- ◆ Many exciting and promising experiments on atomic/molecular scale conductors.
- ♣ Many unknown factors in most experiments.
- ♥ We are developing a tool for first principles modelling (*TranSIESTA*)

## Preliminary Platinum



# **Landauer / McKelvey**

## **Approach to MOSFET Modeling**

Mark Lundstrom  
Electrical and Computer Engineering  
Purdue University, West Lafayette, IN

- 1. Introduction**
- 2. Landauer/McKelvey Theory of the MOSFET**
- 3. The Ballistic MOSFET**
- 4. Back-scattering in MOSFET's**
- 5. Discussion**
- 6. Summary**

Lundstrom

additional information at: [www.ece.purdue.edu/celab](http://www.ece.purdue.edu/celab)

Purdue

### *Acknowledgements*

Professor Supriyo Datta

students:

Zhibin Ren, Ramesh Venugopal, Jung-Hoon Rhew  
Dave Rumsey, Anisur Rahman, Jing Guo, Sayed Hasan

sponsors:

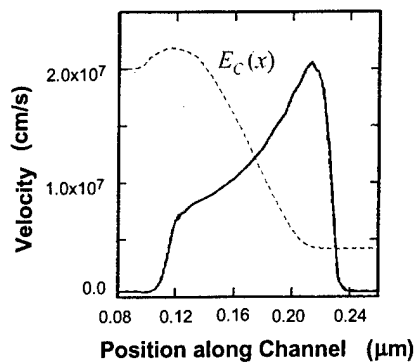
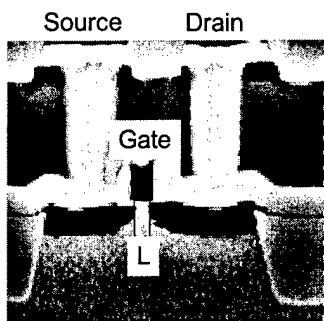
NSF  
SRC  
MARCO/DARPA  
Indiana 21st Century Research and Technology Fund

Lundstrom

Purdue

## 1. Introduction

*nanoscale MOSFETs*



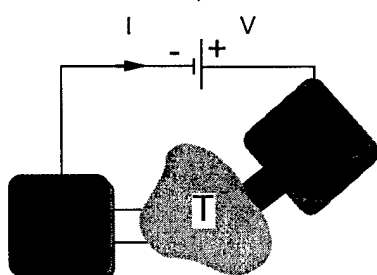
Lundstrom

Purdue

## 1. Introduction

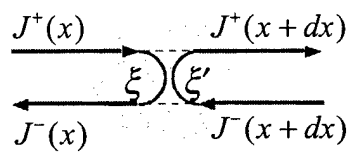
*conceptual approach*

Landauer, 1959



$$G = \frac{2e^2}{h} TM$$

McKelvey, 1961



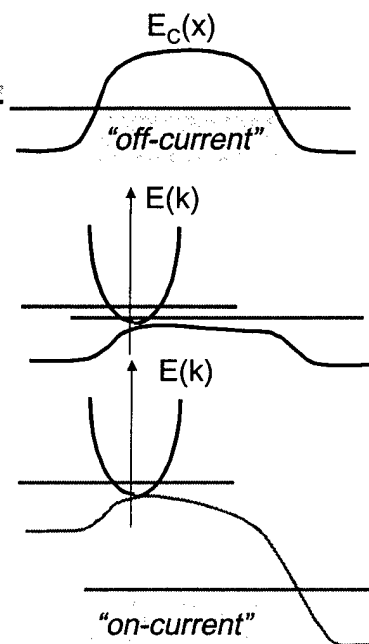
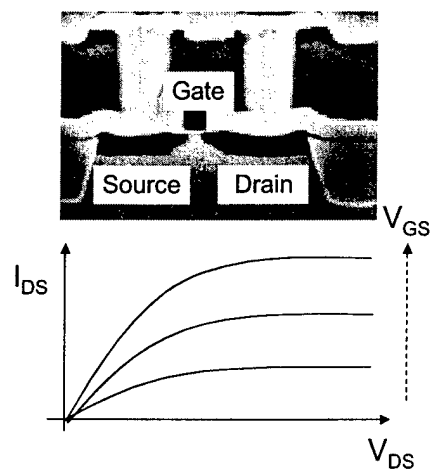
$$\frac{dJ^+}{dx} = -\xi J^+ + \xi' J^-$$

$$\frac{dJ^-}{dx} = -\xi' J^+ + \xi J^-$$

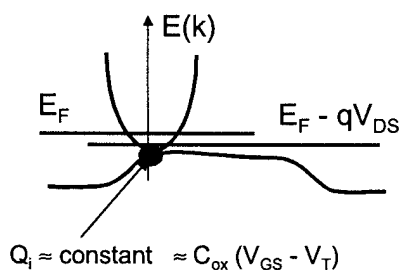
Lundstrom

Purdue

2. Landauer/McKelvey  
Theory of the MOSFET



2. Landauer/McKelvey  
Theory of the MOSFET



$$J^+ = n^+ \tilde{v}_T^+$$

$$n^+ = \frac{m}{2\pi\hbar^2} \ln(1 + e^{\eta_F})$$

$$\tilde{v}_T^+ = \sqrt{\frac{2k_B T}{\pi m}} \frac{F_{1/2}(\eta_F)}{F_0(\eta_F)}$$

$$I_{DS} = WQ_i(V_{GS})\tilde{v}_T \times \left[ \frac{1 - \frac{F_{1/2}(\eta_F - U_{DS})}{F_{1/2}(\eta_F)}}{1 + \frac{F_0(\eta_F - U_{DS})}{F_0(\eta_F)}} \right]$$

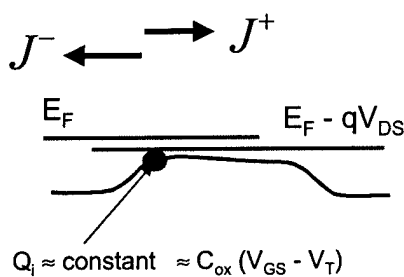
$$I_D = Wq(J^+ - J^-)$$

$$Q_i(V_{GS}) = q(n^+ + n^-)$$

Lundstrom

Purdue

## 2. Landauer/McKelvey Theory of the MOSFET



$$J^+ = n^+ \tilde{v}_T^+$$

$$J^- = (1 - T)J^+ + TJ_{ball}^-$$

$$I_D = Wq(J^+ - J^-)$$

$$Q_i(V_{GS}) = \frac{q(J^+ + J^-)}{\tilde{v}_T^+}$$

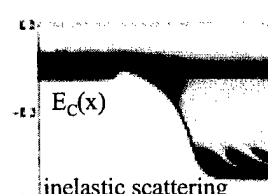
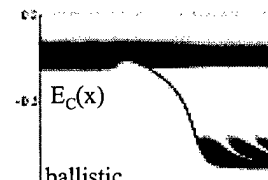
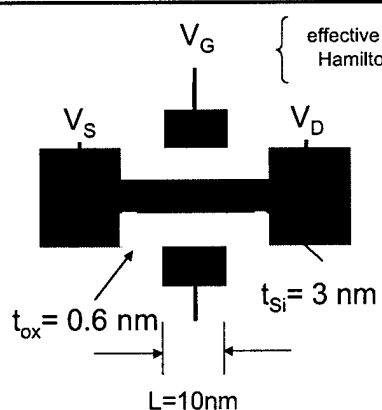
$$I_{DS} = WQ_i(V_{GS})\tilde{v}_T \left( \frac{T}{2-T} \right) \times \left\{ \frac{1 - \frac{F_{1/2}(\eta_F - U_{DS})}{F_{1/2}(\eta_F)}}{1 + \left( \frac{T}{2-T} \right) \frac{F_0(\eta_F - U_{DS})}{F_0(\eta_F)}} \right\}$$

Lundstrom

Purdue

## 2. Landauer/McKelvey Theory of the MOSFET

NEGF Simulations



Zhibin Ren and Ramesh Venugopal (Purdue)  
Dejan Jovanovic (Motorola, Los Alamos)

Lundstrom

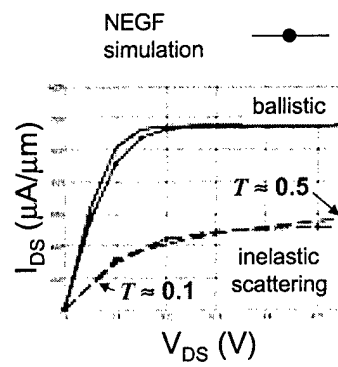
Purdue

## 2. Landauer/McKelvey Theory of the MOSFET

### Landauer/McKelvey model

$$I_{DS} = WC_{ox}(V_{GS} - V_T) \tilde{v}_T \left( \frac{T}{2-T} \right) \times \frac{\frac{F_{1/2}(\eta_F)}{\ln(1+e^{\eta_F})} \times \left\{ \frac{1 - \frac{F_{1/2}(\eta_F - U_{DS})}{F_{1/2}(\eta_F)}}{1 + \left( \frac{T}{2-T} \right) \frac{\ln(1+e^{\eta_F - U_{DS}})}{\ln(1+e^{\eta_F})}} \right\}}{T = \frac{\lambda_o}{\lambda_o + (k_B T / e V_{DS})^\alpha}}$$

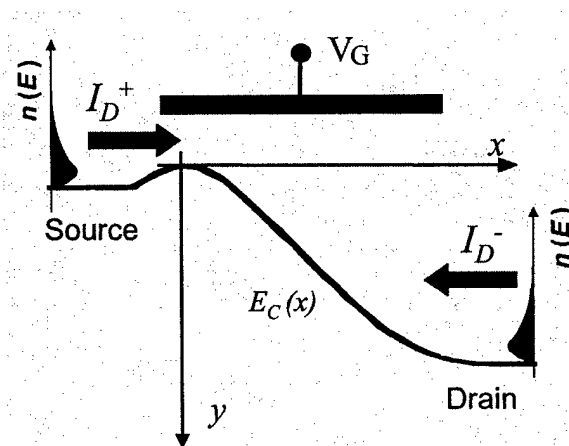
Lundstrom



Purdue

## 3. The Ballistic MOSFET....

thermionic emission

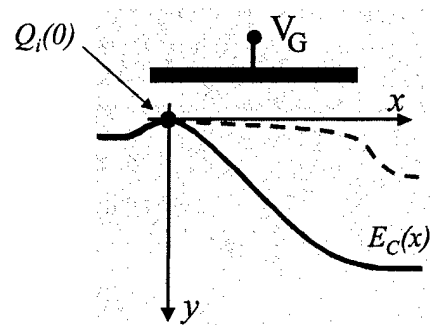


Lundstrom

Purdue

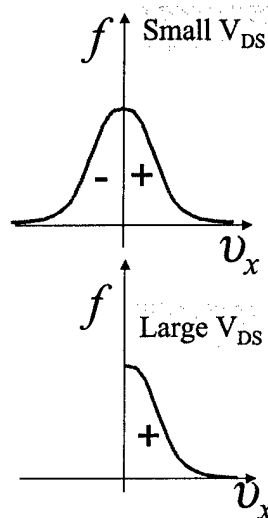
### 3. The Ballistic MOSFET.....

$Q_i(0)$



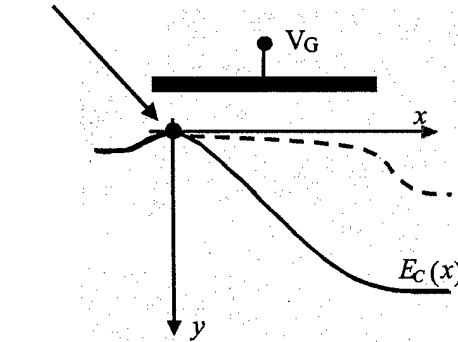
$$f_o = e^{-E/k_B T} \sim e^{-m^* v_x^2 / 2k_B T}$$

Lundstrom

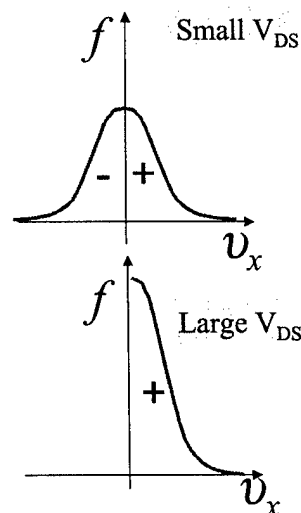


### 3. The Ballistic MOSFET.....

$$Q_i(0) \approx C_{ox} (V_{GS} - V_T)$$

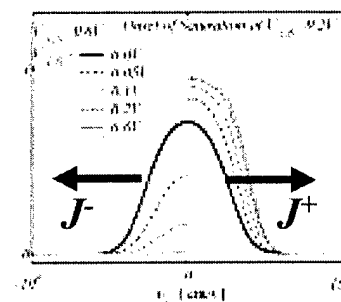
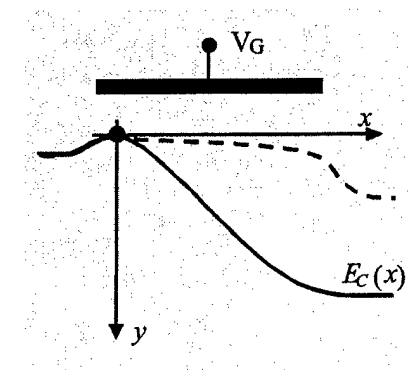


Lundstrom



### 3. The Ballistic MOSFET.....

*numerical solution of the ballistic BTE*



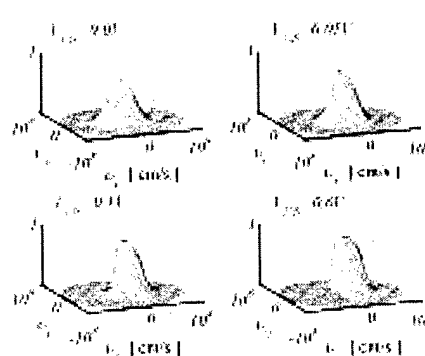
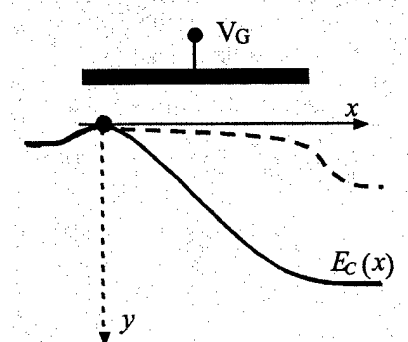
$$R \equiv J^- / J^+$$

Lundstrom

Purdue

### 3. The Ballistic MOSFET.....

*numerical solution of the ballistic BTE*

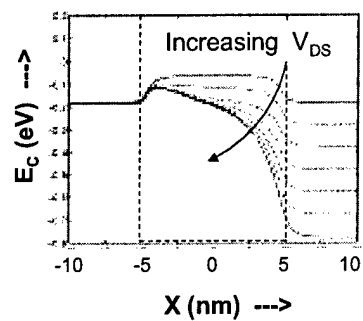


Lundstrom

Purdue

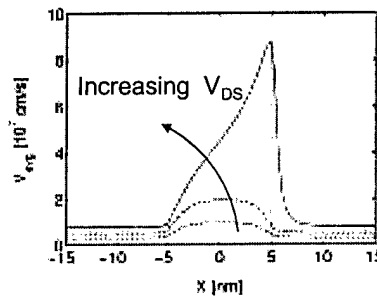
### 3. The Ballistic MOSFET.....

$E_C$  vs.  $x$  for  $V_{GS} = 0.5V$



Lundstrom

- i)  $Q_i(0) \approx \text{constant}$
- ii)  $\langle v(0) \rangle \rightarrow v_T$

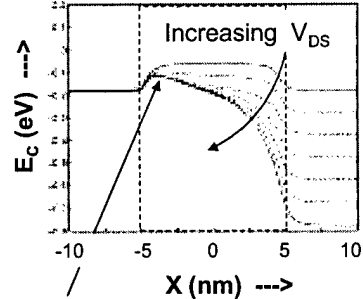


Purdue

### 3. The Ballistic MOSFET....

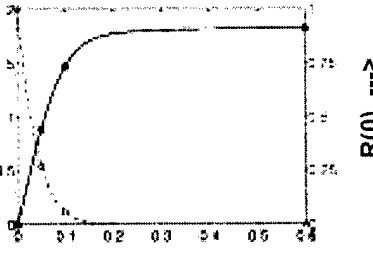
velocity saturation in a ballistic FET

$E_C$  vs.  $x$  for  $V_{GS} = 0.5V$



Lundstrom

- i)  $Q_i(0) \approx \text{constant}$
- ii)  $\langle v(0) \rangle \rightarrow v_T$



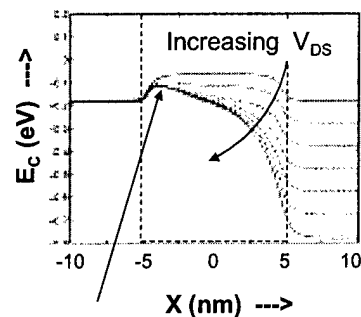
Purdue

$v(0) \rightarrow v_T$

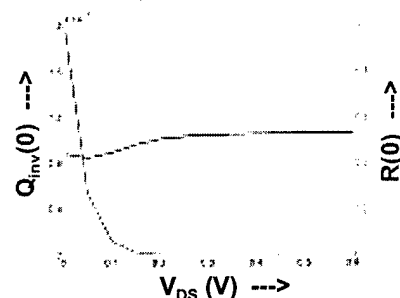
### 3. The Ballistic MOSFET.....

'(2-T) effect'

$E_c$  vs.  $x$  for  $V_{GS} = 0.5V$



- i)  $Q_i(0) \approx \text{constant}$
- ii)  $\langle v(0) \rangle \rightarrow v_T$



The (2-T) effect:  $Q_{\text{inv}} \sim \text{constant}$

Lundstrom

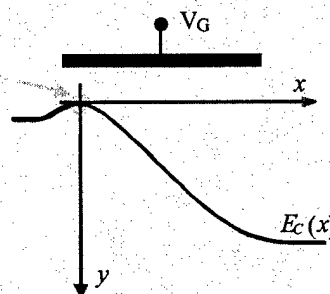
Purdue

### 3. The Ballistic MOSFET.....

quasi-equilibrium

$$n_s(V_{GS}) = C_{eff}(V_{GS} - V_T)$$

(Gradual Channel Approximation  
+ DIBL)



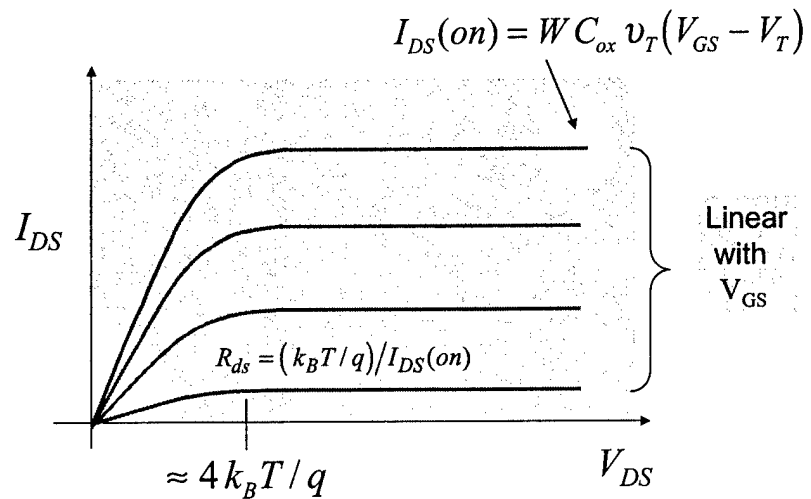
$$I_{DS} = W C_{ox} v_T (V_{GS} - V_T) \left[ \frac{1 - e^{-qV_{DS}/k_B T}}{1 + e^{-qV_{DS}/k_B T}} \right] \quad v_T = \sqrt{\frac{2k_B T}{\pi m^*}}$$

Lundstrom

(Boltzmann statistics and one subband)

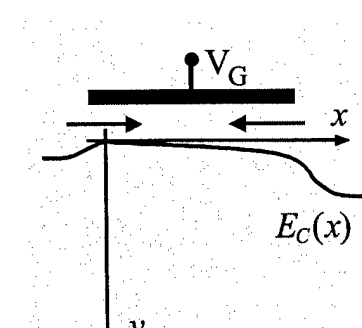
Purdue

### 3. The Ballistic MOSFET.....



### 3. The Ballistic MOSFET.....

Why does a ballistic MOSFET have a finite channel resistance?



$$I_D^- = I_D^+ e^{-qV_{DS}/k_B T}$$

$$I_{DS} = I_D^+ - I_D^-$$

$$I_{DS} = I_D^+ \left(1 - e^{-qV_{DS}/k_B T}\right)$$

$$I_{DS} \approx \frac{I_D^+}{(k_B T / q)} V_{DS}$$

### 3. The Ballistic MOSFET.....

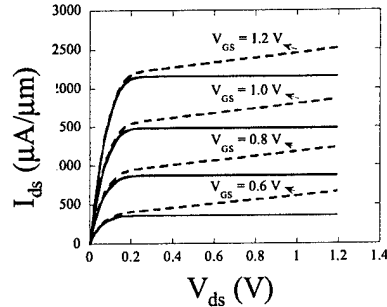
*100 nm technology node....*

$t_{ox} = 1.5 \text{ nm}$

$N_A = 2 \times 10^{18} \text{ cm}^{-3}$

$V_{DD} = 1 \text{ V}$

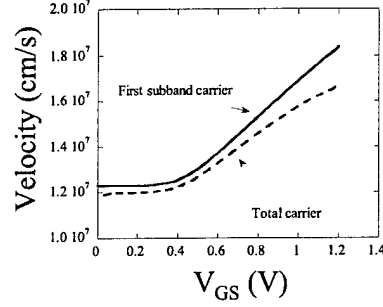
DIBL = 100 mV/V



$$I_{DS} \propto (V_{GS} - V_T)^\alpha$$

$$1 \leq \alpha \leq 1.5$$

Lundstrom



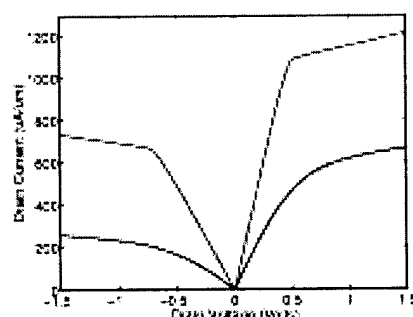
$$I_{DS(on)} / W = q n_s v_T$$

Purdue

### 3. The Ballistic MOSFET.....

*comparison with measurements....*

$L_{eff} = 115/125 \text{ nm}$  technology



ballistic  
(with measured  $R_s$ )

Lundstrom

NMOS: ~ 55% of limit

PMOS: ~ 33% of limit

How can a device with  $L_{eff}$   
~ 6 mfps operate at ~50%  
of the ballistic limit?

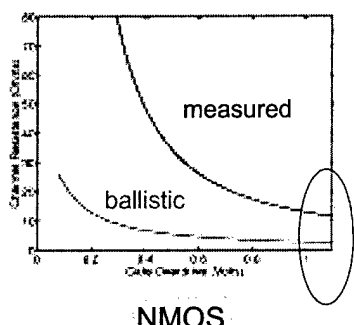
- Farzin Assad, et al. (1999 IEDM)
- Dave Rumsey
- G. Timp, J. Bude, et al., (1999 IEDM)
- A. Lochtefeld, D. Antoniadis (EDL, Feb 2001)

Purdue

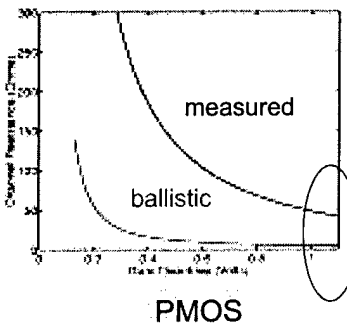
### 3. The Ballistic MOSFET.....

*comparison with measurements.....*

Channel resistance vs.  $V_{GS}$



NMOS



PMOS

$$R_{SD} = R_{par} + R_{ballistic} + R_0 \frac{L}{W}$$

Lundstrom

Purdue

### 3. The Ballistic MOSFET.....

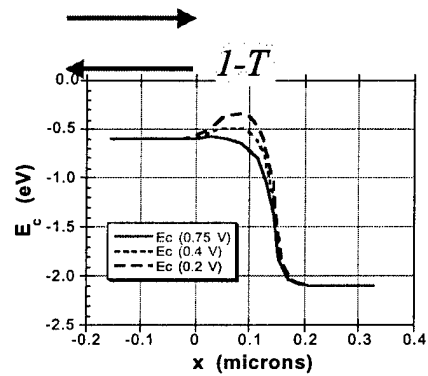
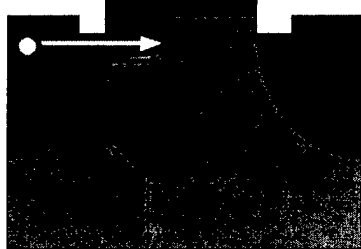
*Summary*

- the ballistic I-V is readily computed and the ballistic MOSFET is readily understood
- present day devices operate at ~ 50% of the ballistic limit
- future devices will have to operate even closer
- **backscattering** limits the performance of realistic devices

Lundstrom

Purdue

#### 4. Back-Scattering in MOSFETs.....

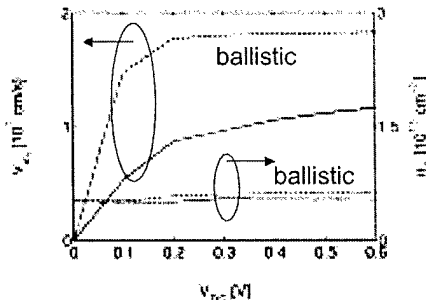
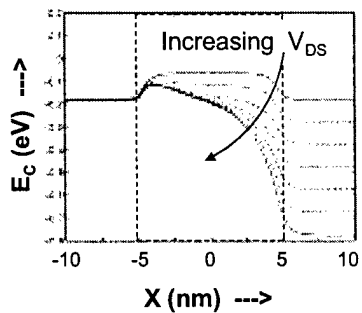


carriers at the top of the barrier: MOS electrostatics  
 carriers that cross the channel: backscattering,  $R=1-T$

Lundstrom

Purdue

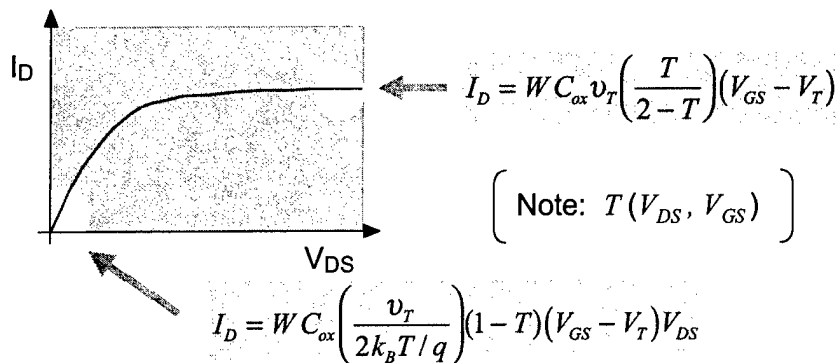
#### 4. Back-Scattering in MOSFETs.....



Lundstrom

Purdue

#### 4. Back-Scattering in MOSFETs....



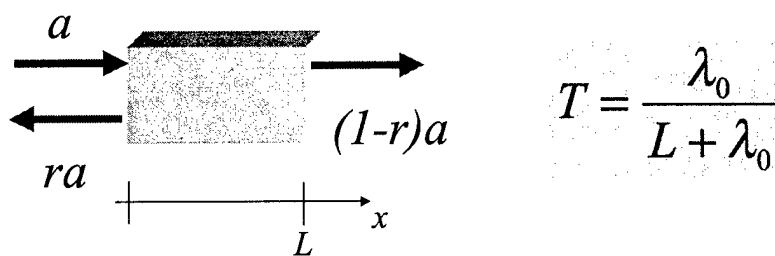
M.S. Lundstrom, "Elementary scattering theory of the MOSFET," *EDL*, 18, 361, 1997  
 S. Datta, et. al, "The MOSFET from a Transmission Viewpoint," *Superlattices and Microstructures*, 1998

Lundstrom

Purdue

#### 4. Back-Scattering in MOSFETs....

computing  $T$ : low  $V_{DS}$



$$I_{DS} = WC_{ox} \left( \frac{v_T}{k_B T/q} \right) T(V_{GS} - V_T)V_{DS}$$

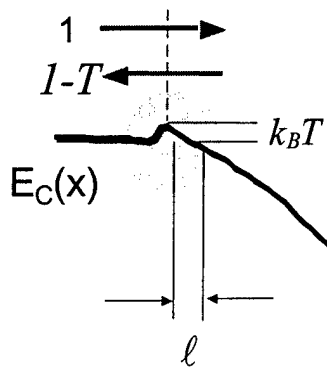
$$\star \quad I_{DS} = \mu_{eff} C_{ox} \left( \frac{W}{L + \lambda_0} \right) (V_{GS} - V_T)V_{DS}$$

Lundstrom

Purdue

#### 4. Back-Scattering in MOSFETs.....

computing  $T$ : high  $V_{DS}$



$$T = \frac{\lambda_o}{\ell + \lambda_o}$$

Bethe condition for a MOSFET:

*ballistic current:  $\ell < \lambda$*

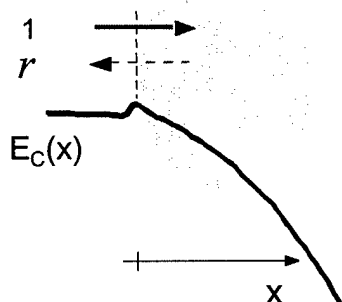
[not:  $L < \lambda$ ]

★ mobility is important for nanoscale FETs

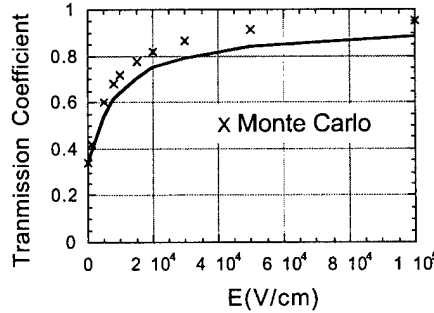
Lundstrom

Purdue

#### 4. Back-Scattering in MOSFETs.....



$$r = \frac{\ell}{\ell + \lambda_o}$$



See:

P.J. Price, *Semiconductors and Semimetals*,  
14, 249-334, 1979  
H. U. Baranger and J.W. Wilkins, *Phys. Rev. B*,  
36, 1487-1502, 1987.

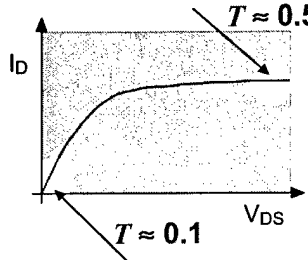
Lundstrom

Purdue

#### 4. Back-Scattering in MOSFETs.....

Landauer/McKelvey model

$$I_D = W C_{ox} v_T \left( \frac{T}{2-T} \right) (V_{GS} - V_T)$$



$$I_D = W C_{ox} \left( \frac{v_T / 2}{k_B T / q} \right) T (V_{GS} - V_T) V_{DS}$$

Lundstrom

$$I_{DS} = W C_{ox} (V_{GS} - V_T) \tilde{v}_T \left( \frac{T}{2-T} \right) \times$$

$$\frac{F_{1/2}(\eta_F)}{\ln(1+e^{\eta_F})} \times \left\{ \frac{1 - \frac{F_{1/2}(\eta_F - U_{DS})}{F_{1/2}(\eta_F)}}{1 + \left( \frac{T}{2-T} \right) \frac{\ln(1+e^{\eta_F - U_{DS}})}{\ln(1+e^{\eta_F})}} \right\}$$

Purdue

## Landauer / McKelvey Approach to MOSFET Modeling

Mark Lundstrom  
Electrical and Computer Engineering  
Purdue University, West Lafayette, IN

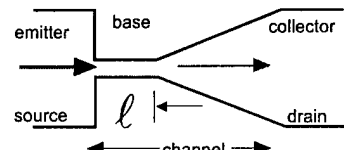
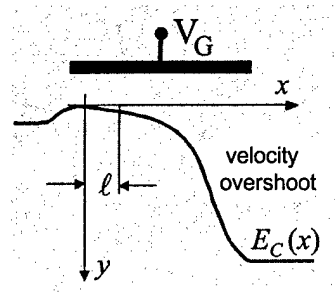
1. Introduction
2. Landauer/McKelvey Theory of the MOSFET
3. The Ballistic MOSFET
4. Back-scattering in MOSFET's
5. Discussion
6. Summary

Lundstrom

Purdue

## 5. Discussion....

*essential physical picture.....*



$$r = (1 - t) = \frac{\ell}{\ell + \lambda_o}$$

See: "Essential physics of carrier Transport in nanoscale MOSFETs," M. Lundstrom, et al.

$$r \approx 50\% \Rightarrow \ell \approx \lambda_o$$

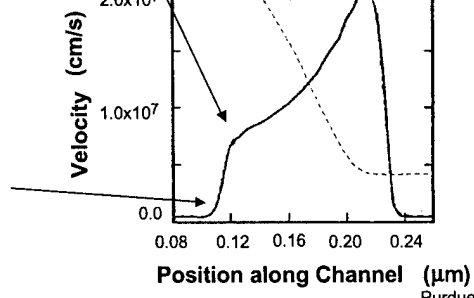
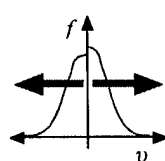
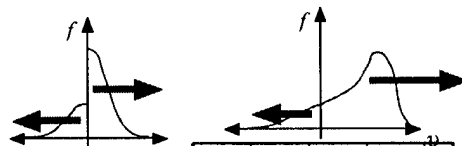
Lundstrom

Purdue

## 5. Discussion....

*interpreting simulations*

$$\langle v(0) \rangle = \left( \frac{T}{2 - T} \right) v_T$$



Lundstrom

Purdue

5. Discussion....

how does  $T$  scale?

$$T = \frac{\lambda}{\ell + \lambda} \approx 50\%$$



$$\ell \approx \lambda$$

How does  $T$  scale?

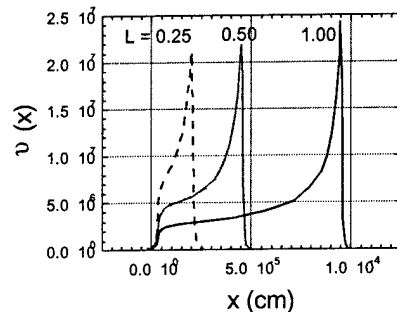
as  $L \downarrow \dots \ell \downarrow$  and  $\lambda \downarrow$



Scaling maintains a constant  $T$  (at min L)

Lundstrom

Purdue



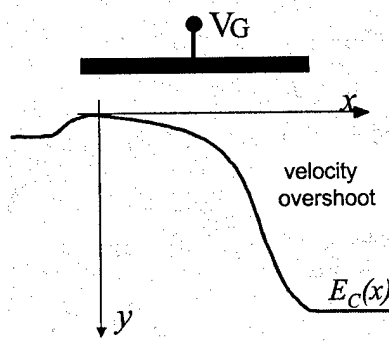
5. Discussion....

How to increase  $T$ ?

To reduce backscattering:

1) increase mfp  $\lambda$  ( $\mu$ )

2) decrease  $\ell$



Lundstrom

Purdue

5. Discussion....

*The role of mobility*

Backscattering is related to  $\lambda_o$  and  $\lambda_o$  is related to mobility

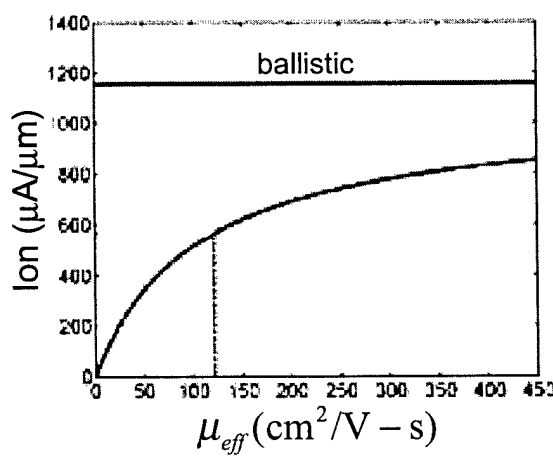
Scattering theory gives:

$$\left. \begin{aligned} \frac{\delta I_D}{I_D} &= \frac{\delta \mu}{\mu} (1 - B) \\ B &\equiv \frac{I_D}{I_D(\text{ballistic})} \end{aligned} \right\} \quad \begin{aligned} \text{i) linear region: } B &\approx 0.2 & \frac{\delta I_D}{I_D} &\approx \frac{\delta \mu}{\mu} \\ \text{ii) saturated region: } B &\approx 0.5 & \frac{\delta I_D}{I_D} &\approx 0.5 \frac{\delta \mu}{\mu} \end{aligned}$$

Lundstrom

Purdue

5. Discussion....



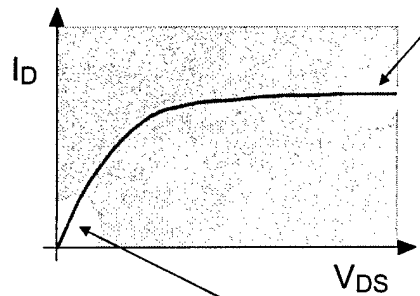
Lundstrom

Purdue

5. Discussion....

*connections to traditional theory*

$$I_D = C_{ox} W v_{sat} (V_{GS} - V_T)$$



$$I_D = C_{ox} \mu_{eff} \left( \frac{W}{L} \right) (V_{GS} - V_T) V_{DS}$$

Lundstrom

Purdue

5. Discussion....

*connections to traditional theory*

Scattering theory

Linear (low  $V_{DS}$ ) drain current

$$\left. \begin{aligned} I_D &= W C_{ox} \left( \frac{v_r}{2k_B T / q} \right) T (V_{GS} - V_T) V_{DS} \\ T &= \frac{\lambda_o}{L + \lambda_o} \end{aligned} \right\}$$

Conventional theory

$$\left. I_D = W \mu_{eff} C_{ox} \frac{W}{(L + \lambda_o)} (V_{GS} - V_T) V_{DS} \right\}$$

Lundstrom

## 5. Discussion....

*connections to traditional theory*

### Scattering theory

$$\left. \begin{aligned} I_D &= WC_{ox}v_T \left( \frac{T}{2-T} \right) (V_{GS} - V_T) \\ T &= \frac{\lambda_o}{\ell + \lambda_o} \quad \ell = \left( \frac{k_B T / q}{V_{DS}} \right) L \end{aligned} \right\}$$

on-current

### Conventional theory

$$\left. \begin{aligned} I_D &= \frac{WC_{ox}v_T m (V_{GS} - V_T) V_{DS}}{1 + m V_{DS}} \\ m &= \left( \frac{\mu}{2L v_T} \right) \end{aligned} \right\}$$

Veeraraghavan and Fossum  
IEEE TED, 35, p. 1866, 1988

Lundstrom

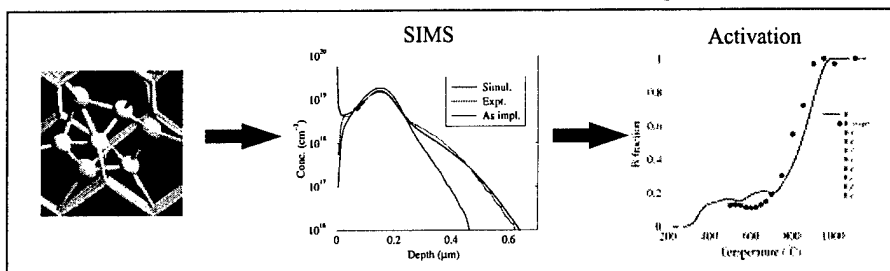
## 6. Summary

- Nanoscale transistor physics is simply understood by beginning at the ballistic limit
- Scattering theory provides a simple, physical view of nanotransistors and compact, analytical models
- Useful for interpreting simulations and guiding experiments
- A bridge to post-CMOS devices

Lundstrom

Purdue

# Diffusion and Clustering of Impurities – “a Problem that Cannot be Ignored”



Wolfgang Windl

*Digital DNA™ Laboratories, Motorola, Inc.  
Austin, TX*

in collaboration with

Benjamin Liu, Dejan Jovanovic, Mike Masquelier (Motorola Labs)  
Blas Uberuaga, Hannes Jónsson, Scott Dunham (UW)

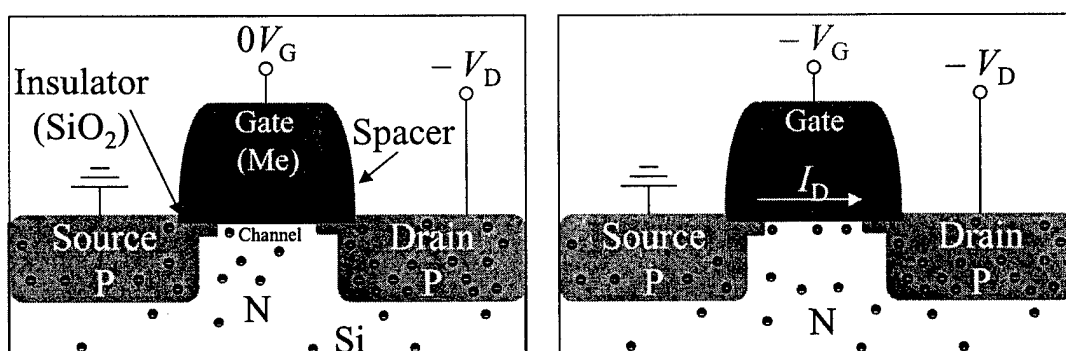


© 2001 Wolfgang Windl (Motorola, Inc.). All rights reserved.



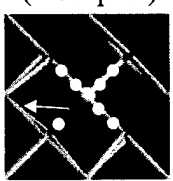
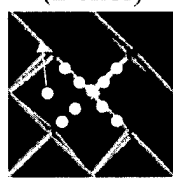
## MOSFET Basics

Metal Oxide Semiconductor Field Effect Transistor



Doping:

N: e⁻, e.g. As      P: holes, e.g. B  
(Donor)                (Acceptor)

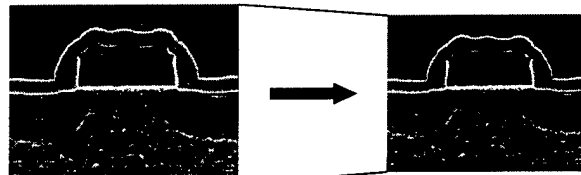


- Analog: Amplification
- Digital: Logic gates

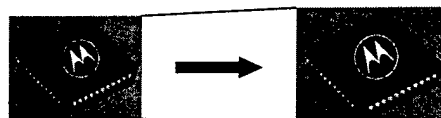


# Semiconductor Technology Scaling

- Feature size shrinks on average by 12% p.a. ( $f = 0.88$ )



- Chip size increases on average by 2.3% p.a. ( $d = 1.023$ )



# of transistors / area ( $\sim d^2 / f^2$ )  $\uparrow$  by 35% p.a.

Switching speed ( $\sim 1/f$ )  $\uparrow$  by 14% p.a.

Overall performance:  $\uparrow$  by ~55% p.a. or  
~ doubling every 18 months ("Moore's Law")

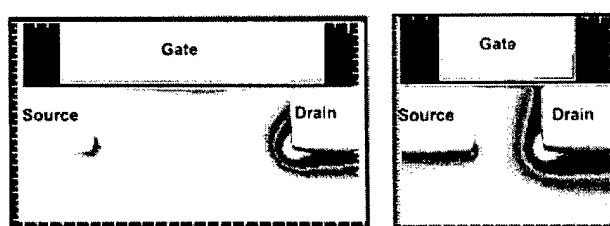
Intelligence  everywhere\*

MOTOROLA digital dna\*



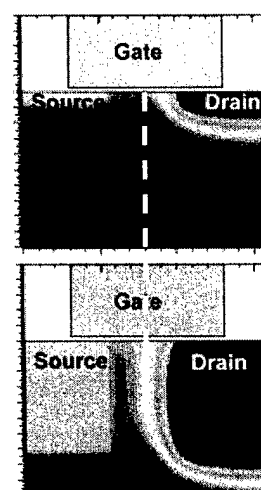
## MOSFET Scaling Challenges

### Shorter Channel



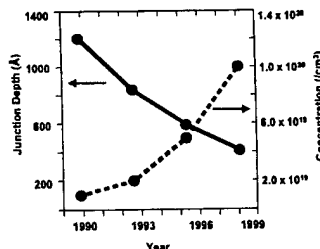
Potential across channel (on)

### Shallower Implant



Better insulation (off)

### Higher Doping



To get enough current with shallow source & drain

Intelligence  everywhere\*

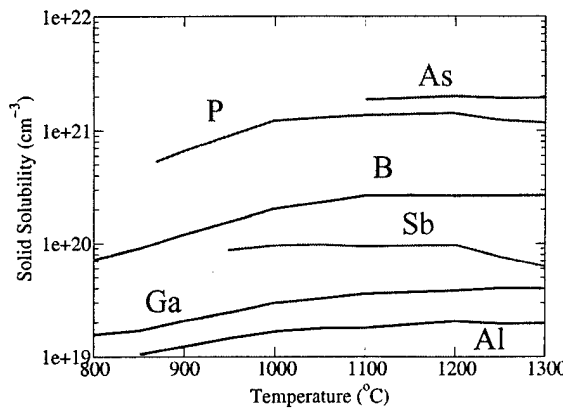
\*P. Packan, MRS Bulletin

MOTOROLA digital dna\*

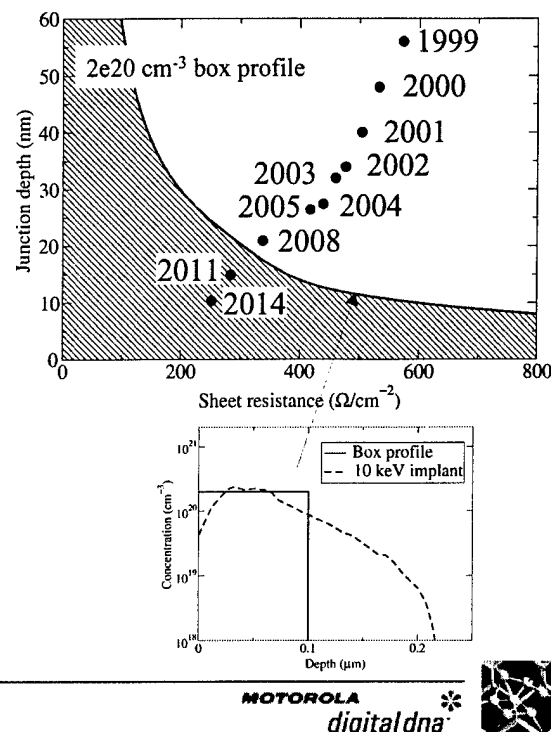


# ITRS Requirements & Solubility Limit

## Solid Solubility of Si Dopants



## ITRS & Solubility Limit

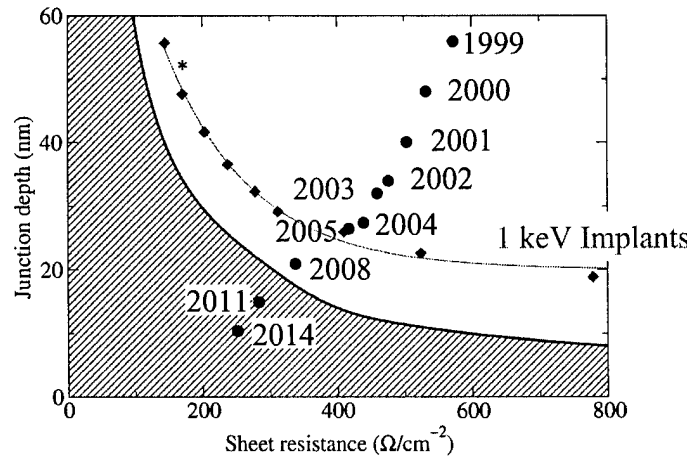


Intelligence everywhere\*

MOTOROLA  
digital dna\*



## How Are We Doing?



- 1 keV implants + optimum anneals can meet 2005 ITRS requirements (100 nm).
- Further reduction in implant energy can perhaps meet 70 nm (2008) needs, but cannot meet needs beyond this node.
- Need to find way to exceed  $2\text{e}20 \text{ cm}^{-3}$  concentration limit for *n* and *p* dopants, or need new device structures (double gate, surround gate, superhalo, etc.).

Intelligence everywhere\*

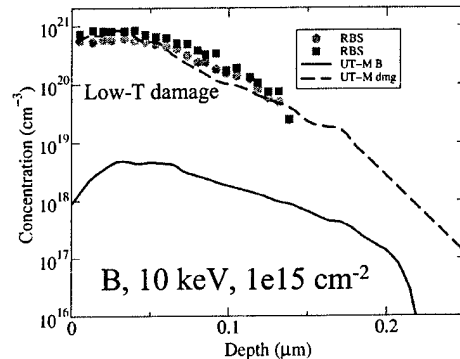
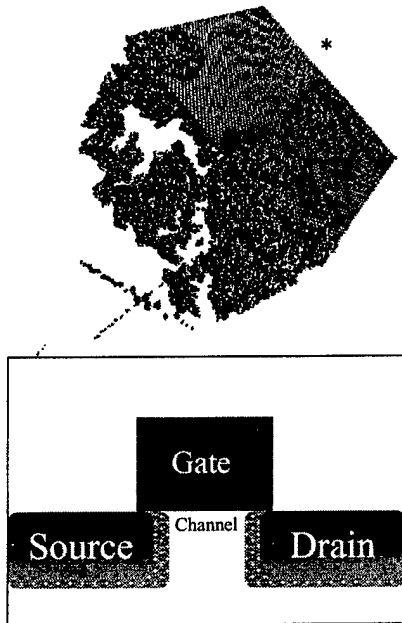
\*Plummer (Stanford)

MOTOROLA  
digital dna\*



# Ion Implantation and Annealing

- Dopants inserted by ion implantation damage
- Damage healed by annealing
- During annealing, dopants diffuse fast (assisted by defects)  
important to optimize anneal



*intelligence*  *everywhere\**

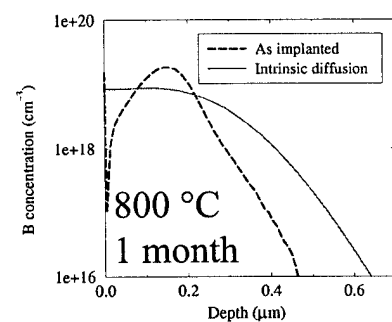
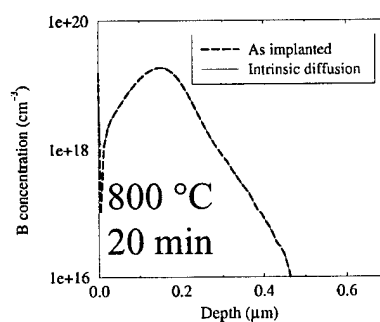
\*S. Srinivasan, K. Beardmore, N. Jensen

**MOTOROLA** 

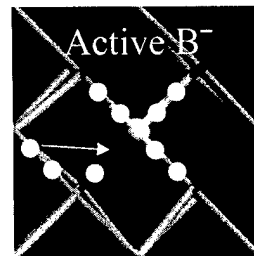
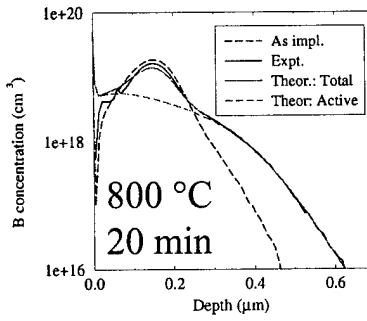


## TED & Deactivation

What you expect:  
Intrinsic diffusion



What you get:  
TED:  
• fast diffusion  
• immob. peak



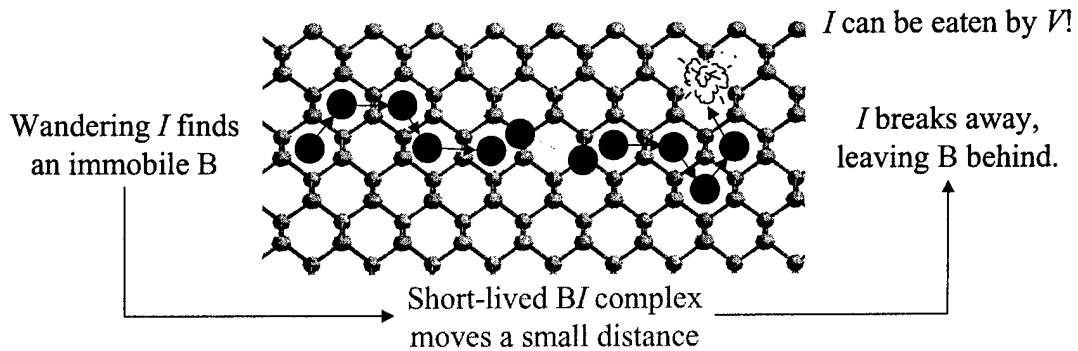
*intelligence*  *everywhere\**

**MOTOROLA** 



## B Diffusion in Bulk Si: Qualitative Picture

- B diffusion exclusively mediated by Si self-interstitials\*
- B diffusion limited by self-interstitial diffusion\*\*



\*A. Ural, P. B. Griffin, and J. D. Plummer, J. Appl. Phys. **85**, 6440 (1999)

\*\* W. Windl, M.M. Bunea, R. Stumpf, S.T. Dunham, and M.P. Masquelier, Proc. MSM99 (Cambridge, MA, 1999), p. 369; MRS Proc. **568**, 91 (1999); Phys. Rev. Lett. **83**, 4345 (1999).

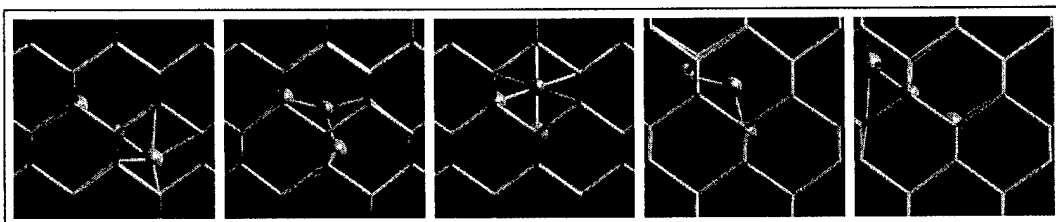
intelligence  everywhere™

MOTOROLA  
digital dna™



## Reason for TED: Implant Damage

Interstitial assisted two-step mechanism:



*Intrinsic diffusion:*

Create interstitial, B captures interstitial, diffuse together

$$\text{Diffusion barrier: } E_{\text{form}}(I) - E_{\text{bind}}(BI) + E_{\text{mig}}(BI)$$
$$4 \text{ eV} \quad 1 \text{ eV} \quad 0.6 \text{ eV} \sim 3.6 \text{ eV}$$

*After implant:*

Interstitials for “free” diffusion barrier  $\sim 0.6$  eV

W. Windl, M.M. Bunea, R. Stumpf, S.T. Dunham, and M.P. Masquelier, Proc. MSM99 (Cambridge, MA, 1999), p. 369; MRS Proc. **568**, 91 (1999); Phys. Rev. Lett. **83**, 4345 (1999).

intelligence  everywhere™

MOTOROLA  
digital dna™



# Reason for Deactivation?

## Phenomenological considerations:

- Boron is smaller than Si     substitutional B strains Si lattice
- Boron crystal structure: Icosahedron (buckyball), threefold coord.  
at higher B concentrations: New structures form,  
bind & deactivate B

## Experimental findings:

- Structures too small to be seen in EM     only “few” atoms
- Clustering dependent on B concentration and *I* concentration  
formation of  $B_mI_n$  clusters postulated;  
experimental estimate:  $m / n \sim 1.5^*$

## Approach:

Calculate clustering energies from first principles up to “max.”  $m, n$   
Build kinetic Monte Carlo / continuum model from it

\*S. Solmi *et al.*, J. Appl. Phys. **88**, 4547 (2000).

Intelligence  everywhere®

MOTOROLA  
digital dna 

# Previous Work - More Motivation

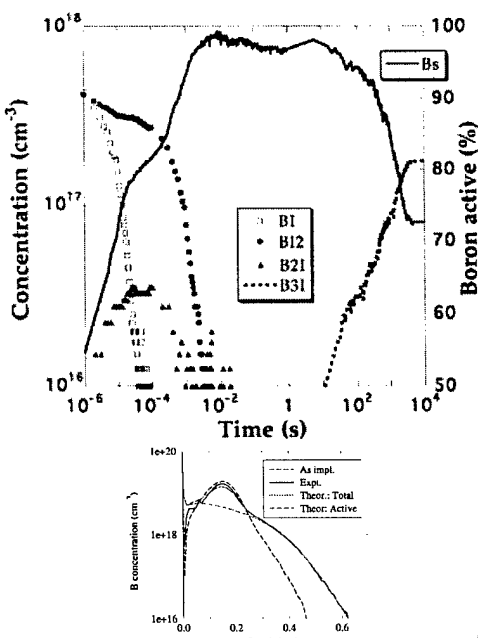
De la Rubia's group (LLNL)  
predicts with *ab initio* based kMC  
model\* (up to  $B_4I_2$ ) a B  
“activation window” for  
annealing activation

\*M. J. Caturla *et al.*, APL **72**, (1998) p. 2736

However:

Experiment\* finds **no** activation  
window, once activated stays  
activated.

\*Mokhberi, Griffin, Plummer (Stanford).



Intelligence  everywhere®

MOTOROLA  
digital dna 

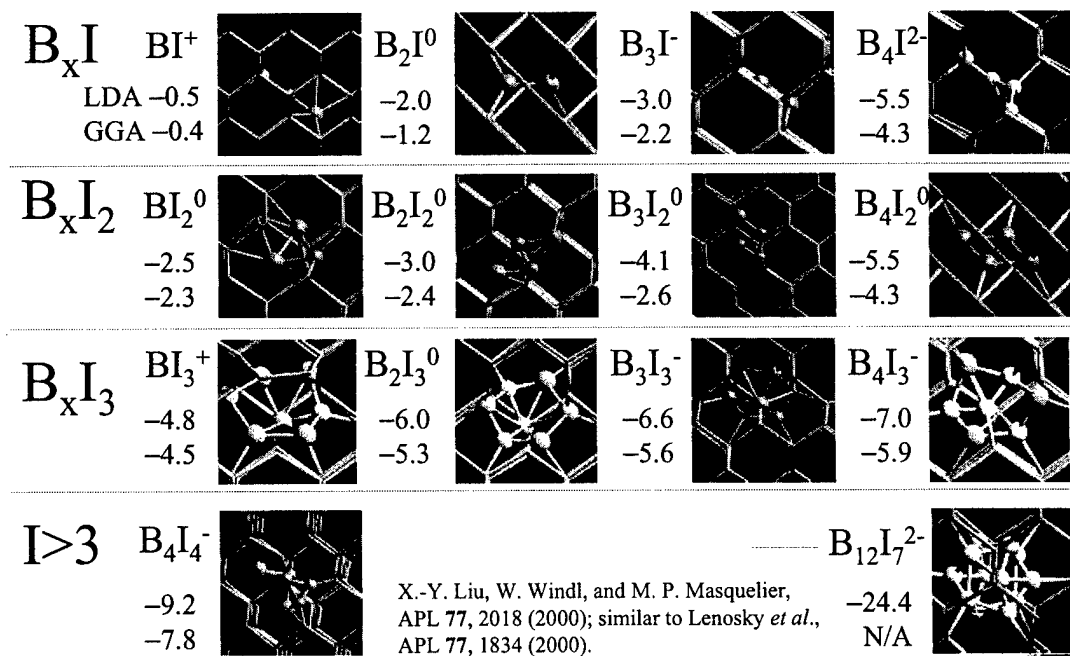
# Calculation of the Clustering Energies

- DFT plane-wave code VASP (Technische Universität Wien), LDA and GGA
- Simulation cells of 64 atoms (converged ~7% vs. 216 atoms),  $E_{\text{cut}} = 230 \text{ eV}$ ,  $4^3 \text{ k-points}$
- Relax many different, “guessed” initial structures for each cluster; dangerous, can miss groundstate!

Intelligence  everywhere®

MOTOROLA  
digital dna 

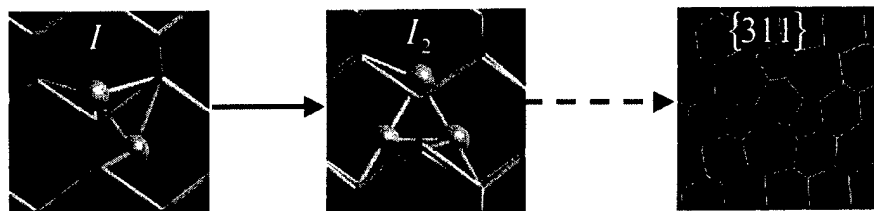
## B-I Cluster Structures from *Ab Initio* Calculations



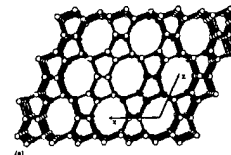
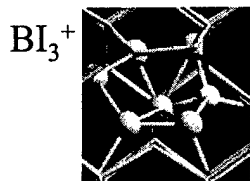
Intelligence  everywhere®

MOTOROLA  
digital dna 

## Influence of B Clustering on I Clustering!?

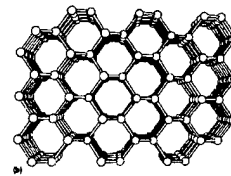


(e.g. Kim, Wilkins,... PRB 1997)



New ring structure for  $I_3$ :

- Without B: Ring  $\sim 0.2$  eV higher than more compact  $I_3$  structures.
- With B: Ring has lowest energies  
B promotes ring growth!?



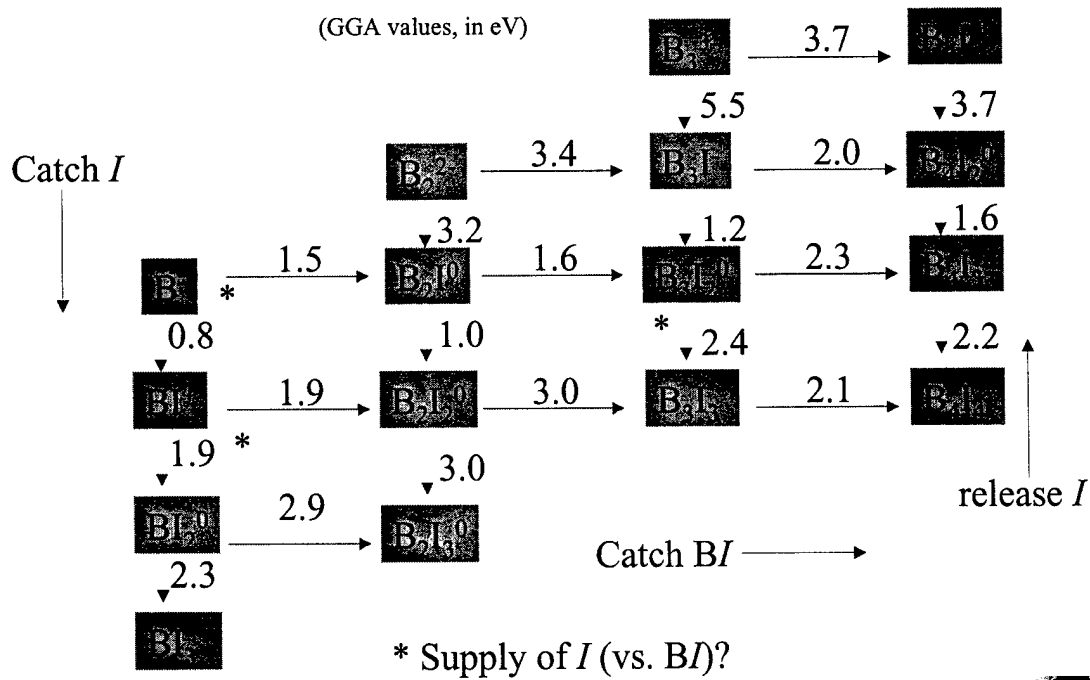
(Demkov, Windl, Sankey, PRB 1996)

Intelligence everywhere\*

MOTOROLA \*  
digital dna



## B-I Clustering Reaction Paths & Binding Energies

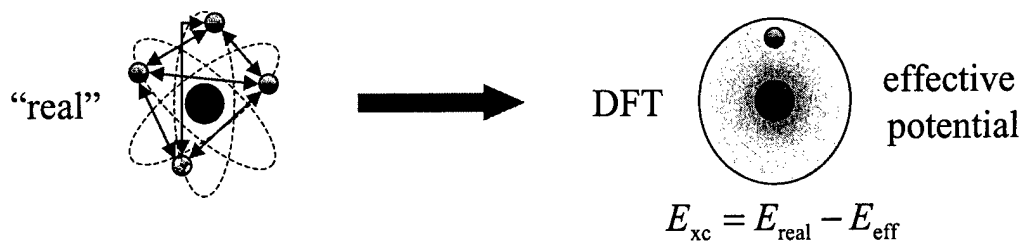


Intelligence everywhere\*

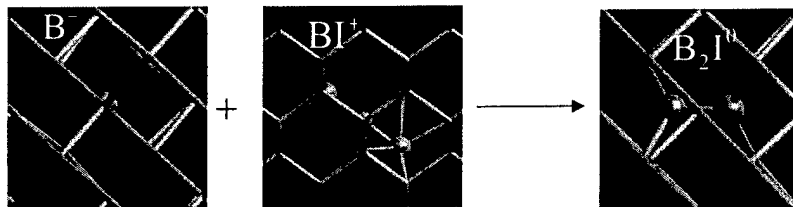
MOTOROLA \*  
digital dna



## DFT Flavors: GGA and LDA



For some cases, energetics differ considerably:



Reaction binding energy: 1.5 eV GGA

0.9 eV LDA.

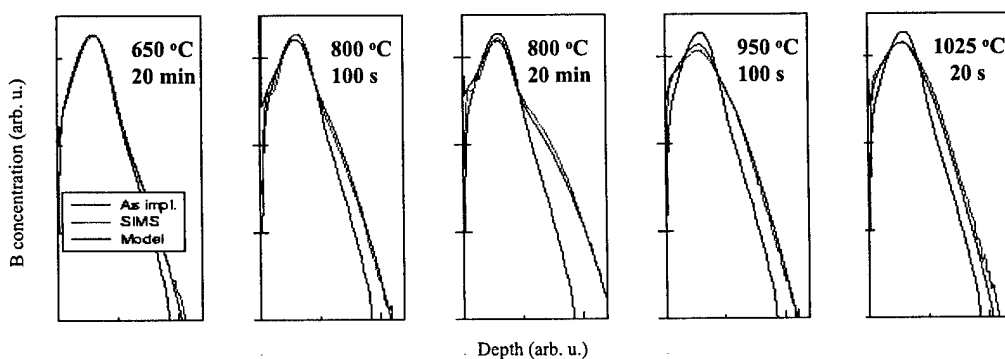
Intelligence  everywhere™

MOTOROLA 



## Calibration with SIMS Measurements

- Continuum model    recalibration of ab initio numbers necessary
- Genetic Algorithm:
  - Start with many random parameter sets within boundaries
  - Select pairs of parameter sets ("parents"), biased by  $\chi^2$
  - Mate parents (mix parameters randomly), add child to population
- Nearly all fitted parameters between LDA and GGA values

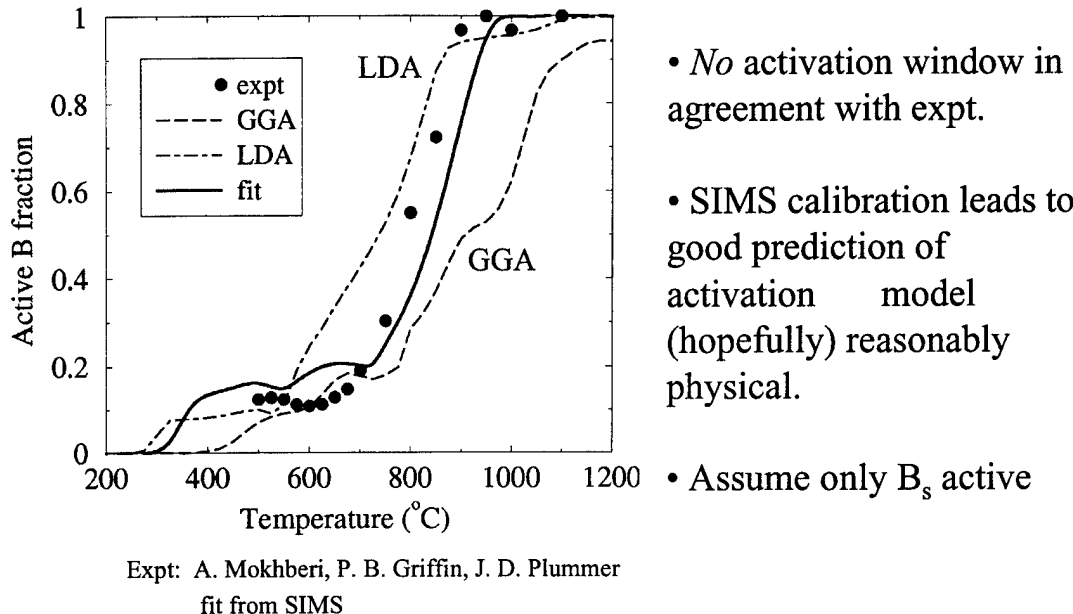


Intelligence  everywhere™

MOTOROLA 



## Activation Results

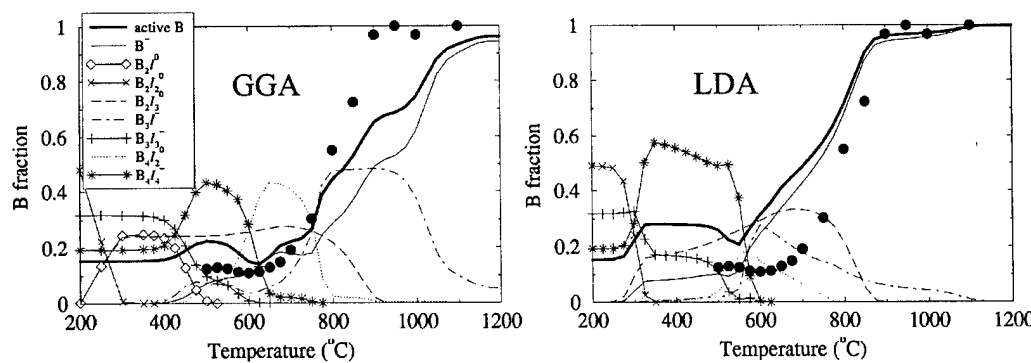


*intelligence everywhere\**

MOTOROLA  
*digital dna*\*



## Activation and Clusters



- LDA, GGA, fit do not give consistent clustering pattern:
- GGA: Dominated by  $B_3I_2^0$  cluster (also  $B_2I_3^0$ )
- LDA: Dominated by  $B_2I_3^0$  cluster (also  $B_3I_2^0$ )
- Fit: Dominated by  $B_4I_2^0$

*intelligence everywhere\**

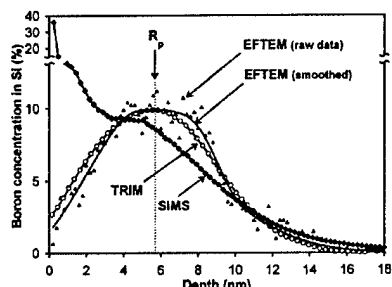
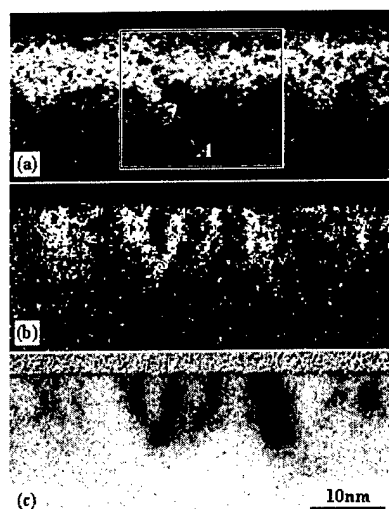
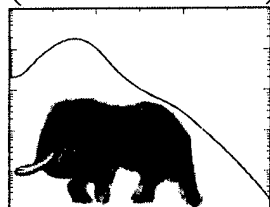
MOTOROLA  
*digital dna*\*



# Uniqueness of Clustering Model!?

“You can fit an elephant with  
21 parameters.”

(Ulrich Schröder)



Energy filtered TEM B maps from (a) as-implanted ( $1 \text{ keV}, 5 \times 10^{15} \text{ cm}^{-3}$ ) and (b)  $900^\circ\text{C}$  annealed sample; (c) bright field image of (b). [Wang *et al.*, APL 77, 3586 (2000)].

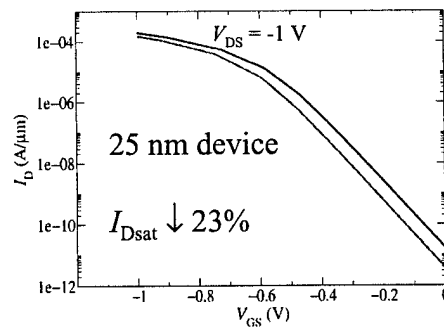
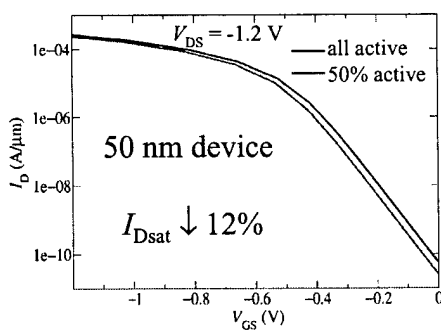
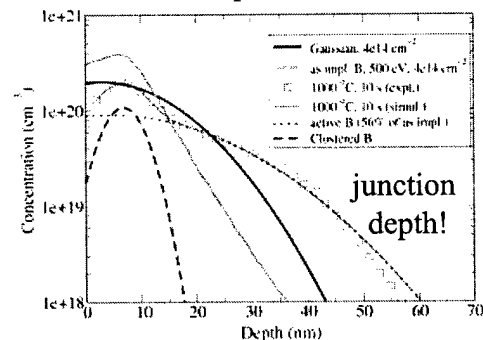
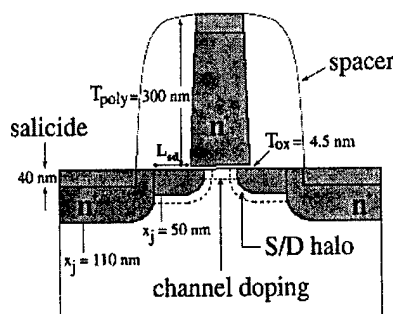
Intelligence everywhere®

MOTOROLA digital dna



## Application: Well Tempered MOSFET (MIT)

B profile



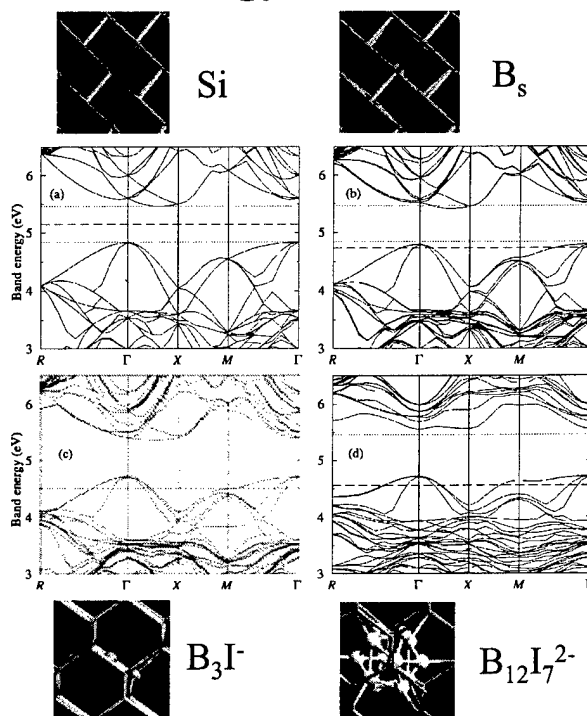
Intelligence everywhere®

MOTOROLA digital dna



# Cluster Energy and Band Structure

DFT gap  
too small  
(0.6 eV)



Cells too small  
(exciton wave  
function ~42 Å)

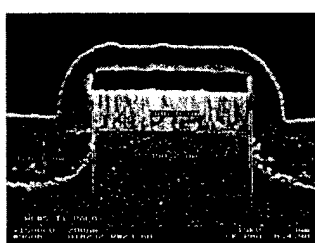
No defect  
states  $\Leftrightarrow$   
more stable

Intelligence everywhere™

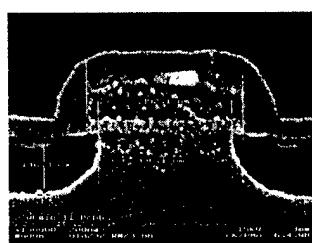
MOTOROLA digital dna



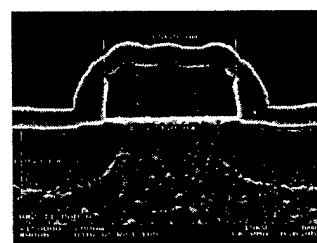
## Evidence of Stress Effect under Metal Gate



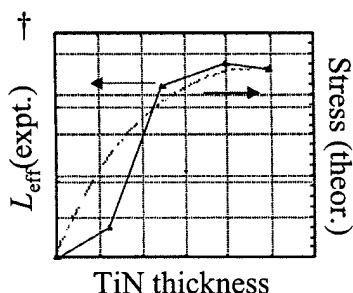
1000 Å TiN/600 Å poly-Si



250 Å TiN/1300 Å poly-Si



Poly-Si



Experiments by Maiti *et al.*:\*

- $L_{\text{eff}}$  function of TiN thickness
- Stress estimate  $\sim L_{\text{eff}}$
- Stress effect

\*B. Maiti *et al.*, IEDM, Session 29, 1998.

Intelligence everywhere™

M. Laudon, N. N. Carlson, M. P. Masquelier,  
M. S. Daw, and W. Windl, APL78 (2001).

MOTOROLA digital dna

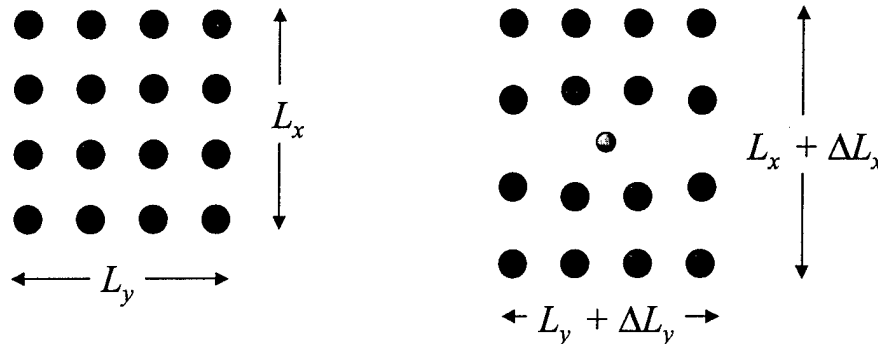


# Stress Dependence of Diffusivities

- Diffusivity:  $D = D_0 \exp(-E/kT)$

- Under hydrostatic pressure:  $E \rightarrow E + p\Delta V$

Perfect Si (or reference sys.): Create defect ( $B_s, I, V, \dots$ )  $\Delta V$ :

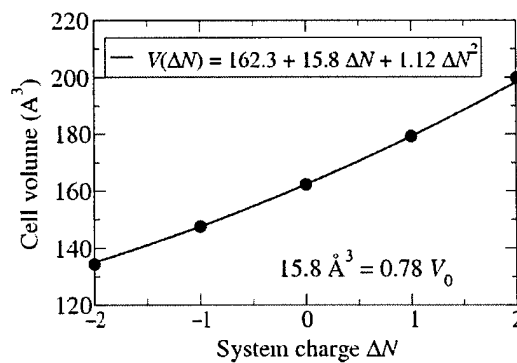


\*M. S. Daw, W. Windl, N. N. Carlson, M. Laudon, and M. P. Masquelier (PRB July 2001).

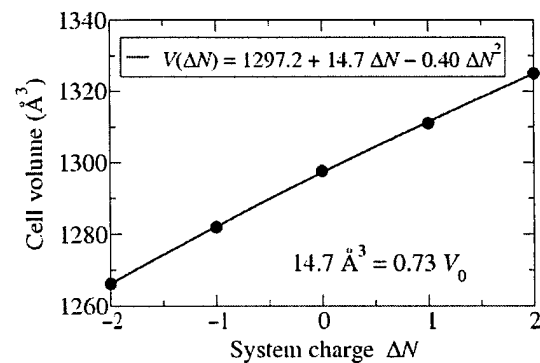


## Cell Volume and Charge in Si

8-atom Si cell



64-atom Si cell



- For all defects, cell sizes, etc., every additional electron adds  $\sim 15 \text{ \AA}^3$  to the volume
- Is this real or an artifact of the charged calculation?

# Electron Volume and Maxwell Relations

- Maxwell relation:  $\frac{\partial V}{\partial N} = \frac{\partial \mu}{\partial p}$

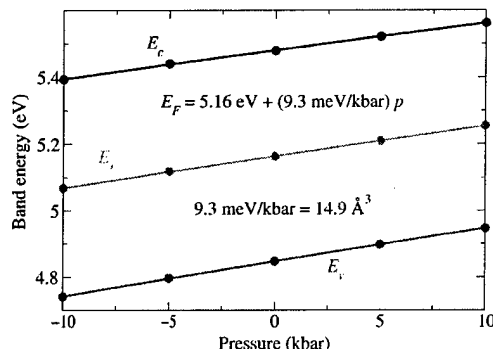
$$E_F(p) = E_F(0) + V_e p$$

- Pressure dependence of bands can be calculated in good agreement with experiment.

TABLE IV. First- and second-order coefficients describing the dependence of the direct band gap at  $T$  ( $E_0$ ) under hydrostatic pressure [ $E_0(P) = E_0 + aP + bP^2$ ] for Si, Ge, and GaAs. The experimental results are from Goñi, Syassen, and Cardona (Ref. 1).

Semiconductor	$E_0$	$a$ (meV/GPa)		$b$ (meV/GPa <sup>2</sup> )	
	Theor.	Expt.	Theor.	Expt.	Theor.
Si	3.273		100.8		0.05
Ge	-0.084	0.795	125.4	121	0.2
GaAs	0.41	1.43	99.1	108	-0.1

Alouani and Wills, PRB 54 (1996).



- We calculate again  $15 \text{ \AA}^3$  for the electron volume in Si seems to be real
- Ferry\*  $\sim 5 \text{ nm}$  (de Broglie).

Intelligence  everywhere\*

\*D. K. Ferry and H. L. Grubin, IEEE 1998.

MOTOROLA 



## Conclusions & Outlook

- Ab-initio methods are being used to provide predictive capability for dopant/defect profile evolution.
- With recalibration, boron clustering model can predict quantitatively activation and SIMS over a wide range of temperatures and annealing times.
- Dopant deactivation can easily be 50%; concentrations  $> 2 \times 10^{20} \text{ cm}^{-3}$  not achievable. Deactivation can easily change  $I_{\text{Dsat}}$  by 10s of percents.
- TED can change junction depth substantially (factor 2 even at “good” annealing conditions) short channel effects; resistance.
- We calculate the volume of an electron in Si to be  $15 \text{ \AA}^3$ .

Intelligence  everywhere\*

MOTOROLA 

